Dihydrogen driven cofactor recycling for use in bio-catalysed asymmetric organic synthesis

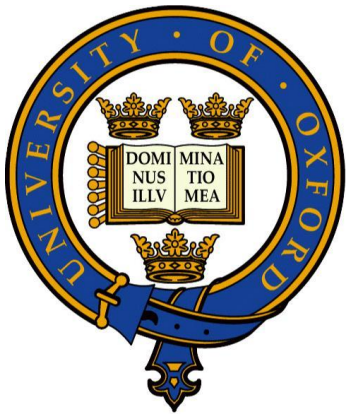

A thesis submitted to the Board of the Faculty of Physical Sciences, for the degree of Doctor of Philosophy, University of Oxford

Thomas H. Lonsdale

Wolfson College, Trinity Term, 2017

Acknowledgments

I would first and foremost like to thank my supervisor Professor Kylie Vincent. Kylie has been inspiration throughout the course of my research life. Her patient guidance and encouragement has been incredibly valuable over the entire course of my D.Phil.

In addition, I would like to thank Dr Holly Reeve for training me in electrochemistry and making particles, four years of help in the lab and for proof reading my thesis.

Dr Jack Rowbotham should be thanked for his uncomplaining assistance with a number of analytical techniques and for his encouragement in the lab during my last year as a D.Phil. student. Additionally, I would like to thank the hard working and conscientious Part II student: Farieha Altaf, for carrying out some experiments under my supervision.

This project wouldn't have been possible without the close collaboration of Dr Oliver Lenz and Dr Lars Lauterbach from the TU Berlin and Dr Frank Hollmann and Dr Caroline Paul from the TU Delft.

I would also like to thank all the members of the Vincent group past and present for making my time spent in the lab pleasant. Ceren and Ricardo deserve a special mention for helping to keep me sane during the last stages of experiments.

I would like to thank the wonderful friends I have had and made throughout my D.Phil. for enriching my life and making me grow as a person over the past four years, in particular Shriya, Mark and Pru, along with all of the SGA crew.

The Engineering and Physical Sciences Research Council are also thanked for funding.

Finally, I would like to thank all of my amazing family for their unwavering support.

Dihydrogen driven cofactor recycling for use in bio-catalysed asymmetric organic synthesis

A Thesis Submitted for the degree of DPhil, Trinity Term, 2017

Thomas H. Lonsdale, Wolfson College

Asymmetric reductions are used to produce chiral molecules which are important precursors for the pharmaceutical industry. Bio-catalytic reductions often display high enantioselectivity without the cost and toxicity associated with metal catalysis. However, unlike metal catalysts which use H_2 directly, many useful redox-enzymes require the hydride donor NADH. NADH is expensive; therefore for a bio-catalytic process to be viable it must be recycled, usually by using a sacrificial carbon based substrate, generating super-stoichiometric amounts of waste.

Two different methods for H_2-driven NADH recycling are explored in this project: using soluble hydrogenases (SH) and, carbon particles modified with a hydrogenase and an NAD^+-reductase moiety. The conductive carbon particles allow electrons from H_2-oxidation to be channelled from the hydrogenase to the NAD^+-reductase for reduction of NAD^+.

This project focuses on four main areas. The first looks at using the enzyme-modified particles for the production of high value chiral amines. A yield of >98% was achieved using the enzyme-modified particles with an L-alanine dehydrogenase for H_2-driven conversion of pyruvate to L-alanine. Moreover, a faster rate of reaction was demonstrated with the L-alanine dehydrogenase immobilised on particles *versus* with the L-alanine dehydrogenase in solution.

The second section focuses on elevated temperature NADH recycling: an SH and an NAD^+-reductase from a thermophilic organism were characterised. The NAD^+-reductase was subsequently used as part of a system for recycling NADH at >35 ^oC. When demonstrated in combination with an enoate-reductase a 62 % yield was obtained for the reduction of 2-methyl-2-cyclopentenone.

In the third strand SHs and enzyme-modified particles were investigated as recycling systems for NADH analogues. This is the first example of an enzymatic system for recycling these reduced analogues.

Finally, selective $^2H_2$-driven deuteration reactions were investigated; deuteriated compounds are high value products. It was possible to demonstrate $^2H_2$-driven production of (S)- and (R)-deuteriated phenylethanol using the enzyme-modified particles with alcohol dehydrogenases.

In summary, this thesis expands the scope for application of H_2-driven biocatalytic reduction reactions.

Abbrevia**tions**

ADH	Alcohol dehydrogenase
AT-ωTA	*Aspergillus terreus ω-transaminase*
BINAP	(2,2'-bis(diphenylphosphino)-1,1'-binaphyl)
BNA^+	1-benzyl-3-carbamoylpyridin-1-ium
BP 2000	Black Pearls 2000
$BuNA^+$	1-butyl-3-carbamoylpyridin-1-ium
BV	Benzyl viologen
COD	Cycloocta-1,5-diene
CE	Counter electrode
CLEA	Cross linked enzyme aggregates
CV	Cyclic voltammogram
D	Deuterium
DIPAMP	Ethane-1,2-diylbis[(2n-methoxyphenyl)phenylphosphane]
DMSO	Dimethyl sulfoxide
DuPHOS	((2R,5R)-1-[2-[(2R,5R)-2,5-diethylphospholan-1-yl]phenyl]-2,5-diethylphospholane)
E	Electrode potential
e	The charge on an electron
ε	Extinction coefficient
E factor	Mass ratio of waste to the desired product
E. coli	*Escherichia coli*
ee	Enantiomeric excess
Eniphos	N1,N2-bis(diphenylphosphanyl)-N1-((R)-1-phenylethyl)-N2-((S)-1-phenylethyl)ethane-1,2-diamine
E_{onset}	Onset potential
FDA	Food and Drugs Administration
FDH	Formate dehydrogenase
FMN	Flavin mononucleotide
FPLC	Fast protein liquid chromatography
GC	Gas chromatography
GDH	Glucose dehydrogenase
H. thermoluteolus	*Hydrogenophilus thermoluteolus*
HOMO	Highest occupied molecular orbital
HoxFU	NAD^+-reducing sub-units of the soluble hydrogenase
HoxHY	Hydrogen cycling sub-units of the soluble hydrogenase
Hox~~HY~~FU	Variant of the *R. eutropha* soluble hydrogenase with an inactivated hydrogen cycling dimer
HoxHYFU	The whole soluble hydrogenase (SH)
HPLC	High performance liquid chromatography
Hyd 1	*Escherichia coli* Hydrogenase 1

Hyd 2	*Escherichia coli* Hydrogenase 2
in vitro	Using isolated enzymes
in vivo	Within a whole living organism
k_{cat}	The turnover number
K_I	Inhibition constant
K_M	Michaelis constant
L-alaDH	L-alanine dehydrogenase
LeuDH	Leucine dehydrogenase
LUMO	Lowest unoccupied molecular orbital
mAC^+	3-acetyl-1-benzylpyridin-1-ium
mCN^+	1-benzyl-3-cyanopyridin-1-ium
$mCOOH^+$	1-benzyl-3-carboxypyridin-1-ium
min	minutes
MNA^+	3-carbamoyl-1-methylpyridin-1-ium
$mNAD^+$	Mimic nicotinamide adenine dinucleotide (oxidised form)
mNADH	Mimic nicotinamide adenine dinucleotide (reduced form)
MV	Methyl viologen
NAD^+	Nicotinamide adenine dinucleotide (oxidised form)
NADH	Nicotinamide adenine dinucleotide (reduced form)
$NADP^+$	Nicotinamide adenine dinucleotide phosphate (oxidised form)
NADPH	Nicotinamide adenine dinucleotide phosphate (reduced form)
NMR	Nuclear magnetic resonance
P450	Cytochrome P450 monooxygenase
PEA	Phenyl ethylamine
PG	Pyrolytic graphite
PGE RDE	Pyrolytic graphite ‘edge’ rotating disc electrode
PLP	Pyridoxal phosphate
PNA^+	3-carbamoyl-1-propylpyridin-1-ium
R. eutropha	*Ralstonia eutropha*
Rh. opacus	*Rhodococcus opacus*
Rt	Retention time
s	Seconds
SCE	Saturated calomel electrode
SDS-PAGE	Sodium dodecyl sulphate polyacrylamide gel electrophoresis
SH	The soluble hydrogenase
SHE	Saturated hydrogen electrode
TOF	Turnover frequency
TRIP	3,3′-Bis(2,4,6-triisopropylphenyl)-1,1′-binaphthyl-2,2′-diylhydrogenphosphate
TsER	*Thermus scotoductus* enoate reductase
TTN	Total Turnover Number
TN	Turnover Number (moles of product per moles of cofactor)
U mg^{-1}	Units mg^{-1}: µmole min^{-1} mg^{-1}

UV-Vis	Ultraviolet-visible
Vf	*Vibrio fluvaris*
V_{max}	Maximum rate of reaction when the enzyme is saturated with substrate
WE	Working electrode
λ_{max}	Absorption maximum

Collaborations and assistance

I would like to thank the following collaborators and research groups for generously providing, assistance, enzymes or chemicals used in this thesis:

- L. Lauterbach, J. Preissler, O. Lenz group (TU Berlin, Germany) for generously hosting me at the TU Berlin and developing the plasmids for expression of the *H. thermoluteolus* SH variants and assistance with microbiological work and for providing NAD^+ reductase samples and soluble hydrogenase.
- Caroline Paul, F. Hollmann group (TU Delft, The Netherlands) for providing the artificial cofactors, *TsER* and YqjM enzyme samples.
- Elena Nomerotskaia, F.A. Armstrong group (Oxford) for preparation of the *E. coli* hydrogenases.
- N. Richter, W. Kroutil group (University of Graz, Austria) for hosting me in Graz and for providing plasmids for the production of the *Vf-ω-transaminase* and samples of the AT-ωTA.
- The L.L Wong Group (Oxford) for GC facilities

Part II and summer students conducted some of the experiments in this thesis under my supervision. The relevant figures are labelled in the thesis itself. I assisted students while carrying out this work by helping plan experiments and develop methodology. Data from previous D.Phil. students is also reproduced and is labelled appropriately throughout the thesis. I was also assisted by Post-Docs in the group for some experiments. Details of assistance received for experimental work is given in the table below.

Section	Figure (F) or Table (T)	Person	Comments
3.6.2		Dr J. Rowbotham (Post-Doc, Vincent group, Oxford University)	Assistance with ^{1}H NMR to determine the *ee* of 1-methyl-3-phenylpropylamine.
4.3	Figure 4-6	Dr S. Frielingsdorf (Post-Doc, TU Berlin)	Assistance with size exclusion chromatography
4.5.6	Figure 4-16, Figure 4-17, Figure 4-18, Figure 4-19	Mr Tim Sudmeier (Summer student)	Determination of affinity constants for *H. thermoluteolus* HoxFU.
4.6	Table 4-4	Dr H. Reeve (Post-Doc, Vincent group, Oxford University) and Dr Z. Idris	K_M and K_I values for the SH from *R. eutropha and Rh. opacus*
6.3	Table 6-2	Ms Farieha Altaf (Part 2: P2)	Percentage conversion of artificial cofactors with GDH and FDH
6.4	Table 6-4	Ms Farieha Altaf (P2)	Specific activities and percentage conversions of the artificial cofactors with *H. thermoluteolus* SH
6.6.1	Table 6-6, Table 6-7, Figure 6-15	Ms Farieha Altaf (P2)	Coupling the SH from *H. thermoluteolus* and *TsER* using artificial cofactors
6.8	Table 6-9	Ms Farieha Altaf (P2)	Percentage conversion with PG particles functionalised with Hyd 2 and *H. thermoluteolus* HoxFU
6.8	Figure 6-29	Dr J. Rowbotham (Post-Doc, Vincent group, Oxford University)	Submitting the sample for LC-MS analysis
6.7.1	Figure 6-21	Dr H. Reeve and Dr Z. Idris	Cyclic voltammograms for reduction of NAD^+
7.5, 7.6	Figure 7-11 (a), Figure 7-15 (a)	Ailun Huang (Summer student)	HPLC for determining the *ee* of the phenylethanol product
Appendix F	Figure A.20	Dr J. Rowbotham (Post-Doc, Vincent group, Oxford University)	Deconvolution to determine the *ee* of 1-methyl-3-phenylpropylamine.
Appendix G	Figure A.22	Dr J. Rowbotham (Post-Doc, Vincent group, Oxford University)	Assistance with NMR experiment to determine the rate of hydrolysis of Maleimide substrates

Publications

1. P. A. Ash, H. A. Reeve, J. Quinson, R. Hidalgo, T. Zhu, I. J. McPherson, M.-W. Chung, A. J. Healy, S. Nayak, T. H. Lonsdale, *et al*., 'Synchrotron-based Infrared Microanalysis of Biological Redox Processes under Electrochemical Control.' Anal. Chem. 2016, acs.analchem.6b00898.

2. C. Zor, H. A. Reeve, J. Quinson, T. H. Lonsdale, L. Thompson, F. Dillon, N. Grobert, K. A. Vincent H_2-driven Biocatalytic Hydrogenation in Continuous Flow using Enzyme-Modified Carbon Nanotube Columns', Chem. Commun., 2017, 53, 9839--9841

In preparation:

3. T. H. Lonsdale, H. A Reeve, F. Altaf, O. Lenz, C. E. Paul, F. Hollmann, K. A. Vincent, 'The *R. eutropha* soluble hydrogenase for hydrogen driven recycling of artificial cofactors' (*in preparation*)

Previous publication:

4. T. H. Lonsdale, L. Lauterbach, S. Honda Malca, B. M. Nestl, B. Hauer, O. Lenz, 2015. 'H_2 -driven biotransformation of n-octane to 1-octanol by a recombinant Pseudomonas putida strain co-synthesizing an O_2-tolerant hydrogenase and a P450 monooxygenase.' Chem. Commun. **2015,** 51, 16173–16175.

Table of contents

1 Introduction

Since the discovery of chirality in 1848 by Pasteur chemists have become increasingly aware of the importance of being able to produce chemicals as single enantiomers.[1] Chirality is particularly important to living organisms which can often distinguish between different enantiomers of a particular compound.[2] Consequently, different enantiomers of flavour compounds can smell or taste different. For example the D-enantiomer of limonene smells of oranges and the L-enantiomer smells of turpentine or lemons.[3]

In addition, chirality is also of substantial importance in the pharmaceutical industry. In 2010, it was expected that over 70 % of pharmaceutical intermediates would contain chiral centres,[4,5] and today most new drugs are marketed as single enantiomers.[6] From a regulatory perspective single enantiomers are important as the FDA (United States Food and Drug Administration) requires extensive studies on both enantiomers of a drug target before granting approval to a racemic drug.[7]

Furthermore, obtaining enantiomerically pure active pharmaceutical ingredients (APIs) is important for the safety and effectiveness of many drugs.[8]

For example L-Dopa (3,4-dihydroxyphenyl-L-alanine) used in the treatment of Parkinson's disease, shows fewer adverse effects than a mixture of L- and D- Dopa, meaning that a higher dosage of active drug can be administered.[9]

1.1 Biocatalysis

As enzymes originate from living systems they are themselves inherently chiral, being entirely composed of L-amino acids.[10,11] They are consequently able to discriminate between enantiomers of racemic substrates[12] as well as being able to carry out oxidative or redox processes in an enantioselective manner.[13]

Biocatalysis is defined as a reaction catalysed by a biological entity, for example whole cells, isolated enzymes or semi purified cell extracts.[14]

The use of biological systems to produce useful products is not new. Fermentation, using yeast, to produce products such as bread, beer and wine has been used for thousands of years.[15] An example of a large scale modern biocatalytic process is the use of immobilised glucose isomerase, which is used to produce millions of tonnes of the sweetener: isoglucose.[16,17]

Biocatalysis has a number of key advantages over traditional synthetic catalytic processes. These include the fantastic selectivity often displayed by enzymes which means that transformations can be performed on complicated molecules containing a number of functional groups with precise regio-, stereo-, and enantio- control.[18]

In addition, biocatalysis allows the use of mild conditions with most reactions operating at ambient temperature and in water. Nowadays, enzymes which are able to act upon a range of substrates are widely available and their substrate scope can be further improved using genetic engineering techniques, possibly even allowing access to new chemical space and new reaction pathways.[13]

Enzymes can also be a cheaper alternative to precious metal catalysts, as although highly purified enzymes are often very expensive,[11] relatively inexpensive crude preparations of enzyme are acceptable for most synthetic organic biocatalytic reactions.[11] This means that they can be produced cheaply in comparison to many chemical catalysts, if a high yielding heterologous expression system in a microbiological host can be developed.[19][20] Enzymes are also produced as additives for washing detergent demonstrating that crude enzyme preparations can be prepared on a large scale very cheaply.[11]

Biocatalysis has already been used in a wide range of industrial settings, including in key steps in the manufacture of a number of drug molecules.[5,21–23]

1.1.1 Hydrolysis and resolution reactions

Enzymatic hydrolysis and resolution reactions are particularly well established methods of generating enantiomerically pure products through biocatalysis.[24] Consequently lipase and protease enzymes are some of the most commonly used in chemical synthesis.[25]

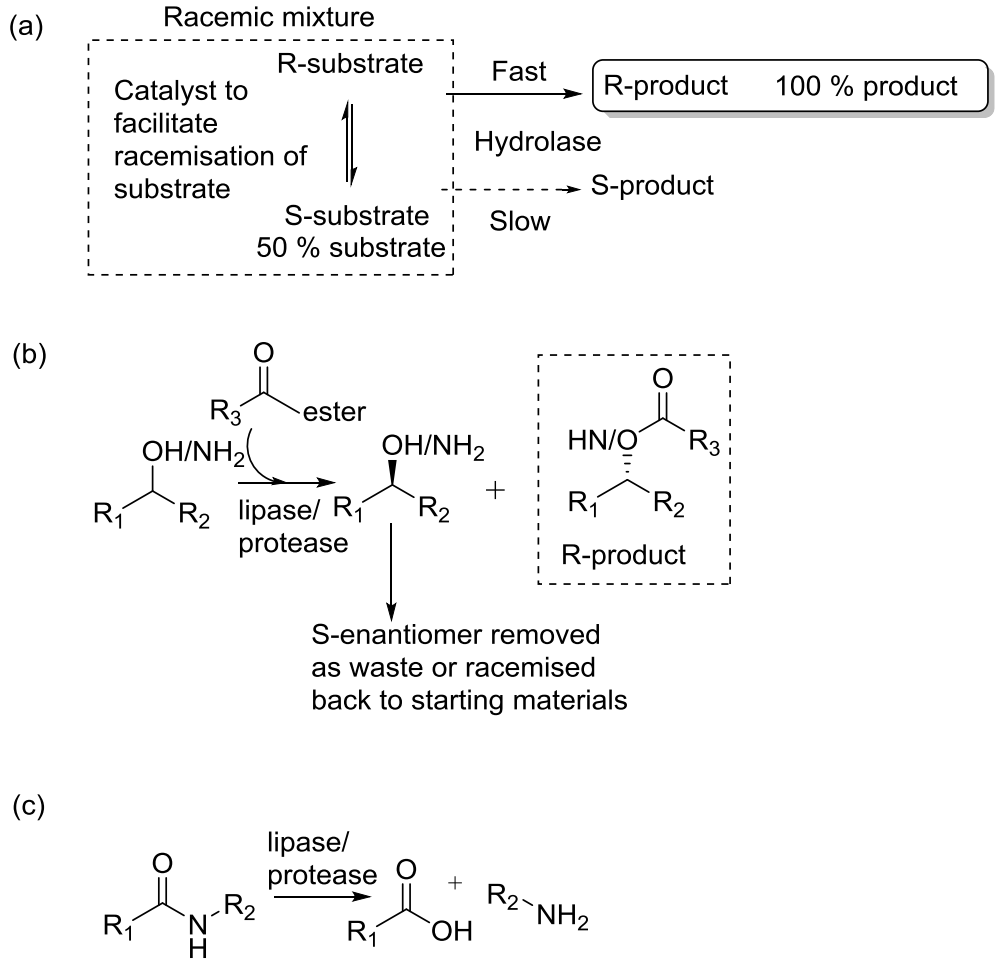

Figure 1-1: (a) A dynamic kinetic resolution of a racemic substrate. The substrate undergoes *in situ* racemisation, so that as the (R)-enantiomer is converted to the (R)-product, the (S)-enantiomer is racemised maintaining 50 % (R)-substrate concentration. (b) An example of a biocatalytic resolution reaction in which an ester is used as a transesterification reagent to obtain a single enantiomer of amine or alcohol product. (c) Amine bond hydrolysis by a lipase. Adapted from Pollard *et al*.[5]

Where possible, dynamic kinetic resolution reactions are used, as shown schematically in Figure 1-1 (a). Here *in situ* racemisation of the starting material gradually increases the amount of substrate recognised by the enzyme catalyst. One very successful example of this is the work of Persson *et al.* on the dynamic resolution of phenylethanol with a lipase and 4-chlorophenyl acetate as the acyl donor. In this work a ruthenium catalyst was used to enhance the rate of racemisation, this led to a yield of >99 % (of (R)-1-phenylethyl acetate) and > 99 % *ee*, see Figure 1-1 (b).[24,26]

Particularly important reactions for the biocatalytic production of chiral amines include the hydrolysis of an amide bond by a protease giving a carboxylic acid and an amine, shown in Figure 1-1 (b). Additionally, resolution of amines can be performed by carrying out selective acylation reactions using esters as the transesterification reagent, see Figure 1-1 (c).[11,24] As these reactions lead to two chemically different molecules, it is possible to separate them using chromatography.

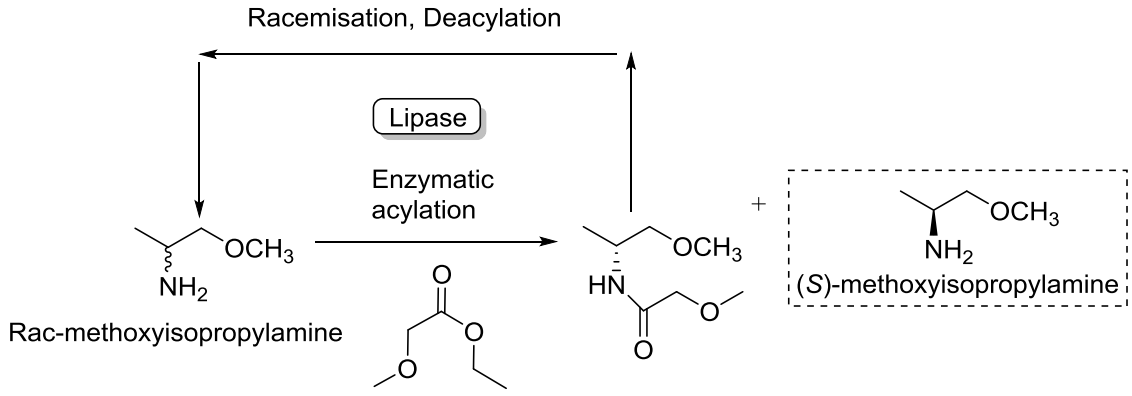

Figure 1-2: The lipase catalysed resolution of (S)-methoxyisopropylamine from a racemic mixture adapter from J. Hagen in Industrial Catalysis: A practical Approach.[27]

One important example of a selective enzymatic acylation used to obtain a chiral amines carried out industrially is in the production of (S)-2-methoxyisopropylamine. This reaction is carried out by BASF on a multi-thousand tonne scale per year as (S)-2-methoxyisopropylamine is a key intermediate in the production of Outlook®, a weed

killer.[27] The chiral resolution of the racemate is carried out by selectively acylating the (R)-enantiomer leaving the desired (S)-enantiomer. The amide can then be separated, deacylated, racemised and recycled.[27] This reaction is shown schematically in Figure 1-2.

1.2 Catalytic chemical methods of asymmetric reduction reactions

Organic reduction reactions involve reducing the oxidation state of a target molecule. These transformations are one of the most important organic reactions.[28] Generally, reduction reactions are preferred over oxidation reactions by the pharmaceutical industry and so starting materials with a higher oxidation states will be chosen and then reduced, rather than oxidising starting materials with a lower oxidation state. This is because oxidants present safety concerns due to their explosion risk and the toxicity of many stoichiometric oxidants.[29] Generally, in other reactions it is possible to prevent fires by not giving the solvent or reactants access to oxidants, in oxidations, however, this is necessary and so the three things necessary for combustion are combined: heat, fuel and an oxidant.[29] One example of a toxic oxidant is OsO_4, which can be used to oxidise C=C double bonds.[29]

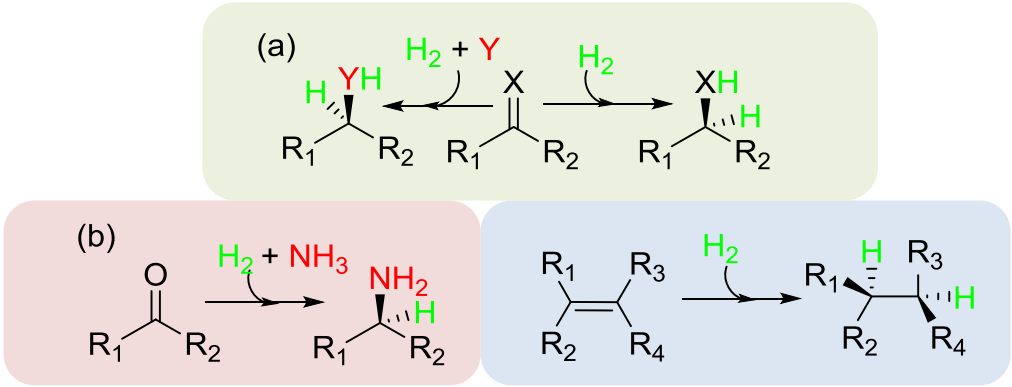

Figure 1-3: Asymmetric hydrogenation reactions (a) Schematic diagram showing the generalised reaction scheme for H_2-driven reduction reaction of C=X double bonds leading to the creation of a chiral centre. Note that as in reductive amination reactions these can be substituted for another species. (b) Red box: reductive amination reaction; blue box: alkene reduction reaction.

The reduction of sp^2 to sp^3 centres is particularly important as it often leads to the introduction of chirality at that position in a molecule;[13] this can include hydrogenation of carbonyls, imines and alkenes, but also the reductive amination of ketones. If a catalyst is employed which is able to control the stereoselectivity of addition this can lead to an enantiopure product. This work focusses in particular on reductive aminations and the reduction of alkene functionalities, see Figure 1-3.

1.2.1 Asymmetric reductive amination reactions

Chiral amines are of significant industrial importance, particularly as chiral building blocks for pharmaceutical synthesis.[30] A general, clean, methodology for the direct synthesis of α-chiral aliphatic amines from prochiral ketones would be highly desirable in synthetic chemistry.[31] A significant number of drugs require chiral amines as building blocks: such as *rivastigmine* used in the treatment of Alzheimer's disease and *sitagliptin*, used in the treatment of diabetes (Figure 1-4).[20]

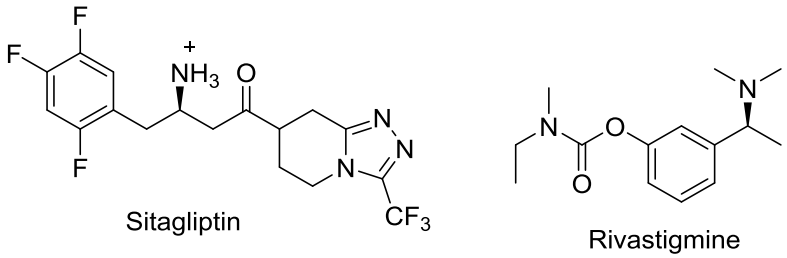

Figure 1-4: The chemical structures of two chiral pharmaceutical compounds containing amine functionalities.

Few methods exist for the efficient synthesis of chiral amines from prochiral ketones. One of the main ways of producing chiral amines is, in fact, still by the resolution of racemic mixtures of amines using chiral carboxylic acids as resolving agents.[20] A one pot synthesis of chiral amines *via* direct reductive amination of ketones, using NH_3 and H_2 gas, would be highly desirable, as it would avoid time-consuming isolation and work up steps.[32]

In traditional synthetic chemistry, two important methods of introducing chiral amine centres from a ketone starting material in a one pot reaction are; transition metal-mediated homogeneous reductive amination and diasteroselective reductive amination.[32]

Transition metal-mediated homogeneous reductive amination makes use of a catalyst with a transition metal centre and often chiral organophosphorus ligands. Blaser and co-workers reported the first example of enantioselective reductive amination.[32] They found that it was possible to carry out the reductive amination of methoxyacetone with 2-methyl-5-ethylaniline using an Ir organometallic catalyst. However, optimal conditions required 80 bar H_2 and 50 ^oC to obtain a product with a 76 % *ee*.[32] Large H_2 overpressures require expensive handling equipment and are also dangerous.

Another good example of this kind of reaction is the reductive amination of a range of substituted acetophenone derivatives using a ruthenium BINAP (2,2-Bis(diphenylphosphino)-1,1-binaphthyl) catalyst, originally developed by Noyori.[33] This method of reductive aminations, using Leuckart–Wallach transfer hydrogenation conditions, was first developed by the groups of Kadyrov (Evonik-Degussa AG) and Börner. An example is shown in Figure 1-5.[34,35]

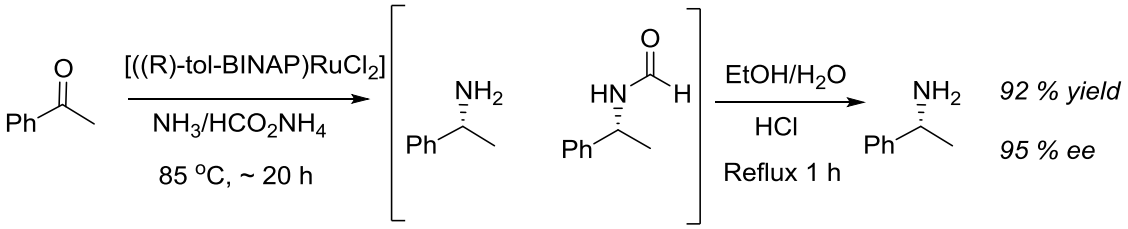

Figure 1-5: The reductive amination of acetophenone (an example of an aryl ketone) to (R)-phenyl ethylamine, using a Ru catalyst along with a chiral BINAP ligand, which is able to control the selectivity of addition of ammonia to the C=O functionality. BINAP = 2,2'-Bis(diphenylphosphino)-1,1'-binaphthyl. This method leads to production of amines and N-formyl amines; however, after work up with ethanol and hydrochloric acid the formyl derivatives could be hydrolysed to the amine giving a 92 % yield with 95 % ee. Adapted from Nugent *et al*. in Chiral amine synthesis.[32]

A range of chiral amine products can be obtained using this method with high enantiomeric excess (*ee*). The catalysts are also generally stable and in the best cases low catalyst loadings of 0.01 mole percent can be used, which would equate to a TTN (Total turnover number) of 10,000.[34] However, even these catalysts require high temperatures (85 ^{o}C). Catalysts used in reductive amination reactions are also expensive to produce, are air and water sensitive and are often highly flammable requiring special handling conditions, such as the use of very pure gas feedstocks.[20][35]

Another method of introducing chiral amine functionality is diasteroselective reductive amination, which uses a chiral amine auxiliary to provide the amine equivalent, hence generating a new chiral primary amine. This method requires the presence of inexpensive chiral amine equivalents, usually (R)- and (S)-phenyl ethylamine (PEA).[34] Nugent and co-workers, for example, have reported on the reductive amination of a range of prochiral ketones using (R)- and (S)-PEA followed by hydrogenolysis, Figure 1-6.[34]

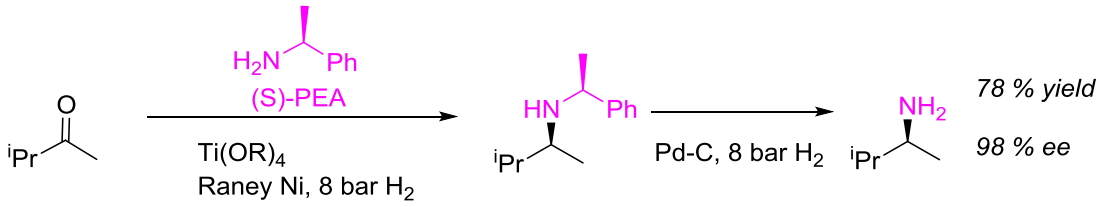

Figure 1-6: Two step chiral primary amine synthesis: reductive amination with the (S)-PEA auxiliary followed by hydrogenolysis. Adapted from Nugent in Chiral Amine Synthesis.[34]

Diasteroselective reductive amination methods are less developed and often give lower *ee* values than asymmetric hydrogenation methods.[20] There are also few chiral amine equivalents, which are acceptable to industry.[34] However, this method avoids the use of difficult to handle metal-organic reagents.

Academic work by List *et al*. has demonstrated that organocatalytic methods can be used for one pot asymmetric reductive amination reactions. In the example shown in

Figure 1-7 an achiral Hantzsch ester was used to reduce the pre-formed achiral iminium cation. This was then protonated by the TRIP (phosphoric acid) catalyst. Due to the chiral nature of the TRIP counter ion the reduction was carried out enantioselectively.[32][36]

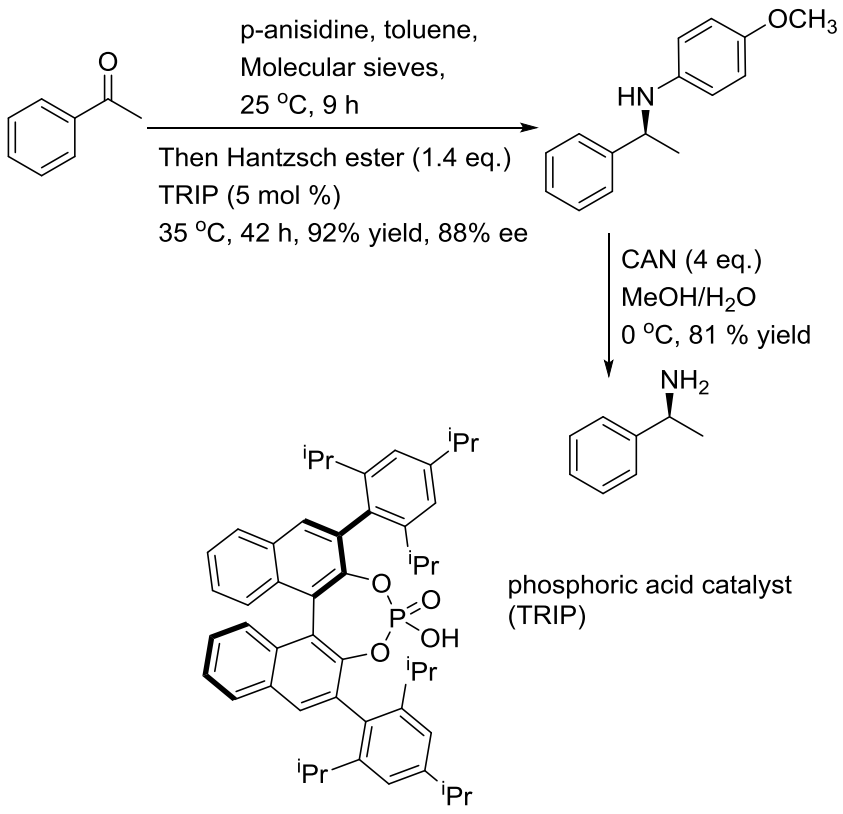

Figure 1-7: TRIP catalysed organocatalytic conversion of a ketone to a chiral amine. This reaction is a two-step reaction and a work-up between the steps is not required. Adapted from Nugent *et al.* [32] **CAN = cerium(IV)ammonium nitrate**

It was possible to obtain the amine product of this reaction with 88 % *ee*. This reaction significantly improves on organocatalytic methods which require imines to be synthesised, then isolated before being reduced to chiral amines. This methodology is also tolerant to a wide variety of functional groups in place of the benzene ring. Organocatalytic reductive amination reactions, however, have yet to be used industrially on a large scale.[34]

1.2.2 Asymmetric reduction of alkenes

Asymmetric reduction of alkenes, otherwise known as asymmetric hydrogenation, is now an advanced field of research.[37] This reaction is often achieved by using precious metal catalysts with a chiral ligand.[38] Rh-catalysed alkene hydrogenation remains a focus of scientific investigation;[38] often chiral phosphorous ligands are used to enable these catalysts to give products with high *ee*. However, these catalysts suffer from the drawbacks of being time consuming to synthesise, costly, and environmentally unfriendly due to the requirement for substantial H_2-overpressures (3-50 bar).[38,39] In addition, although transition metal based *cis*-hydrogenation is a well-developed field, developing effective transition metal catalysts for *trans*-hydrogenation has been more difficult.[40] One example of asymmetric alkene reduction used industrially is in the synthesis of pharmaceutical 3,4-dihydroxyphenyl-L-alanine (L-Dopa) used to treat Parkinson's disease, this methodology was originally developed by W. S. Knowles.[41] An R,R-DIPAMP catalyst (see caption to Figure 1-8) was used for the selective reduction of the C=C double bond which is a key step in the total synthesis of this drug (Figure 1-8).

A range of more effective chiral phosphorous ligands have since been developed, such as DuPHOS ((2R,5R)-1-[2-[(2R,5R)-2,5-diethylphospholan-1-yl]phenyl]-2,5-diethylphospholane).[41] Currently, more than 250 tonnes of L-Dopa are produced per year, mainly using asymmetric hydrogenation catalysis.[42][43] Although, the chemical synthesis of L-Dopa is a demonstration of the success of organometallic catalysis, this method still requires an expensive rhodium metal centre.

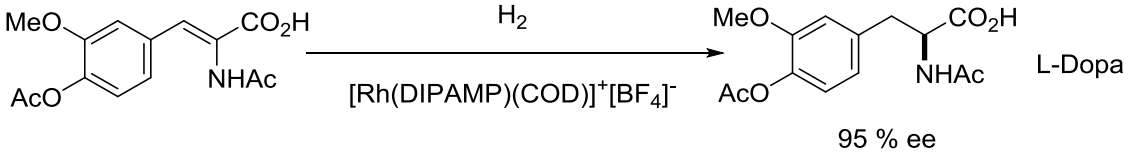

Figure 1-8: An asymmetric alkene reduction which makes up a key step in the synthesis of L-Dopa. Adapted from W. S. Knowles.[41] DIPAMP = Ethane-1,2-diylbis[(2n methoxyphenyl)phenylphosphane]. COD = Cycloocta-1,5-diene.

Typically laboratory preparations of asymmetric hydrogenation catalysts achieve TTNs (total turnover numbers) of *ca.* 2000. However, larger volume processes for the production of L-Dopa have achieved TTNs approaching 1×10^6.[37]

Often state of the art rhodium based asymmetric hydrogenation catalysts achieve turnover frequencies (TOFs) of up to 5000 h^{-1}, which is equivalent to 1.45 s^{-1}.[44] For example acetyl-L-phenylalanine, which is an intermediate in the synthesis of the sweetener aspartame can be synthesised by asymmetric reduction of (Z)-2-acetamido-3-phenylacrylic acid, shown in Figure 1-9. [45] For this process it was possible to achieve TOFs of 5,000 h^{-1} and a TTN of 15,000.[45]

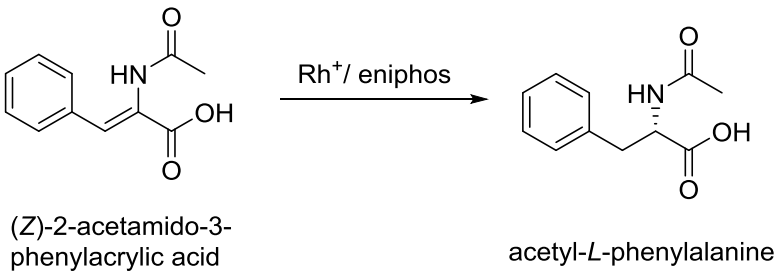

Figure 1-9:Asymmetric alkene reduction in the synthesis of acetyl-L-phenylalanine. Eniphos = N1,N2-bis(diphenylphosphanyl)-N1-((R)-1-phenylethyl)-N2-((S)-1-phenylethyl)ethane-1,2-diamine. Adapted from Blaser *et al.*[45]

1.3 Enzymatic methods for asymmetric hydrogenation reactions

Since 1970 interest in using enzymes in synthesis has steadily increased[11,46] because of their very high selectivity, their ability to function under mild conditions, and in water.[11]

Using enzymes for asymmetric hydrogenation reactions avoids the use of expensive and toxic precious metal based catalysts, as well as high pressures of H_2. Recently, there has been increasing interest in carrying out the final step in the L-Dopa synthesis, shown in Figure 1-8, enzymatically.[39][47]

1.3.1 Asymmetric reductive amination reactions

One particularly desirable reaction for the pharmaceutical industry is the direct reductive amination of prochiral ketones, using ammonia as a nitrogen source and a reducing equivalent.[31]

An example of a true enzymatic reductive amination carried out industrially, just using NH_3 as the amine source is the reductive amination of trimethylpyruvate to give L-tertiary leucine, see Figure 1-10, making use of recombinant leucine dehydrogenase (LeuDH) from *Bacillus stearothermophilus* as the enzymatic catalyst.[48,49] This product is made on a multi-tonne scale by Evonik-Degussa GmbH.

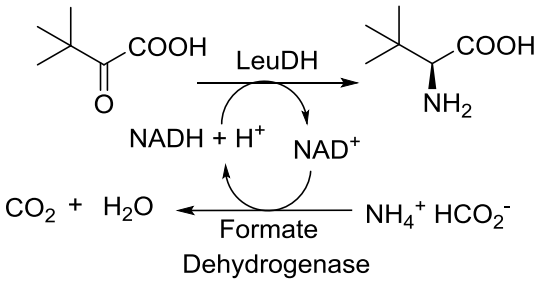

Figure 1-10: The reductive amination of trimethylpyruvate to give L-tertiary leucine, adapted from Bommarius et al.[48]

L-tertiary leucine is used as a precursor in the production of pharmaceuticals used to treat tumours and in the production of anti-retroviral medication.[50] Leucine dehydrogenase has been shown to catalyse the reductive amination of a number of branched chain α-keto acids leading to products ranging from naturally occurring leucine to the non-proteogenic amino acid (S)-β-hydroxy-valine.[51] Amino acid dehydrogenases, however, have the drawback that they are only able to accept

α-ketoacids as substrates and are consequently confined to α-amino acids as products.[13] Additionally, due to their role in amino acid metabolism most amino acid dehydrogenases are highly L-specific, consequently only giving access to one enantiomer of the amino acid product.[13]

ω-Transaminase enzymes, on the other hand, are able to catalyse the redox neutral conversion of a prochiral ketone to a chiral amine at the expense of an amine donor. Recently, a genetically engineered *ω-transaminase* enzyme has been used in the synthesis of the pharmaceutical sitagliptin, a drug used in the treatment of type 2 diabetes.[52,53] By using an *ω-transaminase* enzyme for the final ketone to amine conversion step in this reaction (see Figure 1-11), it was possible to increase the overall yield by 13 %, increase productivity by 53 % and decrease the waste produced by 19 % in comparison to the original route which made use of a rhodium organometallic catalyst:[52] a significant improvement.

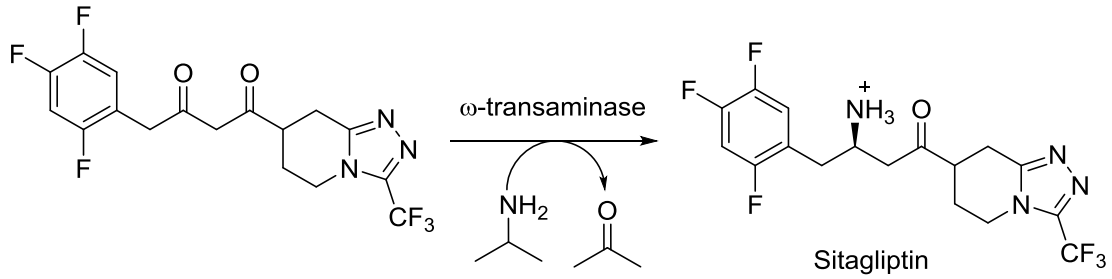

Figure 1-11: The final reductive amination step in the synthesis of Sitagliptin

The *ω-transaminase* enzyme used here is able to make use of the cheap amine donor isopropyl amine. It was engineered to contain 27 mutations both at the active site and at the interface of the enzyme dimer.[52] The engineered *ω-transaminase* is able to tolerate 200 g L^{-1} substrate and 50 % DMSO. The biocatalytic process has now been demonstrated on a pilot scale.[52]

1.3.2 Asymmetric reduction of alkenes

Enzymatic reduction of C=C double bonds may become an important synthetic tool in addition to already established chemical hydrogenation methods, due to the tendency of enzymes to favour trans-hydrogenation.[13,40] The reduction of activated C=C double bonds can be achieved using enoate reductase enzymes (ERs).

Baker's yeast is the first choice biocatalyst for the reduction of a number of activated C=C bonds.[40] One of the best known industrial applications of enoate reductase enzymes is in the reduction of ketoisophorone to (R)-levodione, see Figure 1-12.[11,40] This is used as a precursor in the synthesis of a number of carotenoids, for example astaxanthin and zeaxanthin.[11] These compounds are mainly used as dietary supplements for animals as they impart colour to fish such as salmon. They are also sometime taken by humans because of their alleged ability to retard progress of degenerative conditions of the eye.[54] As enoate-reductases within baker's yeast catalyses the reduction of the alkene bond more quickly than alcohol dehydrogenases within the cells catalyse the reduction of the ketone group, by having relatively short reaction times it is possible to obtain the desired (R)-levodione product in high yields without a significant number of over-oxidation products.[40,54]

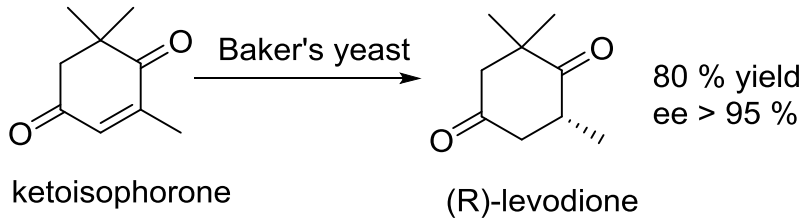

Figure 1-12: Industrial scale reduction of ketoisophorone to (R)-levodione using whole cells of baker's yeast.

More recently a number of isolated enoate reductase enzymes have been shown to be able to reduce ketoisophorone, all giving the (R)-product.[13,55] When the isolated enoate reductase pentaerythritol tetranitrate reductase (PETNr) was used in combination with a

glucose dehydrogenase enzyme as the cofactor recycling system, it was possible to obtain the (R)-levodione product with > 99 % *ee*.[55–57]

1.4 Immobilisation in biocatalysis

Immobilisation allows many of the problems associated with the application of enzymes to be overcome.

Immobilisation can improve the stability of enzymes,[11,58] as trapping an enzyme in a restricted pocket or linking it to a carrier matrix can lead to less movement of the protein.[58][59] Additionally, trapping enzymes on or in some type of support creates a heterogeneous system meaning the enzyme catalyst can be easily removed from the aqueous reaction mixture at the end of a batch process and used in a subsequent process. If the enzyme can be re-used this reduces the cost of the catalyst as a percentage of the overall cost of the reaction.

Depending on the immobilisation technique the properties of the enzyme such a k_{cat} or pH stability may also be affected.[60]

There are a range of immobilisation techniques which are widely applied. Adsorption is one of the simplest methods of immobilisation. There are a number of different adsorption forces including Van der Waals, ionic interactions and hydrogen bonding. These are all relatively weak. Adsorption is generally a simple procedure in which loss of enzyme activity is usually low. However, there is the possibility of desorption or leaching of the enzymes from the carrier surface during the course of a reaction or if the enzymes are to be recycled, in the recycling step. [11,60]

Alternatively, ionic bonding or covalent immobilisation techniques can be used. Ionic based immobilisation techniques are particularly susceptible to changes in pH or the ion concentration of the solution, which can lead to desorption of the enzyme. Covalent

attachment often requires harsh conditions, typically involving using glutaraldehyde solution to cross link enzymes to a carrier matrix.[11] This means that significant enzyme activity is often lost.[61] Additionally, the covalent immobilisation step can be relatively time consuming, meaning that activity of the enzyme may be lost during the immobilisation process.

Enzymes can also be attached to each other *via* cross linking to produce CLEAs (cross linked enzyme aggregates).[62] CLEAs are produced by using salts, water immiscible solvents or non-ionic polymers to precipitate out enzymes from aqueous solution. These are then cross linked with glutaraldehyde solution.[61] This avoids the introduction of a significant mass of inactive carrier. However, the activity of these structures can be limited due to diffusional problems within the aggregates. So far the only commercially available CLEA produced with a redox enzyme is a CLEA with an alcohol dehydrogenase (ADH) from *Rhodococcus erythropolis*, combined with a FDH cofactor recycling system from *Candida boidinii*.[63][61] Only 20 % of the activity of the ADH towards the reduction of p-chloroacetophenone prior to cross linking was retained in the case of this CLEA.[63]

1.5 Cofactor requirements for enzymatic reductions

Metal catalysts are often able to use H_2 directly to produce co-ordinated hydride ligands which then carry out the hydrogenation reaction. Enzymes on the other hand, are not usually able to use H_2 directly for hydrogenation chemistry. Many industrially applicable dehydrogenase enzymes rely instead on a biological transporter molecule to supply a hydride in a form which they can use.[64] They make use of this hydride along with a proton from solution to carry out enzymatic hydrogenation reactions. These biological hydride transporters are known as cofactors. The most commonly required

cofactor is Nicotinamide adenine dinucleotide hydride (NADH) shown in Figure 1-13 and its phosphorylated derivative, NADPH.

NADH enters the active site of the oxidoreductase enzyme and either transfers the hydride from the 4 position of the nicotinamide ring directly to a substrate or to an internally bound redox cofactor within the protein active site (such as FMN, Flavin mono nucleotide). A proton, which originates from solution, but is likely to be delivered from a nearby amino acid, is then added to the other side of the double bond.

When using cofactor dependent enzymes to carry out reductions, stoichiometric amounts of the reduced cofactor NADH (Nicotinamide adenine dinucleotide) or NADPH, are required to provide reducing equivalents. Current prices from Sigma Aldrich for 1 mole of NADH and NADPH respectively are £68,950 and £1,040,000.[65] This means that these cofactors are often more expensive than the desired products of the reactions they are catalysing, therefore it is not economically viable to use nicotinamide cofactors in stoichiometric quantities. Consequently, a system for recycling the reduced cofactor is required.

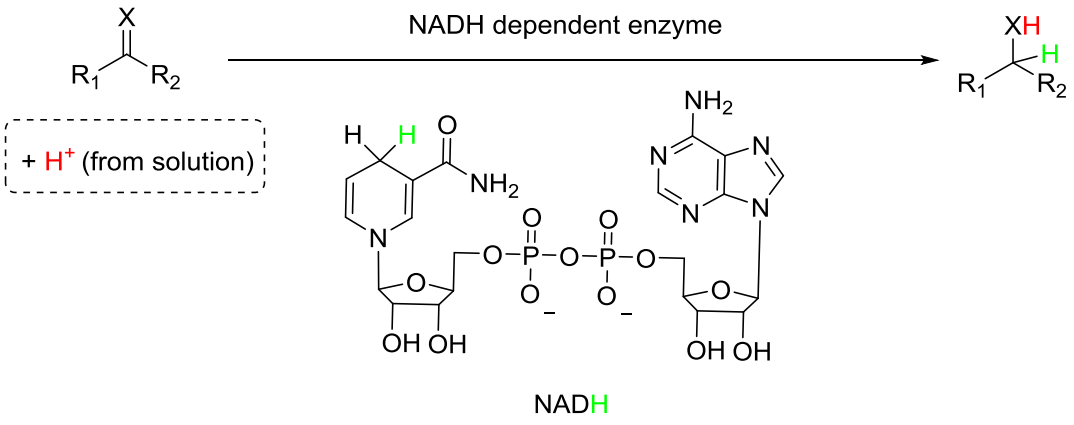

Figure 1-13: A diagram showing NADH being used by an NADH dependent enzyme to carry out the reduction of a double bond. Within the enzyme active site the green hydride at the 4-position of the nicotinamide ring of NADH is added to the double bond of the substrate molecule, a proton (originally from solution) is then added to the other side of the double bond.

Recently, there has been interest in developing artificial cofactors which conserve the nicotinamide group present in NADH, (shown in blue in Figure 1-13) but have simpler side chains. These artificial cofactors can be synthesised in the laboratory and so can cost as little as £300 per mole.[65][66] However, the development of robust recycling systems for these artificial cofactors is still required to prevent the production of super-stoichiometric amounts of carbon based waste, which must be removed from the reaction mixture at the end of the reaction to obtain a pure product.

1.5.1 Using whole cells to satisfy the cofactor requirements of redox processes

One possible way of avoiding adding stoichiometric amounts of natural cofactor is to carry out reactions in whole cells. It is then possible to rely on cellular metabolism to provide the required cofactors which are naturally present within all cells.[11]

Using whole cells, with a redox enzyme overexpressed within them, has a number of advantages over using enzymes *in vitro.* The main advantage is that cellular metabolism can be used to satisfy the cofactor requirements of the oxido-reductase enzyme. In addition, expensive and time consuming purification steps are not necessary to obtain the required enzymes, and enzymes are generally more stable within cells.[11,13,67,68]

When growing cultures are used to carry out biocatalysis glucose is normally used as the source of energy for metabolism. In *E. coli* the pentose phosphate pathway is the main pathway used to produce the cofactor NADPH, which leads to the production of 2 moles of NADPH per mole of glucose.[69] NADH is also produced via glycolysis when the *E. coli* is growing on glucose.[70]

Often however, in order to avoid metabolic by-products contaminating the reaction mixture, resting cells are used. In order to boost yields, cells often have an additional enzyme for cofactor recycling overexpressed within them, such as a formate

dehydrogenase (FDH) or glucose dehydrogenase (GDH).[69] On a laboratory scale it has been possible to demonstrate H_2-driven cofactor recycling in whole cells using the soluble hydrogenase (SH) from *R. eutropha*.[68]

Whole cell processes using alcohol dehydrogenase enzymes (ADH) are very well developed. One example of a whole cell biocatalytic process used industrially is the conversion of ethyl-5-oxo-hexanoate to ethyl (S)-5-hydroxyhexanoate.[71][67] β-Hydroxy acids are versatile chemical building-blocks used in the synthesis of a number of natural products and pharmaceuticals. Pharmaceutical company Bristol-Myers Squibb used whole cells of *Pichia methanolica* to carry out this reduction, while supplementing the reaction medium with glucose. In this reaction they could obtain the product ethyl (S)-5-hydroxyhexanoate with a yield of 90 % and >95 % *ee*, when the reaction was carried out on a gram scale.[67,71]

Whole cells have also been used in the production of amino acids. Evonik-Degussa have developed a whole cell biocatalytic process for the production of L-neopentylglycine from 4,4-dimethyl-2-oxopentanoic acid.[72,73] These bulky non-natural amino acids are important pharmaceutical precursors for medicines used to treat viruses and tumours.[73] Using a 'designer cell' approach with a leucine dehydrogenase enzyme over-expressed within the cell, it was possible to obtain L-neopentylglycine on a 10 kg pilot plant scale with > 95 % conversion and 99.8 % *ee*.

However, using whole cells in biocatalysis generally has a number of disadvantages. These include: low volumetric activity of the catalyst, as whole cells represent a large volume of biomass, much of which is not directly involved in the synthetically useful reaction. Additionally, metabolic processes can lead to the production of undesirable side products, which can complicate isolation of the desired product and lower the yield of the reaction. Heterogeneous enzymes present in the microbial host can also catalyse

side reactions, reducing the *ee* or purity of the product.[13] Whole cells tend not to be tolerant to high concentrations of organic solvent and to high concentrations of organic substrate, thus limiting the possible substrate loading in a reaction.[11]

Additionally, diffusion of substrates and products across cell membranes can limit the productivity of whole cell biocatalytic reactions[74] and whole cell biocatalysis often requires high levels of glucose to maintain cellular metabolism and ensure high yields.

1.5.2 Existing methods for *in vitro* cofactor recycling

Due to the reasons given in the section above for synthetic process which involve few enzymes (<3) there are significant advantages to using isolated enzymes *in vitro*.[17] Using enzymes *in vitro* often leads to higher purity products (as there are no competing side reactions) and higher volumetric yields. However, when redox enzymes are used *in vitro*, time consuming and expensive purification steps are usually necessary and a cofactor recycling strategy is required.[11]

A number of methods currently exist for cofactor recycling, these have been explored in a number of review articles.[75–77] They are outlined in Figure 1-14. Generally, these cofactor recycling strategies rely on the addition of stoichiometric amounts of a sacrificial reagent to provide the reducing equivalents to convert $NAD(P)^+$ back to NAD(P)H.

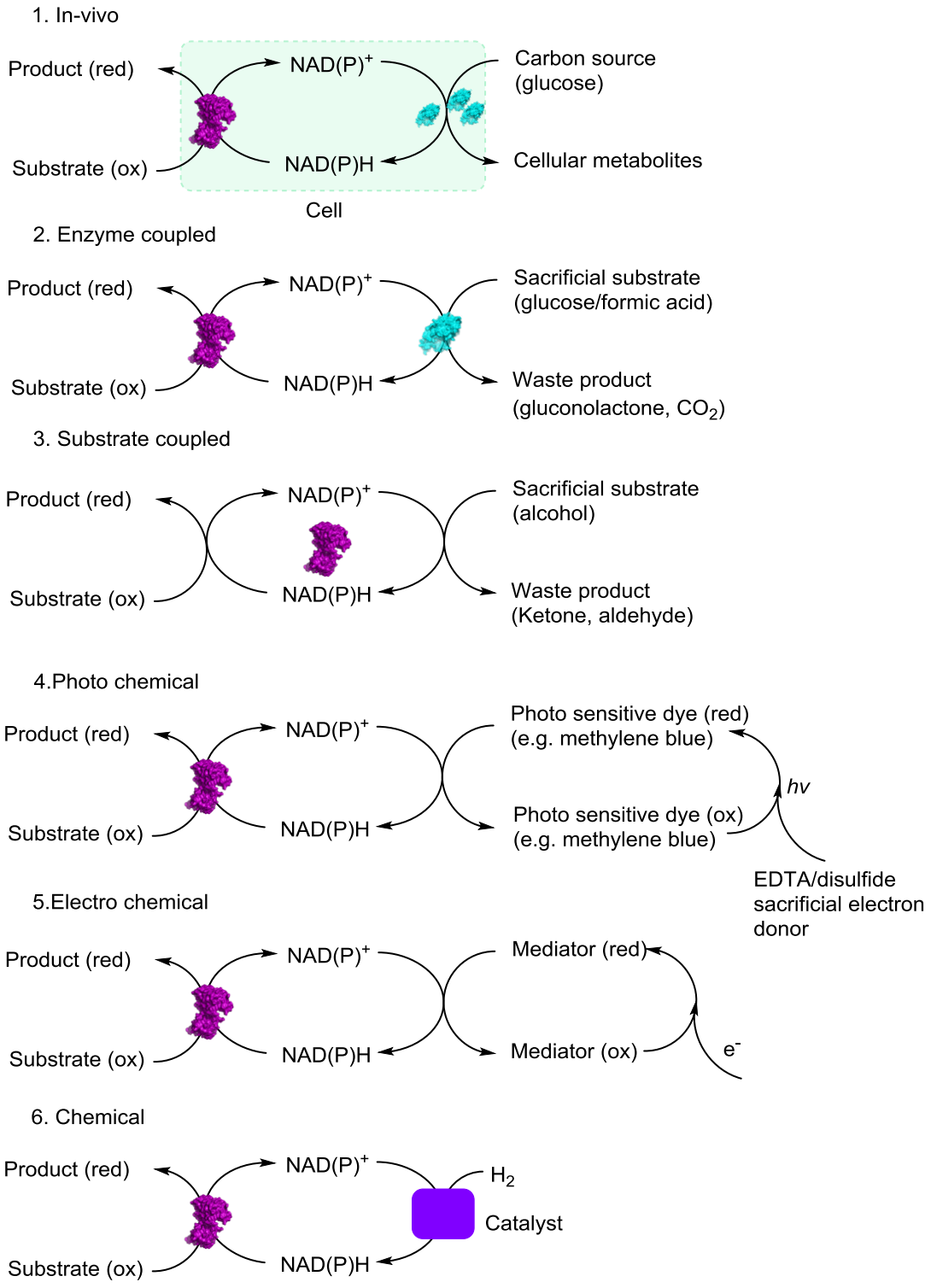

Figure 1-14: Summary of established methods for cofactor recycling adapted from De Wildeman *et al.*[77] and Hollmann *et al.*[78]

Substrate coupled

Substrate coupled cofactor recycling is typically used with ADH enzymes.[76] It involves using the same enzyme to catalyse the desired reaction and to recycle the cofactor. An ADH is able to carry out a desired ketone to alcohol conversion, at the expense of NADH. High quantities of a cheap alcohol substrate (such as isopropanol or ethanol) are also added to the reaction mixture. These can then be consumed by the same ADH enzyme to regenerate NADH from NAD^+, which can then be used to carry out further useful transformations, see Figure 1-15. [76]

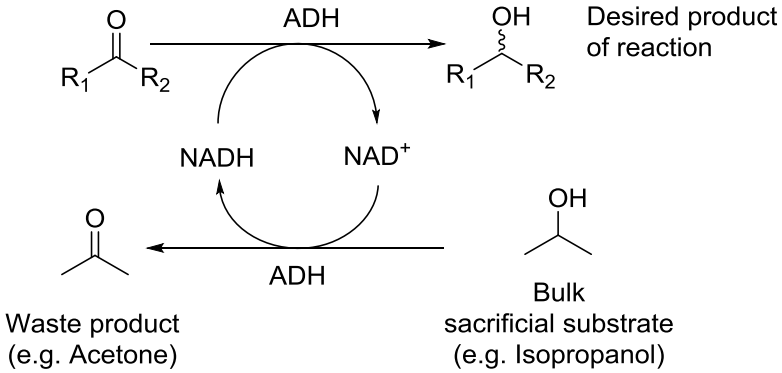

Figure 1-15: The substrate coupled approach to cofactor recycling with an ADH enzyme.

The efficiency of this approach is limited as the ADH enzyme often displays a lower turnover frequency, as its activity is spread between two different substrates. The ADH enzyme is also often more quickly de-activated due to contact with both the high concentration of the co-substrate required for cofactor recycling and the waste product (ketone or aldehyde).[11] Furthermore, enzymes used to carry out reductive amination reactions or enoate reductions are not commonly established as cofactor recycling systems and so this approach is not useful for the reactions of interest in this thesis.

Enzyme coupled

A range of enzyme coupled methods exist for recycling the reduced cofactor NAD(P)H. In enzyme coupled cofactor recycling an auxiliary cofactor recycling enzyme is added to the reaction mixture to recycle the cofactor at the expense of a sacrificial substrate.[76]

All commonly used methods require super-stoichiometric amounts of a carbon based sacrificial substrate, which leads to at least stoichiometric amounts of carbon based waste.[75] Two enzymes which are commonly used for cofactor recycling are formate dehydrogenase (FDH) and glucose dehydrogenase (GDH).

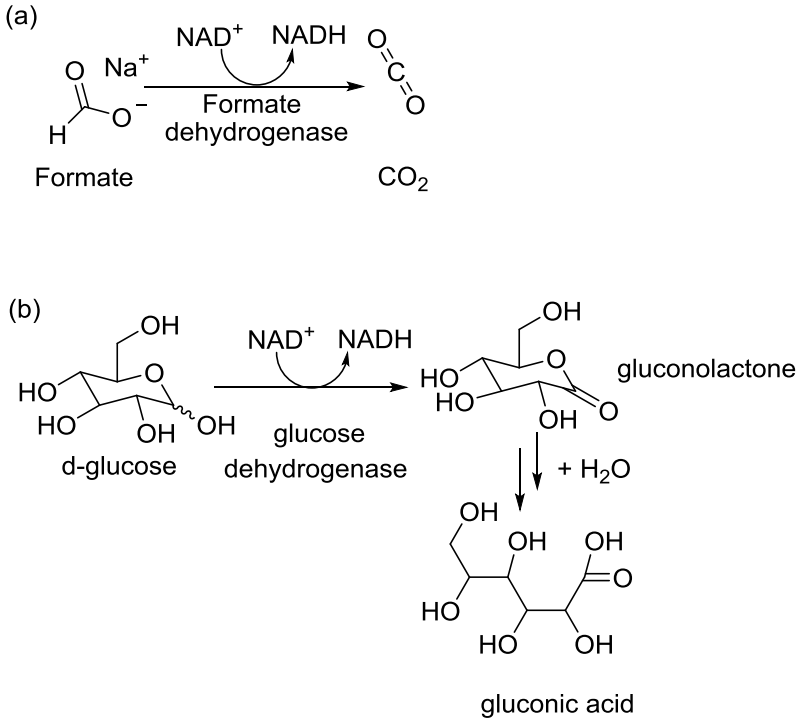

Figure 1-16: (a) The reaction catalysed by FDH producing $CO_{2(g)}$ which is irreversibly lost. (b) The reaction catalysed by GDH, producing gluconolactone which hydrolyses to give gluconic acid, shifting the equilibrium in the direction of the products.

FDH converts formate to CO_2 with the hydride being released in this process being donated to the NAD^+ molecule, see Figure 1-16 (a). The conversion of formate to CO_2 helps drive the equilibrium in the forward direction as CO_2 is lost as a gas. However, this enzyme has a low specific activity and the production of stoichiometric amounts of CO_2 leads to acidification of the reaction mixture.[75] One example where this system is used industrially is in the production of L-tertiary-leucine, see Figure 1-10.[48]

GDH converts glucose to gluconolactone, again transferring a hydride to NAD^+ giving NADH. The irreversible hydrolysis of gluconolactone to gluconic acid forces the equilibrium in the direction of the products, see Figure 1-16 (b).

GDH is often used as a cofactor recycling enzyme industrially.[79] For example Codexis have employed a GDH as the cofactor recycling system for the synthesis of (R)-tetrahydrothiophene-3-ol from tetrahydrothiophene-3-one using an ADH enzyme. (R)-tetrahydrothiophene-3-ol is a component of sulopenem an antibacterial agent being developed by Pfizer. Overall, codexis have produced 1 M Tonne of (R)-tetrahydrothiophene-3-ol in 100 kg batches.[13,80] This is an example of using GDH for cofactor recycling on a huge scale.

However, separation steps are required to remove the stoichiometric gluconic acid waste at the end of the reaction, and obtain just the desired reaction product.

A number of GDH and FDH enzymes have been developed which are able to tolerate elevated temperatures and increased concentrations of organic solvents.[81][82] This makes these enzymes more attractive for use in organic synthesis as they are more robust and can often tolerate greater (organic) substrate loadings, which are sometimes necessary to obtain industrially acceptable volumetric yields.[11]

Summary

Both the enzyme and substrate coupled methods of cofactor recycling usually require the addition of super stoichiometric amounts of a sacrificial substrate to drive the reaction in the direction of the products. They also generate super stoichiometric amounts of carbon based waste. Consequently, they display poor atom economy and the desired products from these types of reaction must be purified to remove the sacrificial substrates and waste products before the product of interest can be used.[75]

Recently phosphite dehydrogenases have been developed as cofactor recycling systems. These enzymes are able to use inexpensive phosphite as a substrate, which is often used as part of the buffer system.[83] However, they display low specific activities and have not yet been used on an industrial scale.[75,83]

1.6 How atom efficient is redox biocatalysis?

Biocatalysis as a technology is often considered green, however the significant amounts of carbon based waste and contaminated water created by biocatalysis are often not included in this evaluation.[84]

It is important that the atom economy and waste produced during biocatalytic processes is critically evaluated.[84] Hollmann and co-workers suggest that the best way of doing this is to examine the E factor for a particular process originally introduced by Sheldon in 1992,[85] which is defined in equation 1-1.[84]

$$E\ factor = \frac{m_{waste}}{m_{product}} \qquad \textbf{1-1}$$

where m_{waste} is mass of waste and $m_{product}$is mass of product. Hollmann and co-workers particularly emphasise that the waste products derived from growing bacteria and producing enzymes should be included in the analysis of the E factor.[84] However, it should be noted that waste from bacterial fermenters can be recycled as crop fertiliser and so should perhaps be considered differently to chemically contaminated waste.[86]

Of particular relevance in this thesis is the waste produced as a result of cofactor recycling processes. Cofactor recycling in itself helps to reduce the E factor of a process as it means that stoichiometric amounts of cofactor are not required.[84] However, most cofactor recycling processes require stoichiometric amounts of carbon based sacrificial substrates to regenerate nicotinamide cofactors, see section 1.5.2.

Electricity is a low cost and atom efficient source of reducing equivalents for cofactor recycling. There have been numerous attempts to develop new cofactor regeneration techniques using a variety of mediators or modified electrode surfaces.[87] Using electrochemical cofactor recycling techniques avoids the usage of stoichiometric reducing agents, meaning there is no carbon based waste, and simplifying isolation of the final product of the reaction.[87] Furthermore, the redox potential of the electrode can be accurately controlled using a potentiostat and the current passed can be monitored to determine the extent of reaction.

H_2 gas can also be used as a source of reducing equivalents for cofactor recycling. Recently, there has been increased research interest in using H_2 as a clean fuel and also as a clean reductant in synthesis.[88] Currently most H_2 is produced from steam gas reforming, this means that H_2 is obtained from natural gas and hence large amounts of CO_2 are released into the atmosphere during its production.[89] It is hoped that in the future cleaner methods of producing $H_{2(g)}$ from the splitting of water will be developed.[88]

When H_2 is used as the source of reducing equivalents for cofactor recycling in combination with an enoate reductase enzyme the reaction is in theory 100 % atom efficient and no additional waste is created as a result of the cofactor recycling process.

1.7 Electrochemical

The overall reaction for electrochemical reduction of NAD^+ is given in equation 1-2.

$$NAD^+ + 2e^- + H^+ \rightarrow NADH \qquad \textbf{1-2}$$

There are three main scenarios for electrochemical recycling of the reduced, NAD(P)H, cofactor. These are direct reduction at an electrode, indirect reduction using mediators and bio-electrocatalytic regeneration using enzyme functionalised electrodes. See

Figure 1-17, for a schematic diagram demonstrating the principals of each of the possible methods for electrochemical cofactor recycling.[78]

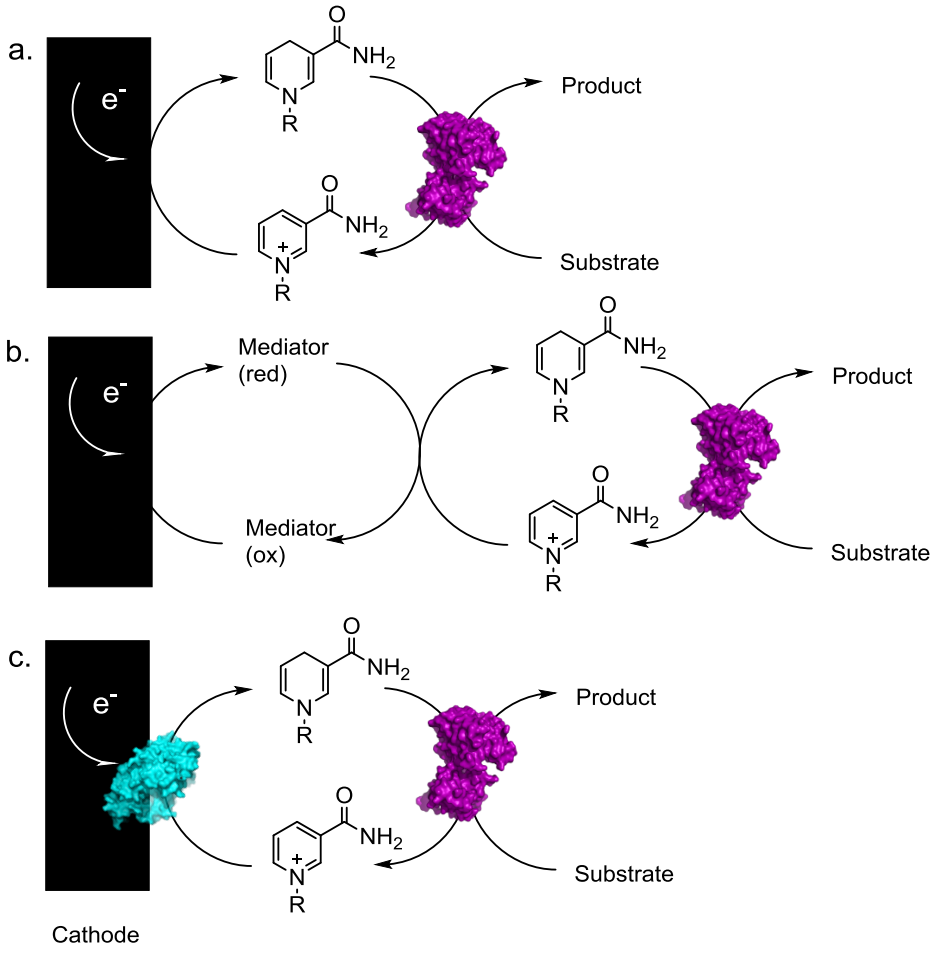

Figure 1-17: Possible methods of electrochemical cofactor recycling. (a) Direct reduction at an electrode. (b) Mediated reduction in which an electrochemical mediator transfers electrons between the electrode and the cofactor. (c) Bio-electrocatalytic reduction in which an enzyme is attached to an electrode and is therefore able to transfer electrons to NAD^+. Adapted from Hollmann *et al.*[78]

Direct reduction

Direct reduction of the $NAD(P)^+$ cofactor at an unfunctionalised electrode would represent the simplest method for the electrochemical recycling of nicotinamide cofactors. However, at unfunctionalised electrode surfaces generally a large overpotential is required to drive the reaction.[87] This is the case when a bare PGE RDE (Pyrolytic graphite edge rotating disc electrode) is used as shown by the blue scan in

Figure 1-18, where E_{onset} is ~ -720 mV *vs* SHE at pH 7 in a 1:1 mixture of NAD^+ and NADH (this represents an overpotential of *ca.* -0.4 V).

This requirement for large overpotentials means that the electrode must be held at very negative potentials in order for appreciable conversions to be achieved. This might also mean that the substrate of the NADH dependent enzyme is reduced directly at the electrode surface leading to unspecific reduction products and possibly lowering the *ee* value obtained from the enzymatic reduction.

In addition, reduction of $NAD(P)^+$ tends to generate the radical NAD(P)•, which rapidly dimerises to $[NAD(P)]_2$, and can lead to electrode fouling.[90] These $[NAD(P)]_2$ dimers are not enzymatically active.

Ali *et al*. have demonstrated that it is possible to produce 100 % enzyme active 1,4-NADH at a glassy carbon electrode functionalised with Pt nanoparticles under certain conditions.[91] Having Pt particles on the electrode surface meant that absorbed $M\text{-}H_{ads}$ species were available at the site of NAD• radical formation meaning that the kinetic barrier to H addition was overcome. However, the optimum potential for this reaction was found to be -1V *vs* SHE, which is a significant overpotential and might lead to direct reduction of substrates when coupled to a synthetically useful reaction.[91]

Indirect reduction using mediators

Using electrochemical mediators can help to avoid some of the problems associated with direct electrochemical reduction of nicotinamide cofactors.[78] A mediator effectively acts as an electron shuttle, which transfers electrons between the electrode and the cofactor.[92] There are a large number of redox mediators which have been used in the mediated regeneration of NADH. These are generally small, soluble molecules able to diffuse quickly between the electrode and the enzyme. This situation is shown schematically in Figure 1-17 (b).[92]

Redox mediators must be reduced at conventional electrodes at a less negative potential than NAD^+, so that the cofactor is not itself reduced at the bare electrode surface. This also means that reduction of the substrate of the NADH dependent enzyme is less likely to occur directly at the electrode. Ideally, redox mediators have no overpotential requirement.

Another key feature of any 2 electron mediator is that it avoids the formation of NAD• radicals because it transfers two electrons at the same time.[78] Mediators must also lead to a high proportion of the enzymatically active 1,4-form of the cofactor as opposed to the 1,2- or 1,6- form, which can also be produced.[78]

Common examples of mediators used for cofactor regeneration on a laboratory scale include viologen molecules, along with organometallic mediators such as: $[Cp^*Rh(bpy)(H_2O)]^{2+}$.[93]

There are several examples in the literature, which have focused on immobilising redox mediators on an electrode.[94] This would mean that the electrode acts as a single heterogeneous electro-catalyst for NAD^+ reduction. One example of this is the poly(Neutral Red) electrodes developed by Karyakin *et al*.[95] Here Neutral Red, which has a structure similar to that of naturally occurring flavins, was electro polymerised onto the surface of a glassy carbon electrode. It was found that these electrodes are able to catalyse the reduction of NAD^+ at a lower overpotential than that at which NAD^+ reduction would occur at an unfunctionalised glassy carbon electrode.[95]

However, mediators are often toxic increasing the environmental cost of the process and they must be removed at the end of the process; as yet, there has been no industrially demonstrated process which make use of redox mediators.[93]

Bio-electrocatalytic regeneration

There are two main scenarios in which bio-electrocatalytic regeneration of NAD(P)H can take place. The first scenario involves using redox enzymes or redox centres as mediators for the transfer of electrons from an electrode to NAD^+. Durliat *et al*. demonstrated this phenomena using the soluble hydrogenase (SH) from *R. eutropha* with a Pt electrode held at -650 mV *vs* SHE.[96,97] In this work, the SH was free in solution and so could take up electrons from the Pt electrode and use these to recycle NAD^+, also present freely in a thin layer of solution and, consequently, able to diffuse to the active site of the SH. This approach was subsequently used by Cantet *et al.* to recycle NADH for use by a an L-glutamate dehydrogenase for the reductive amination of α-keto glutarate to L-glutarate.[98]

Kang *et al*. demonstrated the use of a chemical mediator, methyl viologen. This was reduced at a gold electrode and coupled to the diaphorase from porcine heart for NAD^+ reduction.[99] This reaction was then coupled to a D-lactate dehydrogenase to produce D-lactate from pyruvate. [99]

Some enzymes are able to undergo direct electron transfer with an electrode surface. This is advantageous as it means that electrodes can be developed with enzymes immobilised on them to carry out the selective reduction of NAD^+. These electrodes can generally operate close to the thermodynamic potential and furthermore represent a heterogeneous system for recycling NADH, which can in theory be removed and re-used at the end of the reaction.

Hirst and co-workers have demonstrated the reduction of NAD^+ at a carbon electrode functionalised with sub complex Iλ from bovine complex I.[100,101] This work has been expanded on by Vincent and co-workers who have demonstrated electro-enzymatic cycling of NAD^+/NADH using the NAD^+-reductase from *R. eutropha.* A cyclic voltammogram displaying NAD^+/NADH cycling at a PGE RDE by the NAD^+-

reductase from *R. eutropha* is shown by the red scan in Figure 1-18. This scan cleanly crosses the blank (scan with an unfunctionalised PGE RDE in buffer) demonstrating that there is no overpotential requirement for electro-enzymatic cycling of NAD^+/NADH at an *R. eutropha* NAD^+-reductase functionalised electrode.[102] Reeve *et al*. have gone on to use this as the basis for the construction of high surface area electrodes for bulk electro-catalytic turnover of NADH and were able to demonstrate > 6000 molecules of cofactor turned over per NAD^+-reductase.[103]

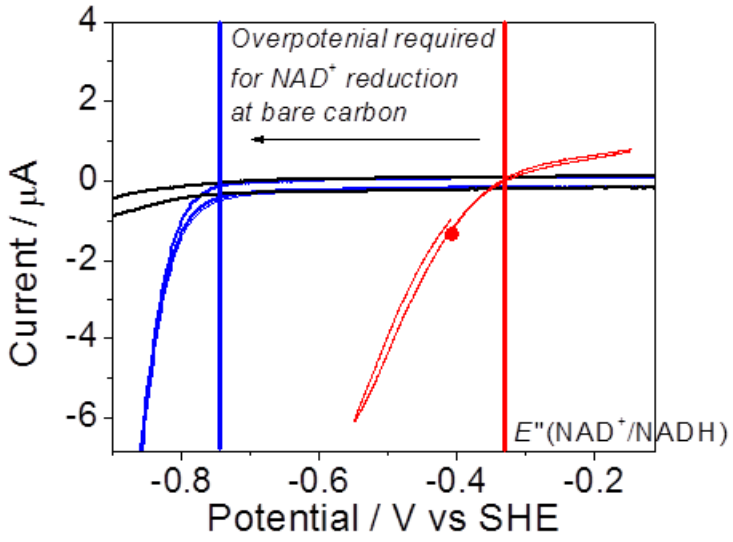

Figure 1-18: Cyclic voltammogram showing electroenzymatic cycling of NAD^+. The trace in red shows an *R. eutropha* NAD^+-reductase functionalised electrode in a mixture of 1 mM NAD^+ and 1 mM NADH in phosphate buffer pH 7. The trace in blue shows a bare PGE RDE in a mixture of 1 mM NAD^+ and 1 mM NADH in phosphate buffer pH 7. The grey scan shows an unfunctionalised PGE RDE in phosphate buffer. Data provided by Dr H Reeve and Dr Z Idris[103]

In this thesis electrochemistry will be used to characterise a novel NAD^+-reductase from a thermophile organism, shown schematically in Figure 1-19 (b), (chapter 4). This enzyme will then be used on a high surface area electrode for bulk conversion of NAD^+ to NADH, see section 5.2 for more information.

1.8 H_2-driven cofactor recycling

A number of hydrogenase enzymes exist in nature, which are able to catalyse the oxidation of H_2. In this project the focus is placed on [NiFe] hydrogenases which have an [NiFe] active site co-ordinated to the rest of the protein by 4 cysteine ligands.[75] The [NiFe] group of hydrogenases are usually more O_2-tolerant than the alternative group of [FeFe] hydrogenases.[75] Cytoplasmic soluble, NAD^+-reducing hydrogenases (SHs) couple the oxidation of H_2 to the reduction of $NAD(P)^+$.[104] In this project, two different approaches will be applied to enable H_2-driven cofactor recycling, these are shown schematically in Figure 1-19 (a and c).

The hydrogenase (and soluble hydrogenase) constructs used in this project all contain a relay of FeS clusters, these facilitate electron transport through these proteins.[105–107]

1.8.1 Soluble hydrogenase

Cytoplasmic soluble, NAD^+-linked hydrogenase enzymes (SHs) are found in a wide range of organisms including *Ralstonia eutropha (R. eutropha), Hydrogenophilus thermoluteolus (H. thermoluteolus)* and cyanobacteria.[108] The SHs from *R. eutropha,*[109] *Rh. opacus*[110] and *Pyrococcus furiosus*[111] have already been well characterised. They are able to reduce NAD^+ selectively to just the 1,4- form of NADH at their FMN containing active sites. They have also been used for *in situ* cofactor recycling, for example Mertens *et al*. demonstrated that the $NAD(P)^+$ reducing hydrogenase from *Pyrococcus furiosus* can be used for the regeneration of NADPH for the conversion of acetophenone to (S)-phenylethanol by an ADH.[112] One of the best characterised SHs is that from *R. eutropha*.[104,109,113,114] This SH has already been demonstrated on a laboratory scale as a cofactor recycling system both *in vivo* and *in vitro.*[68][115][116]

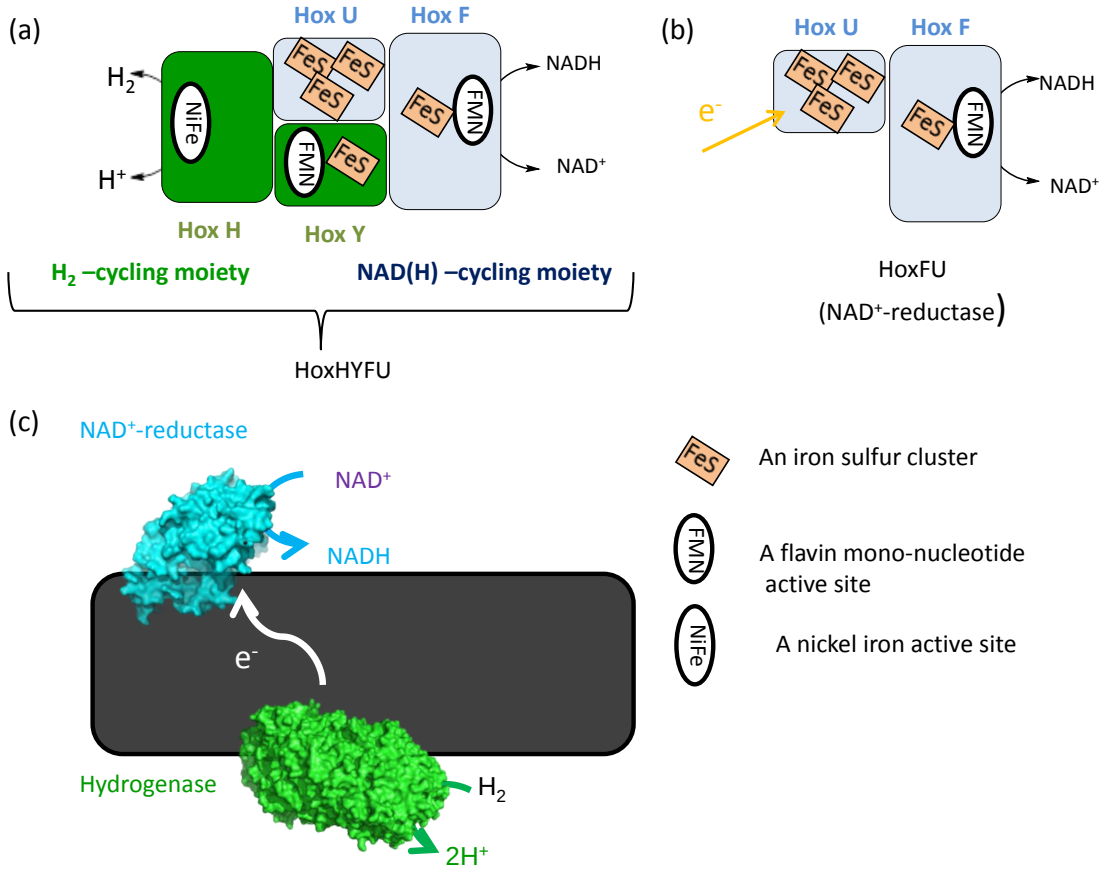

Figure 1-19: Methods of H_2-driven and bio-electrochemical cofactor recycling. (a) The soluble hydrogenase (SH) comprised of the $2H^+/H_2$ cycling (HoxHY) and the NAD^+/NADH cycling (HoxFU) moieties. The two catalytic moieties (HoxHY and HoxFU) of the enzyme can be de-coupled using molecular biology strategies, allowing the HoxFU moiety to be expressed on its own (b) A diagram of the NAD^+ reducing moiety (HoxFU) of the SH, which can be overexpressed without the hydrogenase moiety. This can be immobilised on an electrode for electrochemical cofactor recycling or on particles for H_2-driven cofactor recycling. (c) A schematic diagram of an enzyme-modified particle for H_2-driven cofactor recycling. Dihydrogen gas is reduced to 2 protons by a hydrogenase, which is able to engage in direct electron transfer with the carbon particle. An NAD^+-reductase enzyme such as HoxFU can take up electrons from the particle and use these to reduce NAD^+ to NADH.

The SH from *R. eutropha* is a bidirectional NAD^+-linked [NiFe] hydrogenase. The HoxFU moiety (NAD^+-cycling) part of the SH from *R. eutropha* shows high sequence similarity to the peripheral subunits of mitochondrial and bacterial Complex I.[114] The *R. eutropha* SH is a multimeric enzyme consisting of two catalytic moieties, the HoxHY hydrogenase component, and the HoxFU diaphorase (NAD^+-reducing) component, see Figure 1-19(a). In its native form the SH from *R. eutropha* also contains

two HoxI modules, the physiological role of which is not yet clear.[113] The HoxI is not expressed in the whole SH used as part of this project.

The *R. eutropha* SH contains five FeS clusters and two FMN (Flavin Mononucleotide) centres.[117] FMN-a is found in HoxY and FMN-b is found in HoxF, where it forms the active site of the diaphorase. *In vivo* H_2-oxidation occurs at the [NiFe] active site and electrons are channelled through a series of FeS clusters to FMN-b, where NAD^+ reduction is carried out. FMN-b is tightly bound to the protein; however, FMN-a is labile and selectively released by the SH, under sustained reducing conditions.[117] It is thought that FMN-a plays an essential role in electron transport from the [NiFe] active site of HoxH to the chain of FeS clusters.[117] Therefore, loss of FMN-a leads to complete loss of activity of the SH meaning that the whole SH is often considered relatively unstable.[118] In addition, previous electrochemical characterisation in the Vincent group has shown that the HoxHY part of the *R. eutropha* SH is less stable than the HoxFU moiety.[103]

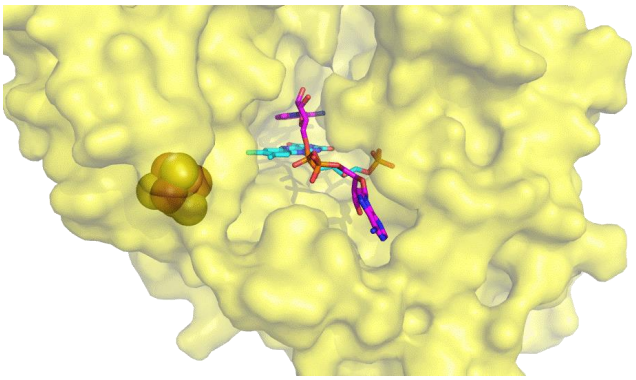

Figure 1-20: A Homology model of *R. eutropha* HoxFU active site, with NAD^+ docked in the active site and a FeS cluster (spheres). Based on PDB: 2FUG, developed by Dr L. Lauterbach from the TU Berlin. The carbon atoms of the FMN at the active site are shown in blue and the carbon atoms of the docked NAD^+ are shown in purple.

The HoxFU, NAD^+ cycling moiety (see Figure 1-19, b) can carry out direct electron transfer with a number of different carbon surfaces,[102,119,120] which has allowed the extensive characterisation of this NAD^+-reductase on a carbon electrode. As yet, no crystal structure has been solved for this enzyme. However, a homology model for the active site has been developed based on Complex I from *Thermus thermophilus*, see Figure 1-20, which shows the binding site of NAD^+ in a model of the surface of the protein structure, along with the first of a chain of FeS clusters involved in the transport of electrons through this enzyme.

The FMN is close enough to the FeS cluster for electrons to be transferred. FMN is able to couple the single electron transfer process from the FeS clusters in the SH, to the two electron process involved in transferring a hydride to NAD^+. The catalytic cycle for FMN is shown in Figure 1-21.

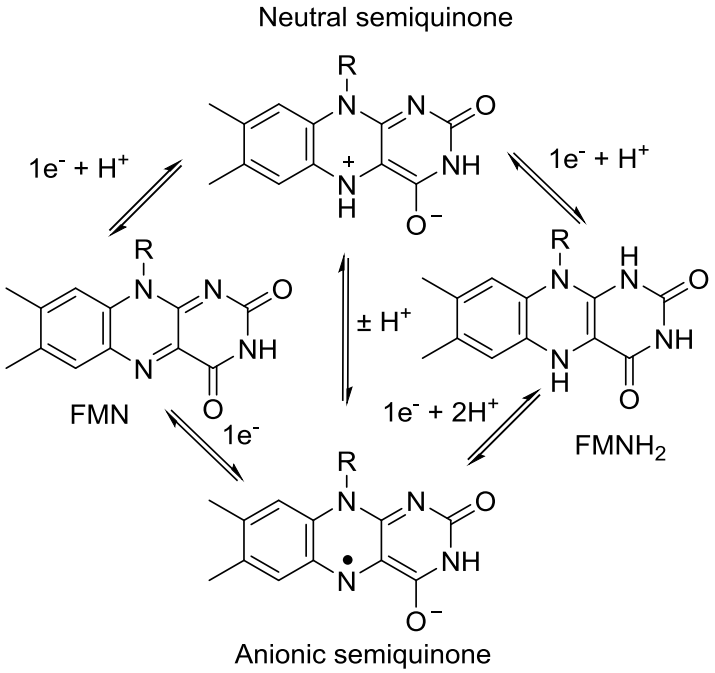

Figure 1-21: Redox cycle of FMN, where R is 2,3,4-trihydroxyhexyl dihydrogen phosphate. Adapted from Frey *et al.* in Enzymatic Reaction Mechanisms.[121]

Two electrons are transferred to the FMN from the FeS cluster, along with a proton from solution. This hydride can then be transferred to NAD^+ giving NADH. The NAD^+ is bond in an orientation, which allows direct transfer of the hydride from the reduced FMN.[102]

It has been shown that the whole SH[113] and the HoxFU[102] moiety from *R. eutropha* are all O_2 tolerant.

1.8.2 Enzyme-modified particles for H_2-driven cofactor recycling

Within the Vincent group a novel approach to H_2-driven cofactor regeneration has been developed.[119] This involves uncoupling the HoxFU (NAD^+-cycling) component of the *R. eutropha* SH from the unstable HoxHY component, see Figure 1-19 (b). The HoxFU component can be co-immobilised on a conducting carbon particle along with a more robust hydrogenase, (such as *E. coli* Hyd 2). This is able to pass electrons to the HoxFU component which is then able to reduce NAD^+ to NADH, see Figure 1-19 (c).

Using the particle-based regeneration system has some advantages over using the whole *R. eutropha* SH. These include the particles being a single heterogeneous catalytic system which can be easily removed from solution and recycled,[119] and that the enzymes used in this system may display greater stability when immobilised on particles. In addition, it is tricky to express some SHs in recombinant hosts with equal ratios of HoxFU and HoxHY. Using the particle system means that optimised ratios of hydrogenase and NAD^+-reductase can be assembled *in vitro*. The particle system is completely modular meaning that different hydrogenase and NAD^+-reductase enzymes can be selected to suit the reaction conditions of interest, for example if it is desirable to run reactions at elevated temperatures, as will be investigated in chapter 5 of this thesis.

Hydrogenases used in this project

In this thesis the hydrogenase, Hyd 2 from *E. coli* was used throughout for construction of enzyme-modified particles. This hydrogenase is an example of a membrane bound, bi-directional NiFe respiratory hydrogenase, which *in vivo* passes electrons to the quinone pool.[122] A cartoon diagram showing the structure of Hyd 2 and the chain of FeS clusters required for electron transport through the protein is shown in Figure 1-22. For experiments conducted in the laboratories of collaborators Hyd 1 from *E. coli* was used, as this enzyme is more tolerant to O_2. This is also a membrane bound hydrogenase.

Figure 1-22 (b) shows a cyclic voltammogram (CV) recorded at an electrode functionalised with Hyd 2 oxidising H_2 under 1 bar H_2 at pH 8. The onset of oxidation occurs at the thermodynamic potential, showing that Hyd 2 is an efficient H_2 oxidising catalyst, as reported by Lukey *et al.*[122]Hyd 1, on the other hand has an overpotential requirement for the oxidation of $H_{2(g)}$ and consequently does not oxidise H_2 at the thermodynamic potential for this reaction.

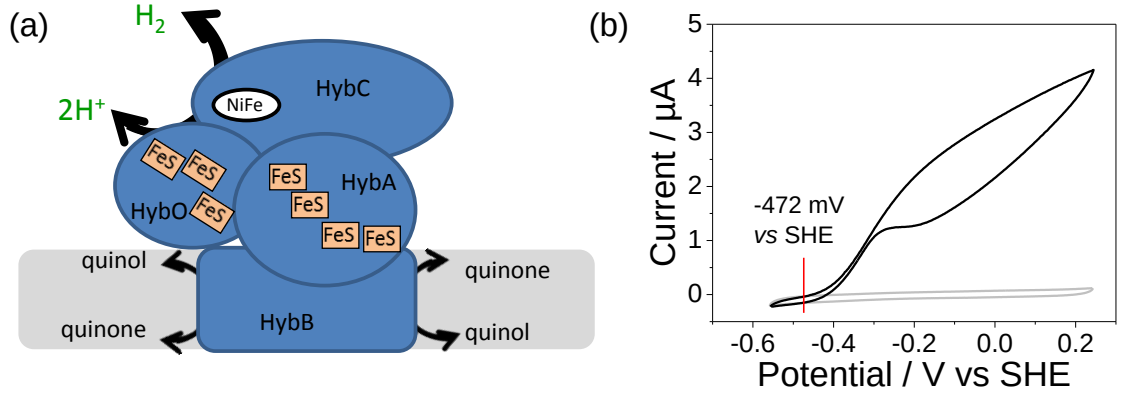

Figure 1-22: *E. coli* Hydrogenase 2. (a) Cartoon representation of Hyd 2 showing the [NiFe] active site of the hydrogenase and the FeS clusters involved in transport of electrons through the protein. (b) Cyclic voltammogram showing H_2 oxidation by Hyd 2 in pH 8 phosphate buffer at 10 mV s^{-1} scan rate with rotation at 2000 rpm, in H_2 saturated buffer at 22 ^oC.

Thermodynamic considerations

Figure 1-23 shows that at pH 8 under 1 bar H_2 pressure the redox potential of the $2H^+/H_2$ couple is -472 mV *vs* SHE. The redox couple for NAD^+/NADH is -438 mV *vs* SHE, at pH 8 when the ratio of [NADH]/[NAD^+] is 1000.

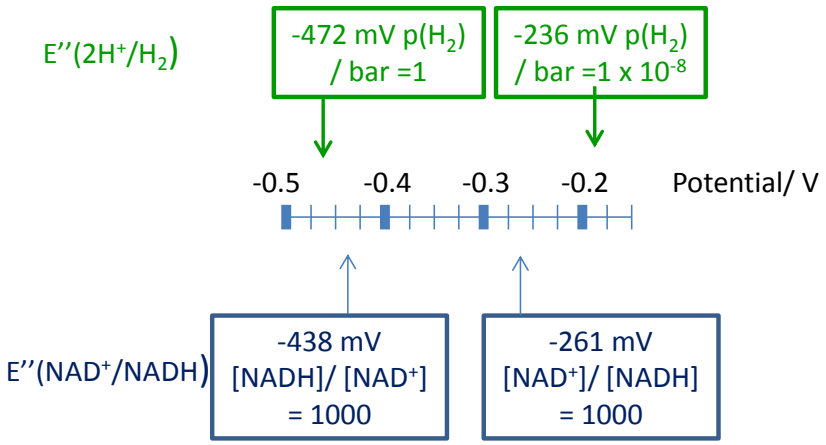

Figure 1-23: The thermodynamic potentials for $2H^+/H_2$ and NAD^+/NADH couples at pH 8 at 298 K.

This means that with an efficient H_2 oxidation catalyst, like Hyd 2, and an NAD^+-reducing catalyst, like the *R. eutropha* NAD^+-reductase it is theoretically possible to drive the reduction of NAD^+ to 99.9% conversion, meaning that it should be possible to observe high conversions using the enzyme-modified particles. In fact Reeve *et al.* have demonstrated that it is possible to achieve > 97 % conversion of NAD^+ to NADH using the enzyme-modified particles.[119] Further details of the thermodynamics of NAD^+ reduction and H_2 oxidation are given in section 2.4.3, particularly under at elevated temperatures and pressures.

1.9 Focus (Aims and scope)

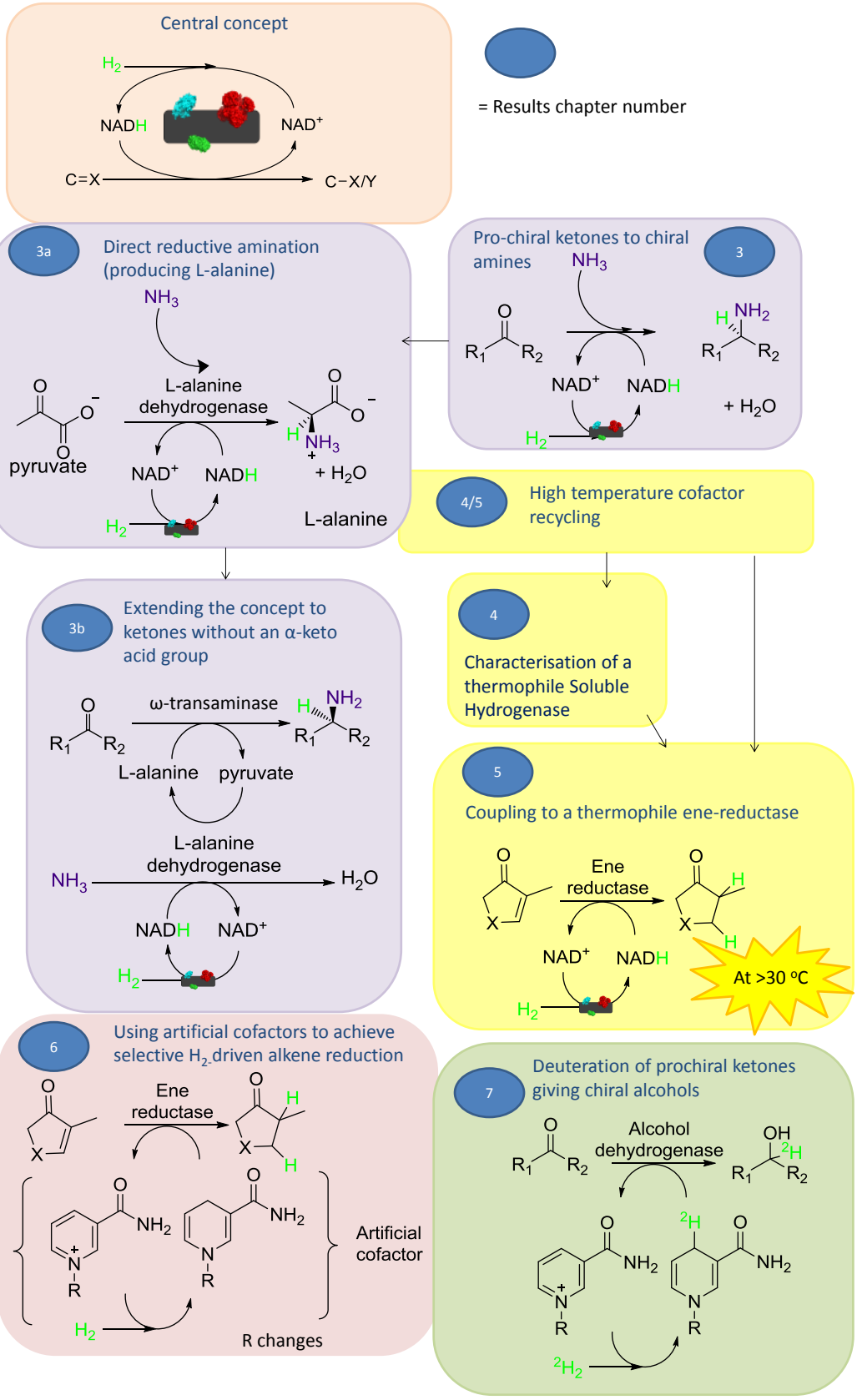

Figure 1-24: A schematic overview of the main areas of focus in this project.

This thesis seeks to investigate the scope of using the H_2-driven cofactor recycling methods outlined in section 1.8. This involves using H_2 gas as a clean, cheap source of reducing equivalents. Particular focus is placed on expanding the scope of the enzyme-modified particles, see Figure 1-19 c. The key areas of focus in this project are outlined in Figure 1-24.

1.9.1 Structure of this thesis

The focus of chapter 3 is on the production of chiral amines, in sections 3.1-3.2 an L-alanine dehydrogenase was coupled to the enzyme-modified particles for production of L-alanine from pyruvate.

In the second section of the Chapter (3.4-3.7), an (S)-selective *ω-transaminase* enzyme was used for the conversion of 4-phenylbutan-2-one to 1-methyl-3-phenylpropylamine.

In section 3.8, an (R)-selective *ω-transaminase* enzyme was used to give access to the (R)-form of 1-methyl-3-phenylpropylamine.

In chapter 4 a NAD^+-reducing soluble hydrogenase (SH) and the HoxFU moiety from the thermophile organism *H. thermoluteolus* were purified and characterised using biochemical and electrochemical methods. Enzymes which are derived from thermophile organisms are often tolerant to higher operating temperatures. These 'thermophile enzymes' are usually more rigid and, therefore often more resistant to physical and chemical degradation.[123]

A large amount of information can be obtained from biochemical and electrochemical characterisation techniques, such as the affinity of this enzyme for a specific cofactor.[102] This information is useful in deciding whether this enzyme is suited to particular biotechnological applications. Characterising the *H. thermoluteolus* HoxFU moiety means that this enzyme can be added to the library of enzymes which can be

used as the NAD^+-reductase part of the enzyme-modified particles, introduced in section 1.8.2.

Chapter 5 examines whether it is possible to use the enzyme-modified particles introduced in section 1.8.2 at elevated temperatures (>30 ^oC).

Being able to carry out enzymatic reactions at elevated temperatures may mean that higher reaction rates can be achieved. Additionally substrate solubility increases as a function of temperature and the viscosity of the solvent decreases.[124] Higher temperatures can also be used to shift the equilibrium of a reaction and working at higher temperatures can reduce the risk of microbial contamination.[124]

Initially, this chapter looks at carrying out NADH recycling using high surface area electrodes modified with the HoxFU from *H. thermoluteolus,* characterised in chapter 4. In order to demonstrate whether the NADH produced is enzymatically active, this system is coupled with the ene reductase enzyme: *TsER* for elevated temperature alkene reduction.

In the next section of this chapter enzyme-modified particles are constructed with the HoxFU from *H. thermoluteolus* and Hyd 2 for H_2-driven cofactor recycling at >30 ^oC. These are then also combined with the ene reductase: *TsER* for H_2-driven elevated temperature alkene reduction.

Artificial cofactors ($mNAD^+$) are synthetic or semisynthetic versions of the natural cofactors NAD^+ or $NADP^+$,[125] which can act as redox mediators for a range of enzymatic reactions. There are currently no well-established enzymatic methods for recycling the reduced forms of the artificial cofactors used in this thesis. In chapter 6, a number of enzymatic methods for recycling a range of reduced artificial cofactors are explored. A particular focus was placed on developing a H_2-driven system for recycling these artificial cofactors.

In chapter 7 it was investigated whether the enzyme-modified particles are able to carry out $^2H_2$-driven selective deuteration of alcohols, as shown in Figure 1-24. Selectively deuteriated chemicals have a number of applications, particularly in the pharmaceutical industry, where deuteriated drugs are being tested to slow down drug metabolism due to oxidative processes within the body.[126]

(S)- and (R)- selective ADHs are used to test whether it is possible to produce selectively deuteriated alcohols in this manner. The conversion of acetophenone to phenylethanol, which has already been shown to be highly efficient using the enzyme-modified particles by Reeve *et al.*, was chosen as the test reaction to demonstrate selective deuteration.[119]

1.9.2 Challenges in biocatalysis and how they are addressed in this project

Table 1-1, illustrates the particular challenges being addressed in each of the chapters.

Table 1-1: A summary of the challenges and aspirations for biocatalytic reactions addressed by each chapter of this thesis.

Chapter number	Name	Challenge in biocatalysis addressed by this chapter
3	Direct reductive amination	• Investigates whether it is possible to achieve the reaction NH_3 + prochiral ketone + 'x' → Chiral amine, which is regarded as "aspirational" by the pharmaceutical and fine chemical industries[31]
4	Characterisation of a thermophile soluble hydrogenase	• Characterisation of a SH from a thermophile organism; this has implications for obtaining a more stable enzyme able to operate at higher temperatures and in organic solvents[11]
5	High temperature cofactor recycling	• Demonstration of an enzyme-modified particle system for recycling cofactors at elevated temperature.
6	Artificial cofactor recycling	• Developing an enzymatic H_2-driven system for recycling artificial cofactors – reduces carbon based waste as artificial cofactors must no longer be supplied in stoichiometric amounts
7	Producing deuteriated alcohols	• Using $^2H_2$ gas to produce selectively deuteriated compounds, cheaper than using deuteriated reagents like d_6-glucose.

2 Methods and Theory

Within this thesis a range of techniques are used to facilitate H_2-driven enzymatic reductions for the production of chiral chemicals. This chapter describes techniques used throughout the thesis. Techniques used or developed in individual experimental chapters are described in more detail in each chapter.

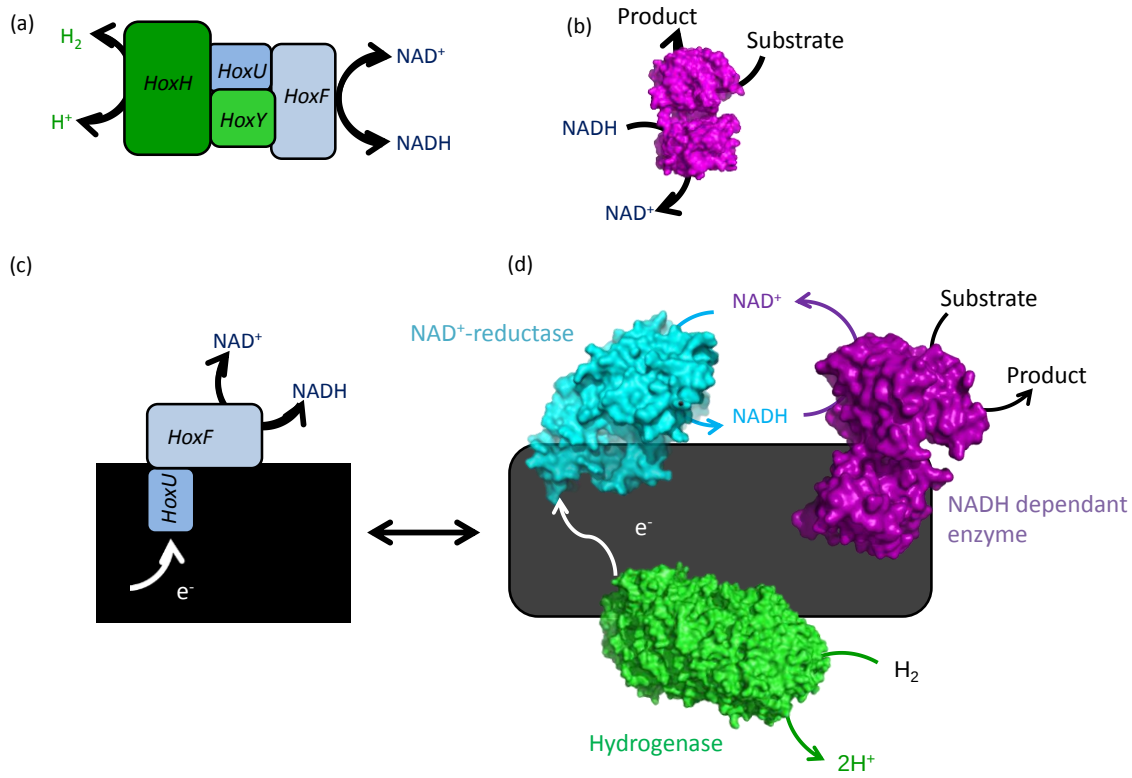

Figure 2-1: Key areas of focus in this thesis. (a) The whole SH which can be used for H_2-driven NADH recycling (b) An NADH dependent enzyme (c) HoxFU immobilised on the surface of a carbon electrode (d) Enzyme-modified particles for H_2-driven NADH recycling.

Figure 2-1 outlines the key systems explored in this thesis. This chapter starts off by outlining the micro-biological techniques relevant to the thesis used to produce the enzymes used. The next section introduces UV-visible spectroscopy and a range of assays which can be used to determine the activity of SH enzymes (Figure 2-1, a), NADH dependent enzymes (Figure 2-1, b) and enzyme-modified particles (Figure 2-1, d). The chapter then goes on to introduce electro-enzymatic methods of characterisation (Figure 2-1, c), which are particularly relevant to chapter 4. This leads

into the idea of co-immobilising a hydrogenase, NAD^+-reductase and NADH dependent enzyme on conductive carbon particles to produce enzyme-modified particles for H_2-driven NADH recycling (Figure 2-1, d), which were introduced in chapter 1, section 1.8.2. This is accompanied by a discussion of the thermodynamics relevant to usage of the enzyme-modified particles. Finally, the analytical techniques used to determine what has been produced during the bio-transformations conducted within this thesis, along with a discussion of general considerations relevant to the work conducted in this thesis is included.

2.1 Enzyme production and molecular biology

This section summarises the details of the established molecular biological techniques used in this thesis. Further details are given in Appendix A and in the references sited.

2.1.1 Enzyme origin

Details of the enzymes used in this project are summarised in Table 2-1 and Table 2-2 and further expanded on in subsequent sections and in Appendix A.

Table 2-1 summarises the details of the enzymes used in this project, which were provided by collaborators or purchased and simply used as provided. Details of the enzymes prepared as part of this project are given in Table 2-2.

Table 2-1: A summary of the details of the enzymes used in this work, which were provided by collaborators or purchased and used as received.

Enzyme	Source organism	Recombinant host	Abbreviation	Properties	Source
Hydrogenase	*E. Coli*	*E. Coli*	Hyd 2	Hydrogenase with a low over potential for hydrogen oxidation	Kindly provided by the Armstrong group, ICL, University of Oxford[122]
	E. Coli	*E. Coli*	Hyd 1	Highly O_2 tolerant hydrogenase	Kindly provided by the Armstrong group, ICL, University of Oxford [122]
NAD^+-reductase	*R. eutropha*	*R. eutropha*	HoxFU	NAD^+-reductase subunits only	Provided by collaborators at the TU Berlin.[102]
SH	*R. eutropha*	*R. eutropha*	HoxHYFU	NAD^+-reducing soluble hydrogenase wild type	Provided by collaborators at the TU Berlin.[127]
L-alanine dehydrogenase [EC 1.4.1]	*Bacillus cereus*	*E. coli*	L-alanine dehydrogenase	-	Sigma Aldrich[65]
Alkene reductase [EC 1.3.1.31]	*Thermus scotoductus*	*E. coli*	TsER	Thermophile alkene reductase	Provided by collaborators at the TU Delft.[66]
Formate dehydrogenase	-	*E. coli*	FDH	Commercial formate dehydrogenase	Evocatal.[128]
			Flavin containing FDH (Mo-FDH)	Formate dehydrogenase with a Flavin mononucleotide active site	Provided by collaborators at the University of Potsdam.[129]
Glucose dehydrogenase	-	*E. coli*	GDH	Commercial glucose dehydrogenase (GDH 102)	Provided by Johnson Matthey catalysis and chiral technologies.[130]
ω -transaminase	*Aspergillus terreus*	*E. coli*	AT ω TA	His-tagged D-alanine dependent (R)-selective *ω-transaminase*	Provided by collaborators at the University of Graz.[115]
Alanine racemase	*Streptomyces coelicolor*	*E. Coli*	SeAlaR	Catalyses the racemisation of L-alanine to a mixture of D- and L- alanine	Provided by collaborators at the University of Graz.[30]
Alcohol dehydrogenase	-	-	ADH101	(R)-selective alcohol dehydrogenase	Provided by Johnson Matthey Catalysis and Chiral Technologies[130]
	-	-	ADH105	(S)-selective alcohol dehydrogenase	Provided by Johnson Matthey Catalysis and Chiral Technologies[130]

Table 2-2: A summary of the details of the enzymes used in this work, which were prepared as part of this project.

Enzyme	Source organism	Recombinant host	Abbreviation	Properties	Source
NAD^+-reductase	*R. eutropha*	*R. eutropha*	Hox~~HY~~FU	HoxHYFU with the mutation I64A, leading to an inactive hydrogenase dimer	Purified at the TU Berlin as part of this project[104]
	H. thermoluteolus	*R. eutropha*	HoxFU	NAD^+-reductase subunits only	Unpublished – first prepared in this work. Cloning and plasmid preparation carried out by Dr L. Lauterbach at the TU Berlin
	H. thermoluteolus	*R. eutropha*	HoxHYFU	NAD^+-reducing soluble hydrogenase wild type	Unpublished – first prepared in this work. Cloning and plasmid preparation carried out by Dr L. Lauterbach at the TU Berlin
ω -transaminase	*Vibrio fluvaris*	*E. coli*	*Vf* TA	His-tagged L-alanine dependent (S)-selective *ω-transaminase*	Prepared and purified in house[115] Plasmid kindly provided by Prof. Wolfgang Kroutil, TU Graz.

Further details of preparation of these enzymes are given in the text of the Methods and Theory section and in Appendix A.

2.1.2 HoxHYFU and HoxFU preparation and purification

During my D.Phil. I spent 2 months working at the TU Berlin in the laboratory of Dr Oliver Lenz where I performed the molecular biological work described here.

This section summarises the preparation of the NAD^+-reductase and SH variants used in this thesis further more complete details are given in Appendix A.

Hox~~HY~~FU

Cloning strategies have made it possible to separate the NAD^+-cycling moiety of the *R. eutropha* SH from the H_2-cycling moiety.[102,131] Additionally, it is possible to inactivate the hydrogenase proportion of the *R. eutropha* SH to obtain Hox~~HY~~FU, by mutating the isoleucine at position 64 to an alanine. This enzyme acts as an NAD^+-reductase; but, shows no hydrogenase activity.[103] *R. eutropha* Hox~~HY~~FU can currently be obtained in higher yields than *R. eutropha* HoxFU.

***H. thermoluteolus* HoxFU**

The plasmid containing the genes for heterologous production of *H. thermoluteolus* HoxFU in *R. eutropha* was provided by Dr Lars Lauterbach and verified by gel electrophoresis following the protocol of Aaij and Borst.[132] This plasmid also contains a gene for kanamycin resistance.

The plasmid for *H. thermoluteolus* HoxFU production was then transformed into competent *E. coli S17-1* (Starlab) cells using a standard Heat shock protocol.[133] Transfer of the *H. thermoluteolus* HoxFU plasmid into *R. eutropha* was carried out using the "Spotmating" technique as described by Eberz *et al.* and further detailed in Appendix A.[134,135]

Growth and purification of the HoxHYFU and HoxFU moieties

The HoxHYFU, Hox~~HY~~FU and HoxFU enzymes were produced in *R. eutropha HF424*, a strain which has been engineered to not produce the native SH.[118] They were

then purified using Strep-tag affinity chromatography, following the protocol used by Lauterbach *et al*. which is described in detail in Appendix A.[102,131][118]

The *R. eutropha* HoxHYFU and Hox~~H~~~~Y~~FU have molecular weights of approximately 177 kDa.[102,131] The amount of protein used is reported in μg throughout this thesis. Approximately, 5.8 pmoles of enzyme are therefore present in a 1 μg portion of *R. eutropha* HoxHYFU.

2.1.3 *Vf ω-transaminase* preparation and purification

The *Vf ω-transaminase* was prepared according to the protocol of Mutti *et al*.[136] See Appendix A for a detailed description of the purification process.

The concentration of the protein was estimated according to the method of Bradford or using a BCA kit, further details are given in Appendix A.[137,138]

2.2 UV-Visible spectroscopy

In this thesis UV-Visible spectroscopy was used extensively to assay the activity of enzymes (chapters 3, 5, 6 and 7). It was also used to determine whether NADH was being produced by the enzyme-modified particles, see Figure 2-1(d), and to determine the rate and percentage conversion of these reactions (chapters 3, 4, 6, 7).

2.2.1 Theory of UV-visible spectroscopy

UV-Visible spectroscopy is a non-destructive technique, which probes the region of the electromagnetic spectrum between 200 – 800 nm. Transitions in the electronic energy levels of the bonds of a molecule, as a result of absorption of electromagnetic radiation in the UV-visible region, lead to the excitation of electrons from the ground state into an excited state.[139]

All molecules absorb UV radiation in the region below 150 nm, as this radiation has energy corresponding to that required to excite the σ-bond framework of molecules.

Electrons in lone pairs and π-bonds require less energy for excitation to their antibonding orbitals than electrons in σ-bonds. Consequently, of particular interest in UV-visible spectroscopy are n > π* and π > π* transitions.[140] Conjugated systems (e.g. polyenes) are often referred to as chromophores; these give rise to characteristic absorptions in the UV-visible spectrum. This is because extending the degree of conjugation progressively narrows the gap between the HOMO and LUMO meaning that the wavelength of radiation required for excitation becomes longer.[140]

NADH absorbs at around 340 nm, due to the n > π* transition of the nicotinamide ring. Both NAD^+ and NADH show absorbance with λ_{max} (Absorption maximum) at 260 nm due to the π > π* transition of the adenine ring, see Figure 2-2.

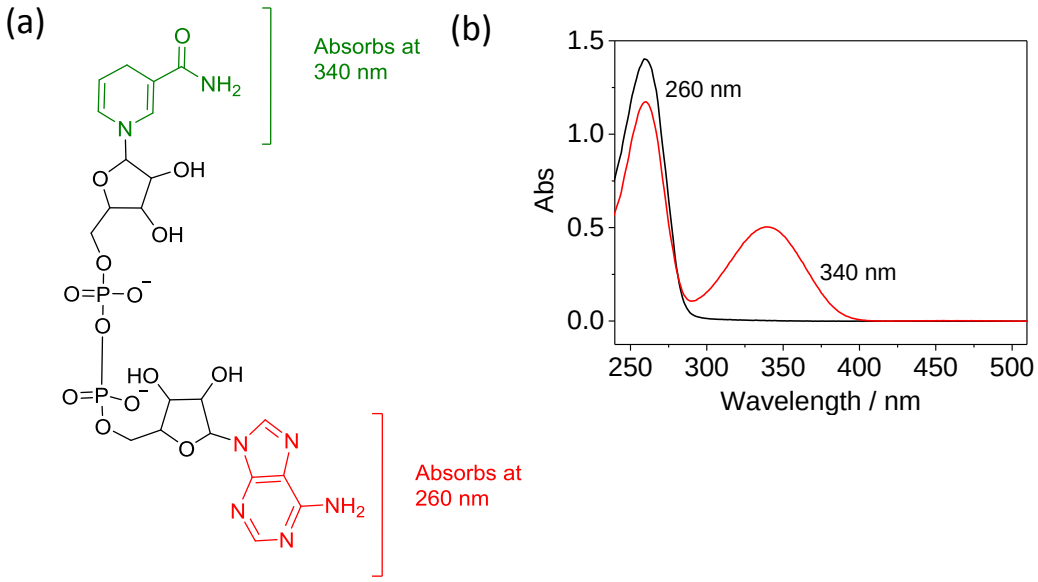

Figure 2-2:(a) Chemical structure of NADH with the nicotinamide functionality which absorbs at 340 nm and the adenine ring which absorbs at 260 nm identified (b) The spectra of 0.1 mM NAD^+ (black) and 0.1 mM NADH (red) in 50 mM Tris-HCl pH 8. The absorbance at 260 nm is clear for both cofactors; however, only NADH displays an absorbance at 340 nm.

The peaks at λ_{max} = 340 nm can be used to distinguish the presence of absence of NADH. Consequently, solutions of NAD^+ and NADH are often studied using UV-visible spectroscopy.

2.2.2 The Beer Lambert Law

UV-visible spectroscopy can be used to determine the concentration of the chromophore in a dilute sample. The absorption and concentration are linked by the Beer Lambert law, equation 2-1:

$$A = \varepsilon c l \qquad \textbf{2-1}$$

where A is the absorption, c is the concentration of the chromophore containing molecule, l is the path length of the cuvette (in cm, most cuvettes have a path length of 1 cm) and ε is the molar absorptivity coefficient. Consequently, the concentration of a sample can be determined if the molar absorptivity coefficient (ε) for that particular molecule is known. The molar absorptivity coefficients of the natural cofactors and mediators used in this project are shown in Table 2-3.

Table 2-3: Literature and experimental values for the molar absorptivity constants used within this thesis.

Sample	Description	Wavelength / nm	ε / mM^{-1} cm^{-1}
NAD^+ [141]	Natural cofactor	260	17.4
NADH[141]	Natural cofactor	260	14.1
		340	6.22
		365	3.4
Benzyl viologen[102]	Redox mediator	578	8.9
Methyl viologen[131]	Redox mediator	605	1.3
Acetophenone[142]	Reaction product	290	0.83

UV-Visible experiments were performed on a Cary 60 spectrometer (Agilent), using a quartz UV-visible cuvette (Helma) with 1 cm pathlength (of 2 mL, 1 mL or 100 µL minimum volume) or a plastic cuvette (Thermofisher). A cell holder (Agilent) with a Peltier element and magnetic stirring element was used for all experiments so that temperature could be accurately controlled and for efficient mixing.

Often, the buffer systems used show some absorbance in the UV-visible range. Consequently, a baseline was always taken of a blank sample just containing buffer, to remove any contributions from the buffer system in subsequent scans. The maximum absorbance which can be measured using the Cary 60 spectrometer is ± 4 Absorbance units. Only absorbances below 2 Absorbance units were used quantitatively.

2.2.3 Calculating enzyme activities

Enzyme activities are often reported as µmoles min^{-1} per mg enzyme (Units mg^{-1} or U mg^{-1}) to allow comparison between the activity of enzymatic systems. Specific activities as a function of molecular weight allow comparison of different batches of the same enzyme.

The activity of metal or molecular catalysts is usually quoted as a total turnover number (TTN), which is the number of moles of product produced per mole of catalyst over the course of a reaction, and turnover frequency (TOF) the number of moles produced per mole of catalyst over a particular time period (usually per second). These figures are also calculated and given where appropriate. The turnover number (TN) is used here to give moles of product per moles of cofactor.

Plate reader

For experiments where repeat readings where required without the requirement for supply of H_2 gas, a plate reader (SPECTROstarNano, BMG LABTECH) was used. This instrument is able to record UV-vis spectra of multiple samples in a 96 well plate at regular intervals. It also contains a heating element allowing assays to be carried out between 25 and 40 ^{o}C. Data from these measurements was initially processed using the SpectroStar Nano data analysis program (Mars), which also gives the value of the pathlength depending on the volume of solution present in each well of the microtiter plated.

Reactions were carried out with a total volume of between 100 – 200 µL. In general, a master mix was prepared containing buffer with the relevant cofactor and substrate. Equal amounts of the master mix were then added to each well using a multi-channel pipette. Reactions were initiated by adding the enzyme solution using a multichannel pipette. The plate was then quickly placed into the plate reader and gently shaken before the first scan was taken. Scans were taken between 300 nm and 600 nm. Scans were corrected for buffer absorbance by taking away the absorbance of a sample just containing the master mix.

2.2.4 Testing the activity of SH enzymes

This section describes methods for assaying the activity of SH enzymes in solution.

Testing the activity of the HoxHYFU enzyme

The specific activity of the whole SH was measured in this thesis by following the H_2 driven conversion of NAD^+ to NADH.

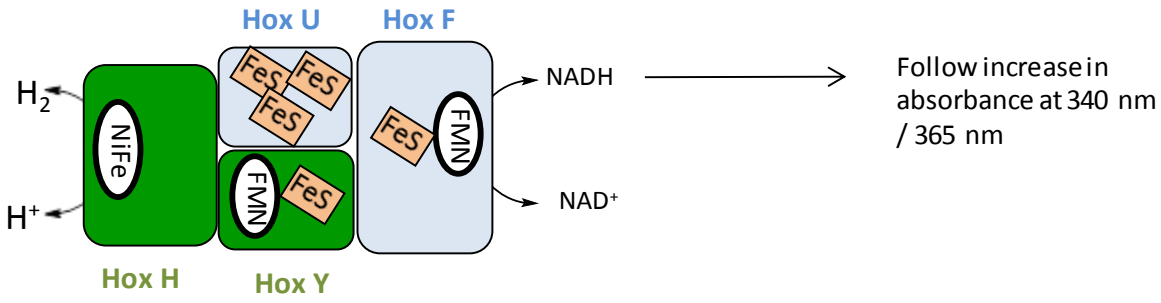

Figure 2-3: Schematic showing the method of measuring the activity of the whole SH.

The H_2-driven reduction of NAD^+ to NADH leads to an increase in absorbance with an absorption maximum at 340 nm. A schematic diagram of the SH is shown in Figure 2-3, showing that the increase in absorbance at 340 nm (or practically 365 nm) is used to follow the reaction.

Practically, SH activity assays were carried out in H_2-saturated buffer, containing NAD^+ (50 mM Tris-HCl pH 8), following the protocol of Schneider *et al.*[113] The buffer was saturated with H_2 by bubbling H_2 gas through the buffer for at least 1 hour. The buffer

was also incubated in a water bath ensuring that it was equilibrated to the desired temperature for the reaction. The assays were carried out on a 2 mL scale in a 3 mL quartz cuvette (Helma) sealed with a rubber bung. The cuvette was subsequently gently sparged with H_2 gas for 2 minutes, to ensure that the reaction mixture was H_2 saturated. A Hamilton syringe was then used to inject an aliquot of SH enzyme (approximately 50 pmoles) to start the reaction. The increase in absorbance was then followed at 365 nm using the Cary kinetics program.

Testing the activity of the HoxFU moiety

In some cases the NADH oxidising activity of the HoxFU domain is analysed indirectly. This assay can be carried out on the whole HoxHYFU moiety or on the HoxFU moiety isolated using molecular biological strategies.

The HoxFU moiety is used within this thesis separately as part of the particle system, as shown in Figure 2-1 (d). The activity of the HoxFU moiety, when assayed in a preparation of HoxHYFU, is sometimes much greater than that of the whole SH (HoxHYFU), due to the HoxHY and HoxFU sub-units dissociating as seen for *Rh. opacus*,[143] or not being produced in equal ratios in the SH.

For this assay redox mediators are used as artificial electron acceptors. These molecules work by binding to the enzyme and accepting electrons. This leads to the mediator changing colour, allowing the reaction to be followed spectrometrically.[144][145]

The activity of the HoxFU moiety was measured using the method of Lauterbach *et al.*,[102] by following the oxidation of NADH, which was used to drive the reduction of benzyl viologen (BV), see Figure 2-4.[109] This assay was carried out outside of a glovebox in the laboratories of Dr O. Lenz at the TU Berlin. The assay was performed in buffer (50 mM Tris-HCl buffer pH 8), which was bubbled with N_2 gas for a least 1 hour in order to eliminate as much O_2 as possible. A 2 mL aliquot of this solution was

then added to a 3 mL quartz cuvette (Helma), which was sealed with a rubber bung and gently sparged with N_2 gas for 2 minutes. Aliquots of NADH (1 mM), BV (5 mM) and sodium dithionite (10 µM) were added to the solution using separate syringes. Addition of sodium dithionite is important in non-anaerobic environments, as this ensures that any O_2 present in the cuvette is reduced ensuring that it cannot abstract electrons from the BV_{red} leading to a lower than expected rate of reaction. The experiment was started by injecting an aliquot of enzyme (*ca.* 50 pmoles) using a syringe. Progress of the reaction was measured by following increase in absorbance at 578 nm, which corresponds to the conversion of BV_{ox} to BV_{red}.

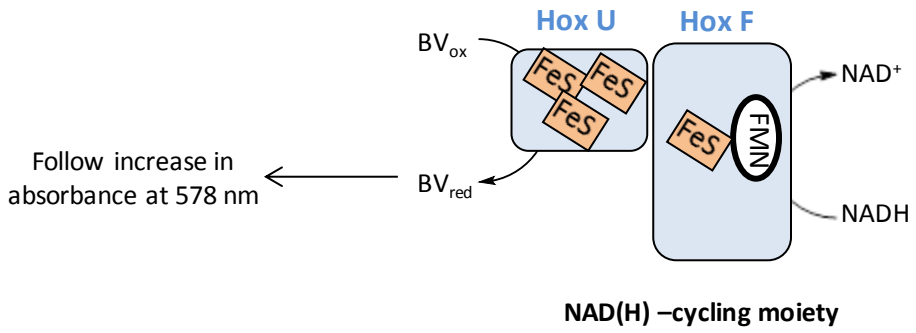

Figure 2-4: A schematic diagram showing the method of measuring the activity of the HoxFU moiety.

Testing the activity of the HoxHY moiety

In chapter 4 section 4.3 the hydrogen cycling ability of the *H. thermoluteolus* SH was determined separately to the NAD^+ cycling ability. This was carried out using the whole HoxHYFU enzyme.

The activity of the HoxHY moiety was measured based on H_2-driven reduction of methyl viologen, (MV) see Figure 2-5 using the method of Lauterbach *et al.*[131] MV was used as the mediator as this allows the activity values determined for the *H. thermoluteolus* HoxHY moiety in this project to be compared to previously measured values in the literature for the isolated HoxHY moiety from *R. eutropha*.[131]

The assay was carried out in 50 mM H_2-saturated Tris-HCl buffer. This was bubbled with H_2 for at least 1 hour in a flask in a temperature controlled water bath. A 2 mL aliquot of buffer was then added to a 3 mL quartz cuvette (Helma) and sealed with a rubber bung. The solution in the cuvette was then gently sparged with H_2 for 2 minutes to ensure the solution was fully H_2 saturated.

Aliquots of MV (5 mM) and sodium dithionite (45 µM) were added to the cuvette using separate Hamilton syringes. The reaction was subsequently started by adding enzyme (*ca.* 50 pmoles) using a separate Hamilton syringe. The reduction of MV_{ox} to MV_{red} can be followed at 605 nm.[146]

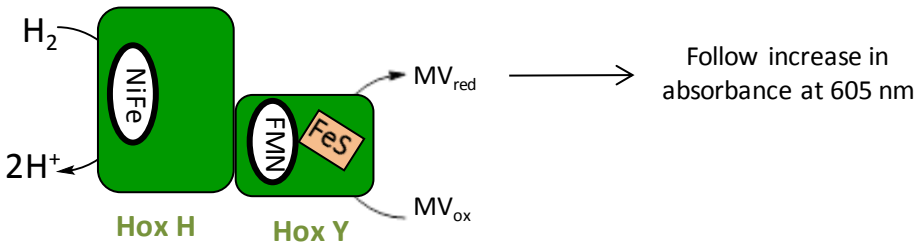

Figure 2-5: A schematic diagram showing the method of measuring the activity of the HoxHY moiety

2.2.5 Testing the activity of enzyme-modified particles.

In Chapter 5, *in situ* measurements of H_2-driven NAD^+ to NADH conversion using enzyme-modified particles were carried out. The activity of the enzyme-modified particles can be measured by following the absorption of NADH at 340 nm, as shown in the diagram in Figure 2-6.

Generally an aliquot of enzyme-modified particles was prepared as described in section 2.4. A 1 mL aliquot of H_2-saturated buffer was added to a cuvette and a 1 mM aliquot of NAD^+ was added to the solution. A micro-stirrer bar of 1 mm diameter was added to the cuvette to ensure efficient mixing. The cuvette was then sealed with a rubber bung and H_2 gas was flowed at a low flow rate (*ca.*5 mL min^{-1}) through the headspace of the

cuvette. An aliquot (containing ≤ 100 µg of BP 2000 particles) of enzyme-modified particles was injected into the cuvette using a syringe to start the reaction. The cuvette was subsequently placed into the spectrometer, with stirring at the maximum possible rate to minimise the effect of particles dropping to the bottom of the cuvette. The reaction was followed by taking sequential UV-visible scans between 200 and 800 nm.

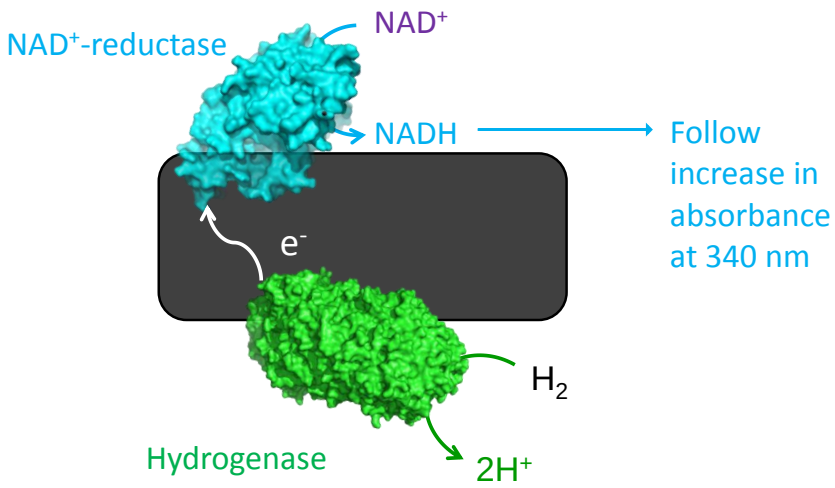

Figure 2-6: A schematic diagram of the enzyme-modified particles. The activity of these particles can be followed in a similar way to the activity of the whole SH, by following the absorption of NADH at 340 nm.

Baseline correction for enzyme-modified particles

Scattering of light in the UV-visible cuvette is caused by the carbon black (BP 2000 particles) added to the reaction mixture.[119] Over time the particles sink, which leads to significant changes in concentration of particles at the point where the sample is analysed (i.e. where the beam goes through the cuvette) and which therefore causes a large change in the baseline (largely independent of the wavelength), due to changes in how much light is scattered.[119] Therefore, changes in absorbance occur both due to changes in the concentration of cofactor over time, but also the concentration of particles, causing scattering of light at the point where the sample is being analysed. Consequently, simple analysis of the absorbance at a single wavelength over time, as

done for the kinetic assays above, does not give an accurate reading of the activity of the particles.[119] Therefore, UV-visible spectra were recorded between 200 and 800 nm over time and a baseline correction was carried out, see Figure 2-7.

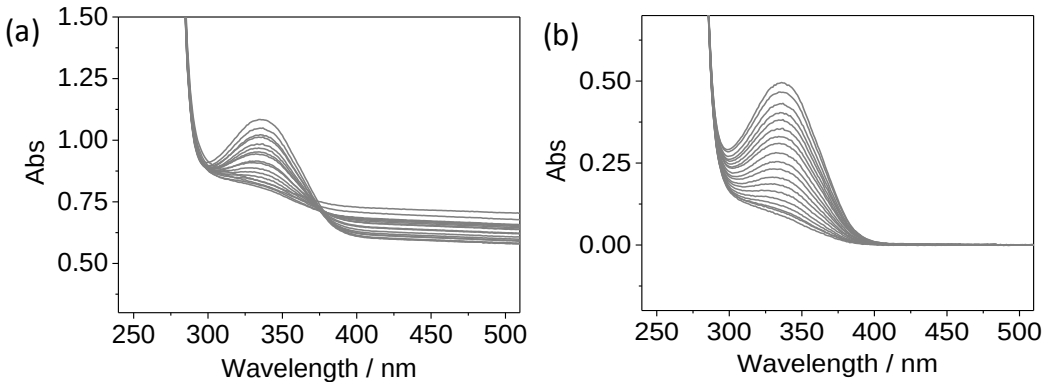

Figure 2-7: The baseline correction method used to analyse NADH production when particles were present in the reaction mixture. (a) Uncorrected spectra, decreasing baseline absorption due to particles falling in solution. (b) Baseline corrected spectra, demonstrating increasing absorption at 340 nm.

Origin software (OriginLab) was used to apply a baseline correction. In general 5 points were taken between 500 and 800 nm, as no absorption due to the cofactor would be expected in this region of the spectrum, meaning that the baseline should be flat. A line was drawn between the 5 points and this was then set to an average value of zero. This method has already been reported by Reeve *et al*.[119] The absorbance at 340 nm can be determined from this baseline corrected figure and can then be plotted as a function of time. This graph can then be used to determine the activity of the particles, by taking a gradient.

2.2.6 Testing the activity of *ω-transaminase* enzymes

ω-Transaminase enzymes are used in chapter 3 of this thesis for the production of chiral amines. These enzymes catalyse the redox neutral transfer of an amine group to a ketone functionality at the expense of a donor amine molecule such as L-alanine, as shown in Figure 1.11. It is important to have a spectroscopic method for assaying the

activity of the *ω-transaminase* enzymes used, as the *Vf ω-transaminase* was produced in house. This method also allows the activity of the *ω-transaminase* to be determined when it was immobilised on carbon particles.

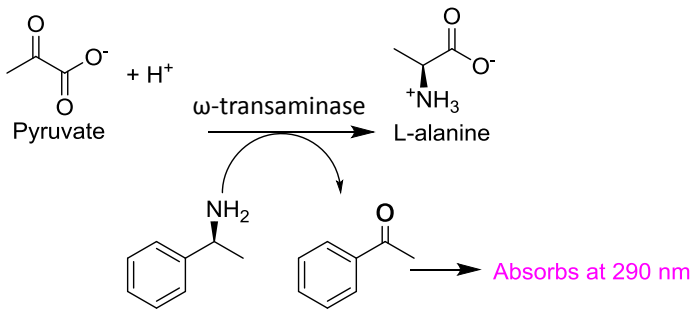

Figure 2-8: A schematic diagram showing the reaction used to determine the activity of *ω-transaminase* enzymes. The deamination reaction was monitored by following the increasing absorption of acetophenone at 290 nm. This reaction is going in the opposite direction to the bio-catalytic reactions carried out in chapter 3 in which L-alanine is used as an amine donor for the amination of 4-phenylbutan-2-one.

The activity of the *ω-transaminase* enzymes was measured by following the (S)-α-methylbenzylamine to acetophenone conversion which leads to an increase in absorption at 290 nm, as shown in Figure 2-8.[147]

This measurement was carried out at room temperature in a 1 mL quartz cuvette (Helma). A 10 µL aliquot of enzyme solution was added with a pipette to the bottom of the cuvette. To start the reaction a 990 µL aliquot of 'master mix' was added. This 'master mix' contains 50 mM potassium phosphate buffer pH 8, 0.1 mM PLP, 10 mM (S)-α-methylbenzylamine and 5 mM sodium pyruvate and was added to the cuvette with a 1 mL pipette. The mixture was pipetted up and down twice to ensure efficient mixing of the solution. The increase in absorption at 290 nm was monitored as a function of time using the Cary kinetics program.[148]

2.3 Electro-enzymatic characterisation methods

In chapter 4, analytical protein film electrochemistry was used to characterise a new NAD^+-reducing soluble hydrogenase variant (HoxFU from *H. thermoluteolus)*.

2.3.1 Analytical electrochemistry

Electrochemistry is a very sensitive technique, which allows the study of electron transfer reactions occurring at electrode surfaces.[149] Protein film electrochemistry (PFE) is a well-established technique for studying redox enzymes that are able to exchange electrons directly with an electrode.[150] In PFE the enzyme is 'directly wired' to the electrode.[151] In the case of the enzymes used in this thesis (NAD^+-reductases and hydrogenases) the active site is linked to the electrode *via* a chain of FeS clusters, see Figure 2-9. For these enzymes intramolecular electron transfer is rapid as the electrode provides a permanent pool of electrons available for reduction, meaning that the rate is limited by the redox process occurring at the enzyme active site, unlike in mediated assays which are often slowed down by diffusion of the mediator.[152][153]

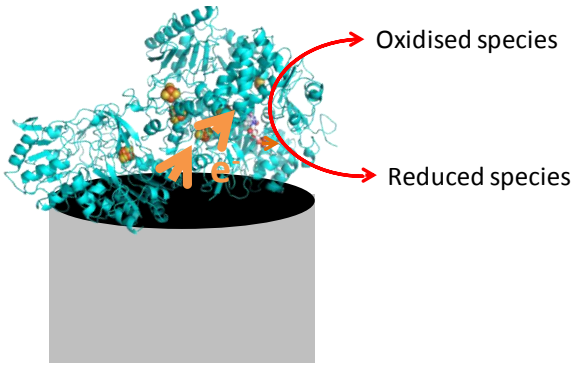

Figure 2-9: A schematic diagram showing the enzyme being directly wired to the surface of an electrode

In this project carbon working electrodes were used, as enzymes can be immobilised directly by absorption on to the carbon surface without further functionalisation or covalent attachment being necessary.[102,131,154,155] This thesis makes use of established protocols for analysing hydrogenase and NAD^+-reductase enzymes adsorbed onto carbon electrodes.[102,122] Carbon has been used in PFE for a number of enzymes.[154] Quinson *et al*. have shown that pyrolytic graphite edge (PGE) electrodes have pockets,

of approximately the same size as the enzymes being tested here, which is thought to aid adsorption.[156]

2.3.1.1 Electrochemical setup

The voltage applied between the working electrode and the reference electrode can be described as:

$$E = (\varphi_m - \varphi_s) + iR + (\varphi_s - \varphi_{ref}) \quad \textbf{2-2}$$

where $(\varphi_m - \varphi_s)$ is the driving force for electrolysis at the surface of the working electrode. Here, *R* is the electrical resistance of the intervening solution, meaning that *iR* describes the voltage drop in solution due to the passage of current. The term $(\varphi_s - \varphi_{ref})$ is the voltage drop at the reference electrode solution interface, which is determined by the chemical composition of the reference electrode.[149]

In voltammetry, we are really interested in measuring *i* as a function of $(\varphi_m - \varphi_s)$. In experiments where small electrodes are used and hence negligible current passes, *iR* is considered negligible and $(\varphi_s - \varphi_{ref})$ is fixed, equation 2-2 therefore simplifies to equation 2-3:

$$E = (\varphi_m - \varphi_s) + Constant \quad \textbf{2-3}$$

This means that changes in potential are directly related to the driving force. However, with larger electrodes *iR* is no longer negligible and so changes in applied potential are not just due to changes in $(\varphi_m - \varphi_s)$.[149] Current flowing through the cell alters the *iR* term and large currents may change the chemical composition of the reference electrode meaning that $(\varphi_s - \varphi_{ref})$ is also no longer zero. Hence, experiments where anything other than a negligible current flows are not possible to interpret. To avoid this problem a three electrode set-up was used in this work. In the three electrode configuration, the current is channelled through an auxiliary counter electrode.[149] A potentiostat

(EcoChemie) was used to precisely control the potential of the working electrode relative to the reference. This functions by virtue of an Op-amp which is able to allow current to flow through the counter electrode, but maintain an accurate potential of the working electrode with respect to the reference.[157] A schematic diagram of the electrical set-up is shown in Figure 2-10.[157] The potentiostat was controlled using the Nova software suite (EcoChemie, Netherlands).

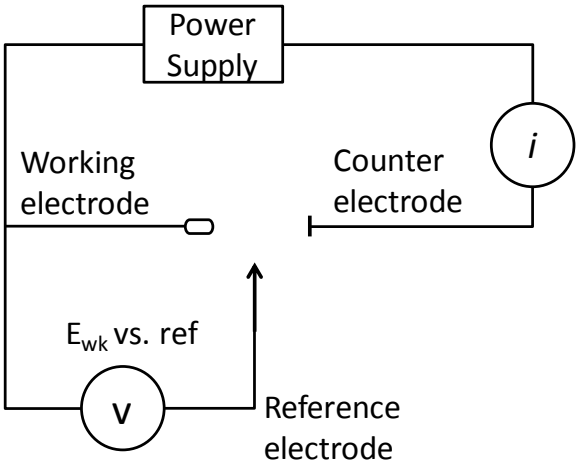

Figure 2-10: A schematic circuit diagram showing the set-up of electrode used in electrochemical experiments in this thesis. Adapted from J. Bard and L. R. Faulkner, Electrochemical Methods: Fundamentals and Applications [157].

2.3.1.2 Counter electrode

The counter electrode is the electrode which takes the current from the working electrode, completing the circuit. For the work conducted in this thesis, a platinum wire (Superpure Chemetals, 99.95 %, 0.4 mm diameter) was used as the counter electrode. For experiments with a large surface area working electrode a platinum gauze or coiled piece of Pt wire was used as the counter electrode, as a larger counter electrode is required to ensure that the process occurring at the counter electrode does not limit the reaction occurring at the working electrode. As the working electrode current in analytical experiments is low, so too is the current generated at the Pt wire. Therefore, in analytical experiments, the amount of product produced as a result of the

corresponding redox process occurring at the counter electrode is low. This means that the presence of this species in the bulk reaction mixture can effectively be ignored.

2.3.1.3 Working electrode

Analytical electrochemistry was carried out using a pyrolytic graphite edge rotating disc electrode (PGE RDE), a material which displays good conductivity.

Pyrolytic graphite sheets were supplied by Momentive Performance, USA. Pyrolytic graphite edge rotating disk electrodes (PGE RDE) were constructed in house. Pyrolytic graphite rods (10 mm, 1 mm diameter), were prepared in the Chemistry department workshops at the University of Oxford by Mr Dennis Chikwanha. A Delrin rotating disc electrode case, with a screw in metal centre was made in the Chemistry department workshops at the University of Oxford by Mr Howard Lambourne. Silver epoxy resin was used to glue a pyrolytic graphite rod to the metal rod running up the centre of the Delrin rotating disc case. Approximately 5 mm of pyrolytic graphite was left protruding from the top of the electrode. This was then sealed in insulating epoxy resin made by mixing Araldite resin and hardener in a 2:1 ratio (Robnor Resins). The electrode was allowed to dry overnight and then sanded to a flat surface using glass paper (Kemet) and polished to a mirror finish using 1 μm alumina powder (Bühler). This leaves a flat graphite circle in the centre of the electrode with an area of 0.03 cm^2, which may be used for enzyme immobilisation.

Preparation of an enzyme film

In PFE (Protein film electrochemistry), a small (*ca.* 0.5 μL equivalent to *ca.* 5 pmoles)[153] sample of enzyme is absorbed directly onto an electrode surface. This allows the rapid characterisation of enzymes with only a tiny amount of protein.[155]

The electrode was prepared following the protocol of Armstrong and co-workers.[158] Before use the working electrode was briefly sanded with a piece of 1600 sandpaper

and then polished with freshly prepared slurry of 1 μM alumina. The electrode was rinsed under a stream of MilliQ water and sonicated for 10s before applying the protein film.

The protein film was applied to the electrode following the procedure used by Idris *et al*.[102] A 0.5 μL aliquot of protein was spread over the carbon surface of the electrode using a 10 μL pipette tip and allowed to dry for 30 seconds until the enzyme was "tacky".

Polishing the electrode generates polar COH and COOH functionalities, which are thought to aid absorption of proteins.[159] To observe catalytic activity, it is essential that proteins retain their native folding and do not denature on an electrode surface. Armstrong and co-workers suggest that the oxygen containing groups which result from polishing the electrode surface form domains which have the ability to hydrogen bond multiple times to the protein. This makes the electrode surface itself more 'biological' in its nature and therefore stabilises the protein adsorbed on the electrode.[152,159]

2.3.1.4 Reference electrode

The reference electrode maintains a constant potential drop across its interface with the solution allowing the voltage of the working electrode to be measured accurately.[149]

For analytical experiments a saturated calomel reference electrode was used. This was corrected to SHE using equation 2.4:

$$E_{SHE} = E_{SCE} + 0.2412 - 6.61 \times 10^{-4}(T-25) - 1.75 \times 10^{-6}(T-25)^2 - 9 \times 10^{-10}(T-25)^3 \quad \textbf{2-4}$$

For experiments where a smaller reference electrode was required, a home-made saturated calomel electrode was constructed following the methods of Hidalgo *et al*.[160] A 5 μL aliquot of mercury was added to a glass-wool fritted plastic tube (Starlab), followed by a 30 mg aliquot of mercury(I) chloride. A short piece of Pt wire was

pushed into the top of the mercury and used to make a connection to the mercury in the tube. The top of the tube was then sealed with araldite resin (Robnor Resins), allowing a small section of the Pt wire to stick out above the resin. A 5 cm long, 2 mm leak free PEEK reference electrode body (Harvard Apparatus, UK) with a fritted bottom was filled with saturated KCl solution and connected to the mercury tube ensuring that the KCl solution was in contact with the bottom of the mercury tube. These tubes were then sealed together with parafilm (Beamis, USA).

2.3.2 Electrochemical cells

Typically, analytical electrochemical experiments were carried out in an electrochemical cell, which has a water jacket allowing precise control of temperature; see Figure 2-11 (a). It was also designed to be gas tight, meaning that gases can be blown into the headspace of the cell, leading to a well-defined gas atmosphere being present in the headspace of the cell.

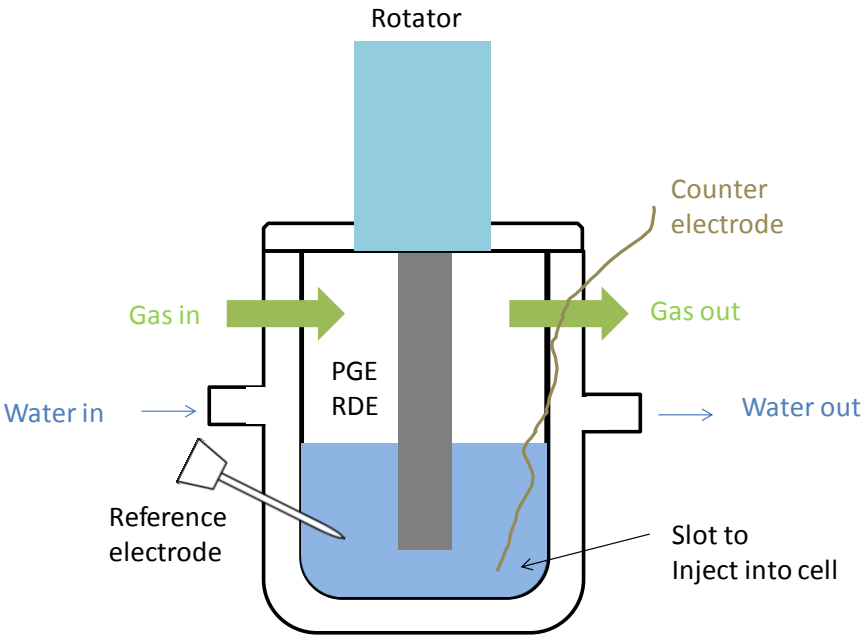

Figure 2-11: A typical electrochemical cell used for analytical electrochemistry in this project. This cell has a water jacket allowing precise control of temperature, it is also able to seal directly onto the rotator meaning that it is gas tight allowing experiments with precise gas mixtures. A side arm allows injections of solution (substrate or inhibitor).

The electrochemical cell was designed to allow a rotating disc electrode to be lowered in and out for analytical chemistry experiments. The cell also contains a sealed side arm for the reference electrode and a side arm or injection port for injection of aliquots of solution (e.g. substrate or inhibitor). This injection port means that the cell solution can be changed without changing the enzyme film.

2.3.3 Electrochemical techniques

Cyclic voltammetry is a technique in which the potential of the working electrode is swept from E_1 to E_2 at a given scan rate. During this process the current is recorded as a function of potential.[149] This is summarised schematically in Figure 2-12 (a).

There are two contributions to the current recorded in a cyclic voltammogram (CV): faradaic and non-faradaic contributions. The non-faradaic component is the background current at the unmodified electrode. This is arises because as the potential of the electrode surface is swept between E_1 and E_2, ions in the solution re-arrange leading to the formation of an electrical double layer which acts as a capacitor.[161] This leads to a background (or blank) contribution to the current recorded. Generally, the electrode was held at the starting potential for 10 s before measuring a CV. During this hold time the non-faradaic current usually drops to approximately < 50 μA. When using a rotating disc electrode decreasing the scan rate also often leads to a drop in the capacitive current. The faradaic current, on the other hand, is the current response that we are actually interested in.

In order to distinguish between the faradaic and non-faradaic contributions to the current a 'blank' scan was always recorded at an unfunctionalised electrode before recording a CV at an enzyme functionalised electrode. An example of a blank is shown in Figure 2-12(b). The blank scans are recorded in the same cell solution as the scans

taken with an enzyme-modified electrode; this ensures that no redox reactions occur for the cell solution at the bare carbon surface in the potential window of interest.

Figure 2-12 (c) shows an NAD^+-reductase functionalised PGE RDE showing NAD^+ reduction (black) against a blank scan carried out with an unfunctionalised PGE RDE.

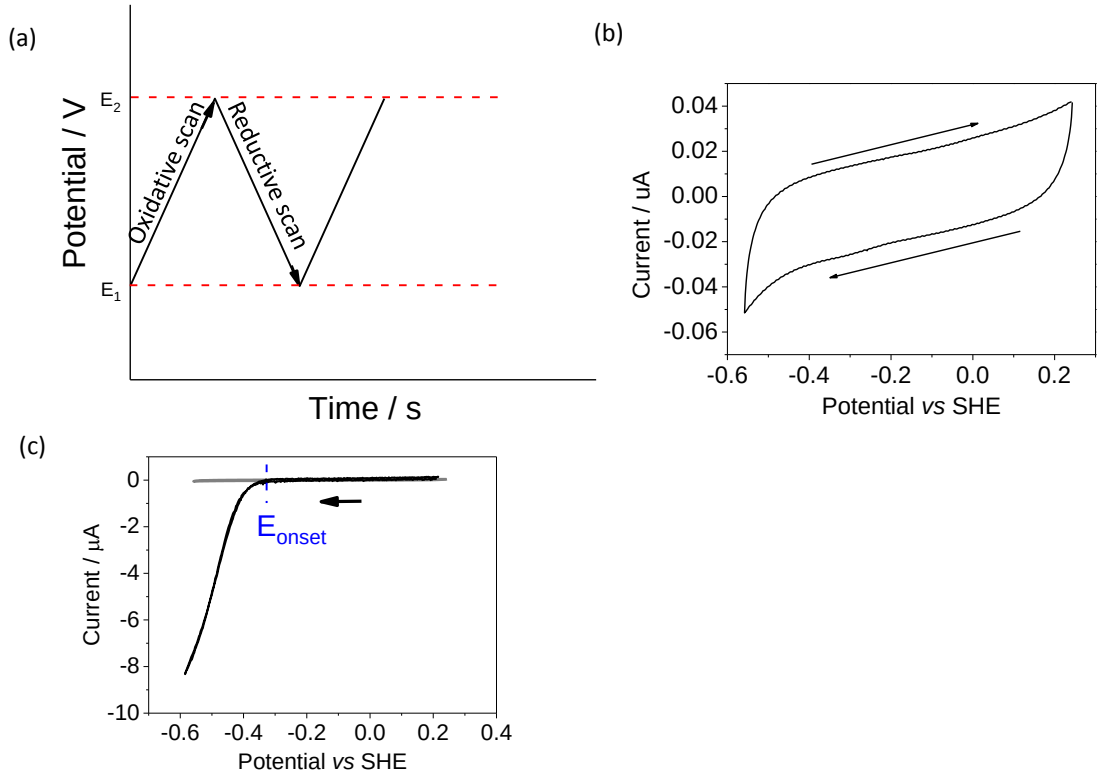

Figure 2-12: Cyclic voltammetry as an analytical tool. (a) Variation of the applied potential as a function of time in a cyclic voltammetry experiment. (b) A typical current *versus* potential plot showing the response at an unmodified PGE electrode to the applied potential. Arrows show scan direction. Conditions: 50 mM Tris-buffer pH 8, scan rate of 10 mV s^{-1}, 2500 rpm rotation rate. (c) Scan of reduction at a *H. thermoluteolus* HoxFU functionalised electrode in 50 mM Tris-HCl pH 8, containing 1 mM NAD^+.

The reductive wave due to NAD^+ reduction at the HoxFU active site (faradaic contribution) can clearly be seen against the blank (non-faradaic contribution).

The scan in Figure 2-12 (c) also demonstrates that in the first section of the CV following the onset potential for NAD^+ reduction, the reductive current increases almost linearly, as the potential becomes more negative. Due to the fast rotation of the electrode fresh substrate (NAD^+) is continually being supplied to the electrode surface.

When the direction of the scan is reversed, the reductive current decreases (almost linearly with current) and importantly no reverse peak is observed for NADH oxidation as all of the NADH in solution has been spun away from the electrode.

The reverse behaviour can be seen for NADH oxidation at a HoxFU functionalised PGE RDE, with the oxidation current increasing the more positive the potential.

The data obtained from cyclic voltammetry experiments like the one above is extremely useful. It allows determination of the potential at which catalysis starts to occur (the onset potential, E_{onset}). In addition the shape of the scan can give information about any inactivation or inhibition processes, which may be occurring.[162] Due to not knowing exactly how much enzyme is immobilised on the electrode surface it is not possible to directly compare the activities between different films of different enzyme. However, by taking averages of the activities of films of the same enzyme it is possible to get an idea of the activity of these films under different conditions (e.g. pH).

Chronoamperometry involves recording the current as a function of time whilst applying a constant potential to the working electrode. This allows the activity of the enzyme to be monitored under constant potential conditions, giving a read out of enzyme activity, which is proportional to the current for a particular enzyme film.

In this work analytical chronoamperometry techniques were mainly used to determine the half-life of enzymes on the electrode, and affinity (K_M) and inhibition constants (K_I), by measuring the activity whilst changing the concentration of substrate or inhibitor see Chapter 4 and section 2.3.4.

2.3.3.1 Electrode rotation

Slow diffusion of the substrate or product to or away from the electrode, can lead to diffusion limiting the catalytic current observed at the electrode.

If the working electrode is stationary this will lead to a diffusion layer around the electrode, where there is a build-up of product and depletion of substrate. This will mean that the concentration of the product at the surface of the electrode will differ to that in the bulk solution.[149]

A rotating disc electrode (RDE) maintains a constant supply of electroactive substrate at the surface of the electrode, as the rotation of this electrode spins the solution away from the electrode surface in a radial direction at the same time as drawing up new solution from the bulk. This ensures that the solution at the surface of the electrode is the same as that found in the bulk.[149]

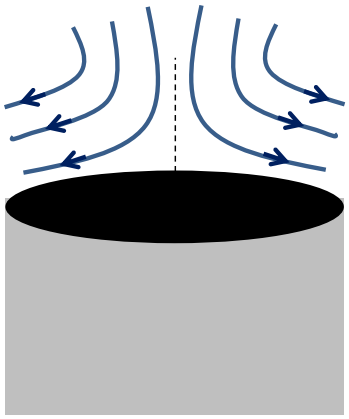

Figure 2-13: The laminar diffusion pattern around a PGE RDE electrode adapted from ref.[161]

Figure 2-13 shows the flow patterns created around a rotating disc electrode. The flow around the electrode can be modelled as laminar. An approximation of the limiting current is obtained when there is no significant increase in current when the rotation rate is increased. In this thesis, the rotation rate was increased until the current stopped increasing. A rotating rate of greater than this value was then used. This ensured that the current was not limited by diffusion considerations, but by the rate of enzyme catalysis for the enzyme of interest. This ensured that substrate was constantly supplied to the electrode surface and that the product of the reaction was rapidly spun away.

2.3.4 Enzyme kinetic measurements

2.3.4.1 Affinity constant determination

The Michaelis constant (K_M) is a measure of the affinity of an enzyme for a particular substrate. This is defined as the substrate concentration at which an enzyme will operate at half of its maximum rate (V_{max}). Generally substrate concentrations of > 10 × K_M are used in industrial processes to ensure that enzymes operate at close to their maximum rates.[11]

Measurements of the K_M are consequently important as they allow appropriate conditions to be selected for a particular bio-transformation.

2.3.4.2 Mathematical background to K_M[163]

A simple enzymatic reaction can be described by equation 2-5:

$$E + S \underset{K_{-1}}{\overset{K_1}{\rightleftarrows}} ES \xrightarrow{K_2} P + E \qquad \textbf{2-5}$$

where E is the enzyme, S is the substrate, ES is the enzyme substrate complex and P is the product. [163] This system can, however, be extended to more complicated enzymatic systems. Assuming the concentration of [ES] doesn't change on the time scale of the reaction solving equation 2-5 for the concentration of [ES] gives equation 2-6:

$$\frac{d\,[ES]}{dt} = K_1[E][S] - K_{-1}[ES] - K_2[ES] = 0 \qquad \textbf{2-6}$$

$K_1, K_{-1}\ and\ K_2$ are the rate constants for forming ES (the enzyme-substrate complex),[163] dissociation of ES back to substrate and enzyme and the rate constant for the conversion of ES to product respectively.[163] Rearranging equation 2-6 for the enzyme substrate complex [ES] gives:

$$[ES] = \frac{K_1[E][S]}{K_{-1} + K_2} \quad \textbf{2-7}$$

Assuming that the starting concentration of the enzyme $[E]_o$ minus the concentration of the enzyme substrate complex [ES] are equal to the enzyme concentration [E] then this gives:

$$[ES] = \frac{K_1[E]_o[S]}{K_{-1} + K_2 + K_1[S]} \quad \textbf{2-8}$$

From equation 2-5 and 2-8 the rate (v) equation can be derived, as the rate of reaction is dependent on the rate of conversion of enzyme-substrate complex to product:

$$v = \frac{d[P]}{dt} = \mathrm{K_2}[ES] = \frac{\mathrm{K_2}K_1[E]_o[S]}{K_{-1} + \mathrm{K_2} + K_1[S]} \quad \textbf{2-9}$$

This simplifies to equation 2-10:[163]

$$v = \frac{\mathrm{K_{cat}}[S][E]_o}{K_M + [S]} \quad \textbf{2-10}$$

In equation 2-10 K_2 has been replaced by K_{cat} (the turnover number) which is the number of cycles per unit time an enzyme can go through.[163]

When the substrate concentration is much higher than K_M then the substrate concentration becomes the dominant term in the denominator of equation 2-10 and the value of K_M can effectively be ignored.[163] Under these conditions the maximum rate (V_{max}) is obtained. Hence:

$$V_{max} = \mathrm{K_{cat}}[E]_o \quad \textbf{2-11}$$

Which gives:

$$v = \frac{V_{max}[S]}{[S] + k_M} \quad \textbf{2-12}$$

when substituted back into equation 2-10, giving the rate in terms of the maximum rate (V_{max}). When the substrate concentration is equal to the K_M equation 2-12 gives equation 2-13:

$$v = 0.5V_{max} \qquad \textbf{2-13}$$

Equation 2-13 is the defining equation for the K_M: The substrate concentration at which the enzyme carries out catalysis at half of its maximum rate (half V_{max}) is equal to the K_M.[163]

The value of the K_M can be most easily determined by plotting activity (normalised current, for electrochemical measurements) against substrate concentration. A Michaelis-Menten fit can then be applied (using the OriginPro software package) and used to determine the value of the K_M. See Figure 2-14 for an example plot.

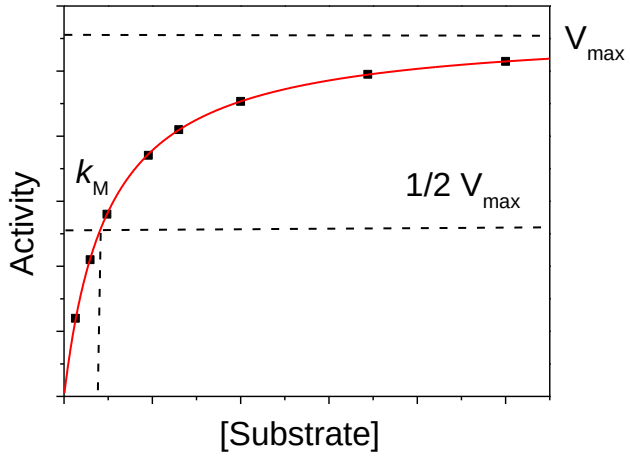

Figure 2-14: An example Michaelis-Menten plot used to determine the value of the K_M. The values of V_{max} and K_M are marked upon the graph.

Determining affinity constants

Biochemical K_M determinations were carried out using UV-visible spectroscopy. These were determined for both the whole *H. thermoluteolus* SH and *H. thermoluteolus*

HoxFU. The activity of the whole SH was determined using H_2-driven NAD^+ reduction at a range of NAD^+ concentrations (> 8 different concentrations). Similarly the activity of the HoxFU moiety was determined using NADH driven reduction of BV at several different concentrations of NADH. These assays are described in more details in section 2.2.4.[102] Data from these assays could be used to calculate the specific activity of the enzyme at a range of concentrations, which can then be plotted against concentration of substrate giving a Michaelis-Menten plot like the example shown in Figure 2-14. A Michaelis-Menten fit can then be applied which gives the value of the K_M.

Electrochemical K_M determinations were carried out using chronoamperometry. To determine the K_M for NAD^+ reduction, an enzyme film was prepared on a PGE RDE. The electrode was then held at an NAD^+-reducing potential (−412 mV *vs* SHE) for approximately 10 s, allowing the current to stabilise. This is in the absence of cofactor so the current tends to zero. Sequential aliquots of NAD^+ (substrate) were then injected into the electrochemical cell through the injection port, using a Hamilton syringe and the current change as a result was measured.[102] The actual number of enzymes undergoing catalysis on the electrode surface is not known, therefore V_{max} cannot be determined using this method. However, as the electrochemical current (i) is directly proportional to the activity (v), then we are able to substitute i for v in the Michaelis-Menten plot, allowing electrochemical determinations of K_M.[102] A similar procedure is followed to determine the K_M for NADH oxidation; here the electrode was held at an NADH reducing potential (−62 mV *vs* SHE) and aliquots of NADH were injected in and the change in current relative to the NADH concentration was recorded.

2.3.5 Inhibition constants[163]

There are a number of different mechanisms which can lead to enzymatic inhibition. Inhibition can be competitive (the inhibitor binds at the same site as the substrate); uncompetitive (the inhibitor binds to the substrate-enzyme complex); or mixed.[163]

Product inhibition means that the product of an enzymatic reaction subsequently goes on to inhibit the enzymatic reaction itself, which it is a product of.[163]

Work carried out by Idris *et al*. has demonstrated that the HoxFU moiety from *R. eutropha* demonstrates competitive product inhibition towards NAD^+ for the oxidation of NADH and towards NADH for the reduction of NAD^+.[164]

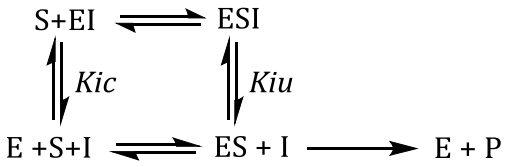

2-14

A schematic which demonstrates the possible routes for inhibition is shown in equation 2-14 where, *I* is the inhibitor and K_{iu} is the uncompetitive inhibition constant and K_{ic} is the competitive inhibition constant, [S] is the substrate concentration and [I] is the inhibitor concentration.[163] An expression for the inhibition derived from the schematic in equation 2-14 is shown in equation 2-15, (based on the Michaelis Menten equation):

$$v = \frac{V_{max}[S]}{K_M\left(1 + \frac{[I]}{k_{ic}}\right) + [S](1 + \frac{[I]}{k_{iu}})} \qquad \textbf{2-15}$$

Taking reciprocals of both sides of equation 2-15, equation 2-16 can be derived:[163]

$$\frac{1}{v} = \frac{K_M + [S]}{V_{max}[S]} + \frac{[I](\frac{K_M}{K_{ic}} + \frac{[S]}{K_{iu}})}{V_{max}[S]} \qquad \textbf{2-16}$$

If two different initial concentrations of substrate are used, the intersection of the two lines can be found when the reciprocal of the rate obtained with $[S]_1$ (substrate

concentration 1) is equal to the reciprocal of the rate obtained with $[S]_2$ (substrate concentration 2).[163]. This therefore results in equation 2-17:

$$\left(\frac{1}{[S]_1}-\frac{1}{[S]_2}\right)\left(1+\frac{[I]}{k_{ic}}\right)=0 \qquad \textbf{2-17}$$

Equation 2-17 shows that a plot of $1/v$ against [I] at a range of different starting substrate concentrations (a Dixon plot), will give the value of the competitive inhibition constant at the point of intersection of the lines (equal to $-K_{ic}$). If the lines are approximately parallel this suggests that there is no competitive inhibition.[163] An example Dixon plot is shown in Figure 2-15 (b).

If $[S]/v$ is plotted against [I] for several values of [S] (a Cornish-Bowden plot) the competitive inhibition constant can be obtained from the point of intersection of the lines (equal to $-K_{iu}$)[163] If the lines are approximately parallel this suggests that there is no uncompetitive inhibition.[163]

Both of these types of plot are shown in Appendix B, for competitive, uncompetitive and mixed inhibition.

Inhibition constant measurement

Measuring the inhibition constant is difficult using UV-assays,[165] generally multiple kinetic measurements must be carried out following pre-incubation of an enzyme sample with an inhibitor.[166] In order to obtain enough points to plot a valid Dixon plot, which is at least 4 different inhibitor concentrations at 4 different substrate concentrations, this would mean running 16 different UV-visible assays.[166] Much less enzyme is required for electrochemical K_i determinations. Furthermore, as this project uses enzymes immobilised on carbon, the conditions which the enzyme experiences on an electrode are much closer to the conditions they will be subjected to when they are immobilised on carbon particles.

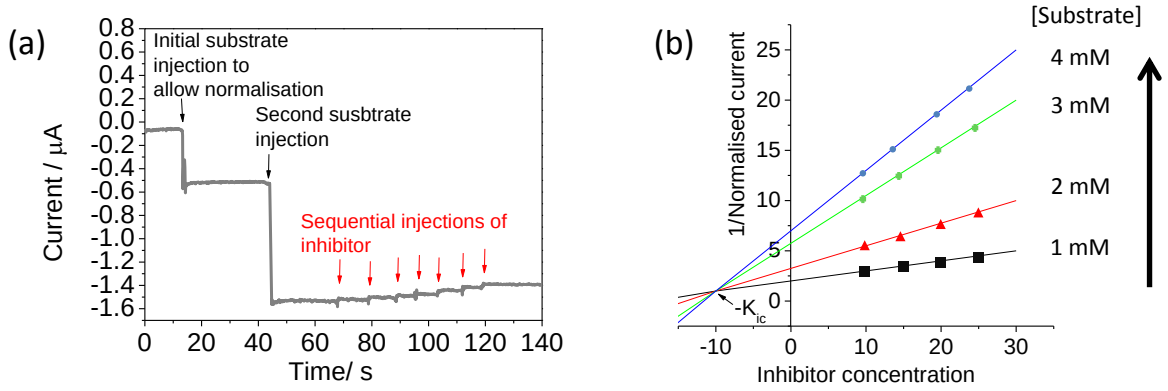

Figure 2-15: An example of a chronoamperogram used to determine the K_i product inhibition of NAD^+ reduction by NADH. (b) An example of a model Dixon plot used to determine the competitive inhibition constant (K_{ic}).

In this thesis the value of K_i was determined electrochemically using chronoamperometry. In order to determine the K_i for product inhibition of NAD^+ reduction by NADH, an enzyme film was prepared on the surface of a PGE RDE. The electrode was then immersed into buffer in the electrochemical cell. The electrode was held at an NAD^+ reducing potential (around −412 mV *vs* SHE). The current was allowed to stabilise for approximately 10 seconds, before an aliquot of NAD^+ (substrate) was injected into the cell through the injection port with a syringe. By injecting in the same concentration of NAD^+ (substrate) at the start of each experiment, it is possible to normalise for the different activities of different enzyme films. A further aliquot of NAD^+ or buffer was then injected to obtain the desired starting concentration of substrate.

Sequential aliquots of NADH (inhibitor) were subsequently injected into the solution and the current drop as a response of this was measured. The NADH solution injected into the cell contained the same amount of NAD^+ as that present in the cell solution to prevent drops in current being observed simply due to dilution effects. An example chronoamperogram used to determine the value of K_i is shown in Figure 2-15 (a).

By making >4 different measurements at different starting concentrations of NAD^+ there is enough data to determine the value of the K_i.

When the inhibition is competitive a Dixon plot can be used to obtain the value of K_{ic} (the competitive inhibition constant).[102] The value of K_{ic} can be determined by taking the negative of the point where all of the lines cross. Similarly a Cornish-Bowden plot can be used to determine the value of K_{iu} which can be determined from the point in the Cornish-Bowden plot where all the lines intersect.

Similar measurements can be carried out to determine the K_i for product inhibition of NADH reduction by NAD^+. These involve holding the electrode at an NADH oxidising potential (around −62 mV *vs* SHE) and injecting in a control step of NADH followed by sequential aliquots of NAD^+ as an inhibitor.

2.4 Enzyme-modified particles

Work in this thesis makes use of enzyme-modified particles for H_2-driven NADH recycling, see Figure 2-1 (d). The enzyme-modified particles were principally used in chapters 3, 5, 6 and 7. These particles have a hydrogenase and NAD^+-reductase co-immobilised on them. The carbon material they are made from is conductive, this means that electrons from H_2 oxidation at the hydrogenase can be channelled through the particles to the NAD^+-reductase where NAD^+ reduction occurs. In this thesis two different types of particles were used: Black Pearls 2000 (BP 2000) particles and Pyrolytic Graphite (PG particles).

2.4.1 Literature review of carbon materials used in particle construction

A range of carbon materials have been reviewed by Quinson *et al*.[156] In this project absorption is used to immobilise enzymes onto carbon particles, this means that the enzymes are directly in contact with the carbon particle surface and that there is no

covalent linker separating the enzymes from the particle, which might lead to less good conductivity.[151] The mesopores of both BP 2000 particles and abraded PG particles have average diameters between 3.5 − 9 nm. Hydrogenases are known to be *ca.* 5 nm in diameter and therefore on the same scale as the pores, which means that the mesoporous network of these particles is accessible to them.[156] Furthermore, as the hydrogenases are of similar size to the pores they are likely to be almost completely surrounded by carbon meaning that their electron relay centres (FeS clusters) are in close contact with the carbon particle and hence that the majority of the enzymes immobilised on the electrode surface is expected to be electroactive.

Electrochemical measurements carried out by Quinson *et al*. show that hydrogenases exchange electrons well with the carbon network of BP 2000 particles when the particles were deposited onto a PGE RDE.[156] In fact, BP 2000 particles showed the highest electrochemical activity per gram of carbon, when a range of different carbon materials were functionalised with *E. coli* Hydrogenase 1 and deposited onto the surface of a PGE RDE by Quinson *et al*.[156]

In addition, BP 2000 particles are a good choice for use in the production of enzyme-modified particles as they have a large surface area to mass ratio (>1000 m^2 g^{-1}) in comparison to other carbon materials.[156] This means that in comparison to other carbon particles, a low mass of carbon is required for a relatively large volume of active enzyme, meaning less energy is required to stir inactive carbon. This large surface area to mass ratio is due to the small diameters of BP 2000 particles (17 – 31 nm, which is smaller than a number of other carbon materials tested by Quinson *et al*.) [156] and the large number of pores present on the particle surface.

2.4.2 Enzyme-modified carbon particles

BP 2000 particles (Black Pearls 2000, Cabot Corporation) were used, in chapters 4, 5 and 7 of this thesis. These particles are a commercially available amorphous carbon black material.[156] They have the advantage that they are an extremely cheap support material, which can be used as obtained from the manufacturer.[119,167]

Pyrolytic graphite (PG) particles were used in experiments with the synthetic cofactor analogues in chapter 6. These particles were produced by sanding a piece of pyrolytic graphite using P400 sand paper (Kemet) inside an anaerobic glovebox.[168] These were then added to a pre-weighed micro-centrifuge tube, which was then re-weighed outside of the glovebox.

Particle preparation was carried out inside an anaerobic glove box; to prevent O_2 from inactivating the enzymes used on the particles (particularly *E. coli* Hyd 2).[122] This also helps to prevent O_2 from becoming absorbed in the particle solution which could lead to direct reduction of O_2 at the carbon particle surface.[155]

A typical procedure for the preparation of enzyme-modified particles is given below, following the procedure of Reeve *et al*.[119].

Buffer was added to carbon particles to obtain a suspension with a concentration of 20 mg mL^{-1}. The particles were then dispersed by sonicating for > 30 minute and then vigorously pipetted to ensure a homogenous suspension.[103] An aliquot of this particle mixture was added to a solution of the required enzymes, usually Hyd 2, an NAD^+-reductase and a NADH dependent enzyme (pre-mixed) and left at 4 ^oC for at least 1 hour allowing the enzymes to adsorb.[103]

After the adsorption step, the particles were washed by centrifuging at 8,000 × g in an Eppendorf MiniSpin® centrifuge. The supernatant was then removed and replaced by a fresh aliquot of buffer. This process was normally repeated several times to ensure that

all unabsorbed enzyme was removed from the solution.[103] An aliquot of particles was then added to the reaction of interest.

2.4.3 Thermodynamic and solubility considerations for H_2-driven NAD^+ reduction[139]

This section summarises the thermodynamic considerations important for operation of the enzyme-modified particles. The enzyme-modified particles used in this thesis couple the oxidation of $H_{2(g)}$ to the reduction of NAD^+. The enzymes used as part of the enzyme-modified particles in this thesis work very close to the thermodynamic potential. This has been shown by Idris *et al*. for the *R. eutropha* HoxFU who recorded CVs which cross the blank scan cleanly at the thermodynamic potential for the NAD^+/NADH couple.[102] Similarly, Lukey *et al*. have shown efficient H_2 oxidation at the thermodynamic potential for Hyd 2.[122]

The Gibbs free energy (ΔG) for an electrochemical reaction can be given by equation 2-17:

$$\Delta G = -nFE_{cell} \qquad \textbf{2-16}$$

where F is the faraday constant, E_{cell} is the thermodynamic potential difference of the couple and n is the number of moles of electrons transferred in the process. For a process to take place spontaneously a favourable (negative) value of ΔG is required.

The value of E_{cell} for H_2-driven NAD^+ reduction can be obtained from equation 2-18:

$$E_{cell} = E\left(\frac{NAD^+}{NADH}\right) - E\left(\frac{H_2}{2H^+}\right) \qquad \textbf{2-18}$$

this can be calculated using the Nernst equation given in equation 2-19:

$$E = E^o - 2.3 \times \frac{RT}{nF} log \frac{[Red]eq}{[Ox]eq} \qquad \textbf{2-19}$$

where E^o is the standard potential, and n is the number of moles. The reduction potential of the NAD^+/NADH couple can therefore be calculated using equation 2-20:

$$E\left(\frac{NAD^+}{NADH}\right) = -0.113 - 2.3 \times \frac{RT}{2F}(pH - log\frac{[NAD^+]}{[NADH]}) \quad \textbf{2-20}$$

Similarly, the reduction potential of the $2H^+/H_2$ couple can be calculated using equation **2-21**:

$$E\left(\frac{H_2}{2H^+}\right) = -2.3 \times \frac{RT}{2F}\log(\frac{P(H_2)_{bar}}{(10^{-pH})^2}) \quad \textbf{2-21}$$

The thermodynamics of H_2 oxidation vary with temperature and pressure. The solubility of H_2 also varies with temperature and pressure. Having less dissolved H_2 in solution and available for the hydrogenase may lead to a decrease in rate. These issues will be considered below.

Using the Nernst equation (equation 2-19) and equation 2-17, it is possible to calculate the ΔG values for the H_2-driven reduction of NAD^+ to NADH under 1 bar H_2 pressure at a number of temperatures. This is shown in Figure 2-17 (a), from which it is clear to see that as the temperature of the reaction is increased, the driving force for reduction of NAD^+ (ΔG) becomes more negative, such that thermodynamically the reaction is more favourable.

Figure 2-17 (a) demonstrates that it is theoretically possible to get increased conversion at higher temperatures. However, even at 40 ^oC, under 1 bar H_2, it is theoretically possible to obtain a ratio of $[NAD^+]/[NADH]$ of $<10^{-4}$ which equates to 99.99 % conversion of NAD^+ to NADH.

Figure 2-17 (b) shows the logarithmic dependence of ΔG on H_2 pressure for H_2-driven reduction of NAD^+ to NADH. Increasing the pressure of H_2 under which the reaction is carried out should mean that the H_2-driven reduction of NAD^+ to NADH becomes more favourable.

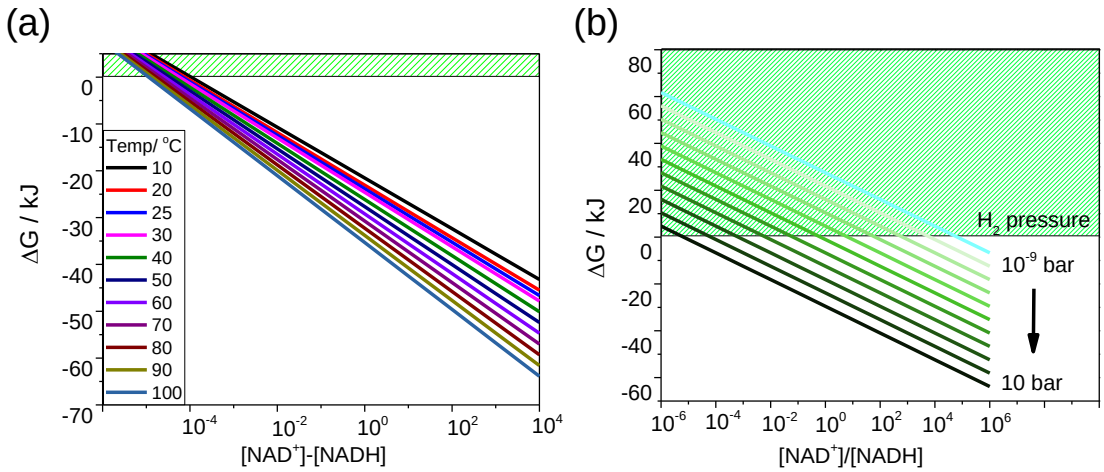

Figure 2-17: Variation in ΔG for the reaction H_2+NAD^+→NADH + H^+. (a) The variation in ΔG as a function of temperature at pH 8 under 1 bar H_2 pressure at temperatures between 10 °C and 100 °C. (b) The variation in ΔG as a function of pressure at pH 8 and 25 °C, pressures shown between 10 bar and 10^{-9} bar. The green sections of each graph shows the region in which ΔG is positive and so the reaction is not thermodynamically favourable.

H_2 solubility considerations

For dilute solutions Henry's law can be used as an approximation for the variation of the solubility of gases with pressure, see equation 2-22.

$$K_{H2} = \frac{C_{H2}}{p_{H2}} \qquad \textbf{2-22}$$

Where K_{H2} is the Henry's law constant for dihydrogen gas, C_{H2} is the concentration of hydrogen gas dissolved in solution and p_{H2} is the partial pressure of H_2 in the vessel. This equation can be rearranged to give equation 2-23:

$$C_{H2} = p_{H2} \times K_{H2} \qquad \textbf{2-23}$$

this indicates that as the partial pressure of H_2 is increased, so too does the solubility of the gas in solution. Meaning that under increased H_2 pressures, more H_2 should be dissolved in the solution.

The Henry's law constant (K_{H2}) is however temperature dependent. The Van't Hoff law given in equation 2-24 can be applied to the Henry's law constant:

$$\frac{d \ln K_{H2}}{d\,(1/T)} = \frac{-\Delta_{sol}H}{R} \qquad \textbf{2-24}$$

where, R is the gas constant, T is the temperature and $\Delta_{sol}H$ is the enthalpy of solvation. This can be integrated to give equation 2-25:

$$K_{H2}(T) = K_{H2}{}^{o} \exp\left[\frac{-\Delta_{sol}H}{R}\left(\frac{1}{T} - \frac{1}{T_o}\right)\right] \qquad \textbf{2-25}$$

Where, T_o is the temperature at which $K_{H2}{}^{o}$ is determined. This indicates that as the temperature goes up solubility of hydrogen will go down. This means that in reactions performed at elevated temperatures less H_2 will be available in solution, which may mean that it is more difficult to obtain full conversion of NAD^+ to NADH.

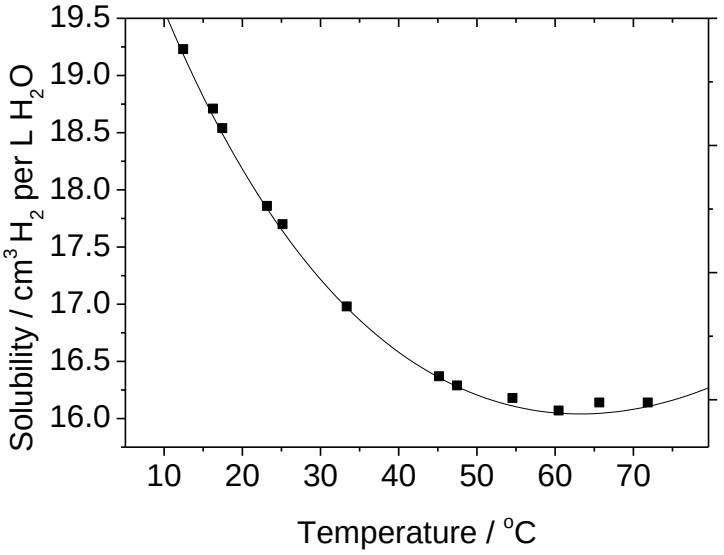

Figure 2-18: Change in the solubility of H_2 as a function of temperature based on experimental data from the IUPAC solubility data series.[169][170] Data recorded under 1 atmosphere H_2 in pure water. Line fitted with the equation Solubility = 10^(-36.25+(1847/T)+12.65×log(T)).

The graph in Figure 2-18, shows the experimentally determined relationship between solubility of H_2 gas and the temperature. This demonstrates that the solubility of H_2 in water decreases from 17 cm^3 per litre at 30 °C (*ca.* 0.7 mM) to approximately 16 m^3 per litre at 60 °C (*ca.* 0.6 mM). This change in solubility is therefore relatively small.

Furthermore, the value of ΔG becomes more negative at elevated temperatures making H_2-driven NAD^+ reduction more favourable. Consequently, it is not expected that operating at temperatures up to 60 ^oC reactions would be limited by supply of $H_{2(g)}$ in solution.

2.5 Analytical methods

2.5.1 NMR spectroscopy

Proton (^1H) NMR spectroscopy was carried out on a 400 MHz Bruker AVIIIHD 400 nanobay instrument. Spectra were acquired in either ^2H_2O or C^2HCl_3 and the signal was referenced internally to the residual protic solvent (^1H). Trace amounts of acetone or tetramethylsilane were added to provide further reference signals. Analysis was carried out at room temperature. Spectra were processed using the MestraNova® 10.0.2 – 15465 software package. Specific details of NMR spectroscopic methods will be given in the relevant chapters (3 and 7). Generally, 64 scans were acquired for proton (^1H) NMR spectra.

2.5.2 HPLC and GC analysis methods

GC analytics

Gas chromatography was performed on a ThermoScientific Trace 1300. The GC was equipped with a flame ionisation detector (FID), suitable for the detection of molecules with low UV-absorbance which could be extracted into organic solvent (ethyl acetate).

Before injection onto the GC, an aliquot of ethyl acetate containing an internal standard was added to the reaction mixture, which was vortexed and then centrifuged. The ethyl acetate layer was subsequently removed and this step was repeated once more. The ethyl acetate fractions were then dried over $MgSO_4$ and filtered through a cotton wool

filter. An aliquot (0.3 – 5 µL) of this ethyl acetate fraction was then injected into the GC for analysis.

To extract the 4-phenylbutan-2-amine from bio-transformations carried out with the *ω-transaminase* enzymes, the aqueous mixtures were basified before extracting into ethyl acetate by adding 70 µL of 10 N NaOH per 300 µL of reaction mixture. Exact procedures for preparing samples for GC analysis vary between experiments and so more details are given in the corresponding experimental chapter and in Appendix C.

In this thesis two different GC columns were used a DB 1701 column (50 m, 0.25 mm I.D., 0.33 µm film) for achiral separations and a CP-Chirasil Dex CB (25 m, 0.25 mm I.D., 0.25 µm film) for chiral separations both produced by Agilent. Details of the exact procedures used for each of the biotransformations are given in Appendix C.

HPLC analysis

HPLC analysis was carried out on a Shimadzu Prominence HPLC, equipped with a dual beam UV detector which recorded 2 pre-defined wavelengths. Molecules with chromophores which absorb in the UV-visible region were analysed using HPLC. Additionally, L-alanine was analysed using HPLC as it cannot be easily extracted into organic solvent without derivatisation.

In this work three columns were used: a Zic-Hilic column (Merck), which contains a zwitterionic packing material for separation of polar molecules; a Chromolith® C18 column (Merck) for reverse phase separation of organic molecules and a Chiralpak IA column (hichrom) chiral C18 column for determination of enantiomeric excess (*ee*).

Samples were prepared prior to injecting into the HPLC column by adding 10% v/v acetonitrile, centrifuging to remove any precipitated protein and then filtering through a 2 µm PTFE filter vial (Thompson). For analysis of samples using the Chiralpak IA

column samples were extracted into hexane. Further details of sample preparations are given in specific results chapters and in Appendix C.

2.6 Gases and reagents

All gasses were obtained from BOC in the highest purity commercially available. Artificial cofactor mimics were provided by Frank Hollmann and Caroline Paul at the TU Delft, Netherlands. BP 2000 particles were kindly provided by Cabot Corporation.[167] Unless specified, other reagents were obtained from Sigma Aldrich or Alfa Aesar.

2.6.1 Gases and ensuring a constant supply of gas

In experiments where the enzyme-modified particles or the whole SH were used, the reaction mixture was normally saturated with H_2 before starting the reaction. This was achieved by bubbling H_2 gas through the buffer for at least one hour at a flow rate of approximately 5 mL min^{-1}. In order to ensure that the buffer remained saturated with H_2 gas, H_2 was either continuously flowed into the head space of the cuvette or the shaker being used for the reaction. Alternatively, a pressure system was used to ensure that the reaction remained sealed in a $H_{2(g)}$ atmosphere see, Figure 2-19 (b).

The shaker case (shown in Figure 2-19, a) used in this project, was specifically designed to accommodate 5 Eppendorf tubes in a compartment with a lid. The lid could be sealed with screws, ensuring that it was airtight. Flowing H_2 gas through the inlet and outlet holes in the lid of the shaker meant that reactions could be conducted under constant H_2 flow. The shaker case was designed to sit on top of and attach to a shaker (IKA) so that the tubes in the reaction could be shaken during the course of an experiment, ensuring that the particles did not sink to the bottom of the tubes during the course of the reaction. Shaking is also important as it ensures that the surface of the

solution is agitated meaning that fresh $H_{2(g)}$ can continue to dissolve in the solution. High sheer forces as a result of rapid stirring are thought to cause enzyme deactivation, Faber and co-workers recommend gentle shaking on a rotary shaker to maintain optimal enzyme stability.[11]

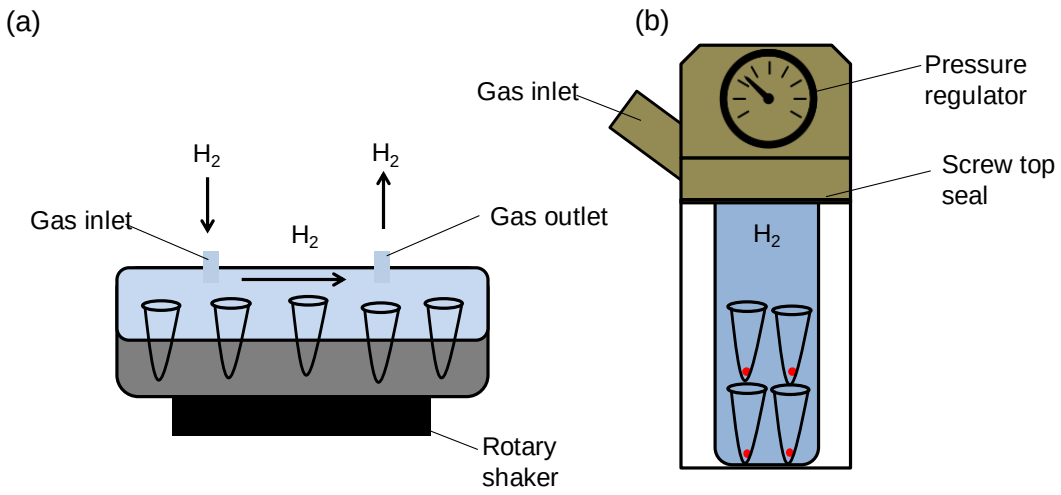

Figure 2-19 Diagrams showing the set-up of (a) a shaker which allows H_2 gas to be continually blown across the top of the reaction vessels and (b) a pressure system used to maintain the reaction vessel under slight H_2 overpressure. This was placed on a shaker to allow adequate stirring during the course of the reaction, to ensure adequate H_2 supply to the solution in the Eppendorf tubes.

The pressure system (tiny clave steel, Büchi, Switzerland) allowed experiments to be conducted under increased H_2 pressure, it is shown schematically in Figure 2-19, b.[171] In this work pressures of 2 bar were routinely used. Micro-stirrer bars were added to each of the tubes in the pressure system and the pressure system was placed on a magnetic stirrer (VWR) to ensure that the solutions in each vessel were agitated during the course of the reaction. This helps to improve mass transport during the course of the reaction and ensures that the particles remain dispersed. Alternatively, for some of this work the pressure system was placed inside an incubator shaker (Thermofisher) with shaking at 100 rpm.

2.6.2 Buffers

Standard electrochemical buffers

Most experiments in this thesis were carried out in buffered solution. This increases the conductivity of the solution meaning that it can be used for electrochemical experiments. Using buffers also ensures that the pH remains constant throughout the course of the reaction. This is important for NAD^+ to NADH conversion, as an H^+ ion is required to balance this reaction. All buffers were prepared with MilliQ® (resistivity 18.2 M Ω) water. Where possible K^+ salts were used in place of Na^+ salts as Schneider and Schlegel have shown that the *R. eutropha* SH is inhibited by Na^+ ions.[109]

Buffers were titrated to the correct pH at the temperature at which they were used, using KOH or HCl and a calomel pH electrode Phosphate buffer was prepared by titrating 50 mM K_2HPO_4 and 50 mM KH_2PO_4 to the required pH.

For pH optima studies, a buffer system that could be used over a wide pH range was required; in this case a mixed buffer system was used. This was prepared following the recipe given in Table 2-4.

Table 2-4: Recipe used to make 100 mL of mixed buffer

Chemical	Mr	Quantity required / g
CHES	207.29	0.31
TAPS	243.28	0.37
HEPES	238.31	0.36
MES	195.23	0.32
Sodium Acetate	82.04	0.12

N_2 gas was bubbled through buffers at approximately 100 mL min^{-1} for at least 2 hours before the buffers were put into the glovebox, in order to remove any dissolved O_2.

2.6.2.1 Deuterated buffers

Deuterated potassium phosphate buffer was made by making up a 50 mM K_2HPO_4 solution with ^2H_2O in the glovebox. DCl solution was then added until the required pH range was achieved, as identified by checking with pH paper. An aliquot of buffer was then removed from the glovebox and tested with a calomel pH electrode (Thermofisher). The pD value was obtained from the pH reading given by adding 0.4 pH units.[172]

2.6.3 Cofactors

NADH and NAD^+ (Prozomix) stocks were made up freshly prior to each experiment to a concentration of 100 mM in N_2-saturated buffer inside a glovebox.

The reduced cofactor NADH contains traces of the oxidised cofactor NAD^+ as an impurity. Although, this is not usually seen in UV-visible spectroscopy, because it absorbs at the same position as NADH and is consequently often ignored in biochemical assays, in electrochemical analysis it is possible to detect minute quantities of NAD^+. Hence, when using commercially obtained NADH it is possible to see NAD^+ reduction by the NAD^+-reductase in electrochemical experiments. Therefore, NADH was purified before use in experiments for determining affinity and inhibition constants using an anion exchange column. Idris *et al*. demonstrated that the HoxFU moiety from *R. eutropha* shows product inhibition by NAD^+ for the oxidation of NADH; hence if NADH which is contaminated with NAD^+ is used this will not give a true reflection of the affinity of the HoxFU for NADH.[102]

A 1 mL AcroSep™ Q Ceramic HyperD F anion exchange column (Pall) was used to purify NADH. The column was first cleaned with 10 mL Tris-HCl pH 8 and then a 1 mL aliquot of 100 mM NADH was applied to the column. This was then washed with a further 5 mL of buffer to remove any unbound impurities and analysed using a

SpectroStar Nano UV-vis (GE Healthcare) spectrometer to determine whether any cofactor had been eluted.

Approximately 5 mL of 0.1 M KCl solution was then added to remove the NAD^+ impurity, again with the eluted sample being collected in 1 mL aliquots and analysed by UV-visible spectroscopy to ensure that no reduced cofactor was also eluted. A 0.5 M solution of KCl was subsequently added to the column to elute the NADH and the solution was collected in 100 µL aliquots and analysed using UV-vis spectroscopy.

A calibration curve was made using un-purified NADH was used to determine the concentration of the purified NADH. Based on the work of Idris *et al*. it was assumed that small aliquots of high concentration KCl do not have any effect on the NAD^+ reductase being tested and so the NADH aliquots were not desalted prior to their use.[102,164]

2.6.4 Glovebox

Unless otherwise stated, experiments in this thesis were carried out in an anaerobic, N_2 filled glovebox (MBraun). For electrochemistry it is essential to carry out experiments at <0.1 ppm O_2, as O_2 reduction at a carbon electrode can be observed at an onset potential of approximately −200 mV *vs* SHE. This is the potential region that we are particularly interested in for studies of enzymatic $2H^+$/ H_2 and NAD^+/NADH cycling, which have thermodynamic potentials of −472 mV and −350 mV *vs* SHE at pH 8. In addition, many hydrogenases, for example *E. coli* Hyd 2, are inactivated by O_2,[122] Therefore, all work carried out using this protein was carried out in an anaerobic glovebox.

2.7 Relation of this chapter to other chapters

In the following chapters techniques introduced in this chapter will be used in a range of projects. The exact experimental details of much of this work will be presented at appropriate points in the course of chapters 3-7.

3 H_2-driven systems for producing chiral amines

3.1 Introduction

Amine functionalities are important components of a wide range of industrially relevant chemicals ranging from pharmaceuticals to fine chemicals and fertilisers.[173] Currently, both industrial and laboratory preparation of amines rely on the reductive amination of pro-chiral ketone functionalities. Often it is difficult to obtain a single enantiomer of a desired chiral amine molecule using conventional synthetic methods. Industry frequently makes use of precious metal catalysts with chiral ligands (see section 1.2.1). However, there remains a large degree of scope for bio-catalytic methods for producing chiral amine targets.[174]

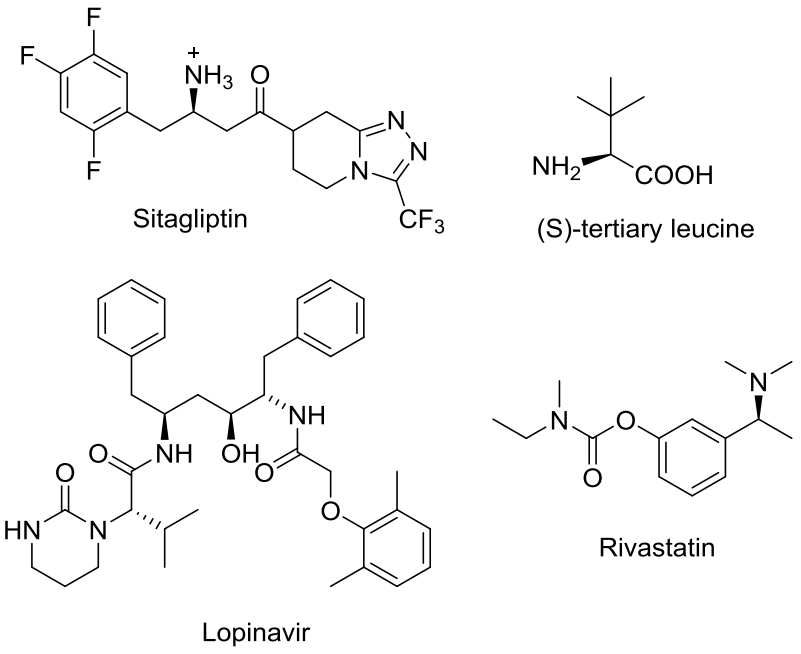

Figure 3-1: Examples of important pharmaceutical molecules, containing chiral amine functionalities.

Figure 3-1, gives some examples of active pharmaceutical reagents or precursors which contain chiral amine functionalities. These include Sitagliptin used in the treatment of type 2 diabetes,[52] (S)-tertiary leucine (used in the production of sterols and a precursor for anti-viral and anti-tumour medication),[175] Rivastatin (used to treat high cholesterol), and Lopinavir (used in the management of HIV).[32] A cleaner synthetic

route to obtain Sitagliptin using biocatalysis is currently being tested at pilot plant scale, see Chapter 1.[52]

Some enzymes exist which are able to catalyse the amination of a ketone moiety just using NH_4^+ and a reducing equivalent. So far amino acid dehydrogenase enzymes are a well-developed and well-studied class of enzymes which carry out these kinds of transformations on a limited set of α-keto acids. Recently, rational mutagenesis on a range of amino acid dehydrogenase enzymes has led to the creation of amine dehydrogenase enzymes which are able to accept a wider range of substrates.[173,176]

3.1.1 Chapter summary

The aim of this chapter is to develop a clean H_2-driven method for the production of a range of chiral amines using the enzyme-modified particles introduced in Chapter 1. Initially, the particles will be used in combination with an L-alanine dehydrogenase for the reductive amination of pyruvate to give L-alanine (section 3.2). In later sections of this chapter the enzyme-modified particles will be used as part of a pyruvate removal system to shift the reaction equilibrium in combination with an (S)- and an (R)-selective *ω-transaminase* enzyme.

The first section of this chapter builds on the work of Reeve *et al.* who have developed the enzyme-modified particles for H_2-driven cofactor recycling and used them in combination with an alcohol dehydrogenase (ADH) to demonstrate the conversion of acetophenone to phenol ethanol.[119] For work focusing on immobilising *ω-transaminase* enzymes comparison is made with the work of Yi *et al*. who have demonstrated the immobilisation of the (S)-selective *ω-transaminase* from *Vibrio fluvialis (Vf)* on chitosan, the *Vf ω-transaminase* enzyme is also used in this chapter.[148] Finally, Holzer *et al.* have demonstrated that the whole *R. eutropha* SH can be used as a cofactor recycling system in combination with an L-alanine dehydrogenase. This

system was demonstrated as a H_2-driven pyruvate removal system for shifting the reaction equilibrium, for use in combination with a number of *ω-transaminase* enzymes.[115] Comparison with this work will be made throughout the sections of this chapter which investigate coupling the *ω-transaminases* to the enzyme-modified particles as a pyruvate removal/alanine recycling system.

3.2 Amino acid dehydrogenases

Over 3 million tons of amino acids are produced worldwide per year.[15] Monosodium glutamate is produced in the largest quantity; however, even L-alanine, the simplest amino acid, is produced on a scale of 500 tons per year.[15]

The most commonly used biocatalytic methods for synthesis of amino acids is the dynamic resolution of a racemic mixture of chemically derived starting material by employing hydrolytic enzymes.[11] However, some amino acid dehydrogenases are already being used to perform reductive aminations on an industrial scale. For example leucine dehydrogenase, which has a broad substrate specificity meaning it can be used in the production of a range of valuable non-proteogenic amino acids, is used on an industrial scale to produce L-tertiary-leucine.[11,175]

This work initially focuses on the simplest amino acid dehydrogenase, L-alanine dehydrogenase, which catalyses the conversion of pyruvate to L-alanine at the expense of NADH and NH_3. L-alanine dehydrogenase enzymes are found in many bacterial species; with high sequence homology being found between enzymes from different bacteria.[177]

The active site of the L-alanine dehydrogenase enzyme contains two distinct domains: the substrate binding and the NAD^+-binding domain.[177] The proposed catalytic mechanism for the L-alanine dehydrogenase from *Bacillus subtilis*, which is based on kinetic data obtained using L-alanine labelled with deuterium at different positions is

shown in Figure 3-2.[178] Initially, the carbonyl group is activated by an acidic amino acid at the active site (XH^+). The ammonia lone pair then attacks into the π* orbital of the C=O group. The OH group is protonated forming a hemiaminal intermediate and H_2O is subsequently eliminated to yield an iminium ion. Direct hydride transfer occurs from NADH, with the nicotinamide ring positioned below the substrate, which results in the formation of L-alanine.[178]

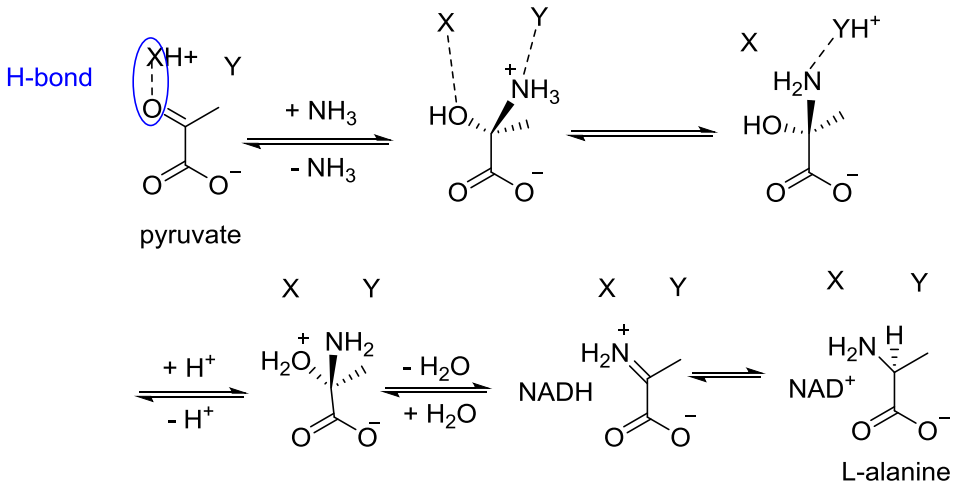

Figure 3-2: The catalytic cycle of the L-alanine dehydrogenase from *Bacillus subtilis*. Based on references [177][178]. X and Y are residues in the active site of the enzyme which are able to act as acid and base catalysts; these are believed to be a histidine and an asparagine residue.

3.2.1 Development of a system for H_2-driven Pyruvate to L-alanine conversion

It was investigated whether it is possible to combine an L-alanine dehydrogenase with the H_2-driven enzyme-modified particles for H_2 driven cofactor recycling, see Figure 3-3. In this system *E. coli* Hyd 2 and *R. eutropha* Hox~~HY~~FU are co-immobilised on carbon particles; where they are able to recycle NADH at the expense of H_2. The NADH produced is then taken up by the L-alanine dehydrogenase (in this case a commercially available L-alanine dehydrogenase from *Bacillus cereus)*, which catalyses the conversion of pyruvate to L-alanine at the expense of NH_3.[11]

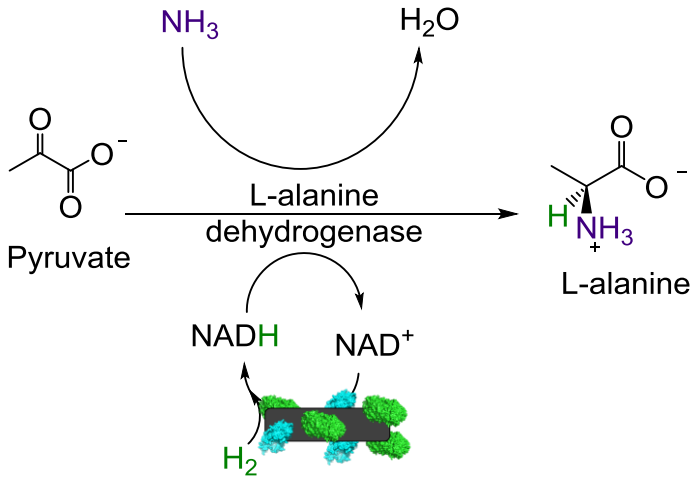

Figure 3-3: Reaction scheme for the reductive amination of pyruvate to L-alanine, when L-alanine dehydrogenase is coupled with the enzyme-modified particle system for H_2-driven cofactor recycling.

Initially, the activity of the L-alanine dehydrogenase was determined in the 50 mM Tris-HCl buffer system (pH 8) by following the consumption of NADH by the L-alanine dehydrogenase using UV-Visible spectroscopy, see Figure 3-4 (a).

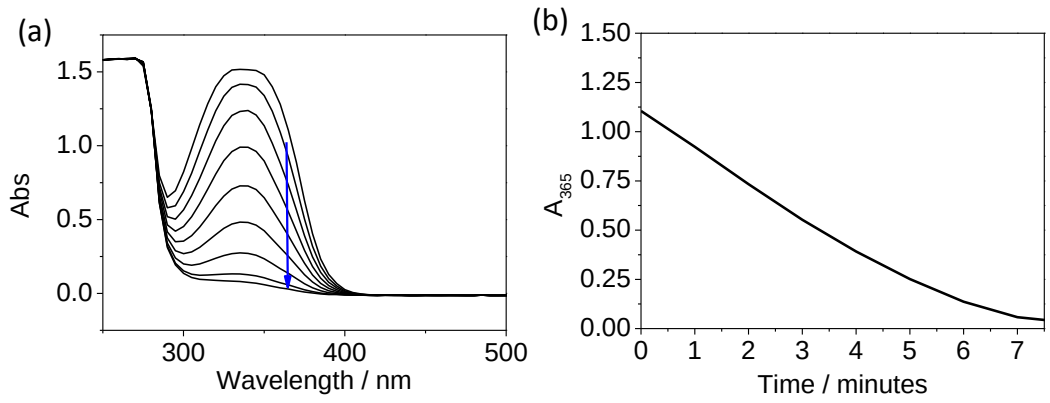

Figure 3-4: (a) A UV-visible absorbance spectrum showing sequential scans taken every minute. The decreased absorbance at 365 nm indicates a decreasing concentration of NADH. The reaction was carried out on a 1 mL scale in 50 mM Tris-HCl buffer pH 8 at 30 °C with a 1 mM concentration of NH_4Cl, 1 mM Pyruvate, 0.6 mM NADH. The reaction was started with a 0.5 µL aliquot of L-alanine dehydrogenase. (b) Kinetics data used to determine specific activity of L-alanine dehydrogenase, scan taken with 1 mM pyruvate, 1 mM NH_4Cl, 0.6 mM NADH and started with a 0.5 µL aliquot of L-alanine dehydrogenase.

From the gradient of the trace in Figure 3-4 (b) the specific activity of the L-alanine dehydrogenase can be calculated as 111 U mL^{-1} (much lower than the figure of > 350 U mL^{-1} given by the manufacturer when the L-alanine dehydrogenase was tested at pH 10

and 30 ^{o}C).[65] The protein concentration of the L-alanine dehydrogenase suspension is not provided by the manufacturers and hence activities are reported as U mL^{-1}. The reported maximum activity of the enzyme-modified-particles for H_2-driven cofactor recycling is 7.8 U mg^{-1} *R. eutropha* Hox~~HY~~FU,[119] meaning that at least 1 µL of L-alanine dehydrogenase is required per 14 µg of immobilised *R. eutropha* Hox~~HY~~FU to ensure that the L-alanine dehydrogenase is not limiting the rate of reaction.

Electrochemistry was used to determine whether L-alanine or NH_4Cl have any inhibitory effects on the NAD^+-reductase, *R. eutropha* Hox~~HY~~FU (see Appendix E). It was found that no inhibitory effect on the NAD^+-reductase was observed for either L-alanine up to a concentration of 17 mM or NH_4Cl up to a concentration of 17 mM.

An experiment was then conducted in which enzyme-modified particles (with Hyd 2 and Hox~~HY~~FU co-immobilised on them) were combined with an L-alanine dehydrogenase. This should allow the conversion of pyruvate to L-alanine just using H_2 and NH_4Cl.

The HPLC traces in Figure 3-5 demonstrate that almost complete conversion of pyruvate to L-alanine is obtained after 18 hours, with the L-alanine peak at 11.7 minutes equating to a > 9.8 mM concentration of L-alanine (determined by comparison of the peak to a set of concentration standards) for samples where the L-alanine dehydrogenase was both immobilised and in solution.

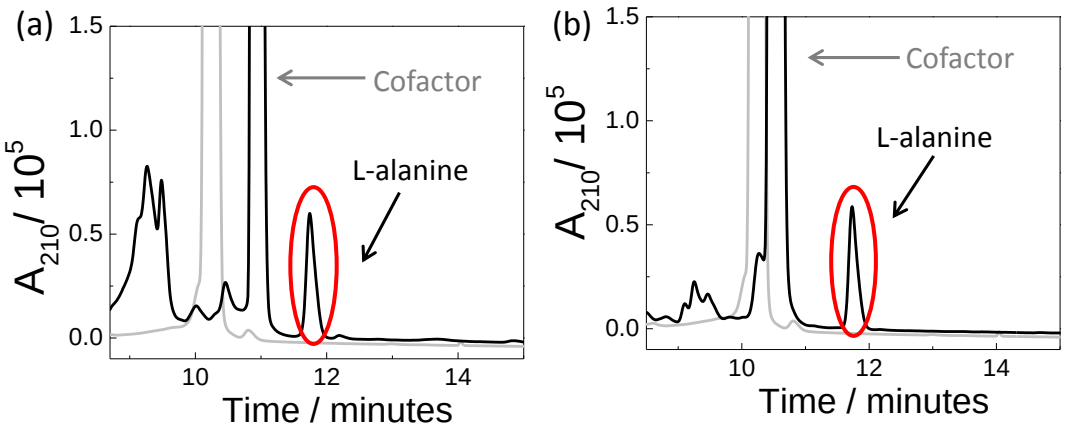

Figure 3-5: HPLC traces demonstrating conversion of pyruvate to L-alanine by L-alanine dehydrogenase; start scans shown in grey, finish scans shown in black. For both experiments particles were made with 0.4 mg BP 2000, 54 µg Hyd 2, 25 µg Hox~~HY~~FU, and left to absorb for one hour at 4 °C. Particles were washed, by centrifuging and replacing the supernatant with buffer twice, before use to remove non-immobilised enzyme. A reaction mixture containing 1 mM NAD^+, 10 mM pyruvate, 15 mM NH_4Cl in 50 mM H_2-saturated Tris-HCl pH 8.0 was then added. (a) A 10 µL aliquot of L-alanine dehydrogenase (*ca.*1.1 U) was added to the reaction mixture. (b) A 10 µL aliquot of L-alanine dehydrogenase was co-immobilised on the particles. Reactions were carried out on a 500 µL scale, with shaking at 500 rpm, under continuous H_2-gas flow for 18 hours. The peaks between 8 – 10 minutes are due to the elution of the cofactors and impurities in the cofactor suspensions used in these reactions.

To further confirm the successful conversion of pyruvate to L-alanine, ^{1}H NMR spectroscopic experiments were also carried out. Figure 3-6 (a) shows the NMR spectrum for an L-alanine standard, which shows a doublet at 1.48 ppm. A doublet is observed due to vicinal coupling of the protons on the methyl group of L-alanine with the single proton on the adjacent carbon (alpha to the NH_2) with a value of approximately ^{2}J = 7.2 Hz. Figure 3-6 (b) shows the NMR spectrum for a pyruvate standard which shows as singlet at 2.38 ppm arising from pyruvate, and a further singlet at 1.48 ppm due to the gem-diol 2,2-dihydroxypropanoic acid (formed when pyruvate is left in aqueous buffer). The signals due to the methyl groups on pyruvate and 2,2-dihydroxypropanoic acid are observed as singlets, as there are no adjacent protons with which to couple to.

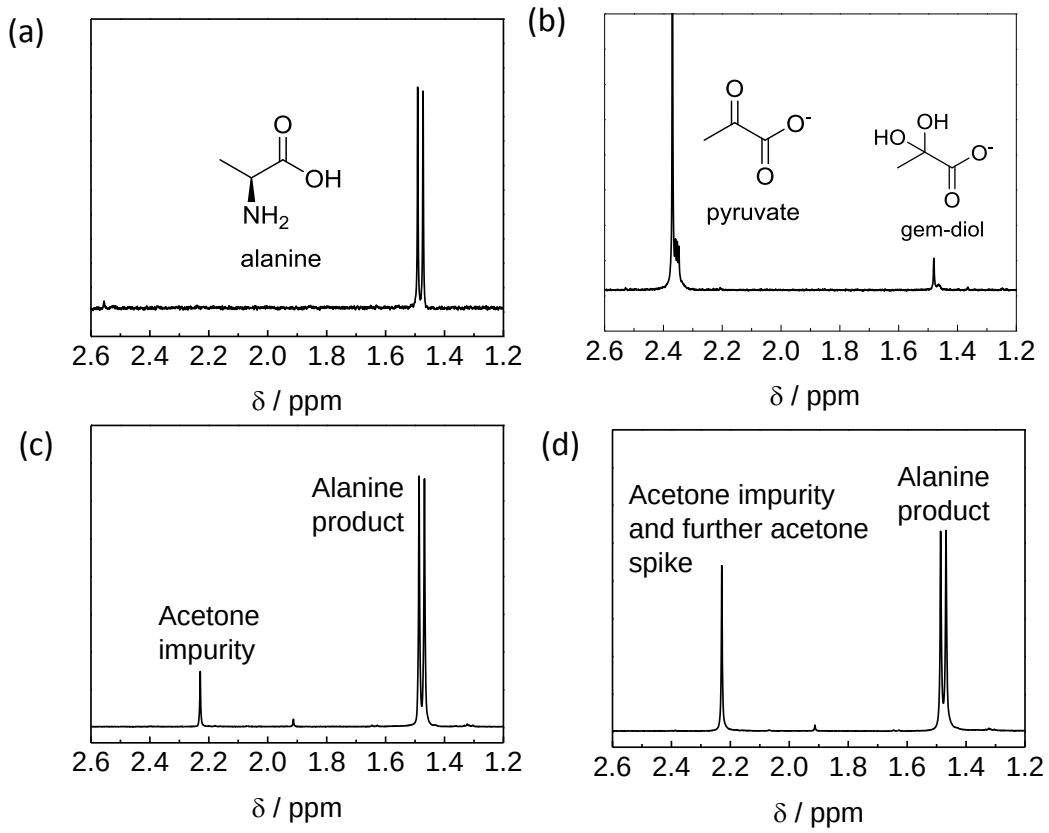

Figure 3-6: ^{1}H NMR experiments to confirm conversion of pyruvate to L-alanine by the L-alanine dehydrogenase. (a) A spectrum of L-alanine in deuteriated phosphate buffer pH 8.0. (b) A spectrum of pyruvate in deuteriated phosphate buffer pH 8.0. (c) A spectrum of the L-alanine sample produced using the enzyme-modified particles with 108 µg Hyd 2, 50 µg Hox~~HY~~FU and 10 µL L-alanine dehydrogenase immobilised on 1.8 mg BP 2000 particles. The reaction was conducted on a 1 mL scale in H_2-Saturated 50 mM phosphate buffer pH 8.0 under a 2 bar H_2 atmosphere. In the reaction mixture was a 1 mM concentration of NAD^+, 10 mM pyruvate and 15 mM NH_4Cl. Particles were washed once before use. After 18 hours, the particles were then removed from the reaction by centrifugation. The residual H_2O was then removed 3 times *via* vacuum distillation on a rotary evaporator and replaced with ^2H_2O. The alanine product peak is clearly visible at 1.48 ppm and a small peak at 2.23 ppm can be seen due to an acetone impurity. (d) The spectrum of the same sample as in (c) spiked with a further aliquot of acetone (to increase the concentration of acetone in the sample to 2mM). The whole spectra are given in Appendix I.

Enzyme-modified particles were prepared by mixing Hox~~HY~~FU, Hyd 2, L-alanine dehydrogenase and BP 2000 particles. The particles were then left at 4 ^oC for 1 hour, prior to centrifuging, removing the supernatant, and re-suspending in fresh buffer. The particles were added to a reaction mixture containing NAD^+, pyruvate and NH_4Cl in H_2-saturated potassium phosphate buffer pH 8.0. The reaction was then left for 18 hours under a pressure H_2 (2 bar), with gentle stirring.

After 18 hours the particles were removed from the reaction mixture. An aliquot of reaction mixture was taken for HPLC analysis, which confirmed conversion of pyruvate to L-alanine of >98 %.

The remainder of the sample was then used for ^{1}H NMR analysis. The buffer was removed *via* reduced pressure evaporation on a rotary evaporator and replaced with $^{2}H_2O$ several times in order to facilitate analysis by ^{1}H NMR spectroscopy.

Figure 3-6 (c) which corresponds to the spectrum of the reaction product in $^{2}H_2O$ shows a doublet at 1.48 ppm (J = 7.2 Hz). From comparison to the spectra of the L-alanine standard in Figure 3-6 (a), this demonstrates that L-alanine has been produced. Moreover, the doublet is symmetrical suggesting that there is no residual signal due to the gem-diol (2,2-dihydroxypropanoic acid) overlapping with this doublet. Furthermore, there is no peak visible at 2.38 ppm, which would be expected if pyruvate was present in significant amounts. All of these findings in combination are indicative of high conversions of the pyruvate starting material to L-alanine, a result confirmed by HPLC (see above).

In Figure 3-6 (c) there is a small impurity peak at 2.23 ppm, due to acetone (used to clean NMR tubes), the chemical shift of which is described in the literature.[179] Figure 3-6 (d) demonstrates that when a further acetone spike is added the intensity of this peak increases confirming that the peak at 2.23 ppm results from an acetone impurity.

According to the manufacturer (Sigma Aldrich) the L-Alanine dehydrogenase used in this work only produces L-alanine.[65] To confirm that this stereochemical preference is maintained, when the enzyme is immobilised on carbon particles, an NMR spectroscopic method was developed to determine the chirality of the alanine product. Here, a chiral shift reagent ((S)-(+)-O-acetylmandelic acid) was employed to break the degeneracy of the two alanine enantiomers in the NMR environment, according to the

methods described by Parker *et al.*[180] However, in the case of D- and L-alanine, the chosen shift reagent did not yield large enough differences in the spectra of the two compounds to allow for their unambiguous assignment in the reaction mixture.

Based on the HPLC traces shown in Figure 3-5 the TTN over an 18 hour period per NAD^+-reductase (*R. eutropha* Hox~~HY~~FU) is 34,000 ± 1000, this figure is, somewhat, lower than that obtained by Reeve *et al*. using the enzyme-modified particles in combination with an alcohol dehydrogenase enzyme for ketone to alcohol conversion, where > 100,000 turnovers were obtained;[119] however, this figure compares favourably with the TTN values obtained for organometallic asymmetric reductive amination catalysts discussed in section 1.2.1.

3.3 Investigating whether immobilisation of the L-alanine dehydrogenase leads to an increase in rate of reaction

Reeve *et al*. have demonstrated already, when investigating the conversion of acetophenone to phenylethanol, that having all enzymes which are part of an enzymatic cascade immobilised in close proximity can lead to increased reaction rates.[119] It is thought that this is a result of substrate channelling,[181] the concept that the substrate (in this case the reduced cofactor) passes quickly between the active sites of the 2 enzymes that catalyse sequential steps in a biosynthetic pathway, here the NAD^+-reductase enzyme (Hox~~HY~~FU) and the NADH dependant enzyme (L-alanine dehydrogenase), without re-entering the bulk solution.[119] This was investigated for H_2-driven L-alanine generation, see Figure 3-7 for a schematic diagram of the two scenarios tested.

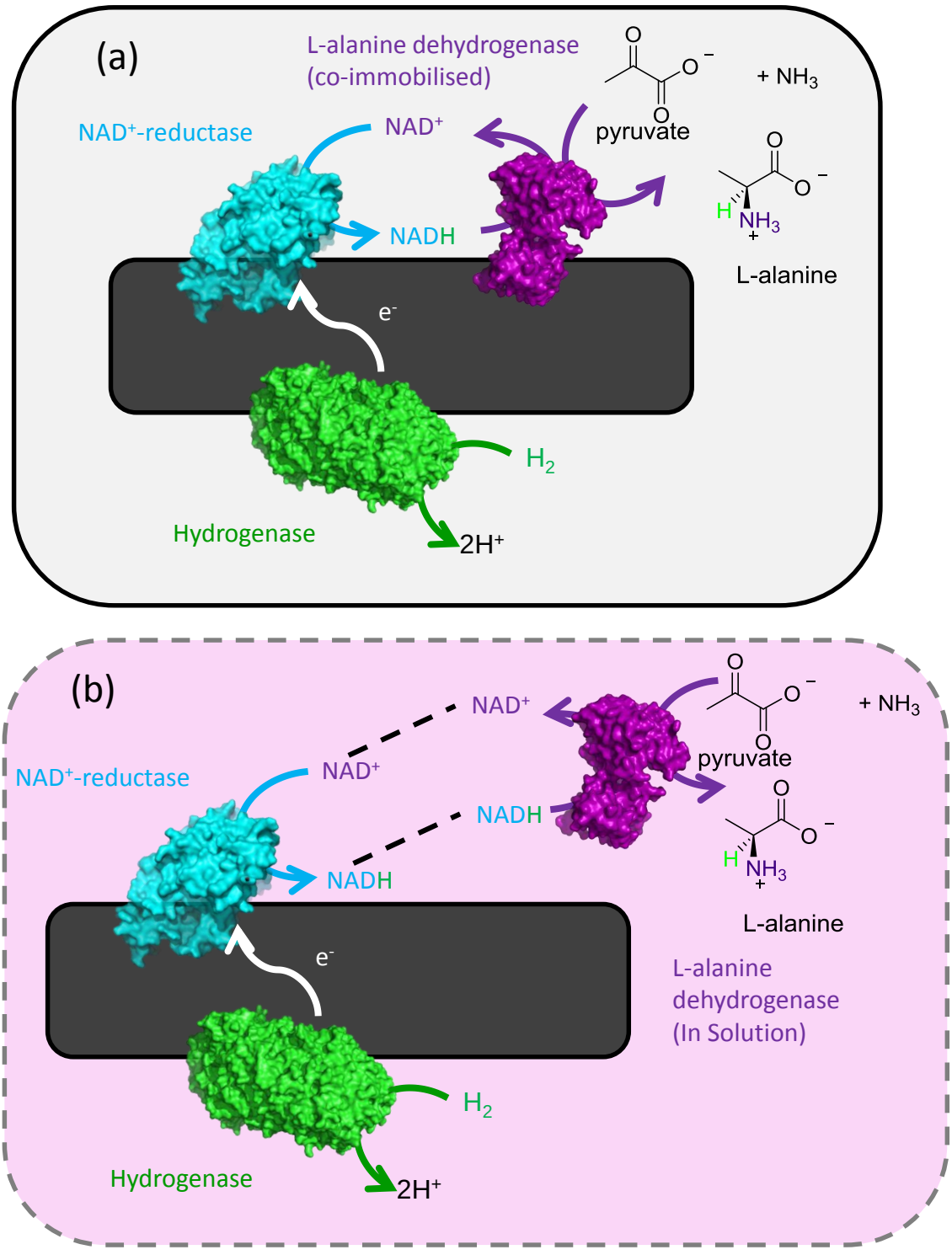

Figure 3-7: A schematic diagram showing the H_2-driven pyruvate to L-alanine conversion system. The hydrogenase and NAD^+-reductase enzymes are co-immobilised on conductive BP 2000 particles. The hydrogenase oxidises H_2 to protons, providing electrons for the NAD^+-reductase to carry out NAD^+ conversion to NADH. This NADH can then be used by the L-alanine dehydrogenase to carry out the reductive amination of pyruvate to L-alanine. The L-alanine dehydrogenase can either be co-immobilised on the particles (a) and therefore in close proximity to the NAD^+-reductase or in solution (b) in which case the NADH must diffuse between the immobilised NAD^+-reductase and the L-alanine dehydrogenase enzyme which is not immobilised on the particles.

Enzyme-modified particles were prepared by mixing Hox~~HY~~FU, Hyd 2 and BP 2000. These particles were split into six sets and L-alanine dehydrogenase was added to three sets. All sets of particles were then left at 4 ^{o}C for 1 hour, before they were centrifuged, the supernatant removed and the particles re-suspended in buffer. To each reaction vessel was then added 500 µL of H_2-saturated buffer, containing 10 mM pyruvate, 15 mM NH_4Cl and 1 mM NAD^+. The same amount of L-alanine dehydrogenase was then added to the tubes where no L-alanine dehydrogenase had been added initially and the same volume of buffer was added to the sets of particles with the L-alanine dehydrogenase immobilised on them, to ensure that the volume of the reaction mixture was the same for all of the sets of particles.

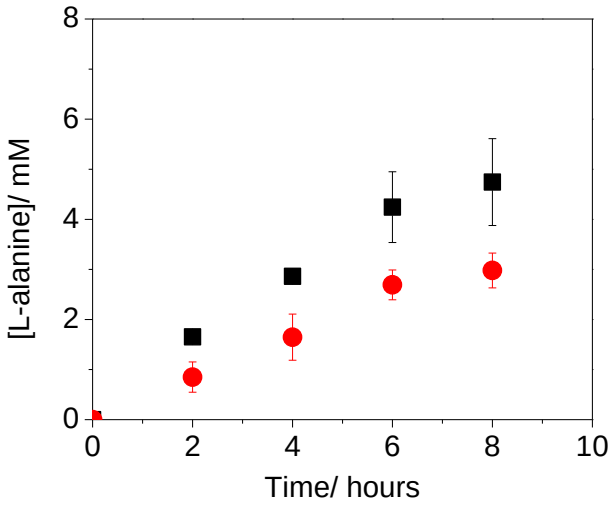

Figure 3-8: Rate of production of L-alanine with the L-alanine dehydrogenase immobilised (black) and in solution (red). Both sets of reactions were performed in triplicate and error bars are shown as 1 standard deviation of the data. Each set of particles was produced by mixing 0.4 mg BP 2000, 30 µg Hyd 2 and 13 µg Hox~~HY~~FU. An 8 µL portion of L-alanine dehydrogenase was added to the aliquots with L-alanine dehydrogenase immobilised. Both sets of particles were then incubated at 4 ^{o}C for 1 hour, then washed three times. Each set of particles was added to 500 µL of reaction mixture containing 1 mM NAD^+, 10 mM pyruvate, 15 mM NH_4Cl in 50 mM Tris-HCl pH 8. An 8 µL portion of L-alanine dehydrogenase was added to the sets of particles without L-alanine dehydrogenase co-immobilised and an 8 µL aliquot of buffer was added to the sets of particles with the L-alanine dehydrogenase co-immobilised. Each time point was taken by removing a 70 µL aliquot of solution and analysing the L-alanine concentration using HPLC.

A 70 µL aliquot was taken every 2 hours from each of the 6 samples to allow analysis by HPLC, ensuring that the solution in each of the reaction vessels was a homogeneous mixture with the particles suspended in it before the samples were taken. The L-alanine concentration was determined by the comparison of the area of the HPLC peak to a standard of known concentration (see Appendix C).

Data in Figure 3-8 demonstrate that a similar effect is observed for H_2-driven pyruvate to L-alanine conversion as that seen by Reeve *et al*. for acetophenone to phenylethanol conversion using the ADH.[119] After 2 hours the yield of L-alanine for the co-immobilised system is approximately twice as large as that observed when the same amount of L-alanine dehydrogenase is in solution.

The turnover frequency (TOF) values for the first 2 hours of reaction shown in Figure 3-8 are 1.8 ± 0.1 s^{-1} for when the L-alanine dehydrogenase is co-immobilised *versus* 0.9 ± 0.3 s^{-1} when the L-alanine dehydrogenase is in solution. Therefore, the initial TOF of L-alanine per NAD^+-reductase when the L-alanine dehydrogenase is immobilised is almost twice the value of the TOF when the L-alanine dehydrogenase is in solution. The TOF for the co-immobilised system is almost certainly an under-estimate, due to some of the L-alanine dehydrogenase being lost in the particle washing steps.[119] This experiment demonstrates that there is a significant advantage to having the L-alanine dehydrogenase immobilised in terms of the rate. Additionally, immobilisation of the entire catalytic system allows the catalyst to be recovered and re-used.

The results from this section, which demonstrate that an increase in reaction rate is observed when the L-alanine dehydrogenase is immobilised on the particles, adds weight to the observations made by Reeve *et al*., who showed this effect with an ADH.[119]

Amino acid dehydrogenase enzymes like the L-alanine dehydrogenase, only accept α-keto acids as substrates. This means that they can only be used in the synthesis of α-amino acids. There is a further of group of enzymes which can be used to produce a wider range of chiral amine products.

3.4 Using *ω-transaminase*s for reductive amination of a wider range of ketone substrates

Introduction

The redox-neutral transfer of an amine group between an amine donor and an acceptor carbonyl group can be catalysed by *ω-transaminase* enzymes.[11]

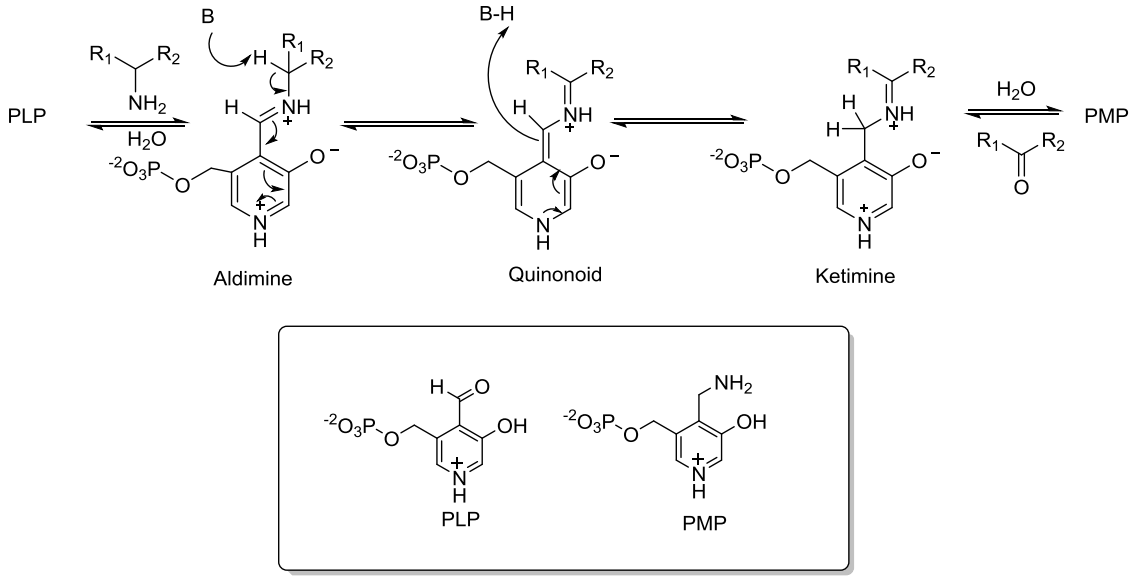

Figure 3-9: Simplified mechanism of *ω-transaminase* catalysed transfer of an amino group adapted from K. Faber in Biotransformations in Organic Chemistry and Höhne et al.[11][20] The PLP cofactor acts as a shuttle which allows the transfer of an amine group. Initially, the PLP forms an aldimine, this goes on to form a ketamine (via a quinonoid intermediate), which when hydrolysed gives the aminated form of PLP, pyridoxamine (PMP). The reverse order of reaction gives access to the desired amine product. B refers to basic residues within the active site of the enzyme (often lysine residues).[182]

The *ω-transaminase* enzymes which are useful for synthetic application are usually group III amino transferase enzymes, which demonstrate high sequence homology with each other.[183] All *ω-transaminase* enzymes are dependent on a PLP (pyridoxal-5'-phosphate) group which acts as a Schiff base, transferring the $-NH_2$ group between the

donor amine molecule and the acceptor ketone group in the *ω-transaminase* catalytic cycle.[11,183,184] A generalised catalytic cycle for *ω-transaminase*s is shown in Figure 3-9.

These enzymes are not able to make use of NH_3, as an amine donor,[13] consequently, a sacrificial amine donor must be supplied. An effective system is required to remove the waste ketone by-product to force the reaction equilibrium in the direction of the products.[13] This is due to the unfavourable thermodynamic equilibrium for this reaction and the inhibition of *ω-transaminase*s by the ketone by-product.[173][185] For example a typical equilibrium constant for the reductive amination of acetophenone to (S)-α-methylbenzylamine with L-alanine as an amine donor is 8.8×10^{-4}.[186] With the commercially available (S)-selective *ω-transaminase* ATA-103. Turner and co-workers demonstrated that with a single equivalent of L-alanine (50 mM) less than 0.5 % conversion of acetophenone to (S)-α-methylbenzylamine could be achieved and even when 10 equivalents of L-alanine were used (500 mM) the maximum conversion was 3 %.[185]

A range of different amine donors can be used with *ω-transaminase*s. Industrially, isopropyl amine is often used as the amine donor, the waste acetone produced is then removed under reduced pressure.[52] However, not all *ω-transaminase*s accept isopropyl amine as an amine donor and reduced pressure gas flow cannot be used in the production of volatile chemicals. In addition, using isopropyl amine as the amine donor generates large amounts of carbon based waste as approximately 10 equivalents of isopropyl amine are required in the reaction mixture to ensure high yields of the desired product of the reaction.[173]

Turner and co-workers have demonstrated that di-amine donors such as ortho-xylylenediamine can be used with a range of *ω-transaminase* enzymes.[187] The

ortho-xylylenediamine is converted to an aminoaldehyde, which spontaneously cyclises and rearranges to the thermodynamically more stable isoindole, consequently meaning that there is no requirement for co-product removal when this system is used. When ortho-xylylenediamine was used as an amine donor only 1.5 equivalents of diamine were required for good conversion.[23,187] However, ortho-xylylenediamine is expensive, toxic and forms a polymer after it aromatises which is difficult to remove downstream.[188] More recently Turner and co-workers have identified a number of *ω-transaminase* enzymes, which are able to accept bio-derived diamines such as putrescine, which will also undergo spontaneous cyclisation on forming amino-aldehydes.[188] This approach has allowed access to a number of pharmaceutically valuable chiral amines, with high *ee* and conversions in the range of 12 – 99%.[188] However, most *ω-transaminase* enzymes will not accept bio-derived diamines.

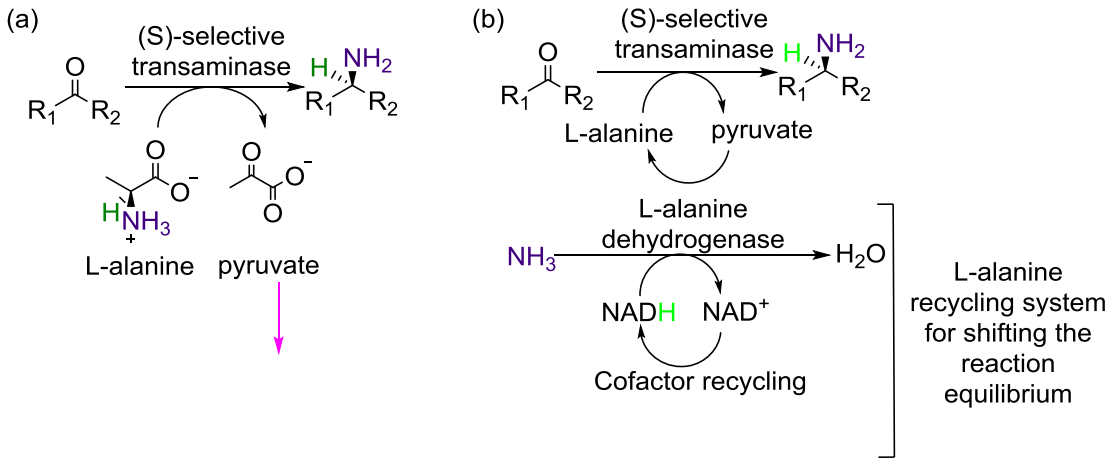

Figure 3-10: (a) A schematic diagram showing the reaction catalysed by an (S)-selective *ω-transaminase* enzyme. The purple arrow emphasizes that the waste product pyruvate must be removed in order for the reaction to proceed in the desired direction due to the unfavourable thermodynamics of this reaction. (b) A reaction scheme for the (S)-selective reduction of a pro-chiral ketone to a chiral amine. L-alanine is used as the amine donor and an L-alanine dehydrogenase is used as a system to remove the waste pyruvate. The L-alanine dehydrogenase recycles pyruvate to L-alanine at the expense of NH_3 and NADH. Consequently, a cofactor recycling strategy is needed.

L-alanine is the preferred amine donor for a range of *ω-transaminase*s. When employed as the amine donor this generates the ketone waste product, pyruvate, which must be removed *in situ* from the reaction mixture, a reaction scheme for this process is shown in Figure 3-10 (a).

One of the best ways of removing the pyruvate co-product to shift the equilibrium in the direction of the desired amine product involves using an L-alanine dehydrogenase, to recycle the pyruvate back to L-alanine as shown in Figure 3-10 (b). However, this in turn requires a cofactor recycling system.

Other groups have used a range of cofactor recycling systems in combination with an L-alanine dehydrogenase as a system for removing the pyruvate co-product (by recycling it to L-alanine) and shifting the *ω-transaminase* reaction equilibrium in the direction of the products; these include formate dehydrogenase (FDH)[136] and glucose dehydrogenase(GDH)[189] among others. When FDH is used as the cofactor recycling system and NH_4HCO_2 as the amine donor, this is effectively a biocatalytic version of the Leuckart-Wallach reaction.[23] The whole soluble hydrogenase (SH) from *R. eutropha* has also been used by Holzer *et al.* for H_2-driven cofactor recycling linked to an L-alanine dehydrogenase for L-alanine recycling in order to shift the *ω-transaminase* reaction equilibrium in the direction of the desired products.[115] Holzer *et al*. demonstrated that it was possible to obtain 86 % conversion of 4-phenylbutan-2-one to 1-methyl-3-phenylpropylamine with 92 % *ee* with the (S)-selective *ω-transaminase* from *Pseudomonas fluorescens* using this system.

In theory, it is possible to use catalytic amounts of L-alanine when an L-alanine dehydrogenase is used to recycle the pyruvate waste product from a *ω-transaminase* reaction back to L-alanine. However, in practice with 0.5 equivalents of L-alanine, both Turner and co-workers and Kroutil and co-workers required prolonged reaction times of

>50 hours to achieved similar yields to after 24 hours when a >5 fold excess of L-alanine was used.[20,185,190] A concentration of >250 mM L-alanine is commonly used in biocatalytic reactions using *ω-transaminases* on a laboratory scale.[115,136,190]

*ω-Transaminase*s have been used industrially to improve upon the efficiency of reductive amination reactions catalysed by precious metal catalysts. A *ω-transaminase* has been used in the final step in the production of the drug Sitagliptin, used in the treatment of type 2 diabetes. This highly evolved *ω-transaminase* variant was able to tolerate 50 vol. % DMSO and meant that use of an expensive Rh catalyst could be circumvented.[52] The enzymatic reaction pathway also led to a 19 % reduction in waste, (for more details see section 1.3.1).[52]

A fourfold excess of isopropyl amine was used as the amine donor in this reaction.[191] However, using sub-stoichiometric amounts of an alternative amine donor could further reduce the waste generated as part of this process.

The next section of this chapter looks at combining a *ω-transaminase* with the pyruvate to L-alanine conversion system developed in section 3.2 and shown in Figure 3-3. When coupling an L-alanine dehydrogenase as an L-alanine recycling system (in order to shift the *ω-transaminase* reaction equilibrium) to the enzyme-modified particles for H_2-driven cofactor recycling system, it is theoretically possible to produce chiral amines with the only side product being water. Although, when NH_4Cl is used as the source of ammonia, additional H^+ and Cl^- ions are also released. The reaction scheme for this process is shown in Figure 3-11.

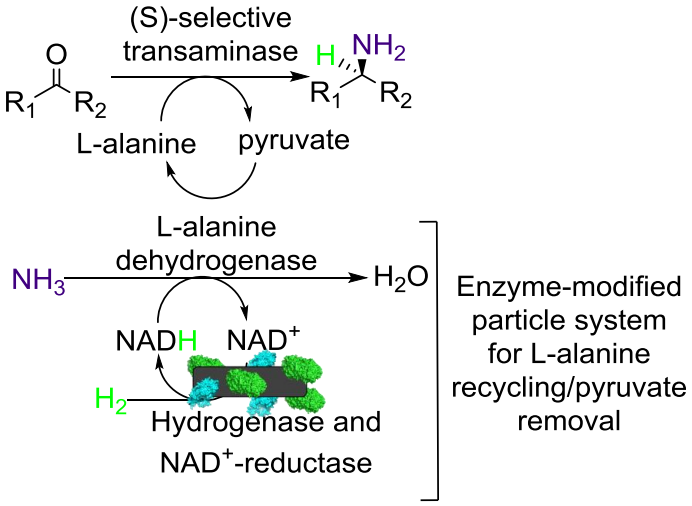

Figure 3-11: A reaction scheme for the (S)-selective reduction of a pro-chiral ketone to a chiral amine at the expense of H_2 and NH_3. In this system the (S)-selective *ω-transaminase* uses L-alanine as the amine donor producing pyruvate. Hydrogenase and NAD^+-reductase enzymes are co-immobilised on carbon particles, to recycle NADH at the expense of H_2. The NADH produced can then be used by an L-alanine dehydrogenase, also co-immobilised on the particles, which catalyses the conversion of pyruvate to L-alanine at the expense of NH_3. Overall, this system theoretically allows the production of chiral amines just using stoichiometric amounts of H_2, NH_3 and the ketone.

3.4.1 Purification of the *Vf ω-transaminase*

The *ω-transaminase* from *Vibrio fluvialis (Vf)* is a well characterised (S)-selective *ω-transaminase* enzyme.[192]

Initially, the *Vf ω-transaminase* was expressed in *E. coli* and purified using His-Tag chromatography nickel affinity chromatography as described in Appendix A, following the protocol of Mutti *et al*.[136] The SDS-PAGE gel shown in Figure 3-12 shows a single band in the purified protein lane at approximately 50 kDa, corresponding to the purified *Vf ω-transaminase* protein.

The activity of *ω-transaminase*s can be assayed by following the (S)-α-methylbenzylamine driven conversion of pyruvate to L-alanine, see Figure 2-8 for a schematic diagram of this process. This is however, the reverse direction to the one of interest for synthetic applications of *ω-transaminase*s. However, having a quick assay to determine the activity of a *ω-transaminase* preparation allows easy comparison of the activity of different batches of the enzyme. In general, specific activities of around

20 ± 10 U mg^{-1} were obtained for batches prepared in this lab. This however is significantly higher than the activity observed in the opposite direction; using L-alanine to drive reductive amination of a prochiral ketone.

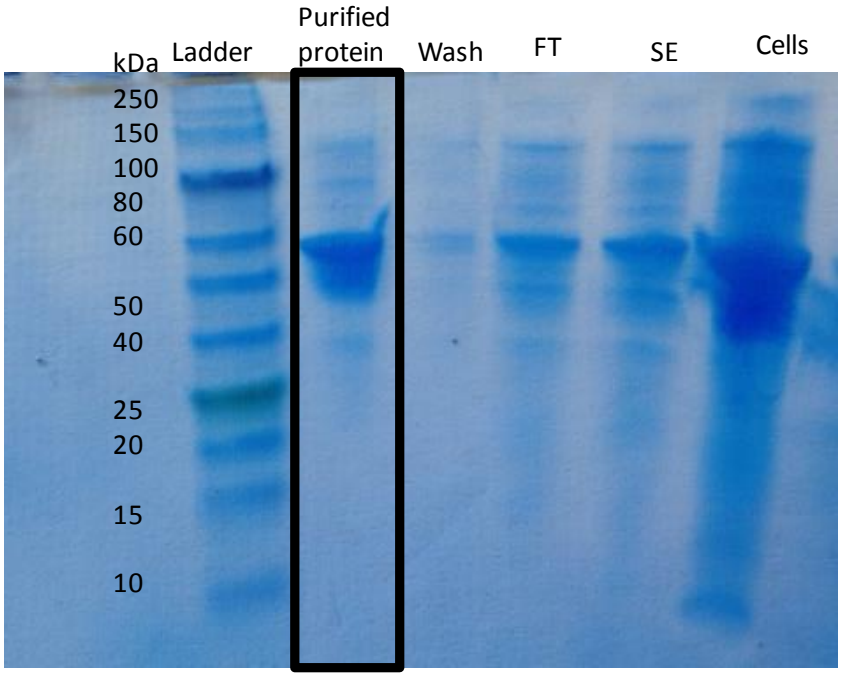

Figure 3-12: An SDS-PAGE gel run after the purification of the *Vf ω-transaminase* protein. Each lane represents the following, from the right hand side, cells: the cell lysate; SE: the 'soluble cell free extract': the soluble fraction of the cells isolate after centrifuging the sonicated cells; FT: 'Flow through': the solution which elutes from the column after loading the protein; Wash: the low imidazole buffer fraction used to wash the His-Tag column; Purified protein: the purified protein eluted from the His-Tag column, after de-salting. A dark band at a molecular weight of around 50 kDa (100 kDa for the native dimer structure)[192] in the purified protein fraction suggests that it has been possible to obtain fairly pure protein.

3.4.2 Using Kinetic assays to optimise conditions for *Vf-ω-transaminase* immobilisation

When the UV-visible assay in section 2.2.6 was used to monitor the activity of the enzyme-modified particles *in situ*, a low concentration of particles must be used to ensure that scattering of light in the cuvette does not cause the spectrometer to reach its absorption maximum.[103] The reaction shown in Figure 2-8 can be used to determine the activity of a *ω-transaminase* immobilised on particles.

Spectra in Figure 3-13 (a) show increasing absorption at 290 nm demonstrating the production of acetophenone by a set of particles with *Vf ω-transaminase* immobilised on them. Figure 3-13 (b) demonstrates that by taking the absorbance at 290 nm as a function of time it is possible to determine the activity of the immobilised *ω-transaminase*.

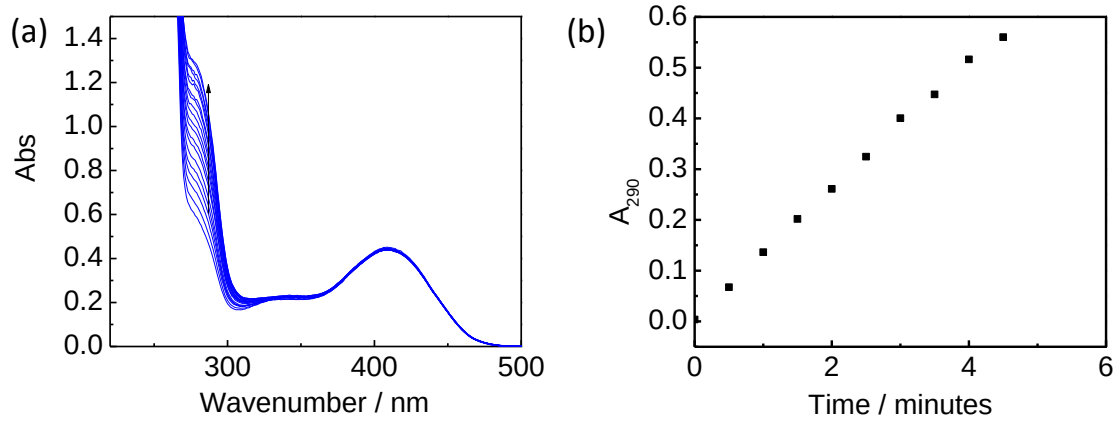

Figure 3-13: Using a (S)-α-methylbenzylamine driven reductive amination of pyruvate to monitor the activity of a *ω-transaminase* enzyme immobilised on particles. (a) A set of particles was constructed with 50 µg BP 2000 and 47 µg *Vf ω-transaminase*. Particles were incubated at 4 °C for 1 hour and subsequently washed once, by centrifuging and removing the supernatant, then adding buffer and repeating this process once. The particles were then added to a cuvette and a 1 mL aliquot of 50 mM phosphate buffer pH 8.0, 5 mM pyruvate, 10 mM (S)-α-methylbenzylamine and 0.1 mM PLP (pyridoxal phosphate) was added quickly. Scans measuring the conversion of (S)-α-methylbenzylamine to acetophenone were taken every 30 seconds. Increasing absorbance at 290 nm indicates production of acetophenone (and therefore activity of the *ω-transaminase*). (b) Points at 290 nm taken from scans in (a), using the gradient from this data it is possible to calculate specific activity values for the particles.

There is significant interest in developing efficient methods for the immobilisation of *ω-transaminase* enzymes, as for expensive enzyme preparations it is essential that the enzyme is recycled if the process is to be economically viable.[193] A number of groups have attempted to immobilise *ω-transaminase* enzymes, for example on chitosan[148][194] and in sol-gels.[193] Yi *et al*. have carried out work which focuses on immobilising the *Vf ω-transaminase* used in this work, on chitosan, therefore this work will be directly compared to results obtained in that paper.[148] Unfortunately, Yi *et al*. do not show data

for producing value-added chiral amines, but instead test their immobilised *ω-transaminase* with (S)-α-methylbenzylamine driven conversion of pyruvate to L-alanine, as shown in section 2.2.6.[148] Activities were calculated in this paper using a HPLC based assay.

Of great encouragement was that the activity of the immobilised *ω-transaminase* on BP 2000 particles obtained here without optimisation (3.9 ± 0.1 U mg^{-1}) was 19 % of that of the enzyme in free solution (20.6 ± 0.5 U mg^{-1}), based on the mass of *Vf ω-transaminase* originally added to the particle suspension. This is similar to the results obtained by Yi *et al* of 17.8 %. The process used in this work is, however, a simple adsorption process; whereas, the process reported by Yi *et al*. involves the use of toxic glutaraldehyde as a cross linking reagent, which may not be suitable for the immobilisation of all enzymes in an enzyme cascade, such as the rest of the L-alanine recycling system required for shifting the *ω-transaminase* reaction equilibrium.[148]

3.4.3 Investigating effects of pH and temperature on the immobilised *Vf ω-transaminase*

Yi *et al*. have also shown that when the *Vf ω-transaminase* was immobilised on chitosan beads, it showed higher activities at elevated temperatures and extreme pHs than when it was in solution.[148] This section examines whether the *Vf ω-transaminase* shows similar enhanced pH and temperature behaviour when immobilised on BP 2000 particles.

The main findings of Figure 3-14 (a) is that the specific activity of the *Vf ω-transaminase* is highest both immobilised and in solution at pH 8.0. At pH 4.0 and pH 11.0, only a tiny amount of the activity observed at pH 8.0 is observed for the immobilised *ω-transaminase*. The pH optimum in the work of Yi *et al*. is seen to be pH 9.0 for both the immobilised and solution preparations of the *ω-transaminase*.[148]

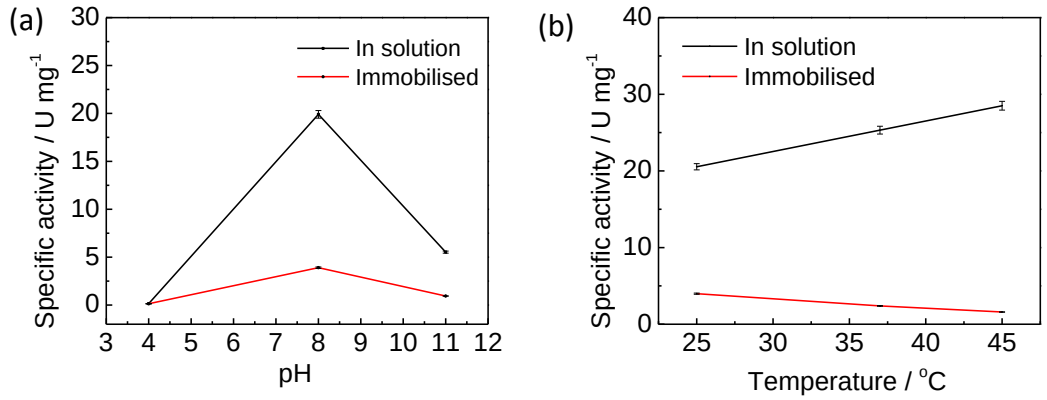

Figure 3-14: Graphs showing the effect of pH (a) and temperature (b) on the activity of the *Vf ω-transaminase* both on immobilised (red) and in solution (black). Assays were carried out with 31 µg of *ω-transaminase* either added to the reaction mixture (solution) or incubated with 100 µg of BP 2000 particles for 1 hour at 4 °C, and washed once as described above. Activity assays were then conducted in phosphate buffer solutions at pH 4.0, 8.0 and 11.0 containing 5 mM pyruvate, 10 mM (S)-α-methylbenzylamine and 0.1 mM PLP (pyridoxal-5'-phosphate). Sequential scans were taken every 30 s and the baseline corrected absorbance at 290 nm was used to determine the activity over the first 5 minutes. In (b) assays were carried out at a series of temperatures in 50 mM phosphate buffer pH 8.0, with particles prepared in the same was as described above. All activities are given in U mg^{-1} of *Vf ω-transaminase* originally added.

However, unlike in the immobilisation process here, Yi *et al*. were able to demonstrate a statistically significant improvement in enzyme activity for their immobilised enzyme preparations at pH 4.0 and pH 11.0, in comparison to the free *ω-transaminase* in solution at pH 4.0 and pH 11.0. Figure 3-14 (b) demonstrates that the temperature stability of the *Vf ω-transaminase* is not improved on immobilisation on BP 2000 particles and that the optimum temperature for biotransformations is <25 °C for the *Vf ω-transaminase* immobilised on BP 2000 particles. In contrast, Yi *et al.* demonstrated that covalent immobilisation led to a shift in temperature optimum to 45 °C for their immobilised preparation of *ω-transaminase*. This is perhaps expected as covalent glutaraldehyde linkages between the enzyme and the support matrix would be expected to hold the enzyme in a more rigid position; whereas, on the BP 2000 particles the *Vf ω-transaminase* is immobilised via adsorption and hence is held in place by a series of weaker interactions with the carbon particle, potentially meaning it is in a less rigid confirmation.[11]

3.5 Biocatalytic reactions

This section describes biocatalytic reactions carried out using the *Vf ω-transaminase* in combination with the enzyme-modified particle system for the recycling of the pyruvate co-product back to L-alanine, in order to shift the *ω-transaminase* reaction equilibrium in the direction of the desired products.

3.5.1 Investigating the quantity of particles required for efficient immobilisation

It was initially important to determine whether the substrate and product being used to test the *ω-transaminase* reaction adsorb to the carbon particles. Samples containing 10 mM 4-phenylbutan-2-one and 1-methyl-3-phenylpropylamine in 50 mM Tris-HCl pH 8.0 were prepared. Each sample was then split into two aliquots (1 mL each), one of which was extracted immediately into ethyl acetate, analysed by GC and used as a standard. To the second sample was added a 2.8 mg portion of BP 2000 particles. It was found that after extracting with ethyl acetate > 95 % of substrate (4-phenylbutan-2-one) and > 80 % product (1-methyl-3-phenylpropylamine) could be recovered from the samples containing BP2000 particles.

The boiling points of the 4-phenylbutan-2-one and 1-methyl-3-phenylpropylamine are 235 ^{o}C and 228 ^{o}C respectively,[65] and both compounds have low predicted vapour pressures.[195] This suggests that evaporation of substrate or product is unlikely to be a problem during the course of an 18 hour bio-transformation. This has been confirmed by tests in the laboratories of collaborators.[196]

In order to test whether using a larger mass of BP 2000 particles to immobilise the *Vf ω-transaminase* leads to more efficient immobilisation and hence a higher yield of product: Hyd 2, Hox~~HY~~FU, L-alanine dehydrogenase and *Vf ω-transaminase* were mixed. Equal aliquots of this solution were then added to Eppendorf tubes containing

1.4, 2.8 and 5.6 mg of BP 2000 particles. These samples were subsequently incubated for one hour at 4 ^{o}C, washed once and the supernatants collected. The supernatants were then subjected to an assay with (S)-α-methylbenzylamine in order to assess their relative activities (see results in Table 3-1).

Table 3-1: The activity of the enzyme mixture on addition of differing amounts of particles.

Mass of particles added (mg)	Mass of particles (μg) / Mass of ω-transaminase (μg)	Relative activity[a] / %	Specific activity / U mg^{-1}[b]
1.4	0.7	73±10	22
2.8	1.5	54±4	16
5.6	2.9	1±0.1	0.3

The activity of the *Vf ω-transaminase* immobilised on different amounts of carbon as a percentage of the activity of the starting mixture. [a]Relative activity of the supernatant = $\left(\frac{\boldsymbol{A_p \times V_p}}{\boldsymbol{A_M \times V_m}}\right) \times \mathbf{100}$, where $\boldsymbol{A_p}$ is the activity of the particle solution containing Hyd 2, Hox~~HY~~FU, L-alanine dehydrogenase and *Vf ω-transaminase* along with an aliquot of particles. $\boldsymbol{V_p}$ is the total estimated volume of the particles solution. $\boldsymbol{A_M}$ is the activity of the enzyme mixture containing Hyd 2, Hox~~HY~~FU, L-alanine dehydrogenase and *Vf ω-transaminase* and $\boldsymbol{V_m}$ is the total volume of the enzyme mixture. Activities were determined from UV-visible assays ((S)-methyl benzyl amine driven reductive amination of pyruvate), errors based on the standard deviation of 2 repeat readings. A master mix of 360 μg Hyd 2, 152 μg Hox~~HY~~FU, 40 μL L-alanine and 7.7 mg *Vf ω-transaminase* was made up. This mixture was then split into 4 and added to the differing masses of BP 2000 particles, with a separate aliquot containing no particles acting as a control experiment. Enzymes were left to absorb on particles at 4 ^{o}C for 1 hour. They were then washed once and the supernatant from each was kept for use in these assays.[b] Specific activity / Unit per mg of *Vf ω-transaminase* added originally to the solution.

The activity of the original enzyme solution (containing Hyd 2, Hox~~HY~~FU, L-alanine dehydrogenase and *Vf ω-transaminase)* used to produce the particles was determined to be 30 U mg^{-1} (per mg *ω-transaminase*) and this was used as a standard against which the relative activity of the supernatants could be determined.

The data shown in Table 3-1 show that the greater the amount of particles added, the less activity is observed in the supernatant. The decrease in activity of the supernatant is therefore taken as indirect evidence for a greater degree of immobilisation of *Vf ω-transaminase* on the carbon support.

In the second stage of this experiment, the washed particles were added to a reaction mixture for the biocatalytic conversion of 4-phenylbutan-2-one to 1-methyl-3-phenylpropylamine and then left to react for 18 hours.

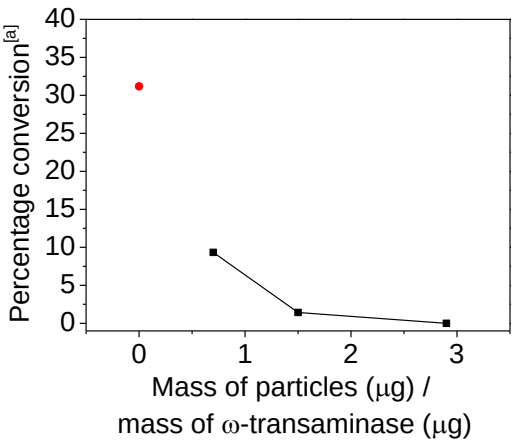

Figure 3-15: Biocatalytic reaction using the same particles from Table 3-1 showing conversion of 4-phenylbutan-2-one to 1-methyl-3-phenylpropylamine, dependent on the H_2-driven enzyme modified particle cofactor recycling system. Red point: control with *ω-transaminase* free in solution. Particles for this reaction were prepared by immobilising 90 µg Hyd 2, 38 µg Hox~~HY~~FU, 10 µL L-alanine on 1.4 mg BP 2000 particles. After the start of the reaction a 1.9 mg aliquot of *Vf ω-transaminase* was added to the reaction vessel. Biocatalytic reactions were carried out on a 300 µL scale, in 50 mM Tris-HCl pH 8.0 containing 10 mM 4-phenylbutan-2-one, 1 mM PLP (pyridoxal-5'-phosphate), 1 mM NAD^+, 150 mM NH_4Cl and 250 mM L-alanine. The reaction vessels were incubated at room temperature under constant H_2-flow for 18 hours with gentle stirring to ensure homogeneous mixing of the suspended particles.[a]Percentage conversion after 18 hours.

The percentage conversions obtained in these bio-transformations are shown in Figure 3-15. The red point represents a comparison with particles with approximately the same amount of Hyd 2, Hox~~HY~~FU and L-alanine dehydrogenase co-immobilised and the *Vf ω-transaminase* free in solution.

The data in Figure 3-15 shows that under these conditions having the *ω-transaminase* in solution (red point) leads to the highest percentage conversion. These effects are discussed further in section 3.7.

In addition, higher percentage conversion figures were obtained when a lower ratio of BP 2000 particles to *ω-transaminase* was used. For example 9 % conversion was obtained with 0.7 µg of BP 2000 per µg of *ω-transaminase versus* 1.4 % conversion

when 1.5 μg of BP 2000 per μg of *ω-transaminase* was used. Data in Table 3-1 shows that the activity of the left-over supernatant is lower when a higher ratio of BP 2000 particles to *Vf ω-transaminase* is used suggesting that more *Vf ω-transaminase* is absorbed when more particles are used. However, the data in Figure 3-15 suggests that despite the fact that more *ω-transaminase* seems to be absorbed when more particles are added, the *ω-transaminase* which is absorbed appears to be less active in the biotransformations.

If more particles are used the Hyd 2 and NAD^+-reductase enzymes will be further apart, perhaps affecting the electronic contact between these two enzymes and consequently the rate of cofactor recycling. Alternatively, the increased distance between the NAD^+-reductase and the L-alanine dehydrogenase could lead to a decrease in the rate of NADH cycling between these enzymes. Additionally, if large amounts of bare carbon are exposed, this may lead to temporary absorption of the substrate meaning that the substrate concentration in solution would be decreased significantly. Immobilising the *Vf ω-transaminase* is investigated further in section 3.7.

These results suggest that it is possible to immobilise active *Vf ω-transaminase* on BP 2000 particles, which can be used in a biotransformation reaction. However, it is not possible simply to use more BP 2000 particles to ensure higher amounts of active *Vf ω-transaminase* are immobilised.

3.5.2 Optimising conditions for *ω-transaminase* driven transformations

A preliminary screen in which a range of conditions were tested was carried out in order to optimise the reaction yield for H_2-driven conversion of 4-phenylbutan-2-one to 1-methyl-3-phenylpropylamine. The results of this work are shown in Table 3-2. This

allowed quick identification of the problems with the reaction set up and key areas of focus in order to optimise the biotransformation yield.

Table 3-2: Preliminary experiments to determine improved conditions for using the *ω-transaminase* enzyme.

Entry	Formate dehydrogenase[a]	Hyd 2[b]	Hox~~HY~~FU[c]	L-alanine dehydrogenase[d]	*ω-transaminase*[e]	[Product] / µM
1	X	X	X	S	S	0
2	X	I	I	I	I	5.1
3	X	I	I	S	S	65
4	S	X	X	I	I	40.9
5	S	X	X	S	S	339
6	X	I	I	X	X	0

[a]1.6 mg Formate dehydrogenase; [b]15 µg Hyd 2; [c] 6 µg Hox~~HY~~FU; [d] 2.5 µL L-alanine dehydrogenase; [e]0.66 mg *Vf ω-transaminase*. Reactions were carried out on a 1 mL scale with 10 mM 4-phenylbutan-2-one, 1 mM NAD^+, 0.5 mM PLP, 1 mM L-alanine and 30 mM NH_4Cl in the case where FDH was not used or 30 mM ammonium formate in combination with FDH. For the immobilised systems 0.4 mg of BP 2000 was added to the reaction mixture. Reactions were left under continuous H_2 flow with gentle shaking for 12 hours. I = immobilised on BP 2000 particles. S = in solution. X = not included The FDH was a commercial preparation from Candida boidinii (2.2 U/mg) obtained from Evocatal.

The first observation which can be made from Table 3-2 is that in the control reaction (Entry 1) no amine product is obtained. Therefore, it is clear that just the L-alanine dehydrogenase and the *Vf ω-transaminase* in solution will not lead to appreciable yields of product. This is further supported by literature observations that a method of removing the pyruvate co-product is required when using *ω-transaminases* in biocatalysis to shift the equilibrium in the direction of the products and generate appreciable yields of the desired chiral amine.[136][187] In addition, Entry 6 shows that just the enzyme-modified particles (modified with Hox~~HY~~FU and Hyd 2) on their own will not yield any 1-methyl-3-phenylpropylamine.

In this work a FDH was used in order to test an alternative cofactor recycling system (Entries 4 and 5) in combination with the L-alanine dehydrogenase (for L-alanine recycling) and the *Vf ω-transaminase.*

Higher yields of 1-methyl-3-phenylpropylamine were obtained when the *ω-transaminase* was free in solution (Entries 3 with the enzyme-modified particles, and 5 with the FDH) than when it was immobilised on BP 2000 particles (Entries 2 with the enzyme-modified particles and 4 with the FDH), re-affirming the findings observed in Section 3.5 and further explored in section 3.7.

The highest yield in this set of experiments (339 μM 1-methyl-3-phenylpropylamine) was obtained when the *Vf ω-transaminase*, L-alanine dehydrogenase and FDH were in solution (entry 5). As it was not possible to obtain as high a yield with the enzyme modified particles in entry 3, this suggests that a higher concentration of enzyme-modified particles are required for the H_2-driven system, if the yield under these conditions is to equal that of the FDH system. However, even with the FDH based system (entry 5) nothing close to complete conversion (10 mM) was achieved. Generally, at least a fivefold excess of L-alanine is required to give good conversion in a 12 hour time period.[20] This finding is therefore supported by the literature discussed in section 3.4, which demonstrates that generally poor yields are achieved over a 12 hour time period with *ω-transaminase* and catalytic amounts of L-alanine.

3.5.3 Investigating H_2-driven *ω-transaminase* reactions under 2 bar $H_{2(g)}$

Preliminary results in the Vincent group have demonstrated that the enzyme-modified particles for H_2-driven cofactor recycling function better under a H_2 pressure of 2 bar.[197] This may be due to the increased solubility of H_2 gas at higher pressures, see Chapter 2, section 2.4.3.

It was found when comparing reactions set up with the same amount of enzyme modified particles and *Vf ω-transaminase* enzyme in the same reaction mixture that the reaction under 2 bar H_2 pressure achieved substantially higher yields than the reaction

conducted under a continuous flow of H_2 gas. Consequently, studies in the later sections of this chapter were carried out using a pressure system under 2 bar H_2. This also has the advantage of allowing easier comparison to the work of Holzer *et al*. whose work with the whole *R. eutropha* SH was conducted under 2 bar H_2.[115]

3.6 Optimised conditions for coupling the *Vf ω-transaminase* with the enzyme-modified particles

The previous sections in this chapter describe experiments carried out under a range of conditions, aiming to optimise the H_2-driven conversion of 4-phenylbutan-2-one to 1-methyl-3-phenylpropylamine using the *Vf ω-transaminase* in combination with the enzyme-modified particles (with L-alanine dehydrogenase co-immobilised) as an L-alanine recycling system.

Significantly higher conversions have been obtained when the *ω-transaminase* was dissolved in solution *versus* when it was immobilised on particles. Part of the reason for this could be due to significant amounts of *ω-transaminase* enzyme not being absorbed on the particles and being lost in washing steps during the immobilisation process.

The highest conversion observed, so far, when using the enzyme-modified particles (with L-alanine dehydrogenase co-immobilised on them) as an L-alanine recycling system in combination with the *Vf ω-transaminase* is 68 %. This was achieved with the *Vf ω-transaminase* in solution and a 250 mM L-alanine concentration, following an 18 hour reaction. The GC trace obtained following this biotransformation is shown in Figure 3-16.

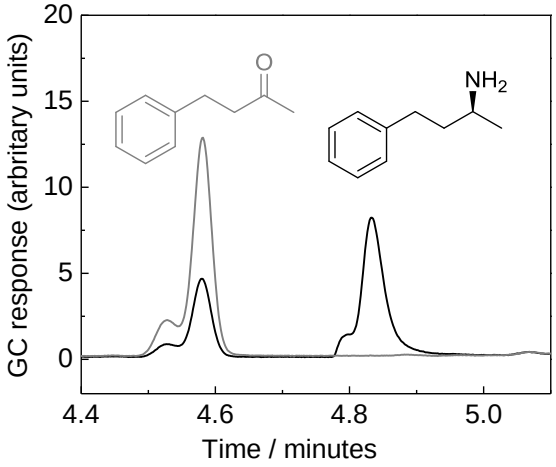

Figure 3-16: A GC trace showing 68 % conversion determined by the ratio of the 4-phenyl-2-butanone to 1-methyl-3-phenylpropylamine peaks. Black: reaction, grey: starting mixture. Particles were made with 81 µg Hyd 2, 38 µg Hox~~HY~~FU (*R. eutropha)*, 10 µL L-alanine dehydrogenase and 1.4 mg BP 2000. This mixture was allowed to immobilise at 4 ^{o}C for one hour. The reaction was carried out in a total volume of 300 µL. The reaction mixture contained 100 mM Tris-HCl pH 8, 1 mM NAD^+, 10 mM 4-phenyl-2-butanone, 0.5 mM PLP, 150 mM NH_4Cl. A 2.8 mg aliquot of *Vf-ω-transaminase* was added to the solution to start the reaction. Reactions were carried out at room temperature under a H_2-pressure of 2 bar.

Over an 18 hour period the TTN (moles of product per moles of NAD^+-reductase) per NAD^+-reductase (*R. eutropha* Hox~~HY~~FU) was calculated to be *ca.* 9,000. This is significantly lower than the value obtained for the pyruvate to L-alanine conversion system above. This TTN is, however, comparable to the figures obtained for transition metal catalysis discussed in section 1.2.1.

In the literature TTN values of *ca.* 1,000-10,000 were reported for the *Vf ω-transaminase* for the conversion of 4-phenylbutan-2-one to 1-methyl-3-phenylpropylamine, when an L-alanine dehydrogenase was used to recycle L-alanine and FDH[136] or the *R. eutropha* SH were used as the cofactor recycling system.[115] This was based on estimating the percentage mass of *ω-transaminase* present in the whole *E. coli* cells used as 4 - 20 % based on the metrics of Kohls *et al.*[198] In this work the TTN per *Vf ω-transaminase* is at least an order of magnitude lower than this value. This suggests that the concentration of *Vf ω-transaminase*

shouldn't be limiting the reaction and that the enzyme-modified particle system is not functioning at its optimum rate under the conditions employed when coupled to the *Vf ω-transaminase* in this reaction.

3.6.1 Investigating using crude cell extracts

There is almost always a balance between the purity of the enzyme preparation used in biocatalysis and its cost.[199] Purified proteins are very expensive because of the time and effort required for the purification process. Consequently, they are rarely used for the production of chemicals and probably only for highly priced fine chemicals such as active pharmaceutical ingredients (APIs).[50] However, cell permiabilisation and disruption is a well-established technique, which can be used to produce a crude (cell free) enzyme extract, which is much cheaper and less time consuming to obtain than a completely purified enzyme.[199]

It was found that crude cell free extract of the *Vf ω-transaminase* (3 mg) could be used in solution, giving a reasonable conversion of 26 % of 4-phenylbutan-2-one to 1-methyl-3-phenylpropylamine after 18 hours under similar conditions to those used in Figure 3-16, above. This soluble extract showed approximately 20 % of the activity per mg of the purified *Vf ω-transaminase* in the assay with (S)-α-methylbenzylamine. Therefore, the percentage conversion obtained per unit activity is larger for the crude enzyme extract than for the purified *ω-transaminase*. Furthermore, no additional side products were observed in the GC-trace as a result of homologous enzymes present in the *E. coli* cells used to produce the *Vf ω-transaminase*.

Hence, with further optimisation the crude cell extract could prove to be a cheaper alternative to using completely purified *ω-transaminase* with the enzyme-modified particles as an L-alanine recycling system.

3.6.2 Determining the *ee* of the 1-methyl-3-phenylpropylamine product

These experiments were performed with the assistance of Dr Jack Rowbotham (Post-doc in the Vincent group)

In order to determine the *enantiomeric excess (ee)* of the product of the *ω-transaminase* reactions NMR spectroscopy was used. Once the *ee* has been determined for a particular cofactor recycling system in combination with L-alanine dehydrogenase for L-alanine recycling, it is expected that this will remain constant regardless of the yield obtained. Different *ee* values are obtained for the same reaction product with the same *ω-transaminase* when different pyruvate removal systems are used (e.g. FDH and L-alanine dehydrogenase and GDH and a lactate dehydrogenase).[136]

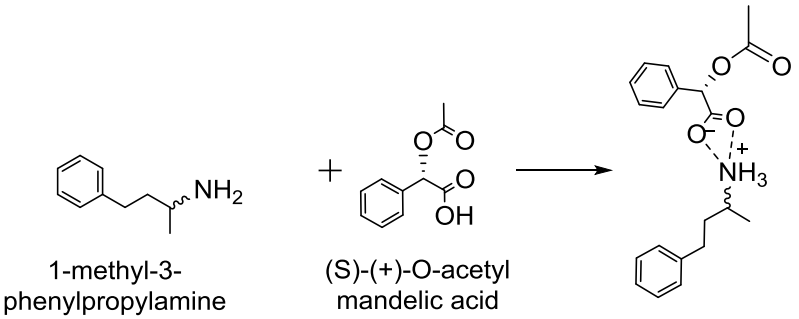

Figure 3-17: Diagram showing the complexation of (S)-(+)-O-acetylmandelic acid with 1-methyl-3-phenylpropylamine, the stereospecific nature of this interaction leads to differences in chemical shifts between the two enantiomers when studied by ^{1}H NMR spectroscopy.

NMR spectroscopy does not differentiate between enantiomers unless such an interaction exists so as to break their degeneracy. In this regard, addition of a coordinating chiral shift reagent converts the mixture of enantiomers into a mixture of diastereoisomeric salts, which can subsequently be distinguished by NMR spectroscopy.[180] Exact experimental details of the procedure used to determine the *ee* of 1-methyl-3-phenylpropylamine are given in Appendix F.

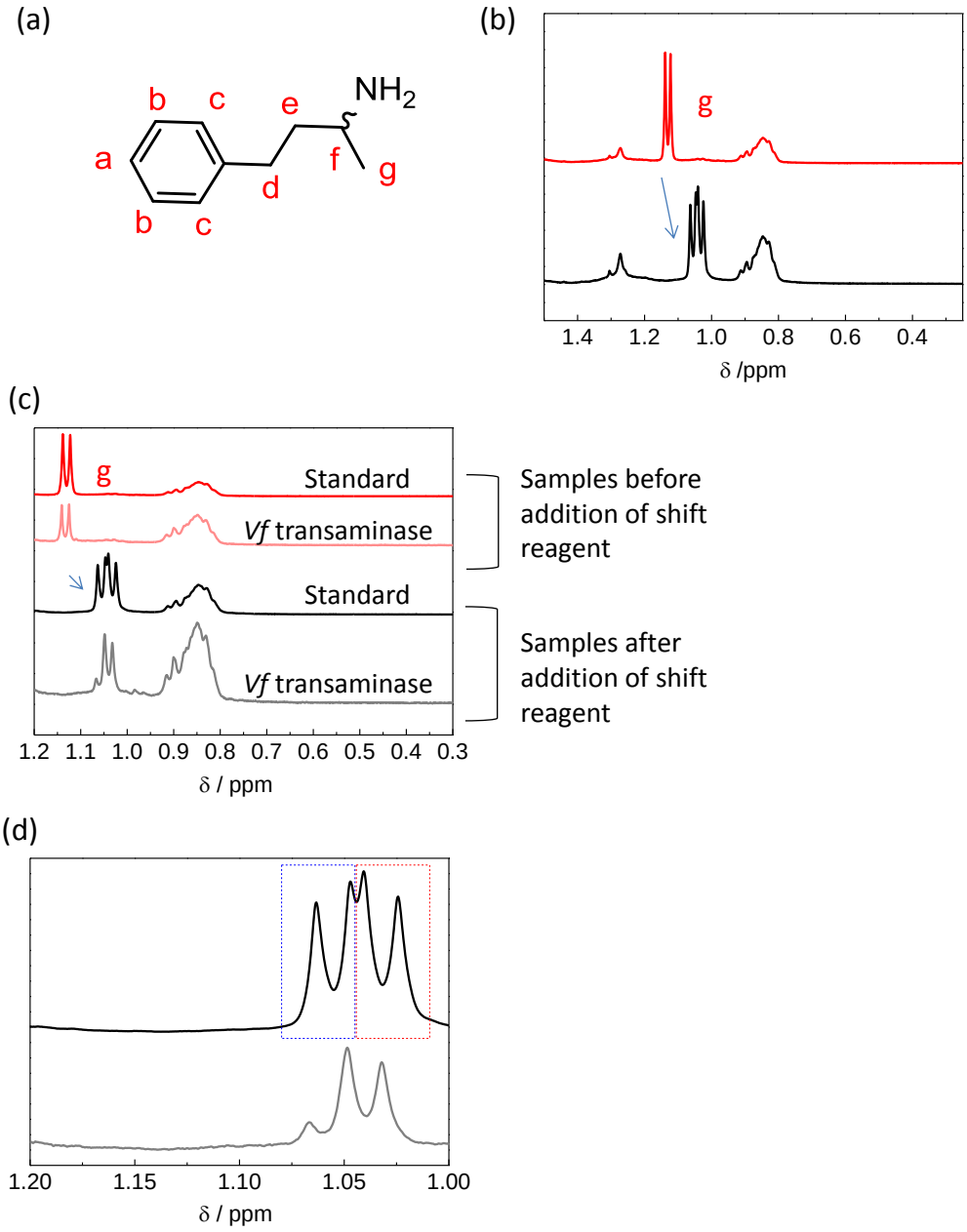

Figure 3-18: ^{1}H NMR spectra used to determine the *ee* of 1-methyl-3-phenylpropylamine product. (a) 1-methyl-3-phenylpropylamine with all of the carbons with protons attached labelled in red (b) ^{1}H NMR spectra of a commercial standard of 10 mM (rac)- 1-methyl-3-phenylpropylamine. Red trace shows a doublet at 1.15 ppm, this signal is assigned to the protons on the methyl group α to the NH_2 (protons on carbon g), with the splitting arising due to scalar coupling (^3J, vicinal) with the single proton on carbon f. Black trace shows this sample after addition of 7.125 mM of chiral shift reagent (S)-(+)-O-acetylmandelic acid added to the solution, breaking the degeneracy of the protons on 'g' leading to a doublet of doublets. (c) ^{1}H NMR spectra of 1-methyl-3-phenylpropylamine, red and black traces as in (b). Pink: sample of 1-methyl-3-phenylpropylamine produced by the *Vf ω-transaminase* biotransformation, showing a doublet corresponding to the protons on carbon 'g'. Grey: sample of 1-methyl-3-phenylpropylamine produced by the *Vf ω-transaminase* biotransformation after addition of (S)-(+)-O-acetylmandelic acid shift reagent. (d) Black and grey traces from (c) zoomed in and overlaid between 1.2 and 1 ppm.

Experimental conditions: The reaction mixture at the end of the biotransformation with the *Vf ω-transaminase* was extracted into C^2HCl_3 by basifying the reaction mixture with 30 µL 10 N NaOH, adding 300 µL C^2HCl_3 to the reaction mixture, vortexing and then centrifuging down and removing the bottom layer. This procedure was repeated twice. NMR samples were 600 µL in volume. ^{1}H NMR spectra were referenced to the residual $CHCl_3$ peak (δ = 7.26 ppm). The two doublets of the racemic sample are indicated by red and blue dashed boxes. Note that due to subtle differences in the samples, the doublet from the ω-TA doesn't overlay directly with the racemic standard.

The *ee* of the 1-methyl-3-phenylpropylamine product of the *Vf ω-transaminase* enzyme reported by Mutti *et al*. is 84 % (S), when an L-alanine dehydrogenase was used for L-alanine recycling and a GDH was used for cofactor recycling.[136] The *ee* determined by Mutti *et al.* was measured by derivatising the product to the acetamide and then using chiral GC, an alternative approach to the NMR spectroscopic methodology utilised in this thesis.

In order to determine whether a similar *ee* could be obtained when the *Vf ω-transaminase* was used with an L-alanine dehydrogenase (for L-alanine recycling) and the enzyme-modified particles as a cofactor recycling system, enzyme-modified particles were produced by combining the following components: BP 2000 particles (1.4 mg), *R. eutropha* Hox~~HY~~FU (38 µg), Hyd 2 (114 µg) and L-alanine dehydrogenase (10 µL). These particles were added together with an aliquot of *Vf ω-transaminase* (6 mg) to a H_2-saturated reaction mixture containing 10 mM 4-phenyl-2-butanone (300 µL total volume). The reaction was then allowed to proceed overnight under 2 bar H_2.

Figure 3-18 (a) shows 1-methyl-3-phenylpropylamine with the carbons with protons attached labelled in red. The red trace in Figure 3-18 (b) shows the characteristic doublet observed for the protons on carbon 'g' in the ^{1}H NMR spectrum of 1-methyl-3-phenylpropylamine. When the chiral shift reagent, (S)-(+)-O-acetylmandelic acid, was added, this doublet is observed to separate into two

separate doublets as the degeneracy of the two enantiomers of the amine is broken upon complexation. This trace is shown in black in Figure 3-18 (b).

In Figure 3-18 (c) the spectra of the product of the reaction described above, in which the enzyme-modified particles were used in combination with the *Vf ω-transaminase* is shown. The trace in pink, is before addition of the shift reagent. This shows that a doublet is obtained at approximately 1.1 ppm, for the product of the reaction. This is identical to the doublet obtained for the racemic standard, shown above in red.

The trace shown in grey in Figure 3-18 (c), was obtained following addition of the (S)-(+)-O-acetylmandelic acid shift reagent to the sample. The shift reagent has caused the peak for the $–CH_3$ protons of 1-methyl-3-phenylpropylamine at 1.1 ppm to shift, as seen for the racemic standard shown by the black trace above in Figure 3-18 (c).

From the zoomed in spectra in Figure 3-18 (d) it is clear that the grey trace (the sample from the *Vf ω-transaminase* reaction) shows one doublet peak centred at 1.03 ppm. The small peak centred around 1.05 ppm is presumed to be due to a small amount of the other product enantiomer. This then allowed a preliminary deconvolution to be performed in order to estimate a value for the *ee* of the reaction, see Appendix F.

Accordingly, a ratio of 10:49 was measured for the intensity of the peak at 1.05 ppm relative to that at 1.03 ppm, this equates to an *ee* of 66 %. This is lower than the 84 % *ee* observed by Mutti *et al*., when a GDH was used for cofactor recycling.[136] However, this is likely to be within the degree of error associated with using chiral solvating agents for *ee* determination.

3.7 Comparing immobilised and non-immobilised *ω-transaminase*s for H_2-driven reductive aminations

Having the *ω-transaminase* co-immobilised on the enzyme-modified particles means that the whole system could potentially be removed from the reaction mixture and re-

used in subsequent batch reactions. Furthermore, an increase in the rate of reaction was seen when the L-alanine dehydrogenase was co-immobilised on the particles *versus* when it was used in solution, see section 3.2 above. It is thought that this increase in rate is probably due to a substrate channelling effect whereby the cofactor is passed very quickly between the L-alanine dehydrogenase and the Hox~~HY~~FU enzyme as suggested in section 3.2, leading to a higher localised concentration of the cofactor at the surface of the particles.

As often more than ten equivalents of L-alanine are required for a high yielding reaction with *ω-transaminase*s,[185][173] if it is possible to increase the localised L-alanine concentration by having the *ω-transaminase* immobilised, this could mean that catalytic amounts of L-alanine could be used in this reaction eliminating the large amounts of unused L-alanine which must be removed from the reaction mixture at the end of the reaction and then treated as waste. The two scenarios tested in this section are outlined in Figure 3-19.

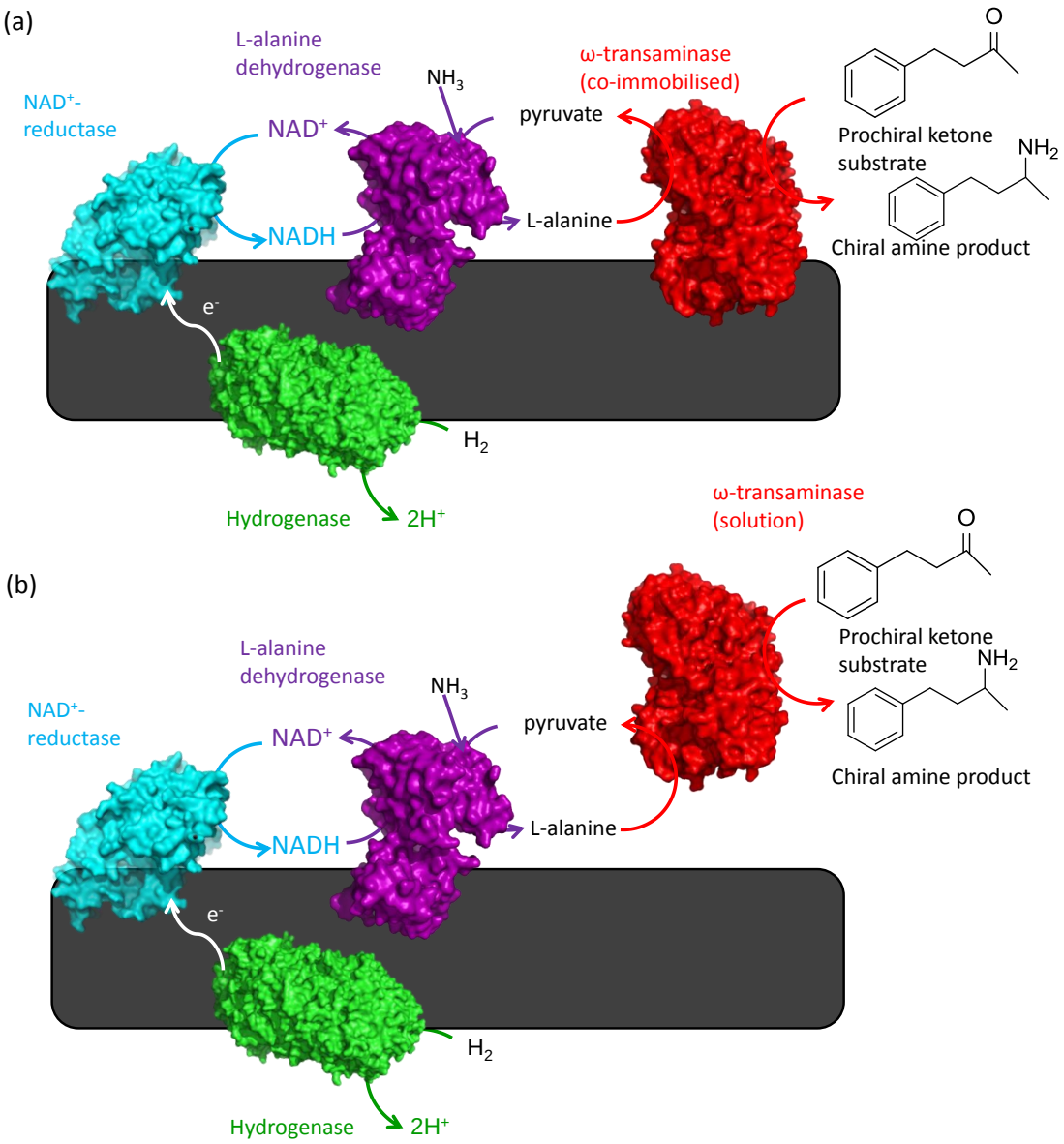

Figure 3-19: Two systems for using an (S)-selective *ω-transaminase* in combination with a H_2-driven system for removal of the pyruvate waste product. (a) All enzymes immobilised on carbon. (b) *ω-transaminase* in solution all other enzymes which are part of the cascade immobilised on particles.

Enzyme-modified particles were prepared by mixing Hox~~HY~~FU, Hyd 2, L-alanine dehydrogenase and BP 2000 particles. These particles were split into eight sets and *Vf ω-transaminase* was added to four sets. Each set of particles were then left at 4 ^{o}C for 1 hour, centrifuged, the supernatant removed, and then re-suspended in buffer. This procedure was then repeated twice more, so that the particles were in total washed three times.

To each set of particles was then added an aliquot of reaction mixture containing 10 mM 4-phenyl-2-butanone. To the sets without *ω-transaminase* co-immobilised, an aliquot of *Vf ω-transaminase* was also added to the solution (an aliquot of buffer of the same volume was added to the samples with the *ω-transaminase* immobilised to ensure that the total volume of the reaction mixture in each case remained the same).

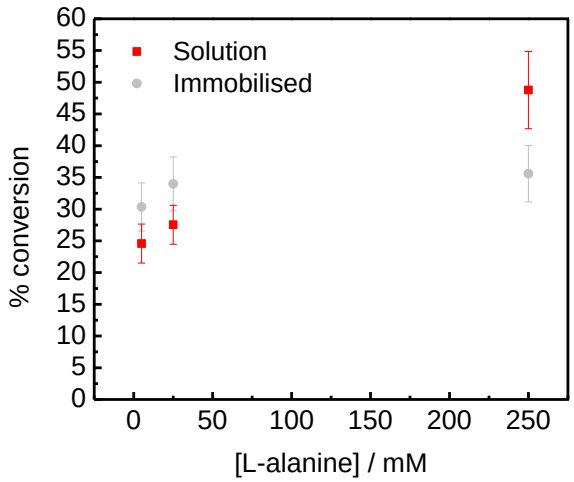

Figure 3-20: A graph comparing the percentage conversion obtained for experiments run in parallel with the *ω-transaminase* enzyme both immobilised and in solution. The concentration of L-alanine in the reaction mixture was varied from 5 mM to 250 mM in sequential reactions. Particles were made with 720 µg Hyd 2, 304 µg Hox~~HY~~FU (*R. eutropha)*, 80 µL L-alanine dehydrogenase, 11.2 mg BP 2000 particles; these were then divided into 8 equal portions and 6 mg of *Vf ω-transaminase* was added to four of the aliquots. The particles were then left at 4 ^{o}C for one hour and washed twice. Reactions were carried out on a 200 µL scale in 100 mM Tris-HCl pH 8.0, containing 1 mM NAD^{+}, 10 mM 4-phenyl-2-butanone, 0.5 mM PLP, 150 mM NH_4Cl and 5, 25 or 250 mM L-alanine. Finally, 6 mg of *ω-transaminase* was added to each of the tubes containing particles which had not had *ω-transaminase* initially immobilised on them (an aliquot of buffer of the same volume was added to the tubes with transaminase immobilised). Reactions were carried out at 22 ^{o}C, under 2 bar H_2-pressure. Error bars estimated at 12 % based on duplicate reading for points at 5 mM.

Data in Figure 3-20 shows that when the *ω-transaminase* is in solution we see higher percentage conversion at high concentrations of L-alanine. A significant decrease in the percentage conversion is seen when the L-alanine concentration is decreased for the experiments in which the *ω-transaminase* was free in the solution (red points). However, when the *ω-transaminase* is co-immobilised on the particles (grey points) alongside the L-alanine dehydrogenase and cofactor recycling system, the percentage

conversion varies less with L-alanine concentration. This leads to a somewhat higher percentage conversion at 5 mM and 25 mM L-alanine concentration when the *ω-transaminase* is immobilised. This could be because of faster transfer of L-alanine and pyruvate between the L-alanine dehydrogenase and the *Vf ω-transaminase*. With further optimisation, immobilisation of the *ω-transaminase* might lead to higher yields at lower L-alanine concentrations. Repeat experiments are shown in Appendix D, they confirm this trend, but again demonstrate the requirement for further optimisation of this system if yields for the immobilised *Vf ω-transaminase* at low L-alanine concentrations are to match yields for the *Vf ω-transaminase* in solution at high L-alanine concentrations.

3.8 Can (R)- chiral amines be accessed using a (R)-selective *ω-transaminase*s?

3.8.1 Initial demonstration of a H_2-driven *ω-transaminase* pyruvate removal system for use with a (R)-selective *ω-transaminase*

This section was conducting at the University of Graz (Austria) in collaboration with Prof. Wolfgang Kroutil. *E. coli* Hyd 1 was used instead of Hyd 2 due to work being conducted outside of an anaerobic glovebox and therefore not perfectly anaerobic conditions.

Investigations into (R)-selective *ω-transaminase*s are of particular interest in the field of bio-catalysis as, to date, these enzymes have not been developed to the same degree as their (S)-selective counterparts.[194,200] There is significant interest in preparing (R)-chiral amines with the high selectivity afforded by *ω-transaminase* enzymes.[200] These enzymes would, however, require D-alanine instead as their amine source. Similar systems have been developed in the literature to remove the waste product pyruvate to drive (R)-selective *ω-transaminase*s in the direction of the products, see Figure 3-21 (a) for an example of a H_2-driven system. These systems do not regenerate the D-alanine, but simply remove the pyruvate waste product.[200]

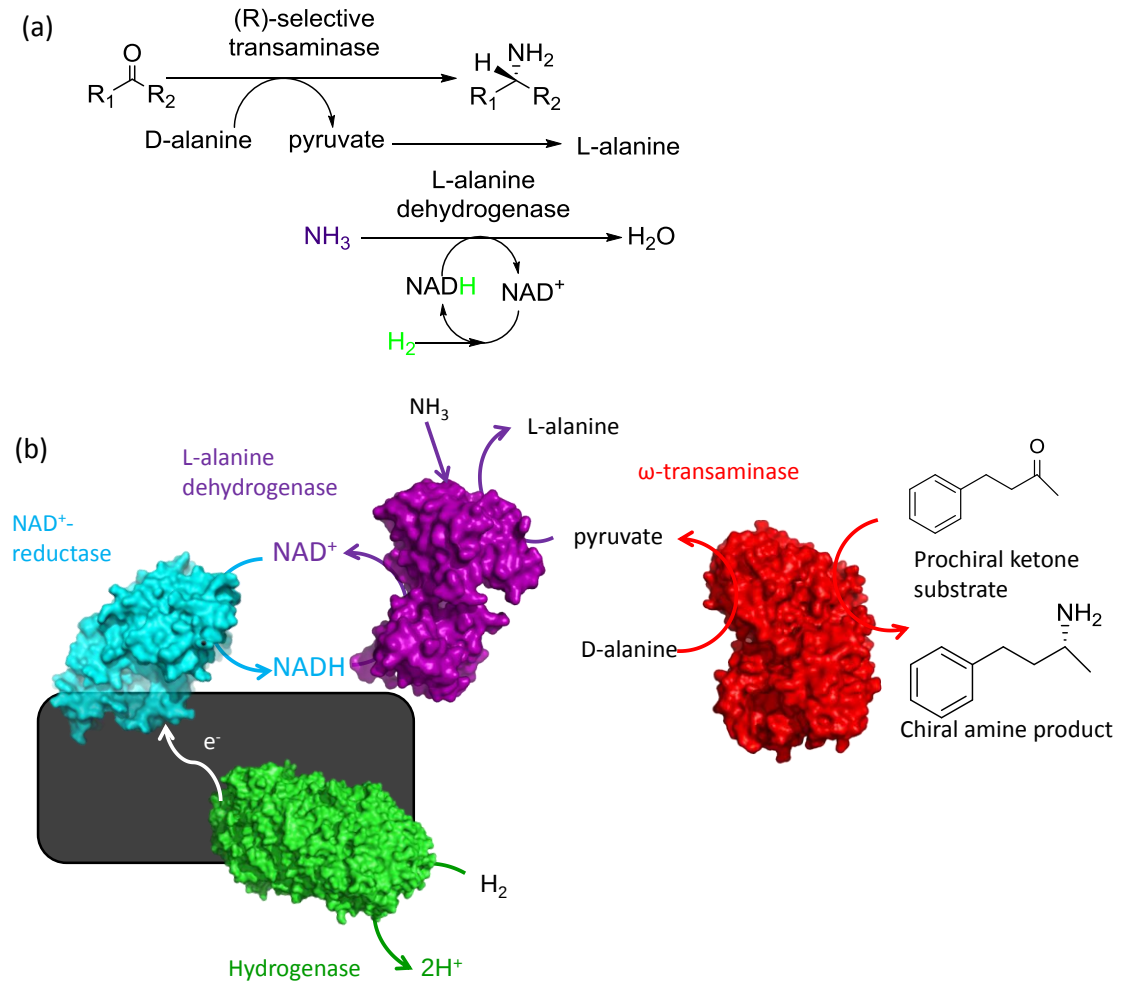

Figure 3-21: A H_2-driven pyruvate removal system for use with (R)-selective *ω-transaminases*. (a) A schematic representation of this system for the production of (R)-chiral amines using an (R)-selective *ω-transaminase* enzyme. Here, super-stoichiometric amounts of D-alanine are added, these are consumed by the *ω-transaminase* to convert the 4-phenyl-butanone (ketone) substrate into (R)-1-methyl-3-phenylpropylamine (the desired chiral product). The waste pyruvate is then converted into L-alanine using an L-alanine dehydrogenase enzyme. The scheme is based on the work of Holzer *et al.*[115] (b) A cartoon representation of the initial test system used to determine whether the (R)-selective *ω-transaminase* could be combined with the enzyme-modified particles for H_2-driven reductive amination.

In order to initially test whether it is possible to couple an (R)-selective *ω-transaminase* (AT ω-TA from *Aspergillus terreus)* with the enzyme-modified particles for H_2-driven reductive amination, a set of particles was prepared by mixing Hox~~HY~~FU, Hyd 1 and BP 2000 particles. These particles were then left at 4 ^{o}C for 1 hour, before adding them to a reaction mixture containing 10 mM D-alanine and 10 mM 4-phenyl-2-butanone. The particles were left to generate NADH for 40 minutes, indicated by increasing

absorption at 340 nm over the first 40 minutes of the reaction, see Figure 3-22. After 40 minutes aliquots of L-alanine dehydrogenase and of AT-ωTA were injected into the cuvette. This led to an instant decrease in absorption at 340 nm, indicative of the L-alanine dehydrogenase consuming some of the NADH in the solution. Hence, it can be concluded that the *ω-transaminase* is using the D-alanine to produce pyruvate and 1-methyl-3-phenylpropylamine. The pyruvate produced is then converted to L-alanine at the expense of NADH by the L-alanine dehydrogenase shifting the equilibrium in the direction of the products, see Figure 3-22.

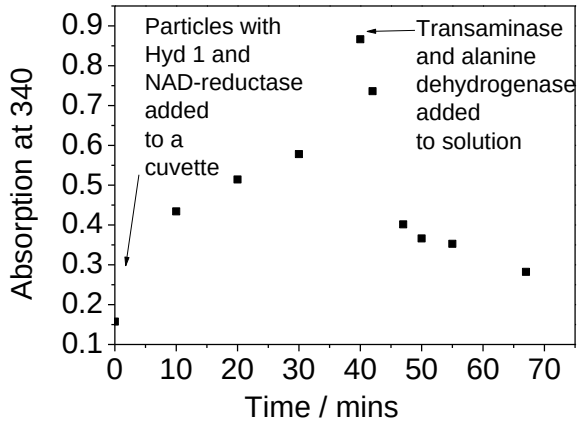

Figure 3-22: At time zero a set of particles with 6 µg Hyd 1 and 2.7 µg Hox~~HY~~FU immobilised on 0.04 mg BP 2000 was added to a cuvette containing 1 mL H_2-saturated 50 mM Tris-HCl pH 8. Also contained in the reaction mixture was 0.2 mM NAD^+, 0.5 mM PLP, 10 mM D-alanine, 10 mM NH_4Cl and 10 mM 4-phenyl-2-butanone. For the first 45 minutes NADH was generated, following this 10 µL of alanine dehydrogenase and 32 µg of Aspergillus terreus *ω-transaminase* (AT-ωTA) were injected into the solution.

3.8.2 Biocatalytic conversion of 4-phenyl-2-butanone to 1-methyl-3-phenylpropylamine using a (R)-selective *ω-transaminase*

The price of D-alanine is £3.68 g^{-1} *versus* £0.59 g^{-1} for the naturally occurring L-enantiomer.[65] This makes it attractive to find a method of using L-alanine instead of D-alanine in combination with (R)-selective *ω-transaminase* enzymes.[30]

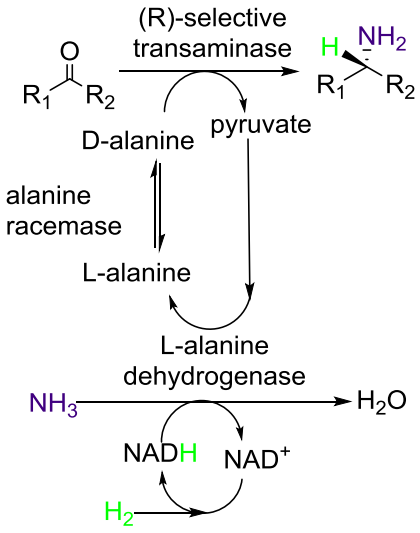

Figure 3-23: Pyruvate removal system for shifting the equilibrium of an (R)-selective *ω-transaminase*. Here an alanine racemase is used to convert comparatively cheap L-alanine to a mixture of D- and L- alanine. The D-alanine can then be used by the (R)-selective *ω-transaminase* to produce (R)-selective chiral amines.[115]

A possible reaction scheme to drive the production of (R)-chiral amines using H_2 and NH_3 is shown in Figure 3-23. L-alanine can also be added at the start, as this is racemised by the alanine racemase (*SeAlaR* from *Streptomyces coelicolor*), meaning that expensive D-alanine is not required.[30,201] Additionally, this cycle has the potential to be catalytic if a *ω-transaminase* with a low enough K_M for alanine can be developed. Enzyme modified particles could be used for cofactor recycling in the system shown in Figure 3-23.

In order to test the (R)-selective *ω-transaminase* with the enzyme-modified particle system for alanine recycling, a set of particles was prepared by mixing Hox~~HY~~FU, Hyd 2, L-alanine dehydrogenase and BP 2000. These particles were then left at 4 ^{o}C for 1 hour before being added to a reaction mixture containing *SeAlaR* and the (R)-selective *ω-transaminase AT-ωTA*.

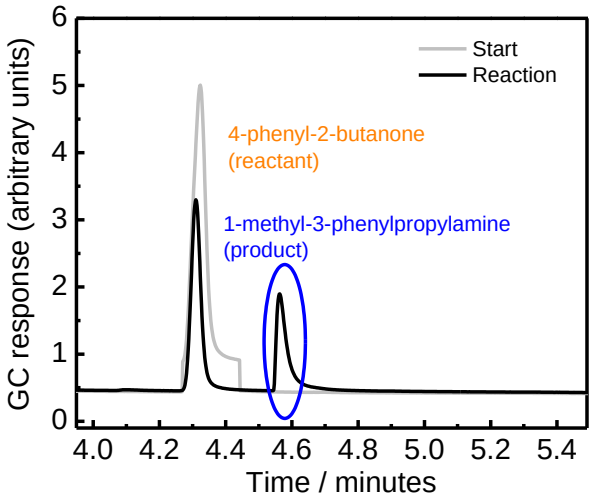

Figure 3-24: Conversion of 4-phenyl-2-butanone to 1-methyl-3-phenylpropylamine using AT-ωTA. Trace in black represents the reaction trace. Grey: starting mixture. The reaction was carried out over 18 hours on a 300 µL scale in H_2-saturated 50 mM Tris-HCl pH 8.0 with gentle stirring under 2 bar H_2 pressure. The reaction was carried out with 81 µg of Hyd 2, 38 µg Hox~~HY~~FU and 10 µL alanine dehydrogenase co-immobilised on 1.4 mg of BP 2000 particles. In addition, 2 mg of alanine racemase and 2 mg AT-ωTA were added to the reaction mixture. A starting concentration of 250 mM L-alanine, 1 mM NAD^+, 0.5 mM PLP, 10 mM 4-phenylbutan-2-one and 150 mM NH_4Cl was used.

The GC trace in Figure 3-24 shows that it is possible to achieve a conversion of 38 % for 4-phenylbutan-2-one to (R)-1-methyl-3-phenylpropylamine, without any optimisation of conditions for this particular *ω-transaminase*. The *ω-transaminase* AT ω-TA typically demonstrates very high *ee* values with the L-alanine dehydrogenase as a pyruvate removal system with either the *R. eutropha* SH or FDH for cofactor recycling.[115,200] The result in Figure 3-24 demonstrates that it is possible to use the H_2-driven enzyme-modified particle system (with L-alanine dehydrogenase co-immobilised on the particles) to remove the pyruvate co-product/recycle alanine, in combination with both (S)- and (R)- selective *ω-transaminase* enzymes. It also demonstrates that it is possible to use H_2 to drive a 5 enzyme cascade reaction and achieve appreciable yields of product. Over the 18 hour reaction period this equates to a TTN of *ca.*5,000 per NAD^+-reductase (Hox~~HY~~FU).

3.9 Conclusion

This chapter describes a proof of concept demonstration of H_2-driven highly selective reductive amination reactions.

In section 3.2 a system has been developed for the production of the amino acid L-alanine from pyruvate just using stoichiometric amount of NH_3 and H_2. It has been possible to demonstrate a TTN of 34,000 ± 1000 for this reaction. Furthermore, it has been demonstrated that there is an advantage, in terms of the rate of reaction, to having the L-alanine dehydrogenase enzyme immobilised *versus* in solution. This supports the work of Reeve *et al.* who made a similar finding when an ADH enzyme was immobilised on the enzyme-modified particles *vs.* in solution.[103] Having all of the enzymes immobilised as a single heterogeneous catalyst also means that the entire bio-catalytic system could theoretically be recycled for use in a subsequent batch process.[61] Although, this has not yet been demonstrated directly for the immobilised L-alanine dehydrogenase system.

In sections 3.4-3.7 the enzyme-modified particles, with L-alanine dehydrogenase co-immobilised on them were used with the (S)-selective *Vf ω-transaminase* as a system to recycle the pyruvate co-product back to L-alanine and to shift the *ω-transaminase* equilibrium in the direction of the desired products. This is a demonstration of a 4 enzyme cascade. It was possible to demonstrate conversion with all of the enzymes immobilised on the particles or with the *Vf ω-transaminase* in solution. The highest conversion obtained, so far, with the *Vf ω-transaminase* when the enzyme-modified particles were used as part of an L-alanine recycling system, was 68 %. This was achieved with the *Vf ω-transaminase* in solution. A 66 % *ee* was obtained for the 1-methyl-3-phenylpropylamine product of this reaction.

In the work of Holzer *et al.*, who used the whole *R. eutropha* SH with an L-alanine dehydrogenase as a L-alanine recycling system, a conversion of 86 % of 4-phenylbutan-2-one to 1-methyl-3-phenylpropylamine, with an alternative (S)-selective *ω-transaminase* was demonstrated.[115] This is higher than the figure obtained here and demonstrates that further optimisation would be required if the enzyme modified particle system for L-alanine recycling is to be competitive with the system demonstrated by Holzer *et al*.. Moreover, the work of Holzer *et al.* is also not currently competitive with established methods of shifting the *ω-transaminase* equilibrium such as using FDH as a cofactor recycling system in combination with an L-alanine dehydrogenase.[23] This demonstrates that H_2-driven bio-catalytic reductive amination reactions using *ω-transaminase* enzymes remain challenging. Potentially the most promising way to improve the atom economy of these reactions is to use a diamine substrate which spontaneously cyclises as described by Turner and co-workers.[188]

In section 3.8 an (R)-selective *ω-transaminase (AT ω-TA)* was used in combination with the enzyme-modified particles as part of a pyruvate removal system. It was possible to obtain a 38 % yield for this reaction, which represents a 5 enzyme cascade. . The promising results without prior optimisation for the system with the *AT ω-TA* are expected as this *ω-transaminase* showed higher yields for the conversion of 4-phenyl-2-butanone to 1-methyl-3-phenylpropylamine in previous publications by Kroutil and co-workers than the *Vf ω-transaminase*, when glucose dehydrogenase was used as the cofactor recycling system and DMSO was used as a co-solvent.[136,200]

3.10 Future work

There are a number of areas in this chapter, which show promise and which merit future experimental work. These are summarised below:

- Investigate whether it is possible to produce a wider range of amino acid products by switching the L-alanine dehydrogenase with a range of other amino acid dehydrogenase enzymes, such as leucine dehydrogenase.
- Coupling the enzyme-modified particles (for H_2-driven cofactor recycling), with recently developed amine dehydrogenase enzymes. These NADH dependent, mutated amino acid dehydrogenase enzymes, could also be used to provide access to a wider range of chiral amine products without the requirement for the addition of a further *ω-transaminase* enzyme.[173]

4 Characterisation of the soluble hydrogenase from *Hydrogenophilus thermoluteolus*

This chapter describes the purification and characterisation of the soluble, NAD^+-linked, hydrogenase (SH, HoxHYFU) from *Hydrogenophilus thermoluteolus* (*H. thermoluteolus*). The NAD^+-reductase (HoxFU moiety) was then expressed independently of the H_2-cycling moiety (HoxHY) and characterised using both electrochemical and biochemical methods. The electrochemical characterisation of the NAD^+-reductase (HoxFU) moiety allows this enzyme to be compared with the HoxFU moieties of *Ralstonia eutropha* (*R. eutropha)* and Rhodococcus opacus (*Rh. opacus)* previously characterised in the Vincent group.[102][103]

By exploring new SHs and NAD^+-reductases it may be possible to find an enzyme which is suited to a particular set of conditions, which may be desirable for a certain set of biocatalytic reactions, for example an enzyme which is able to function at elevated temperatures. Biocatalytic reactions carried out at elevated temperature may be useful in applications where it is important to avoid microbial contamination or where faster rates can be achieved at elevated temperature with cofactor dependent enzymes from thermophile organisms. Additionally, high temperatures are advantageous in some industrial processes where it is desirable to increase the solubility of substrates or products (e.g. biopolymers) or where elevated temperatures can be used for *in situ* removal of volatile products.[202]

4.1 Soluble Hydrogenases

Cytoplasmic soluble, $NAD(P)^+$-linked hydrogenases couple the oxidation of H_2 to the reduction of NAD^+, see Chapter 1, section 1.8.1.[104]

These enzymes are found in a wide range of organisms including *R. eutropha*, *Rh. opacus* and cyanobacteria.[108] Soluble hydrogenases from *R. eutropha*,[109] *Rh. opacus*[110] and from *Pyrococcus furiosus*[111] have already been well characterised. The information obtained from biochemical and electrochemical characterisation is

important, as it gives insight into the optimum conditions required by these enzymes for catalysis. This can then be used as the basis for the implementation of these enzymes in bio-catalytic applications.

4.1.1 Rhodococcus opacus and *Ralstonia eutropha*

The native SH proteins from *R. eutropha* and *Rh. opacus* are similar with respect to a range of catalytic and structural properties.[143] These enzymes show >60 % sequence similarity.[143] The native SH from *Rh. opacus* consists of HoxHYFU, without the HoxI sub-units found in *R. eutropha*. The *Rh. opacus* SH also requires the presence of Ni^{2+} ions, high concentrations of chaotropic salts or buffers with pHs lower than 7 to be used when assaying activity in order to observe any NAD^+-reduction activity. Otherwise the SH from *Rh. opacus* easily dissociates into its two catalytic moieties HoxHY and HoxFU.[143] The *R. eutropha* SH on the other hand, remains intact in alkaline conditions without divalent anions. This means that it is good for using as a whole SH in biocatalytic applications, but that molecular biology strategies are required to separate this enzyme into its two component fragments to study the single functionalities.[203]

4.1.2 Cyanobacteria

A range of cyanobacteria also produce SHs.[204] These enzymes contain an additional subunit, meaning that the SH enzymes produced by them are composed of HoxHYFUE. It is postulated that HoxE participates in electron transfer to the hydrogenase (HoxHY) component.[205] Although, some of these hydrogenases have been isolated from cyanobacteria such as *Anabaena cylindrica*[206] and the phototrophic organism *Thiocapsa roseopersicina*[205], detailed characterisations of these enzymes have not yet been performed. These enzymes are highly sensitive to oxygen and are unstable *in vitro* precluding their use in bio-technological applications.[114,206,207]

4.2 The SH from *Hydrogenophilus thermoluteolus*

Hydrogenophilus thermoluteolus was originally isolated from the soil around a hot spring.[208] This organism is a gram negative knallgas bacterium, which shows optimum growth at temperatures between 50 ^{o}C and 52 ^{o}C. It also produces an SH which may be more stable that the SHs originally from mesophile organisms, particularly at higher temperatures.[102][113][114]

Having access to a thermostable SH has some potential advantages in biotechnological cofactor recycling applications. A thermostable SH could be used as a cofactor recycling system in combination with thermophile NADH dependent enzymes. As a rule of thumb the reaction rate for enzymatic reactions doubles approximately every 10 ^{o}C.[202] Therefore, carrying out enzymatic process at elevated temperatures would potentially increase productivity and shorten process times. Additionally, thermo-stability is additionally often found to go hand-in-hand with other properties desirable for biotechnological applications including: better solvent tolerance and the ability to cope with higher organic substrate concentrations.[11] Similarly to the SHs from *R. eutropha* and *Rh. opacus*, the *H. thermoluteolus* SH is made up of two heterodimeric catalytic sub-units HoxFU (the NAD^+-cycling domain) and HoxHY (the hydrogenase moiety). [209]

4.2.1 Genetic links

Figure 4-1 shows a phylogenetic tree which demonstrates the genetic link between the NAD^+-reducing sub-units within a number of organisms, based on the sequence of their NAD^+-reducing domains (analogous to HoxF in *R. eutropha*).

The phylogenetic tree suggests that the SH from *H. thermoluteolus* is most closely related to the SHs from *R. eutropha* and *Rh. opacus* and is less closely related to the SHs from cyanobacteria like *Anabaena cylindrical* and *Thiocapsa roseopersicina* (*H. thermoluteolus* is, like *R. eutropha*, a protobacteria).[208]

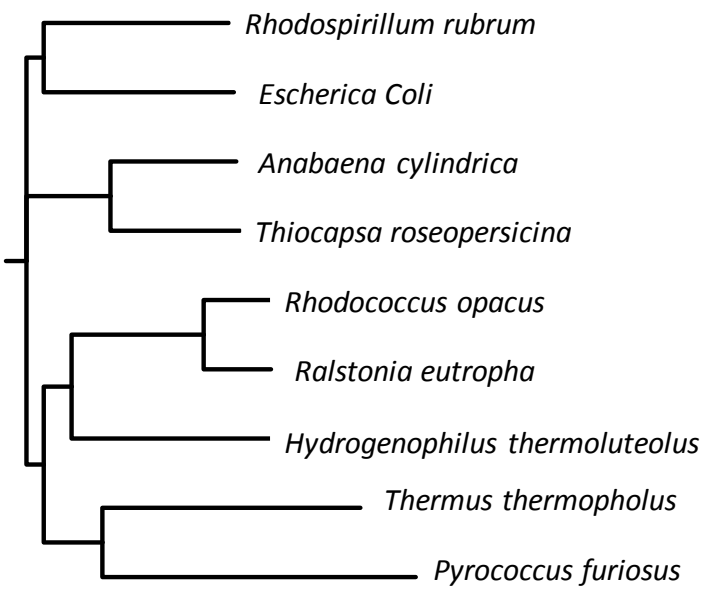

Figure 4-1: A simplified phylogenetic tree developed using the San Diego super computer biology workbench tool and the algorithm CrystalW.[210][211][212] **The tree depicts the closeness of the protein sequences of HoxF or equivalent sub-units found in each of the above organisms. Compared are: *Rhodospirillum rubrum* NADH-quinone oxidoreductase subunit F; Escherichia coli NADH-quinone oxidoreductase subunit F; *Anabaena cylindrica* NAD(P)$^+$-dependent nickel-iron dehydrogenase flavin-containing subunit; *Thiocapsa roseopersicina* Hox1F; *Rhodococcus opacus* NAD$^+$-reducing hydrogenase subunit alpha; *Ralstonia eutropha* HoxF; *Hydrogenophilus thermoluteolus* HoxF; Thermus thermophilus Nqo1; *Pyrococcus furiosus* cytochrome-c3 hydrogenase subunit gamma. Protein sequences were obtained from www.uniprot.org.**

The phylogenetic tree also suggests that the SH from *H. thermoluteolus* diverged evolutionarily before the SHs from *R. eutropha* and *Rh. opacus* did from one another. This may imply that the *H. thermoluteolus* SH is more ancient in origin, than the SHs from *R. eutropha* and *Rh. opacus.* This is common for many enzymes originating from thermophiles and thermophilicity is often thought to be a primitive trait characteristic of early life on earth, meaning that thermophile organisms are often found close to the root of phylogenetic trees.[213]

Figure 4-2 shows a sequence alignment for *R. eutropha* HoxF; *Rh. opacus* NAD$^+$-reducing sub-unit and *H. thermoluteolus* HoxF. The *R. eutropha* HoxF and *Rh. opacus* NAD$^+$-reducing sub-unit are very closely related showing 79 % sequence homology, whereas with *H. thermoluteolus* HoxF they show 38 % and 36 % respectively.

```
R. eutropha          MSGDIKAILERNGSERTRLIDILWDVQHLYG-HIPDEVLPQLADELNLSP
Rh. opacus           MDSRITTILERYRSDRTRLIDILWDVQHEYG-HIPDAVLPQLGAGLKLSP
H.thermoluteolus     ------MTTERQRTAPG-LLAALHQARSRFGRPLDAQALAELSTAFSLPP
                           **  :    *:  * :.:  :*  :   .*.:*.  :.*.*

R. eutropha          LDILETASFYHFFHRKPSGKYRIYLSDTVIAKMNGYQAVHDSLERETGAR
Rh. opacus           LDIRETASFYHFFLDKPSGKYRIYLCNSVIAKINGYQAVREALERETGIR
H.thermoluteolus     GEIAATASFYHFFQTPP-ARYQIHFVDHVVDHHAGVAALCNHLCAAFAIQ
                      :*  ********   * .:*:*:: : *: :  *  *: : *    . :

R. eutropha          FGGTDKTGMFGLFETPCIGLSDQEPAMLIDNVVFTRLRPGTIVDIITQLR
Rh. opacus           FGETDPNGMFGLFDTPCIGLSDQEPAMLIDKVVFTRLRPGKITDIIAQLK
H.thermoluteolus     PGQRTADARLFVGWTACAGLSDQAPAALINGRPMPRLDAARIDALIEKIQ
                      *     . : :  *.* ***** ** **:   :.** .. *  :* :::

R. eutropha          QGRSPEDIANPAGLPSDDVAYVDGVVESNVRTKGPVF-FRGLTDYGRLLE
Rh. opacus           QGRSPAEIANPAGLPSQDIAYVDAMVESNVRTKGPVF-FRGRTDLRSLLD
H.thermoluteolus     -----------AQIPMDQWPTEWFAVTNAIHRHGPLLTWLDTTPAEAVFE
                           * :* :: .     * . :: :**:: : . *    :::

R. eutropha          LCLALRPEQIIDRIIESKLRGRGGAGFSTGLKWQLCRTAVSDDKYIICNA
Rh. opacus           QCLLLKPEQVIETIVDSRLRGRGGAGFSTGLKWRLCRDAESEQKYVICNA
H.thermoluteolus     HPTAHDPDAILQAVTDAGLRGRGGAGFPTATKWRFCRENADPERFLICNA
                          *: ::: : :: *********.*. **::**   . ::::****

R. eutropha          DEGEPGTFKDRVLLTRSPKKVFMGMIIAARAIGSRNGILYLRWEYIYLKD
Rh. opacus           DEGEPGTFKDRVLLTRAPKKVFVGMVIAAYAIGCRKGIVYLRGEYFYLKD
H.thermoluteolus     DEGEPGTFKDRVLLTRYPEHLFAGMILAARAIGADKAILYLRYEYQYLLP
                     **************** *:::* **::** ***. :.*:*** ** **

R. eutropha          YLERQLQELRDEGLLGARIGGQSGFDFDIRIQMGAGAYICGDESALIESC
Rh. opacus           YLERQLQELREDGLLGRAIGGRAGFDFDIRIQMGAGAYICGDESALIESC
H.thermoluteolus     ----QLEAARER-IASAQATVPQAERVTLEIALGAGAYVCGEESALIESL
                         **:  *:  : .       .  . :.* :*****:**:*******

R. eutropha          EGKRGTPRVKPPFPVQEGYLGKPTCVNNVETFAAAARIMEEGPNWFRALG
Rh. opacus           EGKRGTPRVKPPFPVQQGYLGKPTSVNNVETFAAVSRIMEEGADWFRAMG
H.thermoluteolus     EGKPGRPRVRPPYPVTQGYLGHPTVVNNVETLVAVAAIVGNGAAWWRALG
                     *** * ***:**:** :****:** ******:.*.: *: :*. *:**:*

R. eutropha          TPESTGTRLLSVAGDCSRPGIYEVEWGVTLNEVLTTVGARDAR-AVQISG
Rh.  opacus          TPDSAGTRLLSVAGDCSKPGIYEVEWGVTLNEVLAMVGARDAR-AVQISG
H.thermoluteolus     TPDSSGPKLFCVSGDVAQPGLYEFPYGVALGDVVTAARPLGTRYAVQVSG
                     **:*:*.:*:.*:** ::**:**. :**:*.:*:: . . .:* ***:**

R. eutropha          PSGQCVSVAEDG-ERRMAYEDISCNGAFTIFNTERDLLEIVKDFMQFFVD
Rh. opacus           PSGECVSVAKDG-ERKLAYEDLSCNGAFTIFNCKRDLLEIVRDHMQFFVE
H.thermoluteolus     PSGTLLPATPEQLARPLAFEALPCNGTVMVFDVRRDPVAIVHHFARFFAH
                     ***  :..: :   * :*:* :.***:. :*: .** : **:.. :**..

R. eutropha          ESCGICVPCRVGNIDLHKKVELVIAGKACQKDLDDVVSWGALVKKTSRCG
Rh. opacus           ESCGICVPCRAGNVDLHRKVEWVIAGKACQKDLDDMVSWGALVRRTSRCG
H.thermoluteolus     ESCGFCTPCRVGTQLIAKTFEKIAAGYATRFDLERLAPALEAMRLASNCG
                     ****:*.***.*.  : :..* : ** * : **: :..    :: :*.**

R. eutropha          LGATSPNPILTTLDKFPEIYTKRLRKQKKEALLLSFDLDAALG------G
Rh. opacus           LGATSPKPILTTLEKFPEIYQNKLVRHEG-PLLPSFDLDTALG------G
H.thermoluteolus     FGLSAGNPVRDLIAHFRQQLEAQLQPHD---FIPAFSLDAELAATRRLTG
                     :* :: :*:   : :* :    :*  :.   :: :*.**: *.      *
```

```
R. eutropha          YEKALEGLAKEEIK----
Rh. opacus           YEKALKDLEEVTR-----
H.thermoluteolus     RDDPHAHLAQFEQPEVTR
                      :..    * :

                     Consensus key
                     * - single, fully conserved residue
                     : - conservation of strong groups
                     . - conservation of weak groups
                       - no consensus
```

Figure 4-2: Part of amino acid sequence comparison between subunits, HoxF from *H. thermoluteolus*, HoxF from *R. eutropha* SH and the NAD$^+$-reducing sub-domain from *Rh. opacus* using the ClustalW software.[210] The amino acid sequences were obtained from www.uniprot.org.

No full crystal structure has yet been published for an SH; although, the *H. thermoluteolus* SH has been successfully purified from native *H. thermoluteolus* and a crystal has been obtained.[209] From the phylogenetic tree in Figure 4-1 it is clear that the HoxF moiety from *R. eutropha* and the Nqo1 sub-unit of complex 1 from *Thermus thermophilus* are closely related. In fact, the Nqo1 sub-unit of *Thermus thermophilus* complex 1 shows 36 % sequence homology with the *R. eutropha* HoxF[164] Sazanov and co-workers have solved the crystal structure of the soluble domain (Nqo1) of *Thermus thermophilus* complex 1 with NADH bound.[214] Proteins with similar function tend to have conserved protein geometries at their active sites.[215] Therefore, the crystal structure of Nqo1 from *Thermus thermophilus* can be used as the basis for producing homology models of both the NAD$^+$ binding site of the SH from *R. eutropha* and from *H. thermoluteolus*.

From the resolved crystal structure of Nqo1 with NADH bound Sazanov and co-workers were able to identify the residues involved in the binding of NADH.[214] These residues are highlighted in Figure 4-3. Idris *et al*. have compared the positions of amino acid residues involved in binding in Nqo1 and *R. eutropha* HoxF, this work adds *H. thermoluteolus* HoxF to this sequence comparison.[164] The residues highlighted in yellow indicate occasions when these amino acids are conserved in the binding site of *Thermus thermophilus* Complex 1 (Nqo1), *R. eutropha* HoxF and *H. thermoluteolus*

HoxF. The residues highlighted in blue indicate that residues are conserved between two of the species.

```
H. thermoluteolus       HPTAHDPDAILQAVTDAGLRGRGGAGFPTATKWRFCRENADPERFLICNA 230
R. eutropha             QCLLLKPEQVIETIVDSRLRGRGGAGFSTGLKWRLCRDAESEQKYVICNA 248
T. thermophilus         EKT---PDEVIEEVKRSGLRGRGGAGFPTGLKWSFMPKDDGKQHYLICNA 73

H. thermoluteolus       DEGEPGTFKDRVLLTRYPEHLFAGMILAARAIGADKAILYLRYEYQYLLP 280
R. eutropha             DEGEPGTFKDRVLLTRAPKKVFVGMVIAAYAIGCRKGIVYLRGEYFYLKD 298
T. thermophilus         DESEPGSFKDRYILEDVPHLLIEGMILAGYAIRATVGYIYVRGEYRRAAD 123

H. thermoluteolus       ----QLEAARERIASAQATVPQAER-VTLEIALGAGAYVCGEESALIESL 325
R. eutropha             YLERQLQELREDGLLGRAIGGRAGFDFDIRIQMGAGAYICGDESALIESC 348
T. thermophilus         RLEQAIKEARARGYLGKNLFG-TDFSFDLHVHRGAGAYICGEETALMNSL 173

H. thermoluteolus       EGKPGRPRVRPPYPVTQGYLGHPTVVNNVETLVAVAAIVGNGAAWWRALG 375
R. eutropha             EGKRGTPRVKPPFPVQQGYLGKPTSVNNVETFAAVSRIMEEGADWFRAMG 398
T. thermophilus         EGLRANPRLKPPFPAQSGLWGKPTTINNVETLASVVPIMERGADWFAQMG 223
```

Figure 4-3: Part of the amino acid sequence comparison between the HoxF sub-unit of *H. thermoluteolus*, *R. eutropha* HoxF and *T. thermophilus* Nqo1. Analysis was performed using the ClustalW algorithm using the San Diego super computer workbench software.[210] The amino acid sequences were obtained from www.uniprot.org. Letters highlighted in yellow show residues involved in the binding of NADH in Complex 1 conserved in all three proteins. The residues highlighted in blue show residues involved in the binding of NADH conserved in Complex 1 and only one of the other proteins.

It is clear that most of the residues involved in binding of NADH are conserved between *Thermus thermophilus* Nqo1 and *H. thermoluteolus* HoxF. On the occasions when residues are not conserved (these are *Thermus thermophilus* Nqo1 Lysine 202 and Phenyl alanine 205) in the *H. thermoluteolus* HoxF the Lysine is replaced by a similarly positively charged arginine at position 339 and the phenyl alanine at position 342 is replaced by a tyrosine (which has a very similar structure to phenyl alanine, but just contains an OH group on the phenyl ring). This suggests that the binding mode of the NAD^+ in all three of these proteins is very similar.

4.3 Biochemical characterisation of the whole HoxHYFU enzyme from *H. thermoluteolus*

I spent two months at the TU in Berlin working in the group of Dr Oliver Lenz with Dr L. Lauterbach on the expression and characterisation of the SH from H. thermoluteolus. The biochemical characterisation work in this section was carried out there.

This section looks at using biochemical techniques to characterise the whole SH (HoxHYFU) from *H. thermoluteolus.* The procedures used in this chapter are detailed in the Methods and Theory chapter, section 2.2.

Dr L. Lauterbach from the group of Dr O. Lenz in Berlin has heterologously expressed the SH from *H. thermoluteolus* in *R. eutropha.* Despite *E. coli* being a more commonly used heterologous host organism, *R. eutropha* possesses a series of maturation proteins to allow it to successfully assemble a functional SH.[216] A strep affinity tag was added to allow purification of the whole SH (HoxHYFU).

In this work, *R. eutropha* cultures were grown at 30 ^{o}C in minimal media containing fructose (as described in Methods and Theory chapter and the appendix). The cells were harvested *via* centrifugation and re-suspended in 50 mM phosphate buffer pH 8 containing 5% glycerol. Protein isolation and purification was carried out as described in the Methods and Theory chapter. The concentration of the protein was determined *via* a Bicinchoninic acid assay using a 96 well plate reader, measuring the absorption at 562 nm following the procedure of Laemmli *et al*.[137] SDS-PAGE (Sodium dodecyl sulphate polyacrylamide gel electrophoresis) was further used to determine the molecular weight of the sub-units of the SH present in the eluted fractions.[217]

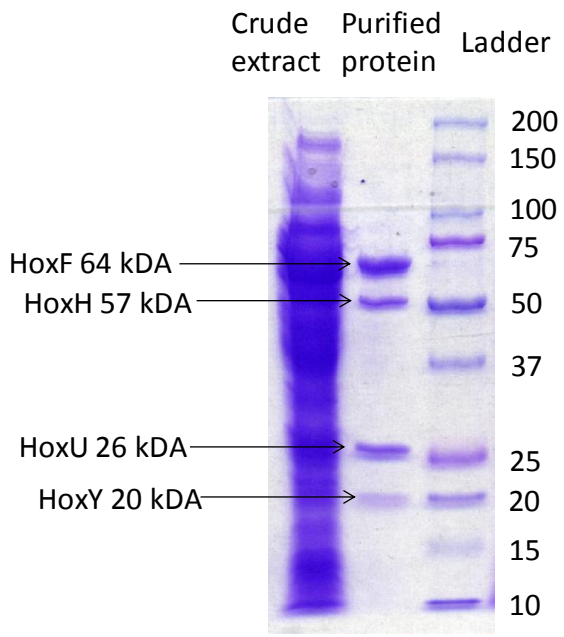

Figure 4-4: An SDS PAGE gel showing the presence of bands at the correct molecular weights for each of the hydrogenase sub-units comprising HoxHYFU, based on the protein sequence from www.uniprot.org using the 'Protein Molecular Weight calculator' function.[218]

The SDS PAGE (Sodium dodecyl sulphate polyacrylamide gel electrophoresis) gel in Figure 4-4 shows bands at the expected molecular weights (determined from the protein sequence) corresponding to all of the sub-units present in the *H. thermoluteolus* SH (HoxHYFU).

It was then important to determine the specific activity of this protein to ensure that it is active. On the day of purification a specific activity of 0.47 U mg^{-1} was recorded, at 30 ^{o}C in 50 mM H_2-saturated Tris-HCl pH 8 containing 1 mM NAD^+. This activity is relatively low in comparison to the SH from *R. eutropha*, which often shows activities of >54 U mg^{-1}.[109] However, this may be due to the purification procedure not yet being optimised for this enzyme.

4.3.1 Investigating the temperature dependence of the SH from *H. thermoluteolus*

The optimum temperature for operation of the SH from *H. thermoluteolus* may differ from that of mesophilic SH enzymes (e.g. those from closely related *R. eutropha* and

Rh. opacus). The activity of the SH was therefore assayed at temperatures between 30 °C and 70 °C in order to determine the temperatures at which this SH displays the highest specific activity.

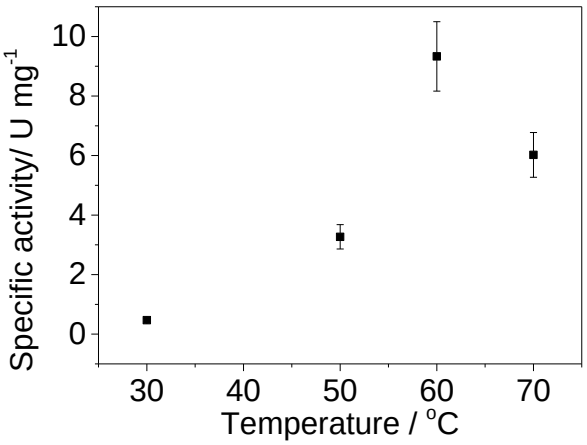

Figure 4-5: Specific activity of the HoxHYFU protein at temperatures between 30 and 70 °C. The activity was tested by following the increase in absorption of NADH at 340 nm in a 2 mL cuvette containing H_2-saturated 50 mM Tris-HCl buffer pH 8 with 1 mM NAD^+. The reaction was in each case started by the addition of 4.5 µg of enzyme and the activity gradient was followed over a 30 minute period. Error bars are set at 12.5 % based on data for repeat readings at 60 °C.

It is clear from data in Figure 4-5 that the optimum temperature for H_2-driven NADH production is around 60 °C. However, relatively high activity is still seen even at 70 °C. Enzymes harvested from thermophiles are often optimally active close to the host organism's optimal growth temperature (here 50 °C to 52 °C).[208,219] This is a clear initial demonstration that this enzyme may be useful in biotechnology for high temperature cofactor recycling applications.[11] This contrasts with the *R. eutropha* SH for which the temperature at which the highest specific activity is observed has been reported as 33 °C.[113]

4.3.2 Investigating the activity of individual components of the SH from *H. thermoluteolus*

It is possible to assay the activity of the 2 catalytic moieties (HoxFU and HoxHY) of the SH (HoxHYFU) individually, while they are linked together in the whole SH.

However, artificial electron acceptors must be used. The activity of the HoxFU moiety can be assayed by following the NADH driven reduction of benzyl viologen at 578 nm (see section 2.2.4) and the activity of the HoxHY moiety can be determined by following the H_2-driven reduction of MV at 605 nm (see section 2.2.4).

Data in Table 4-1 show that much higher specific activities were observed for the individual diaphorase and hydrogenase moieties, in these mediated assays than for H_2-driven NAD^+ reduction using the whole SH. However, it should be noted that the binding site of the mediators used remains uncertain.[220] Consequently, the specific activity values recorded here may not be easily replicated in bio-catalytic reactions. Nevertheless, as much greater specific activities are observed for the reactions of each component moiety than for the activity of the whole enzyme (H_2-driven NAD^+ reduction), it appears that the whole SH may be dissociating into its component catalytic moieties (HoxHY and HoxFU) during purification.

Table 4-1: The specific activities of the whole HoxHYFU hydrogenase enzyme compared to the specific activities of the component HoxFU and HoxHY moieties.

Portion being tested	Test	Specific activity/ U mg^{-1}
HoxHYFU	H_2 -> NADH	0.27
Diaphorase	NADH -> BV	61
Hydrogenase	H_2 -> MV	39

These activity assays were carried out at 60 ^oC, after snap-freezing the enzyme. For H_2 driven NAD^+ reduction a 2 mL cuvette containing H_2-saturated Tris-HCl buffer pH 8 with 2 mM NAD^+ and 10 µM FMN, along with 50 µM $NiCl_2$ and 5 mM $MgCl_2$. The reaction was started with 2.5µg enzyme. Conditions for NADH driven benzyl viologen reduction: 50 mM Tris-HCl pH 8 (N_2 saturated), 2 mM NADH, 5 mM Benzyl viologen (oxidized), 90 µM dithionite and the reaction was started with 2.5µg enzyme. Dihydrogen-driven methyl viologen reduction 5 mM methyl viologen was added to a 2 mL cuvette containing H_2-saturated Tris-HCl buffer pH 8 and started with 2.5µg of enzyme. Further details of the experimental methods are given in the Methods and Theory chapter.

Such a large discrepancy between the specific activity for the component SH moieties and the whole SH is not seen for *R. eutropha*,[113] consequently this was further investigated using size exclusion chromatography (FPLC: Fast protein liquid chromatography) following the protocol described in the review by Barth *et al*.[221] This

technique separates molecules, in this case proteins, by their size. The procedure was carried out using a Superfix column with buffers 50 mM Tris-HCl pH 8 and 100 mM KCl. A salt gradient was used to determine whether it is possible to separate the HoxHY proportion (77 kDa) of the SH from the HoxFU portion (90 kDa).

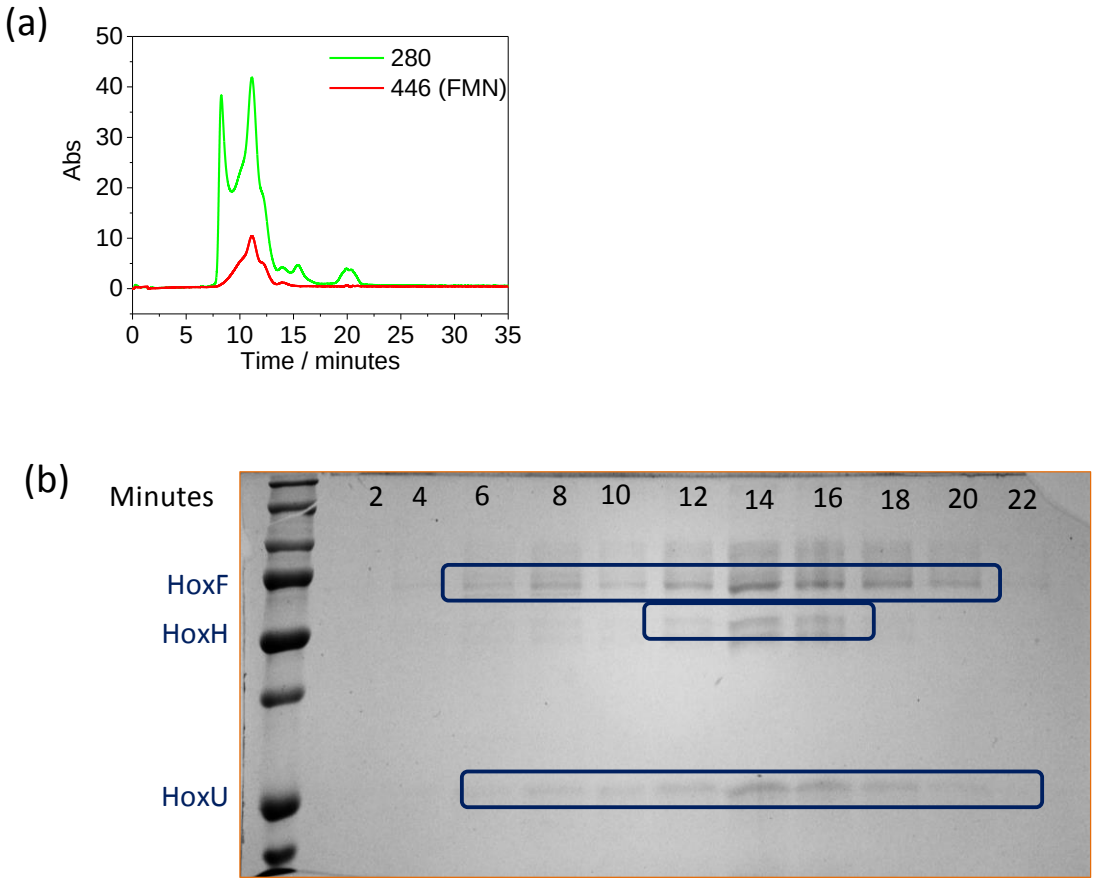

Figure 4-6: Size exclusion experiments to determine whether the HoxFU and HoxHY sub-units of the *H. thermoluteolus* easily dissociate. (a) A graph showing the absorption of fractions obtained after the strep column. Absorption at 280 nm suggests protein is eluting and absorption at 446 nm suggests FMN (either bound in the protein or not) is eluting. (b) SDS PAGE gel with each of the fractions following size exclusion chromatography. Numbers at the top correspond to minutes after being added to the column. This experiment was performed with the assistance of Dr Stefan Frielingsdorf from the group of Oliver Lenz at the TU Berlin.

The trace in green in Figure 4-6 (a), shows absorption at 280 nm which correlates with elution of protein. In contrast, the trace in orange shows absorption at 446 nm indicating elution of Flavin Mononucleotide (FMN). The green trace shows two peaks suggesting that the protein is eluting at two different points, only one of which contains an FMN

peak, likely to correspond to the FMN which is tightly bound at the active site of the HoxFU portion of the SH.

Each of the fractions, for which UV absorbance at 280 nm was observed, was then added to an SDS PAGE gel, which is shown in Figure 4-6 (b), to investigate the composition of each of the eluted fractions. The SDS PAGE gel in Figure 4-6 (b) is not conclusive. It appears that in bands 6 to 20 some trace of HoxFU is observed. HoxHY in contrast is only observed in the bands 12, 14 and 16 (HoxY is not easily visible on the gel). This suggests that non-stoichiometric amounts of HoxFU and HoxHY of the *H. thermoluteolus* SH are being produced by the *R. eutropha* heterologous host.

4.3.3 Investigating the O_2 tolerance of the SH from *H. thermoluteolus*

The SH from *R. eutropha* is O_2 tolerant, retaining 100 % of its H_2-driven NAD^+ reduction activity in the presence of an atmospheric concentration of O_2.[113][127] It was of interest to investigate whether the SH from *H. thermoluteolus* displays the same degree of O_2 tolerance as the SH from *R. eutropha*, particularly as the *H. thermoluteolus* SH shows relatively high sequence homology with the *R. eutropha* SH, as demonstrated by the sequence alignment in Figure 4-2.

The experiments in Table 4-2 were carried out by mixing H_2-saturated and O_2-saturated buffers. Data in Table 4-2 demonstrate that the SH from *H. thermoluteolus* exhibits no inhibition at 10 % O_2 concentration and only a slight decrease in specific activity is observed at 20 % O_2 concentration.

Table 4-2: The O_2 tolerance of HoxHYFU from *H. thermoluteolus*.

Percentage O_2	Activity (U mg^{-1})
0 % O_2	32 ± 4
10 % O_2	36 ± 0.7
20 % O_2	26 ± 5

Experiment conducted in a mixture of O_2/H_2 saturated 50 mM Tris-HCl buffer at pH 8 containing 2 mM NAD^+ and 10 µM FMN. Along with 0.5 mM $NiCl_2$ and 5 mM $MgCl_2$. All measurements were taken at 60 ^oC. Experiments used 4.5 µg SH in a 2mL reaction volume. Experiments were carried out following the protocol of Shäffer *et al.* for determining O_2-tolerance.[222]

This again suggests that the SH from *H. thermoluteolus* may be useful in a range of cofactor recycling applications, particularly if this enzyme is employed in tandem with an enzyme which requires O_2 as a substrate, for example P450 mono-oxygenase enzymes. P450 mono-oxygenases have wide ranging applications for the insertion of an oxygen atom into an unfunctionalised C-H bond in an extensive range of hydrocarbon substrates.[223] Although, these enzymes catalyse an oxidative insertion reaction, they require the reduced cofactor NAD(P)H to reduce O_2 to O^-. Recently these enzymes have been used in the industrial production of a range of flavour compounds.[224]

4.3.4 Affinity constant determination for the whole SH from *H. thermoluteolus*

The K_M value is the substrate concentration at which the rate is half of the maximum possible rate; an overview of the derivation of K_M is shown in the Methods and Theory chapter, section 2.3.4.1. An important factor in biocatalysis is the relationship between the activity of the enzyme and the substrate concentration. This is particularly important for a cofactor recycling enzyme, because as the nicotinamide cofactor is expensive it is desirable to use as low a concentration of cofactor as possible. Consequently, a low affinity constant is desirable. In general a concentration of at least $5 \times K_M$ of substrate is used in biocatalysis to ensure that enzymes function at their maximum rate.[225]

The K_M for NAD^+ reduction was determined using the H_2-driven activity assays, as described in section 2.2.4 of the Methods and Theory section, at various NAD^+ concentrations. The rate of reaction was monitored by following absorbance at 365 nm.

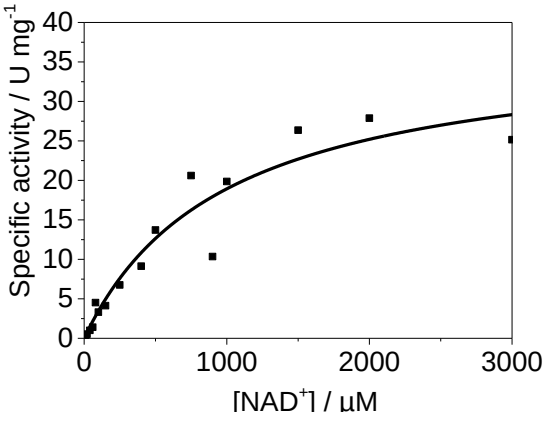

Figure 4-7: A Michaelis-Menten plot used to determine the K_M of the whole SH towards NAD^+ reduction. This experiment was carried out at 60 °C in 2 mL of H_2-saturated 50 mM Tris-HCl pH 8.0, with 0.5 mM $NiCl_2$ and 5 mM $MgCl_2$ in a 3 mL cuvette sealed with a rubber bung. The concentration of NAD^+ was increased with each run and each run was started by injecting 4.5 µg of enzyme.

From data in Figure 4-7, the Michaelis constant for this enzyme was determined to be 990 µM, this is slightly larger than that for the SH from *R. eutropha* which has a K_M value of 560 µM. However, these K_M values both have the same order of magnitude.

4.4 Biochemical characterisation of the HoxFU moiety from *H. thermoluteolus*

This section looks at using biochemical techniques to characterise the diaphorase (HoxFU) portion of the SH, this is carried out by following the NADH driven reduction of benzyl viologen, the method used for this assay is shown in more detail in the Methods and Theory chapter, section 2.2.4.

Dr L. Lauterbach *et al*. have already shown that is possible to use molecular biological strategies to separate the HoxFU moiety from the HoxHY moiety in *R. eutropha*.[102,131]

To produce just the *H. thermoluteolus* HoxFU a plasmid containing the genetic

information expressing the *H. thermoluteolus* HoxFU moiety along with the appropriate promotor genes was provided by Dr L. Lauterbach.

The plasmid was brought into *E. coli* cells using a heat shock protocol detailed in Appendix A.[133] The spot mating technique was then used to transfer the plasmid from the E. coli cells into *R. eutropha* (the heterologous host).[134,135] Cell cultures of *R. eutropha* containing the plasmid for overexpression of the *H. thermoluteolus* HoxFU moiety were grown according to the method of Schwartz *et al*.[226] Purification was carried out as described in Appendix A.

After Strep-affinity column purification an SDS PAGE gel shown in Figure 4-8 was used to determine that subunits of the expected size had been produced. This gel shows bands at molecular weights of 64 kDa and 26 kDa corresponding to the HoxF and HoxU fragments respectively.

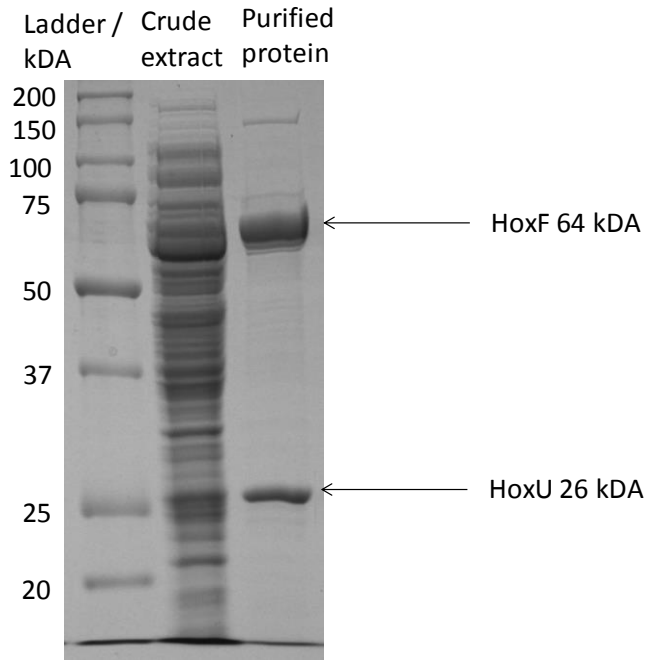

Figure 4-8: SDS PAGE gel showing bands at the correct molecular weights for HoxFU. This suggests that the correct enzyme fragment has been produced. The molecular weights of each of the bands in the ladder are given on the left hand side of the gel.

The specific activity of the HoxFU fragment was tested at 30 ^{o}C, in order to allow easy comparison to the biochemical characterisation data for *R. eutropha* HoxFU.[102] The activity of the HoxFU moiety was assayed by following the NADH driven reduction of benzyl viologen. This gave a value of 2.2 U mg^{-1}; this is low in comparison to the values obtained for the HoxFU fragment from *R. eutropha*, where 59 U mg^{-1} have been observed.[227] No activity could be determined for the HoxFU fragment towards the phosphorylated NADH derivative NADPH in short activity assays. This strong specificity for a particular nicotinamide cofactor was also observed by Schneider and Schlegel for the *R. eutropha* SH and it is now known that the *R. eutropha* HoxFU has a K_M for NADP$^+$ of 8 mM.[164,228]

4.4.1 Temperature optimum determination for the *H. thermoluteolus* HoxFU

The option temperature for the whole *H. thermoluteolus* SH has been determined to be around 60 °C, see section 4.3.1. As the optimum specific activity for the HoxFU moiety may be seen at a different temperature a temperature optimum determination was carried out for just the HoxFU moiety.

Data in Figure 4-9 show that this enzyme fragment shows optimum activity at around 60 ^{o}C, which is similar to the value obtained for the whole SH. This assay however is based solely on short (<60 minute) activity assays and consequently does not report on longer-term stability of the HoxFU moiety under these conditions.

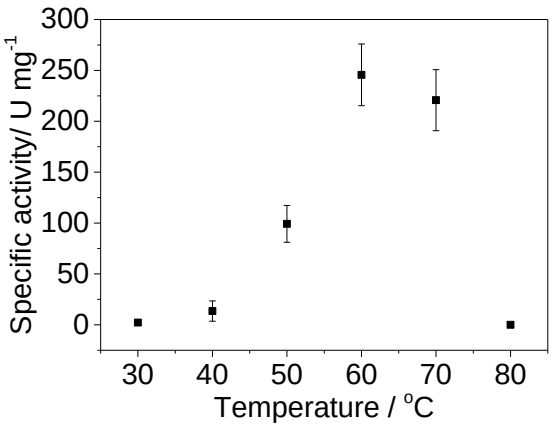

Figure 4-9: A graph demonstrating the specific activity of the HoxFU moiety towards NADH-driven benzyl viologen reduction at a range of different temperatures. The reaction was carried out in a 2 mL cuvette containing 50 mM Tris-HCl pH 8.0 (N_2 saturated) titrated to pH 8.0 at each temperature, 2 mM NADH, 5 mM benzyl viologen (oxidized) and 90 µM dithionite. A protein aliquot of 4.5 µg was used in each assay to start the reaction. Error bars are based on one standard deviation of 3 repeats.

The activity of the *H. thermoluteolus* HoxFU moiety is 245 U mg^{-1} at 60 °C, which is 100 times greater than the specific activity at 30 °C (2.2 U mg^{-1}) and ca. 5 times higher than the highest specific activity observed for the whole SH (section 4.3). The higher specific activity observed for the HoxFU moiety could mean that better activities could be obtained for this enzyme on an electrode, or on the enzyme-modified particles (introduced in the introduction) than for the whole SH.

4.4.2 pH optimum determination for the HoxFU moiety

Schlegel *et al*. report that the optimum pH for the SH from *R. eutropha* is pH 8.[109] Similarly the pH optimum of the SH from *Rh. opacus* is between 7.8-8.0, in the presence of Ni^{2+} ions. In the absence of Ni^{2+} no activity is recorded above pH 7.[228]

The pH optimum for NADH driven benzyl viologen reduction was determined at 60 °C using a mixed buffer system, details of the composition of which are given in the Methods and Theory chapter, section 2.6.2. Using a mixed buffer means that the same buffer can be used for all pH values tested, so that there is not a large variation in buffer composition over the pH range tested.

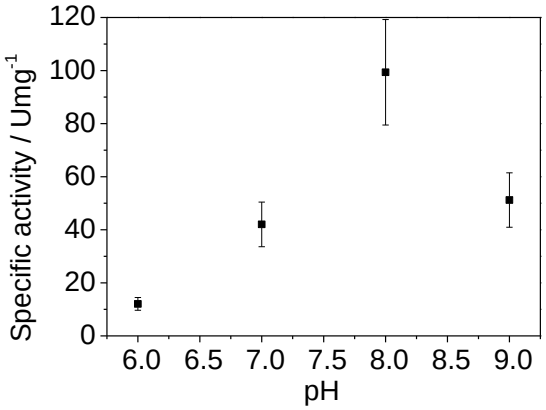

Figure 4-10: The specific activity of the HoxFU moiety at pH values between 6.0 and 9.0. This experiment was conducted in 2 mL sealed cuvettes containing 50 mM N_2 saturated mixed buffer (see Methods and Theory section) at 60 °C. Benzyl-viologen and dithionite were added to each cuvette to give a concentration of 5 mM and 90 µM respectively and the reaction was started with 6 µg of enzyme.

Data in Figure 4-10 show that the HoxFU moiety in solution was most active at pH 8.0. This is the same as the pH optimum for the whole SH and for the whole SH from *R. eutropha*. However, the HoxFU moiety from *R. eutropha* shows a pH optimum at pH 10.0; although, it loses activity after 30 seconds at this non-physiological pH.[102] *H. thermoluteolus* is a soil bacterium, so its optimum growth pH is around neutral, implying that the SH is likely to be most active around a neutral pH.[208]

4.4.3 Affinity constant determination for the HoxFU moiety from *H. thermoluteolus*

The K_M of the HoxFU fragment for NADH reduction was determined using NADH driven benzyl viologen activity assays, as described in section 2.2.4 of the Methods and Theory section, at various NADH concentrations. The rate of reaction was monitored by following the absorbance at 578 nm. The K_M of the HoxFU fragment for NADH reduction is important as the HoxFU moiety can be used on its own in applications such as electrochemical NAD^+ recycling or as part of the enzyme-modified particles. Determining this value in solution also allows comparison with the HoxFU moiety from

R. eutropha and comparison between the K_M values determined electrochemically later in this chapter.

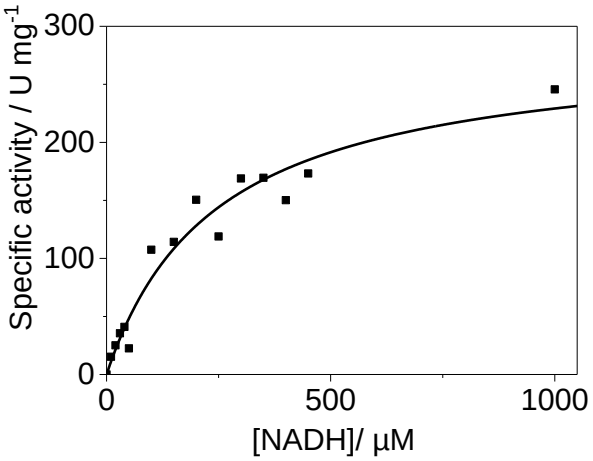

Figure 4-11: A Michaelis-Menten plot used to determine the K_M for HoxFU from *H. thermoluteolus* for NADH using benzyl viologen as an electron acceptor. The experiment was conducted in 2 mL sealed cuvettes containing 50 mM N_2 saturated Tris-HCl pH 8 at 30 °C. A concentration of 5 mM Benzyl-viologen and 90 µM dithionite was added to each cuvette and the reaction was started with 6 µg of enzyme.

The K_M was determined to be 245 µM, again higher than the value for *R. eutropha* HoxFU (56 µM): a plot of the Michaelis-Menten curve used to determine the K_M value is shown in Figure 4-11.[102]

4.5 Electrochemical characterisation of the HoxFU moiety from *H. thermoluteolus*

This section describes an electrochemical characterisation of the HoxFU moiety of the SH from *H. thermoluteolus.* A range of HoxFU moieties have already been characterised electrochemically.[102][111] Electrochemical characterisation is useful as it avoids the use of soluble artificial electron donors/acceptors, which are often unreliable and cannot easily be used to test the activity of the HoxFU fragment in both catalytic directions.[102] Furthermore, it more closely approximates the conditions under which the enzymes would be operating when immobilised onto carbon particles. During electrochemical characterisation of the HoxFU moiety the enzyme was immobilised on

a pyrolytic graphite edge electrode, and electrons were passed directly from an electrical circuit to the enzyme. The HoxFU moiety from *R. eutropha* possesses four FeS clusters, which electrically connect the buried FMN active site to the surface of the protein.[102,155] Preliminary crystallographic studies by Taketa *et al.* have demonstrated that the SH from *H. thermoluteolus* also possesses the same number of FeS clusters as the *R. eutropha* SH.[209]

The protocols for the electrochemical testing of the *H. thermoluteolus* HoxFU moiety follow those of Idris *et al.* and more details are given in the Methods and Theory chapter section 2.3.[102] Throughout most of this electrochemical characterisation section purified NADH was used. This is because 'as purchased' NADH contains trace impurities of NAD^+ and electrochemistry is able to detect minute quantities of NAD^+. The method of NADH purification is described in the Methods and Theory Chapter, section 2.6.3.

4.5.1 Electrocatalytic cyclic voltammograms for *H. thermoluteolus* HoxFU at 30 °C

To confirm that the HoxFU moiety from *H. thermoluteolus* is able to exchange electrons directly with a PGE RDE (Pyrolytic graphite edge rotating disc electrode), cyclic voltammetry experiments were performed, initially at 30 °C, following the same protocol as Idris *et al*. to allow easy comparison with data from *R. eutropha*.[102] A 0.5 μg aliquot of enzyme was spotted onto the PGE RDE and allowed to dry for approximately 30 seconds. The electrode was subsequently placed in an electrochemical cell with buffer containing cofactor in it. The potential was then swept from a region at which no catalytic activity would be expected to a region at which oxidation or reduction of the cofactor would be expected to occur.

The CVs shown in Figure 4-12 demonstrate that the HoxFU portion of the SH from *H. thermoluteolus* is able to exchange electrons with a PGE RDE, as shown already for *R. eutropha* and *Rh. opacus*.[102][103] The current observed in a CV (Cyclic Voltammogram) is proportional to the activity of the enzyme film on the electrode at that potential. Therefore, in Figure 4-12 (a) as the potential is swept to a more negative value the current increases, demonstrating an increase in the rate of NAD^+ reduction at the electrode.

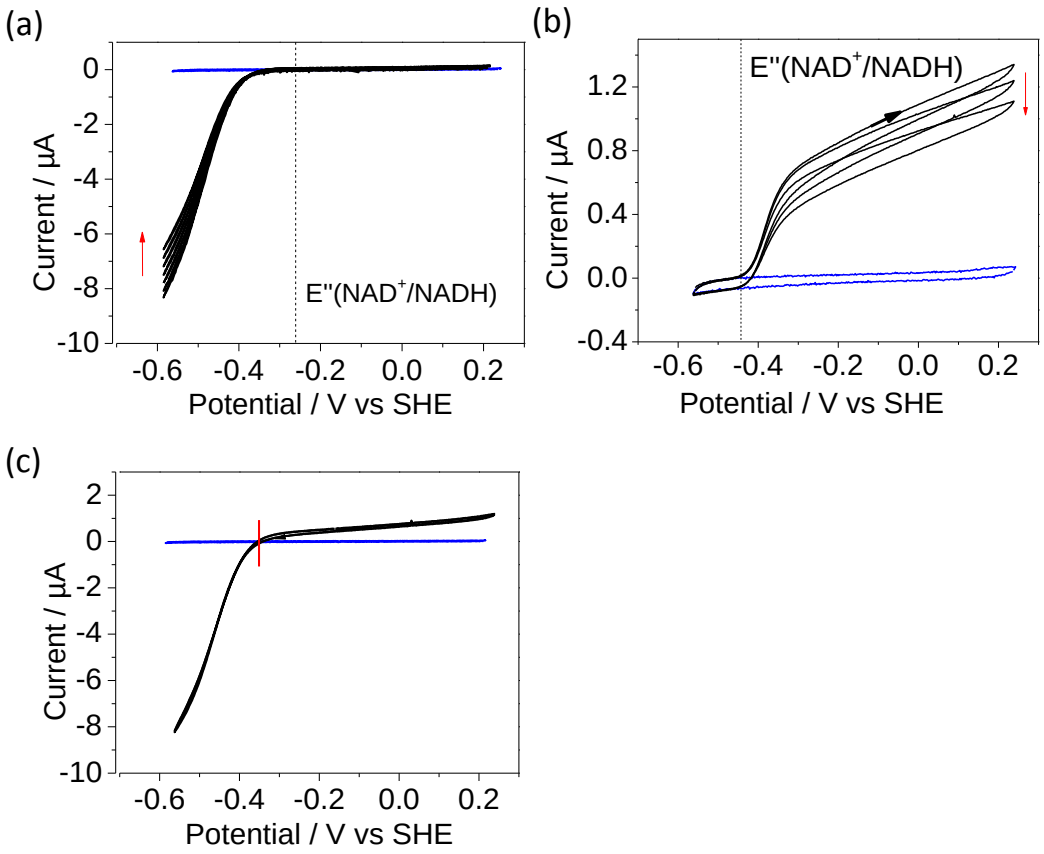

Figure 4-12: (a) CVs for an electrode modified with HoxFU showing catalysis of (a) NAD^+ reduction and (b) NADH oxidation. The electrochemical cell contained (a) 1 mM NAD^+ and (b) 1 mM NADH (c) 1 mM NADH and 1 mM NAD^+. The red line in this scan indicates the potential at which the CV crosses the blank. Experiments were performed in 50 mM Tris-HCl pH 8 at 30 °C. A scan rate of 10 mV s^{-1} was used and the electrode was rotated at 2000 rpm. In each case a scan with an unmodified electrode, without HoxFU immobilised (blank), is shown in blue. Black arrows indicate the direction of the scan. Red arrows indicated subsequent scans in this direction.

The CVs demonstrate the onset of reduction of NAD^+ at close to -280 mV *vs* SHE, and NADH oxidation at -450 mV *vs* SHE: the same as the values observed for HoxFU from

R. eutropha.[102] These values are close to the expected thermodynamic values: for example the thermodynamic couple for NAD^+/NADH at pH 8 in a ratio of 1000:1 NAD^+ to NADH is -261 mV *vs* SHE and -443 mV *vs* SHE for a ratio of 1000:1 NADH to NAD^+; which are shown on the CVs in Figure 4-12 (a and b) as dotted lines.

Figure 4-12 (c) shows a CV at 30 ^oC in 1 mM NADH and 1 mM NAD^+. This cuts the axis at around -350 mV *vs* SHE (shown by the red line) exactly at the thermodynamic potential for this reaction at pH 8. This clearly demonstrates that the *H. thermoluteolus* HoxFU is a thermodynamically efficient catalyst catalysing oxidation of NAD^+ and reduction of NADH exactly at the thermodynamic potential for this reaction.

4.5.2 Electrocatalytic cyclic voltammograms for *H. thermoluteolus* HoxFU at 60 ^oC

Protein film electrochemistry allows a continual 'read out' of the activity of an enzyme immobilised on the electrode under constant conditions, unlike the biochemical assays. This means that it is possible to use electrochemical methods to get an idea of the stability of an enzyme.

The cyclic voltammograms in Figure 4-13 demonstrate that the HoxFU moiety from *H. thermoluteolus* is able to exchange electrons with a PGE RDE at 60 ^oC. Figure 4-13 (a) shows NAD^+ reduction, with an onset potential of around -300 mV *vs* SHE at pH 8 and Figure 4-13 (b) demonstrates NADH oxidation with an onset potential of -450 mV *vs* SHE at pH 8, the same as the values seen at 30 ^oC.

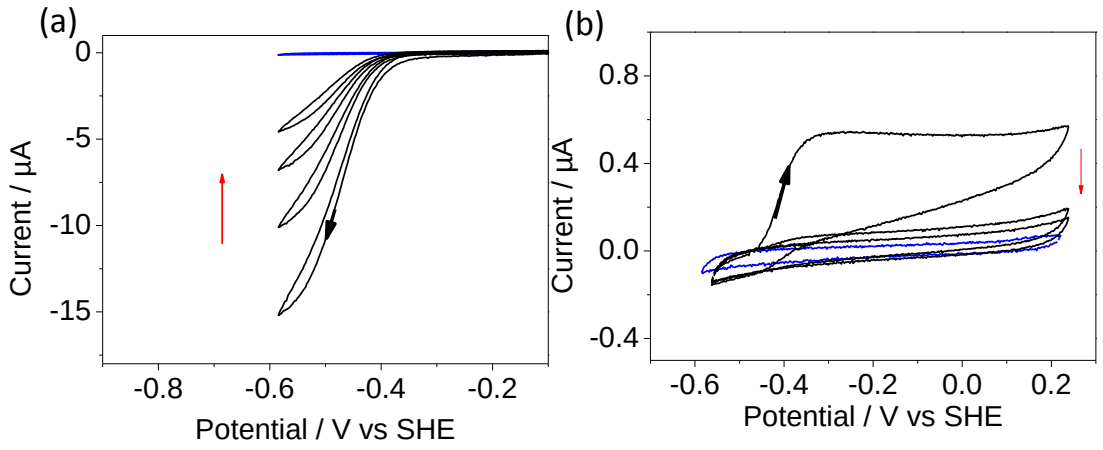

Figure 4-13: (a) Cyclic voltammograms for an electrode modified with HoxFU showing catalysis of (a) NAD^+ reduction and (b) NADH oxidation. The electrochemical cell contained (a) 1 mM NAD^+ and (b) 1 mM NADH. Experiments were performed in 50 mM Tris-HCl pH 8 at 60 ^oC. A scan rate of 10 mV s^{-1} was used and the electrode was rotated at 2000 rpm. In each case the unmodified electrode (blank) scan is shown in blue. Black arrows indicate the direction of the scan. Red arrows indicated subsequent scans in this direction.

The catalytic waves at 30 ^oC (Figure 4-12) and 60 ^oC (Figure 4-13) are very different. The maximum current for NAD^+-reduction is significantly higher at 60 ^oC than that seen in at 30 ^oC; however, this could be simply a result of variation between different enzyme films. For the CVs at 60 ^oC, we see a large drop in current between subsequent scans. This is much less pronounced for scans at 30 ^oC, where there is less difference between the maximum current between subsequent CVs. A variety of factors may be contributing to the decrease in activity. This could be a result of greater enzyme instability (faster inactivation or denaturation) at 60 ^oC. Alternatively, this may be a result of the phenomenon 'film loss' occurring between subsequent scans due to enzyme desorbing from the electrode or re-positioning of some of the enzyme from an active to in-active orientation on the electrode surface.[229] These two different contributions to loss of catalytic current cannot easily be separated and it is not possible to obtain a quantitative measure of the enzyme stability on an electrode just using CVs.

4.5.3 Electrochemical half-life determination of the HoxFU moiety

To obtain a quantitative measure of the stability of the *H. thermoluteolus* HoxFU at a number of different temperatures, the half-life of the enzyme during electro-catalytic NAD^+ reduction or NADH oxidation was investigated on a PGE RDE using chronoamperometry (a technique in which the electrode is held at a constant potential). A 0.5 μg aliquot of enzyme was spotted onto the PGE RDE and allowed to dry for approximately 30 seconds. The electrode was subsequently placed in an electrochemical cell with buffer containing cofactor in it. The electrode was held at -410 mV *vs* SHE for NAD^+ reduction or -160 mV *vs* SHE for NADH oxidation, in a solution of cofactor (1 mM), with rotation at 2000 rpm. The electrode was held at the required potential for 10 s before beginning the measurement. The half-life was determined by fitting an exponential decay function to the chronoamperometry trace obtained following the experiment. Data in Table 4-3 show that the half-life of the HoxFU from *H. thermoluteolus* for NAD^+ reduction does decrease with increasing temperature, as suggested by the data from the CVs above. A decrease in stability with increasing temperature is generally seen for most enzymes.[230] Interestingly the half-life for NADH oxidation is approximately half of that observed for NAD^+ reduction at 30 ^oC, suggesting that this SH is less stable when acting in the oxidation direction or at high potential.

The decrease in stability of the enzyme film as the temperature increases could be due to faster denaturation of the enzyme. However, there may also be contributions from film loss: the enzyme desorbing from the electrode or moving into an inactive configuration (discussed in section 4.5.2). It is difficult to separate these two contributions when assessing the stability of an enzyme on a PGE RDE.

Table 4-3: Table showing the half-life of the *H. thermoluteolus* HoxFU moiety on a PGE RDE.

Organism	***H. thermoluteolus***		***R. eutropha***	
Temperature / ^{o}C	Half-life for NAD^+ reduction / minutes	Half-life for NADH oxidation / minutes	Half-life for NAD^+ reduction / minutes	Half-life for NADH oxidation / minutes
22	ND	ND	21	ND
30	51	33	ND	ND
40	19	ND	ND	ND
60	6	ND	ND	ND

The electrode was rotated at 2000 rpm in 1 mM solutions of cofactors. For NAD^+ reduction the electrode was held at -410 mV *vs* SHE, for NADH oxidation the potential was held at -159 mV *vs* SHE. Data for *R. eutropha* determined by Dr H. Reeve[103] ND = not determined. To determine the half-life the chronoamperometry trace was fitted with the following equation $y=y_o+Ae^{-x/\tau}$, where y_o is the y offset of the trace, A is the amplitude at time zero and τ is the time constant. Multiplying τ by the natural logarithm to the base 2 returns the value of the half-life $t_{1/2}$.

Although, the highest activity of the *H. thermoluteolus* HoxFU is observed at 60 ^{o}C, this result shows instability at these elevated temperatures might preclude its use in biotechnological applications at 60 ^{o}C.

Fortunately, however the half-life of the HoxFU moiety from *H. thermoluteolus* at 40 ^{o}C is comparable to that of the HoxFU moiety from *R. eutropha* at 22 ^{o}C,[164] this finding is promising for future applications of this enzyme in cofactor recycling at elevated temperatures, where 40 ^{o}C would be a compromise temperature.

4.5.4 pH optimum determination

The pH is known to have a profound influence on enzyme stability and catalytic activity, as it may affect the protonation state of amino acids which make up the protein. Changes to the ionisation state of the amino acids can affect the enzyme conformation and have large effects on enzyme substrate recognition at the enzyme active site. At extreme pHs the enzyme may also become inactive, or may display activity for a limited time period.[11]

In order to assess the pH optimum for electrochemically driven reduction of NAD^+ and oxidation of NADH, CVs were performed in mixed buffer containing 1 mM NAD^+ and

1 mM NADH, at pH values from 5.0 – 9.0 with a *H. thermoluteolus* HoxFU modified PGE RDE. A typical CV is shown in Figure 4-14 (a) and scans at a number of different pH values are shown in Figure 4-14 (b). Different protein films were used for each CV meaning that direct comparison of the current at each pH would not give on accurate representation of the activity at that pH, as different enzyme films display different activities at the electrode, partly due to different amounts of active enzyme being immobilised on the surface of the electrode (discussed in the Methods and Theory chapter, section 2.3.4).[162] In order to avoid this problem the average of 3 scans was used, to obtain an average activity at that pH. As the same protein sample was used to make each protein film and scans were performed on the same day this treatment is acceptable to provide an estimate of the relative activity at each pH on carbon.

The data shown in Figure 4-14 (c and d) demonstrates that the HoxFU moiety is active over a wide range of pH values for both NAD^+ reduction and NADH oxidation. Additionally, as observed for the *R. eutropha* SH and Bovine heart complex I reversible catalysis of electrocatalytic NAD(H) interconversion was observed over the pH range 5.0-9.5.[100,164]

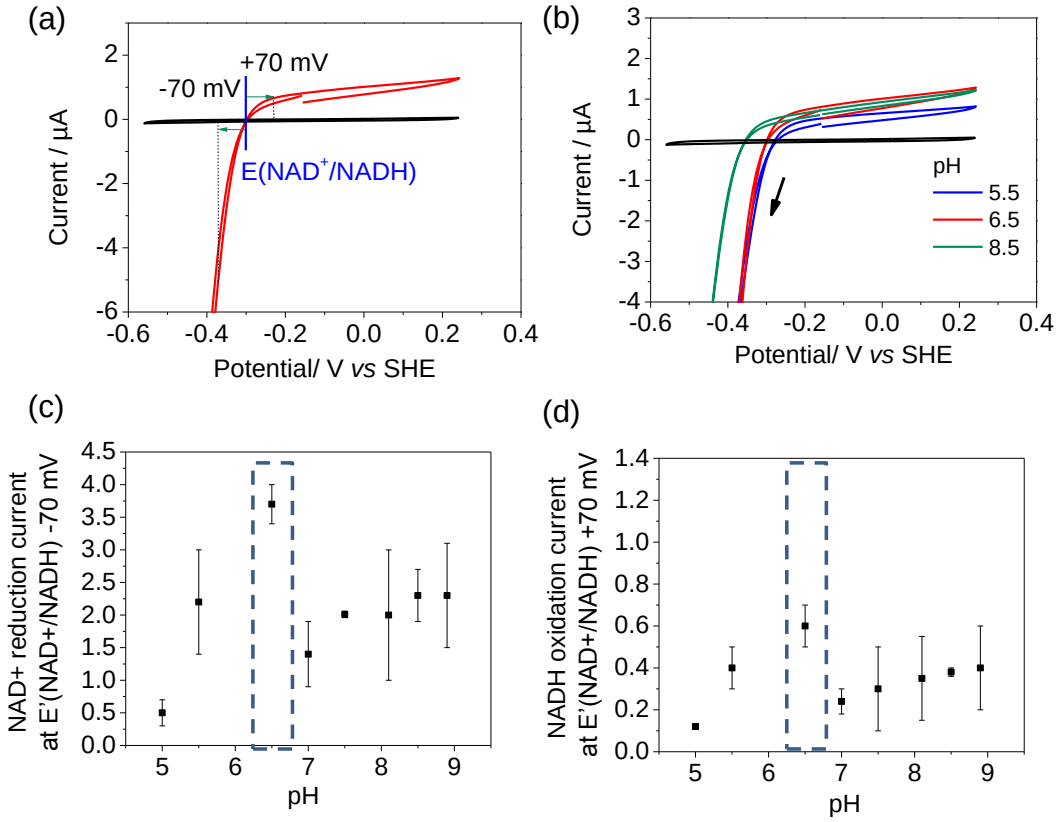

Figure 4-14: Determining the pH optimum for electrochemical NAD^+ reduction and NADH oxidation. CVs were recorded in mixed buffer containing 1 mM NAD^+ and 1 mM NADH. (a) Method of determining pH optimum from cyclic voltammogram, by taking the current at – 70 mV from the thermodynamic potential for NAD^+ reduction and at +70 mV from the thermodynamic potential for NADH oxidation. Blank scan with an unfunctionalised PGE RDE recorded in buffer solution shown in black (b) Example CVs showing reductive sweeps followed by sweeping the potential to an oxidising potential at three different pHs. A scan with an unfunctionalised electrode at pH 8.0 (blank) is shown in black. The electrode was rotated at 2000 rpm and a scan rate of 10 mV s^{-1} was used. (c) The catalytic current measured at – 70 mV from the thermodynamic potential of the NAD^+/NADH redox couple for 3 repeated scans and used to give an indication of the catalytic current for NAD^+ reduction at each pH. (d) The catalytic current was measured at + 70 mV from the thermodynamic potential of the NAD^+/NADH redox couple for 3 repeated scans and used to give an indication of the average catalytic current for NADH oxidation at each pH.

At higher pHs NADH oxidation occurs at a more negative potential, due to the thermodynamic potential of the NAD^+/NADH couple shifting to a more negative value this is clearly demonstrated by the scans in Figure 4-14 (b). To account for this, the current at -70 mV from the thermodynamic potential was used to determine the activity towards NAD^+ reduction. Similarly, the current at a +70 mV from the thermodynamic

potential for the reaction was used to assess the activity towards NADH oxidation at a particular pH.

For NAD^+ reduction the optimum pH can be estimated as 6.5. This is slightly lower than those observed in biochemical mediated assays in section 4.4.2 and could be a result of the HoxFU moiety being in a slightly different conformation when immobilised on a PGE RDE, than when it is in solution.

Figure 4-14 (c) demonstrates that the pH optimum for NADH oxidation also occurs at around pH 6.5. At high non-physiological pHs such as pH 10 the enzyme film on the electrode is very unstable, leading to a significant decrease in catalytic current in the second scan (not shown), hence pHs above 9 were not investigated. Idris *et al.* have observed a similar low stability of the *R. eutropha* HoxFU at high pHs on the electrode. These trends have also been seen by Lauterbach *et al*. in biochemical assays of the HoxFU moiety from *R. eutropha*.[164][102]

4.5.5 Catalytic bias determination

The catalytic bias of the HoxFU moiety was determined using cyclic voltammetry following the method of Idris *et al*.[102] Cyclic voltammograms were obtained with a HoxFU functionalised PGE RDE in a cell containing a total cofactor concentration of 2 mM, but with the relative quantities of NAD^+ and NADH being varied. This is similar to the concentration of NAD^+/NADH found in the cytoplasm of bacterial cells under physiological conditions.[231]

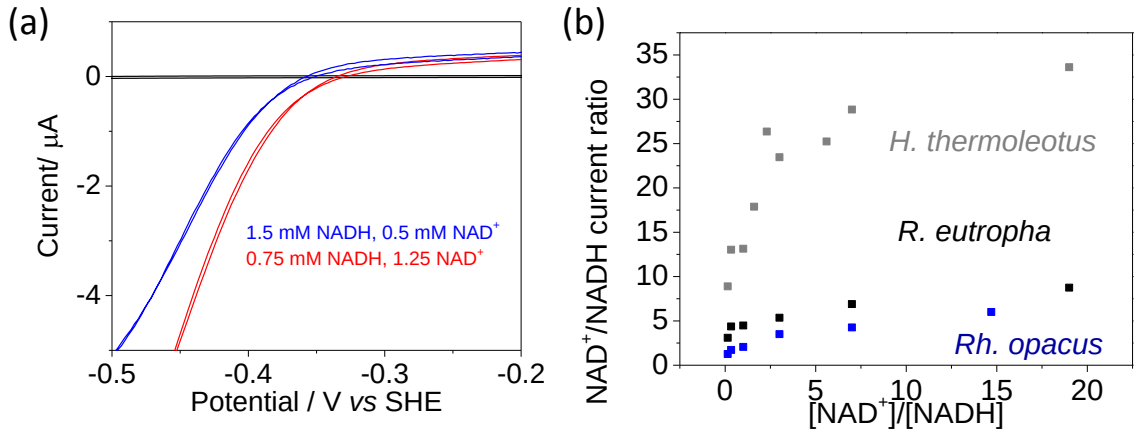

Figure 4-15: (a) Cyclic voltammograms used to determine the catalytic bias of HoxFU from *H. thermoluteolus:* The current response for a HoxFU-modified electrode in the presence of 1.5 mM NADH and 0.5 mM NAD^+ (blue) and 0.75 mM NADH and 1.25 mM NAD^+ (red), blank scan with an unfunctionalised PGE RDE in buffer shown in black. (b) The ratio of the current at ±140 mV from the thermodynamic potential against the ratio of NAD^+ and NADH concentrations. Results for the HoxFU moiety from *H. thermoluteolus* are compared to similar experiments for *R. eutropha* and *Rh. opacus.* Data for *Rh. opacus* and *R. eutropha* were provided by Dr Z Idris and Dr H Reeve.[103,164] These experiments were performed at 30 ^{0}C, at 2000 rpm rotation with a scan rate of 10 mV s^{-1} in 50 mM Tris-HCl pH 8.

In order to allow different HoxFU films to be compared, the current at ±140 mV either side of the thermodynamic potential, was determined from the cyclic voltammograms at different cofactor concentrations. The ratio of these two current values was then plotted *vs* the concentration ratio of NAD^+ and NADH. This was compared to values obtained for the *R. eutropha* and *Rh. opacus* HoxFU moieties already tested in the Vincent group, shown by the graph in Figure 4-15 (b).[102][103] From Figure 4-15 (b) it is clear that like the HoxFU moieties from *R. eutropha* and *Rh. opacus*, the *H. thermoluteolus* HoxFU shows a bias towards NAD^+ reduction. This bias is more significant for the *H. thermoluteolus* HoxFU than for HoxFU moieties from other organisms. This may mean that this enzyme construct is more useful for applications in reduction reactions, as it favours production of NADH. This thesis focuses on reduction reactions, therefore this is desirable here.

4.5.6 Affinity constant determination

This work was carried out by Tim Sudmeier (Summer student) under my supervision

Michaelis-Menten constant determination for NAD^+ reduction

This K_M for NAD^+ reduction by *H. thermoluteolus* HoxFU was carried out at 30 ^oC, in order to allow easier comparison with the electrochemical K_M determination for the HoxFU moiety from *R. eutropha* which was carried out at 30 ^oC.[102] In addition, the HoxFU moiety from *H. thermoluteolus* is more stable at 30 ^oC, meaning that electrochemical chronoamperometry plots are easier to interpret as they are less affected by film loss and enzymes denaturing. It was found that at higher temperatures it was much more difficult to determine K_M values accurately, as the catalytic current after each injection was found to be significantly less stable. The K_M determination was carried out as described in the Methods and Theory chapter (section 2.3.4), following the method of Idris *et al*.[102,164]

Figure 4-16 (a) shows a CV recorded in 1 mM NAD^+ with a *H. thermoluteolus* HoxFU functionalised PGE. The blue arrow shows the potential at which the electrode was held during the K_M determination. At this potential there is a significant current due to NAD^+ and importantly no other side reactions are observed to occur at the PGE RDE.

A typical chronoamperogram used to determine the K_M is shown in Figure 4-16 (b). At the beginning of this trace the current is approximately zero, as there is no substrate (NAD^+) present. Sequential aliquots of NAD^+ were injected into the solution leading to an increase in the magnitude of the catalytic current. By taking away the capacitive current when no NAD^+ is present at the start of the reaction a corrected current can be obtained. As the corrected current is directly proportional to the activity of the enzyme film, plotting the corrected current against the concentration of NAD^+ gives a Michaelis-Menten plot.

Figure 4-16 (c) shows a typical example of a Michaelis-Menten plot. The K_M can be determined from this plot by fitting the data to the Michaelis-Menten equation, see section 2.3.4. This experiment was repeated 9 times, which gave an average K_M value of 360 ± 69 µM. This value is slightly higher than the value of 197 ± 28 µM obtained for *R. eutropha*.[102]

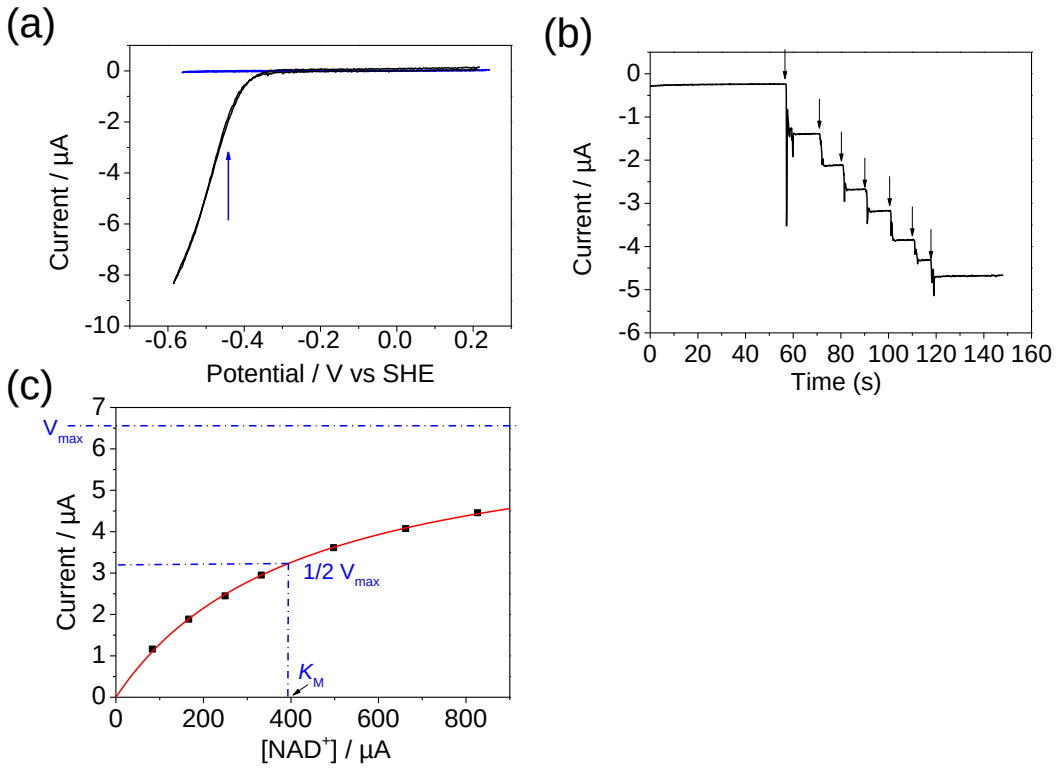

Figure 4-16: Electrochemical determination of the K_M for NAD^+ reduction. (a) A cyclic-voltammogram in 1 mM NAD^+ in Tris-HCl pH 8.0, blue arrow indicates the potential at which the chronoamperometry was performed. (b) Chronoamperometry trace from a typical experiment designed to determine the K_M for NAD^+ reduction. A HoxFU modified electrode was poised at -412 mV *vs* SHE and the current was recorded as sequential aliquots of NAD^+ were injected into the cell, leading to an increase the NAD^+ concentration. The concentration of NAD^+ in the cell was increased to 83, 166, 249, 322, 497, 662, 826 µM at the times indicated by the arrows. (c) A Michaelis-Menten plot used to calculate the K_M value, by plotting the catalytic current against the NAD^+ concentration.

This K_M value is, however, significantly less than the one obtained for the whole SH using biochemical methods (shown in section 4.3.4), suggesting that it may be possible to use lower NAD^+ concentrations with the enzyme-modified particles or with an

electrochemical set up, than when using the whole *H. thermoluteolus* SH by employing HoxFU alone.

Michaelis-Menten constant determination for NADH oxidation

Similar techniques to those used in the section above can be used to determine the substrate affinity constant for NADH. A cyclic voltammogram showing NADH oxidation is shown in Figure 4-17 (a), with the blue arrow indicating the potential at which the electrode was held in the chronoamperometry experiments to determine the K_M for NADH oxidation. An example chronoamperogram is shown in Figure 4-17 (b). The Michaelis-Menten plot for this experiment gave a K_M value of 293 µM and is shown in Figure 4-17 (c).

From the Michaelis-Menten plots, based on 9 independent electrochemical K_M determinations, a value of 256 ± 117 µM was obtained. This figure is again larger than the figure for *R. eutropha* HoxFU. This value is in good agreement with the K_M value determined using biochemical methods (254 µM) for NADH driven reduction of benzyl viologen. Idris *et al*. observed a similar agreement when they characterised the HoxFU moiety from *R. eutropha* (Biochemical: 56 µM, Electrochemical: 58 ± 18 µM).[102] The K_M value obtained for NADH oxidation is lower than that for NAD^+ reduction. However, the catalytic bias of this enzyme strongly favours NAD^+ reduction, suggesting this enzyme may be better for applications in this direction, despite its lower affinity for NAD^+.

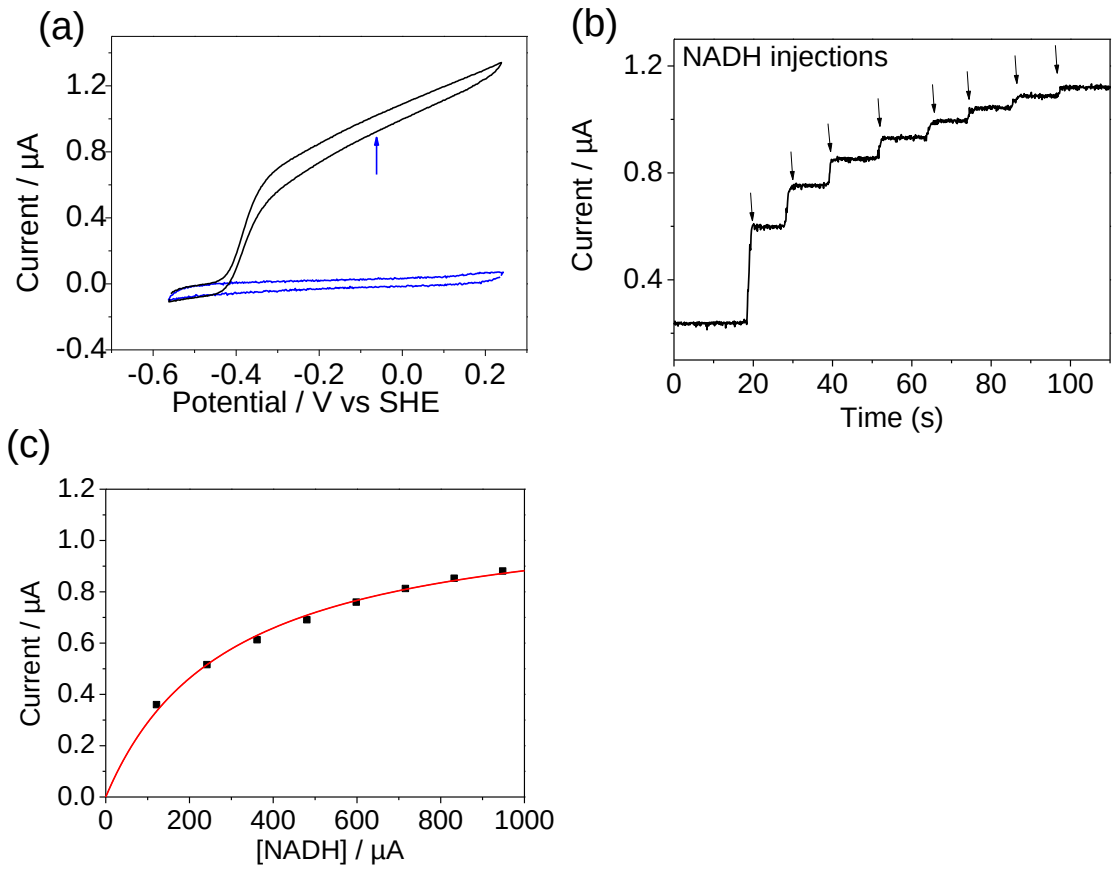

Figure 4-17: Determining the K_M for NADH oxidation by the *H. thermoluteolus* HoxFU (a) A cyclic-voltammogram in 1 mM NADH in 50mM Tris-HCl pH 8.0, blue arrow indicates the potential at which the chronoamperometry was performed. (b) A chronoamperometry trace for an experiment in which a HoxFU functionalised PGE RDE was poised at -62 mV *vs* SHE and sequential aliquots of NADH were injected into the cell to give a concentration of 121, 242, 361, 480, 598, 716, 832, 948 µM at the time points indicated by the arrows. Conditions: 50 mM Tris-HCl pH 8, rotation rate 2000 rpm (c) A Michaelis-Menten plot; the asymptote of this graph can be used to determine K_M.

4.5.7 Inhibition constant determination

Product inhibition of NAD^+ reduction

The SH from *R. eutropha* suffers from product inhibition. This effect can impact the utility of an enzyme in biochemical processes.[102] Therefore, it is important to determine the K_i for both inhibition of NAD^+ reduction by NADH and inhibition of NADH oxidation by NAD^+. Both of these values can be determined electrochemically. Electrochemical K_i determinations were carried out following the methods of Idris *et al.* which are discussed more fully in section 2.3.5[102,164] Initially, a HoxFU functionalised PGE RDE was immersed into an electrochemical cell containing buffer.

A control step of NAD^+ (substrate) was injected into the cell after approximately 20 seconds and an increase in the catalytic current was observed. The control step allows all experiments to be normalised to the current at the same NAD^+ concentration, which allows direct comparison between different enzyme films used in subsequent experiments This is necessary in order to be able to produce Dixon and Cornish-Bowden plots.

Subsequently, a further second aliquot of NAD^+ or buffer was injected in to the cell so that a final desired concentration of NAD^+ was reached. Aliquots of NADH (inhibitor) were then sequentially injected into the electrochemical cell. The NADH aliquots contained the same concentration of NAD^+ as that present in the electrochemical cell, to prevent dilution effects leading to a drop in current, which could be mistaken for product inhibition. The resulting decrease in current was used to determine the K_i values for inhibition of NAD^+ reduction by NADH.

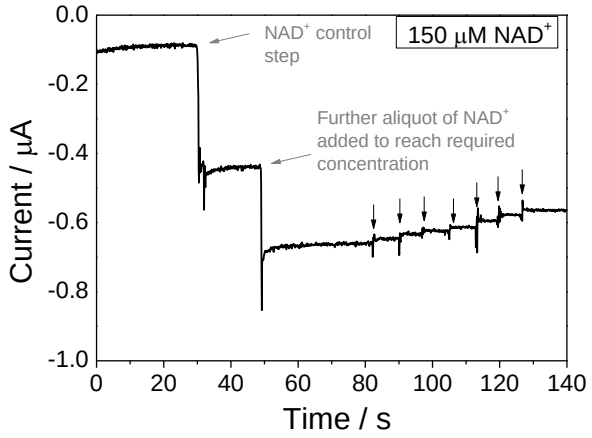

Figure 4-18: A typical chronoamperometry plot to determine the inhibition of NAD^+ reduction by NADH. The electrode was poised at -460 mV, an NAD^+ reducing potential. A control injection of NAD^+ (taking the concentration of NAD^+ in the cell to 50 µM) was followed by a second injection to reach the desired substrate concentration; in this example 150 µM. Sequential injections of NADH (the product of the reaction, containing 150 µM NAD^+ to prevent dilution effects) causing inhibition, leads to a decrease in catalytic current. Inhibitor (NADH) concentrations used were: 49 µM, 97 µM, 145 µM , 193 µM, 287 µM, 380 µM, 472 µM.

Figure 4-18 shows a typical chronoamperometry trace used to determine the K_i for NADH inhibition of NAD^+ reduction. The electrode was held at an NAD^+ reducing potential (-460 mV *vs* SHE). Initially, the negative current was observed to increase in magnitude as the first two injections of NAD^+ were added to the electrochemical cell, indicating NAD^+ reduction. Subsequently, aliquots of NADH (containing the same amount of NAD^+ as in the cell solution, in order to avoid dilution effects) were injected into the cell solution. These led to a decrease in magnitude of the current implying some degree of inhibition of NAD^+ reduction. By carrying out similar experiments at a number of different NAD^+ starting concentrations it is possible to determine the inhibition constant.

A Dixon plot can be constructed from this data by plotting the reciprocal of the normalised current against the concentration of NADH for a number of starting NAD^+ concentrations, see Figure 4-19 (a). Similarly a Cornish-Bowden plot can be constructed by plotting the concentration of NAD^+ over the normalised current *versus* the concentration of NADH, see Figure 4-19 (b). The lines in the Dixon plot cross, suggesting that there is a competitive component to the inhibition. From the Cornish-Bowden plot in Figure 4-19 (b) it is clear to see that the lines on the graph are approximately parallel. This suggests that uncompetitive inhibition does not play a particularly significant role in the product inhibition of the HoxFU moiety from *H. thermoluteolus*. This is expected, as the reduced cofactor (NADH) competes for binding at the same active site as the oxidised cofactor (NAD^+).

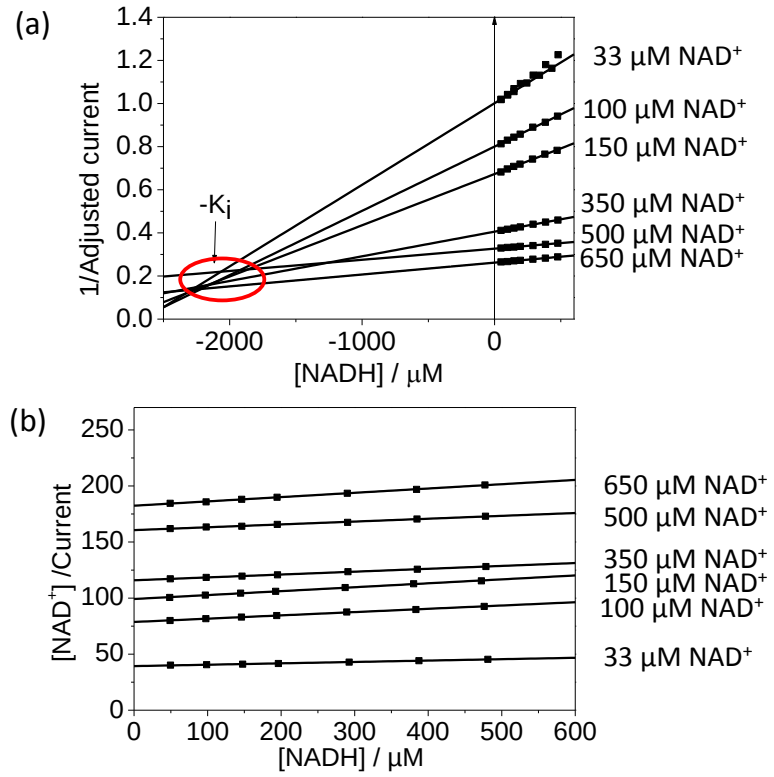

Figure 4-19: Electrochemical determination of the inhibition constant for NAD^+ reduction $K_{I(NAD+)}$ (a) Dixon plot, which plots 1/current against inhibitor concentration. The point at which the lines cross gives the inhibition constant. (b) A Cornish-Bowden plot of Substrate/current vs inhibitor concentration; the line on this graph are parallel suggesting that the inhibition experience by this enzyme is mainly competitive Experiments were performed at 30 °C, with electrode rotation rate of 2000 rpm in 50 mM Tris-HCl buffer pH 8.0. NADH was purified using an anion exchange column.

Delarosa *et al*. first demonstrated in 1981 that NAD^+ competitively inhibits NADH oxidation at a the active site of a diaphorase, in their case the NADH cytochrome c reductase diaphorase isolated form the spinach NADH-nitrate reductase complex.[232] Subsequently, Idris *et al*. demonstrated that the closely related *R. eutropha* HoxFU moiety is competitively product inhibited both in the NADH oxidation direction and in the NAD^+ reduction direct.[102] Similar findings were demonstrated by Reeve *et al*. for *Rh. opacus.*[103]

From Figure 4-19 (a), it appears that the lines in the Dixon plot converge around 2200-1800 µM. This implies that the value of K_{ic} for product inhibition of NAD^+ reduction by NADH is 2200-1800 µM.

Product inhibition of NADH oxidation

A similar experiment was performed to determine the inhibition constant for NADH oxidation by NAD^+, see Figure 4-20. Here, a HoxFU functionalised electrode was immersed into an electrochemical cell containing buffer and held at an NADH oxidising potential (-62 mV *vs* SHE). A control step of NADH was injected into the electrochemical cell, followed by a further step to once again increase the NADH concentration; allowing different concentrations of NADH to be used. Sequential aliquots of NAD^+ (containing the same amount of NADH as present in the cell solution) were then injected into the cell, leading to a decrease in magnitude of the catalytic current; again suggesting product inhibition.

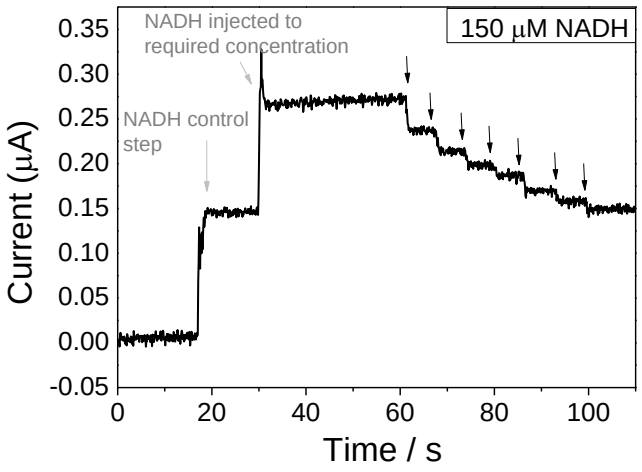

Figure 4-20: Electrochemical determination of the inhibition constant, $k_{i(NADH)}$ for *H. thermoluteolus* HoxFU. A chronoamperogram used to determine the inhibition of NADH oxidation by NAD^+. The electrode was poised at -62 mV, an NADH oxidising potential. Initially, there was no substrate (NADH) in solution, a control step of NADH was then injected (50 µM) to normalise each experimental run. An aliquot of NADH was subsequently injected to reach the required concentration. Sequential aliquots of inhibitor, shown by the black arrows (NAD^+, containing the desired concentration of substrate) were then injected causing inhibition, leading to a decrease in catalytic current. Inhibitor (NAD^+) concentrations used were: 49 µM, 97 µM, 145 µM , 193 µM, 287 µM, 380 µM, 472 µM.

Figure 4-21 (a) shows a Dixon plot, with the lines converging at about 500 – 800 µM. This demonstrates that the inhibition is competitive and suggests that the value of K_{ic} for

product inhibition of NADH oxidation, by NAD^+ is 500 - 800 µM, shown by a circle on the plot. Figure 4-21 (b), shows a Cornish-Bowden plot used for determining the value of K_{iu} (the uncompetitive inhibition constant). In this plot the lines are almost parallel; however, there is a weak uncompetitive component to the inhibition here.

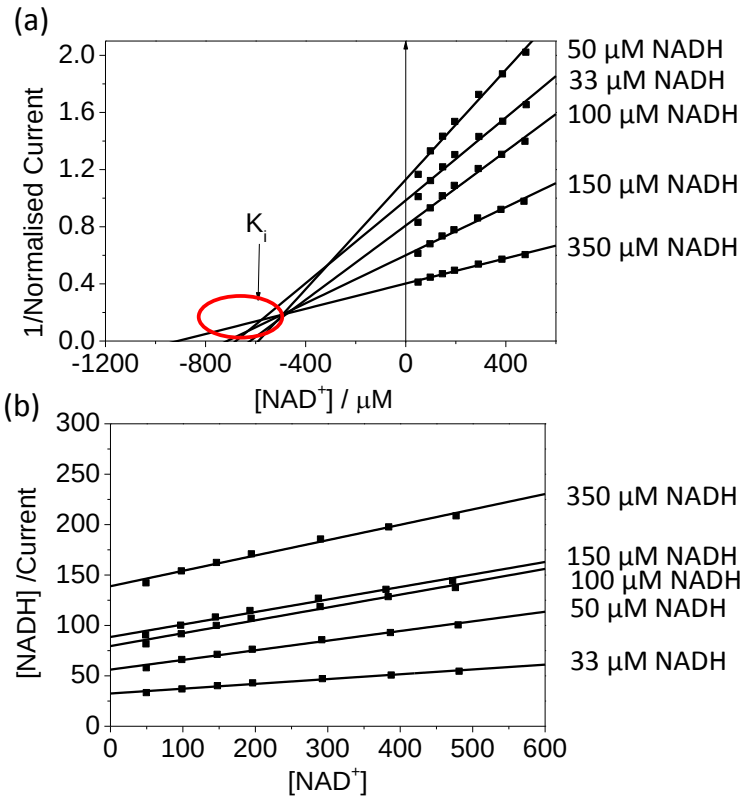

Figure 4-21: (a) A Cornish-Bowden plot demonstrating that inhibition here is mainly competitive, the competitive inhibitions constant is given by the negative of the intercept (point at which all the lines cross). (b) A Dixon plot displaying the data from experiments with different final NADH concentrations and the same NAD^+ injections.

4.6 Comparison of the affinity constants to other electrochemically characterised HoxFU moieties

A number of HoxFU moieties from different organisms have been characterised in the Vincent group; this section seeks to provide a comparison of the affinity and inhibitor concentrations determined electrochemically.

All the K_M values shown in Table 4-4 are within an order of magnitude. The K_M for NAD^+ reduction is higher for *H. thermoluteolus* than for the other two HoxFU variants:

however, it is still within the same order of magnitude. The K_M for NADH oxidation is similar to that for *Rh. opacus*; although, again higher that for *R. eutropha*. Due to the strong catalytic bias of the *H. thermoluteolus* SH for NAD^+ reduction it is unlikely that this enzyme would be used in the reductive direction in biocatalytic applications. The K_I value for NAD^+ inhibition by NADH is significantly larger for *H. thermoluteolus* than for *Rh. opacus* and *R. eutropha* fitting with the bias of this enzyme towards NAD^+ reduction. Therefore, the *H. thermoluteolus* enzyme is not significantly inhibited at high concentrations of NADH. This could be advantageous for biocatalytic reactions where the NADH-dependent enzyme has a high K_M for NADH requiring high levels of reduced cofactor to allow it to function at it optimal rate.

The *H. thermoluteolus* HoxFU shows similar values to *R. eutropha* and *Rh. opacus* HoxFU for inhibition of NADH oxidation by NAD^+.

Table 4-4: A table comparing Michaelis-Menten and inhibition constants for the SH from *R. eutropha, Rh. opacus and H. thermoluteolus*

HoxFU from:	K_M^{NAD+}	K_M^{NADH}	K_I^{NADH}	K_I^{NAD+}
R. eutropha[164]	197 ± 28	58 ± 18	100-300	200-300
Rh. opacus[103]	131 ± 17	311 ± 92	600-900	850-950
H. thermoluteolus	360 ± 68.5	256 ± 117	500-800	2200-1800

Data for *R. eutropha* determined by Dr Z. Idris, data for *Rh. opacus* determined by Dr H. Reeve. [103,164]

4.7 Summary

This chapter has detailed the first biochemical characterisation of the SH from *H. thermoluteolus.* This SH shows an optimum activity at 60 °C and is tolerant to atmospheric oxygen concentrations.

The chapter has also shown that the *H. thermoluteolus* HoxFU moiety can be expressed actively on its own. The *H. thermoluteolus* HoxFU moiety also shows its highest activity at 60 °C in biochemical assays.

Electrochemical characterisation of the *H. thermoluteolus* HoxFU has demonstrated that like *R. eutropha* and *Rh. opacus* this enzyme can undergo direct electron transfer on an electrode and reversibly catalyse the NAD^+/NADH couple at the thermodynamic potential. The *H. thermoluteolus* HoxFU is strongly biased towards NAD^+ reduction and displays a low product inhibition constant for NAD^+ reduction, which may be advantageous for some applications where working at high concentrations of NADH is required (i.e. when coupling to an NADH-dependant enzyme with a low K_M for NADH).

The *H. thermoluteolus* HoxFU moiety shows a half-life of 19 minutes at 40 ^oC, which is similar to the half-life of the *R. eutropha* HoxFU at 22 ^oC.

Both the SH and HoxFU are suitable for NADH recycling applications and may have advantages for operation at elevated temperatures. These applications will be explored in chapters 5 and 6.

5 Elevated temperature cofactor recycling

5.1 Introduction

This chapter focuses on developing a H_2-driven cofactor recycling system for use at elevated temperatures.

Generally, thermophile enzymes (enzymes originally isolated from thermophile micro-organisms) have a range of features which leads to them being more stable than mesophilic enzyme variants. These include extra hydrogen bonds, disulphide bridges and less conformational strain. This leads them to being more rigid than mesophile variants, meaning that they are often more resistant to chemical and thermal degradation.[123][233]

Generally, the high temperature stability of these enzymes is retained if they are expressed in mesophilic hosts, for example *R. eutropha*, which is used as the heterologous host for production of HoxFU from *H. thermoluteolus,* the purification and characterisation of which is described in chapter 4. [123] The thermal stability of these enzymes often means that they can be easily purified by heat treatment of the solubilised cell fractions, which can reduced the cost of obtaining pure enzymes for biocatalytic applications.[202,234]

Thermophile enzymes are already used in a range of industrial settings. In general thermophile enzymes work at elevated temperatures of around 40 ^{o}C – 70 ^{o}C. A key example of the industrial use of thermophile enzymes is in the production of high glucose-fructose syrup from starch in the food industry. Here elevated temperatures are required for the liquidation and scarification of the starch.[235] A pullulanase thermozyme which specifically targets the α-1,6-linked branches of the amylopectin structure is then required for the next step of starch degradation.[236]

The increased temperature stability of thermophile enzymes often goes hand in hand with other desirable properties. One such property is increased stability in the presence

of organic solvents and other protein denaturants.[11] It is often desirable to use high concentrations of organic substrates in industrial reactions to optimise the volumetric yield. Therefore, research into thermophile enzymes is of great interest to industry.[235][237]

The field of thermophile proteases is highly developed.[235] These enzymes catalyse the hydrolysis of proteins and have been added to detergents since 1913.[238] Today the serine protease from thermophilic bacterium *Coprothermobacter proteolyticus* is used frequently by detergent manufacturers because of its stability at high temperatures, its preference for alkaline pHs and its ability to tolerate high concentrations of detergent.[239] Due to their increased stability and ability to carry out catalysis under a wide range of different conditions, Antranikian and co-workers suggest thermophile enzymes are the 'biocatalysts of choice for future green industries'.[235]

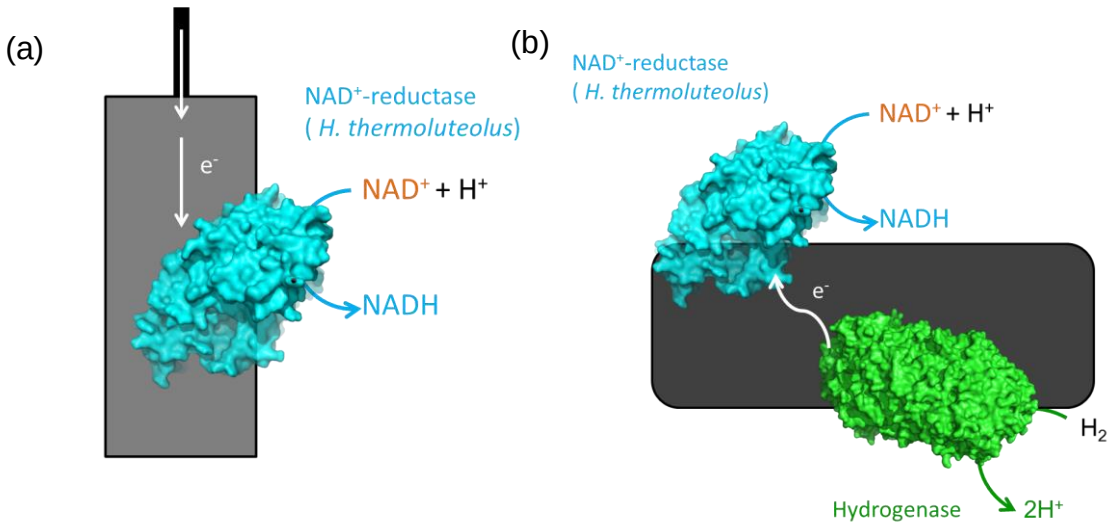

Figure 5-1: Two possible systems for cofactor recycling at elevated temperatures. (a) An electrochemical system for cofactor recycling with HoxFU from *H. thermoluteolus* immobilised on a carbon paper electrode. (b) Enzyme-modified particles with the HoxFU moiety from *H. thermoluteolus* and Hyd 2 from *E. coli* co-immobilised such that they are in electronic contact.

An area where there is emerging interest in using thermophile enzymes is in redox catalysis.[240] As these enzymes are dependent on NADH or NADPH cofactors, there is a requirement for high temperature cofactor recycling systems. After the promising

results obtained in Chapter 4, which suggest that the HoxFU moiety from *H. thermoluteolus* could be a good candidate for high temperature cofactor recycling. This chapter examines whether it is possible to use this enzyme as part of a cofactor recycling system to reduce NAD^+ to NADH at elevated temperatures.

Two systems for cofactor recycling at elevated temperatures, shown as schematic diagrams in Figure 5-1, will be explored in this chapter. One approach involves using a high surface area carbon electrode functionalised with *H. thermoluteolus* HoxFU, building upon the characterisation work carried out in chapter 4, to carry out the reduction of NAD^+ to NADH using electrons from a circuit as the source of reducing equivalents (these electrons originally come from a oxidation process occurring at the Pt counter electrode). The second system shown in Figure 5-1 (b) uses *H. thermoluteolus* HoxFU and *E. coli* Hyd 2 co-immobilised on conductive carbon particles. Building on the work in chapter 3, both of these systems will be combined with an enoate-reductase enzyme from *Thermus scotoductus* (*TsER*), which has a reported optimum temperature of 65 °C and retains more than 70 % of its activity at 80 °C.[241]

5.1.1 The *Thermus scotoductus* enoate reductases (*TsER*)

The *TsER* catalyses the reaction shown in Figure 5-2. The *TsER* is able to reduce a wide range of activated carbon-carbon double bonds.

Similarly to the SH it also contains a FMN at its active site. This enzyme operates via a ping-pong bi-bi- mechanism, with both the substrate and the cofactor binding at the same FMN active site.[242] The NAD(P)H cofactor initially adds a hydride to the oxidised FMN. This leads to the production of reduced $FMNH^-$. The alkene substrate then enters the same active site and is reduced by the $FMNH^-$ giving an alkane and

FMN (at the active site), see Figure 1-21.[243] The *TsER* is also able to accept reducing equivalents from both NADH and NADPH.[241]

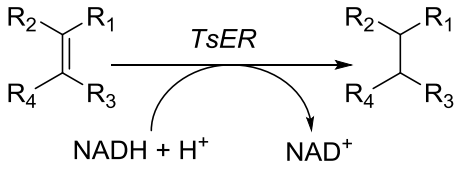

Figure 5-2: The reaction catalysed by the *TsER* enzyme.

5.1.2 Confirming that *TsER* shows increased activity at elevated temperatures

In the literature, Opperman and co-workers have determined that the TsER is optimally active at 65 ^{o}C.[241] The activity of the *TsER* was determined over a range of temperatures in order to determine the activity under the experimental conditions used in this thesis.

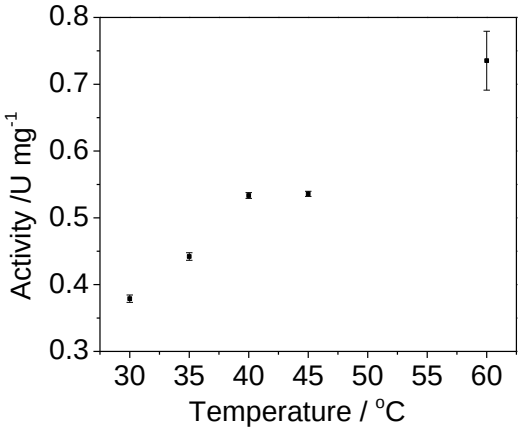

Figure 5-3: A graph showing the activity of the *TsER* enzyme between 30 ^{o}C and 60 ^{o}C. Results from 30 -45 ^{o}C, were measured using a plate reader (path length 2.4 mm), with all 3 scans being repeated in triplicate. Activity was determined by monitoring the consumption of NADH determined from the decreasing absorption at 340 nm with a baseline correction based upon the absorbance at 450 nm. Error bars are shown as one standard deviation of the data. As the plate reader cannot be used to measure activities at temperatures over 45 ^{o}C; a UV-visible spectrometer was used to determine the activity at 60 ^{o}C, the error bar for this reading was estimated at 6 % based on the errors observed with previous activity measurements with the Cary 60 spectrometer. All of the reactions were carried out on a 100 µL scale in 50 mM Tris-HCl pH 8, with 0.3 mM NADH and 2 mM 2-methyl-2-cyclopentenone.

Data in Figure 5-3 confirms that the activity of the *TsER* enzyme increases as a function of temperature up to 60 ^{o}C under the conditions used in this thesis, in agreement with the findings of Opperman and co-workers. Therefore this enzyme is a good candidate for testing with an elevated temperature cofactor recycling system.

5.1.3 Investigating whether the substrates of the *TsER* are reduced directly at carbon

Hollmann *et al*. have reported that the *TsER* enzyme can reduce a wide range of molecules containing activated double bonds which have adjacent electron withdrawing groups.[66] A number of possible substrates which have been shown to be accepted by the *TsER* are shown in Figure 5-4.

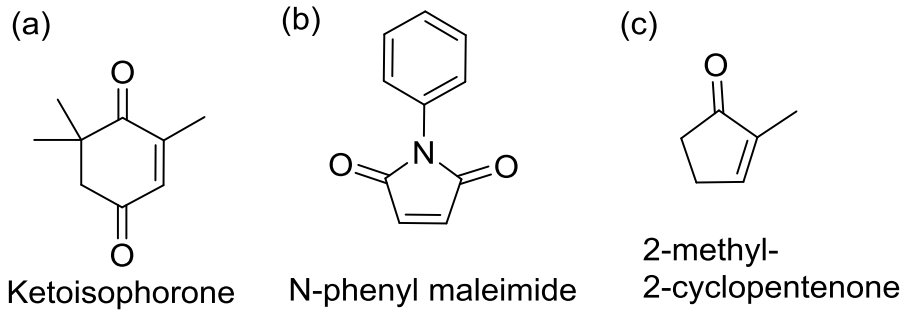

Figure 5-4: (a) The chemical structure of a number of substrates accepted by the *TsER* : (a) Ketoisophorone, (b) N-phenyl maleimide, (c) 2-methyl-2-cyclopentenone.

Electrochemical characterisation of the *H. thermoluteolus* HoxFU in chapter 4 has demonstrated that this enzyme will catalyse the reduction of NAD^+ at the thermodynamic potential for this reaction (see section 4.5.1).

When the enzyme-modified particles are used for high temperature cofactor recycling, introduced in section 1.8.2 of this thesis, the hydrogenase and NAD^+-reductase channel electrons between each other through the carbon particles.[64] This means that the enzyme-modified particles 'sit' at potential between the $2H^+/H_2$ and NAD^+/NADH couples. If the *TsER* substrates of interest are reduced at bare carbon surfaces at potentials between the two couples, it is possible than non-selective reduction of the

substrates would lead to the generation of side-products, since reduction reactions at unfunctionalised electrodes tend not to display good enantioselectivity.[244] Therefore, control experiments investigating the potential at which the *TsER* substrates are reduced at a bare PGE RDE were carried out.

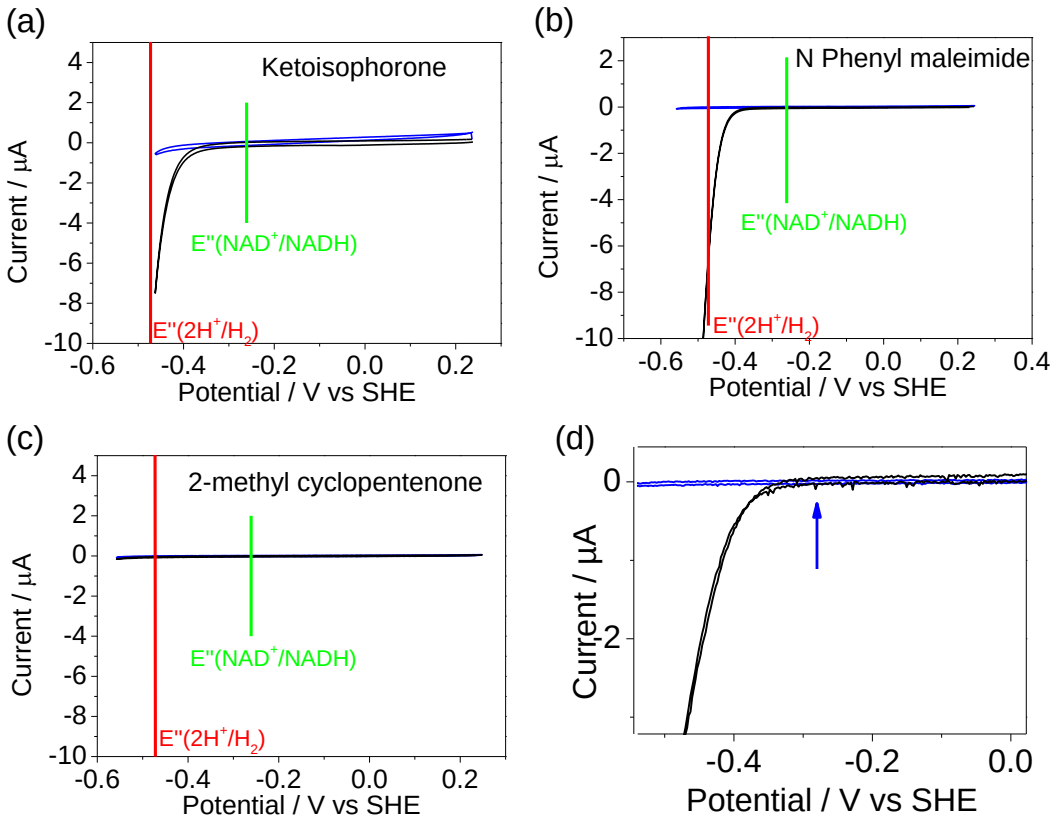

Figure 5-5: Cyclic voltammograms demonstrating the electrochemical behaviour of the *TsER* substrates in Figure 5-4 at an unfunctionalised PGE RDE. (a) 2.2 mM ketoisophorone (black), (b) 6 mM N-phenyl maleimide (black), (c) 6.8 mM 2-methyl-2-cyclopentenone (black). As a comparison a blank scan of an unfunctionalised PGE RDE in buffer, without any substrate, is shown in blue. The green line shows the potential of the NAD^+/NADH redox couple at a 1000:1 concentration of NAD^+ and NADH at pH 8. The red line indicates the potential of the $2H^+/H_2$ redox couple at pH 8 under 1 bar H_2. (d) A CV showing enzymatic cycling of NAD^+/NADH at a *H. thermoluteolus* HoxFU functionalised PGE RDE in a solution containing 1 mM NAD^+. The blue arrow indicates E_{onset} for NAD^+ reduction at -280 mV. The CVs were recorded at 10 mV s^{-1} in 50 mM Tris-HCl pH 8 at 30 °C, with rotation at 2000 rpm.

Control experiments were performed to determine whether reduction of any of the substrates in Figure 5-4 occurs directly at a bare carbon PGE RDE in the potential region of interest, that is between *ca.* -280 mV *vs* SHE (E_{onset} for NAD^+ reduction at a HoxFU functionalised PGE RDE in 1 mM NAD^+) and -472 mV (the H^+/H_2 couple of at

1 bar H_2, pH 8). Cyclic voltammograms were measured between 240 and -560 mV *vs* SHE with an un-functionalised (blank) PGE RDE in the presence of each substrate shown in Figure 5-4 in solution.

The black CV in Figure 5-5 (a) shows that reduction of ketoisophorone occurs at a more positive potential than the $2H^+/H_2$ couple under 1 bar H_2 at pH 8. Therefore, if ketoisophorone was used as the *TsER* substrate in combination with the enzyme-modified particles it is possible that reduction of ketoisophorone would occur directly at the bare carbon surface of the particles and not at the *TsER* active site.

The black CV in Figure 5-5 (b) shows that N-phenyl maleimide is also reduced directly at a bare PGE RDE in the potential region sampled. For N-phenyl maleimide, E_{onset} is approximately -350 mV *vs* SHE. This is again more positive than the potential at which H_2 oxidation will occur under 1 bar H_2 at pH 8. Figure 5-5 (d) shows a CV from chapter 4, which demonstrates that E_{onset} for the reduction of NAD^+ by the *H. thermoluteolus* HoxFU in a 1 mM solution of NAD^+ is approximately -280 mV. As the value of E_{onset} for N-phenyl maleimide at bare carbon is *ca.* -350 mV *vs* SHE there is a small potential window at which it would be possible to use the *H. thermoluteolus* HoxFU to reduce NAD^+ at a carbon electrode; but, at which reduction of N-phenyl maleimide would not occur at the bare electrode. This means that this substrate could possibly be used in a system in which NADH is recycled electroenzymatically, if the electrode was held at a less negative potential than -350 mV *vs* SHE.

The black scan in Figure 5-5 (c), shows an un-functionalised PGE RDE in a solution containing 2-methyl-2-cyclopentenone. From this CV it is clear that reduction of 2-methyl-2-cyclopentenone does not occur in the potential range tested. Therefore, reduction of 2-methyl-2-cyclopentenone at bare carbon occurs at a significantly more negative potential that the thermodynamic potential for the $2H^+/ H_2$ couple under 1 bar

H_2. This means that direct reduction of 2-methyl-2-cyclopentenone is unlikely to occur at the surface of the enzyme-modified particles in presence of 1 bar H_2.

From the results in Figure 5-5 it is clear that 2-methyl-2-cyclopentenone is the best substrate to use as a test system for cofactor recycling by either an enzyme-modified electrode, or using enzyme-modified particles, as it is not reduced at bare carbon at the relevant potential.

5.2 Elevated temperature electrochemical NADH generation

The previous section demonstrated that 2-methyl-2-cyclopentenone is a suitable substrate to use for development of an electroenzymatic approach to NADH recycling using the NAD^+-reductase. However, so far, only small surface area analytical electrodes have been discussed and used for characterisation work (chapter 4). In this section, high surface area electrodes that allow incorporation of larger quantities of NAD^+ reductase are detailed.

5.2.1 High surface area electrodes

The PGE RDE has a surface area of only 0.03 cm^2. A maximum of approximately 5 pmoles of enzyme can be immobilised on this surface area.[153] Where it is desirable to obtain high conversions of NAD^+ to NADH, electrodes with higher surface areas are required, which can incorporate higher loadings of enzyme.

Vincent and co-workers have reviewed a number of strategies for the construction of high surface area carbon electrodes.[156,245,246] In this thesis, carbon paper was used as a scalable method for the construction of high surface area electrodes.

Carbon paper is made from combining carbon nanofibers into flat carbon sheets. It has been used as a support for a variety of enzymatic fuel cells, as well as for precious metal catalysts.[155] The carbon paper used in this thesis displays high conductivity and chemical stability,[247] and has a large surface area (in comparison to the PGE RDE).

The surface of the carbon fibre itself, however, is not functionalised[247] which may mean that the enzyme sticks less well to this surface than to carbon surfaces used more commonly in the Vincent group.[103,119,156,248] For example polishing of the PGE RDE with an alumina slurry leads to the creation of a rough hydrophilic surface, with many acid oxide groups on it, which are thought to aid enzyme immobilisation.[153]

Fabrication of high surface area electrodes

High surface area electrodes were constructed following a similar protocol to that used by Reeve *et al*.[103] Initially, a rectangular piece of carbon paper (Fuel Cell Earth, USA) of *ca.* 1 cm^2 area was cut out with a scalpel. This was then attached to a piece of carbon fibre laminating the carbon fibre and paper using laminating film. The piece of carbon fibre could subsequently be connected to a crocodile clip and thus incorporated into a circuit. The carbon paper is hydrophobic, consequently if enzyme is applied directly to the paper it won't stick. Therefore, the paper was soaked in water for a 1 hour period, and subsequently excess water was removed under a stream of N_2 gas. An aliquot of enzyme (10 µL, 6 pmoles) was then directly applied to one side of the carbon paper electrode.

The electrode was then left for 20 minutes in a 15 mL centrifuge tube to allow the enzyme to absorb onto the carbon paper. To ensure a moist atmosphere a small amount of water was added to the bottom of the centrifuge tube.

As the carbon paper cannot be rotated, in this experiment a magnetic stirrer (Thermofisher) was instead used to aid mass transport of substrate and product to the electrode surface.

Electrochemical NAD^+ reduction

A typical cyclic voltammogram taken with a high surface area electrode in buffer containing NAD^+ is shown in Figure 5-6 (a). The scan in blue was taken with the

unfunctionalised carbon paper electrode, before absorbing enzyme onto its surface. This shows that the non-faradaic (capacitive) contributions to the CV are more significant for the carbon paper electrode due to the much larger electrode surface area. Nevertheless, the scan in black showing the *H. thermoluteolus* HoxFU functionalised electrode demonstrates that the maximum current obtained from the carbon paper (*ca.*-60 μA), shown in Figure 5-6 (a), is approximately 5 times larger than that obtained at a PGE RDE (*ca.*-8 μA), with the CV shown in Figure 5-6 (b) for reference.

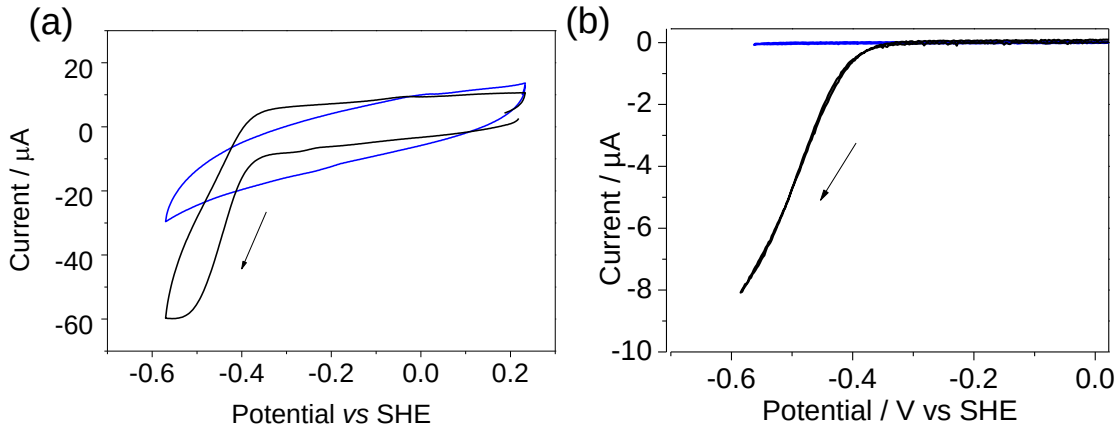

Figure 5-6: Cyclic voltammograms showing reduction of NAD^+ at a *H. thermoluteolus* HoxFU functionalised electrode. (a) A CV taken with a high surface area carbon paper electrode. Scan in blue unfunctionalised carbon paper electrode in 50 mM Tris-HCl pH 8.0, containing 1 mM NAD^+ and 2 % DMSO at 40 °C. Black trace: carbon paper functionalised with *H. thermoluteolus* HoxFU under the same conditions. A magnetic stirrer was added to the cuvette, which was used as the electrochemical cell for these experiments, to support mass transport in the solution (b) A CV showing enzymatic cycling of NAD^+/NADH at a *H. thermoluteolus* HoxFU functionalised PGE RDE in 50 mM Tris-HCl pH 8.0 containing 1 mM NAD^+. Scan in blue shows a 'blank' or unfunctionalised PGE RDE in the same solution. The electrode was rotated at 2000 rpm

The catalytic current for the immobilised HoxFU moiety has a similar shape to that observed for the *H. thermoluteolus* HoxFU on a PGE RDE, suggesting that immobilising the HoxFU from *H. thermoluteolus* on carbon paper does not significantly alter the electrochemical behaviour of the HoxFU moiety. The CV, however, shows a flat curve between -500 and -600 *vs* SHE suggesting substrate limitations, probably due to the electrode being mass transport limited, as it is not being rotated at 2000 rpm; but

instead relying on a small magnetic stirrer to replenish the solution at the surface of the electrode.

5.2.2 Chronoamperometry methods

Chronoamperometry was used to drive and monitor the enzyme-electrolysis (bio-electrolysis) reactions carried out.

For bulk electrolysis a fritted counter electrode was used. Here a coiled Pt wire was placed in a heat shrink tube with a vycor porous glass frit (Gamry Instruments) sealed into the bottom of the tube.[249] This tube was then filled with the same buffer as that used in the experiment. This ensures that the reaction mixture is isolated from any oxidative processes occurring at the counter electrode, meaning that the product or cofactor isn't re-oxidised at the counter electrode before it can be used.[249]

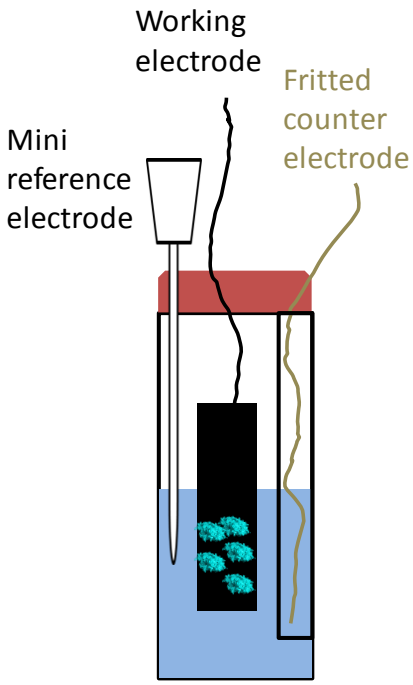

Figure 5-7: A UV-vis cuvette set up, used in Spectro-electrochemistry experiments and in bulk electrolysis experiments.

Spectro-electrochemical experiments and bulk electrolysis reactions were carried out using a plastic cuvette (Thermofisher) as the electrochemical cell, shown diagrammatically in Figure 5-7.[250] This allowed monitoring of the production of

NADH at 340 nm during experiments. The cuvette was sealed with a rubber septum. A home-made miniature calomel electrode was used as the reference electrode, construction of which is described in the Methods and Theory section. Temperature control of the set-up was provided by a Peltier element, and mixing was achieved by using a built-in magnetic stirrer with a mini stirrer bar (Thermofisher, diameter *ca.* 1 mm).

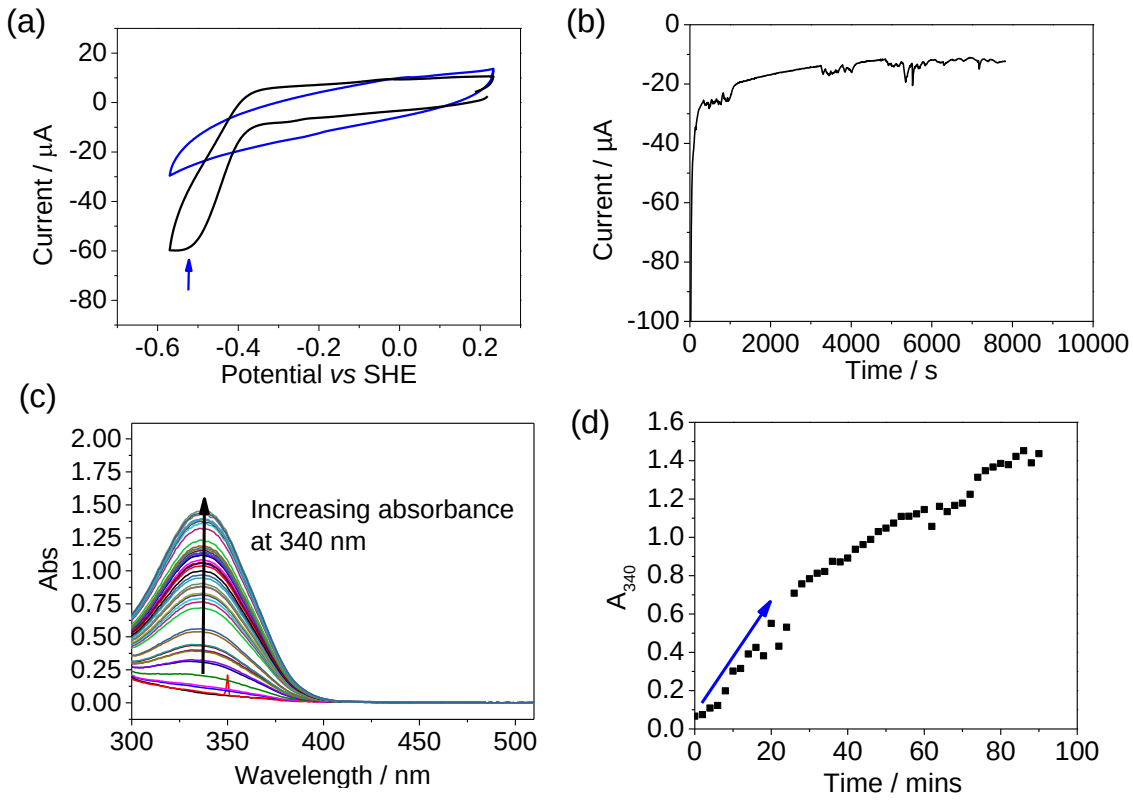

Figure 5-8: Electrochemical generation of NADH using a *H. thermoluteolus* HoxFU carbon paper functionalised electrode. (a) Cyclic voltammogram (from Figure 5-6) of a *H. thermoluteolus* HoxFU functionalised carbon paper electrode in 1 mM NAD^+ with the blue arrow showing the potential at which the carbon paper working electrode was held during the chronoamperometry experiment (b) A chronoamperometry trace taken over the course of the reaction. The reaction was carried out by applying 11 µg of *H. thermoluteolus* HoxFU to a carbon paper electrode (*ca.* 100 mm^2) and then concentrating the enzyme onto the electrode surface *via* evaporation for 15 minutes. The electrode was then submerged into a cuvette containing 1 mL of 50 mM Tris-HCl pH 8 and 1 mM NAD^+. The electrode was held at -520 mV *vs* SHE over a period of 70 minutes, during which time the Peltier accessory was used to provide stirring and to maintain a temperature of 40 ^oC. (c) Sequential scans taken every 2 minutes, showing increasing absorption at 340 nm, corresponding to increasing NADH concentration. (d) Points at 340 nm from (c) plotted as a function of time, used to calculate the activity from the gradient over the first 20 minutes.

Electro-enzymatic generation of NADH using the *H. thermoluteolus* HoxFU was carried out at 40 ^{o}C, as data in chapter 4 (section 4.5.3) show that the half-life of *H. thermoluteolus* HoxFU at 40 ^{o}C is 19 minutes, which is very similar to the half-life for *R. eutropha* HoxFU at 22 ^{o}C, the half-life at higher temperatures being too short for practical applications. Figure 5-8 (a) shows a CV from Figure 5-6 (a) with a black arrow showing the potential at which the high surface area electrode was held on the CV.

The trace in Figure 5-8 (b) shows the chronoamperogram for the reduction of NAD^+ by the HoxFU functionalised high surface area electrode and figure (c) shows sequential scans taken every two minutes demonstrating increasing NADH concentration. Figure (d) was obtained by plotting the absorbance at 340 nm from (c) as a function of time.

By virtue of the fact that the charge passed (Q) is equal to the current (I) multiplied by time (t), by integrating the current over the course of a reaction it is possible to determine the total charge passed. This charge figure can then be used to calculate the number of electrons passed; hence, giving the theoretical amount of product produced. This can then be used to determine the current efficiency of the electrochemical process under consideration.[251]

After 70 minutes (4200 s) a charge of 0.068 C had passed which corresponds to 0.34 mM of NADH produced. A concentration of 0.23 mM NADH was obtained from the UV-visible data shown in Figure 5-8 (c). This suggests that the transfer of electrons to generate NADH in solution is 68 % efficient. This is probably a result of some of the NADH adsorbing on to the carbon. There is evidence in the literature that both NAD^+ and NADH absorb on a variety of carbon materials.[162,252] For example NAD^+ is known to absorb to glassy carbon.[162]

By fitting a line of best fit to the points in Figure 5-8 (d) a gradient can be determined, this can be used to calculate the specific activity per HoxFU in this experiment. A specific activity of 0.3 U mg^{-1} (U = μmoles of product per minute) per HoxFU immobilised on the carbon paper or a TOF (turnover frequency) of 0.5 moles of product per mole of enzyme, per second was obtained. Although, these figures are significantly lower than the value obtained for the whole SH in solution, see Chapter 4, it is probably the case that not all of the enzyme supplied was absorbed on the electrode and that some of the enzyme that was absorbed was not in the correct orientation to carryout electro-catalysis.[152] In addition, the scan in Figure 5-8 (a) demonstrates that at the potential at which the electrode was held in this experiment, cycling of NAD^+ and NADH at the electrode surface is mass transport limited and this is likely to become more significant over the course of the reaction.

5.2.3 Testing whether the electrochemically generated NADH is enzyme active

Many electrochemical methods of NAD^+ reduction lead to the production of inactive forms of NADH, such as radicals, dimers or regio-isomers of NADH.[92] It is therefore important to demonstrate that the NADH produced using this electrochemical method can actually be accepted by an NADH dependent enzyme.

After 76 minutes an aliquot of 2-methyl-2-cyclopentenone (1 mM) was added to the reaction mixture, followed by a 57 μg aliquot of *TsER* and the electrode was held at -520 mV *vs* SHE for a further 56 minutes at 40 ^oC. An aliquot of the reaction mixture was then removed for analysis by GC.

Figure 5-9 shows the GC trace used to determine how much product was produced, when coupling the *TsER* to electrochemical NADH generation using the *H. thermoluteolus* HoxFU. Peaks are seen both at 5.7 minutes and at 8.2 minutes

corresponding to the 2-methyl-cyclopentanone product and 2-methyl-2-cyclopentenone substrate respectively.

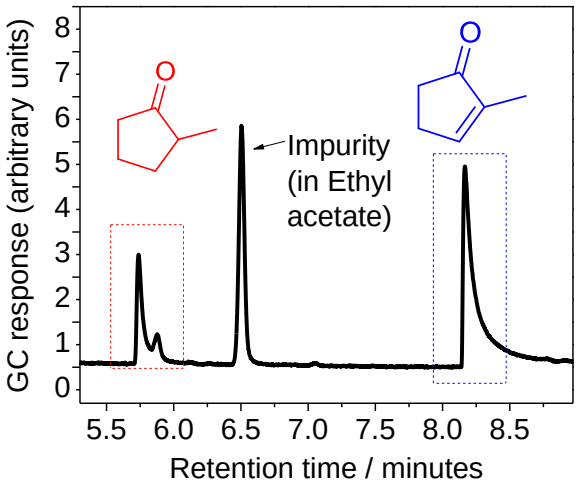

Figure 5-9: A GC trace demonstrating the conversion of 2-methyl-2-cyclopentenone to 2-methyl-cyclopentanone, using the electrochemically generated NADH.

Comparison of the area of the peak at 5.7 minutes in Figure 5-9, which corresponds to the 2-methyl-cyclopentanone product, to standards gives a product concentration of 0.4 mM. This would correspond to 40 % conversion and clearly demonstrates that the NADH which has been produced electrochemically using the *H. thermoluteolus* HoxFU functionalised electrode can be used by the *TsER* to convert 2-methyl-2-cyclopentenone to 2-methyl cyclopentanone. Overall during the course of this experiment 0.1148 C of current were passed this would equate to approximately 0.57 mM of NADH being produced, meaning that at the end of this reaction the overall current efficiency for the *TsER* coupled reaction is 70 %, this similar to the current efficiency obtained for NADH production.

The CV in Figure 5-6 demonstrates that there are mass transport limitations which affect the rate of catalysis when a carbon paper electrode is used. Therefore, it was decided not to continue with investigations into elevated temperature electrochemical

NADH reduction coupled to the *TsER* and instead focus on H_2-driven elevated temperature NADH recycling using enzyme-modified particles.

5.3 H_2-driven cofactor recycling at elevated temperatures

Product and substrate evaporating

This section examines how much of the 2-methyl-2-cyclopentenone substrate and the 2-methyl-cyclopentanone product evaporate under the reaction conditions used for cofactor recycling with the H_2-driven particles.

To ensure that reaction mixtures remain saturated with H_2 gas, the standard procedure in the laboratory involves constantly flowing H_2 gas over the top of the reaction mixture, see Methods and Theory chapter, section 2.6. For volatile substances this presents a problem. It was therefore important to be able to estimate the volatility of the 2-methyl-2-cyclopentenone substrate and the 2-methyl-cyclopentanone product, when left for 18 hours open to the air.

Table 5-1: A table showing the percentage of substrate and product retained after being left for 18 hours either at 40 ^{o}C (in a water bath) with the lid closed and at 40 ^{o}C (in a water bath) with the lid open in comparison to a sample left at 4 ^{o}C with the lid closed. All tubes initially had 1 mL of solution in them, containing 10 mM substrate or 10 mM product in pH 8 50 mM Tris-HCl.

	[2-methyl-cyclopenten-one] / % retained (substrate)	**[2-methyl-cyclopentanone] / % retained (product)**
Closed vessel	72	68
Open vessel	81	37

% retained values were determined by comparison of the peak areas with those of the standards incubated at 4 ^{o}C.

Data in Table 5-1 show that at 40 ^{o}C significant amounts of 2-methyl-cyclopentanone were lost from the solution after incubation in a vessel open to the atmosphere (63 % loss). The evaporation of the 2-methyl-2-cyclopentenone substrate is less significant.

Some substrate and product was also lost from the vials with the closed lids, i.e. not open to air. This is likely to be due to the vessels not being cooled before the samples were extracted into ethyl acetate for GC analysis.

Absorbtion of 2-methyl cyclopenten-1-one and 2-methyl cyclopentanone on carbon

This section investigates whether the 2-methyl-2-cyclopentenone substrate and the 2-methyl-cyclopentanone product absorb onto BP 2000 particles.

Activated carbons are often used to remove organic molecules from aqueous solutions.[253] Therefore, it is important to be able to determine whether 2-methyl-2-cyclopentenone (substrate) and 2-methyl-cyclopentanone stick to the carbon surface of BP 2000 particles, and whether it is ultimately possible to extract them into ethyl acetate to allow GC analysis of conversion.

Solutions containing 2-methyl-2-cyclopentenone and 2-methyl-cyclopentanone in 50 mM Tris-HCl pH 8.0 were incubated with BP 2000 particles (carbon black) for one hour. Samples were prepared containing both 1 mM and 10 mM concentrations of 2-methyl-2-cyclopentenone and 2-methyl-cyclopentanone.

Table 5-2: Amount of substrate or product it was possible to extract as a percentage of the amount of substrate or product extracted from solutions not containing particles

Starting concentration of solution / mM	[2-methyl-cyclopenten-one] / mM (substrate)	[2-methyl-cyclopentanone] / mM (product)
1	98	95
10	>99	>99

400 µg of BP 2000 particles were added to Eppendorf tubes containing 500 µL of each of the solutions in 50 mM Tris-HCl pH 8. Particles were incubated for 1 hour. Extraction of the product was achieved by adding the ethyl acetate (500 µL), vortexing to ensure efficient mixing, centrifuging, separating the layers, and then repeating the process twice to give a total volume of 1 mL of ethyl acetate. The collected ethyl acetate fractions were then dried using excess $MgSO_4$ and filtered through cotton wool.

The data in Table 5-2 shows that in all cases it was possible to obtain at least 95 % of 2-methyl-2-cyclopentenone and 2-methyl-cyclopentanone back from samples with BP 2000 particles in them, after extracting with ethyl acetate. This shows that both 2-methyl-2-cyclopentenone and 2-methyl-cyclopentanone do not stick to the bare surface of the BP 2000 particles or at least that it is possible to remove 2-methyl-2-cyclopentenone and 2-methyl-cyclopentanone from the surface of the particles by

extracting into ethyl acetate. Hence, this substrate is suitable for use with the enzyme-modified particles.

5.3.1 Enzyme-modified particles for high temperature cofactor recycling

In this subsection, the rate of NADH production by particles with *H. thermoluteolus* HoxFU and Hyd 2 co-immobilised was tested at temperatures between 30 ^{o}C and 60 ^{o}C. The reaction set-up is shown in Figure 5-1 (b).

Testing the particles over a range of temperatures

In Figure 5-10 (a) the concentration of NADH at each time point has been calculated based on the change in absorption at 340 nm over time. These data show that the particles continue to work up to 50 ^{o}C and that the rate of reaction is faster over the first 20 minutes with increasing temperature. They also demonstrate that the particles are stable at 50 ^{o}C over this time period. These results are highly promising as they suggest that the *H. thermoluteolus* HoxFU moiety is a good candidate for part of a H_2-driven cofactor recycling system for use at elevated temperatures and that Hyd 2 also displays activity at these elevate temperatures.

Data in Figure 5-10 (b) shows the specific activity calculated for a series of repeated measurements between 30 ^{o}C and 60 ^{o}C. For each set of data it is clear that the activity per mg HoxFU increases as the temperature is increased, with the optimum activity being at 60 ^{o}C, as observed for the whole *H. thermoluteolus* SH in chapter 4. It is also clear that the activity decreases from set one to set two, suggesting that the particles become less active over time, while they are being stored. The average specific activities per mg of *H. thermoluteolus* HoxFU are: 1.2 ± 0.3 U mg^{-1}, 2.1 ± 0.2 U mg^{-1}, 3.6 ± 0.4 U mg^{-1} and 5.5 ± 0.2 U mg^{-1} at 30 ^{o}C, 40 ^{o}C, 50 ^{o}C and 60 ^{o}C respectively. This compares favourably with reported activity values for the system with Hyd 2 and *R. eutropha* NAD^+ reductase.[119]

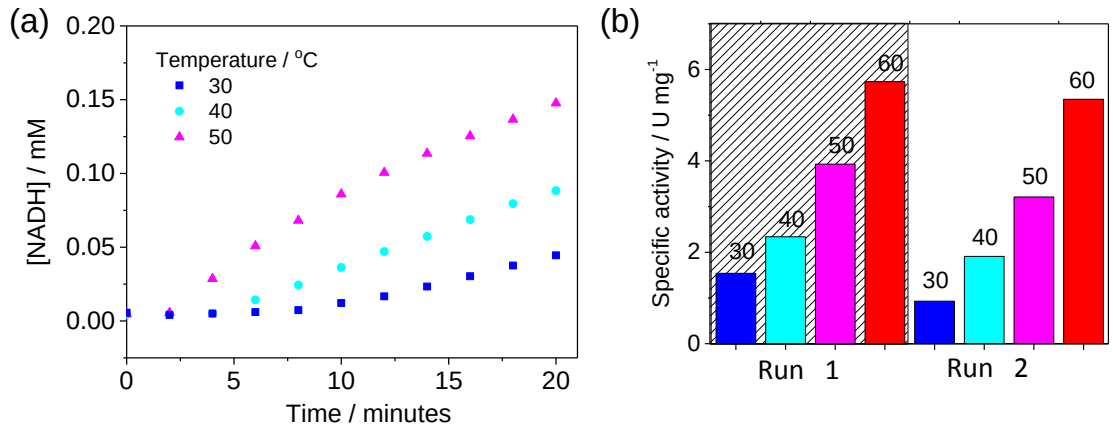

Figure 5-10: H_2-driven NADH production between 30 °C and 60 °C. (a) A comparison between the amount of NADH generated by particles at 30 °C, 40 °C and 50 °C as a function of time (c) The specific activities of repeated experiments carried out at different temperatures. The temperature at which each run was conducted is shown above each bar, the activity is given as U mg^{-1} of HoxFU. Reactions were carried out in 50 mM MOPS buffer pH 7, approximately 55 µg of *E. coli* Hyd 2 and 22 µg of *H. thermoluteolus* HoxFU were added to 0.6 mg of BP 2000 particles in a total volume of 70 µL. Each reaction used 5 µL of a particle suspension; these were injected into a cuvette containing 1 mM NAD^+ in H_2-saturated MOPS buffer. The reactions were stirred rapidly throughout.

These specific activities correspond to TOFs of 1.8 ± 0.5 mol s^{-1}, 3.2 ± 0.3 mol s^{-1}, 5.4 ± 0.5 mol s^{-1}, 8.3 ± 0.3 mol s^{-1} at 30 °C, 40 °C, 50 °C and 60 °C respectively. These values compare favourably with the TOFs obtained for asymmetric hydrogenations of alkenes using organometallic catalysts, discussed in section 1.2.2.

5.3.2 Coupling the *TsER* to the H_2-driven NADH recycling system

This section investigates whether the enzyme-modified particles developed in section 5.3.1 can be used as a cofactor recycling system in combination with an NADH dependent thermophile enzyme: the *TsER* , at elevated to temperatures.

Initial experiments

Initially, a number of control reactions were performed. Table 5-3 details control experiments performed with the enzyme-modified particles and the *TsER* ; the first two entries are initial demonstrations that it is possible to obtain conversion of 2-methyl-2-cyclopentenone-one to 2-methyl-cyclopentanone using the *TsER* at 40 °C, either by

adding stoichiometric quantities of NADH or by using GDH as the cofactor recycling system.

The two controls (entries 3 and 4) with unfunctionalised BP 2000 particles and with particles with only Hyd 2 immobilised on them demonstrated that reduction of 2-methyl-2-cyclopentenone does not occur at the bare carbon of the BP 2000 particles. This supports the electrochemical results in Figure 5-4 (d), as it demonstrates that the 2-methyl-2-cyclopentenone substrate cannot be reduced at bare carbon at a potential more positive than -472 mV *vs* SHE (the potential for the $2H^+/ H_2$ couple under 1 bar H_2 at pH 8).

Table 5-3: A summary of controls for H_2-driven coupling reactions with particles and the *TsER* at 40 ^oC

Entry	Conditions	TsER / µg	Approx. number of Units[a]	Initial Substrate Conc / mM	Final Product Conc/ mM[b]	Comments
NADH	250 µL scale, Cuvette left open to the atmosphere NADH added over time (5 mM total)	60	$33x10^{-3}$	5.0	2.7	Evaporation of the 2-methyl-cyclopentanone is likely to have occurred as the reaction was carried out over 6 hours in open air
GDH	Sealed vial with 10 mL headspace. Reaction carried out at 40 ^oC, not cooled before extracting (ca. 1.6 mg GDH, 5 mM glucose).	60	$33x10^{-3}$	5.0	1.0	Relatively low conversion. Suggests significant loss of product on opening the sealed vial without cooling.
BP 2000	500 µL reaction scale, with the reaction carried out in a 10 mL sealed vial filled with H_2 gas, 0.6 mg BP 2000 particles.	-	-	5.0	0	No reaction. Control demonstrates no side reactivity observed with BP 2000 carbon particles on their own
Hyd 2, BP 2000	Hyd 2 (20 µg immobilised on 0.8 mg BP 2000 particles) reaction carried out in a 10 mL sealed vial filled with H_2 gas.	-	-	5.0	0	No reaction. Control demonstrates no side reactivity observed with BP 2000 particles just functionalised with Hyd 2. Meaning no reduction is occurring at the bare carbon surface of the particles.

[a]Number of units estimated based on activity of *TsER* as 40 ^oC (Units = µmoles min^{-1}). [b]Product concentration based on standards, see Appendix C.

Table 5-4: A summary of experiments for H_2-driven coupling reactions with particles and the *TsER* at 40 ^oC

Entry	Conditions	HoxFU /µg	TsER / µg	Approx. number of Units[a]	Substrate Conc / mM	Product Conc / mM[b]	Percent yield[c]	Comments
1	H_2 constantly equilibrating in headspace of a 1 mL UV-vis cuvette, overnight, 150 µL scale	3.5	20	11 $x10^{-3}$	10	0.022	0.22	Low conversion, likely due to evaporation and not enough HoxFU
2	H_2 constantly equilibrating in the headspace of a UV-vis cuvette, overnight, 500 µL scale (0.3 mM NAD^+)	16	60	$33x10^{-3}$	5	0.24	4.8	Evaporation still likely to be a problem, Although larger volume and more HoxFU seem to have led to an increased yield
3	In a sealed UV-vis cuvette for 18 hours, 500 µL scale (0.3 mM NAD^+), H_2 topped up every two hours for first 6 hours.	16	60	$33x10^{-3}$	5	0.6	12	H_2 now probably limiting the system
4	Sealed 10 mL vial, overnight, 500 µL scale (1 mM NAD^+), Samples cooled in ice prior to extraction. Reaction carried out in a water bath with shaking at 100 rpm.	55	60	$33x10^{-3}$	5	0.76	15.2	Product produced, evaporation still a significant problem. Also, potentially not enough H_2 available in sealed vial set up, with rubber septum as sealing device.
5	2 bar H_2, in a pressure system on a 200 µL scale for 12 hours. Reaction was carried out in a conical centrifuge tube inside the pressure system and the pressure system was cooled prior to extraction. Reaction carried out in a water bath with shaking at 100 rpm.	22	100	55 $x10^{-3}$	5	1.1	22	Product evaporation still seems to be a problem even in the pressure system. Furthermore, limited shaking in a water bath may have meant that the reaction mixture did not remain hydrogen saturated.

[a]]Number of units of *TsER* estimated based on activity of *TsER* as 40 ^oC (Units = µmoles min^{-1}). [b]Product concentration based on standards, see Appendix C.
[d]Isolated yield, based on concentration of product obtained

Entries 1 to 5 in Table 5-4 summarise experiments designed to couple the *TsER* to the H_2-driven enzyme-modified particle system for cofactor recycling at 40 ^{o}C. Entries 1 and 2 demonstrate that it is possible to obtain some conversion of 2-methyl-2-cyclopentenone to 2-methyl-cyclopentanone; but that with constant H_2 gas flow into the headspace of the cuvette used to carry out these experiments a significant amount of substrate and product evaporated from the reaction vessel, as would be expected from the findings in section 5.3.

Entry 3 demonstrates an increase in the amount of product produced, when H_2 is not constantly flowed over the top of the reaction vessel. Theoretically, a volume of >500 µL H_2 at 1 bar pressure in the headspace of the cuvette represents a super-stoichiometric amount of $H_{2(g)}$ for the reduction of 500 µL of 5 mM 2-methyl-2-cyclopentenone. The surface area of the liquid-gas interface in the cuvette is 40 mm^2. It is likely that, large amounts of this $H_{2(g)}$ escaped through the septum of the cuvette and without constant H_2-gas flow were not replenished, even though the reaction was topped up with $H_{2(g)}$.

In entry 4 a larger reaction vessel was used. This led to a greater amount of product being produced confirming the hypothesis that $H_{2(g)}$ supply was limiting in entry 3.

However, Paul *et al*. managed to achieved a percentage yield of >93% with the *TsER* using this substrate when simply providing the *TsER* with stoichiometric amounts of NADH.[66] This, implies that supply of H_2 gas is still limiting the reaction, leading to a limited supply of NADH. This is again probably due to $H_{2(g)}$ leaking out of the rubber septum used to seal the vessel.

Finally, a test was carried out in a pressure system (entry 4), which ensured that the reaction vessel could be effectively sealed and that elevated pressures (2 bar) could be used to ensure that the amount of H_2 dissolved in solution was increased in comparison

to reactions run under atmospheric pressure. This reaction gave a promising conversion of 1.1 mM product equivalent to a 22 % yield. However, evaporation of the product and substrate remained a problem even when the reaction was carried out in a pressure system with a limited internal volume.

Further controls

Because of the promising yields that could be achieved when using the pressure system experiments were carried out in order to try to optimise this reaction set-up further. On increasing the temperature by 10 ^{o}C going from 30 to 40 ^{o}C; it is expected that the solubility of $H_{2(g)}$ in solution would go down from around 0.7 mM to 0.65 mM. However, Henry's law states that there is a linear dependence on the partial pressure of a gas and its concentration in a dilute solution. Therefore, carrying out reactions with the enzyme-modified particles under 2 bar H_2 pressure should more than offset the decrease in solubility of $H_{2(g)}$ due to the increase in temperature. See Methods and Theory chapter section 2.4.3 for further discussion.

Table 5-5: Control reactions to demonstrate how much product and substrate can be retained after a reaction in the pressure system.

Entry	Conditions[a]	2-methyl-cyclopenten-one (substrate)/ %[b]	2-methyl-cyclopentanone (product)/ %[b]
1	10 mM substrate and product in separate pressure systems. Each vessel contained 200 µL of mixture in 15 mL conical centrifuge tube inside the pressure system	59	24
2	In pressure system (5 mM substrate and 5 mM product in same system) 500 µL added to system without a conical centrifuge tube inside the system.	76	77

[a]All reactions were carried out in pH 8 50 mM Tris-HCl buffer at 40 ^{o}C for 18 hours, under 2 bar H_2 with shaking at 100 rpm. The size of the pressure system glass vial is 25 cm^3.
[b]Percentage of product or substrate retained as a percentage of that extracted from samples stored at 4 ^{o}C, in sealed Eppendorf tubes.

Table 5-5 shows a series of controls carried out in the pressure system in an attempt to optimise the reaction set up, in order to minimise evaporation of the 2-methyl-cyclopentanone product during the course of a reaction. The two reaction set-ups are shown schematically in Figure 5-11.

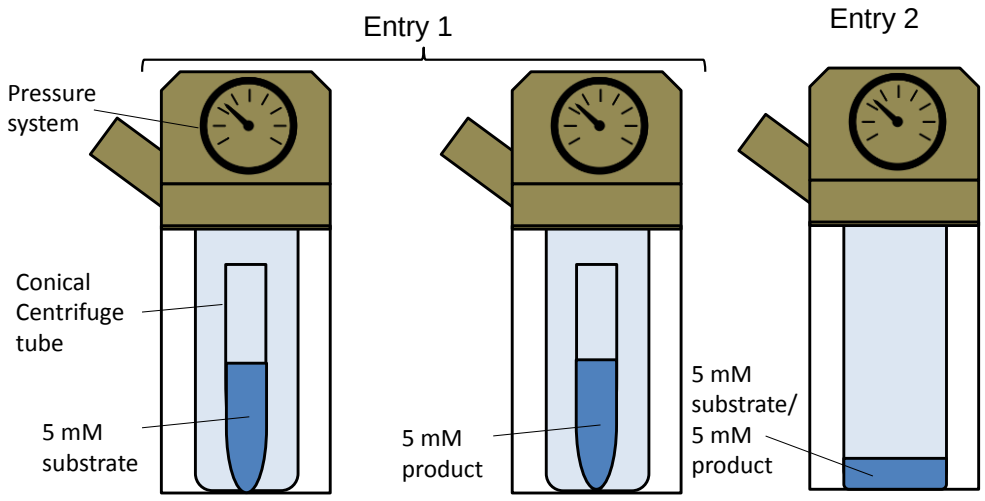

Figure 5-11: A schematic diagram showing the controls carried out to investigate reducing evaporation of 2-methyl-2-cyclopentenone and 2-methyl-cyclopentanone.

In entry 1, two pressure systems were used. A conical centrifuge tube was used inside each pressure vessel containing a 200 µL aliquot of 10 mM substrate or product and a piece of parafilm was loosely placed on top of the tube. Despite the pressure systems being cooled in ice for 1 hour before the product and substrate were extracted for GC

analysis only *ca.* 60 % of the substrate and only *ca.* 25 % of the product could be seen on the GC trace in comparison to standards, which were extracted and run at the start of the reaction.

In entry 2, however, a slightly larger reaction volume of 500 µL was used and the substrate and product were both inside the same pressure system. Additionally, the substrate and product mixture was added directly to the base of the glass body of the pressure system, without a conical centrifuge tube inside. Following 18 hours at 40 ^{o}C, the pressure system was cooled in ice for 1 hour before the substrate and product were extracted into ethyl acetate for analysis. In this set-up 77 % of the product could be retained, this is a significant improvement on previous reaction set-ups.

The data in entry 2 suggests that it is possible to reduce evaporation of 2-methyl-cyclopentanone (or at least ensure that the product re-condenses back into the reaction phase) by having the reaction mixture directly in the body of a well-sealed pressure system and by cooling the whole pressure system in ice before extracting the reaction mixture.

Biotransformation

Following the positive result in entry 2 in Table 5-5, a biotransformation was set up to couple the *TsER* to the enzyme-modified particles for elevated temperature cofactor recycling. A 500 µL aliquot of reaction mixture was added directly to the base of the pressure system to ensure that as in entry 2 (Table 5-5), as much substrate or product as possible condenses back down into the reaction vessel if it evaporates. In this reaction, the pressure system was, in addition, placed in an incubator at 40 ^{o}C to ensure fast enough agitation, to avoid limiting H_2 supply to the enzyme-modified particles.

After 14 hours the pressure system was cooled in ice and the sample was extracted into ethyl acetate for analysis by GC. The GC trace is show in Figure 5-12.

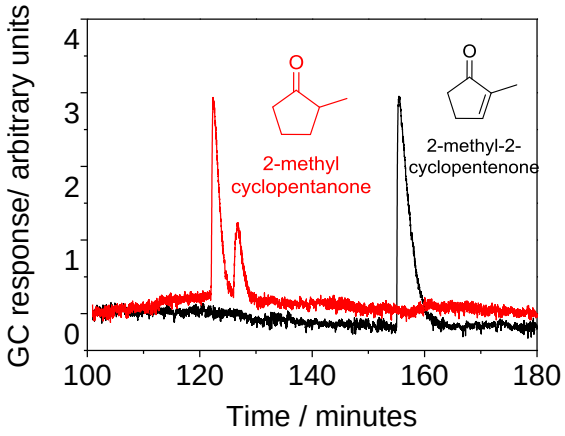

Figure 5-12: (a) A chiral GC trace demonstrating production of 2-methyl-cyclopentanone. Trace in black shows the starting mixture, the trace in red is of a sample following the reaction. The enzyme-modified particles were made using 105 µg Hyd 2, 33 µg *H. thermoluteolus* HoxFU and 1.2 mg BP 2000, which were pre-mixed and then left at 4 °C for one hour. The particles were then added to a reaction mixture (total volume 500 µL) containing 1mM NAD^+, 5 mM 2-methyl-2-cyclopentenone and 2 % DMSO in H_2-saturated 50 mM Tris-HCl pH 8. An aliquot of 150 µg of *TsER* was subsequently added to the reaction mixture. The reaction mixture was then added directly to the glass base of the pressure system and incubated under 2 bar H_2-pressure for 14 hours in an incubator at 40 °C with shaking at 100 rpm. The sample was then extracted into 1 mL ethyl acetate (the extraction procedure was performed twice with 500 µL ethyl acetate with toluene as the internal standard) and analysed using chiral GC. The yield was determined based on a racemic standard assuming the GC response factor for both enantiomers is the same. Further details are given in Appendix C.

The chiral GC trace in Figure 5-12 shows no substrate peak at 160 minutes in the red trace corresponding to the reaction mixture, this suggests >99 % conversion. The area of the peaks at 120-130 minutes would correspond to a concentration of 3.14 mM 2-methyl-cyclopentanone based on a series of racemic standards, where it has been assumed that the GC response factor for each enantiomer is the same. This corresponds to an isolated yield of 62 % of the 5 mM concentration of starting material added; however, from the controls in Table 5-5 it would be expected that the percentage yield would be lower than the percentage conversion as it is likely that some of the volatile 2-methyl-cyclopentanone product is lost on depressurising the pressure system.

The *ee* of the product shown here, based on the relative areas of the peaks for each enantiomer is 50 %. This is lower than the value of > 99 % *ee* ((S)-enantiomer)

obtained for this product by Paul *et al*. using stoichiometric amounts of NADH with the *TsER* enzyme.[66]

Scrutton and co-workers have already reported on the poor enantiopurity of products with stereogenic centres alpha to a carbonyl from biocatalytic reactions with an alternative ene reductase (PETNR).[57] They concluded that this was due to a non-enzymatic process and that loss of enantiopurity was greater if reactions were carried out over 24 hours and at pH values > 7.[57] It is likely that deprotonation at the stereogenic centre leading to the formation of an sp^2 hybridised intermediate leads to the racemisation. At pH 7 Scrutton and co-workers found that with (R)-levodione (a molecule containing a six member ring with a stereogenic centre alpha to a carbonyl) a decrease in enantiopurity of approximately 3 %ee/h was observed.[57] Therefore, they emphasise that short reaction times are critical to improving the enantiopurity of ene reductase products with a stereogenic centre alpha to a carbonyl.[57]

Over the course of the 14 hour reaction, this racemisation process is likely to be responsible for the drop in *ee* seen here in comparison to the work of Paul *et al*. Assuming that the *TsER* with the enzyme-modified particles as a cofactor recycling system displays perfect enantioselectivity, this suggests that over the course of the 14 hour reaction half of the product has undergone racemisation.

However, overall the impressive conversion of 2-methyl-2-cyclopentenone to 2-methyl-cyclopentanone demonstrates the effectiveness of the *H. thermoluteolus* HoxFU enzyme-modified particles for elevated temperature cofactor recycling when coupled with the *TsER.*

5.4 Investigating whether a layer of immiscible organic solvent could be used in combination with the enzyme-modified particles

Water is avoided as a solvent in most reactions performed by synthetic organic chemists, due to the limited solubility of organic compounds in water, the difficulties associated with removing water and the possibility of other side reactions occurring in water, such as hydrolysis, racemisation, polymerisation and decomposition of substrates and products.[11]

Conventional biocatalysis is generally performed in aqueous systems.[11] However, using organic solvents can lead to the following advantages: it is possible to obtain higher concentrations of poorly soluble products and substrates in organic solvents, reaction equilibria can be shifted favourably and hydrolysis of substrate and product can be prevented.[254]

There are two possible classes of organic solvent-aqueous systems: class 1 Water, water miscible organic solvent systems, leading to a homogeneous reaction mixture, and class 2 water, water immiscible organic solvent systems giving a two layer biphasic system.[254] High concentrations of miscible organic solvent in bio-catalytic systems often give rise to inhibition, decreased specificity and denaturation.[255] Using biphasic systems can avoid a lot of these disadvantages and has the added advantages that recovery of product and biocatalyst can be facilitated *in situ* by a biphasic system.[254,255] Additionally, *in situ* product removal can lead to lower concentrations of inhibitor in the aqueous environment.

This work focuses on a water, water immiscible organic solvent system, in which a layer of undecane was added as a second layer.

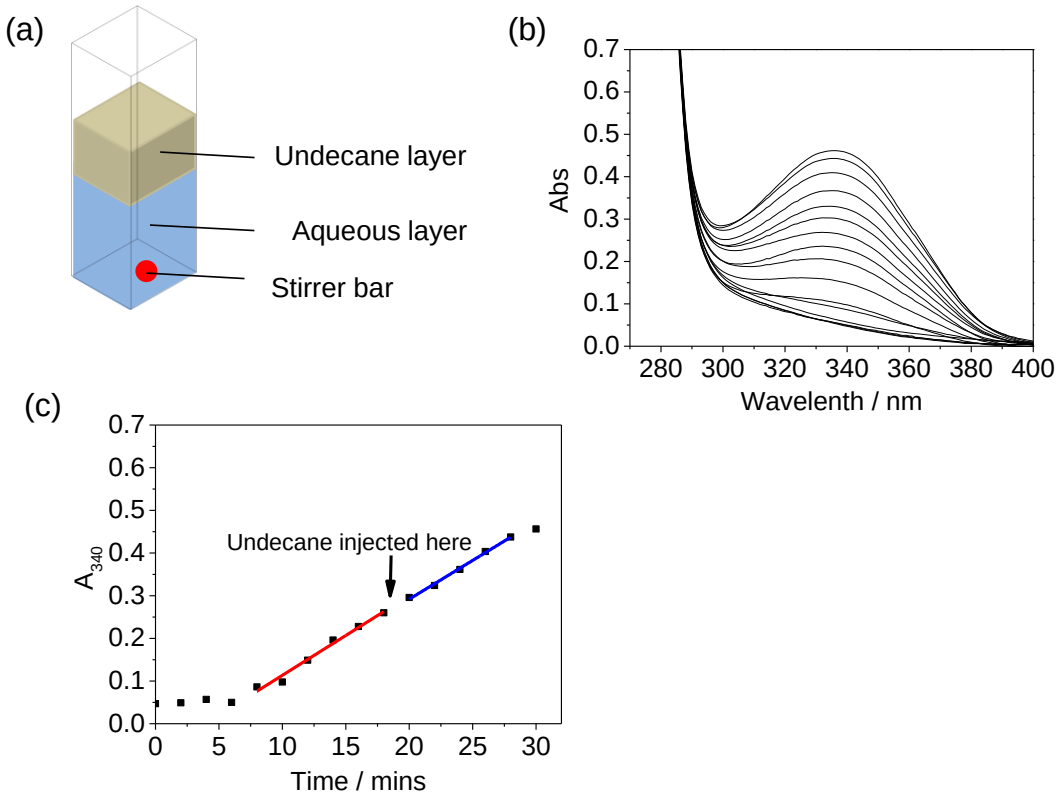

Figure 5-13: Solvent tolerance experiments. (a) A schematic diagram showing a UV-visible cuvette containing buffer with particles in (aqueous layer) and a layer of undecane injected on top. (b) Sequential scans taken before and after addition of undecane. (c) The absorption at 340 nm taken from (c), the point at which undecane was injected is shown with an arrow.

An experiment was carried out in which particles were prepared with *H. thermoluteolus* HoxFU, Hyd 2 and BP 2000 particles. Aliquots of particles were then added to a cuvette containing 1 mL 1 mM NAD^+ in H_2-saturated 50 mM Tris-HCl pH 8. The H_2-driven generation of NADH was followed by taking UV-visible scans every 2 minutes. Activities were determined by plotting the absorption at 340 nm from baseline corrected spectra as a function of time. In the first run no organic solvent was injected into the cuvette and the reaction was allowed to run for 30 minutes.

In three subsequent experiments particles were added to a cuvette containing H_2-saturated buffer and 1 mM NAD^+; with fast stirring of the solution in the cuvette. After 14 minutes, 200 µL of undecane was quickly added to the cuvette. The solution in the cuvette was pipetted up and down several times, so that it perturbed the solution.

The reaction was then run for another 16 minutes. The activity of the particles after injecting undecane was compared to the activity for the period before giving a percentage activity value, see Figure 5-13.

Table 5-6: A comparison of the activity of particles at 40 ^{o}C before and after addition of the organic solvent undecane.

	Percentage activity retained after solvent injection at 14 minutes / %
No injection	99.1
Fast stirring	87 ± 12
Slow stirring	87 ± 10

Similar experiments were repeated with slow stirring. The rate of reaction before and after 14 minutes was also measured for a sample in which no solvent was injected. Data in Table 5-6 show that the percentage activity of the 16 – 30 minute time points *versus* the 0 -14 minute time points is 99 % for the measurements where no undecane was injected into the cuvette. This demonstrates that the rate of NADH generation is fairly constant over a 30 minute time period.

The drop in activity on application of an organic undecane layer was low (*ca.* 0 - 20 %), for both the situation where the mixture was stirred quickly and where it was stirred slowly. The activity values obtained when an organic solvent layer was added are equal to the activity when no organic solvent layer was added within the degree of experimental error of this experiment. This suggests that these particles can be considered to be tolerant to immiscible organic solvents. This may be useful for bio-catalytic reactions where an immiscible second phase is useful to act as a reservoir of substrate or product.[255]

5.5 Summary

This chapter has built upon the characterisation of the *H. thermoluteolus* SH in chapter 4 and the use of enzyme-modified particles in chapter 3. In this chapter two cofactor recycling systems for use at elevated temperatures have been developed. These systems complement other whole hydrogenase based systems such as hydrogenase 1 (SH) from *Pyrococcus furiosus* used in NADPH recycling[116] and the whole SH from *H. thermoluteolus* characterised in Chapter 3, which can be used for H_2-driven cofactor recycling at elevated temperatures.

The first system: an electrochemical cofactor recycling system, involved immobilising *H. thermoluteolus* HoxFU onto a high surface area electrode. It was possible to demonstrate conversion of NAD^+ to NADH at 40 ^oC using this system and to show that the NADH produced was enzymatically active, leading to a 40 % yield of product when coupled to the *TsER* enzyme.

Subsequently, enzyme-modified particles were developed with the *H. thermoluteolus* HoxFU co-immobilised on them along with *E. coli* Hyd 2. It was possible to achieved increasing activity from 30 ^oC to 60 ^oC with the enzyme-modified particles.

The enzyme-modified particles were then coupled with the *TsER* enoate reductase at 40 ^oC, where it was possible to achieve an isolated yield of 62 % 2-methyl-cyclopentanone.

Having a cofactor recycling system which can function at elevated temperatures facilitates the easier application of cofactor dependent thermophile enzymes in biotechnology. This is important as there are a number of processes where using elevated temperatures would be advantageous, particularly where it is desirable to reduce the viscosity of solution or to increase the solubility of a substrate.

The next chapter describes work extending the electrochemical and enzyme-modified particle approach for recycling a number of artificial cofactors.

6 Artificial cofactor recycling

6.1 Introduction

This chapter investigates recycling the reduced form of a range of synthetic nicotinamide derivatives or artificial cofactors (mNADH)[125] enzymatically. In section 6.3 it will be investigated whether it is possible to use two commercially available NAD^+ recycling systems to regenerate a number of these artificial cofactors. The chapter then goes on to explore using SH enzymes in section 6.4, and the Mo containing formate dehydrogenase (Mo-FMN) from *Rhodobacter capsulatus* in section 6.5, as systems for recycling artificial cofactors. Section 6.6 explores whether these enzymes can be coupled to an enoate reductase (*TsER*) for selective reduction of conjugated double bonds. Finally, in sections 6.7 and 6.8 electro-enzymatic cycling and using the enzyme-modified particles for H_2-driven cofactor recycling are explored as means of recycling the artificial cofactors. This chapter builds on the work in chapters 4 and 5 as the *H. thermoluteolus* SH is trialled as an artificial cofactor recycling system. Additionally enzyme-modified particles will be used as demonstrated in chapters 3 and 5.

6.2 Background

There is increasing interest in artificial cofactors, where the nicotinamide ring moiety of NADH is conserved, but the side groups are different, following expansion in the field of bio-catalytic redox reactions.[256] The artificial cofactors ($mNAD^+$) investigated in this chapter are shown in Figure 6-1. Throughout this chapter the artificial cofactors are referred to using the recognised abbreviations $mNAD^+$ for the oxidised cofactor and mNADH for the reduced cofactor (where m stands for mimic).[125]

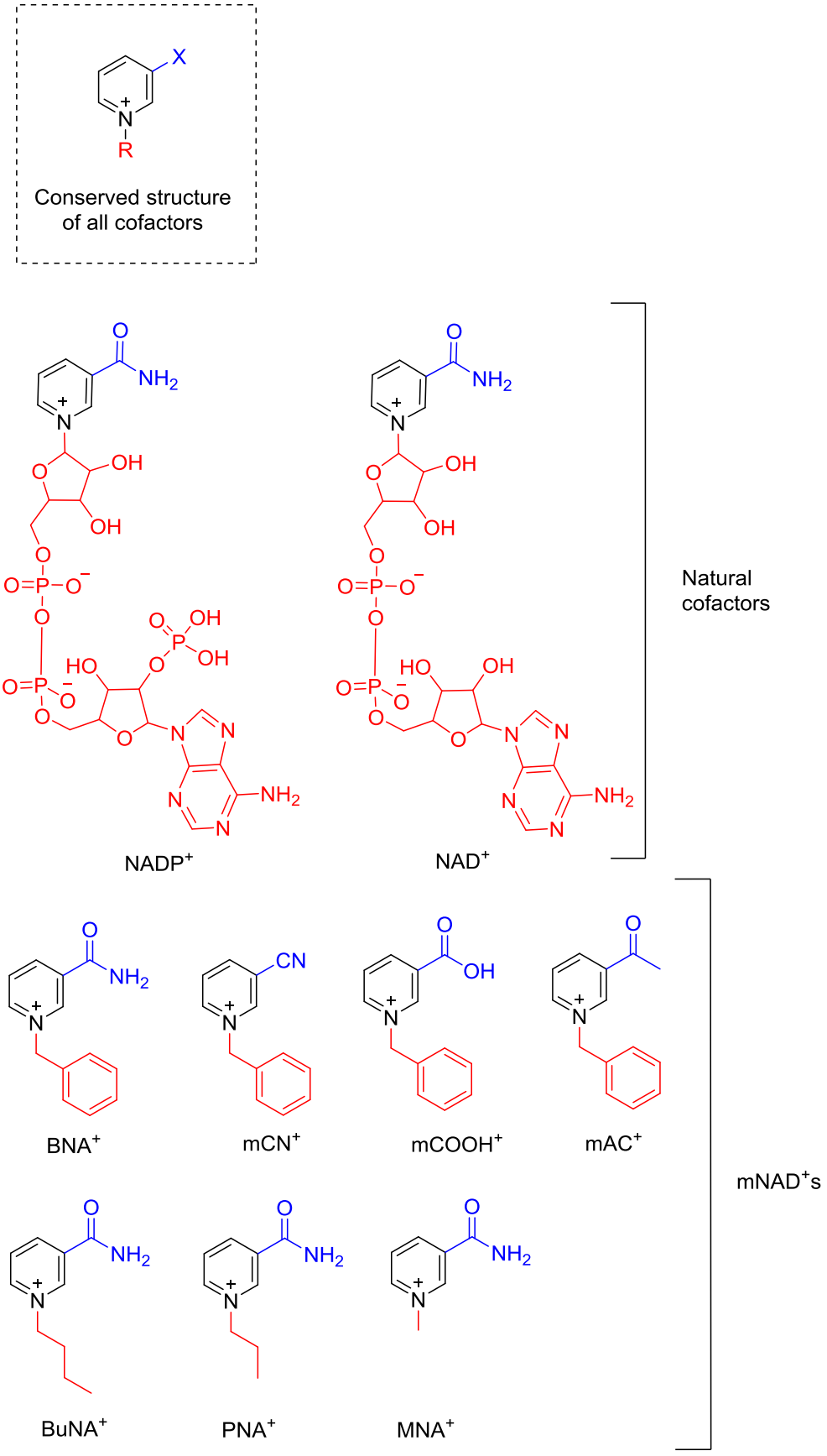

Figure 6-1: The structure of the cofactors used in this chapter.

Table 6-1: A table showing the artificial cofactors used in this chapter along with their absorbance maximum values and extinction coefficients

Simplified name[a]	A_{max} (reduced form)[b]	ε [c]	Cost per mol / £[d]	TN (moles of product per moles of artificial cofactor) required to bring cost below £10/ mol product
$NADP^+$	340	6.3	500000	50000
NAD^+	340	6.22	14000	1400
BNA^+	360	7.3	300	30
mAC^+	378	10.83	580	58
mCN^+	342	5.93	340	34
$mCOOH^+$	283	8.99	750	75
$BuNA^+$	364	6.45	322	32
PNA^+			-	-
MNA^+			-	-

[a]name of the oxidised cofactor used within the laboratory, BNA^+=benzyl nicotinamide, mAC^+: mimic acetyl, mCN^+: mimic cyano, $mCOOH^+$:mimic carboxylic acid, $BuNA^+$:butyl nicotinamide, PNA^+:propyl nicotinamide, MNA^+:methyl nicotinamide; [b]for the naturally occurring cofactors this is the secondary absorption maximum as a result of the UV-Visible absorption from the reduced nicotinamide ring.[c] Extinction coefficients for the secondary maximum of the reduced form of the natural cofactors were obtained from Bergmeyer *et al*.[257] and for the mNADHs values were obtained from Knaus *et al*.[258]; [d]prices calculated based on the value of commercially available reagents from Sigma Aldrich, based on the synthetic procedures used by Paul *et al*.[65][66]

Column six in Table 6-1 demonstrates that the natural nicotinamide cofactors (NAD^+ and $NADP^+$) remain expensive, with one mole of NAD^+ costing about £14,000 based on the current prices from the Sigma Aldrich catalogue.[65] This means that in order to reduce the cost of the cofactor to below £10, for a mole of product it must be recycled at least 1,400 times. In contrast, the artificial cofactors are significantly cheaper to produce as they can be synthesised in the laboratory.[259] For example one mole of BNA^+ only costs £300 to produce; therefore, to reduce the cost of the cofactor to under £10 per mole it must only be recycled 30 times.

Artificial cofactors are only accepted by certain enzymes, meaning that the bio-orthogonality of these cofactors can be exploited in biocatalysis. Consequently,

crude preparations of enzymes (soluble lysates), which might contain other naturally occurring redox enzymes from the recombinant host, can be used in biotransformations as the other redox enzymes (which catalyse undesirable processes) are unlikely to be able to accept a hydride from an mNADH.[66] Additionally, these artificial cofactors are more soluble in organic solvents, which could be a significant benefit if working with enzymes in non-aqueous media.

Nevertheless, recycling artificial cofactors remains an important challenge, in order to avoid producing super stoichiometric amounts of carbon based waste during bio-catalytic redox processes and to keep costs down. Furthermore, it is desirable to be able to produce a highly pure product. If the cofactor can be recycled >100 times, this means that the product will have contamination due to the cofactor of <1%; therefore, further purification steps are often unnecessary.[237] Currently, there is no robust system for recycling the reduced version of these artificial cofactors.[256]

6.2.1 Enzymes able to use artificial cofactors

A range of enzymes with internally bound redox groups (FMN, haem etc.) have already been shown to be able to accept some of the artificial cofactors shown in Figure 6-1. These include enoate reductases such as the enoate reductase from *Thermus scotoductus* (*TsER*) first introduced in chapter 5, modified $P450_{BM3}$ enzymes and 2-hydroxybiphenyl 3-monooxygenase enzymes.[11][260][261] This work focuses on developing an artificial cofactor regeneration system for coupling with the *TsER*.

The TsER has an active site containing FMN and is able to accept reducing equivalents from both NADH and NADPH.[241] Hollmann and co-workers have shown that the *TsER* is able to use all of the artificial cofactors shown in Figure 6-1.[234,258] Additionally, it has been demonstrated that the rate of the reductive half-reactions using

BuNAH is elevated compared to the natural cofactor NADPH for a number of enoate reductase enzymes including the *TsER*.[258] In fact, with the enoate reductases XenA (enoate reductase xenobiotic reductase A) and PETNr higher catalytic efficiency (k_{cat}/K_M) was demonstrated with the artificial cofactor BuNAH for the conversion of the substrate 2-cyclohexenone to 2-cyclohexanone, than with the natural cofactor NADPH i.e. the synthetic cofactors outperforming the natural ones.[258]

6.2.2 Existing systems for recycling artificial cofactors

Glucose dehydrogenases, formate dehydrogenases and alcohol dehydrogenases

Glucose dehydrogenases (GDH), formate dehydrogenases (FDH) and alcohol dehydrogenases (ADH) have been used widely in biotechnological processes where recycling of the natural cofactors NADH and NADPH is required, see section 1.5.2.[13] Recent work by Okamoto *et al*. hypothesises that these enzymatic systems for cofactor recycling cannot be used in combination with the artificial cofactors shown in Figure 6-1, as the lack of binding interactions between the artificial cofactor and residues in the active site of these enzymes leads to extremely high K_M values, which precludes the utility of these enzymes with artificial cofactors in biocatalytic applications.[262,263] It is expected that this will not be the case for enzymes in which the cofactor is required to reduce a tightly bound prosthetic group, such as FMN or haem, as the ring staking interactions between the nicotinamide ring and the prosthetic group within the enzyme would be expected to be conserved.[262] This means that despite the artificial cofactors not having the adenosine diphosphate group, meaning that they will not display the same interactions with the amino acid residues at the enzyme active site, they will still display the same interactions with the prosthetic group at the active site.

In stark contrast to this hypothesis, work by Fish and co-workers appears to demonstrate that horse liver ADH (HLADH) is able to accept the reduced form of BNAH to carry out the reduction of 4-phenylbutan-2-one to 4-phenylbutan-2-ol, suggesting that this enzyme could be used as a regeneration system for the oxidised form of BNA^+.[264] These results could not, however, be replicated with pure, NAD(P)H free samples, of HLADH in the laboratories of our collaborators.[234] In their review paper, Paul *et al*. suggest that the enzyme preparation used in the study by Fish and co-workers possibly contained samples of the natural cofactor NADH.[256,265] It was demonstrated in 1976 by Taylor and Jones that C-4 H-exchange between NADH and various 1,4-dihydropyridines is possible.[266]

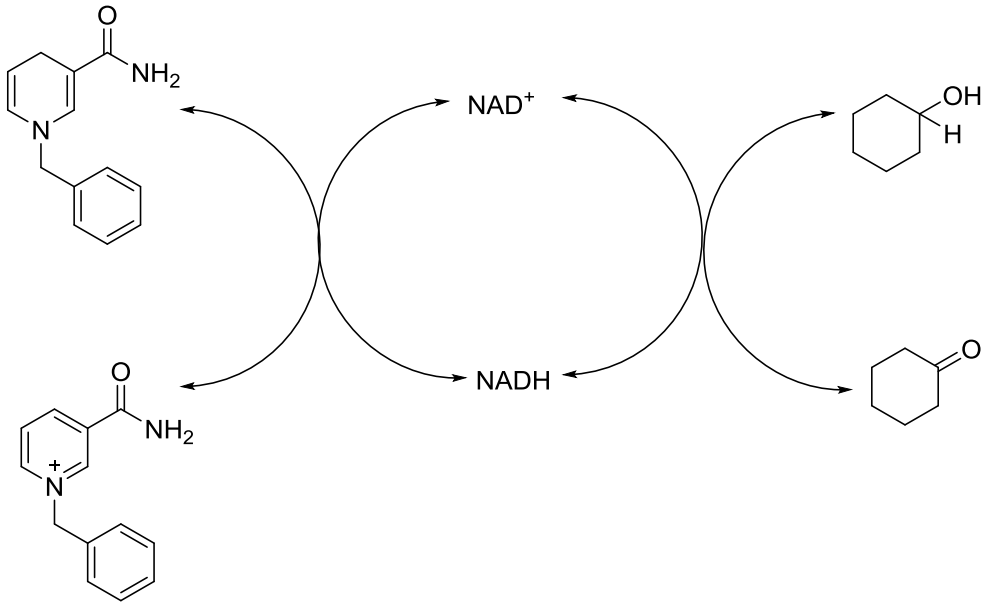

Figure 6-2: *In-situ* regeneration of NADH and NAD^+ using stoichiometric amounts of the nicotinamide mimic BNAH or BNA^+. The natural cofactor could then be used by a HLADH for the oxidation of cyclohexanol or the reduction of cyclohexanone.

A schematic diagram showing the reaction with BNAH is shown in Figure 6-2. Consequently, it is possible that in the work of Fish and co-workers small impurities of the natural cofactor were able to accept a hydride from BNAH leading to regeneration of BNA^+. The natural cofactor could then be oxidised at the active site of the HLADH.

Section 6.2.3 investigates whether the artificial cofactors used in this chapter can be used with commercially available FDH and GDH preparations. This work is important to confirm the hypothesis of Okamoto *et al*. that these enzymes do not accept the artificial cofactors and to add further weight to the hypothesis that it is indeed necessary for enzymes which are able to accept artificial cofactors to contain an internally bound redox prosthetic group.[263]

Other methods of recycling the reduced form of artificial cofactors

In 1955 Mauzerall *et al*. demonstrated that sodium dithionite could be used to reduce the artificial cofactor BNA^+ to BNAH.[259] Using sodium dithionite is approximately 95 % efficient in supplying a hydride to the 1,4-position of the nicotinamide ring, producing the reduced form of the cofactor.[256] However, for a cofactor recycling system to be considered efficient, it must display at least 99.9% conversion to the 1,4-product, as otherwise the build-up of 1,6- and 1,2- product will lead to reduced rates of reaction, due to gradual loss of cofactor.[256] In addition, sodium dithionite is a potent reducing agent (E" for the couple HSO_3^-/SO_2^- at pH 7, 25°C is -0.66V) and so may lead to the non-specific reduction of alkenes if used to regenerate the artificial cofactor *in situ* in a coupled reaction with an enoate reductase enzyme for selective alkene reduction.[267] Gaillard *et al*. demonstrated that 1,4-dihydroquinolines possessing a chiral sulfoxide group at C-3 can also be used to reduce BNA^+ to BNAH. However, again it was only possible to achieve a 95 % yield of the 1,4 product.[268]

Precious metal catalysts have also been shown to be able to recycle some of the artificial cofactors in Figure 6-1. Lo *et al.* have shown that rhodium catalysis can be used to regenerate cofactors, for example $[Cp^*Rh(bpy)H]^+$ has been used to regenerate NADH and a range of artificial cofactors using formate as the stoichiometric hydride source.[256] In addition, Wagenknecht *et al*. have demonstrated that it is possible to use

H_2 in combination with a $[RuCl_2(TPPTS)_2]_2$ (TPPTS = Tris(m-sulfonatophenyl)-phosphine) catalyst obtaining 11 turnovers per ruthenium centre and a 75 % yield of BNAH from BNA^+. It has also been possible to use precious metal systems to carry out the photocatalytic reduction of BNA^+, with the catalyst $[Ru(trpy)(bpy)(py)](PF_6)_2$ (where trpy = 2,2' : 6',2''-terpyridine, bpy = 2,2'-bipyridine, py = pyridine) where *ca.* 100 % selectivity for 1,4-BNAH was achieved, but low total turnover numbers (TTNs) of <5 per catalytic centre.[269]

However, all of these catalysts suffer from low TTNs and require expensive precious metal centres.[263] Additionally, interaction of the catalyst metal with the mNADH dependent enzyme can lead to inactivation of the enzyme.[256]

Recently, Okamoto *et al*. have demonstrated that an artificial transfer hydrogenation catalyst with an Iridium metal centre can be used to regenerate the reduced artificial cofactor mACH with each Ir centre being able to recycle the cofactor 2000 times over the entire course of the reaction.[263] In this work the Ir was attached to an organometallic framework shown in Figure 6-3.

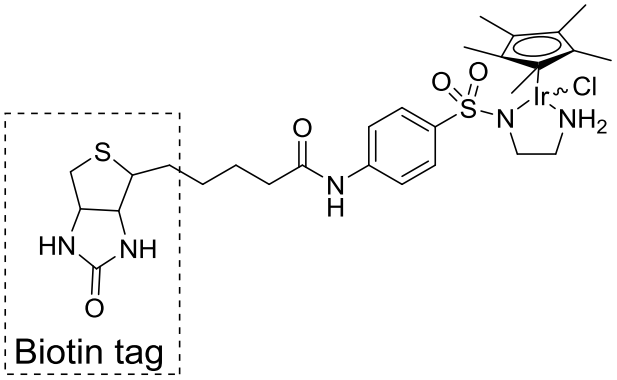

Figure 6-3: The Ir-metal complex used in the artificial transfer hydrogenation catalyst developed by Okamoto et al. [263]

In order to overcome the issues associated with the incompatibility of synthetic transition-metal catalysts and enzymes, this organometallic complex was then trapped

inside a streptavidin protein, making use of the affinity of the streptavidin protein for the biotin tag attached to the end of the organometallic complex.[263] This system was able to use formate to recycle BNAH, MNAH, mACH, $mCOOH_{red}$ and mCNH from their oxidised forms. The system was demonstrated for *in situ* artificial cofactor recycling in combination with the *TsER* enzyme. The best results were obtained with the artificial cofactor mACH and the *TsER* substrate N-ethyl 3-methyl maleimide. It was possible to obtain a yield of >99 % and an *ee* of 95 %. This equates to a TTN per Ir metal centre of >1980. A 3 mM concentration of artificial cofactor was used with 30 mM substrate, meaning that a total of 10 turnovers of artificial cofactor could be achieved using this artificial metalloenzyme.[263]

However, this method requires an expensive and potentially toxic precious metal centre which compromises the green credentials of biocatalysis. Furthermore, the formate hydride donor required leads to the production of stoichiometric amounts of carbon waste. Nevertheless, as this system is the most convincing example of an artificial cofactor recycling system demonstrated so far, it will be used as a comparison throughout this chapter and referred to as an artificial metalloenzyme.[263] It is however, desirable to develop enzymatic methods for recycling the reduced form of these artificial cofactors as enzyme engineering can be used to optimise these catalysts.[270]

Enzymatic methods for the regeneration of the oxidised forms of the cofactors BNA^+ and MNA^+ have been developed using the water-forming NADH oxidase from *Lactobacillus pentosus.*[125,270] This FAD containing enzyme is able to convert BNAH to BNA^+ which couples the conversion of O_2 to H_2O_2.[125]

6.2.3 Formate dehydrogenase and glucose dehydrogenase

FDH enzymes are a structurally diverse class of enzymes which catalyse the oxidation of formate to CO_2, coupled to the reduction of NAD^+ to NADH.[129]

Commercial preparations of NAD^+ dependent FDHs are usually related to the FDH from *Candida boidinii*.[11,76] The mechanism of the FDH from *Candida boidinii* was proposed by Lamzin and Popov using the structure of the apo-protein and the enzyme-NAD^+- azide ternary complex, shown in Figure 6-4 (a).[82,271] Mechanistically the hydride ion is donated directly from the formate ion to the C 4 position of the nicotinamide ring. [271] Figure 6-4 (b) shows a mechanistic diagram showing this reaction.

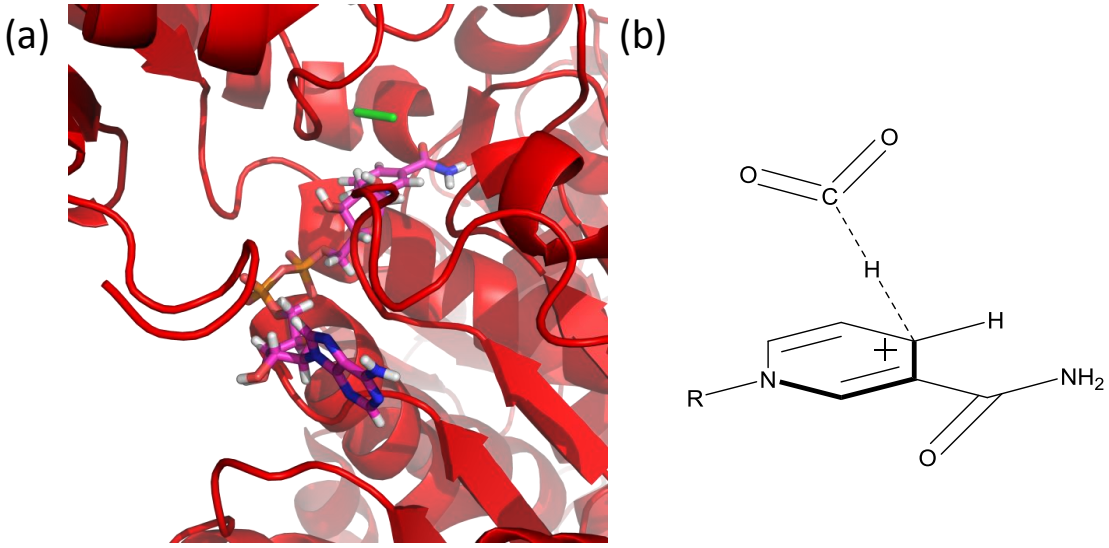

Figure 6-4: The structure of the FDH active site. (a) Crystal structure of the related formate dehydrogenase, *Candida boidinii* FDH (PDB: 5DN9), with NAD^+ (carbon atoms shown in purple) and N_3^- (shown in green) co-crystallised at the active site. There is no bound redox co-factor in this enzyme meaning that hydride delivery must occur directly between the formate and the nicotinamide cofactor.[272] (b) The structure of the formate dehydrogenase transition state during the transfer of a hydride from formate to the nicotinamide ring.[271]

The cofactor (NAD^+) and formate molecule are held in place due to electrostatic interactions with the amino acids at the active site. The artificial cofactors do not possess the same side chains as NAD^+. Consequently, they are not likely to bind in the

active site of the FDH meaning that these enzymes are unlikely to be able to recycle the artificial cofactors.[263] This will be investigated further in section 6.3.

GDHs couple the reduction of NAD^+ to the oxidation of glucose to gluconolactone, which hydrolyses to gluconic acid meaning that the reaction is driven irreversibly in the direction of the products. Commercial preparations of GDH are often derived from the *Bacillus* species and belong to the family of short chain dehydrogenases.[273] GDH 102 used in this work is also a member of the family of short chain dehydrogenases and is likely to be derived from the *Bacillus* species.[130]

A crystal structure has been published for the GDH from *Bacillus megaterium* with both NADH and glucose bound, see Figure 6-5.[274] As occurs in the FDH enzyme, in the GDH the glucose substrate is held in place by hydrogen bond interactions between glucose and amino acids at the active site of the enzyme. The NAD^+ molecule also binds in an extended conformation at the Rossmann fold.[275] Both NAD^+ and glucose are held in close proximity allowing a hydride to be easily passed between carbon 1 of glucose and the 4-position of the nicotinamide ring on NAD^+, as shown in Figure 6-5(b).[274]

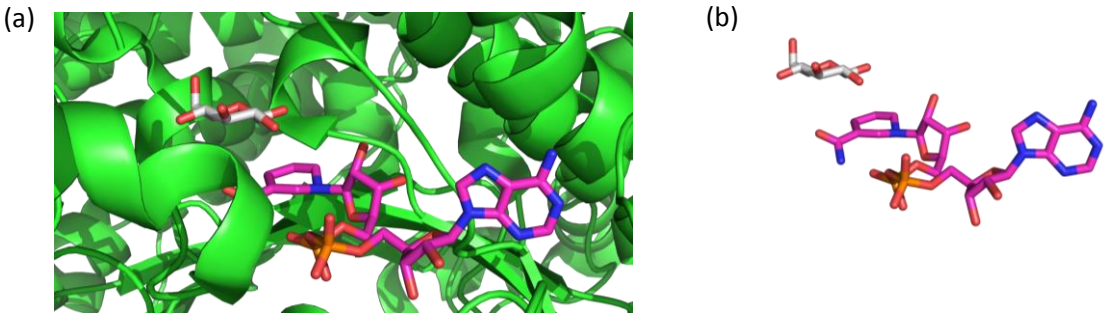

Figure 6-5: Crystal structure of *B. megaterium* GDH with glucose and NAD^+ co-crystallised (PDB: 3AY6). (a) The structure of the active site surrounded by the protein (b) The position of glucose and NAD^+ at the active site, with the carbons of the glucose shown in grey and the NAD^+ in purple. This enzyme is believed to be structurally similar to GDH 102, here it is clear to see that the hydride from the C_1 position of glucose is transferred directly to the nicotinamide ring of NAD^+, without any intermediate redox prosthetic group.[274]

Hydrogen bonds between the adenine ribose moiety and the pyrophosphate moiety are important in stabilising the NAD^+ in a confirmation close to the glucose in the active site of the GDH enzyme.[275] These interactions would not be possible for the artificial cofactors with the GDH as they do not possess the adenine ribose pyrophosphate moiety.

6.2.4 Soluble hydrogenase and Mo-Formate dehydrogenase

Work in this chapter makes use of the SHs from *R. eutropha* and *H. thermoluteolus*, shown schematically, as a recap, in Figure 6-6 (a) both introduced in chapter 1.

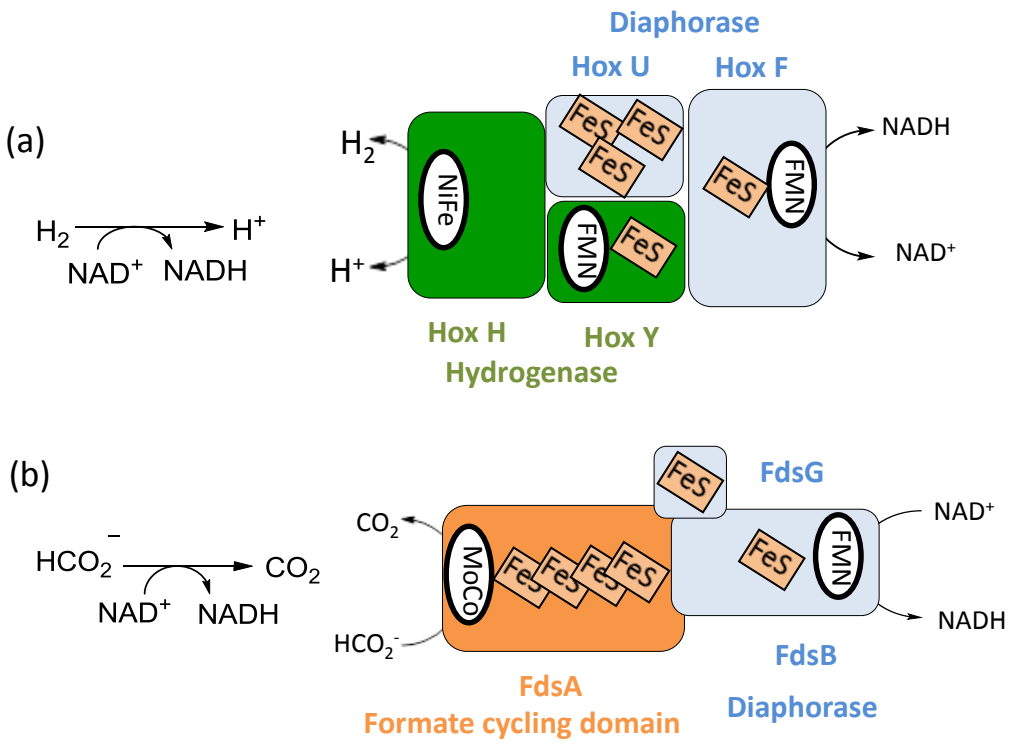

Figure 6-6: (a) The SH from *R. eutropha* or *H. thermoluteolus*. These enzymes also possess two catalytic moieties: at the hydrogenase (HoxHY) H_2 is oxidised to give 2 protons, the electrons released from this process are then channelled through a series of FeS clusters to the diaphorase or NAD^+-cycling moiety, here NAD^+ is reduced to NADH at a FMN active site.[113] (b) The formate dehydrogenase (Mo-FDH) from *Rhodobacter capsulatus,* this enzyme has two catalytic moieties a formate cycling centre (FdsA) and a diaphorase consisting of the NAD^+-reductase sub-unit (FdsB). This enzyme catalyses the oxidation of formate at a molybdenum active site, the electrons from this process are then transferred through a chain of FeS clusters to a Flavin mononucleotide active site (FMN) where they are transferred to NAD^+ as the terminal electron acceptor.[276]

These enzymes have an FMN prosthetic group at their active site which is where the NAD^+ cofactor is reduced. The *R. eutropha* SH has a much greater affinity for NAD^+ than $NADP^+$. It has been shown that the electrochemically determined K_M value for the *R. eutropha* SH for NAD^+ is 197 µM and for $NADP^+$ it is 8 mM.[25,33] For the *H. thermoluteolus* SH the K_M for NAD^+ is 360 µM. Finally, the *Rhodobacter capsulatus (R. capsulatus)* Mo-FDH enzyme with an FMN active site will be tested to see whether this can be used to reduce the artificial cofactors. This enzyme is shown schematically in Figure 6-6 (b).

The Mo-FDH from *R. capsulatus* possesses a bis-molybdopterin–guanine dinucleotide (Moco) active site at which the oxidation of formate to CO_2 occurs. This is electronically linked by a series of FeS clusters to the Mo-FMN active site where NAD^+ reduction occurs, see Figure 6-6(b). *R. capsulatus* is a facultative anaerobic bacterium and the Mo-FDH enzyme from this organism has been shown to be O_2 tolerant.[129] There is a 36 % sequence homology between the β-sub-unit of the *R. capsulatus* Mo-FDH and HoxF from *R. eutropha.* Due to coupling of structural changes during evolution, the structure of proteins with similar functions tend to be similar even when they display sequence homologies of <50%.[215] This implies that the parts of both enzymes at which oxidation or reduction of the cofactor takes place are similar in the *R. capsulatus* FdsB and *R. eutropha* HoxF.

This implies that if the SH is able to reduce some of the artificial cofactors, it can be hypothesised that the *R. Capsulatus* Mo-FDH with its similar active site architecture is likely to also be able to do so too.

6.3 Common methods of cofactor regeneration applied to artificial cofactor regeneration

These experiments were carried out by Farieha Altaf (Part II) under my supervision

Recycling of the artificial cofactors was initially attempted using a commercially available FDH 203 from Evocatal. and GDH 102 from Johnson Matthey Catalysis and Chiral Technologies.[128,130] The results for these reactions are shown in Table 6-2.

Table 6-2: Recycling artificial cofactors using conventional cofactor recycling systems

	FDH				**GDH**			
Cofactor	**1 mM concentration**		**5 mM concentration**		**1 mM concentration**		**5 mM concentration**	
	Percentage conversion after 1 hour	Specific activity/ U mg^{-1}	Percentage conversion after 1 hour	Specific activity/ U mg^{-1}	Percentage conversion after 1 hour	Specific activity/ U mg^{-1}	Percentage conversion after 1 hour	Specific activity/ U mg^{-1}
NAD^+	>70	0.2 ±0.01	> 20	0.26 ±0.04	>99	1.07 ± 0.06	>90	1.18 ±0.01
BNA^+	0	0	0	0	0	0	0	0
mAC^+	0	0	0	0	0	0	0	0
mCN^+	0	0	0	0	0	0	0	0
$mCOOH^+$	0	0	0	0	0	0	0	0
$BuNA^+$	0	0	0	0	0	0	0	0

Reactions were carried out on a 100 µL scale at 30 ^oC in 50 mM Tris-HCl buffer pH 8 in a 96 well plate. FDH: to each reaction mixture was added 0.2 mg FDH (FDH 230 from Evocatal), 10 mM sodium formate, and either 1 or 5 mM oxidized cofactor along with 2 % DMSO. GDH: reactions were carried out on a 100 µL scale at 30 ^oC in 50 mM Tris-HCl buffer pH 8 in a 96 well plate. To each reaction mixture was added 0.2 mg GDH (GDH 102 Johnson Matthey Catalysis and chiral technologies,) 10 mM glucose, and either 1 or 5 mM oxidized cofactor along with 2 % DMSO.

The results in Table 6-2 demonstrate that with commercial FDH no reaction is seen with any of the five artificial cofactors tested, whereas conversion of NAD^+ to NADH is observed, with >70 % of the NAD^+ in a 1 mM sample being converted to NADH in 1 hour. Similarly, the GDH also only demonstrates activity with the natural cofactor NAD^+, but not with any of the artificial cofactors. This supports the findings of Okamoto *et al*. who suggest that these commonly used commercial methods of recycling cofactors cannot be used in combination with artificial cofactors.[262,263]

6.4 The SH as a regeneration system for the reduced form of artificial cofactors

This section details experiments carried out to determine whether the *R. eutropha* SH can be used to reduce $mNAD^+$ (the oxidised form of the artificial cofactors or cofactor mimics, where m stands for mimic) to mNADH (the reduced form of the artificial cofactors or cofactor mimics, where m stands for mimic), shown in Figure 6-1.[125]

Determining percentage conversion

In Figure 6-7 experiments were carried out to determine which, if any of the artificial cofactors shown in Figure 6-1 can be reduced by the *R. eutropha* SH regenerating the reduced form of the artificial cofactor and the maximum possible conversion which can be achieved under these conditions over the course of 18 hours.

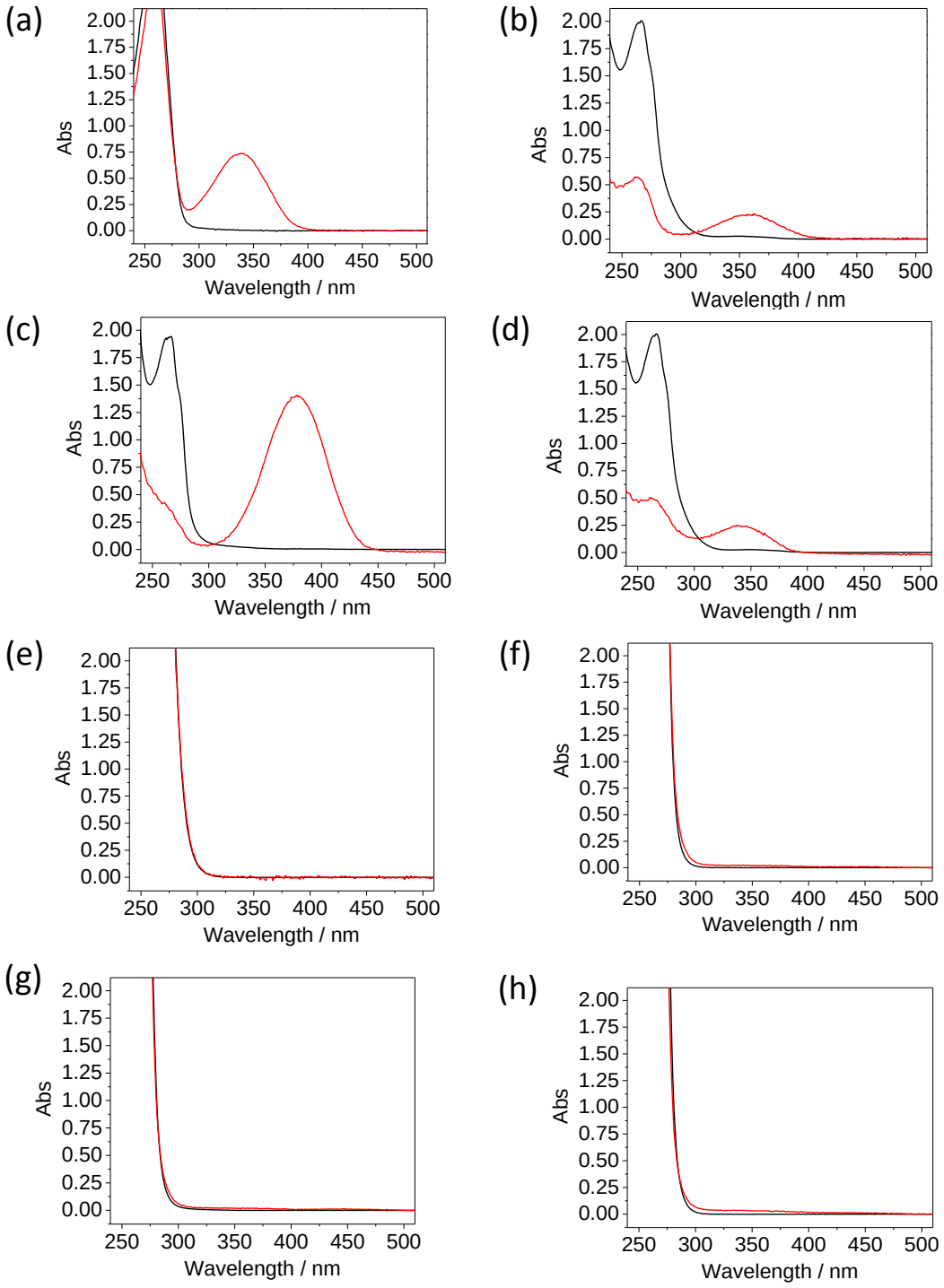

Figure 6-7: Spectra of the conversion achieved by the *R. eutropha* SH after 18 hours. Black: start scan, red: scan after 18 hours. Experiments were carried out in 50 mM Tris-HCl pH 8 at 30 °C. An aliquot of 9 µg of *R. eutropha* SH (0.5 µg for NAD^+) was added to 120 µL of H_2-saturated buffer containing 2 mM cofactor. (a) NAD^+ (finish scan at 1:10 dilution), (b) BNA^+ (finish scan at 1:10 dilution), (c) mAC^+ (finish scan at 1:10 dilution), (d) mCN^+ (finish scan at 1:10 dilution), (e) $mCOOH^+$, (f) $BuNA^+$, (g) MNA^+, (h) PNA^+. Conversion figures based on ratio of the peaks at 260 nm and 340 nm for NAD^+ and intensity of the secondary absorption maximum at *ca.* 340 nm for the artificial cofactors.

From Figure 6-7, it is clear that the SH from *R. eutropha* is able to reduce the artificial cofactors: BNA^+, mAC^+ and mCN^+. However, no product peak was observed in the case of $mCOOH^+$, $BuNA^+$, MNA^+ and PNA^+ indicating that no reduced mNADH has been produced. Control reactions were carried out which demonstrated that no reduction of the artificial cofactors is seen without the SH. The percentage conversion values are presented in Table 6-3, and discussed there. This is an exciting result, as it demonstrates the first purely enzymatic system for recycling the reduced versions of these artificial cofactors.

Determining the specific activity of the *R. eutropha* SH with BNA^+, mAC^+ and mCN^+

This sub-section details experiments carried out to determine the specific activity of the *R. eutropha* SH with BNA^+, mAC^+ and mCN^+. The graph in Figure 6-8 (a) shows scans taken every minute for a reaction with the *R. eutropha* SH and the artificial cofactor BNA^+. Increasing absorbance at 360 nm indicates an increasing concentration of BNAH.

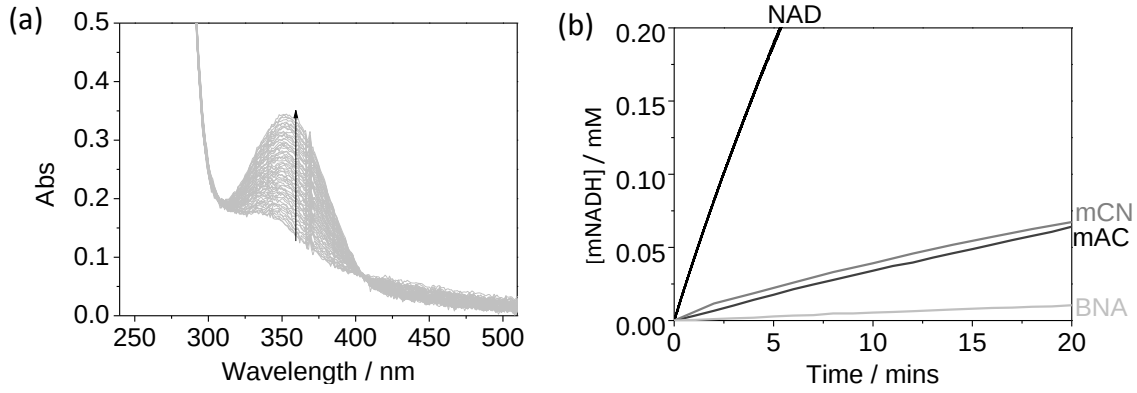

Figure 6-8: Specific activity determination of the artificial cofactors with the SH from *R. eutropha*. (a) Reduction of BNA^+ by the SH from *R. eutropha*. Sequential scans taken every 1 minute showing increasing absorption at 360 nm, indicating an increasing concentration of BNAH over time. (b) Comparison of traces used to determine the specific activity for the artificial cofactors BNA^+, mAC^+, mCN^+ with NAD^+. Reactions were carried out with 2 mM starting concentration of cofactor, 2 % DMSO and 9 µg of *R. eutropha* SH. For the NAD^+ trace 0.5 µg of *R. eutropha* SH was used.

By plotting the absorbance at 360 nm divided by the extinction co-efficient for BNAH as a function of time, it is possible to produce a rate plot, as shown in Figure 6-8 (b).The traces shown in Figure 6-8 (b) were used to determine the rate of reaction for the artificial cofactors BNA^+, mAC^+, mCN^+. The trace for NAD^+ is shown as a comparison.

Summary of percentage conversion and specific activities achieved with the R. *eutropha* SH

This sub-section summarises the results obtained from the experiments detailed above to obtain the conversion and specific activities using the SH from *R. eutropha.*

Table 6-3:The SH from *R. eutropha* as a system for recycling artificial cofactors.

Cofactor	% conversion	Specific activity	Activity as a percentage of activity with NAD^+
NAD^+	(60)[a] >99[b]	15.9	100
BNA^+	15	0.01 ±0.001	0.06
mAC^+	65	0.05 ± 0.01	0.3
mCN^+	20	0.08 ± 0.02	0.5
$mCOOH^+$	0	0	0
$BuNA^+$	0	0	0
MNA^+	0	0	0
PNA^+	0	0	0

Reactions were carried out with 2 mM starting concentration of cofactor, 2 % DMSO and 9 µg of *R. eutropha* SH on a 120 µL scale. For the NAD^+ trace 0.5 µg of *R. eutropha* SH was used. Conversions were measured by leaving samples for 18 hours and then analysing the absorbance of the secondary absorption maximum peak for a 1:10 diluted sample in 50 mM Tris-HCl pH 8. [a]Figure achieved here with 5 % of the amount of *R. eutropha* SH used in the assays with $mNAD^+$. [b]Figure achieved for coupled system in the literature.[75]

Data in Table 6-3 show that the specific activity with all of the cofactors is significantly lower than with the natural cofactor NAD^+. However, promisingly, a 65 % conversion of mAC^+ to mACH could be demonstrated after 18 hours. This was the highest

conversion obtained with any of the artificial cofactors. The highest specific activity, however, was obtained with the artificial cofactor mCN^+, which gave a specific activity of 0.08 U mg^{-1}; this is 0.5 % of the activity of the *R. eutropha* SH towards NAD^+.

Interestingly, all of the artificial cofactors which can be reduced by the SH have a phenyl group on the nitrogen of the nicotinamide ring. The phenyl ring is generally thought of as inductively electron withdrawing. Therefore, it would be expected that the redox couple ($mNAD^+$/mNADH) of the cofactors containing a benzyl R-group would be less negative than those with an alkyl chain R-group. This means that it would be expected that there would be a larger potential driving force for H_2-driven reduction of the cofactors containing an aryl R-group than those with an alkyl R-group.

This is supported by the literature, as the redox potential of BNA^+ has been determined using the cyanide affinity method first demonstrated by Wallenfels and Gellrich to be -361 mV *vs* SHE,[256,266,277] this is less negative than the potentials reported for the cofactors PNA^+ (-387 mV)and MNA^+ (-403 mV).[256] Meaning there should be a greater driving force for H_2-driven reduction of BNA^+ than PNA^+ or MNA^+.

These results are highly significant because they, conclusively, demonstrate the first purely enzymatic system for recycling the reduced form of these particular artificial cofactors and they support the hypothesis that FMN containing enzymes are able to accept the artificial cofactors, in contrast to the commercial GDH and FDH enzymes used in section 6.3.

Comparison of artificial cofactor recycling with the SH from *H. thermoluteolus* and the SH from *R. eutropha*

It was also of interest to see whether the SH from *H. thermoluteolus* can carry out reduction of artificial cofactors. This enzyme has relatively high sequence homology

with the SH from *R. eutropha* as discussed in Chapter 4 (a sequence alignment is shown in Figure 4-2), it also has an FMN at the active site where reduction of NAD^+ occurs. Results shown in Table 6-4 demonstrate that the SH from *H. thermoluteolus* is also able to reduce the same artificial cofactors as the SH from *R. eutropha*.

As discussed in Chapter 3 the specific activity of the *H. thermoluteolus* SH for NAD^+ is generally lower than that for the SH from *R. eutropha.* Interestingly, however, data in Table 6-4 shows that the SH from *H. thermoluteolus* shows higher specific activities for the artificial cofactors BNA^+ and mAC^+ than the *R. eutropha* SH. Generally, however, lower percentage conversions were obtained with the *H. thermoluteolus* SH following an overnight reaction and similar TTNs were obtained. The total turnover number (TTN, number of molecules of reduced cofactor produced per enzyme) for an overnight reaction with both the *R. eutropha* and *H. thermoluteolus* SH with the artificial cofactor mAC^+ is >3000 turnovers per enzyme, this is an improvement on the highest TTN figure of *ca.* 2000 TTNs per catalyst centre previously reported by Okamoto *et al*. for the artificial metalloenzyme coupled to the *TsER* for artificial cofactor driven reduction of N-phenyl-3-methylmaleimide discussed in section 6.2.2 of this chapter.[263]

Table 6-4: Summary table showing the percentage conversion and specific activities of the SHs from *R. eutropha* and *H. thermoluteolus* for a variety of cofactors.

	R. eutropha SH					*H. thermoluteolus SH*[a]				
	% conversion	Specific activity	% activity[b]	TOF[c]	TTN[d]	% conversion	Specific activity	% activity[b]	TOF[c]	TTN[d]
NAD^+	-	15.9	-	-	-	99	0.97	-	2.7	-
BNA^+	15	0.01	0.06	0.03	700	15	0.12	12.4	0.3	2000
mAC^+	65	0.05	0.3	0.15	3100	24	0.14	14.4	0.4	3200
mCN^+	20	0.08	0.5	0.23	1000	9.4	0.03	3.1	0.0835	1200
$mCOOH^+$	0	0	-	-	-	0	0	-	-	-
$BuNA^+$	0	0	-	-	-	0	0	-	-	-
MNA^+	0	0	-	-	-	0	-	-	-	-
PNA^+	0	0	-	-	-	0	-	-	-	-

Reactions with the *R. eutropha* SH were carried out under the following conditions: 50 mM Tris-HCl pH 8 at 30 ^oC. An aliquot of 9 µg of *R. eutropha* SH was added to 120 µL of H_2-saturated buffer containing 2 mM cofactor. For rate calculations data from the first linear phase of the reaction were used; conversions were measured by leaving samples for 18 hours and then analysing the height of the secondary absorption maximum due to the reduced version of the cofactor (analogous to the peak at 340 nm for NADH) for a 1:10 diluted sample in 50 mM Tris-HCl pH 8. Reactions with *H. thermoluteolus* were carried out under the following conditions: H_2-saturated 50mM Tris-HCl buffer, pH 8 containing 2 % DMSO. To determine conversion reactions were carried out on a 100 µL scale with 2.5 µg of enzyme under 2 bar H_2-pressure, with 2 mM oxidised cofactor at 40 ^oC. Reactions were run overnight. To determine the rate 5 µg of enzyme was used with NAD^+, BNA^+ and mCN^+ and 2.5 µg of enzyme with mAC^+, 1 mM of oxidised cofactor was added to each of the reactions and constant H_2 flow was maintained throughout the course of the reaction.[a]Reactions carried out by Farieha Altaf (Part II student under my supervision)[b] Specific activity as a percentage of the activity of the protein for NAD^+.[c]TOF is number of product per enzyme per second.[d]TTN is total number of molecules of reduced product per enzyme over the course of the experiment.

6.4.1 Determination of the affinity constant of the *R. eutropha* SH for artificial cofactor mAC+

As detailed in the Methods and Theory section of this thesis, the K_M value provides details about the affinity of the active site for a particular substrate. According to the Michaelis-Menten equation the rate of reaction is given by equation 6-1:

$$v = \frac{k_{cat}\,[E]_o[A]}{k_M + [A]} \qquad \textbf{6-1}$$

where v is the rate, k_{cat} is the catalytic constant, $[E]_o$ is the starting concentration of enzyme and [A] is the concentration of substrate. For enzymatic reactions which obey Michaelis-Menten kinetics a high K_M will give rise to a slow rate except at very high substrate concentrations.

When mAC^+ is substituted into the homology model for HoxF in the place of NAD^+, see Figure 6-9 (c), it appears that nicotinamide ring will interact with the loop of amino acids 221-224 and tyrosine 336 in a similar way to the natural cofactor. However, no additional interactions would be expected as a result of the phenyl group with the other amino acids thought to be involved in the binding of NAD^+ at the active site of HoxF. Consequently, it would be expected that the affinity of the SH active site would be significantly lower for mAC^+ than for NAD^+, resulting in a much higher K_M value.

In order to test this hypothesis a K_M determination was carried out. Initially, a K_M determination was carried out using UV-visible spectroscopy (see Methods and Theory chapter, section 2.2) for the natural cofactor NAD^+, in order to determine that this enzyme preparation demonstrates the same substrate affinity as previous preparations of this enzyme described in the literature (not shown). From this measurement a K_M value of 0.50 mM was obtained for the whole SH from *R. eutropha*, this agrees well with the K_M value of 0.56 mM originally obtained by Schneider and Schlegel.[109]

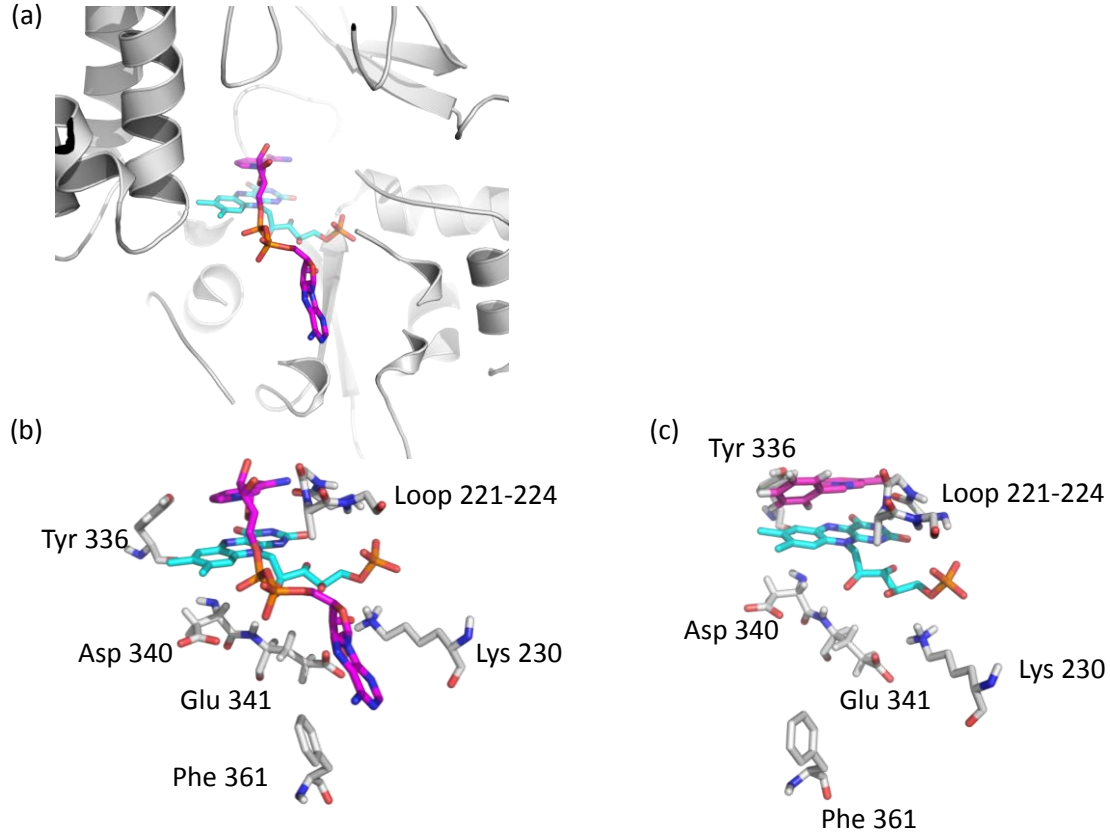

Figure 6-9: Active site models of the HoxF portion of the SH from *R. eutropha*. HoxF homology model originally prepared by L. Lauterbach based on Complex 1 from *Thermus thermophilus* Nqo1 PDB: 2FUG. The carbon atoms in the FMN in the active site are coloured in turquoise and those of the cofactor in purple. The key amino acids involved in protein binding are shown in each of the figures. The loop of amino acids consists of a glycine rich loop containing glycine 221, glycine 222 and alanine 223. (a) The active site of HoxF with the amino acid chain shown as a cartoon representation. (b) The NAD^+ binding in the active site of HoxF with the key residues involved in binding labelled. (c) mAC^+ binding in the active site of the HoxF homology model, binding mode based on the binding seen in crystal structure 2FUG, mAC^+ superimposed in the same position as NAD^+ without conducting a docking study.

A K_M determination was then carried out with the artificial cofactor mAC^+. This cofactor was selected because data in Table 6-3 demonstrates that the *R. eutropha* SH exhibits the highest conversion with this artificial cofactor and a relatively high specific activity.

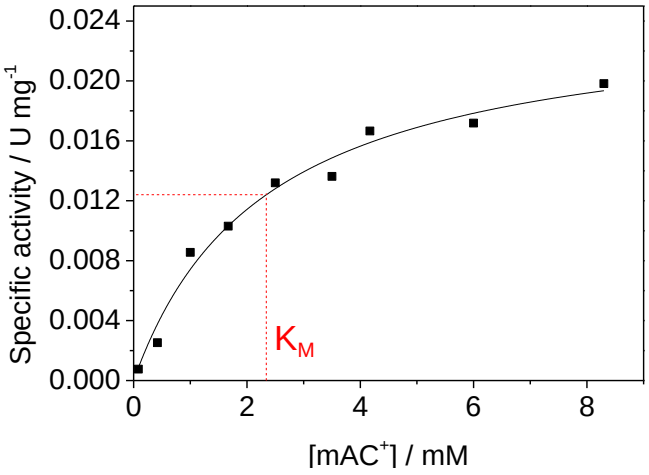

Figure 6-10: A Michaelis-Menten plot used to determine the K_M for the *R. eutropha* SH towards the H_2-driven reduction of mAC^+ to mACH. Activities were determined from the initial activity of the SH over the first 10 minutes of reaction. Measurements were carried out in a 120 µL volume in pre-H_2-saturated 50 mM Tris-HCl pH 8 buffer at 30 °C (2% DMSO). Each reaction was started with 9 µg of enzyme. Kinetic scans were taken at 378 nm in order to determine the increase in mACH concentration. H_2 gas was blown across the top of the cuvette at approximately 1 mL min^{-1} for the duration of the reaction. The black line represents a fit of the data using a Michaelis-Menten fit, which was used to determine the K_M.

Figure 6-10 shows a Michaelis-Menten plot used to determine the K_M value for H_2-driven reduction of mAC^+ by the *R. eutropha* SH. A K_M value of 2.34 ± 0.4 mM was determined. This is larger than that for NAD^+, which is unsurprising, as from Figure 6-9 it would be expected that there would be fewer interactions with the cofactor mAC^+ at the active site of HoxF than for NAD^+. Thus, leading to a decreased substrate affinity and therefore an increased K_M. Due to the low cost of the artificial cofactors, see Table 6-1, using a 2.3 mM concentration of the cofactors is likely to be acceptable for bio-catalytic applications, particularly as at high substrate concentrations, where this would correspond to low mole ratio of cofactor to substrate.

6.5 The Mo-FDH as a regeneration system

This section investigates whether the Mo-FDH from *R. capsulatus* can be used to reduce the $mNAD^+$ to mNADH.

Determining percentage conversion

The experiments in this sub-section were carried out by Farieha Altaf (part II) under my supervision

The UV-visible scans in Figure 6-11, were used to determine which artificial cofactors can be reduced by the Mo-FDH and the percentage conversion, which it was possible to achieve.

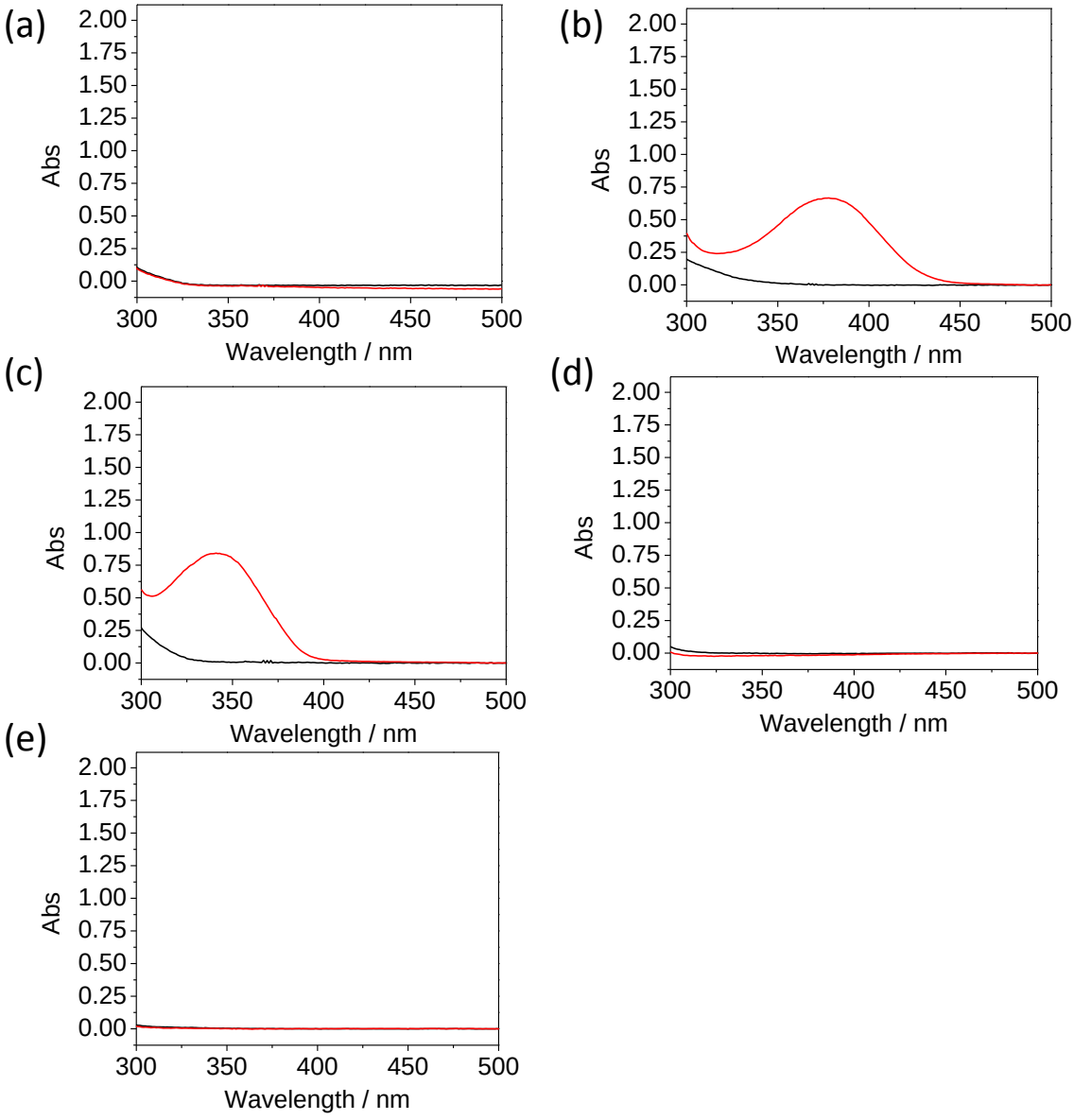

Figure 6-11: Spectra of the conversion of cofactors by *R. capsulatus* FDH. Conversion reactions were performed in 50 mM Tris-HCl pH 8 with 10 mM formate, 1 mM oxidized cofactor, 2 % DMSO and 12 µg FDH at 40 °C, in a 100 µL total volume. Black: start scan, red: scan after 6 minutes (a) BNA^+ (b) mAC^+ (c) mCN^+ (d) $mCOOH^+$ (e) MNA^+. Reactions were carried out in a plate reader at 40 °C, with a pathlength of 2.4 mm.

The scans in Figure 6-11 demonstrate that the Mo-FDH is able to reduce the cofactors mCN^+ and mAC^+. However, surprisingly no conversion was observed for the Mo-FDH with the artificial cofactor BNA^+. This is in contrast to the results obtained with the SH enzymes.

The percentage conversion values for the Mo-FDH with mCN^+ and mAC^+ are presented in Table 6-5, and discussed there. It should however, be noted that these scans were obtained after 6 minutes; however, no further conversion was observed after a further four hours of reaction.

Determining the specific activity of the *R. capsulatus* Mo-FDH with mAC^+ and mCN^+

This sub-section details experiments carried out to determine the specific activity of the *R. capsulatus* Mo-FDH with the artificial cofactors mAC^+ and mCN^+.

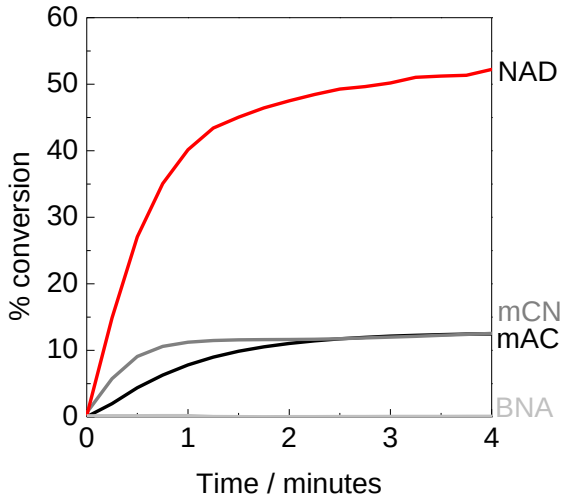

Figure 6-12: Time courses for the reduction of $mNAD^+$ to mNADH by *R. capsulatus* Mo-FDH. Experiments carried out in 50 mM Tris-HCl pH 8 containing 2 % DMSO, with 1 mM oxidised cofactor in the presence of 10 mM formate, and monitored *in situ* using UV-visible spectroscopy kinetics at the secondary absorption maximum for each reduced cofactor. Experiments were carried out on a 200 µL scale at 30 °C with 12 µg of Mo-FDH. Artificial cofactors mCN^+ (grey) and mAC^+ (black) are compared to the biological cofactor, NAD^+ (red).

The traces in Figure 6-12 were used to determine the rate of reaction of the Mo-FDH with the artificial cofactors. The trace for natural cofactor NAD^+ is shown on the graph for comparison. Interestingly, the activity of the Mo-FDH with all of the cofactors (including the natural cofactor NAD^+) appears to tail off after *ca.* 2 minutes. Therefore, activities were determined from data from the first 30 s. The initial characterisation work carried out by Hartmann *et al*. on this enzyme only reports on the initial activity values and not on the stability under catalytic turnover conditions.[276] However, it is known that many FDH enzymes display instability.[129] The observed tailing off of activity for all of the cofactors, including the natural cofactor NAD^+, suggests that the Mo-FDH is not a particularly good candidate for use as a recycling system for the artificial cofactors tested in this chapter.

However, promisingly this work again further supports the hypothesis that FMN containing enzymes are able to reduce the artificial cofactors.

Summary of percentage conversion and specific activities achieved with the *R. capsulatus* Mo-FDH

This sub-section summarises the results obtained from the experiments detailed above to obtain the conversion and specific activities using the *R. capsulatus* Mo-FDH.

Results in Table 6-5 summarise both the results for the rates of reaction and show the maximum conversion which was achieved after 6 minutes is 59 % for the artificial cofactor mCN^+. A maximum conversion of 26 % was achieved for the artificial cofactor mAC^+. This is in contrast to the SH enzymes, where a higher total conversion was obtained with mAC^+ than with mCN^+. No increase in percentage conversion was observed after a further four hours of reaction.

Table 6-5: Specific activity and conversion of the *R. capsulatus* Mo-FDH.

Cofactor	% conversion[a]	Specific activity[b]	% activity[c]	TTN
NAD^+	-	9.3± 1	-	-
BNA^+	0	0	0	-
mAC^+	26	1.3± 0.2	14	300
mCN^+	59	2.8± 0.3	30	800
$mCOOH^+$	0	0	-	-
MNA^+	0	0	-	-

Conversion reactions were performed in 50 mM Tris-HCl pH 8 with 10 mM formate, 1 mM oxidized cofactor and 2 % DMSO and 12 µg FDH at 40 ^oC, in a 100 µL total volume. For specific activities reactions were carried out on a 200 µL scale with 2 % DMSO, 1 mM cofactor, 10 mM sodium formate, 10 mM potassium nitrate and 12 µg of Mo-FDH at 30 ^oC.
[a]Percentage conversion after 6 minutes
[b]Specific activity in U mg^{-1}; determined from initial activity over the first 30 s of the assay.
[c]Specific activity as a percentage of the activity of the protein for NAD^+.

The specific activities obtained for both the artificial cofactors mAC^+ (1.3 U mg^{-1}) and mCN^+ (2.8 U mg^{-1}) are both less than that seen for NAD^+ (9.3 U mg^{-1}) with the Mo-FDH as expected; however, they are significantly higher than the specific activity values obtain for the SH enzymes tested in section 6.4. Interestingly, a higher activity is obtained for mCN^+ reduction, than for mAC^+. As the Mo-FDH appears to only display reduction activity over a limited time period, this faster rate of reaction for mCN^+ *versus* mAC^+ may be what leads to a higher percentage conversion being observed for mCN^+. Subsequent experiments using lower concentrations of Mo-FDH led to lower conversion. However, further work would be required to demonstrate what is causing Mo-FDH activity to drop off after 4 – 6 minutes.

6.6 Coupling

This section contains details of experiments which investigate using the SHs from *R. eutropha* and *H. thermoluteolus* and the Mo-FDH from *R. capsulatus* as recycling systems for the artificial cofactors. It was investigated whether it is possible to couple

these systems to the *TsER*, introduced in chapter 5, for selective alkene reduction reactions with artificial cofactor recycling.

6.6.1 Coupling the *TsER* with the *H. thermoluteolus* SH for artificial cofactor recycling

The experiments in this section were carried out by Farieha Altaf (part II) under my supervision

Initial attempts at coupling enzymatic recycling of the artificial cofactors with the *TsER* for selective alkene reduction were carried out using the SH from *H. thermoluteolus*, see Figure 6-13 for a schematic diagram of the reaction under consideration. This builds upon the characterisation work in chapter 4 of this thesis. These attempts are summarised in Table 6-6.

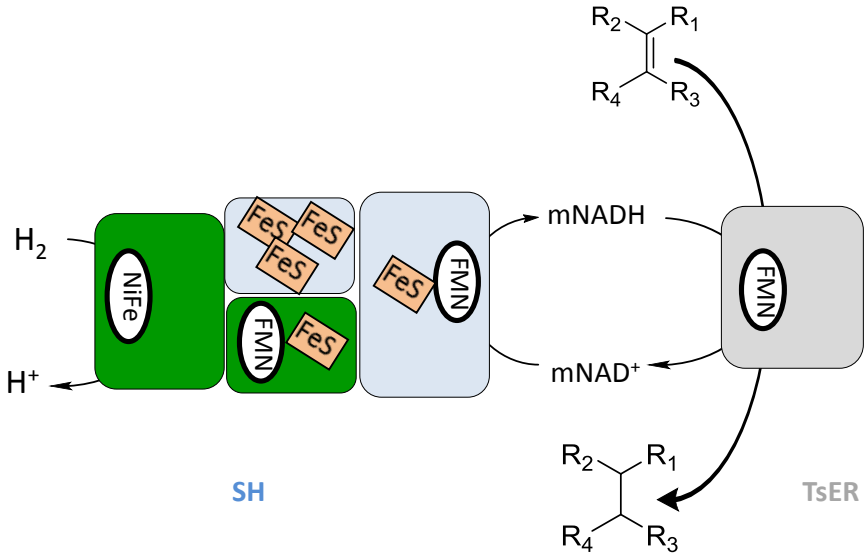

Figure 6-13: A schematic diagram of the H_2-driven recycling of the artificial cofactors (mNADH) by the *H. thermoluteolus* SH coupled to the *TsER* for selective alkene reduction.

Initial studies using 2-methyl-2-cyclopentenone

The experiments detailed in entries 1-4 in Table 6-6 were carried out with the substrate 2-methyl-2-cyclopentenone, as this was used in Chapter 5. Entries 1 and 2 were carried out with constant H_2 flow over the top of the reaction vessel, with the SH being used to supply the reduced cofactor in entry 1 and stoichiometric amounts of reduced cofactor

being used in entry 2. In both of these reactions significant loss of substrate was observed supporting the hypothesis from chapter 5 that 2-methyl-2-cyclopentenone evaporates readily under conditions of constant gas flow or if the vessel is open to the air. Entries 3 and 4 were conducted under H_2-atmospheres in order to limit evaporation. Some conversion was observed in the case of entry 4; although, even in the pressure system which has a 25 cm^3 total there appears to have been significant loss of substrate due to evaporation, which probably limited the conversion.

Table 6-6: Summary of coupling reactions trailed with the SH from *H. thermoluteolus* and *TsER* using the 2-methyl-2-cyclopentenone substrate

Entry	Conditions[a]	TsER / µg	SH / µg	Cofactor / mM	Conversion	Comments
1	H_2 constantly equilibrating in headspace, shaking at 150 rpm, 1 mL volume	500	5	1 mM, BNA^+	-	Significant loss of substrate
2	Reaction provided with reduced cofactor, 1 mL volume	500	-	10 mM BNAH	-	Significant loss of substrate
3	Reaction was conducted in a 10 mL vial with1 bar H_2 sealed in headspace, 1 mL reaction volume, shaking at 100 rpm	600	10	2 mM BNA^+	-	Significant loss of substrate due to evaporation and reaction was potentially limited due to supply of $H_{2(g)}$
4	Reaction conduced on a 100 µL scale in a micro-centrifuge tube in the pressure system under 2 bar H_2	120	10	2 mM BNA^+	Some conversion	Significant loss of substrate due to evaporation

[a]Reactions were carried out at 40 °C, in 50 mM Tris-HCl pH 8 with an initial concentration of 10 mM 2-methyl-2-cyclopentenone and 2 % DMSO. Reactions were left overnight.

In this project the supply of the SH enzyme was a limiting factor. As the specific activities of the SH enzymes are much lower with the artificial cofactors than with the natural cofactors in order to obtain appreciable conversion it was necessary to use small reaction volumes and higher catalyst loading, over extended time periods.

It was also found that it is particularly necessary when working with artificial cofactors to ensure that the reaction mixture remains well saturated with $H_{2(g)}$ throughout the course of the reaction, either by carrying out the reactions under 2 bar H_2 or with constant $H_{2(g)}$ flow and with the solution requiring sufficient agitation to ensure that the supply of H_2 gas dissolved in solution can be replenished from the H_2 present in the headspace of the vessel. Due to these requirements, 2-methyl-2-cyclopentenone is not a particularly suitable substrate to initially demonstrate high TTNs for artificial cofactor recycling.

Coupling to the *TsER* with the N-phenyl maleimide substrate

As this work was carried out with the whole *H. thermoluteolus* SH and not the enzyme-modified particles system, it was not necessary to avoid substrates which are reduced directly at carbon. Consequently, N-phenyl maleimide was trialled as a substrate in combination with the *H. thermoluteolus* SH. N-phenyl maleimide is a solid at room temperature and has a much lower predicted vapour pressure,[195] than 2-methyl-2-cyclopentenone.[195] The results of initial studies investigating coupling the *H. thermoluteolus* SH for artificial cofactor recycling to the *TsER* for reduction of N-phenyl maleimide are summarised in Table 6-7.

All of the reactions in Table 6-7 led to some conversion; however, it was noted that significant amounts of substrate were lost during the course of the reaction due to hydrolysis, even in entry 3 where the natural cofactor NAD^+ was used conversion remained low.

Table 6-7: Summary of coupling reactions trailed with the SH from *H. thermoluteolus* and *TsER* using the N-phenyl maleimide substrate

Entry	Conditions[a]	[Substrate] /mM	TsER / µg	SH / µg	Cofactor / mM	Conversion [b]	Comments
1	H_2 constantly flowing through the headspace of a cuvette. Constant stirring of reaction mixture.	10	100	5	1 mM BNA^+	4 %	Significant loss of substrate due to hydrolysis
2	Micro-centrifuge tube in a pressure system under 2 bar H_2 with shaking at 100 rpm.	2	116	10	2 mM BNA^+	1 %	Loss of substrate due to hydrolysis
3	In a 10 mL vial with H_2 sealed in the headspace, with shaking at 100 rpm.	10	200	2.5	2 mM NAD^+	6 %	Significant loss of substrate due to hydrolysis

[a]Reactions were carried out on a 200 µL scale at 40 °C in 50 mM Tris-HCl pH 8 containing 2 % DMSO. All values reported for 24 hour reactions [b]Conversion figures based on comparison of the product peak to a standard curve.

These findings suggest that N-phenyl maleimide is not stable on the 24 hour time scale used for these reactions. This was found to be consistent with the literature.[278] A mechanism for base catalysed maleimide hydrolysis is shown in Figure 6-14.[278][279]

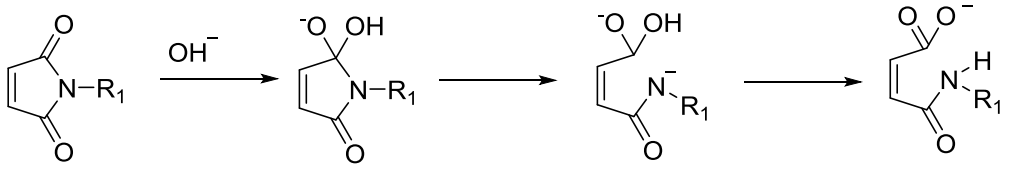

Figure 6-14: The mechanism of hydrolysis of maleimide substrates in alkaline media, with addition of HO^- to the carbonyl (the rate determining step) and subsequent formation of a tetrahedral intermediate.[278]

Coupling the TsER with the *H. thermoluteolus* SH for artificial cofactor recycling using stoichiometric amounts of artificial cofactor

In order to minimise the amount of time the N-phenyl maleimide was left in alkaline buffer, a reaction was set up in which H_2 gas was blown across the top of the reaction vessel for 15 hours, allowing reduction of stoichiometric amounts of the artificial cofactor mAC^+ (2 mM starting concentration) giving mACH. After leaving the reaction for 15 hours, an aliquot of *TsER* and N-phenyl maleimide (2 mM concentration) was then added and the conversion was measured after the reaction was allowed to proceed for a further hour.

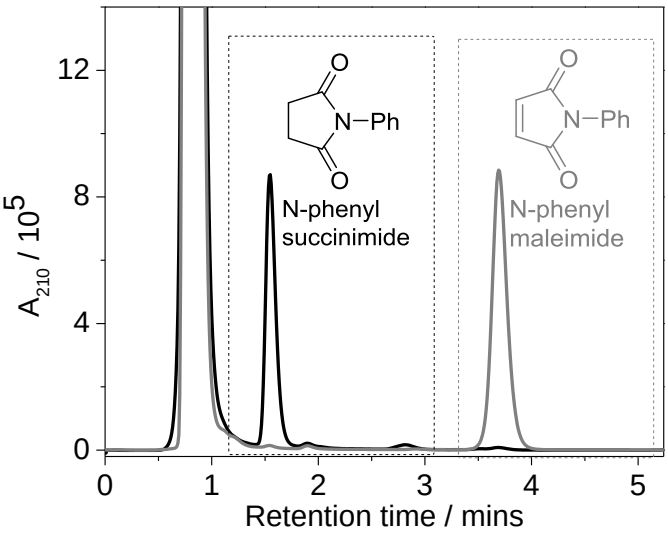

Figure 6-15: Coupling of artificial cofactor reduction by the *H. thermoluteolus* SH with the *TsER* for reduction of N-phenyl maleimide. Start: grey, finish: black. The reaction was carried out on a 100 µL scale, in 50 mM Tris-HCl pH 8 at 40 °C. For the first 15 hours of the reaction H_2 gas was blown over the top of a solution containing 5 µg of SH, 2 mM mAC^+ and 2 % DMSO. After 15 hours an aliquot of *TsER* (100 µg) was added to the solution, followed by an aliquot of N-phenyl maleimide to take the total concentration of the solution up to 2 mM N-phenyl maleimide. The reaction was then allowed to continue for 1 hour and analysed using HPLC.

Results in Figure 6-15 demonstrate a 92 % conversion of N-phenyl maleimide to N-phenyl succinimide on the basis of the concentration of the product detected. No substrate was found in the reaction mixture at the end of the reaction and no extra side

products could clearly be identified from the HPLC trace. This is a promising demonstration of the possibilities afforded by the *H. thermoluteolus* SH as an artificial cofactor reduction system. The TTN per SH here is > 6,000 (moles product per mole SH), this is a more than three times increase on the best TTNs achieved in the work Okamoto *et al*. using the artificial metalloenzyme catalyst, outlined in section 6.2.2 of this chapter.[263] To our knowledge, this is the best TTN of the reduced form of an artificial cofactor ever achieved for a recycling system.[125,263] However, as stoichiometric amounts of mAC^+ were used in this work, the artificial cofactor is not being used in catalytic quantities.

6.6.2 Coupling the *TsER* with the *R. capsulatus* Mo-FDH

This section investigates using the *R. capsulatus* Mo-FDH as an artificial cofactor recycling system in combination with the *TsER*, with the *TsER* being used for selective reduction of N-phenyl maleimide. The overall reaction is summarised as a schematic diagram in Figure 6-16.

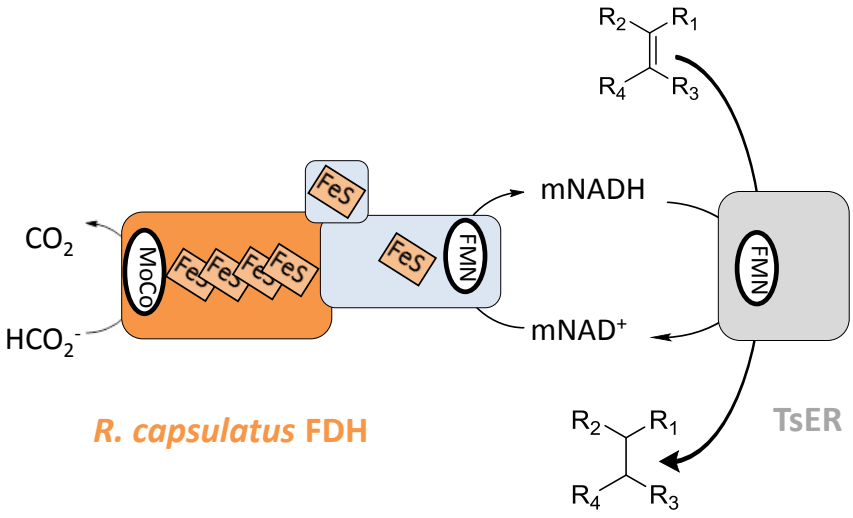

Figure 6-16: A schematic diagram of the formate driven recycling of the artificial cofactors (mNADH) by the *R. capsulatus* FDH coupled to the *TsER* for selective alkene reduction.

The best result achieved, when using the Mo-FDH as an artificial cofactor recycling system was with the artificial cofactor mCN^+. A HPLC chromatogram showing the trace at the end of the reaction is shown in Figure 6-17.

The product peak at 1.5 minutes in Figure 6-17 corresponds to a concentration of 0.91 mM N-phenyl succinimide. There is no peak at *ca.* 3.5 minutes demonstrating that the remaining N-phenyl maleimide has hydrolysed. A product concentration of 0.91 mM equates to a relatively impressive TN of 9 and a TTN of *ca.* 1300 moles of product per mole Mo-FDH.

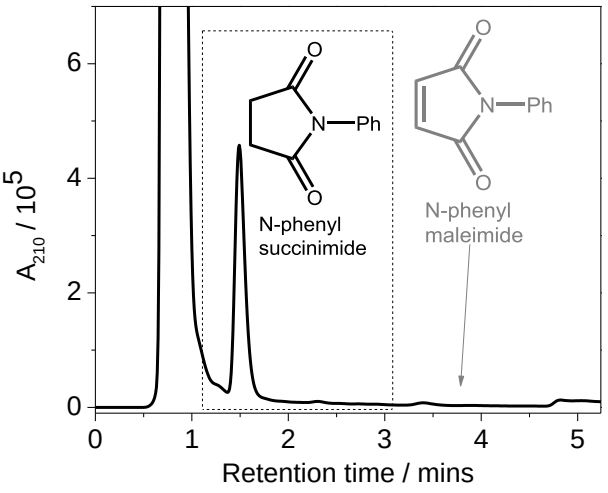

Figure 6-17: Coupling of artificial cofactor reduction by the *R. capsulatus* Mo-FDH with the *TsER* for reduction of N-phenyl maleimide. The reaction was carried out on a 100 µL scale, in 50 mM Tris-HCl pH 8 at 22 °C. The reaction mixture contained 15 mM sodium formate, 2 % DMSO, 0.1 mM mCN^+, 12 µg of Mo-FDH and 150 µg of TsER. The reaction was started by adding a 1 mM aliquot of N-phenyl maleimide. After 4 hours a further 1 mM aliquot of N-phenyl maleimide was added to the solution. The area of the N-phenyl succinimide product peak at 1.5 minutes equates to a 0.91 mM concentration of N-phenyl succinimide. The reaction was analysed after 18 hours using HPLC.

This is a promising initial demonstration of using the Mo-FDH as an artificial cofactor recycling system. However, due to the limited period of activity displayed by the Mo-FDH further experimental work focused on coupling the *R. eutropha* SH, as an artificial cofactor recycling system, to the *TsER*.

6.6.3 Coupling the *TsER* with the *R. eutropha* SH as an artificial cofactor recycling system

The SH from *R. eutropha* has been extensively characterised[102,109,220] and showed similar TTNs to the SH from *H. thermoluteolus* for mAC^+ conversion overnight. In this work the cofactor mAC^+ was used, this is because the *R. eutropha* SH shows the highest conversion (following an overnight experiment) and a relatively high specific activity with this artificial cofactor. It has already been possible to determine high TTNs per enzyme with the *H. thermoluteolus* SH; work in this section therefore, particularly focuses on optimising TN (moles of product per moles of artificial cofactor) possible during the course of a reaction. This is an important goal, as it is necessary to obtain a TN of at least 30 (moles of product per mole of artificial cofactor) in order for them to be economically viable, see Table 6-1.

Table 6-8: Summary of initial coupling reactions trailed with the SH from *R. eutropha* and *TsER* with the N-phenyl maleimide substrate. Reactions were carried out in 50 mM Tris-HCl pH 8 at 22 °C.

Entry	Conditions	TsER / µg	SH / µg	Cofactor / mM	[Initial Substrate] / mM	% conv.[a]	[Product] / mM	Comments
1	2 bar H_2 pressure, 200 µL scale, 18 hours reaction time.	15	9	0.5 mM mAC^+	5	11 (After 4 hours)	0.55	Loss of substrate due to hydrolysis
						12 (After 7 hours)	0.59	
2	2 bar H_2 pressure, 200 µL scale, 18 hours reaction time.	37	9	0.5 mM mAC^+	5 mM added at 0 minutes, 5 mM added after *ca.* 1 hour, then 5 mM added after *ca.* 4 hours (15 mM total)	5	0.72	Increased *TsER* appears to increase the yield of the reaction, but still loss of substrate due to hydrolysis despite gradual addition
3	2 bar H_2 pressure, 200 µL scale, 10 hours reaction time.	15	18	0.3 mM mAC^+	2 mM injected every 2 hours up to a total concentration of 6 mM	6.6	0.13	Complete hydrolysis of substrate observed, despite gradual addition of N-phenyl maleimide

[a]Conversion figures based on comparison of the product peak to a standard curve.

Initial optimisation work investigating coupling the *R. eutropha* SH as an artificial cofactor recycling system to the *TsER* was carried out with the substrate N-phenyl maleimide. Entries in Table 6-8 summarise these attempts. A maximum of 1.4 cofactor turnovers was obtained in this work (Table 6-8, entry 2). Again, as seen in section 6.6.1 there were significant issues experienced with the N-phenyl maleimide substrate hydrolysing on the time scale of the reactions. However, more promisingly it was possible to obtain *ca.* 3000 turnovers of N-phenyl maleimide to N-phenyl succinimide per SH enzyme (see entry 2), this is a higher number of turnovers than that obtained in recent work by Okamoto *et al*. with an artificial metalloenzyme, discussed in the introduction to this chapter, although not quite as good as the result obtained for the SH from *H. thermoluteolus,* above; however, in this case sub-stoichiometric amounts of artificial cofactor are being used.[263]

N-ethyl maleimide as a substrate

Due to the problems experienced as a result of the hydrolysis of the N-phenyl maleimide substrates in sections 6.6.1, 6.6.2 and the beginning of this section, an NMR study was conducted in order to determine whether maleimide or N-ethyl maleimide hydrolyse less rapidly than N-phenyl maleimide. These compounds are also accepted as substrates by the *TsER*.[234] The data from this study is shown in Appendix G. After 8 hours approximately 30 % of the maleimide or N-ethyl maleimide would be expected to undergo hydrolysis in comparison to 60 % of the N-phenyl maleimide in deuteriated 50 mM Tris-HCl buffer pD 8.1. The N-ethyl maleimide substrate hydrolyses slightly less quickly than maleimide. These findings about the relative rates of hydrolysis are supported by the findings of Matsui *et al*. in the literature.[279]

In order to try and avoid the hydrolysis of the N-phenyl maleimide substrate, N-ethyl maleimide was trialled as a substrate. However, preliminary experiments using this substrate were disappointing.

The highest conversion achieved was 4 % after 4 hours when a reaction was carried out on a 200 μL scale, with 1 mM mAC^+ and 10 mM N-ethyl maleimide in combination with the *R. eutropha* SH (9 μg) and *TsER* (30 μg) with H_2 gas being continually blown across the top of the reaction mixture. However, the percentage conversion did not increase after 18 hours, and hydrolysis of the substrate was still observed to be a significant competitive reaction.

Cyclohexenone as a substrate

To avoid the hydrolysis problems experienced with the N-phenyl maleimide and N-ethyl maleimide substrates used in the sections above an alternative substrate, cyclohexenone was used. Cyclohexenone has a high boiling point of *ca.*171^oC[65] and is not able to hydrolyse. It also has a lower predicted vapour pressure than 2-methyl-2-cyclopentenone.[195]

Initial tests were carried out to determine that the substrate and product do not disappear when incubated at 30 ^oC in uncapped vessels. Two samples containing cyclohexenone (substrate, 10 mM) and cyclohexanone (product, 10 mM) were produced. These samples were each divided into two 500 μL aliquots, half of the sample was extracted at time zero and analysed using GC. The other half was left open to the air, shaking (300 rpm), at 30 ^oC for nine hours. For the cyclohexenone sample 99 % of the cyclohexenone was retained in the mixture after incubation and for the cyclohexanone mixture 84 % was retained. This demonstrates that cyclohexenone is unlikely to display significant evaporation when it is used as the substrate in low volume reactions with

constant gas flow across the top of the reaction vessel or in the pressure system with a 25 cm^3 H_2-atmosphere.

It was subsequently investigated whether it is possible to get good conversion of cyclohexenone to cyclohexanone when supplying stoichiometric amounts of mACH to the *TsER* enzyme. Using sequential UV-visible scans the *TsER* was demonstrated to have an initial activity of 1.19 U mg^{-1} with mACH and the cyclohexenone substrate.

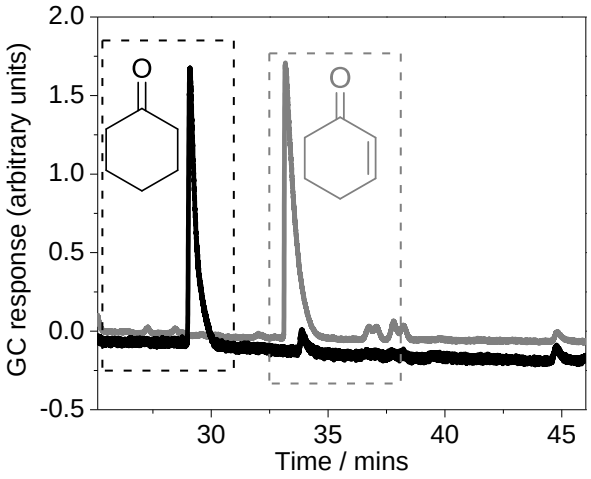

Figure 6-18: Final GC trace showing conversion of cyclohexenone (R.t.=33.875 mins) to cyclohexanone (R.t.=29.09 mins), shown in black on top of the starting mix shown in grey. Reaction was conducted on a 120 µL scale in 50 mM Tris-HCl pH 8 with 15 µg *TsER*. At the start of the reaction 5 mM cyclohexenone was added to the reaction mixture. Sequential aliquots of mACH in a 50 % DMSO solution were then added to the mixture until the total concentration of mACH was 6 mM. Peaks were assigned by comparison to authentic standards.

The HPLC trace in Figure 6-18 demonstrates a 95 % conversion of alkene to alkane with slight excess of reduced artificial cofactor (mACH). This suggests that cyclohexenone is a good candidate for further coupling work with the SH from *R. eutropha* as it is possible to achieve high conversions when just providing the *TsER* with the reduced cofactor. The literature also reports good conversions for the 1-methyl form of this substrate with the *TsER*, which could be used to determine whether the *TsER* retains its enantioselectivity when coupled with the SH as a mNADH recycling system.[263]

An experiment was carried out on a 120 µL scale with 2 mM mAC^+ in 50 mM Tris-HCl containing 2 % DMSO. The SH was left for 18 hours with just the mAC^+ in solution under 2 bar H_2. Subsequently an aliquot of *TsER* and cyclohexenone were added to the solution and the reaction was left to react for a further 2 hours. Under these conditions it was possible to obtain a final concentration of 0.83 mM cyclohexanone from this experiment (41 % conversion), which equates to a TTN of > 2,000 moles of product per mole SH. This is a lower TTN than the result obtained for the *H. thermoluteolus* SH. However, this is still a promising proof of concept and comparable to the work of Okamoto *et al*.[263]

Subsequently, a reaction was set up in which the *R. eutropha* SH was used to reduce mAC^+ to mACH. A UV-visible scan was taken after 30 minutes to confirm that mACH was being successfully produced, see Figure 6-19.

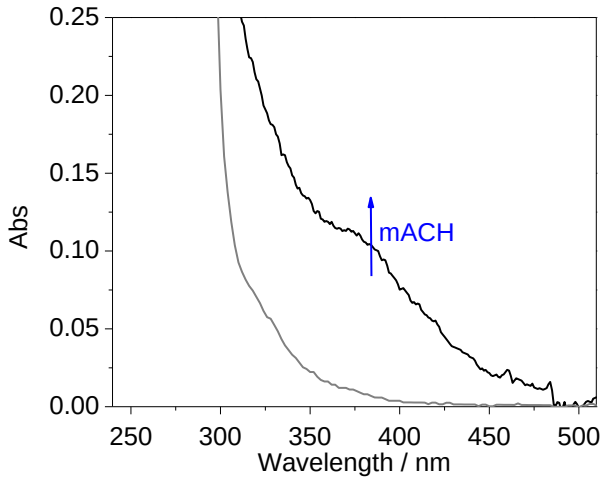

Figure 6-19: Scan of reaction mixture after 30 minutes to ensure mACH is being produced, shown in black (start scan shown in grey). Reaction conducted on an 80 µL scale, with 36 µg *R. eutropha* SH, 0.1 mM mAC^+, 5 mM cyclohexanone. The reaction was conducted under 2 bar H_2 in 50 mM Tris-HCl pH 8 with 2 % DMSO, under continuous H_2-flow.

The scan in Figure 6-19 shows an increase in absorbance at 378 nm, which equates to production of approximately 30 µM of mACH. Aliquots of *TsER* and cyclohexenone were then added to the reaction mixture and the reaction vessel was incubated under 2

bar H_2-pressure with shaking at 120 rpm for a further 8 hours before an aliquot was taken for GC analysis. GC traces used to determine the results of this experiment are shown in Figure 6-20.

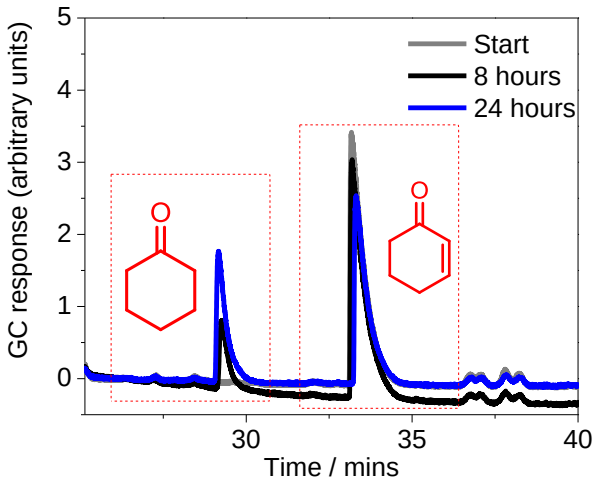

Figure 6-20: Coupling H_2-driven mAC^+ reduction by the SH to reduction of cyclohexenone by the *TsER*. The reaction was carried out on an 80 µL scale, with 36 µg SH, 0.1 mM mAC^+, 5 mM cyclohexenone and 87 µg *TsER*. The reaction was conducted under 2 bar H_2 in 50 mM Tris-HCl pH 8 with 2 % DMSO. Aliquots (20 µL) were taken after 8 and 24 hours for GC analysis.

Data in Figure 6-20 shows the product peaks for cyclohexanone (r.t. = 29.09) for samples taken after both 8 and 24 hours. After 8 hours, a 0.87 mM concentration of cyclohexanone equivalent to 17 % conversion was observed. The conversion increased to 38 % corresponding to a concentration of 1.9 mM cyclohexanone after 24 hours. Due to the starting concentration of mAC^+ being 0.1 mM the result after 24 hours equates to a TN (moles of product per moles of artificial cofactor) of 19. To our knowledge this is the highest TN of reduced artificial cofactor ever seen with a catalytic system and, additionally, this is a demonstration that very low concentrations of artificial cofactor can be used with both the *R. eutropha* SH and *TsER* enzymes. The TTN per SH enzyme is *ca.* 900 mAC^+ molecules per enzyme. However, it should be noted that the loading of SH in this example is relatively high, due to the low concentration of cofactor. It is likely that the TTN per SH could be improved for this system if lower enzyme loading

was used and a higher concentration of artificial cofactor. In addition, in contrast to the work of Okamoto *et al*. with an artificial metalloenzyme, this system makes use of a natural enzyme and hence avoids all of the problems associated with toxicity and cross reactivity when a catalyst containing a non-natural precious metal is used.[263]

6.7 Electrochemical studies

6.7.1 Reduction at bare carbon electrodes

The natural cofactor NAD^+ can be reduced a bare carbon PGE RDE, but with a large overpotential requirement relative to the thermodynamic NAD^+/NADH couple (-353 mV *vs* SHE at pH 8).[164] Idris *et al*. have shown that onset of reduction occurs at -800 mV *vs* SHE for a PGE RDE, in a mixture of 1 mM NAD^+ and 1 mM NADH. Oxidation on the other hand occurs at +400 mV *vs* SHE in a 1 to 1 mixture of NAD^+ and NADH at pH 7, see Figure 6-21 (a).

The large overpotential requirement has also been demonstrated for a range of other materials.[280] When cofactors are reduced directly at conventional electrodes dimers and inactive forms of the reduced cofactor are often produced.[256] This is because although, the 1-4-dihydropyridine versions of the artificial cofactors are thermodynamically more stable than the 1,2- or 1,6- versions[91,256], it is likely that the process of forming a radical cofactor ($mNAD^{\cdot}$) will be significantly faster than the subsequent protonation step. Consequently, due to kinetics it is statistically more likely that dimers will be formed than the enzymatically acceptable 1,4-form.[91] Ali *et al.* have demonstrated this with the natural cofactor NAD^+, this is because the addition of a proton and electron to $NAD^{\cdot}$ is a slow process whereas dimerization occurs rapidly,[91] see section 6.8 for more discussion.

In contrast, Figure 6-21 (b) shows a scan recorded at an electrode functionalised with HoxFU from *R. eutropha*. Enzymes are often very efficient electrocatalysts operating at

very close to the thermodynamic potential.[155] This is shown by the fact that the CV taken in a 1:1 ratio of NAD^+ and NADH (Figure 6-21, b) cleanly crosses the blank scan at the expected thermodynamic potential, represented by the red line. Reduction of NAD^+ by HoxFU leads to the enzymatically active form (1,4-NADH) of the cofactor, and as reduction of the cofactor won't occur at the bare electrode at potentials more positive than -472 mV, this means that when HoxFU is coupled to Hyd 2 on enzyme-modified particles reduction of NAD^+ must occur at the HoxFU active-site, not at the bare carbon surface of the particles. Consequently, the NADH produced by the enzyme-modified particles will be enzymatically active.

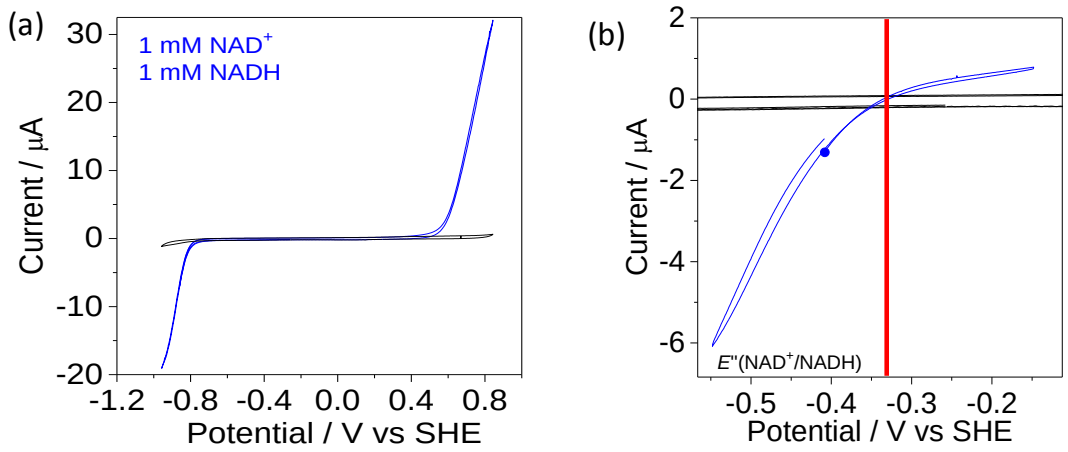

Figure 6-21: Cyclic voltammograms of NADH oxidation and NAD^+ reduction in a 1 mM NADH and 1 mM NAD^+ mixture (a) at a bare PGE RDE (b) at a *R. eutropha* HoxFU functionalised electrode, shown in green. Black line represents an unfunctionalised PGE RDE in buffer without cofactor. All scans were carried out in 50 mM phosphate buffer pH 7 at 30 °C. Rotation speed 2000 rpm, scan rate 10 mV s^{-1}. Data provided by Dr H. Reeve and Dr Z. Idris.[103,164]

When similar experiments were carried out for the artificial cofactor BNA^+ the onset of reduction is observed at a bare carbon electrode at approximately -600 mV *vs* SHE in a1 mM solution of BNA^+, see Figure 6-22.

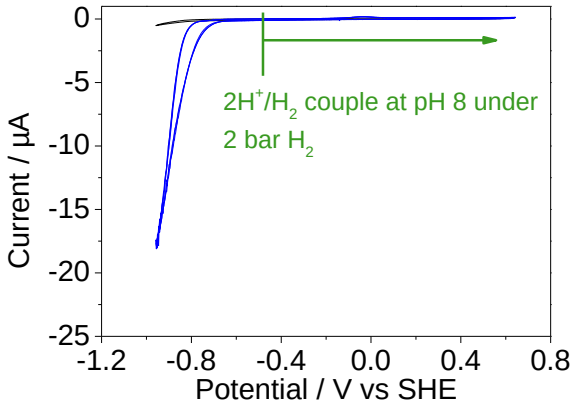

Figure 6-22: BNA^+ reduction at a bare PGE RDE. (a) Blue line: CV showing BNA^+ reduction at a bare carbon PGE RDE in 1 mM BNA^+ in 50 mM Tris-HCl buffer pH 8.0 containing 1 % DMSO at 22 ^oC, with a rotation rate of 2000 rpm, scan rate 10 mV s^{-1}. Black line represents a blank scan, with an unfunctionalised PGE RDE in 50 mM Tris-HCl buffer pH 8.0 containing 1 % DMSO at 22 ^oC.

When the electrode is rotated rapidly, as shown in Figure 6-22 just a single peak is observed demonstrating reduction of BNA^+. This is because at fast rotation rates, solution at the surface of the electrode rapidly exchanges with the bulk solution, meaning that the product of BNA^+ reduction, BNAH (although not necessarily the enzymatically acceptable 1,4-form of BNAH) does not builds up at the electrode surface. The green line on the CV shows the thermodynamic coupled for $2H^+/H_2$ at pH 8 under 2 bar H_2. As the onset of reduction occurs at a more negative potential than the thermodynamic couple, it is not possible to couple H_2 oxidation to reduction of BNA^+ at bare carbon under these conditions. This means that if the enzyme-modified particles were used as a recycling system for BNAH reduction of BNA^+ is unlikely to occur directly at the bare carbon surface of the particles.

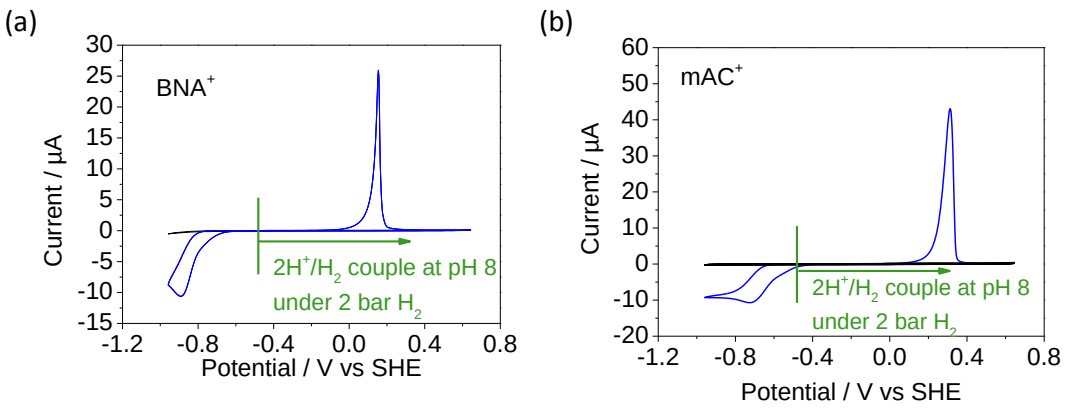

Figure 6-23: Reduction of artificial cofactors at bare PGE RDEs. CVs taken in buffer shown in black, CVs taken with the artificial cofactor present shown in blue (a) CV in 5 mM BNA^+ (b) CV in 5 mM mAC^+. All scans were performed in 50 mM Tris-HCl buffer, with 1 % DMSO at pH 8 at 23 ^oC with the electrode stationary. The black line represents a blank scan taken in solution not containing any cofactor. A scan rate of 10 mV s^{-1} was used.

Figure 6-23 (a) shows that in 5 mM BNA^+, when the electrode is not rotated a reverse peak for the oxidation of BNAH at the bare carbon electrode can be observed at approximately 200 mV *vs* SHE. This is because at low rotation rates the reaction becomes diffusion limited, consequently BNAH builds up at the electrode surface and at more positive potentials will undergo oxidation back to BNA^+, leading to a reverse peak in the CV.

Similar redox waves were observed in Figure 6-23 (b), which shows the reduction and re-oxidation of mAC^+. However, for mAC^+ the onset potential of reduction at the bare carbon PGE RDE is less negative than the thermodynamic couple for $2H^+/H_2$ at pH 8 under 2 bar H_2, shown by the green line on each of the scans. This means mAC^+ does not have the same overpotential requirement for reduction at a bare carbon electrode as BNA^+ or NAD^+, meaning that it may be possible to carry out H_2-driven reduction of mAC^+ at the carbon surface of the enzyme-modified particles, possibly leading to non-specific reduction products.

6.7.2 Electro-enzymatic cycling of artificial cofactors

As mAC^+ has a less negative E_{onset} potential than BNA^+ at bare carbon, which could mean that reduction of this cofactor occurs at the bare carbon surface of a PGE RDE rather than at the NAD^+-reductase active site, investigations into electro-enzymatic cycling of the artificial cofactors was initially only carried out with BNA^+. Analytical electrochemical experiments led to an extremely low current for reduction and oxidation of BNA^+ at a *H. thermoluteolus* HoxFU functionalised electrode. Even at scan rates of 1 mV s^{-1}, it was particularly difficult to distinguish between the contribution to the faradaic current from reduction and oxidation of the BNA^+/BNAH cofactor at the HoxFU active site and the contribution to the current as a result of the redox behaviour of the bound FMN cofactor within the HoxFU enzyme. Consequently, these results could not be used to reliably confirm electro-enzymatic cycling of BNA^+ at a HoxFU functionalised PGE RDE.

6.7.3 Bulk electro-enzymatic reactions

Using high surface area electrodes allows the reduction of larger amounts of cofactor, than is possible at the surface of a PGE RDE. This means that it is possible to significantly alter the composition of reduced and oxidised cofactor in the electrochemical cell solution. This allows the reaction to be monitored both by measuring the current passed from the chronoamperogram, but also by measuring the increase in UV-visible absorbance at 360 nm, see chapter 5 section 5.2 for more information about bulk electro-enzymatic methods. The UV-visible measurement provides additional evidence that electrochemical BNA^+ reduction is occurring at the electrode. High surface area carbon paper electrodes were produced as described in Chapter 5, see section 5.2. These were then functionalised with NAD^+-reductase (*H. thermoluteolus* HoxFU). Data in Figure 6-24 (a) shows a chronoamperometry trace.

Here the HoxFU functionalised electrode was held at a potential of -510 mV *vs* SHE for a period of 12.5 hours.

Figure 6-24 (b) shows the UV-visible scan of the cell solution after the chronoamperometry experiment. This scan shows an increase in absorption at 360 nm, this corresponds to generation of BNAH. The increase in absorption at 360 nm is equal to 35 µM BNAH being produced. This agrees well with the amount of current passed during the chronoamperometry experiment, which would correspond to a 39 µM concentration of BNAH having been produced. The transfer of electrons to generate BNAH in solution is therefore 90 % efficient.

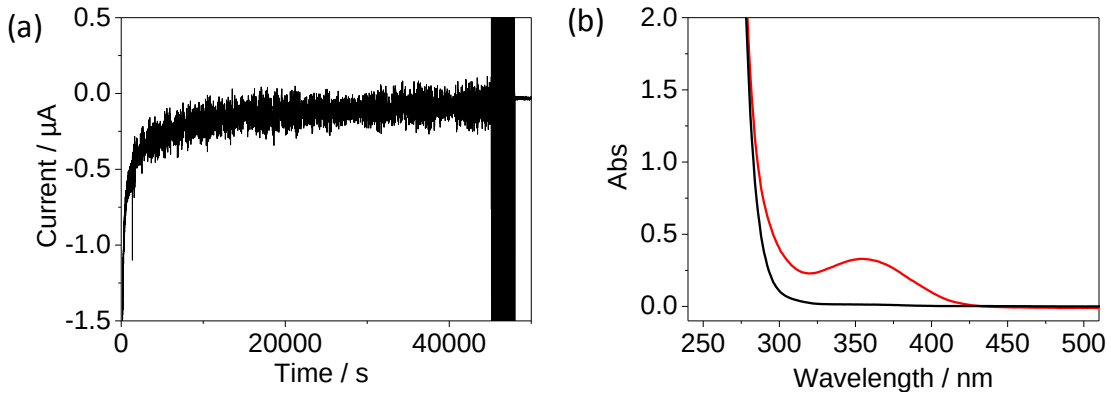

Figure 6-24: Electro-enzymatic production of BNAH (a) Overnight chronoamperometry trace for a *H. thermoluteolus* HoxFU functionalised carbon paper electrode. Electrode held at -510 mV *vs* SHE in 100 mM Tris-HCl pH 8.0 containing 1 mM BNA^+ and 2 % DMSO in a total volume of 1 mL. A mini calomel electrode was used as the reference and a coiled Pt wire was used as the counter electrode, in a fritted compartment separated from the main cell. The reaction was carried out at 40 ^oC. (b) UV-Visible scans; black: start scan, red: following the overnight electrochemical reaction.

This suggests that electrochemical reduction of BNA^+ to BNAH with a HoxFU functionalised electrode could be a feasible method of recycling BNAH for use in bio-catalysis, although, it would be desirable to improve the yield of BNAH for this.

As BNAH can be recycled at a carbon surface functionalised with NAD^+-reductase, this also suggests that it may also be possible to use the H_2-driven enzyme-modified particles as an artificial cofactor recycling system.

6.7.4 Determining whether BP 2000 particles are suitable to be used with the artificial cofactors

In order to determine whether the BP 2000 particles used in previous chapters of this thesis are suitable for use for making enzyme-modified particles for recycling artificial cofactors, BP 2000 particles were immobilised onto a PGE RDE and a CV was taken in buffer containing BNA^+.

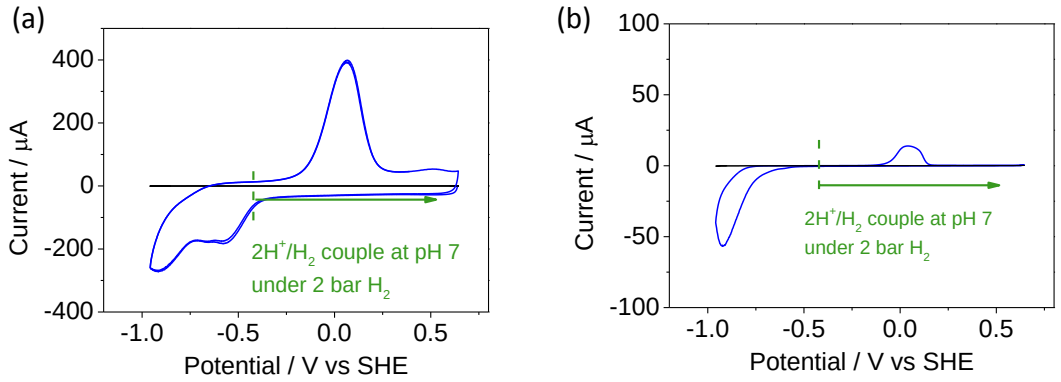

Figure 6-25: (a) CV at an electrode comprising BP 2000 particles immobilised on a PGE RDE. (b) CV at an electrode comprising PG particles immobilised on a PGE RDE. CVs were taken in 50 mM Phosphate buffer pH 7 containing 1 % DMSO. Blue traces: the electrode was rotated at 2000 rpm in a solution containing 5 mM BNA^+. Black traces: a CV for an unfunctionalised PGE RDE in 50 mM Phosphate buffer pH 7 containing 1 % DMSO. Particles were immobilised onto the PGE RDE by taking a 100 µg aliquot of particles suspended in buffer and allowing this to dry onto the surface of the electrode for 20 minutes.

The scan in Figure 6-25 (a) shows a CV taken in a solution containing 5 mM BNA^+ at a PGE RDE functionalised with BP 2000 particles. This demonstrates that reduction of BNA^+ has a less negative E_{onset} than the thermodynamic couple for $2H^+/H_2$ at pH 7, at the surface of the BP 2000 particles. Meaning that reduction of BNA^+ could occur at bare carbon surface of BP 2000 particles functionalised with *E. coli* Hyd 2, potentially leading to non-specific reduction products. This means that BP 2000 particles may show alternative redox activity with the artificial cofactors and hence are not suitable to be used as the basis for enzyme-modified particles for artificial cofactor recycling.

In contrast, in Figure 6-25 (b) a PGE RDE has been functionalised with home-made pyrolytic graphite (PG) particles. PG particles can be produced by simply abrading a piece of pyrolytic graphite with course sandpaper. These particles do not show reduction of BNA^+ at a potential less negative than the thermodynamic potential for the $2H^+/ H_2$ couple. In addition, the shape of the scan is similar to that of Figure 6-23 (a), which shows a bare PGE RDE, demonstrating that the electrochemical behaviour of BNA^+ at the surface of PG particles and a PGE RDE is essentially the same.

In subsequent work with enzyme-modified particles PG particles were used in order to reduce the possibility of direct reduction of the artificial cofactors occurring at the surface of the carbon particles, when they are modified with Hyd 2.

6.8 Artificial cofactor recycling using H_2-driven enzyme-modified particles

This section looks at using the enzyme-modified particles as a system for recycling the artificial cofactors.

There are a number of advantages of using the H_2-driven enzyme-modified particle system, first demonstrated in Chapter 3, over the native SH. The hydrogenase component of the SH from *R. eutropha* is less stable than the HoxFU moiety.[103,220] Therefore, one key advantage of using the particles is that the stable HoxFU moiety can be coupled with a more stable hydrogenase enzyme such as Hyd 2 from *E. coli*. Additionally, using particles means that all of the enzymes required for the cofactor recycling step are co-immobilised. Hence the particles are a single heterogeneous catalyst for this cofactor recycling step and can be easily removed and re-used at the end of the reaction.[119]

Initially, a control was carried out in which just *E. coli* Hyd 2 was immobilised on a set of PG particles, these were then added to H_2-saturated buffer containing BNA^+ and left to react overnight. The results for this control are shown in Figure 6-26 (a). The start

and finish scan directly overlay on top of one another demonstrating that reduction of BNA^+ does not occur at the surface of carbon particles functionalised with *E. coli* Hyd 2. Subsequently *H. thermoluteolus* HoxFU and Hyd 2 were co-immobilised on particles. These particles were then tested to determine whether it was possible to use the enzyme-modified particle cofactor recycling system to carry out BNA^+ reduction, see Figure 6-26 (b).

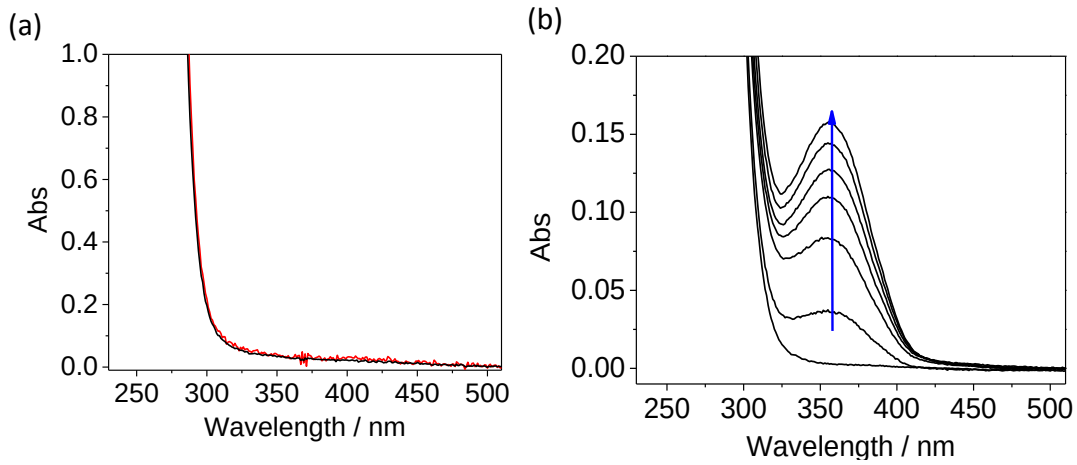

Figure 6-26: (a) A control showing PG particles (180 µg) with 27 µg Hyd 2 immobilised on them. These particles were left in H_2-saturated 50 mM Tris-HCl pH 8 containing 2 mM BNA^+ and 2 % DMSO overnight. Start scan: black, Finish scan: red. The reaction was carried out on a 500 µL scale. (b) BNAH generation by *H. thermoluteolus* HoxFU and Hyd 2 functionalised particles. Scans were taken every hour demonstrating increasing absorbance at 360 nm indicating increasing BNAH concentration. This reaction was carried out on a 1 mL scale at 40 ^oC in 50 mM Tris-HCl buffer pH 8. Particles were prepared by co-immobilising 5 µg H. *thermoluteolus* HoxFU along with 7.5 µg Hyd 2 on 100 µg of PG particles.

Figure 6-26 (b) shows increasing absorption at 360 nm over time. This shows that the concentration of BNAH is increasing. This is expected as it has been possible to demonstrate electro-enzymatic cycling of BNA^+ at a HoxFU functionalised electrode, see section 6.7, and in this experiment, H_2 was simply being used as an alternative electron source.

The rate of BNAH production is slower than that obtained using the whole *H. thermoluteolus* SH, with a turnover number of 0.1 s^{-1} or 0.07 U mg^{-1}. However, this

figure could probably be improved upon if the ratio of *H. thermoluteolus* HoxFU and Hyd 2 from *E. coli* was further optimised for this reaction.

It was also of interest to determine if it was possible to carry out the reduction of artificial cofactors using the Hox~~HY~~FU from the mesophile *R. eutropha* on particles. The whole *R. eutropha* SH is able to reduce BNA^+. Therefore, as the active site of the NAD^+ cycling domain of these two enzymes is identical, it would be expected that BNA^+ reduction should also be possible with the *R. eutropha* Hox~~HY~~FU immobilised on particles. This was initially tested by leaving enzyme-modified particles functionalised with *R. eutropha* Hox~~HY~~FU overnight in H_2-saturated buffer containing BNA^+.

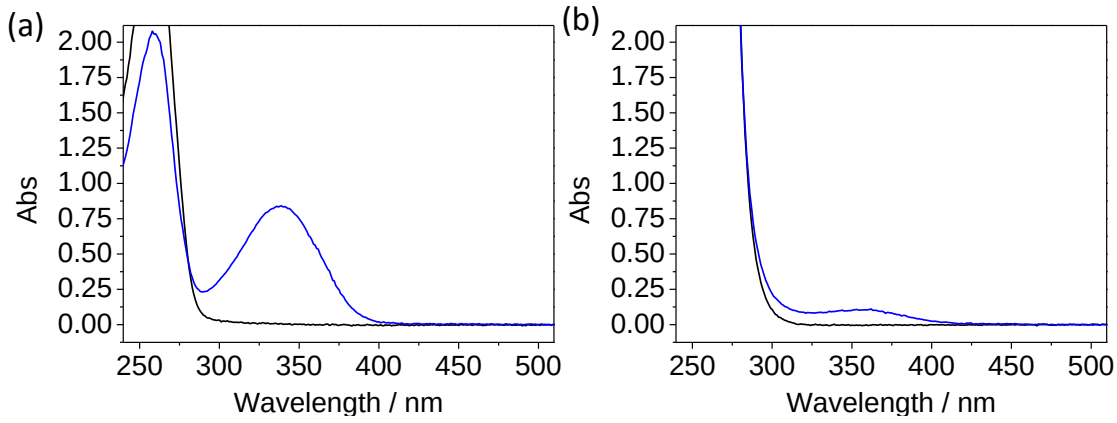

Figure 6-27: Start and finish scans comparing reduction of NAD^+ and BNA^+ by the same amount of particles prepared in the same batch. Particles were made with 0.4 mg PG particles, 13 µg Hox~~HY~~FU, 27 µg Hyd 2. Black: start scan. Blue: end scan. Reaction were left for 18 hours in pre-H_2 saturated 50 mM Tris-HCl pH 8, containing 2 % DMSO under 2 bar H_2 pressure (a) 2 mM NAD^+ (Scan shown 1:10 dilution of starting mix and product). (b) 2 mM BNA^+.

The scans in Figure 6-27 demonstrate that it is possible to use the mesophilic Hox~~HY~~FU from *R. eutropha* to reduce BNA^+ to BNAH. A drastically lower conversion is observed with BNA^+ than with NAD^+, during the course of an overnight reaction with the same amount of particles. This is however, to be expected as the specific activity of the *R. eutropha* SH is much lower with the artificial cofactors, as shown in section 6.4.

Using the enzyme-modified particles with other artificial cofactors

This section summarises the reactions and controls carried out with enzyme-modified particles in order to determine whether they can be used as an efficient artificial cofactor recycling system with all of the artificial cofactors shown in Figure 6-1.

Table 6-9: Reduction of cofactors using PG particles. The numbers in the table are percentage conversion (%) values following overnight reactions.

		1	*2*	*3*	*4*	*5*	*6*	*7*
	Cofactor	**Particles only**	**Hyd 2 only**	**Hyd 1 + particles**	**Hyd 2 + particles**	**Particles + Hyd 2 + Hox~~HY~~FU**	**Particles + Hyd 2 + *H. thermoluteolus* HoxFU**	***R. eutropha* SH**
1	NAD^+	✘	✘	✘	✘	90[a]	*ca.* 20 [b]	-
2	BNA^+	✘	✘	✘	✘	0.68	3[b]	12
3	mAC^+	✘	✘	0.67	3.8	4.3	5.5[b]	65
4	mCN^+	✘	✘	✘	✘	2.2	0.65[b]	20
5	$mCOOH^+$	N.D.	✘	N.D.	N.D.	✘	✘ [b]	✘
6	$BuNA^+$	N.D.	✘	N.D.	N.D.	✘	✘ [b]	✘
7	PNA^+	N.D.	✘	N.D.	N.D.	✘	✘ [b]	✘
8	MNA^+	N.D.	✘	✘	✓	✓	N.D.	✘

✘: no reaction. ✓:Conversion. N.D.: Not Determined. Percentage conversion (%) figures given following an overnight reaction. Reactions were carried out on a 200 µL scale in 50 mM Tris-HCl pH 8 at room temperature, with 2 % DMSO and 2 mM starting concentration of cofactor. A 800 µg aliquot of PG particles was added to each reaction containing just particles. In the case of the Hyd 2 only 60 µg of Hyd 2 was added. Particles with Hyd 1 contained approximately 80 µg Hyd 1 and 800 µg PG. Particles with Hyd 2 contained approximately 60 µg Hyd 2 and 800 µg PG. Particles with Hyd 2 and Hox~~HY~~FU contained approximately 54 µg Hyd 2, 25 µg Hox~~HY~~FU and 800 µg PG. Particles with Hyd 2 and *H. thermoluteolus* HoxFU contained approximately 54 µg Hyd 2, 20 µg *H. thermoluteolus* HoxFU and 800 µg PG, these reactions were carried out at 40 ^oC, all other reactions were carried out at room temperature. All reactions were carried out in a pressure system under 2 bar H_2. [a]Conversion figure based on ratio of peaks at 260 nm and 340 nm [b]Reactions carried out by Farieha Altaf (Part II student under my supervision)

A range of artificial cofactors were tested with the enzyme-modified particles for H_2-driven artificial cofactor recycling, as shown in Table 6-9. Controls were also performed to show that the NAD^+-reductase was catalysing reduction of the artificial cofactors and that they are not reduced by the particles themselves or by any of the component sections of the particle system.

Column one in Table 6-9 demonstrates that no activity was observed with any of the artificial cofactors with just the PG particles themselves under H_2 gas. Similarly column 2 demonstrates that none of the artificial cofactors were reduced directly by the hydrogenase enzyme, *E. coli* Hyd 2.

Columns three and four, however, show that the artificial cofactor mAC^+ was reduced at particles functionalised with only *E. coli* Hyd 1 and only *E. coli* Hyd 2. MNA^+ was also reduced at particles functionalised with only *E. coli* Hyd 2. Both of these cofactors were not reduced by *E. coli* Hyd 2 on its own, consequently they must be being reduced directly at the carbon surface of the particles, potentially leading to unspecific reduction products (such as 1,6-mNADH or dimers).

E. coli Hyd 2 catalyses the oxidation of H_2 at the thermodynamic potential for this reaction; whereas, *E. coli* Hyd 1 requires an overpotential of 50 mV to begin catalysis.[122] The fact that MNA^+ is only reduced at *E. coli* Hyd 2 functionalised particles, suggests that E_{onset} for reduction of MNA^+ at bare PG carbon occurs at close to the thermodynamic potential for the H_2 oxidation under 2 bar H_2.

E_{onset} for reduction of mAC^+, on the other hand, occurs at a more positive potential than for MNA^+. The reduction of mAC^+ at carbon particles supports the electrochemical data in Figure 6-23, which show that E_{onset} for mAC^+ reduction at a bare carbon PGE RDE occurs at a more positive potential than the thermodynamic potential for the $2H^+/ H_2$ couple at pH 8 under 2 bar H_2.

Data in column 5 show that the percentage conversion figures achieved following an overnight reaction with the enzyme-modified particles functionalised with *R. eutropha* Hox~~HY~~FU are significantly lower than the percentage conversion figures achieved with the whole *R. eutropha* SH, shown in Table 6-4, for all of the artificial cofactors.

Column 6 demonstrates that again significantly lower conversions are achieved with the H. *thermoluteolus* HoxFU functionalised particles, than for the whole *H. thermoluteolus* SH, shown in Table 6-4.

However, it is likely that these figures could be improved upon through optimisation of the system for reduction of the specific cofactor. Currently, however, both the whole *R. eutropha* SH or the whole *H. thermoluteolus* SH present better options in terms of artificial cofactor recycling. The magnitude of the conversion figures for the particles functionalised with *R. eutropha* Hox~~HY~~FU, do however follow the same trend as seen for the whole *R. eutropha* SH with the highest conversion being seen for mAC^+ and the lowest for BNA^+ for the artificial cofactors.

Date in Table 6-9 demonstrates that it would be feasible to use particles as a system for recycling mCNH and BNAH which are not directly reduced at the carbon surface of Hyd 2 functionalised particles. However, for mAC^+, reduction of the cofactor is observed at the bare carbon particle surface, which is often associated with unspecific reduction products (e.g. 1,6-mNADH or dimers).[91] Furthermore, similar yields of reduced mACH (which may not be the enzymatically acceptable form of 1,4-mACH) were obtained with carbon particles only modified with Hyd 2 and carbon particles modified with Hyd 2 and *R. eutropha* Hox~~HY~~FU. This suggests that even in the case of the particles modified with Hyd 2 and *R. eutropha* Hox~~HY~~FU the majority of the reduced mACH product is being produced at the carbon surface of the particles and not at the HoxF active site.

6.8.1 LC-MS detection of the product of reduction of mAC^+ at bare carbon

This experiment was performed with assistance from J. Rowbotham (Post doc. in the Vincent group).

In order to conclusively determine the product of mAC^+ reduction at the bare carbon surface of the PG particles modified with Hyd 2, an LC-MS experiment was performed on a sample produced using just *E. coli* Hyd 2 functionalised PG particles.

Two possible products of the reduction of mAC^+ at bare carbon are shown in Figure 6-28, the dimer and the 1,4-form of mACH along with their predicted m/z and splitting patterns for the $[M+H^+]$ ions.

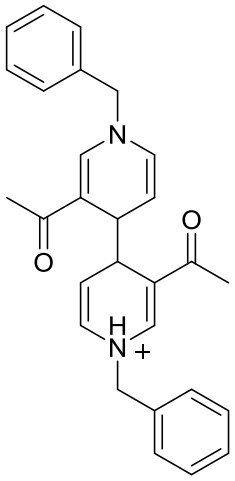

Chemical Formula: $C_{28}H_{29}N_2O_2^+$
Exact Mass: 425.22
Molecular Weight: 425.55
m/z: 425.22 (100.0%), 426.23 (30.3%), 427.23 (2.7%), 427.23 (1.7%)

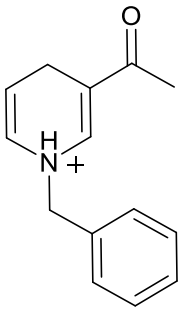

Chemical Formula: $C_{14}H_{15}NO^+$
Exact Mass: 213.11
Molecular Weight: 213.28
m/z: 213.11 (100.0%), 214.12 (15.1%), 215.12 (1.1%)

Figure 6-28: Chemical structures of two possible $[M+H^+]$ ions which could result from ionisation of the reduction products from direct reduction of mAC^+ at the bare surface of the carbon particles.

The spectrum in Figure 6-29 (a) shows a UV-visible spectrum taken of the product at the end of an overnight reaction in which Hyd 2 modified PG particles were added to a H_2 saturated solution of buffer containing mAC^+. The increased absorbance at 378 nm in the spectrum shown in Figure 6-29 (a) demonstrates that some conversion of mAC^+ to a reduced form of mACH (although, not necessarily the enzymatically acceptable

form 1,4-mACH) has been achieved in this reaction. This mixture was then analysed using LC-MS.

The HPLC chromatogram from the liquid chromatography stage of the LC-MS analysis is shown in Figure 6-29 (b), there is one major peak corresponding to a single major reduced product.

The mass spectrum corresponding to the time point for the major peak in the HPLC chromatogram (ca. 3.5 mins) is shown in Figure 6-29 (c). This trace shows a major m/z peak at 425 which corresponds exactly with the expected mass of the mAC-mAC dimer, shown in Figure 6-28. The idea that this major peak is the dimer is further supported by the presence of additional peaks at 426 and 427, shown more clearly in Figure 6-29 (d), which is an enlargement of the m/z region between 410 and 440 Da in Figure 6-29 (c). These additional peaks are expected due to the presence of carbon isotopes in the skeleton of the dimer.

Electrochemical reduction of the natural cofactor NAD^+ at a bare carbon surface occurs as a two-step process.[91] The first step is the formation of $NAD^{\cdot}$ radical. This is then reduced once more and protonated to give NADH in a subsequent step.[91] The protonation of the radical is significantly slower than the first step (the addition of an electron). In fact, radical recombination of two $NAD^{\cdot}$ radicals forming a dimer is significantly faster at most conventional electrodes than forming the 1,4-form of the cofactor *via* the protonation step. This leads to yields of less than 1 % of the active form of 1,4-NADH when it is reduced directly at a glassy-carbon electrode.[91]

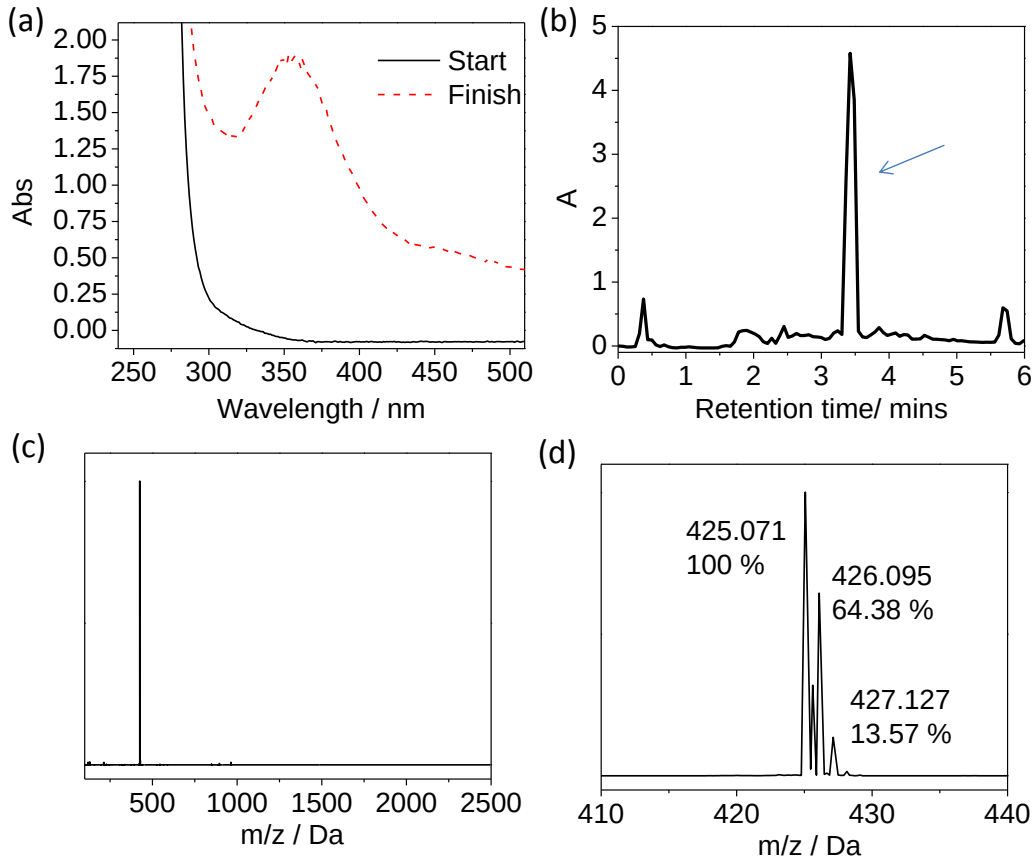

Figure 6-29: Use of LC-MS to determine the product of direct reduction of mAC^+ at Hyd 2 functionalised PG particles. (a) Start and finish scans of the reaction mixture used to produce reduced mAC^+ showing the characteristic absorbance at 378 nm. The reaction was performed in pre-H_2-saturated 25 mM phosphate buffer pH 7 containing 2 % DMSO and 3 mM mAC^+. The reaction was performed on a 3 mL scale with 150 µg Hyd 2 immobilised on 2 mg PGE particles. The vessel was stirred gentle for 18 hours under a 2 bar H_2-atmosphere at room temperature (b) LC-MS was performed using a Waters LCT Premier XE equipped with electrospray interface. The LC column was an ACE equivalence C18. Details of the LC program are given in Appendix H. Electrospray ionisation in the positive mode was used by the LCMS. LC trace showing peaks for the main components in the reaction mixture following the reaction. (c) Full mass spectrometry splitting pattern for the large peak shown in the HPLC trace (indicated with an arrow). (d) Mass spectrogram zoomed in on the large peak at m/z 425.

The dimer product, which is not enzymatically active, is also the majority product formed when mAC^+ is reduced directly at carbon. Consequently, the enzyme-modified particle system is not suitable for recycling mACH, unless a blocking strategy can be developed to block bare sites of the particles, perhaps using another enzyme which can be produced cheaply and in bulk like bovine serum albumin, ensuring that reduction of mAC^+ occurs only at the active site of the HoxF moiety.

6.9 Discussion

All of the enzymes demonstrated to be able to recycle the artificial cofactors in this chapter (SHs, Mo-FDH) contain the bound redox cofactor FMN at their active sites where cofactor reduction occurs. The work carried out in this chapter therefore supports the hypothesis that enzymes with tightly bound internal redox groups such as FMN are able accept artificial cofactors;[262] whereas, those without internal redox centres, such as the commercial FDH and GDH tested in section 6.3 cannot accept the artificial cofactors.

Table 6-10 summarises the specific activities and TTNs (mol reduced artificial cofactor/mol enzyme) obtained for each of the artificial cofactor recycling systems, when just used to reduce the artificial cofactors.

Entries in Table 6-10 show that the behaviour of both SHs are similar in that they both accept the three artificial cofactors BNA^+, mAC^+ and mCN^+. Similar specific activity values were obtained with both the *R. eutropha* and *H. thermoluteolus* SHs. In contrast, the *R. capsulatus* Mo-FDH behaves differently in that it will not reduce the artificial cofactor BNA^+. In addition, significantly higher specific activities were seen with the Mo-FDH than with either of the SHs for the artificial cofactors mAC^+ and mCN^+. However, this higher activity was not sustained over time and consequently higher TTNs were also obtained with the SH enzymes with all of the artificial cofactors. It has not yet been possible to isolate the reduced forms of the artificial cofactors produced by the SH enzymes and to determine their structures using NMR spectroscopy, mainly due to the requirement for large amounts of SH enzyme to produce the reduced version of cofactor on the required scale for ^1H NMR analysis.

Table 6-10: Overall summary table of activities and total turnover numbers per enzyme when used to reduce the artificial cofactors

							Particles	
	***R. capsulatus* Mo-FDH** [a]		***R. eutropha* SH**		***H. thermoluteolus* SH**		***R. eutropha* Hox~~HY~~FU** [b]	***H. thermolu-teolus* HoxFU** [c]
	Activity	TTN	Activity	TTN	Activity	TTN	TTN	TTN.
NAD^+	9.3	-	15.9	-	0.97	Ca. 14,000	-	-
BNA^+	0	0	0.01	700	0.14	2000	19	53
mAC^+	1.3	300	0.05	3100	0.12	3200	122[d]	100[d]
mCN^+	2.8	800	0.08	1000	0.03	1200	62.3	12
$mCOOH^+$	0	0	0	0	0	0	0	0
$BuNA^+$	-	-	0	0	0	0	0	0
PNA^+	-	-	0	0	0	0	0	0
MNA^+	0	0	0	0	0	0	✓	-

Activity = initial specific activity, U mg^{-1} TTNs (Total turnover number) moles of reduced artificial cofactor produced per mole of enzyme. [a]TTN after 6 minutes; [b] *R. eutropha* Hox~~HY~~FU immobilised on PG particles with Hyd 2. TTNs given per Hox~~HY~~FU enzyme. [c] *H. thermoluteolus* HoxFU immobilised on PG particles with Hyd 2 TTNs given per HoxFU moiety [d] Reduction probably occurring at the bare carbon surface of the particle.

It was also possible to use the enzyme-modified particles with Hyd 2 and either the *R. eutropha* Hox~~HY~~FU or *H. thermoluteolus* HoxFU to recycle the artificial cofactors BNA^+ and mCN^+ (grey columns). Although, mAC^+ was reduced directly at the surface of the carbon particles leading to the production of dimers, this was verified using LC-MS in section 6.8.1.

The total turnover numbers obtained after an overnight reaction with the enzyme-modified particles were generally lower than those obtained when using the

whole SHs. This suggests that using the whole SH from either *R. eutropha* or *H. thermoluteolus* is the most promising recycling system for the artificial cofactors mAC^+, mCN^+ and BNA^+.

In section 6.4.1 the K_M of the *R. eutropha* SH was determined with the artificial cofactor mAC^+. Extensive work has already been carried out to improve the affinity of the *R. eutropha* SH for the phosphorylated version of NAD^+, $NADP^+$. Rational mutagenesis has led to a significant decrease in the K_M of this enzyme for $NADP^+$ from its native value of 8 mM.[164] This is based on work already carried out on NuoF from *E. coli* complex I, which shows high sequence homology with the *R. eutropha* SH. For NuoF mutation of a single glutamic acid residue led to a 220 fold increase in the affinity of the complex for NADPH from 1870 µM to 25 µM.[281] Consequently, a rational mutagenesis approach, could help to improve the affinity of the SH from *R. eutropha* for a particular artificial cofactor, to improve the K_M making this enzyme more attractive for biotechnological applications and providing a viable enzymatic strategy for recycling artificial cofactors.

The electrochemical studies carried out as part of this chapter suggest that electrochemical regeneration of BNAH at a HoxFU functionalised electrode is also feasible. An electrochemical approach towards artificial cofactor regeneration could also perhaps be used in combination with the artificial cofactor mCN^+, which is not reduced at bare carbon particles at a potential more positive than the $2H^+/H_2$ couple (at pH 8 under 2 bar H_2), but, is reduced by HoxFU. This suggests that there is a potential window at which mCN^+ reduction can occur at HoxFU, but at which the mCN^+ will not be reduced at bare carbon.

Table 6-11: Overall summary table of TTNS per recycling enzyme (SH or Mo-FDH) when used to recycle the artificial cofactors coupled to the TsER for alkene reduction.

Recycling enzyme	Artificial cofactor	TsER substrate	TTN (per recycling enzyme)	TN (of artificial cofactor)
***H. thermoluteolus* SH**	mAC^+	N-phenyl maleimide	>6000	-
***R. eutropha* SH**	mAC^+	N-phenyl maleimide	Ca. 3,000	1.4
	mAC^+	Cyclohexenone	>2000	-
	mAC^+	Cyclohexenone	900	19
***R. capsulatus* Mo-FDH**	mCN^+	N-phenyl maleimide	Ca. 1300	9

TTN: Total Turnover Number, moles of product per mole of recycling enzyme. TN: Turnover Number, moles of product per mole of cofactor.

Table 6-11 shows data for reactions where the SHs from *R. eutropha* or from *H. thermoluteolus*, or the Mo-FDH was used to recycle the reduced version of one of the artificial cofactors which was then used by the *TsER* for selective reduction of activated alkenes.

The highest TTN (moles of alkane produced per mole of SH) was achieved with the *H. thermoluteolus* SH using N-phenyl maleimide as the *TsER* substrate. With the *R. eutropha* SH total TTNS of >2000 were achieved when both N-phenyl maleimide and cyclohexenone were used as substrates for the *TsER*. A maximum TN of 19 was achieved with the *R. eutropha* SH and cyclohexenone as the *TsER* substrate. This also clearly demonstrates that the reduced forms of the artificial cofactors produced by the recycling enzymes used in this project are accepted by the *TsER*.

6.10 Summary and outlook

This chapter presents the first enzymatic methods for recycling the reduced versions of the artificial cofactors BNA^+, mAC^+ and mCN^+. SH enzymes from two organisms along with the Mo-FMN from *R. capsulatus* have been demonstrated to reduce a number of artificial cofactors. It has also been possible to observe the highest TTNs

(moles of artificial cofactor reduced per mole of enzyme or catalyst) ever observed in this work: >3000 for both the *R. eutropha* and *H. thermoluteolus* SH.[258,263]

Work in this chapter then goes on to demonstrate that it is possible to couple both SHs from *R. eutropha* and from *H. thermoluteolus,* and the Mo-FDH from *R. capsulatus* (as artificial cofactor recycling systems) with the *TsER* enoate-reductase enzyme for selective alkene reduction. Coupling the *TsER* with the SH from *R. eutropha* led to the highest TN of mNADH (moles of product per moles of artificial cofactor) ever observed with a catalytic system (19 in total).[256,263] In addition, when coupling the *H. thermoluteolus* SH to the *TsER* it was possible to obtain TTNs of >6000 moles of product per mole of SH enzyme.

These systems consequently present a viable solution to recycling the reduced forms of the artificial cofactors for use with enoate reductase enzymes, avoiding the need for metal catalysts or sodium dithionite used previously as recycling systems for the reduced forms of the artificial cofactors.[263] This study supports the use of further rational mutagenesis work to improve the substrate affinity of the SH from *R. eutropha* or *H. thermoluteolus* for the reduction of a range of artificial cofactors in order to increase the substrate affinity of the SHs for a particular artificial cofactor.

7 Producing selectively deuteriated alcohols using $^{2}H_2$-driven cofactor recycling

All complete NMR spectra for results discussed in this chapter are provided in Appendix J.

7.1 Introduction

This chapter demonstrates a possible application of the enzyme-modified particles for the production of deuteriated alcohols. Use of the enzyme-modified particles was first demonstrated in Chapter 3. In this chapter, initially, the enzyme-modified particles were used for ^{2}H-driven NAD$^+$-reduction, this allowed the selectivity of hydride addition to NAD$^+$ by the *R. eutropha* Hox~~HY~~FU moiety to be determined by comparison to spectra obtained by Hirst and co-workers.[282] Subsequently, ^{2}H-driven cofactor recycling was demonstrated for the production of deuteriated (R)- and (S)-phenylethanol using (R)- and (S)- selective alcohol dehydrogenase enzymes, as a proof of concept demonstration. This is the first demonstration of ^{2}H-driven cofactor recycling. Finally, it was demonstrated that the enzyme-modified particles are able to carry out ^{2}H-driven cofactor recycling in unbuffered ^2H_2O.

7.2 Uses of deuteriated molecules

Deuterium-labelled compounds are highly useful in a variety of scientific and pharmaceutical applications. In addition, deuteriated compounds are often very expensive. For example L-alanine-2-d, which is mainly used in research applications, is priced at £653.00/g from Sigma Aldrich compared to non-deuteriated L-alanine which is around £10/g.[65] Benzaldehyde-α-d_1 sells for £233.50/g, whereas non-deuteriated benzaldehyde costs £0.34/g. Similarly, 1-phenylethan-d_1-ol is £67/g *versus* approximately £1/g of unlabelled 1-phenylethanol.[65]

Deuteriated water (^2H_2O) can readily be obtained for well under £1/mL from mainstream chemical vendors. It is envisaged that $^2H_2$ could be produced from the ^2H_2O

solvent *in situ via* electrolysis (for example using established technologies like the H-Cube®), to provide the $^{2}H_2$ gas required for hydrogen-driven cofactor recycling.[283,284] Provided that production costs of the particles could be minimised, for example by mass producing the enzymes required, selective bio-catalytic deuteration (reduction with $^{2}H^{-}$) of cheap starting materials, presents a lucrative potential application for the hydrogen-driven enzyme-modified particles.

7.2.1 Research uses of deuterium labelled compounds

Deuterium is the only stable, heavy, non-radioactive, isotope of hydrogen, which is present on the Earth's surface at a ratio of 150×10^{-6}:1.[285] Deuteriated compounds are used as reference materials in mass spectrometry and in neutron scattering experiments.[286][287]

In addition, deuteriated molecules are often used to study mechanism. For example deuteriated proteins can display altered stretching frequencies of bands within a protein active site, particularly reporter groups such as CN and CO, but also C-^{2}H bonds which can be observed using IR spectroscopy.[288] Moreover, as a result of variations in rate due to the kinetic isotope effect for C-^{2}H *versus* C-H bonds deuteriated compounds can be used in mechanistic studies for enzymes such as cytochrome P450.[289]

7.2.2 Pharmaceutical uses of deuterium labelled compounds

Deuteriated compounds are used widely in biomedical research. Combining selectively deuterium labelled compounds with mass spectrometry can be used for metabolic studies required for the regulatory clearance of pharmaceuticals.[290,291] One example of where selectively deuteriated compounds were used in tandem with mass spectrometry was to study the *in vivo* metabolic breakdown of benzylamine in rats.[291] The rats were dosed with an equimolar mixture of $d_0 - d_7$ benzylamine, this allowed the oxidative

breakdown pathway of benzylamine to benzaldehyde to be confirmed, as 2 of the deuterium atoms were lost during the metabolic process.[291] The benzaldehyde was then rapidly converted to the carboxylic acid, conjugated with glycine and excreted as Hippuric acid.[291] Dietary cholesterol absorption can, also, be measured effectively using selectively deuteriated cholesterol.[292] This can be carried out by administering selectively deuteriated cholesterol to patients over a seven day period and monitoring the composition of their faeces samples over this period (using mass spectrometry). The amount of deuteriated cholesterol in faeces samples with respect to a deuteriated internal standard (sitostanol), administered to patients at the same time as the cholesterol, can be used to determine how much cholesterol is absorbed by the patient.[292]

A second emerging use of deuteriated compounds within medicine is in deuteriated drug molecules. Because of the kinetic isotope effect (^{2}H-X bonds having a lower zero point energy than the equivalent ^{1}H-X bonds), C-^{2}H bonds are stronger than C-^{1}H bonds.[126] Therefore, replacing a C-^{1}H bond with a C-^{2}H bond can help to shield a pharmaceutical molecule from unwanted metabolic effects (particularly oxidation of C-H bonds by cytochrome P450 enzymes within the body),[293] whilst avoiding changes to the uptake and method of action of the drug in the body.[126]

Adding deuterium to drugs can also help to reduce the side effects of the drug. For example, '*Concert Pharmaceuticals'* are working on a deuteriated version of dextromethorphan, a drug used in combination with quinidine to treat pseudobulbar disorder.[293] Quinidine's side effects mean that it increases risks for patients with cardiovascular disorders. Using the deuteriated form of dextromethorphan has been shown to reduce the amount of quinidine required, as the deuterium slows down

metabolism of the dextromethorphan. This therefore should lead to a reduced chance of side effects for patients with cardiovascular risk factors.[293]

Deuteriated drugs may also reduce inter patient variability, particularly between patients of different genders and ethnicities. It is known that some groups are 'fast metabolisers', i.e. they are able to break down drugs through oxidative pathways more quickly than other groups, leading to faster clearance of drugs in these groups.[126] Deuterating C-H bonds can help shut down these oxidative metabolic pathways leading to clearance of the drug being achieved through more universal pathways in all groups.[126]

Another innovative approach to using deuterium in pharmaceutical molecules is being pioneered by the biopharmaceutical company DeuteRx.[293] They have developed a deuteriated form of the (R)-enantiomer of the anti-diabetic compound pioglitazone, see Figure 7-1.

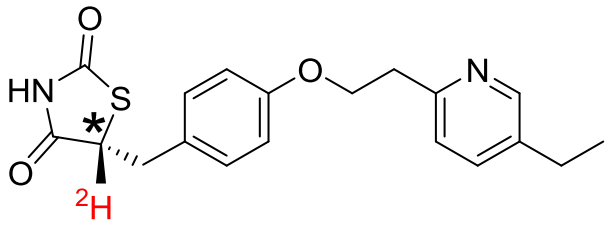

Figure 7-1: The deuteriated (R)-enantiomer of pioglitazone.

In this molecule the deuterium at the chiral centre (marked with a star) slows down the rate of formation of the enol intermediate.[293] When the enol is formed this facilitates interconversion between the two enantiomers of this molecule, meaning that the *ee* of the drug will decrease over time. It has been shown that the (S)-enantiomer of pioglitazone has the side effect of possible weight gain, whereas the (R)-enantiomer displays the desired mitochondrial function without the negative side effects.[293]

Recently, the first deuteriated drug molecule has been approved by the FDA: Austedo or deutetrabenazine.[294] The chemical structure of this molecule is shown in Figure 7-2.

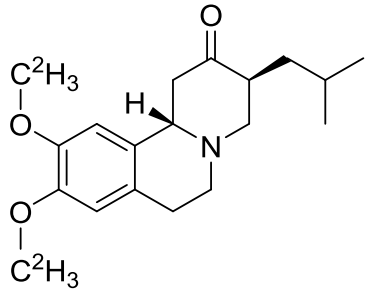

Figure 7-2: The chemical structure of Austedo.

Austedo is used in the treatment of Huntington's chorea, adding deuteriums to the methoxy-groups on this molecule slows down metabolism, meaning that the methoxy groups are demethylated more slowly. This leads to slower clearance of the drug from the body.[294]

7.3 Methods of production of deuteriated compounds

All deuterium on Earth is originally obtained from heavy water.[295] This is obtained from normal water, which on average contains about 0.0013 % H^2HO.[295] Most commonly the Girdler sulphide process is used to enrich the deuterium content of water.[296] This process involves chemical exchange between H_2O and H_2S *via* the following reaction:

$$H_2O + H^2HS \rightleftarrows H_2S + H^2HO \qquad \textbf{7-1}$$

At 303 K the equilibrium constant for this reaction is 2.33 and at 403 K it is 1.8.[296] The discrepancy in equilibrium constants can be exploited by having a cold tower where the concentration of deuterium in water is enriched and a hot tower where a constant flow of non-enriched water is maintained. In the hot tower H^2HS will be produced, which is then circulated to the cold tower preferentially giving H^2HO. The enriched water can then be removed and the process repeated again until pure ^2H_2O is produced.[296]

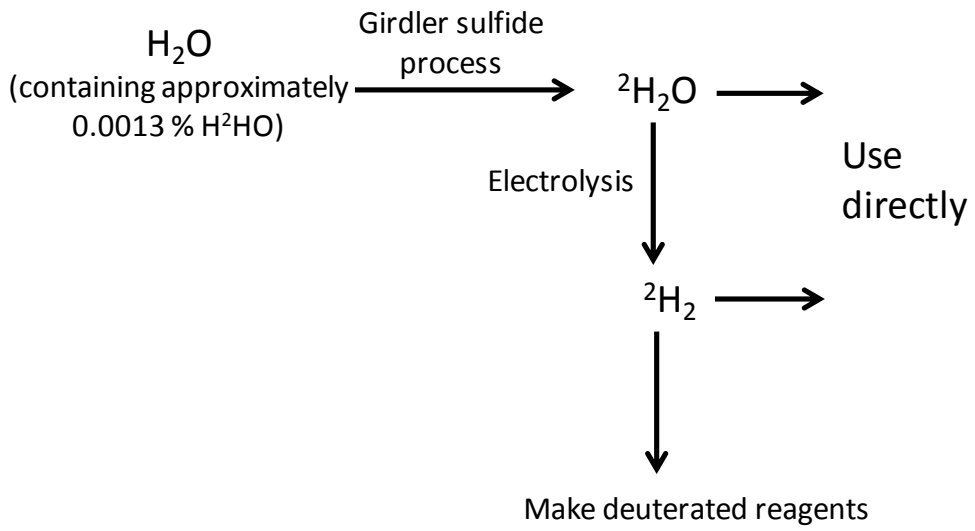

Figure 7-3: A schematic diagram showing the pathway to making deuteriated compounds used in research and the pharmaceutical industry.

The $^{2}H_2O$ obtained from this process can then either be used directly in synthetic processes or used to produce $^{2}H_2$ gas, which can again be used directly or converted into sacrificial reagents for carrying out deuteration reactions, see Figure 7-3.[297]

The main methods of producing deuteriated fine chemicals are summarised in Figure 7-4. Perhaps the easiest method conceptually is direct addition of $^{2}H_2$ across a double bond, with $^{2}H_2$ being produced electrochemically from $^{2}H_2O$ as required, see Figure 7-4 (a).[284] The second common method involves the reduction of a carbonyl group with a sacrificial deuteride source such as $NaB^{2}H_4$, see Figure 7-4 (b).[298][299] It is worth noting $^{2}H_2O$ is approximately 40-fold cheaper than $NaB^{2}H_4$ (Prices from Sigma Aldrich £1.05/g and £40.90/g respectively).[65,297]

Another common method involves activation of a C-H bond and subsequent exchange with a deuteriated reagent, usually the solvent, which is often $^{2}H_2O$. This could be simply keto enol tautomerisation or as in Figure 7-4 (c) by the action of a precious metal catalysed exchange process.[300–305]

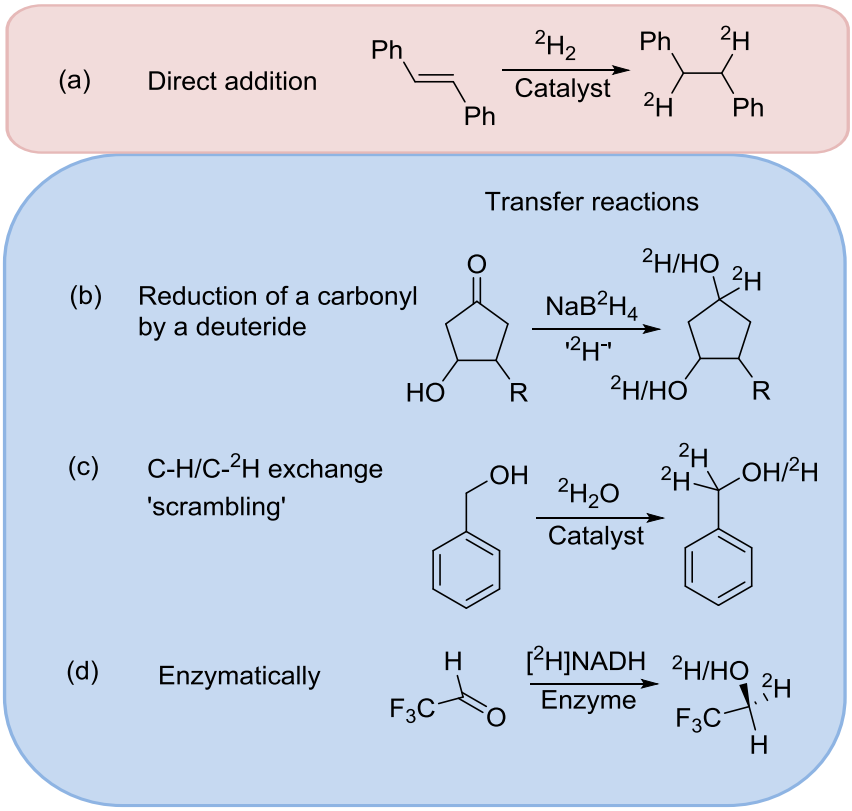

Figure 7-4: The main routes towards producing deuteriated fine chemicals. Examples of reactions taken from (a)[284] (b)[298] (c)[306] (d)[307]. The two main routes involve catalytic hydrogenation (pink box) or a variety of transfer reactions (blue box), these are carbonyl reduction by a deuteride donor, C-H, C-^{2}H exchange with the solvent and enzymatic deuterium addition.

Enzymatic methods of producing deuteriated molecules show great promise.[307] For example the ketone reduction shown in Figure 7-4 (d). As already discussed in detail in the introduction to this thesis, many dehydrogenase enzymes are able to use the cofactor, NADH, for highly enantio-selective hydride transfer. If [^{2}H]NADH is used instead, selective ^{2}H- addition can be achieved. Currently, GDH or FDH enzymes tend to be used as the cofactor recycling systems for these deuteration reactions. These enzymes require super stoichiometric amounts of expensive sacrificial deuteriated formate or α-deuteriated glucose for cofactor recycling systems to produce [^{2}H]NADH, which cost £20.80 and £125.00 per gram respectively from Sigma Aldrich.[65,282,307,308]

7.4 Producing deuteriated NADH

Except whether otherwise stated experiments in this chapter were performed in deuteriated phosphate buffer pD 6.9-8.5.

Initial experiments were performed to determine if it is possible to produce deuteriated NADH ([^{2}H]NADH) using the hydrogen-driven enzyme-modified particles by replacing H_2 and H_2O with $^2H_2$ and ^2H_2O (in deuteriated buffer). An NMR spectrum of commercially available (non-deuteriated) NADH in deuteriated phosphate buffer is shown in Figure 7-5. Peaks corresponding to protons on the nicotinamide ring are labelled in red. The peaks which are essential for determination of whether or not deuteriated NADH has been produced are found between 2.5-2.8 ppm (marked as 'a' in Figure 7-5 a), these peaks correspond to the peaks resulting from the ^{1}H nuclei on the 4-position of the nicotinamide ring.[282] Figure 7-5 (b) shows a close up of this region of the spectrum. The degeneracy of the two protons in position 'a' of the ring is broken due to asymmetry in the rest of the molecule, with the *pro*-(S) proton (a_S) being in closer proximity to the adenosine moiety than the *pro*-(R) proton (a_R). As a consequence, germinal coupling is observed between the two protons ($^2J_{(a_S,a_R)}$ = 18.4 Hz), as well as differences in vicinal coupling to proton "b" (Hirst and Co-workers report that $^2J_{(b,a_R)} < {}^2J_{(b,a_S)}$).[309]

To determine whether it is possible to produce deuteriated NADH using the enzyme-modified particles the following experiment was carried out. Deuteriated phosphate buffer (pD = 6.9, 50 mM) was prepared inside a glove box with N_2 saturated ^2H_2O. Enzyme modified particles were prepared as outlined in the Methods and Theory chapter (section 2.4) and added to pre-$^2H_2$-saturated buffer containing NAD^+. After 18 hours the mixture was analysed using UV-visible spectroscopy to determine the conversion of NAD^+ to NADH. ^{1}H NMR spectroscopy was then used to determine if

the reduced product contained ^1H or ^2H on the methylene carbon (C4) of the dihydro-nicotinamide ring.

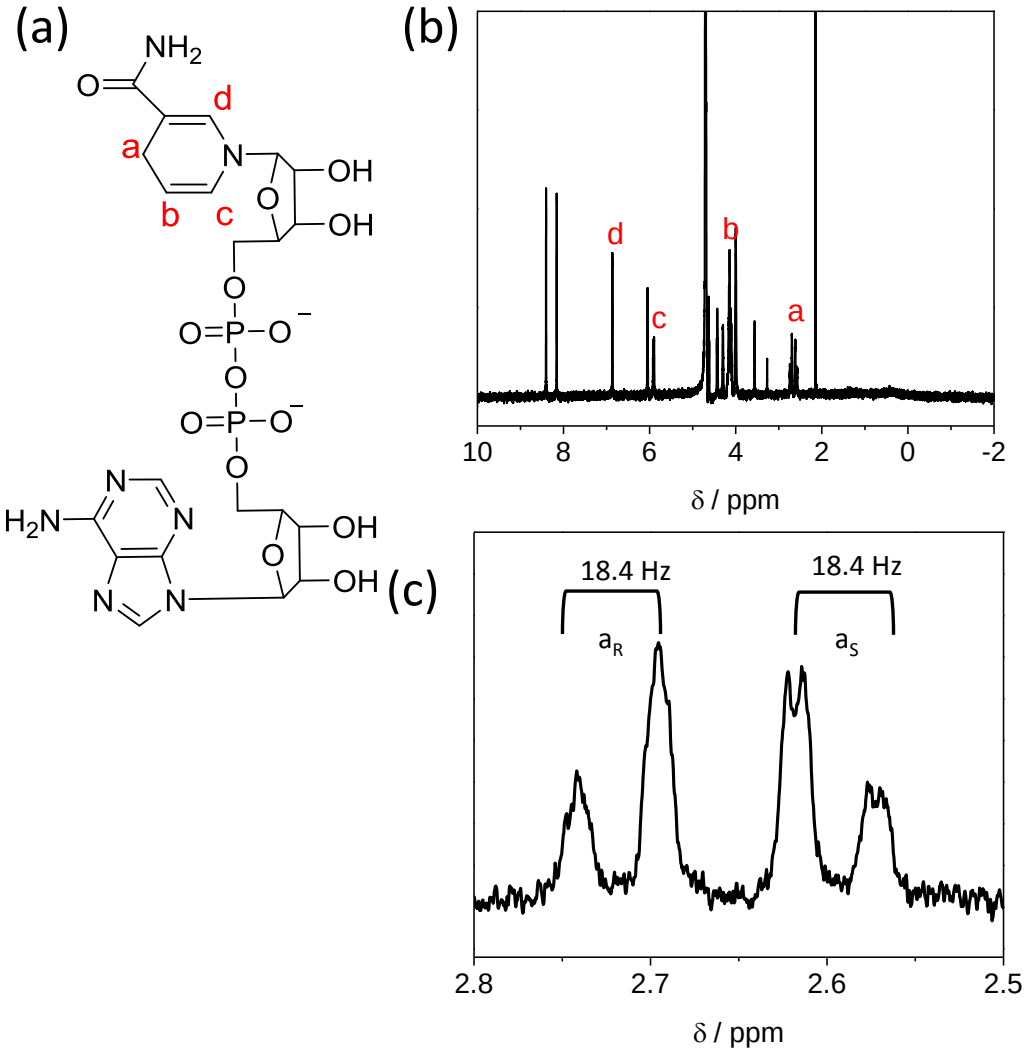

Figure 7-5: (a) NADH with the carbons on the nicotinamide ring labelled in red (b) ^{1}H-NMR spectrum of NADH. Key peaks due to the protons on the nicotinamide ring are labelled in red. (c) Close up of the spectrum between the regions 2.5 and 2.8 ppm, the peaks shown are due to the protons on carbon a (scalar coupling constants for the germinal coupling shown above the peaks).

The UV-visible spectrum obtained at the end of the $^2H_2$-driven reduction of NAD^+ using the enzyme-modified particles is shown in Figure 7-6. The peak at 340 nm indicates that NADH had been produced. Approximately 99 % conversion of NAD^+ to NADH has been achieved based on the ratio of the peaks at 260 nm and 340 nm.

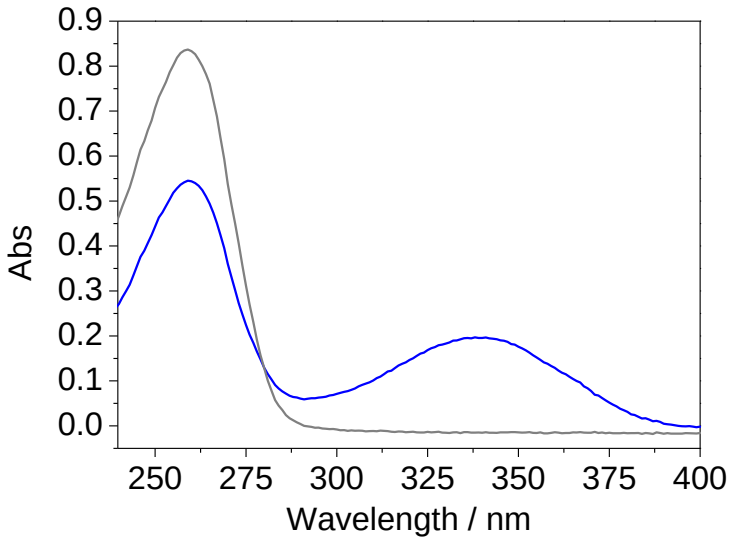

Figure 7-6: UV-visible spectrum showing the absorption spectra of a 1:20 diluted sample of NADH produced by $^2H_2$-driven cofactor reduction using the enzyme-modified particles. Grey: starting mixture, Blue: Final scan. Particles were prepared as outlined in the Methods and Theory chapter (section 2.4), with 52 µg Hyd 2 and 25 µg *R. eutropha* Hox~~HY~~FU co-immobilised on 0.7 mg of BP 2000 particles. The particles were washed once, by centrifuging and removing the supernatant, then re-suspended in 50 µL of deuteriated phosphate buffer. The reaction was carried out on a 3 mL scale with NAD^+ at a concentration of 2 mM in $^2H_2$ saturated buffer. The reaction vessel was then placed inside a pressure system under 2 bar $^2H_2$ for 18 hours, with fast stirring. The particles were removed by centrifugation (14,000 × g for 2 minutes) and by passing the solution through a cotton wool filter. A commercial membrane filter was not used as these filters introduce glycerol impurities into the sample which complicates analysis by NMR spectroscopy.

In the work by Hirst and co-workers,[282] ^{1}H NMR spectra were obtained for singly labelled [^{2}H]NADH with the deuteride in both the *pro*-(R) and *pro*-(S) positions, reproduced in Figure 7-7(a). In the case of [^{1}H]NADH the germinal coupling constant ($^2J_{HH}$) between the two ^{1}Hs on carbon 4 of the nicotinamide ring is large (17.5 Hz)[282] and the vicinal coupling constant is 3.5 Hz for the *pro*-(S) and is too small be resolved for the *pro*-(R).[282] Consequently, in the case of in [4R-^{2}H]NADH where ^{2}H is *pro*-(R) and ^{1}H *pro*-(S) the vicinal coupling between the ^{1}H at the 4 position of the nicotinamide ring is 3.5 Hz, Figure 7-7 (a, ii). In the case of [4S-^{2}H]NADH, where ^{1}H is *pro*-(R) and ^{2}H is *pro*-(S) no coupling can be resolved, shown in Figure 7-7 (a, iii).

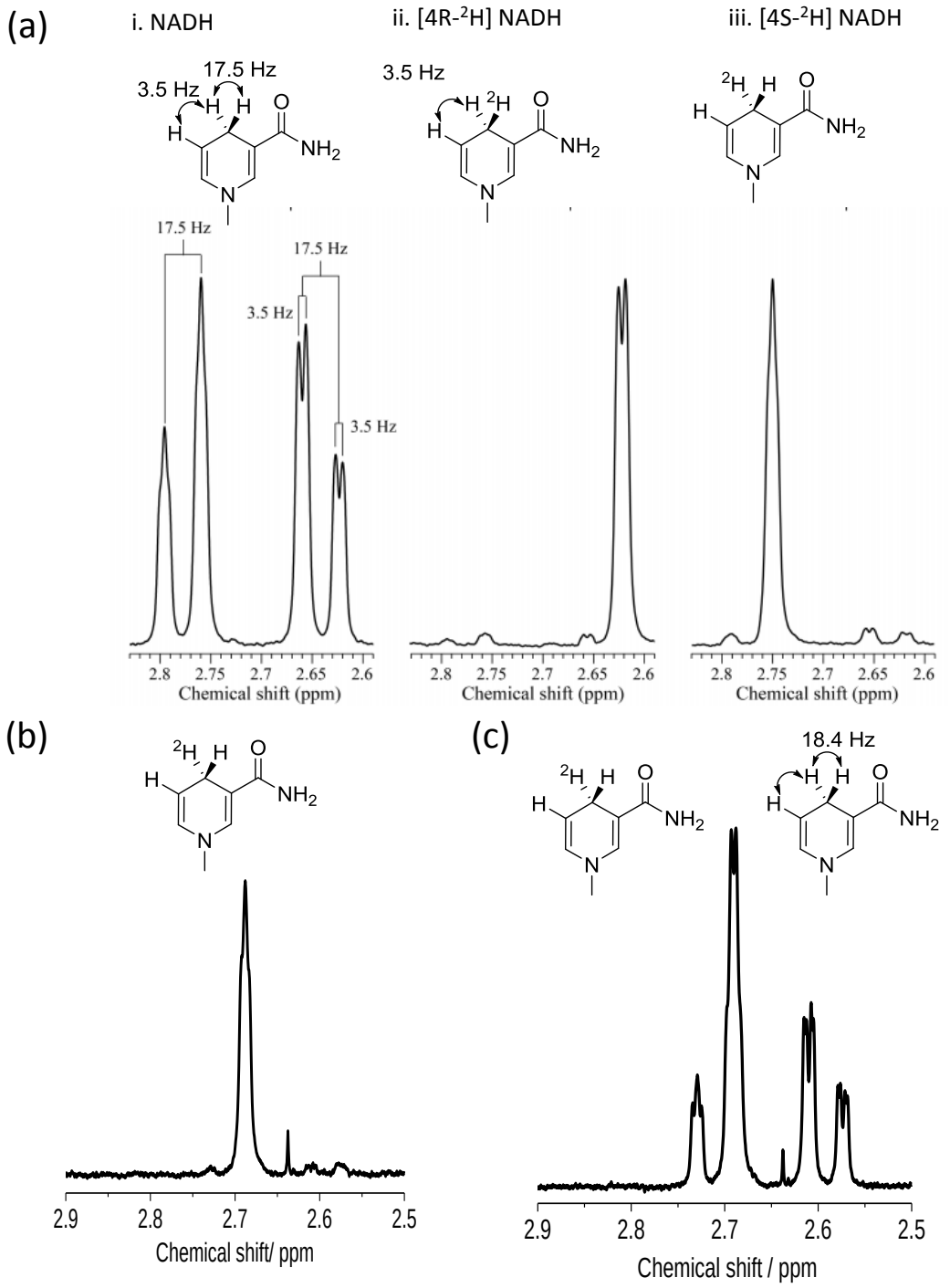

Figure 7-7: Determination of the enantiomer of deuteriated NADH produced by the Hox~~HY~~FU when used as part of the enzyme-modified particles for $^2H_2$-driven NADH generation. (a) Spectra from Hirst and co-workers in reference: *Investigation of NADH Binding, Hydride Transfer, and NAD$^+$ Dissociation during NADH Oxidation by Mitochondrial Complex I Using Modified Nicotinamide Nucleotides*[282] *©ACS 2013 (http://pubs.acs.org/doi/abs/10.1021%2Fbi3016873, further permissions related to the material excerpted should be directed to the ACS). This is an unofficial adaptation of an article that appeared in an ACS publication. ACS has not endorsed the content of this adaptation or the context of its use* (b) Section of an NMR spectrum showing the peak for [^{2}H]NADH produced by the particle system. (c) Spectrum of the same sample as shown in (b), but spiked with 0.5 mM [^{1}H]NADH (i.e. two ^{1}Hs on carbon 4 of the nicotinamide ring).

Figure 7-7 (b) shows an NMR spectrum of the reaction mixture from the experiment described in the caption of Figure 7-6, only a single peak can be observed in the region of the NMR spectrum between 2.6 and 2.8 ppm relating to the protons on carbon 4 of the nicotinamide ring of NADH. The lack of germinal coupling suggests that there is only a single ^{1}H present on this carbon, implying that a deuteride ($^{2}H^{-}$) ion has been added, instead of a hydride (^{1}H-) ion. Using the assignments of Hirst *et al.*,[282] it could be demonstrated that the method described in this thesis yields [4S-^{2}H]NADH, indicating that the *R. eutropha* HoxHYFU moiety is selectively adding the deuteride (or hydride) to the *si*- face of the NAD^{+} molecule. It would be expected the whole *R. eutropha* SH should also display the same selectivity.

The spectrum in Figure 7-7 (c) was recorded after addition of a non-deuteriated [^{1}H]NADH (0.5 mM) spike to the sample. This caused smaller peaks to appear around 2.6 ppm corresponding to peaks from the second proton on C4 present in non-deuteriated [^{1}H]NADH. The appearance of peaks at a lower ppm values than in Figure 7-7 (b) is further evidence that [4S-^{2}H]NADH and not [4R-^{2}H]NADH has been produced.

The pymol homology model of HoxF from *R. eutropha* shown in Figure 7-8 demonstrates that due to the way in which NAD^{+} binds in the active site it is always the *si*-face of the molecule which is above the FMN. The black arrow shows that the H^{-} is therefore always transferred from the FMN cofactor to the *si*-face of the NAD^{+} meaning that that hydride is in the *pro*-(S) configuration in the resulting NADH molecule. This shows that [4S-^{2}H]NADH production is theoretically predicted by the homology model of this enzyme.

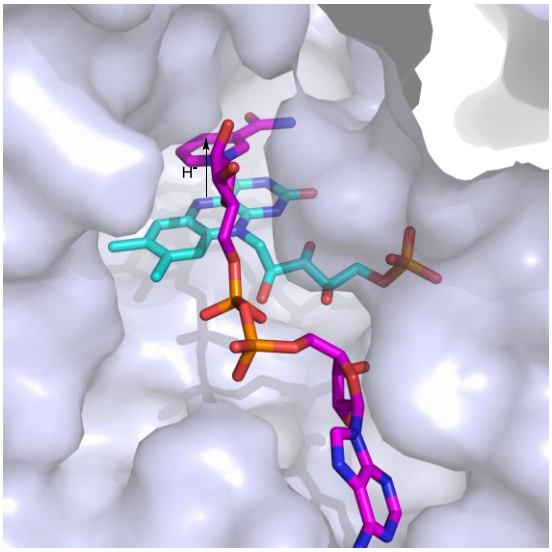

Figure 7-8: Active site of the HoxF portion of the SH from *R. eutropha,* the HoxF homology model was originally prepared by Dr L. Lauterbach (TU Berlin) based on Complex 1 from Thermus thermophilus Nqo1 (PDB: 2FUG). The carbon atoms in the FMN active site are coloured in turquoise and those of the cofactor are in purple. The surface of the protein clearly shows the shape of the HoxF binding site.

7.5 Determining whether [4S-^{2}H] NADH can be used to produce deuteriated alcohols

HPLC determination of enantiomeric excess in this section was performed by Ailun Huang (summer student) under my supervision.

There are already a number of methods for producing [^{2}H]NADH (deuteriated NADH):[307] glucose dehydrogenase can used with ^{2}H-glucose-d_1 as the substrate to produce [4S-^{2}H]NADH and horse liver alcohol dehydrogenase (HLADH) with 2-propanol-d_8 to give [4R-^{2}H]NADH.[282] In this section the [4S-^{2}H]NADH produced by the enzyme-modified particle system will be used in combination with an (R)- and an (S)-selective ADH to produce phenylethanol from acetophenone, as a proof of concept reaction. The alcohol dehydrogenases ADH 101 ((R)-selective) and ADH 105 ((S)-selective) from Johnson Matthey Catalysis and Chiral technologies will be used.[119]

Many ADH enzymes contain a zinc atom, which acts as a Lewis acid to activate the substrate ketone moiety, thereby promoting transfer of the hydride from the NADH to

the carbonyl carbon.[77,310] There are 4 possible orientations for the hydride attack, which are shown in Figure 7-9.

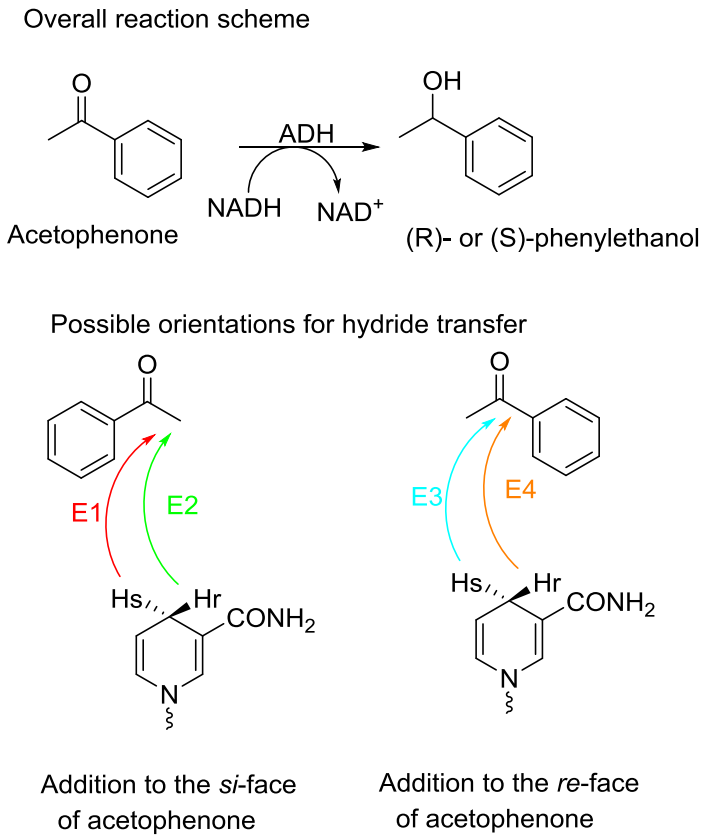

Figure 7-9: Acetophenone to phenyl ethanol conversion. The 4 possible orientations of hydride transfer from NADH to acetophenone. E1 and E2 show anti-Prelog specificity with attack of the hydride taking place on the *si*-face giving the (R)-alcohol. E3 and E4 follow Prelog's rule with attack of the hydride taking place on the *re*-face of the ketone, leading to the (S)-alcohol. Pathways E1 and E3 involve the transfer of the *pro*-(S) hydride of NADH, and pathways E2 and E4 involve transfer of the *pro*-(R) hydride. Adapted from De Wildemann *et al.*[77]

Generally, (S)-selective ADHs follow the E3 mechanism shown in Figure 7-9. [77] Therefore, when using the [4S-^{2}H]NADH produced by the enzyme-modified particles with the (S)-selective ADH (ADH 105), incorporation of ^{2}H into the phenylethanol product wouldn't be expected, as this enzyme uses the *pro*-(R) hydride of the dihydronicotinamide ring to carry out the ketone reduction reaction.[77] In contrast, the (R)-selective ADH (ADH 101) belongs to the short chain dehydrogenases family,[130] which typically follow the E2 mechanism, (with transfer of the 4-*pro*-(S) hydride from the nicotinamide cofactor to the ketone substrate).[77,311]

Therefore, it is expected that a deuteriated product should only be observed when the (R)-selective ADH is used with [4S-^{2}H]NADH, but not when the (S)-selective ADH is used.

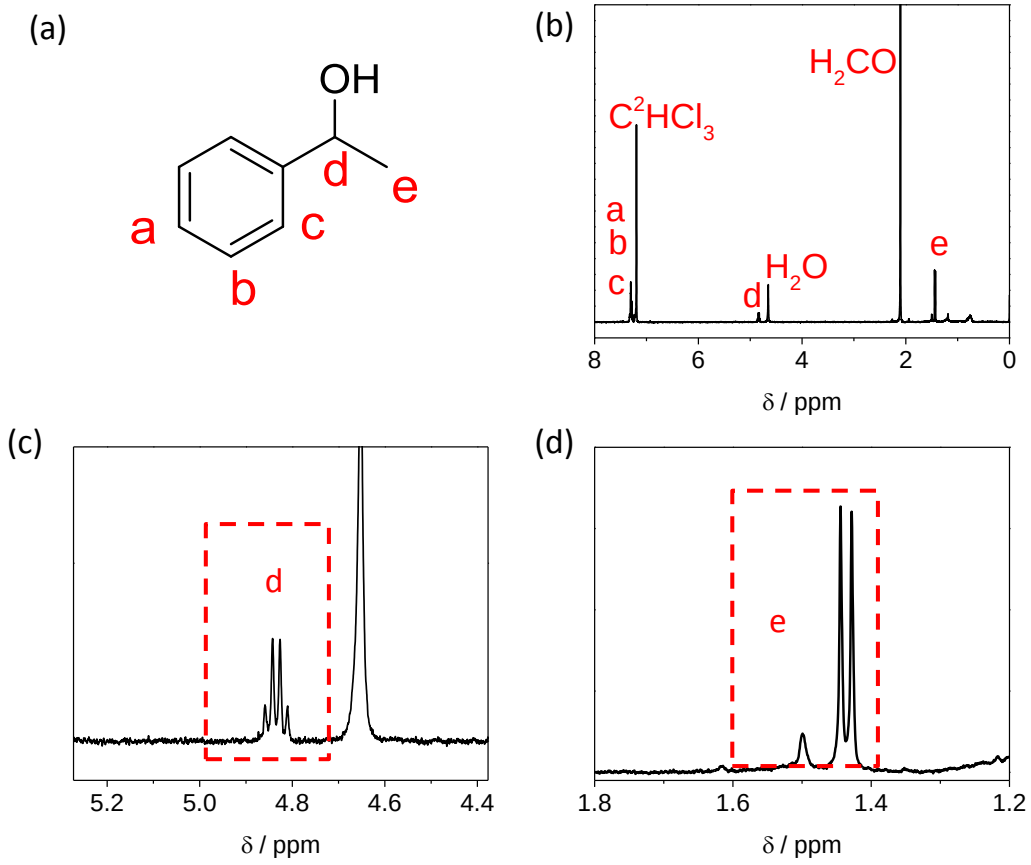

Figure 7-10: The NMR spectrum of a phenylethanol standard (a) Phenylethanol with detectable protons labelled in red. This work was carried out as part of this project and is not taken from the literature. (b) The ^{1}H NMR spectrum of phenylethanol in C^2HCl_3. Peaks corresponding to the protons on each carbon in figure (a) are labelled in red. (c) Section of the NMR spectrum showing the quartet peak for the proton α to the alcohol group in phenylethanol. (d) Section of the NMR spectrum showing the doublet peak from the methyl group protons 'e'.

Figure 7-10 (b) shows the peaks present in the ^{1}H NMR spectrum of phenylethanol. The quartet between 4.8-4.9 ppm corresponds to the proton present on the carbon α to the OH group (labelled **'d'**) shown in Figure 7.7(c). This peak is key in determining whether deuteriated phenylethanol has been produced. In addition, the peak at approximately 1.4 ppm corresponds to the protons on the methyl group β to the OH group (labelled '**e**'). In non-deuteriated phenylethanol this peak should be a doublet,

owing to the vicinal coupling between protons **d** and **e** ($^3J_{d,e}$), as shown by the spectrum in Figure 7-10 (d). However, if a deuterium is present α to the OH group instead of a proton, it is expected that the peak corresponding to the methyl protons would appear as a singlet instead (as the ^2H atom nucleus relaxes too quickly to observe).

In order to determine whether the ^2H from [4S-^{2}H]NADH is incorporated into the (R)-enantiomer of phenylethanol, an experiment was conducted in which both the (S)- and (R)- selective ADHs were given stoichiometric amounts of [4S-^{2}H]NADH. Controls were also carried out with [^{1}H]NADH (non-deuteriated NADH) to ensure that the enantioselectivity of the ADHs remains the same with [4S-^{2}H]NADH. The experiment was conducted on a 1500 µL scale, with 2 mM acetophenone (substrate) and 1 mg ADH added to each reaction vessel.

The vessels were incubated at 25 ^oC for 5 hours, with shaking at 300 rpm. The phenylethanol was extracted from the aqueous reaction mixture into C^2HCl_3 for NMR analysis and heptane for HPLC analysis. The reactions were analysed using HPLC to quantify enantiomeric excess (*ee*), and ^1H NMR spectroscopy to determine the amount of deuterium incorporated into the product.

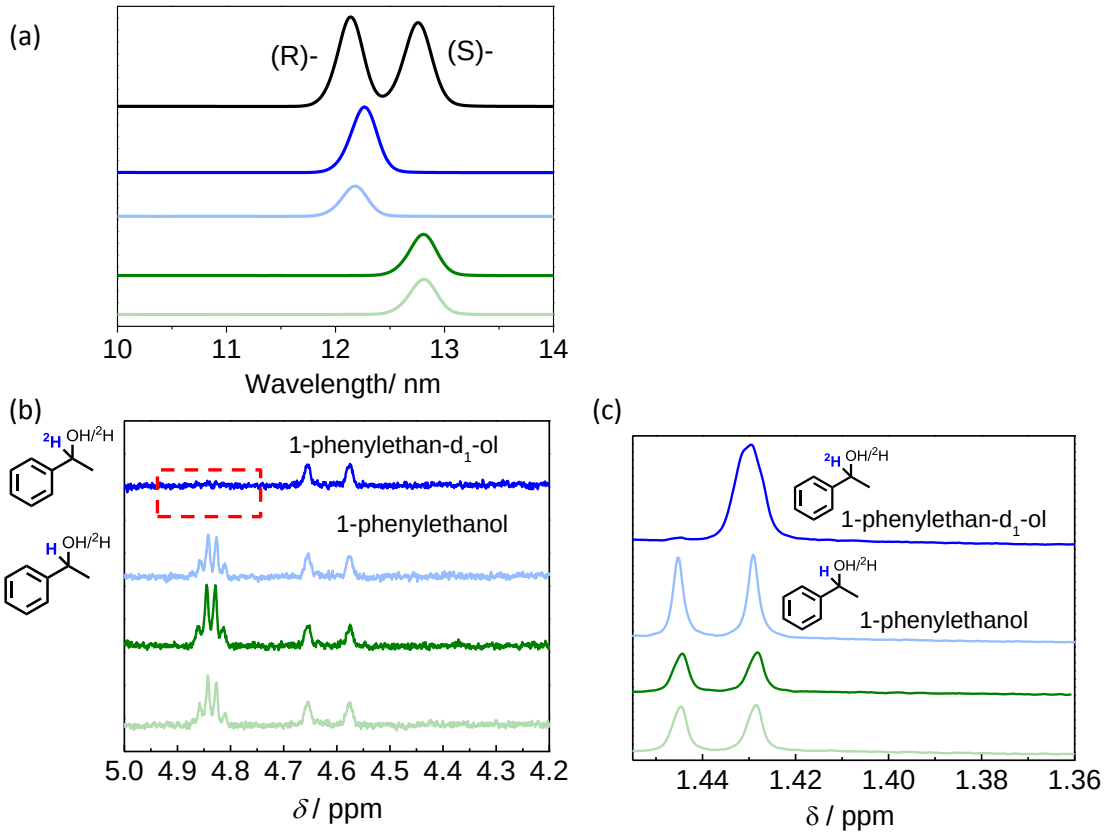

Figure 7-11: Data for acetophenone to phenylethanol conversion with addition of stoichiometric amounts of non-deuteriated [^{1}H]NADH (light) and deuteriated [4S-^{2}H]NADH (dark), with an (R)-selective ADH (blue) and an (S)-selective ADH (green). (a) HPLC trace showing peaks demonstrating production of the expected enantiomer in all cases (blue: (R), green: (S)). (R)-enantiomer r.t. = 12.4 minutes, (S)-enantiomer r.t. = 12.7 minutes. The black trace corresponds to a standard of commercially available racemic phenylethanol. (b) NMR spectra showing the characteristic quartet splitting for the hydrogen α to the -OH group, for all cases apart from where deuteriated [4S-^{2}H]NADH was used in combination with the (R)-selective ADH (dark blue line). (c) Portion of the same spectra as in (b), showing the characteristic doublet splitting pattern for the methyl group α to the alcohol, apart from the case where deuteriated [^{2}H]NADH was used in combination with the (R)-selective ADH (dark blue line), which leads to a deuterium being incorporated onto the carbon α to the OH group, causing no splitting and hence a singlet signal at 1.43 ppm in the NMR spectrum. The reaction mixtures were extracted into heptane for HPLC analysis (from a 200 µL aliquot, by performing the extraction procedure twice with 100 µL of heptane) and C^{2}HCl$_3$ for NMR analysis (from an 800 µL aliquot, by performing the extraction procedure twice with 400 µL of C^{2}HCl$_3$).

The chiral HPLC traces shown in Figure 7-11 (a) show that both the (R) (traces shown in blue) and (S)-selective (traces shown in green) ADH enzymes produced their respective enantiomers of phenylethanol with *ee* values of >99 % when both [^{2}H]NADH and [^{1}H]NADH were used. Both ADH 101 ((R)-selective) and ADH 105 ((S)-selective) show >99 % *ee* when glucose dehydrogenase is used as a cofactor

recycling system for acetophenone to phenylethanol conversion, see Appendix K. Consequently, as only a single peak indicating > 99 % *ee* is observed in both of the dark HPLC traces, this suggests that using [^{2}H]NADH, produced by the enzyme-modified particles, does not affect the enantioselectivity of either the (R)- or (S)- selective ADHs. The section of the NMR spectra between 5.0 ppm and 4.2 ppm shown in Figure 7-11 (b) demonstrates that only the (R)-selective ADH with [4S-^{2}H]NADH leads to addition of deuterium to the carbon α to the OH group, shown by the dark blue trace. This can be clearly seen, due to the absence of the quartet peak between 4.8-4.9 ppm seen in all other samples. Figure 7-11 (c) provides further confirmation of this result, as a doublet is observed for the methyl protons in all cases except where [4S-^{2}H]NADH is used in combination with the (R)-selective ADH, (shown by the dark blue trace). In this case only a singlet is observed, as vicinal ($^{3}J_{HH}$) coupling between the methyl protons and the deuterium atom is not observed.

On removal of $^{x}H^{-}$ from either the *pro*-(R) or *pro*-(S) position of the deuteriated NADH, either deuteriated or non-deuteriated NAD^{+} should be produced. The nature of the remaining NAD^{+} was subsequently investigated using NMR to determine if the ^{2}H-label remains on the cofactor when the (S)-selective ADH is used. Since the NAD^{+} is not extracted into $C^{2}HCl_{3}$, the aqueous portion from the spectra in Figure 7-11 was used; this ensured that the NMR spectrum was clear of peaks due to acetophenone and phenylethanol.

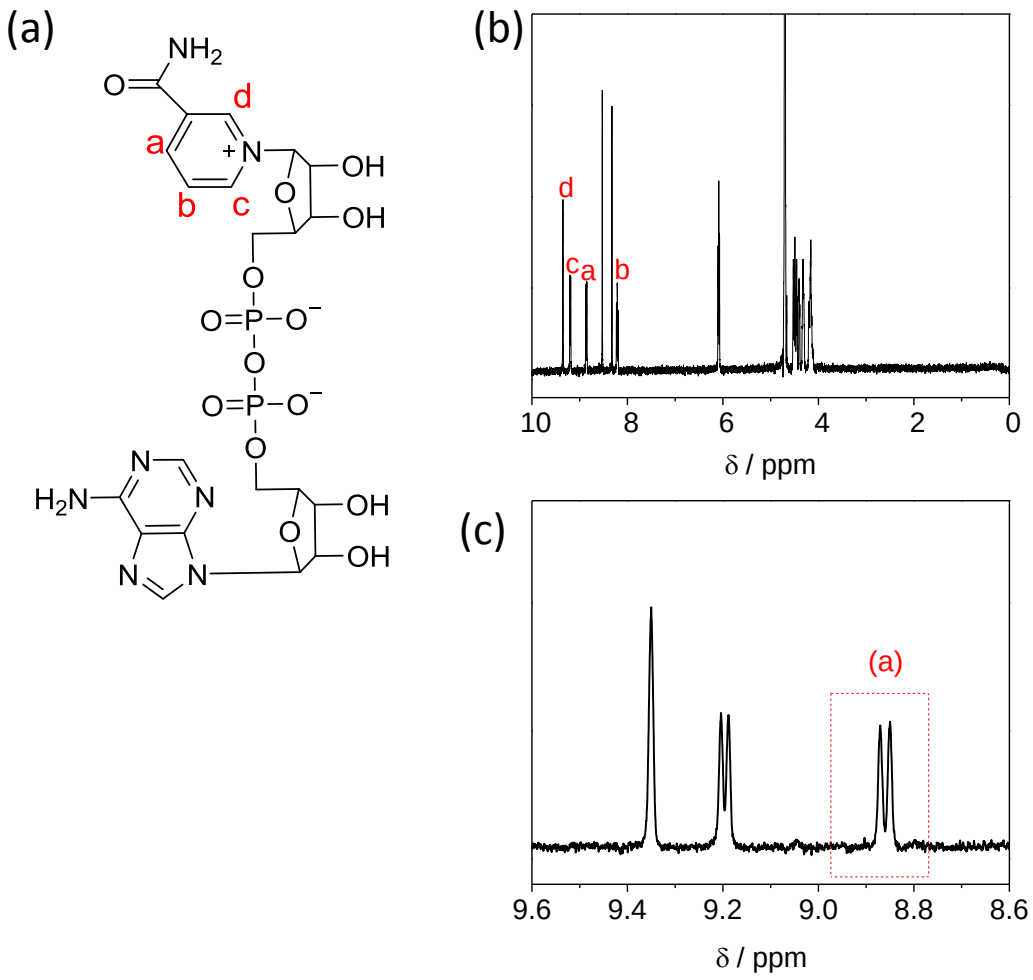

Figure 7-12: (a) NAD^+ with the carbons on the nicotinamide ring labelled in red (b) ^1H NMR spectrum of NAD^+ in deuteriated phosphate buffer. The key peaks for the nicotinamide ring are labelled in red. (c) Section of the ^1H NMR spectrum between 9.6 and 8.6 ppm showing the key doublet for the proton in the 4-position of the nicotinamide ring in NAD^+ at 8.85 ppm.

Figure 7-12 (a) shows the chemical structure of NAD^+ with the carbons on the nicotinamide ring labelled in red. Figure 7-12 (b) shows the ^1H NMR spectrum for as-purchased (non-deuteriated) NAD^+ in deuteriated phosphate buffer. The peaks for the key nicotinamide region of this molecule are labelled in red. The peak between 8.8-8.7 ppm (a) corresponds to the proton at the 4 position (relative to the nitrogen) of the nicotinamide ring. This region of the NMR spectrum is shown in more detail in Figure 7-12 (c).

For the case where ([4S-^{2}H]NADH) was used with the (S)-selective ADH, the ^{2}H (in the *pro*-(S) position) remains present on the NAD^{+}, as the original ^{1}H (in the *pro*-(R) position) has been used by the ADH. This should result in the absence of a doublet peak between 8.8-8.7 ppm. In contrast for the case where ([4S-^{2}H]NADH) was used with the (R)-selective ADH, the ^{2}H is used by the ADH, meaning that ^{1}H remains present on the NAD^{+}. This should result in a doublet peak between 8.8-8.7 ppm, as observed for the NAD^{+} standard in Figure 7-12 (c).

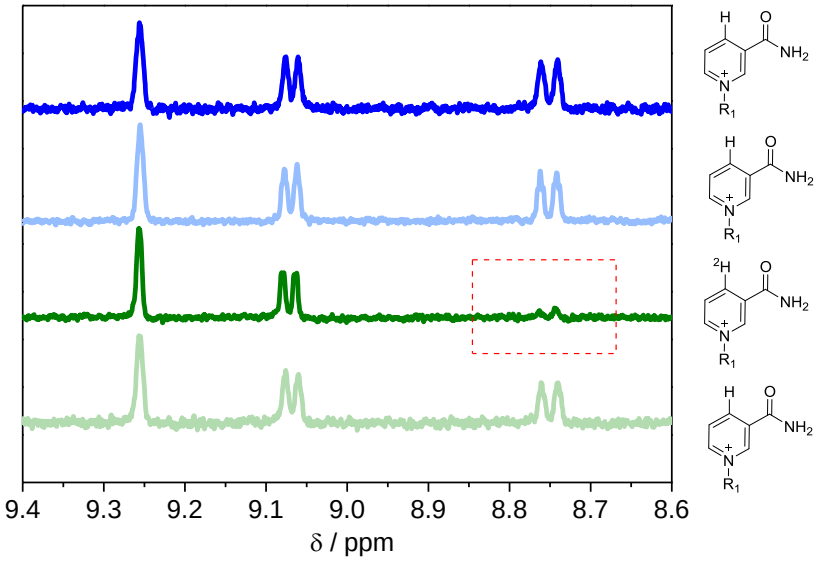

Figure 7-13: NMR spectrum showing the aqueous fraction just containing the cofactor. Spectra for addition of stoichiometric amounts of deuteriated [^{2}H]NADH (dark) and [^{1}H]NADH (light), with an (R)-selective ADH (blue) and an (S)-selective ADH (green) Notice the absence of the characteristic peak for the ^{1}H in the 4-position where [^{2}H]NADH was used in combination with an (S)-selective ADH, (dark green).

From the spectra shown in Figure 7-13, it is clear that all spectra apart from the sample made by the (S)-selective ADH with deuteriated [4S-^{2}H]NADH show a doublet peak between 8.8-8.7 ppm. This is not present for the example when the (S)-selective ADH was used with deuteriated [^{2}H]NADH (shown in dark green in Figure 7-13) showing that the (S)-selective ADH has used the ^{1}H originally on the NAD^{+}, producing [4-^{2}H]NAD^{+} or NAD^{+} deuteriated at the C4-position of the nicotinamide ring.

This section demonstrates the development of an effective method for accessing deuteriated (R)-enantiomers of alcohols. It also confirms the selectivity of the Hox~~HY~~FU enzyme moiety and that using deuteriated NADH does not affect the enantioselectivity of the ADH enzymes ADH 101 and ADH 105.

7.6 Cofactor recycling to produce deuteriated (S)- and (R)-selective alcohols

Having access to a method of producing deuteriated [4S-^{2}H]NADH opens up the possibility of producing a range of selectively deuteriated chemicals.

The results in section 7.5 demonstrate that the (R)-selective ADH always uses the deuterium on the 4-, *pro*-(S) position of [4S-^{2}H]NADH. In the case of the (S)-selective ADH, the 4-, *pro*-(R) hydrogen is used. However, if the Hox~~HY~~FU enzyme moiety (as part of the enzyme-modified particles) is then again used to re-reduce the NAD^+, a deuterium will be added to the 4-, *pro*-(S) position, leading to di-deuteriated [4R-^{2}H]-[4S-^{2}H]-NADH. Therefore, on the second turnover of the cofactor both the positions on the dihydronicotinamide ring will be doubly deuteriated. Consequently, only a deuteride ($^2H^-$) will be available to the (S)-selective ADH on subsequent cofactor recycles.

Thus, with *in situ* cofactor recycling, and catalytic loadings of NAD^+ (<10%), both enantiomers of deuteriated phenylethanol should be observed. This was trialled in a subsequent experiment. A schematic diagram summarising the reaction set up is shown in Figure 7-14.

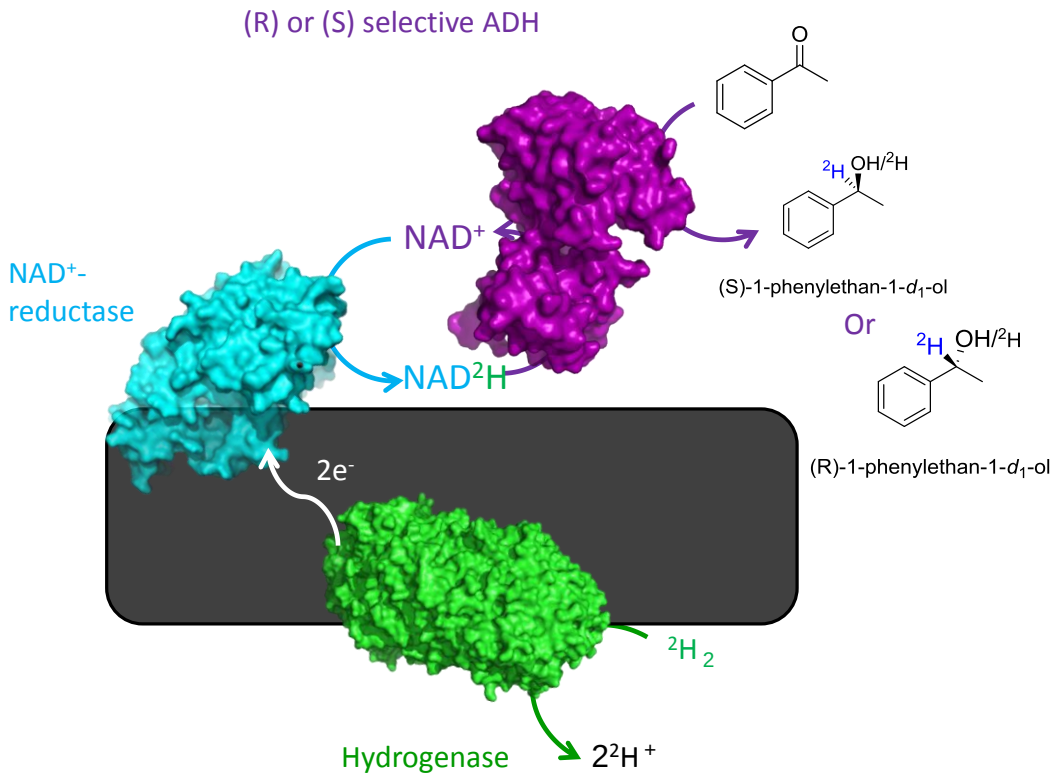

Figure 7-14: A schematic diagram demonstrating the production of both enantiomers of deuteriated phenylethanol, with *in situ* $^2H_2$-driven cofactor recycling.

Two aliquots of enzyme-modified particles were prepared to which were added ADH 101((R)-selective) and ADH 105 ((S)-selective) respectively. These particles were then added to a reaction mixture in deuteriated phosphate buffer containing acetophenone (3 mM) and a low loading of NAD^+ (0.1 mM).

The HPLC spectra in Figure 7-15 (a) again show >99% *ee* for both of the ADHs for the phenylethanol product, with the enzyme-modified particles as an *in* situ cofactor recycling system. This demonstrates that using the enzyme-modified particles for *in* situ cofactor recycling doesn't lead to a reduction in the *ee* in comparison to the results obtained in section 7.5, where NADH was added in stoichiometric amounts.

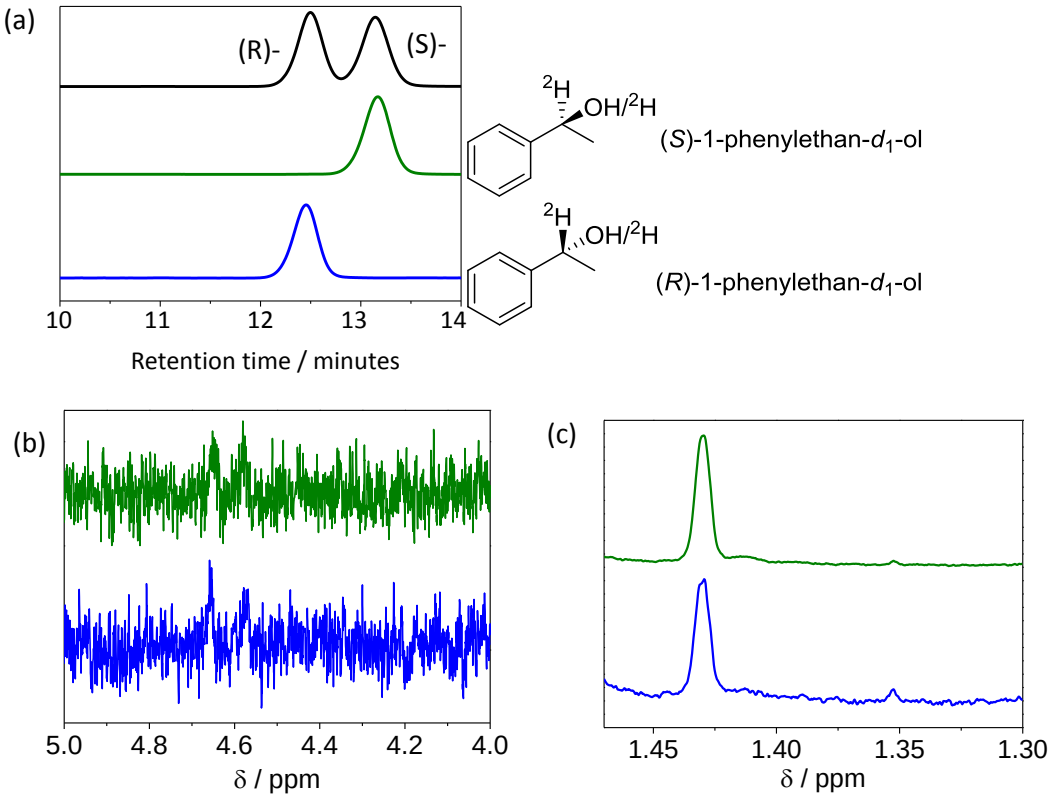

Figure 7-15: Phenylethanol enantiomers produced with *in situ* cofactor recycling in the presence of $^2H_{2(g)}$. This experiment was performed on a 1000 µL scale. Deuteriated phosphate buffer (pD = 7.5, 50 mM) was prepared inside an anaerobic glove box. Each set of particles was produced as outlined in the Methods and Theory Chapter (Section 2.4), with 63 µg Hyd 2, 25 µg Hox~~HY~~FU and 1 mg ADH pre-mixed, and then co-immobilised on 0.8 mg of BP 2000 particles. The mixture was then left for 1 hour to immobilise. The particles were washed once, re-suspended in 50 µL deuteriated phosphate buffer and added to a pre-H_2 saturated reaction mixture containing 0.1 mM NAD^+ and 3 mM acetophenone (3.3 mol % cofactor). The reaction was carried out under 2 bar $^2H_2$ with gentle stirring for 18 hours. Following the reaction the particles were then removed by centrifugation at 14,000 × g for 2 minutes and then by passing the solution through a homemade cotton wool filter. The reaction products were analysed using chiral HPLC to quantify conversion and enantiomeric excess, and NMR spectroscopy to determine the amount of ^2H incorporated. Acetophenone and phenylethanol were extracted into heptane for HPLC (from a 200 µL aliquot, 2 × 100 µL of heptane) and C^2HCl_3 for NMR (from an 800 µL aliquot, with 2 × 400 µL of C^2HCl_3)

The olive green trace represents the (S)-selective ADH; bright blue the (R)-selective ADH. (a) HPLC traces showing that the correct enantiomer of the product was produced. (R)-enantiomer r.t. = 12.4 minutes, (S)-enantiomer r.t. = 13.2 minutes. (b) A section of NMR spectra showing no characteristic quartet for the ^1H α to the alcohol, suggesting that the phenylethanol (in the case of both enantiomers) is deuteriated. (c) The same spectra as shown in (b), this section, however, demonstrates the presence of a singlet for the methyl group, with no observable coupling to neighbouring protons.

The NMR spectra shown in Figure 7-15 (b), show that there is no peak present between 4.8-4.9 ppm, the characteristic peak for the ^1H on the carbon α to the OH group (see,

Figure 7-10). This shows that both of the enantiomers of phenylethanol produced by the (R)-selective and (S)-selective ADHs are deuteriated at the carbon α to the OH group. Similarly the spectra presented in Figure 7-15 (c) show a characteristic singlet at 1.43 ppm, indicating that the protons of the methyl group do not show observable coupling to another proton on an adjacent carbon. This is good confirmation that both deuteriated enantiomers of phenylethanol have been produced.

Table 7-1: Percentage conversion and number of NADH turnovers obtained from the HPLC traces shown in Figure 7-15 (a).

	(S)-selective (ADH 105)	**(R)-selective (ADH 101)**
[Product] / mM	1.9	0.7
Number of cofactor turnovers	19	7
Incorporation of D	No ^{1}H product observed	No ^{1}H product observed

Data in Table 7-1 demonstrates that it is possible to obtain nineteen cofactor turnovers with the (S)-selective ADH. The 1:19 portion of non-deuteriated phenylethanol, which results from the original ^{1}H on NAD^{+} cannot be observed in the splitting pattern of the phenylethanol methyl group in Figure 7-15 (c).

7.7 Carrying out deuteration reactions in unbuffered solutions

In all of the previous work in this chapter, the reactions have been carried out in buffered media. Deuteriated buffers add significant expense to these reactions with dipotassium deuterium phosphate costing £13.40 / g from Sigma Aldrich.[65] Reeve *et al*. have already shown that it is possible to produce phenylethanol using ADH 105 in combination with the hydrogen driven cofactor recycling system in unbuffered water.[119]

This work investigates whether it is possible to produce deuteriated phenylethanol in unbuffered $^{2}H_2O$. Enzyme-modified particles were made as described in the methods

and theory section, with Hyd 2, Hox~~HY~~FU and ADH 105. The particles were then added to solutions containing NAD^+ and acetophenone in either unbuffered ^2H_2O or in unbuffered ^1H_2O.

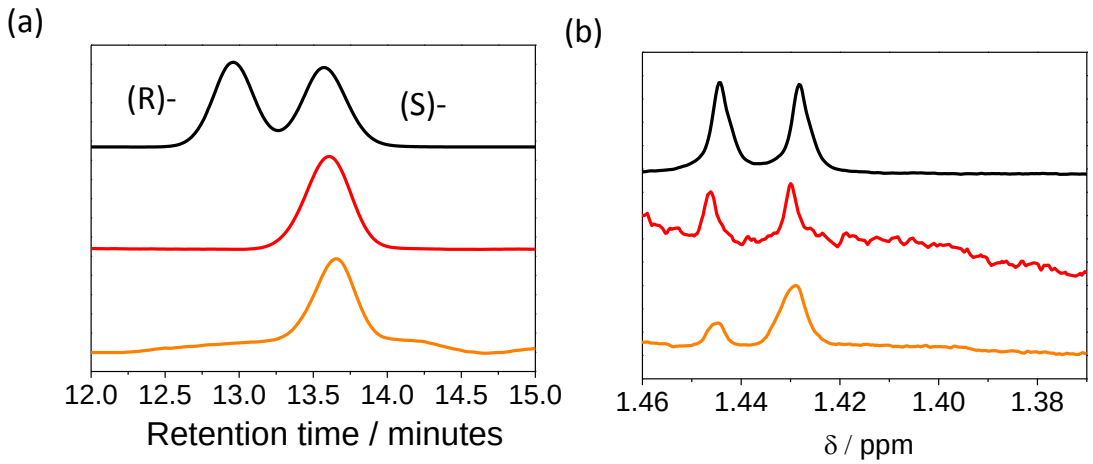

Figure 7-16: (S)-phenylethanol produced with *in situ* cofactor recycling in the presence of $^2H_2$. Orange reaction carried out in ^2H_2O. Red (control) carried out in H_2O. Black traces correspond to a phenylethanol standard. Two sets of particles were prepared one set in ^2H_2O and the other, a control, in ^1H_2O. Particles were constructed as outlined in the Methods and Theory chapter (Section 2.4), with 27 µg Hyd 2, 11 µg Hox~~HY~~FU and 1 mg ADH 105 pre-mixed, and then co-immobilised on 0.4 mg of BP 2000 particles. The mixture was then left for 1 hour to immobilise. The particles were centrifuged down and the supernatant removed. A 1 mL aliquot of $^2H_2$-saturated ^2H_2O (orange) or ^1H_2O (red), containing 0.1 mM NAD^+ and 10 mM acetophenone was then added to each set of particles respectively. The reactions were then left overnight under constant deuterium flow in a shaker for 18 hours, with shaking at 500 rpm. (a) HPLC traces showing that the (S)-enantiomer of the product was produced. (R)-enantiomer r.t. = 12.7, (S)-enantiomer r.t. = 13.4. (b) A section of the NMR spectrum between 1.46- 1.37 ppm showing a doublet for the methyl protons in the standard (non-deuteriated) sample of phenylethanol (black). A doublet for the reaction performed in H_2O (red), as there is a ^1H α to the OH group and a singlet with a shoulder due to the doublet from the first NADH equivalent in the case of the reaction performed in ^2H_2O (orange).

The HPLC trace shown in Figure 7-16 (a) shows that both reactions, regardless of whether performed in ^1H_2O or ^2H_2O produce the (S)-phenylethanol product, as expected. When the reaction was performed in ^1H_2O a characteristic doublet peak is observed showing that a proton has been added to the position α to the OH group on phenylethanol, shown in Figure 7-16 (b), red trace. In contrast when the reaction is performed in ^2H_2O there is a singlet peak with a shoulder (orange trace). With the (S)-selective ADH for the first equivalent of [4S-^{2}H]NADH, the *pro*-R ^{1}H will be added

to the acetophenone, leading to a doublet peak in the NMR spectrum due to the methyl group protons coupling with this ^{1}H α to the OH group. However, when the [4-^{2}H]NAD^{+} is re-reduced giving [4R-^{2}H]-[4S-^{2}H]-NADH this will then lead to addition of a deuterium to the carbonyl carbon, leading to a singlet at *ca.*1.43 ppm as the coupling between the methyl protons and the deuterium α to the OH group cannot be resolved. Due to the relatively low conversion obtained in this reaction, the peak resulting from the non-deuteriated phenylethanol can still be clearly seen. However, this is a promising proof of concept demonstration that it is possible to carry out these reactions in unbuffered $^{2}H_2O$ and obtain the desired product.

7.8 Conclusions and Outlook

This chapter represents a promising demonstration that the enzyme-modified particles can be used to produce a single enantiomer of deuteriated NADH: [4S-^{2}H]NADH. This is interesting from a mechanistic point of view and supports the binding of NAD^{+} shown in the homology model for the active site of *R. eutropha* HoxF.

Furthermore, using the enzyme-modified particles to recycle [4S-^{2}H]NADH *in situ* in combination with a NADH-dependent redox enzyme means that $^{2}H_2$ gas can be used directly as the source of deuterium, significantly reducing the costs of conventional redox processes used to incorporate deuterium into chiral molecules used as building blocks. The enzyme-modified particles, in combination with (R)- and (S)- selective ADHs have been used to produce deuteriated phenylethanol, as a proof of concept. This is the first example of a $^{2}H_2$-driven enzymatic system for the production of selectively deuteriated alcohols. Additionally, the enzyme-modified particles could be used to give access to a range of chiral alcohols and potentially a range of other deuteriated products, which demonstrates the ability of the enzyme-modified particles in combination with an NADH-dependent enzyme to act as a clean and cheap method for

producing selectively deuteriated compounds. In addition, by using *in situ* cofactor recycling both enantiomers of the product can be accessed.

Furthermore, this chapter demonstrates that it is possible to produce deuteriated alcohols in unbuffered ^2H_2O. This technology could also be extended for use with a range of NADH-dependent enzymes, such as amino acid dehydrogenases, for the production of deuteriated amino acids. Additionally, it would of interest to investigate whether this technology could be expanded to incorporate ^3H into a range of chemicals. Chemicals containing ^3H have applications in radiopharmaceuticals.

The approach used in this chapter could also be harnessed to produce deuteriated artificial cofactors, like the ones recycled in Chapter 6. These could be useful for mechanistic studies into the catalytic mechanism of FMN containing enzymes which are able to accept these cofactors.

8 Conclusion

The work in this thesis set out to expand the scope of H_2-driven biocatalysis for application under a wider range of conditions and for a number of different asymmetric reduction reactions. This work is particularly relevant to the pharmaceutical and fine chemicals industries where chiral molecules are of significant importance.

A limitation of biocatalysis for these reactions is the requirement for complex and expensive biological hydride sources, usually the biological cofactors NADH and NADPH.

This works makes use of whole soluble hydrogenase (SH) enzymes which natively couple H_2 oxidation to NADH recycling, as well as a system of enzyme-modified particles in which a non-native, and more robust, hydrogenase is coupled to an NAD^+-reductase by co-immobilising both enzymes on electronically conducting particles. In each case, the use of H_2 gas as the reducing equivalent offers benefits over the existing methods for cofactor recycling: these include improved atom economy of the overall reaction, improvements in final product purity and a decrease in the costs associated with NADH-dependent biocatalysis. The use of enzymes immobilised on carbon has further benefits including the ability to reuse the enzymes.

This thesis demonstrates some of the many possibilities presented by H_2-driven NADH recycling coupled to an NADH dependent enzyme for highly selective biocatalysis.

Chapter 3 focused on H_2-driven biocatalytic reductive amination reactions, for conversion of ketones (C=O) to chiral amines (CH-NH_2). This is an essential reaction class for the pharmaceutical industry, a recent report suggests that 40 % of drug targets contain at least one chiral amine component in their structure, with amines often helping to make drugs more soluble.[312] Being able to carry out reductive amination reactions just using NH_3 and H_2 is an "aspirational reaction" for the pharmaceutical industry.[31] By combining the enzyme-modified particles with an L-alanine

dehydrogenase enzyme, it was possible to develop a system for H_2-driven production of L-alanine from pyruvate and ammonium. Conversions of >98 % pyruvate to L-alanine were achieved using this system. By comparing sets of particles with the L-alanine dehydrogenase co-immobilised on the particles and sets with the L-alanine dehydrogenase in solution, it was demonstrated that there is an advantage to having the L-alanine dehydrogenase co-immobilised on the particles rather than in solution. It is hypothesised that this is likely to be due to faster transfer of the NADH between the NAD^+-reductase and the co-immobilised L-alanine dehydrogenase enzyme (which are in close proximity, when both are immobilised on the particles), than the transfer between the NAD^+-reductase and the L-alanine dehydrogenase in solution. Reeve *et al*. obtained similar results in work, which used an ADH in combination with the enzyme-modified particles.[119] This section demonstrated that the H_2-driven enzyme-modified particle system is suitable for highly atom efficient reductive amination reactions relying on only H_2 and NH_3, generating only H_2O as a waste product. Although only demonstrated for production of L-alanine, it is likely that this system could also be implemented for production of a range of native and non-native amino acid dehydrogenases and perhaps the new class of related amine dehydrogenases in the future.

In the second part of this chapter a system was developed for bio-catalytic production of a range of chiral amines from prochiral ketone substrates, using (S)- and (R)- selective *ω-transaminase* enzymes. Advantageously these enzymes expand the substrate scope of biocatalytic reductive amination; however, they require a more sophisticated amine donor such as L-alanine or D-alanine. The enzyme-modified particles with the L-alanine dehydrogenase co-adsorbed (developed in the first part of Chapter 3) were used as a system for converting the pyruvate produced by the *ω-transaminase* back to

L-alanine and shifting the thermodynamically unfavourable equilibrium of the *ω-transaminase* enzyme to the side of the products. It was possible using this system to produce 1-methyl-3-phenylpropylamine with a yield of 68 % and an *ee* of *ca.* 66 %. Although, this is not yet competitive with more established pyruvate removal systems used in combination with *ω-transaminase* enzymes, it provides further demonstration of the scope of H_2-driven biocatalysis for reductive amination.[23]

The fourth chapter of this thesis focused on the characterisation of an SH from a thermophilic organism: *Hydrogenophilus thermoluteolus*. Work conducted in this chapter demonstrates that the *H. thermoluteolus* SH shows its highest activity at 60 ^{o}C in solution and shows no inhibition at 10 % O_2 concentration. Electrochemical characterisation of the HoxFU portion of the *H. thermoluteolus* SH demonstrates that the SH shows greater catalytic bias towards NAD^+ reduction than the *R. eutropha* SH, which means that this enzyme favours NAD^+ reduction compared to NADH oxidation (i.e. much higher currents are obtained for the *H. thermoluteolus* HoxFU on a PGE RDE when this enzyme is operating in the NAD^+ reducing direction than when it is operating in the NADH oxidation direction). Electrochemical measurements also demonstrate that the *H. thermoluteolus* HoxFU is active on an electrode at temperatures up to 60 ^{o}C, with a half-life of 19 minutes at 40 ^{o}C (similar to the half-life of the *R. eutropha* HoxFU at 22 ^{o}C). Following the characterisation of the *H. thermoluteolus* HoxFU, Chapter 5 looked at using this NAD^+-reductase for cofactor recycling at elevated temperatures. Chapter 5 initially demonstrated electrochemical reduction of NAD^+ to NADH at 40 ^{o}C. Subsequently, enzyme-modified particles were used for H_2-driven NAD^+-reduction. Using particles modified with the *H. thermoluteolus* HoxFU and Hyd 2, it was possible to demonstrate increasing activity for NAD^+ to NADH conversion from 30 ^{o}C to 60 ^{o}C. This particle system was then used as a

cofactor recycling system to supply the enoate reductase, TsER at 40 ^{o}C, demonstrating elevated temperature H_2-driven alkene reduction. It was possible to achieve 62 % yield of 2-methyl-2-cyclopentenone to 2-methyl cyclopentanone with 50 % *ee*. This result demonstrates the modularity of the enzyme-modified particles system. Together, Chapters 4 and 5 detail methods for rapidly characterising new NAD^+-reductase constructs and exploiting them for increasing the range of conditions that can be used for H_2-driven biocatalysis.

In chapter 6, the first enzymatic methods for recycling the reduced form of several artificial cofactors were developed. There are a number of existing non-enzymatic methods for regenerating the reduced form of these artificial cofactors. These include using transition metal catalysts and reducing agents such as sodium dithionite.[256] However, metals are often incompatible with the enzymes able to accept the artificial cofactors to carry out useful reduction reactions and sodium dithionite is a potent reducing agent and as such can lead to the unselective reduction of the substrate of the enzymatic reaction.[256] The most promising strategy developed so far for recycling the reduced form of the artificial cofactors has involved using an artificial metalloenzyme, with an Ir metal centre incorporated into a streptavidin framework. TTNs of >1980 per Ir centre have been achieved with this system and a TN of 10 (moles of product per moles of artificial cofactor).[263]

Using the SH from either *H. thermoluteolus* or *R. eutropha* it was possible to obtain a TTN of >3000 (moles of reduced cofactor per mole of SH), for the reduction of the artificial cofactor mAC^+ to mACH. In the second section of the chapter it was possible to couple the SH from both *R. eutropha* and *H. thermoluteolus* with the *TsER* to demonstrate H_2-driven reduction of alkenes using artificial cofactors. Using the *H. thermoluteolus* SH it was possible to obtain a TTN of >6,000 (moles product per

mole SH) when coupled to the *TsER* for reduction of N-phenyl maleimide. With the *R. eutropha* SH it was possible to obtain a TN (moles of product per mole of artificial cofactor) of 19 for the artificial cofactor mACH. This is within the range required to make the use of the mACH cofactor economically acceptable and is better that the highest TN obtained for the artificial metalloenzyme discussed above. Not only does this work represent the first enzymatic systems for recycling artificial cofactors, but successful demonstrations with the SH enzymes from *H. thermoluteolus* and *R. eutropha* have the added advantage that the reducing equivalents are supplied by H_2 and hence a stoichiometric carbon based reducing agent is not required. This work also adds support to the hypothesis of Kara *et al.* that enzymes with a tightly bound redox prosthetic group such as FMN are able to accept artificial cofactors (like the SH enzymes here), whereas enzymes without internal redox cofactors have K_M values which preclude their operation with artificial cofactors.[262] It is possible that future mutagenesis studies on the SH enzymes could be used to further improve the affinity of the *R. eutropha* SH or *H. thermoluteolus* SH for the artificial cofactors.

Chapter 7 investigated the use of the enzyme-modified particles to produce [4S-^{2}H]NADH in ^2H_2O with $^2H_2$ gas as the source of the reducing equivalents. By coupling this system with an (R)- and (S)-selective ADH enzyme, it was possible to gain access to both (R)- and (S)- phenylethanol, selectively labelled with deuterium. This demonstrates a powerful new strategy for carrying out a range of selective biocatalytic reduction reactions in order to incorporate deuterium into a range of molecules. Deuteriated molecules have applications in tracing and in pharmaceuticals. For example deuteriated molecules are often used in combination with mass spectrometry to study breakdown of metabolites. Currently using deuterium in pharmaceuticals is a hot topic of research, with the first deuteriated drug ‘Austedo’

(deutetrabenazine) being recently approved by the FDA.[294] In the future, it would be interesting to explore whether it is possible to harness this approach for the incorporation of ^{3}H in a range of chemicals, as compounds which incorporate ^{3}H have applications as radiopharmaceuticals.[313]

Overall, this thesis has explored a range of possibilities offered by H_2-driven cofactor recycling. The work has successfully demonstrated that the enzyme-modified particle system can be used to access a number of useful products, most significantly chiral amines and deuteriated alcohols. In addition, a system has been successfully developed for elevated temperature H_2-driven cofactor recycling and for the recycling of artificial cofactors. Thus, this thesis not only expands the scope of H_2-driven biocatalysis but opens up new opportunities that can be further explored and expanded on in the future.

References

[1] H. D. Flack, *Acta Crystallogr. Sect. A* **2009**, *65*, 371–389.

[2] R. Noyori, *Nobel Prize Lecture*, "Asymmetric Catalysis: Science and Technology". Nobelprize.org. Nobel Media AB 2014. Web.http://www.nobelprize.org/nobel_prizes/chemistry/laureates/2001/noyori-Lecture.html. **May 2017**

[3] D. J. Willock, in *Molecular Symmetry*, Wiley, Chichester, **2009**, p. 41.

[4] M. J. Abrahamson, E. Vázquez-Figueroa, N. B. Woodall, J. C. Moore, A. S. Bommarius, *Angew. Chem. Int. Ed.* **2012**, *124*, 4036–4040.

[5] D. J. Pollard, J. M. Woodley, *Trends Biotechnol.* **2007**, *25*, 66–73.

[6] P. Mansfield, D. Henry, A. Tonkin, *Clin. Pharmacokinet.* **2004**, *43*, 287–290.

[7] L. A. Nguyen, H. He, C. Pham-Huy, *Int. J. Biomed. Sci.* **2006**, *2*, 85–100.

[8] R. N. Patel, A. Banerjee, L. J. Szarka, *J. Am. Oil Chem. Soc.* **1995**, *72*, 1247–1264.

[9] W. F. Gellad, P. Choi, M. Mizah, C. B. Good, A. S. Kesselheim, *Am. J. Manag. Care* **2014**, *20*, 90–97.

[10] S. Caddick, K. Jenkins, *Chem. Soc. Rev.* **1996**, *25*, 447–456.

[11] K. Faber, *Biotransformations in Organic Chemistry: A Textbook*, Springer, Heidelberg, **2011**.

[12] A. L. Margolin, *Enzyme Microb. Technol.* **1993**, *15*, 266–280.

[13] F. Hollmann, I. W. C. E. Arends, D. Holtmann, *Green Chem.* **2011**, *13*, 2285.

[14] T. Hudlicky, J. W. Reed, *Chem. Soc. Rev.* **2009**, *38*, 3117.

[15] A. L. Demain, *Ind. Biotechnol.* **2007**, *3*, 269–283.

[16] M. K. Turner, *TIBTECH* **1995**, *13*, 253–258.

[17] K. Buchholz, V. Kasche, U. T. Bornscheuer, *Biocataysis and Enzyme Technology*, Wiley, Weinheim, **2005**, p. 370–406.

[18] C. M. Clouthier, J. N. Pelletier, *Chem. Soc. Rev.* **2012**, *41*, 1585.

[19] O. Kirk, T. V. Borchert, C. C. Fuglsang, *Curr. Opin. Biotechnol.* **2002**, *13*, 345–351.

[20] M. Höhne, U. T. Bornscheuer, *ChemCatChem* **2009**, *1*, 42–51.

[21] A. S. Wells, G. L. Finch, P. C. Michels, J. W. Wong, *Org. Process Res. Dev.* **2012**, *16*, 1986–1993.

[22] J. M. Choi, S. S. Han, H. S. Kim, *Biotechnol. Adv.* **2015**, *33*, 1443–1454.

[23] M. Fuchs, J. E. Farnberger, W. Kroutil, *European J. Org. Chem.* **2015**, *2015*, 6965–6982.

[24] K. M. Koeller, C. H. Wong, *Nature* **2001**, *409*, 232–240.

[25] B. G. Davis, V. Boyer, *Nat. Prod. Rep.* **2001**, *18*, 618–640.

[26] B. A. Persson, A. L. E. Larsson, M. Le Ray, J. E. Backvall, *J. Am. Chem. Soc.* **1999**, 1645–1650.

[27] J. Hagen, *Industrial Catalysis: A Practical Approach*, Wiley-VCH, Weinheim, **2015**, p. 94–105.

[28] J. Magano, J. R. Dunetz, *Org. Process Res. Dev.* **2012**, *16*, 1156–1184.

[29] S. Caron, R. W. Dugger, S. G. Ruggeri, J. A. Ragan, D. H. B. Ripin, *Chem. Rev.* **2006**, *106*, 2943–2989.

[30] N. Richter, J. E. Farnberger, D. Pressnitz, H. Lechner, F. Zepeck, W. Kroutil, *Green Chem.* **2015**, 2952–2958.

[31] D. J. C. Constable, P. J. Dunn, J. D. Hayler, G. R. Humphrey, J. L. Leazer, Jr., R. J. Linderman, K. Lorenz, J. Manley, B. A. Pearlman, A. Wells, et al., *Green Chem.* **2007**, *9*, 411.

[32] T. C. Nugent, M. El-Shazly, *Adv. Synth. Catal.* **2010**, *352*, 753–819.

[33] R. Noyori, T. Ohkuma, M. Kitamura, H. Takaya, N. Sayo, H. Kumobayashi, S. Akutagawa, *J. Am. Chem. Soc.* **1987**, *109*, 5856–5858.

[34] T. C. Nugent, *Chiral Amine Synthesis*, Wiley-VCH Verlag GmbH & Co. KGaA, Weinheim, **2010**, p. 225–245.

[35] R. Kadyrov, T. H. Riermeier, *Angew. Chem. Int. Ed.* **2003**, *42*, 5472–5474.

[36] S. Hoffmann, A. M. Seayad, B. List, *Angew. Chem. Int. Ed.* **2005**, *44*, 7424–7427.

[37] W. S. Knowles, R. Noyori, *Acc. Chem. Res.* **2007**, *40*, 1238–1239.

[38] S. E. Lewis, *Annu. Rep. Prog. Chem., Sect. B* **2010**, *106*, 34–75.

[39] W. S. Knowles, *Acc. Chem. Res.* **1983**, *1445*, 106–112.

[40] R. Stuermer, B. Hauer, M. Hall, K. Faber, *Curr. Opin. Chem. Biol.* **2007**, *11*, 203–213.

[41] W. S. Knowles, *Angew. Chem. Int. Ed.* **2002**, *41*, 1999–2007.

[42] S. A. Patil, O. A. Apine, S. N. Surwase, J. P. Jadhav, *Advances in Parkinson's Disease.* **2013**, *2*, 81–87.

[43] K. Min, D. H. Park, Y. J. Yoo, *J. Biotechnol.* **2010**, *146*, 40–44.

[44] H.-U. Blaser, C. Malan, B. Pugin, F. Spindler, H. Steiner, M. Studer, *Adv. Synth. Catal.* **2003**, *345*, 103–151.

[45] H. U. Blaser, F. Spindler, M. Studer, *Appl. Catal. A Gen.* **2001**, *221*, 119–143.

[46] P. K. Robinson, *Essays Biochem.* **2015**, *59*, 1–41.

[47] T. Koyanagi, T. Katayama, H. Suzuki, A. Onishi, K. Yokozeki, H. Kumagai, *Biosci. Biotechnol. Biochem.* **2014**, *73*, 1221–1223.

[48] A. S. Bommarius, M. Schwarm, K. Drauz, *J. Mol. Catal. B: Enzym.* **1998**, *5*, 1–11.

[49] K. Drauz, H. Groeger, O. May, *Enzyme Catalysis in Organic Synthesis*, Wiley-VCH, Weinheim, **2012**, p. 1186.

[50] A. S. Bommarius, B. R. Riebel, *Biocatalysis*, Wiley-VCH, Weinheim, **2004**.

[51] A. S. Bommarius, M. Schwarm, K. Stingl, M. Kottenhahn, K. Huthmacher, K. Drauz, *Tetrahedron: Asymmetry* **1995**, *6*, 2851–2888.

[52] A. A. Desai, *Angew. Chem. Int. Ed.* **2011**, *50*, 1974–1976.

[53] P. J. Dunn, *Chem. Soc. Rev.* **2012**, *41*, 1452.

[54] H. G. W. Leuenberger, W. Boguth, E. Widmer, R. Zell, *Helv. Chim. Acta* **1976**, *59*, 1832–1849.

[55] C. K. Winkler, G. Tasnádi, D. Clay, M. Hall, K. Faber, *J. Biotechnol.* **2012**, *162*, 381–389.

[56] H. S. Toogood, N. S. Scrutton, *Curr. Opin. Chem. Biol.* **2014**, *19*, 107–15.

[57] A. Fryszkowska, H. Toogood, M. Sakuma, J. M. Gardiner, G. M. Stephens, N. S. Scrutton, *Adv. Synth. Catal.* **2009**, *351*, 2976–2990.

[58] B. M. Brena, F. Batista-Viera, *Methods in Biotechnology: Immobilization of Enzymes and Cells*, Springer, Heidelberg, **2006**, p. 15–26.

[59] C. Mateo, J. M. Palomo, G. Fernandez-Lorente, J. M. Guisan, R. Fernandez-Lafuente, *Enzyme Microb. Technol.* **2007**, *40*, 1451–1463.

[60] N. R. Mohamad, N. H. C. Marzuki, N. A. Buang, F. Huyop, R. A. Wahab, *Biotechnol. Biotechnol. Equip.* **2015**, *29*, 205–220.

[61] R. A. Sheldon, *Adv. Synth. Catal.* **2010**, *349*, 1289–1307.

[62] *http://www.cleatechnologies.com/products*, **Jan 2017**.

[63] R. Schoevaart, M. W. W. Wolbers, M. Golubovic, M. Ottens, A. P. G. P. G. Kieboom, F. van Rantwijk, L. A. M. A. M. van der Wielen, R. A. A. Sheldon, *Biotechnol. Bioeng.* **2004**, *87*, 754–762.

[64] H. A. Reeve, P. A. Ash, H. Park, A. Huang, M. Posidias, C. Tomlinson, O. Lenz, K. A. Vincent, *Biochem. J.* **2017**, *474*, 215–230.

[65] *www.sigmaaldrich.com*, **Feb. 2016**.

[66] C. E. Paul, S. Gargiulo, D. J. Opperman, I. Lavandera, V. Gotor-Fernández, V. Gotor, A. Taglieber, I. W. C. E. Arends, F. Hollmann, *Org. Lett.* **2013**, *15*, 180–183.

[67] K. Goldberg, K. Schroer, S. Lütz, A. Liese, *Appl. Microbiol. Biotechnol.* **2007**, *76*, 249–255.

[68] T. H. Lonsdale, L. Lauterbach, S. Honda Malca, B. M. Nestl, B. Hauer, O. Lenz, *Chem. Commun.* **2015**, *51*, 16173–16175.

[69] S. Siedler, S. Bringer, M. Bott, *Appl. Microbiol. Biotechnol.* **2011**, *92*, 929–937.

[70] W. Lee, M. Kim, Y. Jin, J. Seo, **2013**, 2761–2772.

[71] V. B. Nanduri, R. L. Hanson, A. Goswami, J. M. Wasylyk, T. L. LaPorte, K. Katipally, H. J. Chung, R. N. Patel, *Enzyme Microb. Technol.* **2001**, *28*, 632–636.

[72] *http://www.pharmtech.com/industrial-applications-whole-cell-biocatalysis*, **May 2017**.

[73] H. Gröger, O. May, H. Werner, A. Menzel, J. Altenbuchner, *Org. Process Res. Dev.* **2006**, *10*, 4–7.

[74] S. Riva, W.-D. Fessner, *Cascade Biocatalysis Integrating Stereoselective and Environmentally Friendly Reactions : Integrating Stereoselective and Environmentally Friendly Reactions*, Wiley-VCH, Weinheim, **2014**, p. 235.

[75] L. Lauterbach, O. Lenz, K. A. Vincent, *FEBS J.* **2013**, *280*, 3058–3068.

[76] W. A. van der Donk, H. Zhao, *Curr. Opin. Biotechnol.* **2003**, *14*, 421–426.

[77] S. M. A. De Wildeman, T. Sonke, H. E. Schoemaker, O. May, *Acc. Chem. Res.* **2007**, *40*, 1260–1266.

[78] F. Hollmann, A. Schmid, *Biocatal. Biotransformation* **2004**, *22*, 63–88.

[79] X. Wang, H. H. P. Yiu, *ACS Catal.* **2016**, *6*, 1880–1886.

[80] J. Liang, E. Mundorff, R. Voladri, S. Jennet, L. Gilson, A. Conway, A. Krebber, J. Wong, G. Huisman, S. Truesdell, et al., *Org. Process Res. Dev.* **2010**, *14*, 188–192.

[81] E. Vázquez-Figueroa, J. Chapparro-Riggers, A. S. Bommarius, *ChemBioChem* **2007**, *8*, 2295–2301.

[82] V. I. Tishkov, V. O. Popov, *Biomol. Eng.* **2006**, *23*, 89–110.

[83] T. W. Johannes, R. D. Woodyer, H. Zhao, *Biotechnol. Bioeng.* **2007**, *96*, 18–26.

[84] Y. Ni, D. Holtmann, F. Hollmann, *ChemCatChem* **2014**, *6*, 930–943.

[85] R. A. Sheldon, *Green Chem.* **2007**, *9*, 1273.

[86] R. A. Sheldon, *Green Chem.* **2017**, *19*, 18–43.

[87] W. R, D. Vasic-Racki, *Adv. Biochem. Eng. Biotechnol.* **2005**, 225–260.

[88] G. W. Crabtree, M. S. Dresselhaus, M. V. Buchanan, *Phys. Today* **2004**, *57*, 39–44.

[89] *https://www.theguardian.com/environment/2012/oct/11/hydrogen-economy-climate-change*, **April 2016.**

[90] R. Devaux-Basseguy, A. Bergel, M. Comtat, *Enzyme Microb. Technol.* **1997**, *20*, 248–258.

[91] I. Ali, M. McArthur, N. Hordy, *Int. J. Electrochem.* **2012**, *7*, 7675–7683.

[92] P. M. Allen, W. R. Bowen, *Trends Biotechnol.* **1985**, *3*, 145–149.

[93] V. Uppada, S. Bhaduri, S. B. Noronha, *Curr. Sci.* **2014**, *106*, 946–957.

[94] H. Wu, C. Tian, X. Song, C. Liu, D. Yang, Z. Jiang, *Green Chem.* **2013**, 1773–1789.

[95] A. A. Karyakin, Y. N. Ivanova, E. E. Karyakina, *Electrochem. commun.* **2003**, *5*, 677–680.

[96] H. Durliat, M. Comtat, J. L. Seris, *Anal. Lett.* **1991**, *24*, 1471–1482.

[97] H. Durliat, M. Comtat, J.-L. Seris, *Process for the Electrochemical Regeneration of Pyridine Cofactors*, **1988**, Patent number: US 5538867 A.

[98] J. Cantet, A. Bergel, M. Comtat, *Enzyme Microb. Technol.* **1996**, *18*, 72–79.

[99] Y. W. Kang, C. Kang, J. S. Hong, S. E. Yun, *Biotechnol. Lett.* **2001**, *23*, 599–604.

[100] Y. Zu, R. J. Shannon, J. Hirst, *J. Am. Chem. Soc.* **2003**, 6020–6021.

[101] C. D. Barker, T. Reda, J. Hirst, *Biochemistry* **2007**, *46*, 3454–3464.

[102] L. Lauterbach, Z. Idris, K. A. Vincent, O. Lenz, *PLoS One* **2011**, *6*, e25939.

[103] H. A. Reeve, *D.Phil Thesis, University of Oxford*, **2015**.

[104] T. Burgdorf, A. L. De Lacey, B. Friedrich, *J. Bacteriol. Virol.* **2002**, *184*, 6280–6288.

[105] J. C. Fontecilla-Camps, A. Volbeda, C. Cavazza, Y. Nicolet, *Chem. Rev.* **2007**, *107*, 4273–4303.

[106] M. Horch, L. Lauterbach, O. Lenz, P. Hildebrandt, I. Zebger, *FEBS Lett.* **2012**, *586*, 545–556.

[107] P. M. Vignais, *Chem. Rev.* **2007**, 4206–4272.

[108] A. Hansel, P. Lindblad, *Appl. Microbiol. Biotechnol.* **1998**, *50*, 153–160.

[109] K. Schneider, H. G. Schlegel, *Cell* **1976**, *452*, 66–80.

[110] K. Karstens, *PhD Thesis, Humboldt University Berlin*, **2014**.

[111] *https://www.hydrogen.energy.gov/pdfs/review14/bes005_jones_2014_o.pdf*, **Jan 2016**.

[112] R. Mertens, L. Greiner, E. C. D. Van Den Ban, H. B. C. M. Haaker, A. Liese, *J. Mol. Catal. B: Enzym.* **2003**, *24–25*, 39–52.

[113] K. Schneider, H. G. Schlegel, *Biochim. Biophys. Acta* **1976**, *452*, 66–80.

[114] T. Burgdorf, O. Lenz, T. Buhrke, E. van der Linden, A. K. Jones, S. P. J. Albracht, B. Friedrich, *J. Mol. Microbiol. Biotechnol.* **2006**, *10*, 181–196.

[115] A. K. Holzer, K. Hiebler, F. G. Mutti, R. C. Simon, L. Lauterbach, O. Lenz, W. Kroutil, *Org. Lett.* **2015**, *17*, 2431–2433.

[116] R. Mertens, A. Liese, *Curr. Opin. Biotechnol.* **2004**, *15*, 343–348.

[117] E. van der Linden, B. W. Faber, B. Bleijlevens, T. Burgdorf, M. Bernhard, B. Friedrich, S. P. J. Albracht, *Eur. J. Biochem.* **2004**, *271*, 801–808.

[118] T. Burgdorf, E. van der Linden, M. Bernhard, Q. Y. Yin, J. W. Back, A. F. Hartog, A. O. Muijsers, C. G. de Koster, S. P. Albracht, B. Friedrich, *J. Bacteriol. Virol.* **2005**, *187*, 3122–3132.

[119] H. A. Reeve, L. Lauterbach, O. Lenz, K. A. Vincent, *ChemCatChem* **2015**, *7*, 3480–

3487.

[120] H. A. Reeve, L. Lauterbach, P. A. Ash, O. Lenz, K. A. Vincent, *Chem. Commun.* **2012**, *48*, 1589.

[121] P. Frey, A. Hegeman, *Enzymatic Reaction Mechanisms*, Oxford University Press, Oxford, **2007**, p. 160.

[122] M. J. Lukey, A. Parkin, M. M. Roessler, B. J. Murphy, J. Harmer, T. Palmer, F. Sargent, F. A. Armstrong, *J. Biol. Chem.* **2010**, *285*, 3928–3938.

[123] J. G. Zeikus, C. Vieille, A. Savchenko, *Extremophiles* **1998**, *2*, 179–183.

[124] H. García-Arellano, B. Valderrama, G. Saab-Rincón, R. Vazquez-Duhalt, *Bioconjug. Chem.* **2002**, *13*, 1336–1344.

[125] C. E. Paul, F. Hollmann, *Appl. Microbiol. Biotechnol.* **2016**, *100*, 4773–4778.

[126] T. G. Gant, *J. Med. Chem.* **2014**, *57*, 3595–3611.

[127] L. Lauterbach, O. Lenz, *J. Am. Chem. Soc.* **2013**, *135*, 17897–17905.

[128] *http://www.evocatal.com/en/products/evozymes/cofactor-regeneration.html*, **July 2016**.

[129] T. Hartmann, P. Schrapers, T. Utesch, M. Nimtz, Y. Rippers, H. Dau, M. A. Mroginski, M. Haumann, S. Leimkühler, *FEBS J.* **2013**, *280*, 6083–6096.

[130] *http://www.jmfinechemicals.com/products/biocatalysts/*, **Jan 2017.**

[131] L. Lauterbach, J. Liu, M. Horch, P. Hummel, A. Schwarze, M. Haumann, K. A. Vincent, O. Lenz, I. Zebger, *Eur. J. Inorg. Chem.* **2011**, *2011*, 1067–1079.

[132] C. Aaij, P. Borst, *Biochim. Biophys. Acta* **1972**, *269*.

[133] *https://www.neb.com/*, **Aug. 2016**.

[134] G. Eberz, C. Hogrefe, C. Kortluke, A. Kamienski, B. Friedrich, *J. Bacteriol.* **1986**, *168*, 636–641.

[135] R. Simon, U. Priefer, A. Puhler, *Biotechnol. J.* **1983**, *1*, 784–791.

[136] F. G. Mutti, C. S. Fuchs, D. Pressnitz, N. G. Turrini, J. H. Sattler, A. Lerchner, A. Skerra, W. Kroutil, *European J. Org. Chem.* **2012**, *2012*, 1003–1007.

[137] P. K. Smith, R. I. Krohn, G. T. Hermanson, A. K. Mallia, F. H. Gartner, M. D. Provenzano, E. K. Fujimoto, N. M. Goeke, B. J. Olson, D. C. Klenk, *Anal. Biochem.* **1985**, *150*, 76–85.

[138] M. M. Bradford, *Anal. Biochem.* **1976**, *72*, 248–254.

[139] P. Atkins, J. De Paula, *Atkins' Physical Chemistry*, Oxford University Press, Oxford, **2010**.

[140] L. M. Harwood, T. D. W. Claridge, *Introduction to Organic Spectroscopy*, Oxford University Press, Oxford, **1997**, p. 13–22.

[141] A. Gopalan, D. Ragupathy, H. T. Kim, K. M. Manesh, K. P. Lee, *Spectrochim. Acta Mol. Biomol. Spectrosc.* **2009**, *74*, 678–684.

[142] A. K. Holzer, W. Kroutil, Masters Thesis, University of Graz, Austria, **2014**.

[143] C. Grzeszik, M. Lubbers, M. Reh, H. G. Schlegel, *Microbiology* **1997**, *143*, 1271–1286.

[144] M. Lou Fultz, R. A. Durst, *Anal. Chim. Acta* **1982**, *140*, 1–18.

[145] L. H. Eng, M. B. M. Lewin, H. Y. Neujahr, *Photochem. Photobiol.* **1993**, *58*, 594–599.

[146] T. Watanabe, K. Honda, *J. Phys. Chem.* **1982**, *86*, 2617–2619.

[147] S. Schätzle, M. Höhne, E. Redestad, K. Robins, U. T. Bornscheuer, *Anal. Chem.* **2009**, *81*, 8244–8248.

[148] S.-S. Yi, C. Lee, J. Kim, D. Kyung, B.-G. Kim, Y.-S. Lee, *Process Biochem.* **2007**, *42*, 895–898.

[149] A. C. Fisher, *Electrode Dynamics*, Oxford University Press, Oxford, **1996**.

[150] C. F. Blanford, *Chem. Commun.* **2013**, *49*, 11130–2.

[151] J. Hirst, F. A. Armstrong, *Anal. Chem.* **1998**, *70*, 5062–5071.

[152] C. Léger, P. Bertrand, *Chem. Rev.* **2008**, *108*, 2379–438.

[153] O. Hammerich, J. Ulstrup, *Bioinorganic Electrochemistry*, Springer, Dordrecht, **2008**.

[154] K. A. Vincent, A. Parkin, F. A. Armstrong, *Chem. Rev.* **2007**, *107*, 4366–4413.

[155] J. A. Cracknell, K. A. Vincent, F. A. Armstrong, *Chem. Rev.* **2008**, *108*, 2439–2461.

[156] J. Quinson, R. Hidalgo, P. A. Ash, F. Dillon, N. Grobert, K. A. Vincent, *Farad. Discuss.* **2014**, *172*, 473–496.

[157] A. J. Bard, L. R. Faulkner, *Electrochemical Methods: Fundamentals and Applications*, Wiley, New York, **2000**.

[158] F. A. Armstrong, J. N. Butt, A. Sucheta, *Methods Enzymol.* **1993**, *227*.

[159] F. A. Armstrong, P. A. Cox, H. A. O. Hill, V. J. Lowe, B. N. Oliver, *J. Electroanal. Chem.* **1987**, *217*, 331–366.

[160] R. Hidalgo, P. A. Ash, A. J. Healy, K. A. Vincent, *Angew. Chem. Int. Ed.* **2015**, 7110–7113.

[161] R. Compton, C. E. Banks, *Understanding Voltammetry*, Imperial College Press, London, **2011**.

[162] P. N. Bartlett, *Bioelectrochemistry*, Wiley, Chichester, **2008**.

[163] A. Cornish-Bowden, *Fundamentals of Enzyme Kinetics*, Portland Press, London, **2004**.

[164] Z. Idris, D.Phil Thesis, Oxford University, **2012**.

[165] A. B. Kotlyar, V. D. Sled, A. D. Vinogradov, *Biochim. Biophys. Acta* **1992**, *1098*, 144–150.

[166] N. H. Gokhale, J. A. Cowan, N. Hooper, A. Turner, L. Skeggs, J. Kahn, N. Shumway, E. Miller, A. Samuels, E. Haber, et al., *Chem. Commun.* **2005**, *10*, 5916–5918.

[167] *http://www.cabot-corp.com/Rubber-CarbonBlacks/Products/PR201101241227PM3639/*, **July 2014.**

[168] M. Duca, J. R. Weeks, J. G. Fedor, J. H. Weiner, K. A. Vincent, *ChemElectroChem* **2015**, *2*, 1086–1089.

[169] C. L. Young, in *IUPAC Solubility Data Series: Hydrogen and Deuterium*, Pergamon Press, Oxford, **1981**, p. 2.

[170] T. J. Morrison, F. Billett, *J. Chem. Soc.* **1952**, 3819.

[171] *https://www.buchiglas.com/en/products/pressure-reactors-stirred-lab-autoclaves.html*, **Jan 2017**.

[172] R. Larralde, M. P. Robertson, S. L. Miller, *Proc. Natl. Acad. Sci.* **1995**, *92*, 8158–8160.

[173] T. Knaus, W. Bohmer, F. G. Mutti, *Green Chem.* **2016**, 1463–9262.

[174] S. Flitsch, *Oxford University Organic Chemistry Lecture series: "De novo" design of biosynthetic reaction cascades*, **Dec 2016.**

[175] U. Kragl, D. Vasic-Racki, C. Wandrey, *Bioprocess Eng.* **1996**, *14*, 291–297.

[176] F. G. Mutti, M. Breuer, N. J. Turner, *Science* **2015**, *224015*, 1525–1529.

[177] D. Ågren, M. Stehr, C. L. Berthold, S. Kapoor, W. Oehlmann, M. Singh, G. Schneider,

J. Mol. Biol. **2008**, *377*, 1161–1173.

[178] C. E. Grimshaw, P. F. Cook, W. W. Cleland, *Biochemistry* **1981**, *20*, 5655–5661.

[179] H. E. Gottlieb, V. Kotlyar, A. Nudelman, **1997**, *3263*, 7512–7515.

[180] D. Parker, *Chem. Rev.* **1991**, *91*, 1441–1457.

[181] E. W. Miles, S. Rhee, R. Davies, E. W. Miles, S. Rhee, D. R. Davies, *J. Biol. Chem.* **1999**, 12193–12197.

[182] E. Kasner, C. A. Hunter, D. Ph, K. Kariko, D. Ph, *Biochim Biophys Acta.* **2013**, *70*, 646–656.

[183] B. Y. Hwang, B. K. Cho, H. Yun, K. Koteshwar, B. G. Kim, *J. Mol. Catal. B: Enzym.* **2005**, *37*, 47–55.

[184] P. K. Mehta, T. I. Hale, P. Christen, *Eur. J. Biochem.* **1993**, *214*, 549–561.

[185] M. D. Truppo, J. D. Rozzell, J. C. Moore, N. J. Turner, *Org. Biomol. Chem.* **2009**, *7*, 395–398.

[186] M. Höhne, S. Kühl, K. Robins, U. T. Bornscheuer, *ChemBioChem* **2008**, *9*, 363–365.

[187] A. P. Green, N. J. Turner, E. O'Reilly, *Angew. Chem. Int. Ed.* **2014**, *53*, 10714–10717.

[188] J. L. Galman, I. Slabu, N. J. Weise, C. Iglesias, F. Parmeggiani, R. C. Lloyd, N. J. Turner, *Green Chem.* **2017**, *19*, 361–366.

[189] D. Koszelewski, M. Göritzer, D. Clay, B. Seisser, W. Kroutil, *ChemCatChem* **2010**, *2*, 73–77.

[190] D. Koszelewski, I. Lavandera, D. Clay, G. M. Guebitz, D. Rozzell, W. Kroutil, *Angew. Chem. Int. Ed.* **2008**, *47*, 9337–9340.

[191] C. K. Savile, J. M. Janey, E. C. Mundorff, J. C. Moore, S. Tam, W. R. Jarvis, J. C. Colbeck, A. Krebber, F. J. Fleitz, J. Brands, et al., *Science* **2010**, *329*, 305–309.

[192] J.-S. Shin, H. Yun, J.-W. Jang, I. Park, B.-G. Kim, *Appl. Microbiol. Biotechnol.* **2003**, *61*, 463–471.

[193] D. Koszelewski, N. Müller, J. H. Schrittwieser, K. Faber, W. Kroutil, *J. Mol. Catal. B: Enzym.* **2010**, *63*, 39–44.

[194] H. Mallin, U. Menyes, T. Vorhaben, M. Höhne, U. T. Bornscheuer, *ChemCatChem* **2013**, *5*, 588–593.

[195] *http://www.chemspider.com*, **June 2016.**

[196] N. Richter, *Personal communication*, **Aug 2014.**

[197] H. Park, *Personal communication*, **Jan 2016**.

[198] H. Kohls, F. Steffen-Munsberg, M. Höhne, *Curr. Opin. Chem. Biol.* **2014**, *19*, 180–192.

[199] A. Goswami, J. D. Stewart, *Organic Synthesis Using Biocatalysis*, Elsevier B.V., Amsterdam, **2016**.

[200] F. G. Mutti, C. S. Fuchs, D. Pressnitz, J. H. Sattler, W. Kroutil, *Adv. Synth. Catal.* **2011**, *353*, 3227–3233.

[201] U. Strych, M. J. Benedik, *J. Bacteriol.* **2002**, *184*, 4321–4325.

[202] K. S. Siddiqui, *Biotechnol. Adv.* **2015**, *33*, 1912–1922.

[203] K. Schneider, R. Cammack, H. G. Schlegel, *Eur. J. Biochem.* **1984**, *142*, 75–84.

[204] L. F. Wu, M. A. Mandrand, *FEMS Microbiol. Lett.* **1993**, *104*, 243–269.

[205] G. Rákhely, Á. T. Kovács, G. Maróti, D. Barna, G. Csanádi, D. Latinovics, L. Kornél, T. Kova, *Appl. Environ. Microbiol.* **2004**, *70*, 722–728.

[206] G. D. Ewart, G. D. Smith, *Arch. Biochem. Biophys.* **1989**, *268*, 327–337.

[207] O. Schmitz, G. Boison, R. Hilscher, B. Hundeshagen, W. Zimmer, F. Lottspeich, H. Bothe, *Eur. J. Biochem.* **1995**, *233*, 266–276.

[208] N. R. Hayashi, T. Ishida, A. Yokota, T. Kodama, Y. Igarashi, *Int. J. Syst. Bacteriol.* **1999**, 783–786.

[209] M. Taketa, H. Nakagawa, M. Habukawa, H. Osuka, K. Kihira, H. Komori, N. Shibata, M. Ishii, Y. Igarashi, H. Nishihara, et al., *Acta Crystallogr. Sect. F* **2015**, *71*, 96–99.

[210] *http://workbench.sdsc.edu/*, **Jan 2017**.

[211] N. Chatterjee, D. Sinha, M. Lemma-Dechassa, S. Tan, M. A. Shogren-Knaak, B. Bartholomew, *Nucleic Acids Res.* **2011**, *39*, 8378–8391.

[212] D. G. Higgins, A. J. Bleasby, R. Fuchs, *Comput. Appl. Biosci.* **1992**, *8*, 189–91.

[213] M. W. W. Adams, R. M. Kelly, *TIBTECH* **2000**, *7799*, 329–332.

[214] L. A. Sazanov, P. Hinchliffe, *Science* **2006**, *311*, 1430–1436.

[215] C. Chothia, A. M. Lesk, *EMBO J.* **1986**, *5*, 823–6.

[216] O. Lenz, *Personal communication*, **Mar 2014**.

[217] U. K. Laemmli, *Nature* **1970**, *227*, 680–685.

[218] *http://www.bioinformatics.org/sms/prot_mw.html*, **Jan 2017**.

[219] C. Vieille, G. J. Zeikus, *Microbiol. Mol. Biol. Rev.* **2001**, *65*, 1–43.

[220] E. van der Linden, T. Burgdorf, M. Bernhard, B. Bleijlevens, B. Friedrich, S. P. J. Albracht, *J. Biol. Inorg. Chem.* **2004**, *9*, 616–626.

[221] H. G. Barth, B. E. Boyes, C. Jackson, *Anal. Chem.* **1996**, *68*, 445–466.

[222] C. Schäfer, B. Friedrich, O. Lenza, *Appl. Environ. Microbiol.* **2013**, *79*, 5137–5145.

[223] E. M. Isin, F. P. Guengerich, *Biochim. Biophys. Acta* **2007**, *1770*, 314–29.

[224] *http://oxfordbiotrans.com/*, **Jan 2017.**

[225] A. Liese, K. Seelbach, C. Wandrey, in *Ind. Biotransformations*, Wiley-VCH, Weinheim, **2000**, p. 93–171.

[226] E. Schwartz, U. Gerischer, B. Friedrich, *J. Bacteriol.* **1998**, *180*, 3197–3204.

[227] L. Lauterbach, *PhD Thesis, Humboldt University Berlin*, **2013**.

[228] K. Schneider, H. G. Schlegel, K. Jochim, *Eur. J. Biochem.* **1984**, *138*, 533–541.

[229] V. Fourmond, T. Lautier, C. Baffert, F. Leroux, P.-P. Liebgott, S. Dementin, M. Rousset, P. Arnoux, D. Pignol, I. Meynial-Salles, et al., *Anal. Chem.* **2009**, *81*, 2962–2968.

[230] G. Gundlach, E. Luttermann-Semmer, *Clin. Chem. Lab. Med.* **1987**, *25*, 441–446.

[231] B. Bennett, E. Kimball, M. Gao, *Nat. Chem. Biol.* **2009**, *5*, 593–599.

[232] F. F. Delarosa, E. Palacian, *Plant Sci. Lett.* **1981**, *21*, 1–8.

[233] K. Dumorné, D. C. Córdova, M. Astorga-Eló, P. Renganathan, *J. Microbiol. Biotechnol.* **2017**, *27*, 649–659.

[234] C. E. Paul, *Personal communication*, **May 2016.**

[235] S. Elleuche, C. Schäfers, S. Blank, C. Schröder, G. Antranikian, *Curr. Opin. Microbiol.* **2015**, *25*, 113–119.

[236] C. Bertoldo, G. Antranikian, *Curr. Opin. Chem. Biol.* **2002**, *6*, 151–160.

[237] K. Faber, Opening Lecture BioCat. 2016, TU Hamburg, **Aug 2016.**

[238] O. Röhm, *US Patent WO1998032908 A1*, **1913**.

[239] A. Toplak, B. Wu, F. Fusetti, P. J. L. M. Quaedflieg, D. B. Janssena, *Appl. Environ. Microbiol.* **2013**, *79*, 5625–5632.

[240] H. Radianingtyas, P. C. Wright, *FEMS Microbiol. Rev.* **2003**, *27*, 593–616.

[241] D. J. Opperman, L. A. Piater, E. van Heerden, *J. Bacteriol.* **2008**, *190*, 3076–3082.

[242] M. Hall, C. Stueckler, H. Ehammer, E. Pointner, G. Oberdorfer, K. Gruber, B. Hauer, R. Stuermer, W. Kroutil, P. Macheroux, et al., *Adv. Synth. Catal.* **2008**, *350*, 411–418.

[243] R. M. Kohli, V. Massey, *J. Biol. Chem.* **1998**, *273*, 32763–32770.

[244] E. Klabunovskii, G. Smith, Á. Zsigmond, *Heterogeneous Enantioselective Hydrogenation: Theory and Practice*, Springer, Dordrecht, **2006**, p. 267–274.

[245] A. J. Healy, H. A. Reeve, A. Parkin, K. A. Vincent, *Electrochim. Acta* **2011**, *56*, 10786–10790.

[246] P. A. Ash, K. A. Vincent, *Chem. Commun.* **2012**, *48*, 1400–9.

[247] T. Kuwahara, H. Ohta, M. Kondo, M. Shimomura, *Bioelectrochemistry* **2008**, *74*, 66–72.

[248] R. Hidalgo-González, D.Phil. Thesis, University of Oxford, **2016**.

[249] *http://www.gamry.com/application-notes/electrodes-cells/care-of-vycor-porous-glass-frits/*, June 2016.

[250] *http://www.thermofisher.com/uk/en/home.html*, Jan 2017.

[251] C. E. Bricker, *J. Chem. Educ.* **1989**, *66*, 954.

[252] W. B. Nowall, W. G. Kuhr, *Anal. Chem.* **1995**, *67*, 3583–3588.

[253] C. Moreno-Castilla, *Carbon* **2004**, *42*, 83–94.

[254] L. E. S. Brink, J. Tramper, *Biotechnol. Bioeng.* **1985**, *27*, 1258–1269.

[255] G. Carrea, *Trends Biotechnol.* **1984**, *2*, 102–106.

[256] C. E. Paul, I. W. C. E. Arends, F. Hollmann, *ACS Catal.* **2014**, *4*, 788–797.

[257] H. U. Bergmeyer, *Z. Klin. Chem. Klin. Biochem.* **1975**, *13*, 507–508.

[258] T. Knaus, C. E. Paul, C. W. Levy, S. de Vries, F. G. Mutti, F. Hollmann, N. S. Scrutton, *J. Am. Chem. Soc.* **2016**, *138*, 1033–1039.

[259] D. Mauzerall, F. Westheimer, *J. Am. Chem. Soc.* **1955**, *77*, 2261–2264.

[260] J. D. Ryan, R. H. Fish, D. S. Clark, *ChemBioChem* **2008**, *9*, 2579–2582.

[261] J. Lutz, F. Hollmann, T. V. Ho, A. Schnyder, R. H. Fish, A. Schmid, *J. Organomet. Chem.* **2004**, *689*, 4783–4790.

[262] S. Kara, J. H. Schrittwieser, F. Hollmann, M. B. Ansorge-Schumacher, *Appl. Microbiol. Biotechnol.* **2014**, *98*, 1517–29.

[263] Y. Okamoto, V. Köhler, C. E. Paul, F. Hollmann, T. R. Ward, *ACS Catal.* **2016**, *6*, 3553–3557.

[264] H. C. Lo, O. Buriez, J. B. Kerr, R. H. Fish, *Angew. Chem. Int. Ed.* **1999**, *38*, 1429–1432.

[265] H. C. Lo, R. H. Fish, *Angew. Chem. Int. Ed.* **2002**, *41*, 478–481.

[266] K. E. Taylor, J. B. Jones, *J. Am. Chem. Soc.* **1976**, 5689–5694.

[267] S. G. Mayhew, *Eur. J. Biochem.* **1978**, *85*, 535–547.

[268] S. Gaillard, C. Papamicaël, F. Marsais, G. Dupas, V. Levacher, *Synlett* **2005**, 441–444.

[269] O. Ishitani, N. Inoue, K. Koike, *Chem. Commun.* **1994**, *5*, 367–368.

[270] C. Nowak, B. Beer, A. Pick, T. Roth, P. Lommes, V. Sieber, *Front. Microbiol.* **2015**, *6*, 1–9.

[271] V. S. Lamzin, Z. Dauter, V. O. Popov, E. H. Harutyunyan, K. S. Wilson, *J. Mol. Biol.* **1994**, *236*, 759–785.

[272] Q. Guo, L. Gakhar, K. Wickersham, K. Francis, A. Vardi-Kilshtain, D. T. Major, C. M. Cheatum, A. Kohen, *Biochemistry* **2016**, *55*, 2760–2771.

[273] T. Pongtharangkul, P. Chuekitkumchorn, N. Suwanampa, P. Payongsri, K. Honda, W. Panbangred, *AMB Express* **2015**, *5*, 68.

[274] T. Nishioka, Y. Yasutake, Y. Nishiya, T. Tamura, *FEBS J.* **2012**, *279*, 3264–3275.

[275] K. Yamamoto, G. Kurisu, M. Kusunoki, S. Tabata, I. Urabe, S. Osaki, *J. Biochem.* **2001**, *312*, 303–312.

[276] T. Hartmann, P. Schrapers, T. Utesch, M. Nimtz, Y. Rippers, H. Dau, M. A. Mroginski, M. Haumann, S. Leimkühler, *Biochemistry* **2016**, *55*, 2381–2389.

[277] K. Wallenfels, M. Gellrich, *Justus Liebigs Ann. Chem.* **1959**, *255*, 149–165.

[278] M. Machida, M. I. Machida, Y. Kanaoka, *Chem. Pharm. Bull.* **1977**, *25*, 2739–2743.

[279] S. Matsui, H. Aida, *J. Chem. Soc. Perkin Trans. 2* **1978**, 1277.

[280] H. Jaegfeldt, *J. Electroanal. Chem. Interfacial Electrochem.* **1980**, *110*, 295–302.

[281] K. Morina, M. Schulte, F. Hubrich, K. Dorner, S. Steimle, S. Stolpe, T. Friedrich, *J. Biol. Chem.* **2011**, *286*, 34627–34634.

[282] J. A. Birrell, J. Hirst, *Biochemistry* **2013**, *52*, 4048–4055.

[283] *http://www.pynnco.com/im/201002/201022111018505*, **Mar 2016**.

[284] I. M. Mándity, T. A. Martinek, F. Darvas, F. Fülöp, *Tetrahedron Lett.* **2009**, *50*, 4372–4374.

[285] C. Lecuyer, P. Gillet, F. Robert, *Chem. Geol.* **1998**, *145*, 249–261.

[286] J. Atzrodt, V. Derdau, T. Fey, J. Zimmermann, *Angew. Chem. Int. Ed.* **2007**, *46*, 7744–7765.

[287] *http://www.fz-juelich.de/jcns/EN/Leistungen/Conference*, **Jan 2017**.

[288] A. Barth, C. Zscherp, *Q. Rev. Biophys.* **2002**, *35*, 369–430.

[289] Q. Wang, X. Sheng, J. H. Horner, M. Newcomb, *J. Am. Chem. Soc.* **2009**, *131*, 10629–10636.

[290] R. Pony Yu, D. Hesk, N. Rivera, I. Pelczer, P. J. Chirik, *Nature* **2016**, *529*, 195–199.

[291] A. E. Mutlib, *Chem. Res. Toxicol.* **2008**, *21*, 1672–1689.

[292] D. Lütjohann, C. O. Meese, J. R. Crouse, K. von Bergmann, *J. Lipid Res.* **1993**, *34*, 1039–1046.

[293] *http://www.rsc.org/chemistryworld/2016/06/deuterium-deuterated-drugs-approval*, **Apr 2017**.

[294] *http://blogs.sciencemag.org/pipeline/archives/2017/04/04/the-first-deuterated-drug-arrives*, **May 2017.**

[295] A. I. Miller, *Can. Nucl. Soc. Bull.* **2001**, *22*, 1–14.

[296] H. K. Rae, *Mater. Sci. Forum* **1978**, *31*, 19–38.

[297] E. Khaskin, D. Milstein, *ACS Catal.* **2013**, *3*, 448–452.

[298] B. L. Cowley, *US Patent 4,002,663*, **1977**.

[299] A. Guaragna, S. Pedatella, V. Pinto, G. Palumbo, *Synthesis* **2006**, *2006*, 4013–4016.

[300] S. S. Bokatzian-Johnson, M. L. Maier, R. H. Bell, K. E. Alston, B. Y. Le, E. A. Cioffi, *J. Label. Compd. Radiopharm.* **2007**, *50*, 380–383.

[301] K. L. Breno, D. R. Tyler, *Organometallics* **2001**, *20*, 3864–3868.

[302] T. Maegawa, Y. Fujiwara, Y. Inagaki, Y. Monguchi, H. Sajiki, *Adv. Synth. Catal.* **2008**, *350*, 2215–2218.

[303] Y. Fujiwara, H. Iwata, Y. Sawama, Y. Monguchi, H. Sajiki, *Chem. Commun.* **2010**, *46*, 4977.

[304] M. Albrecht, M. M. Lindner, *Dalton Trans.* **2011**, *40*, 8733–8744.

[305] W. Bai, K. H. Lee, S. K. S. Tse, K. W. Chan, Z. Lin, G. Jia, *Organometallics* **2015**, *34*, 3686–3698.

[306] M. Takahashi, K. Oshima, S. Matsubara, *Chem. Lett.* **2005**, *34*, 192–193.

[307] C. Wong, G. M. Whitesides, *J. Am. Chem. Soc.* **1981**, 4890–4899.

[308] J. Szymańska, M. Kańska, *J. Chem. Chem. Eng.* **2014**, *8*, 2014.

[309] N. J. Oppenheimer, L. J. Arnold, N. O. Kaplan, *Proc. Natl. Acad. Sci.* **1971**, *68*, 3200–5.

[310] S. Ramaswamy, H. Eklund, B. V Plapp, *Biochemistry* **1994**, *33*, 5230–5237.

[311] K. L. Kavanagh, H. Jörnvall, B. Persson, U. Oppermann, *Cell. Mol. Life Sci.* **2008**, *65*, 3895–3906.

[312] D. Ghislieri, N. J. Turner, *Top. Catal.* **2014**, *57*, 284–300.

[313] R. Marques, R. Helmy, D. Waterhouse, *J. Label Compd. Radiopharm*. **2015**, 2014–2016.

[314] R. M. Atlas, *Handbook of Microbiological Media*, Taylor & Francis Group, Washington DC, **2004**.

[315] H. C. Birnboim, J. Doly, *Nucleic Acids Res.* **1979**, *7*, 1513–1523.

[316] D. Hanahan, *J. Mol. Biol.* **1983**, *166*, 557–580.

[317] T. G. M. Schmidt, A. Skerra, *Nat. Protoc.* **2007**, *2*, 1528–1535.

[318] D. Parker, R. J. Taylor, *Tetrahedron* **1987**, *18*, 5451–5456.

[319] R. Taylor, PhD Thesis, University of Durham, **1987**.

[320] http://www.sigmaaldrich.com/spectra/fnmr/FNMR009210.PDF, **Nov 2017**

[321] K. Moozeh, S. M. So, J. Chin, *Angew. Chem. Int. Ed.* **2015**, *54*, 9381–9385

Appendix

Appendix A **Molecular biology**

A.1 Growth media and buffer composition used in this section

The growth media described in Table A.0-1 were used throughout this thesis for growth of bacteria to produce proteins.

Table A.0-1: Media used for growth of bacterial strains in this project

Media	Composition
H16 buffer	25 mM $Na_2H(PO_4)$, 11 mM $KH_2(PO_4)$ pH 7.0
H16 medium	25 mM $Na_2H(PO_4)$, 11 mM $KH_2(PO_4)$ pH 7.0 with addition of 37.4 mM NH_4Cl, 0.81 mM $Mg(SO_4).7H_2O$, 0.068 mM $CaCl_2.2H_2O$, 18 µM $FeCl_3.6H_2O$, 1 µM $ZnCl_2$, 1 µM $NiCl_2$ and SL6[314]
FGN	H16 medium containing 0.05 % w/v fructose and 0.4 % v/v glycerol
FN	H16 medium containing 0.4 % w/v fructose
NB	8 g L^{-1} Nutrient broth
LB	10 g L^{-1} tryptone, 10 g L^{-1} NaCl, 5 g L^{-1} yeast extract
SOC	20 g L^{-1} Tryptone, 5 g L^{-1} Yeast Extract, 4.8 g L^{-1} $MgSO_4$, 3.603 g L^{-1} dextrose, 0.5 g L^{-1} NaCl, 0.186 g L^{-1} KCl
Agar	Agar was prepared by adding 15 g of Bacto agar per litre of medium before autoclaving.

A.2 Determination of protein concentration

The concentration of the protein was estimated according to the method of Bradford with BSA-solution (Thermofisher) in a concentration range of 0 to 1000 µg mL^{-1} used as a standard, see Figure A.1 for a typical calibration curve.[138] Calibration curves were performed freshly each time the assay was performed.

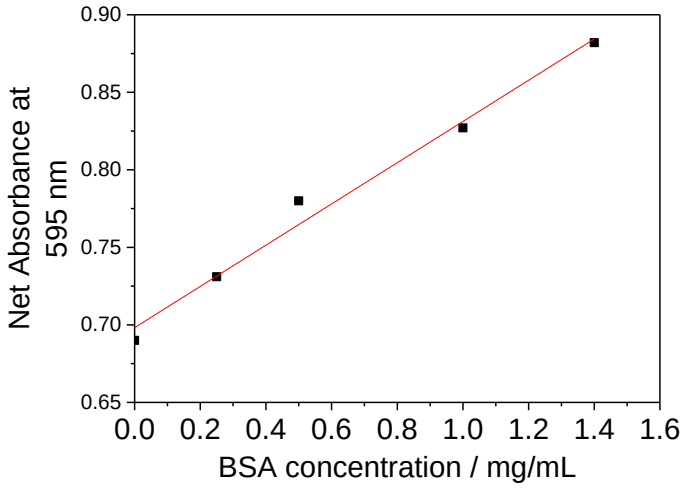

Figure A.1: A typical Bradford calibration curve used to determine protein concentration.

The calibration curve in Figure A.1 has an R^2 value of 0.98 and a gradient of 0.133.

Alternatively, the concentration of the protein was estimated using a BCA kit (Thermofisher). This was carried out following the manufacturer's instructions at a wavelength of 562 nm in a 96 well plate using a spectromax 340 plate reader. BSA-solution in a concentration range between 0 – 1000 µg mL^{-1} (Sigma Aldrich) was used as the internal standard

A.3 Preparation of HoxFU from Hydrogenophilus thermoluteolus

This work was carried out in collaboration with the group of Dr Oliver Lenz at the TU Berlin.

In chapter 4 of this thesis the HoxFU moiety from *H. thermoluteolus* was characterised. This organism is a thermophile, therefore, it requires growth temperatures of around 50 ^{o}C. To avoid this requirement the HoxFU was expressed recombinantly in *R. eutropha* which naturally produces a similar SH and so contains the necessary maturation machinery to produce an active SH. It is not trivial to transfer DNA directly into *R. eutropha* therefore a plasmid was isolated from *E. coli* and sequenced. It was subsequently transferred back into *E. coli* and established cross mating techniques were used to transfer the plasmid into *R. eutropha* as described below*:*

Plasmid isolation of H. thermoluteolus HoxFU

Initially, the *H. thermoluteolus* HoxFU plasmid was isolated from *E. coli* using a modified version of the protocol used by Birnboim and Doly 1979.[315] A 1.5 mL overnight culture was harvested by centrifuging at 9,000 × g for 5 minutes. The remaining solution was discarded and the cell pellet was re-suspended in 100 µL of buffer 1, see

Table A.0-2. A 200 µL aliquot of buffer 2, was used to lysis the cells. This was subsequently neutralised by addition of 200 µL of buffer 3. This also causes precipitation of the protein. The tube was then centrifuged at 15,000 × g for 3 minutes and the supernatant transferred to a fresh Eppendorf tube. The DNA was precipitated by addition of 1000 µL of EtOH (0 ^{o}C) and centrifuging at 15,000 × g for 7 minutes. The DNA pellet was then washed with 70 % EtOH and dried under vacuum. Finally, it was dissolved in 50 mM Tris-HCl pH 8.

Table A.0-2: The buffers required for Birnboim plasmid isolation

Buffer	Contents
1	25 mM Tris-HCl, 10 mM EDTA 100 mg/mL RNase pH 8
2	0.2 N NaOH,1 % (w/v) SDS
3	3 M Potassium acetate pH 4.8

Gel electrophoresis was used to check that the plasmid was of the correct molecular weight following the protocol of Aaij and Borst.[132]

Recombinant expression of *H. thermoluteolus* HoxFU in *R. eutropha*

Initially, the plasmid for *H. thermoluteolus* HoxFU production was transformed into *E. coli S17-1* using the standard Heat shock protocol from NEB Biolabs.[133] This involved thawing a 50 µL aliquot of competent *E. coli S17-1* cells (Starlab) on ice, adding 1 µL (*ca.*1µg) of the plasmid DNA isolated above and leaving on ice for 30 minutes. A heat

shock was then applied and the cells were heated to 42 ^{o}C for 30 seconds. The cells were subsequently placed back on ice for a further 2 minutes before being incubated for 1 hour at 37 ^{o}C with 9000 µL of SOC medium,[316] with 450 rpm rotation. The plasmid containing the HoxFU genes contains a kanamycin resistance cassette. Following incubation for 60 minutes the cells were plated onto an LB agar plate containing 150 µg mL^{-1} kanamycin and grown at 37 ^{o}C overnight.

Transfer of the HoxFU plasmid into *R. eutropha* was carried out using the "Spotmating" technique.[134,135] The *E. coli S17-1* donor strain was used to transfer the plasmid to *R. eutropha.* The *E. coli S17-1* strain containing the HoxFU plasmid and *R. eutropha* were cultivated in a 10 mL LB_{kan} or NB cultures overnight respectively.

Cultures were then centrifuged at 6000 rpm for 4 minutes and the supernatant discarded. Each cell pellet was then washed in 10 mL of H16 buffer (see Table A.0-2) and again centrifuged at 6000 rpm for 4 minutes. The supernatant was again discarded and the cells were re-suspended in 10 mL of H16 buffer. A 200 µL aliquot of each strain was then plated onto the same NB plate and left to grow for 5 hours at 37 ^{o}C. As both *E. coli* and *R. eutropha* can grow on NB this step allows transfer of the plasmid between the *E. coli* cells and *R. eutropha.*

Following this 5 hour incubation period the bacterial colonies were scrapped up with a sterile pipette tip and re-suspended in 5 mL H16 buffer. The pellet was then washed twice in 5 mL H16 buffer. Finally the 5 mL solution of pellet was diluted by a factor of 100 and 100 µL was plated onto an FN plate containing 150 µg mL^{-1} kanamycin. The plates were then left to grow for 48 hours.

A colony was subsequently picked and a streaked onto another FN_{kan} plate. Following incubation for 24 hours a further colony was picked and added to 10 mL a H16

overnight culture. A 1 mL aliquot of this culture was then used to create a glycerol stock for this new bacterial strain (*R. eutropha_H. thermoluteolus* HoxFU).

Growth and purification of the HoxFU moiety

R. eutropha cultures were grown at 30 ^{o}C with shaking at 120 rpm. Overnight cultures containing 10 mL FN medium in a 100 mL conical flask were used to inoculate 5 L baffled Erlenmeyer flasks containing 4 L of FGN medium, with the required antibiotics (150 µg mL^{-1} kanamycin for HoxFU and HoxHYFU strains, 50 µg mL^{-1} tetracycline for Hox~~HY~~FU). These cultures were then grown for 5 to 7 days until an OD_{436} (optical density at 436 nm) of 10 ±1 was achieved.

Cultures were then harvested at 6000 rpm for 12 minutes at 4 ^{o}C in an F9S-4x1000y centrifuge (Thermofisher), the wet weight of the cell pellets was determined before shock freezing in liquid N_2. Cell pellets were stored at – 80 ^{o}C

Protein purification was carried using Strep-Tag II affinity chromatography at 4 ^{o}C.[317] Cell pellets were defrosted on ice and re-suspended in re-suspension buffer (50 mM potassium phosphate buffer pH 7.0 containing 5 % glycerol) in the ratio 10 mL buffer to 5 g cells with 1 Roche EDTA free protease inhibitor tablet per 20 mL of solution. Argon was then used to remove air from the headspace of the mixture.

Lysis of the cells was achieved by two passages through a cooled French press, followed by centrifuging at 100,000 × g in an ultracentrifuge (Thermofisher) to sediment the cellular debris.

The soluble extract was then transferred to a 2 mL Strep-Tactin superflow-column (IBA) pre -washed with 15 mL of resuspension buffer. The soluble extract was washed with 10 mL of the resuspension buffer with protease inhibitor added and eluted with 12 mL of elution buffer (50 mM potassium phosphate buffer pH 7.0, 5 % glycerol + 5 mM Destiobiotin). .

The activity of the hydrogenase was determined on the day of purification. The protein was then aliquoted and snap frozen in liquid N_2.

Sodium dodecyl sulphate polyacrylamide gel electrophoresis (SDS PAGE) was carried out following the method of Laemmli.[217] This method allowed determination of whether subunits of the correct molecular weight are present in the purified protein, as well as protein purity.

The HoxHYFU samples prepared in this thesis were prepared using the same method as that used for HoxFU.

A.4 Vf *ω-transaminase* preparation and purification

A plasmid for overproduction of *Vf ω-transaminase*[115] was transformed into a set of chemically competent *E.coli* BL21 (DE3) cells (from Invitrogen) following a standard protocol from New England Biolabs.[133]

A 100 µL aliquot of the cells following the transformation were then added to an $LB_{Amp\ 100\ \mu g/mL}$ agar plate and allowed to grow for 24 hours at 37 ^{o}C. A colony from this plate was picked, grown in 10 mL of LB $_{Amp\ 100\ \mu g/mL}$ in a 50 mL sterile conical centrifuge tube for 18 hours at 37 ^{o}C with rotation at 120 rpm. A 1 mL aliquot of this solution was then added to 0.3 mL sterile glycerol in an Eppendorf tube and frozen at -80 ^{o}C to create a glycerol stock, which was used to inoculate all future batches of *Vf ω-transaminase* cultures.

A 10 mL initial culture of LB medium was set up in a 50 mL sterile conical centrifuge tube, containing 100 µg mL^{-1} Ampicillin. This was inoculated with a 2 µL aliquot from the glycerol stock and allowed to grow overnight at 37 ^{o}C, 120 rpm.

A 5.5 mL aliquot of initial culture was inoculated into a sterile 1L baffled Erlenmeyer flask containing 330 mL LB medium containing 100 µg mL^{-1} Ampicillin. The culture was grown at 30 ^{o}C, 120 rpm for 5 hours (OD_{600} = Ca. 0.5). The culture was then

induced with 0.2 µg mL^{-1} Anhydrotetracycline from a 1.3 mg mL^{-1} stock in pure ethanol. The culture was left to grow at 20 ^{o}C, 120 rpm for a further 18 hours.

Cells were then harvested in 50 mL conical centrifuge tubes at 9,000 rpm for 20 mins and frozen in liquid N_2. Pellets were then stored at – 80 ^{o}C.

For purification cells were re-suspended in 100 mM HEPES buffer pH 8 containing 1 mM PLP with a volume of 2.5 mL of buffer per 1 g cell wet weight. Disruption was achieved by sonicating for 2 minutes, 1 second sonication 4 seconds pause at 40 % amplitude followed by a 2 minute pause. This was repeated 4 times and the vessel containing the cells was cooled on ice throughout.

The cell solution was then centrifuged at 9,500 rpm and passed through an amnicon 2 µg filter to remove cell membrane fractions.

Purification was carried out using an automatic AKTA system (GE lifesciences). A 1 mL His-Trap HP column (GE lifesciences) was pre-equilibrated with 50 mL of 100 mM HEPES buffer pH 8 containing 1 mM PLP and 10 mM imidazole. The soluble extract was then loaded on to the column and washed with 50 mL HEPES buffer pH 8 containing 0.1 mM PLP and 20 mM imidazole at a rate of 1 mL per minute. Finally, the protein was eluted with 25 mL HEPES buffer pH 8 containing 0.1 mM PLP and 300 mM imidazole at a rate of 0.5 mL per minute.

The protein was concentrated in a 30 kDa 50 mL centrifuge concentrator (amnicon) and desalted by passing through a PD 10 desalting column (GE lifesciences) using 10 mM HEPES pH 8 buffer containing 1 mM PLP as the desalting buffer.

Appendix B **Dixon plots and Cornish-Bowden plots for the different types of possible enzymatic inhibition**

Biocatalysis can be limited by enzymatic inhibition. This concept covers a number of different situations, which are summarised below:

- Competitive: the substrate and inhibitor both bind to the active site of the enzyme i.e. they 'compete' for access to the enzyme active site. The inhibitor therefore cannot bind at the same time as the substrate.
- Uncompetitive: the inhibitor binds to the enzyme-substrate complex.
- Mixed: the inhibitor can bind to either the free enzyme or the enzyme-substrate complex.

Figure A.2 shows model plots for competitive, uncompetitive and mixed inhibition. The top figures (a) and (b) show competitive inhibition: K_{ic} can be determined from the Dixon plot (a) and the lines of the Cornish-Bowden plot are parallel (b). The middle figures (c) and (d) show mixed inhibition, with K_{ic} able to be determined from where the lines cross on the Dixon plot (c) and K_{iu} from the Cornish-Bowden plot (d).[163] Finally, the case of uncompetitive inhibition, in the last two figures in the table (e) and (f). Here, the value of K_{iu} can be determined from the Cornish-Bowden plot (f) and the lines of the Dixon plot are completely parallel (e).[163] The NAD^+-reductase from *R. eutropha* has been shown to display competitive product inhibition.[164]

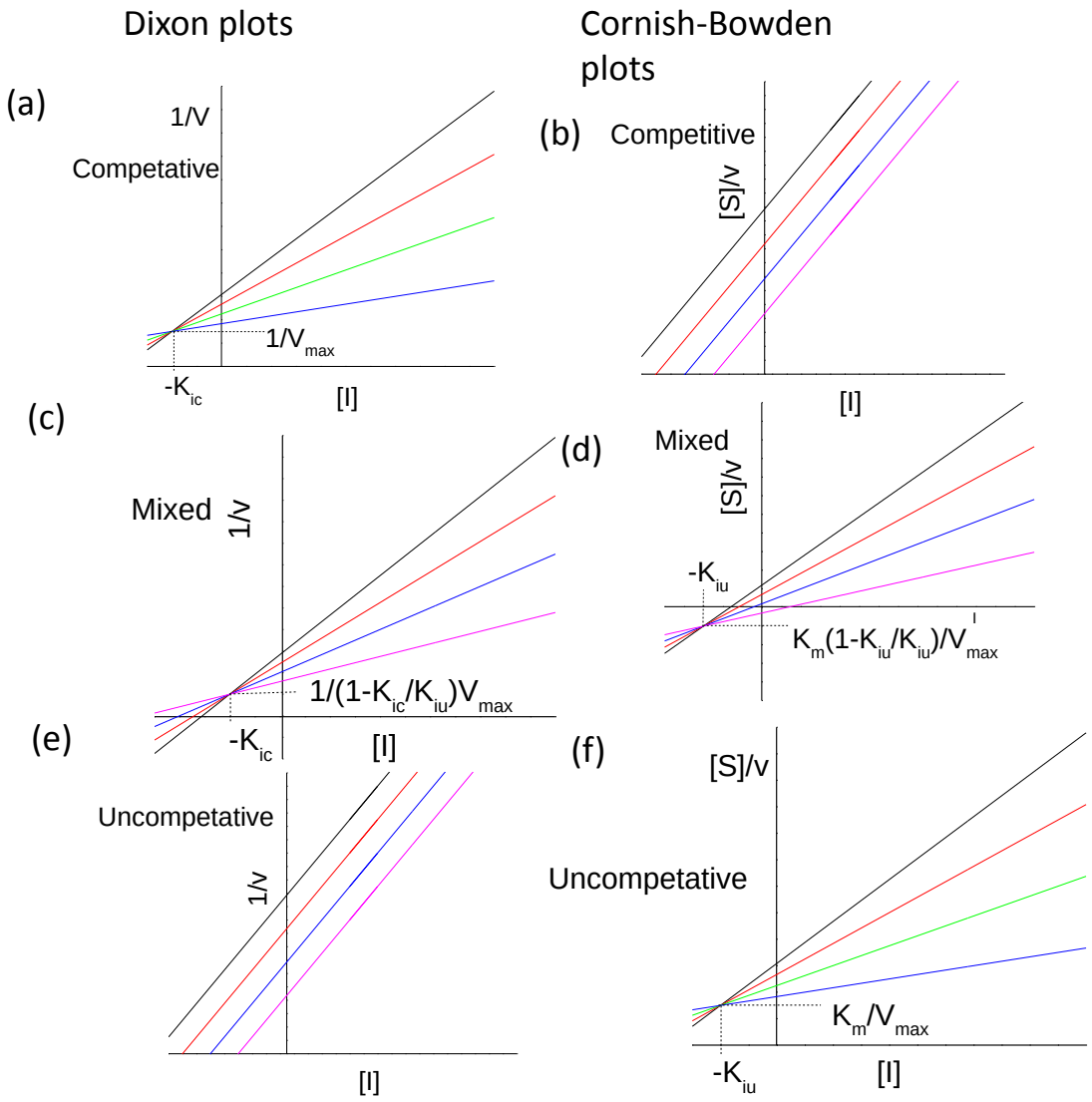

Figure A.2: Determination of competitive and uncompetitive inhibition constants. On the left hand side, figures a, c and e show Dixon plots, where 1/current is plotted against concentration of inhibitor. These can be used to determine the competitive inhibition constants. On right hand side, figures b, d, and f show Cornish-Bowden plots where inhibition concentration is plotted against substrate concentration over current. These graphs can be used to determine the uncompetitive inhibition constant. Adapted from Fundamentals of Enzyme Kinetics (A Cornish-Bowden).[163]

Appendix C **Calibration curves**

The following HPLC and GC calibration curves were used to determine the amount of product produce in the bio-catalytic reactions throughout this thesis.

HPLC calibration curves

The HPLC protocols used throughout this thesis are detailed in this section. In general, a new calibration curve was produced for every set of experiments and example calibration curves are shown in this section. All HPLC was conducted on a Shimadzu UFLC LC-20AD prominence liquid chromatograph.

C.1 N-phenyl maleimide to N-phenyl succinimide

The concentration of N-phenyl succinimide was analysed by HPLC using a Chromolith Performance 100-3 mm column (Merck) using the following procedure: Solvent A (acetonitrile), Solvent B (MilliQ® Water). Isocratic 80 % B, 20 % A for 7.5 minutes. Flow rate 1 mL min^{-1}.

The separation was monitored by measuring the absorbance at 210 nm.

Figure A.3 shows peaks at 1.3 minutes for N-phenyl succinimide (the product of the reaction) and at 2.4 minutes for N-phenyl maleimide (the substrate) at various concentrations.

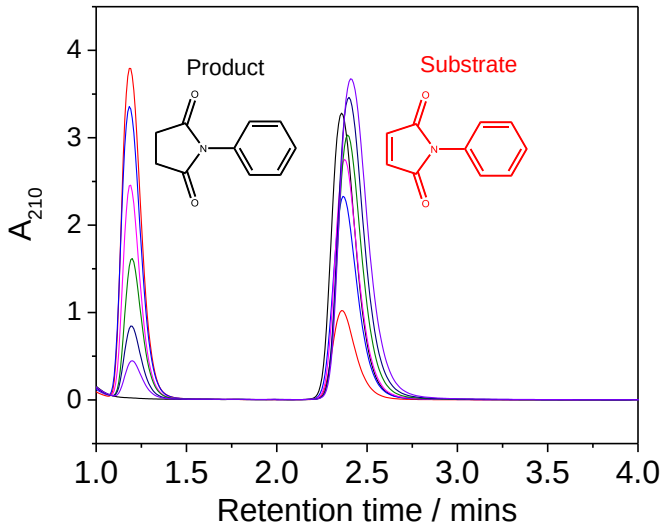

Figure A.3: HPLC trace showing the retention times for N-phenyl maleimide (2.4 mins) and N-phenyl succinimide (1.2 min). An 80 µL aliquot of reaction mixture was removed and diluted with 80 µL of acetonitrile and 200 µL of water. The sample was then centrifuged to remove any particles present and trace amounts of enzyme were removed using spin filter (life technologies, 3 kDa cut off). A 40 µL aliquot of sample was then injected into the HPLC for analysis. Absorbance at 210 nm was used to identify the peals. Samples of concentration 0.0, 0.5, 1.0, 2.0, 3.0, 4.0 mM N-phenyl succinimide from black to red are shown.

The data in Figure A.3 was used to produce the calibration curve in Figure A.4.

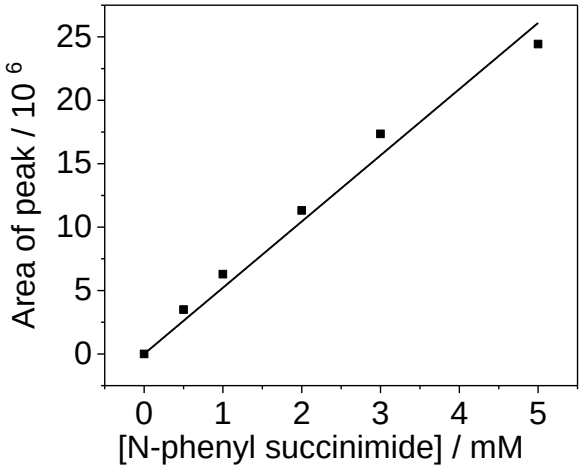

Figure A.4: Standards of N-phenyl succinimide against the area of the peaks observed in the 210 nm trace in the HPLC chromatogram. The R^2 value for this data is 0.99 and the gradient of the line is 5.22×10^6.

The data in Figure A.4 shows a plot of the concentration of N-phenyl succinimide in samples of known concentration against the area of the peak at 210 nm. This can be used to determine the concentration of product produced in a sample from a biotransformation.

C.2 Pyruvate to L-alanine conversion

Pyruvate and L-alanine were separated using a ZIC®-HILIC (150 × 2.1 mm, 5 µm, 200 Å) SeQuant® using the following procedure:

Solvent A (acetonitrile), Solvent B (MilliQ® Water). Starting conditions 95 % A, 5 % B, linear gradient over 20 minutes to 20 % A and 80 % B. At 20.1 minutes return to 95 % A, 5 % B for 9.9 minutes. Flow rate 0.75 mL min^{-1}.

Absorbance was measured at 210 nm and used to identify the peaks due to L-alanine and pyruvate.

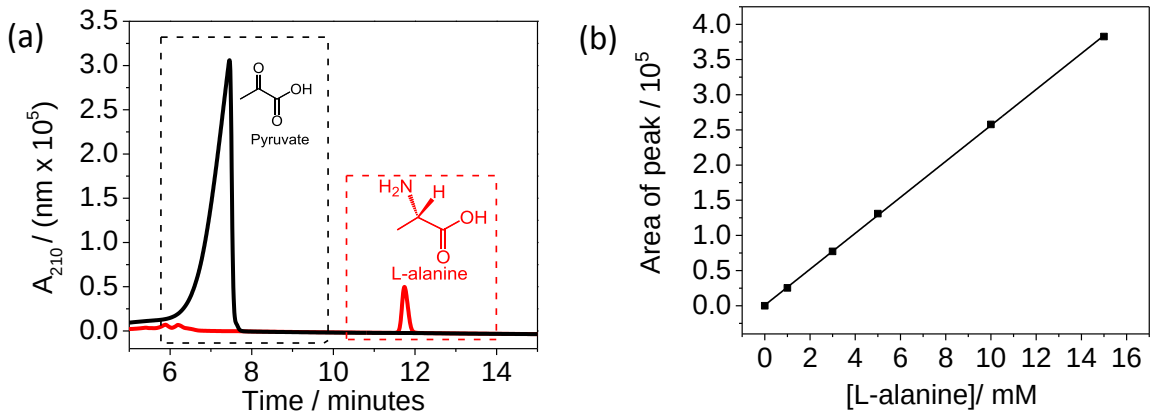

Figure A.5: (a) HPLC trace showing the retention times for pyruvate (7.45 min) and L-alanine (11.7 min). The L-alanine concentration of samples was measured by removing a 70 µL aliquot of the reaction mixture. This was then diluted 1:2 with 50 mM Tris-HCl buffer and then adding 14 µL of acetonitrile. Particles were removed from samples via centrifugation and trace amounts of enzyme were then removed using a spin filter (life technologies, 3 kDa cut off). A 40 µL aliquot of sample was then injected into the HPLC for analysis. The concentration was determined by monitoring the UV-visible absorbance at 210 nm. (b) The areas of the L-alanine peaks measured at

210 nm for the following concentrations of L-alanine: 0, 1, 3, 5, 10, 15 mM. A linear fit can be applied to this data, which gave an R^2 value of 0.998. This fit can be used to determine the concentration of L-alanine. The gradient of the line is 25554.

The retention times of pyruvate and L-alanine are around 7.45 minutes and 11.7 minutes respectively. Linear fits of the peaks for L-alanine gave an R^2 value of 0.999. The area of the L-alanine peak could therefore be used to determine the concentration of an unknown sample.

C.3 Acetophenone to phenylethanol conversion

The concentration of phenylethanol was analysed using HPLC using a Chiralpak IA column using the following procedure:

Solvent A (Heptane), Solvent B (Isopropanol). Isocratic 99 % A, 1 % B for 20 minutes.

Flow rate 1 mL min^{-1}

The trace in Figure A.6 shows a typical HPLC trace at 245 nm showing the retention times of acetophenone and phenylethanol. A number of samples of known concentration of phenylethanol were injected into the HPLC in order to produce a calibration curve, shown in Figure A.6 (b).

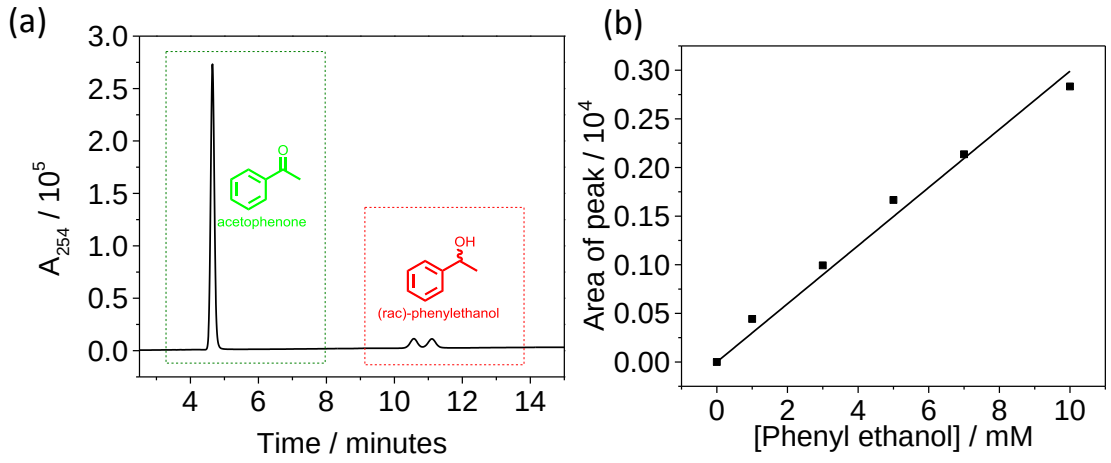

Figure A.6: (a) HPLC trace showing the retention times of acetophenone (4.6 mins) and phenylethanol (S) 10.6 mins, (R) 11.2 mins). Samples were prepared using the following method: A 500 µL aliquot of heptane was added to 500 µL of aqueous reaction mixture. The solutions were then vortexed to ensure efficient mixing and centrifuged to separate the organic and aqueous layers. The organic layer was then removed. A 10 µL aliquot of the organic layer was then injected into the HPLC for analysis. The absorbance of the solution flowing through the HPLC was analysed by monitoring the UV-visible absorbance at 254 nm (b) Concentration standards of phenylethanol. These were used to determine the concentration of samples of unknown concentration. This trace was constructed by plotting the concentration of known standards against the area of the phenylethanol peak at 254 nm. A liner fit of this data gave an R^2 value of 0.997 and a gradient of 29908.

Calibration curves were generally performed after each set of experiments. The calibration curve in Figure A.6 (b) can be used to calculate the concentration of unknown samples containing phenylethanol. The retention time for acetone is 5.0 minutes and for phenylethanol 10.6 minutes for the (S)-enantiomer and 11.2 minutes for the (R)-enantiomer. Due to changing retention times of phenylethanol a racemic standard was always run at the same time as analysis of experimental results.

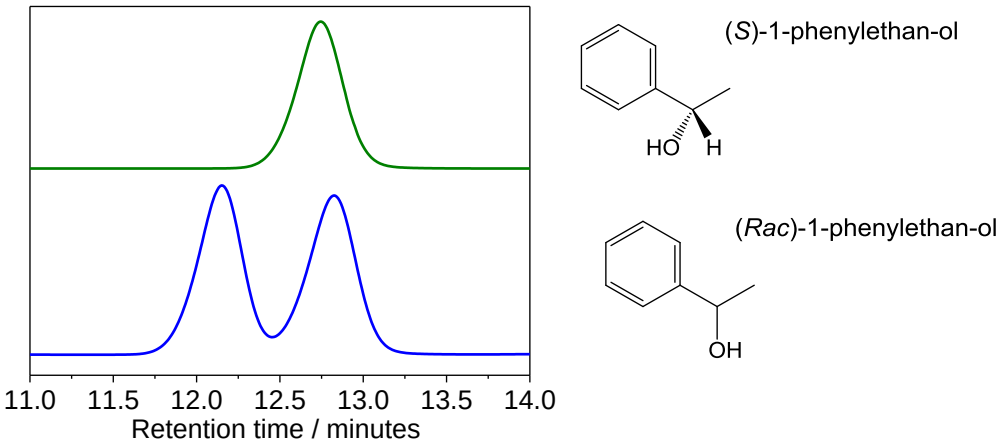

Figure A.7: The retention times of (S)-1-phenylethanol and racemic 1-phenylethanol.

Figure A.7 demonstrates that when chiral HPLC is carried out on the same day with racemic and (S)-phenylethanol the (S)- phenylethanol peak has a longer retention time than the (R)-peak.

GC calibration curves

The GC protocols used throughout this thesis are detailed in this section. In general, a new calibration curve was produced for each set of experiments and example calibration curves are shown in this section. All GC was conducted on a ThermoScientific Trace 1300 gas chromatograph equipped with an FID.

The protocols for each product analysed in this project using GC are given in Table A.0 3.

Table A.0-3: GC retention times to determine conversion and *ee*

Column[a]	Program[b]	Injector temperature/ °C	Helium carrier gas flow rate/ mL min^{-1}	Compound	Retention time (min)
A	Initial temp. 100 °C/hold time 2 min /slope 1 °C per min/temp 130 °C/ hold time 5 min/ slope 10 °C per min/temp. 160 °C/ hold time 10 min.	250	1.7	N-ethyl maleimide N-ethyl succinimide	13.3 22.8
B	Initial temp. 40 °C/hold time 2 min /slope 0.5 °C per min/temp 62 °C/ hold time 2 min/ slope 10 °C per min/temp. 160 °C/ hold time 3 min.	250	0.25	cyclohexenone cyclohexanone	28.2 32.9
B	Initial temp. 120 °C/hold time 5 min /slope 5 °C per min/temp 140 °C/ hold time 2 min/ slope 30 °C per min/temp. 220 °C/ hold time 2 min.	250	1.5	4-phenyl-2-butanone 1-methyl-3-phenylpropylamine	4.9 5.3
B[b]	Initial temp. 50 °C/hold time 2 min /slope 5 °C per min/temp 100 °C/ hold time 0 min/ slope 60 °C per min/temp. 220 °C/ hold time 2 min.	250	1.5	2-methyl cyclopentanone 2-methyl-2-cyclopentenone	5.7 8.2
A[c]	Initial temp. 30 °C/hold time 10 min /slope 0.1 °C per min/temp 35 °C/ hold time 10 min/ slope 0.1 °C per min/temp. 40 °C/ hold time 60 min/ slope 20 °C per min/temp. 160 °C/ hold time 5 min.	250	0.5	2-methyl cyclopentanone 2-methyl-2-cyclopentenone	153 120, 125

[a] **A**: CP-Chirasil Dex CB (25 m, 0.25 mm I.D., 0.25 µm film). **B**: DB 1701 column (50 m, 0.25 mm I.D., 0.33 µm film)
[b]Achiral method. [c]Chiral method.
Detector settings: 1= FID temperature 150 °C, Air flow 350 mL min^{-1}, Hydrogen flow 35 mL min^{-1}, Make-up gas (N_2) 40 mL min^{-1}

C.4 N-ethyl maleimide to N-ethyl succinimide

Figure A.8 shows a typical GC trace showing the retention times for N-ethyl succinimide and N-ethyl maleimide. By injecting samples of known concentration of N-ethyl succinimide and N-ethyl maleimide it is possible to produce a calibration curve, shown in Figure A.8 (b). Comparison of the areas of the N-ethyl succinimide peak to this standard curve was used to determine the concentration of N-ethyl succinimide in samples of unknown concentration.

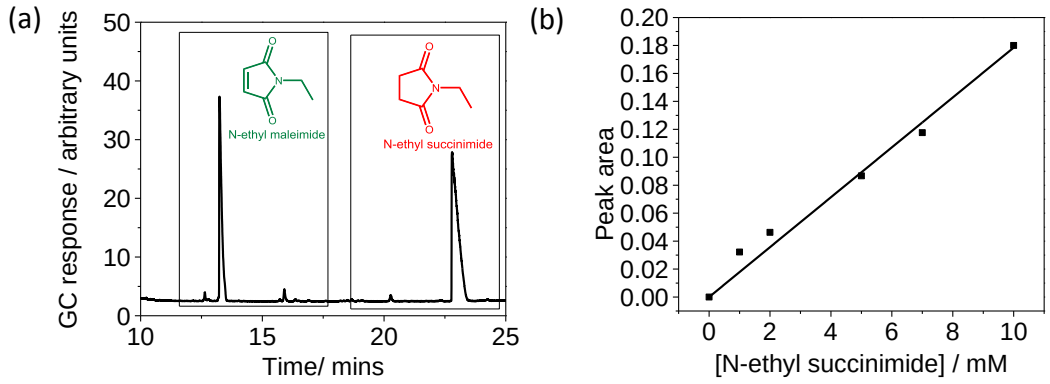

Figure A.8: (a) GC trace showing the retention times for N-ethyl maleimide (13.3 min) and N-ethyl succinimide (22.8 min). Samples were prepared using the following method: A 200 µL aliquot of ethyl acetate (containing 0.1 µL/mL phenyl butanone as an internal standard) was added to a 100 µL aliquot of reaction mixture. Extraction of the product was achieved by adding the ethyl acetate, vortexing to ensure efficient mixing, centrifuging, separating the layers, and then repeating the process several times to give a total volume of 400 µL of ethyl acetate. The collected ethyl acetate fractions were then dried using excess $MgSO_4$ and filtered through cotton wool. A 0.3 µL injection was used for GC analysis. (b) GC-FID response for different standard concentrations of N-ethyl succinimide (normalised against the area of the internal standard peak in each case). A linear fit was applied to this data with an R^2 value of 0.999 and a gradient of 0.0178. This trace was used to calculate the concentration of unknown samples of N-ethyl succinimide

C.5 Cyclohexenone to cyclohexanone

Figure A. shows a typical GC trace showing the retention times for cyclohexanone and cyclohexenone.

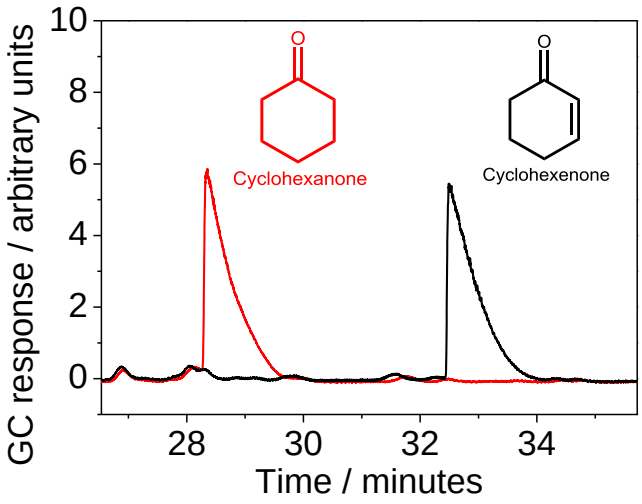

Figure A.9: (a) A GC trace showing the retention times for cyclohexenone (28.5 min) and cyclohexanone (32.8 min). Samples were prepared using the following method: A 100 µL aliquot of ethyl acetate (containing 0.1 µL/mL toluene as an internal standard) was added to a 15 µL aliquot of reaction mixture. Extraction of the product was achieved by adding the ethyl acetate, vortexing to ensure efficient mixing, centrifuging, separating the layers, and then repeating the process several times to give a total volume of 200 µL of ethyl acetate. The collected ethyl acetate fractions were then dried using excess $MgSO_4$ and filtered through cotton wool. A 0.3 µL injection was used for GC analysis.

The retention time for cyclohexenone is 28.5 minutes and that of cyclohexanone is 32.9 minutes. By injecting samples of known concentration it is possible to produce a calibration curve, shown in Figure A.10.

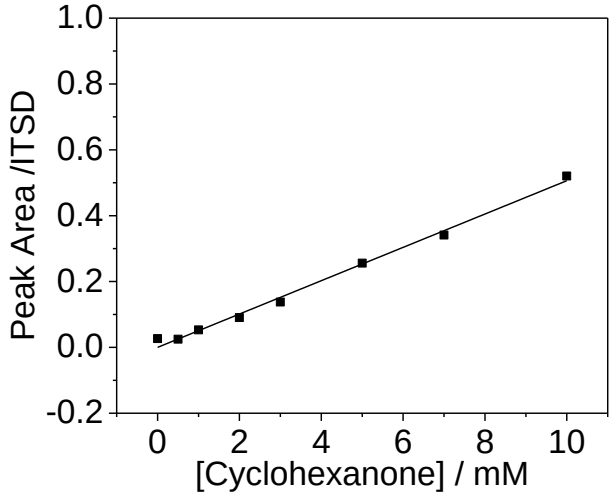

Figure A.10: GC-FID response for different standard concentrations of cyclohexanone (normalised against the area of the internal standard peak in each case). A linear fit was applied to this data with an R^2 value of 0.998 and a gradient of 0.05. This trace was used to calculate the concentration of unknown samples of cyclohexanone

The calibration curve shown in Figure A.10 was used to determine the concentration of cyclohexanone in an unknown sample.

C.6 4-phenyl-2-butanone to 1-methyl-3-phenylpropylamine

Figure A.11 was prepared by injecting samples of known concentration into the GC, the retention times for 4-phenyl-2-butanone and 1-methyl-3-phenylpropylamine are 4.9 and 5.3 minutes respectively.

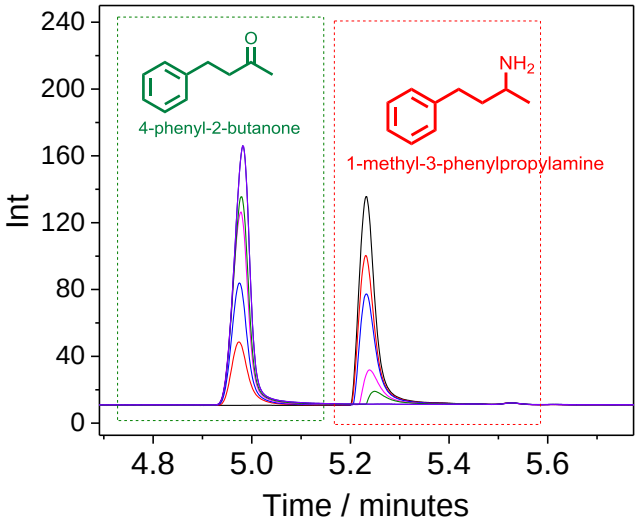

Figure A.11: GC trace showing the retention times for 4-phenyl-2-butanone (4.9 min) and 1-methyl-3-phenylpropylamine (5.3 min) The samples were prepared using the following procedure: A 100 µL sample of reaction mixture was basified by adding 30 µL of 10 N NaOH. A 100 µL aliquot of ethyl acetate (containing 0.1 µL/mL toluene as an internal standard) was added to the reaction mixture. Extraction of the product was achieved by adding the ethyl acetate, vortexing to ensure efficient mixing, centrifuging, separating the layers, and then repeating the process several times to give a total volume of 200 µL of ethyl acetate. The collected ethyl acetate fractions were then dried using excess $MgSO_4$ and filtered through cotton wool. A 1 µL injection was used for GC analysis. 1-methyl-3-phenylpropylamine samples of concentration 10.0, 7.0, 5.0, 2.0, 1.0, 0.5 and 0 mM (black to purple) and 4-phenyl-2-butanone samples of concentration 10.0, 9.5, 9.0, 8.0, 5.0, 3.0 and 0 mM (purple to black) are shown.

Using the peak areas from Figure A.11 is was possible to construct the calibration curves shown in Figure A.12.

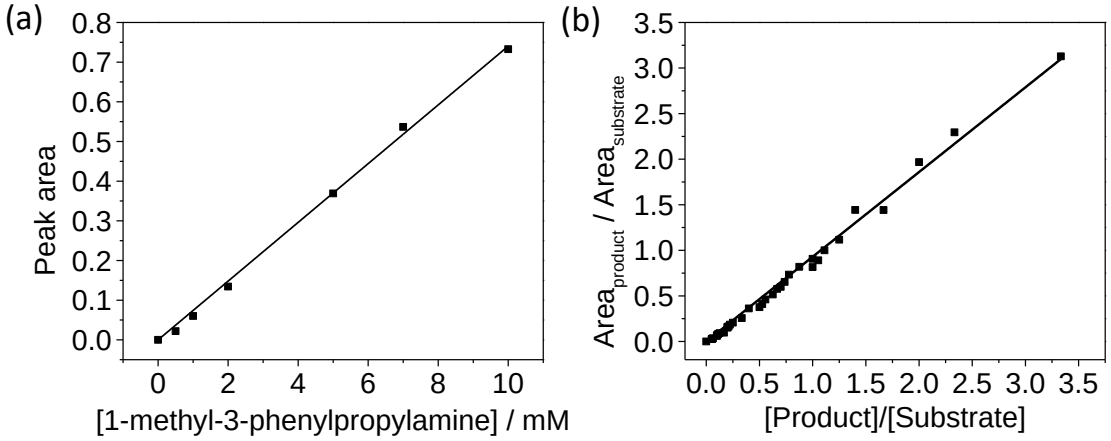

Figure A.12: (a) Standards of 1-methyl-3-phenylpropylamine against the area of the peaks observed in the FID trace in the GC chromatogram. A linear fit was applied to this data with an R^2 value of 0.999 and a gradient of 0.07403. This trace was used to calculate the concentration of unknown samples of 1-methyl-3-phenylpropylamine (b) A ratio of the area of substrate and product peaks, this graph was used to determine the percentage conversion of unknown samples. The linear fit applied to this data has a gradient of 0.929 and an R^2 value of 0.998

The calibration curve shown in Figure A.12 (a) was used to determine the concentration of 1-methyl-3-phenylpropylamine in an unknown sample. The plot of [1-methyl-3-phenylpropylamine] / [4-phenyl-2-butanone] *vs* the area of the peak for 1-methyl-3-phenylpropylamine / the area of the peak for 4-phenyl-2-butanone shown in Figure A.12 (b) was used to determine the percentage conversion.

C.7 2- methyl-2-cyclopentenone to 2-methyl cyclopentanone

Two methods were used to determine the concentration of 2-methyl cyclopentanone in unknown samples: Achiral GC (for routine analysis) and chiral GC (for samples in which the *ee* of the reaction was required).

Achiral GC

The retention times of 2-methyl cyclopentanone and 2-methyl-2-cyclopentenone (5.7 min) and (8.2 min) respectively are shown in Figure A.13.

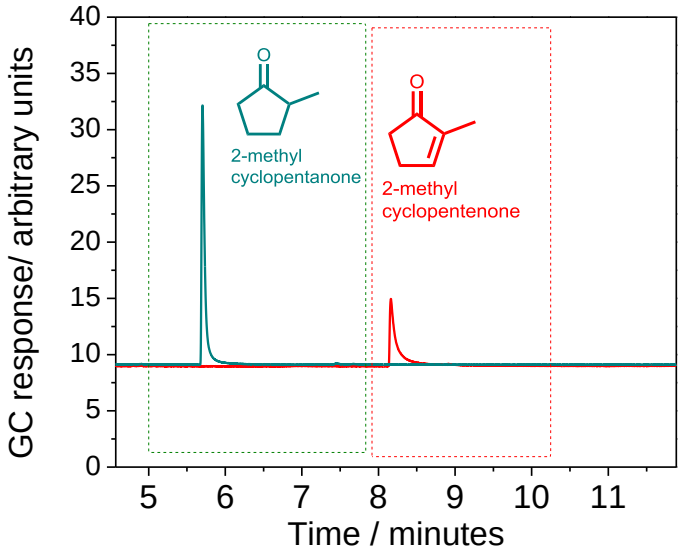

Figure A.13: (a) GC trace showing the retention times for 2-methyl cyclopentanone (5.7 min) and 2-methyl-2-cyclopentenone (8.2 min). Samples were prepared using the following method: A 100 µL aliquot of reaction mixture was extracted into 200 µL of ethyl acetate (containing 0.1 µL/mL toluene as an internal standard). Extraction of the product was achieved by adding the ethyl acetate, vortexing to ensure efficient mixing, centrifuging, separating the layers, and then repeating the process several times to give a total volume of 400 µL of ethyl acetate. The collected ethyl acetate fractions were then dried using excess $MgSO_4$ and filtered through cotton wool. A 1 µL injection was used for GC analysis.

By injecting samples of known concentration it was possible to produce the calibration curves shown in Figure A.14.

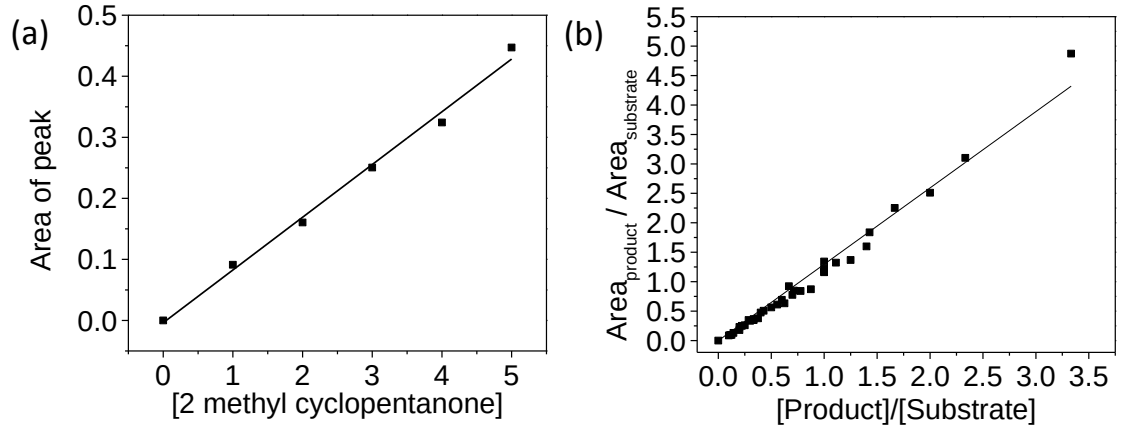

Figure A.14: (a) Injections of standards of known concentration of 2-methyl cyclopentanone against the area of the peaks observed in the FID trace (normalised by the internal standard). Concentrations of 0, 2, 5, 7, and 10 mM 2-methyl cyclopentanone were used. A linear fit was applied to this data with an R^2 value of 0.999 and a gradient of 0.0177. This trace was used to calculate the concentration of unknown samples of 2-methyl cyclopentanone (b) A ratio of the area of substrate and product peaks (corrected for the internal standard), this graph was used to determine the percentage conversion of unknown samples. The line of best fit displays an R^2 value of 0.98 and a gradient of 1.1.

The calibration curve shown in Figure A.14 (a) was used to determine the concentration of 2-methyl cyclopentanone in an unknown sample. The plot of [2-methyl cyclopentanone] / [2-methyl-2-cyclopentenone] *vs* the (area of the peak for 2-methyl cyclopentanone) / (the area of the peak for 2-methyl-2-cyclopentenone) shown in Figure A.14(b) was used to determine the percentage conversion. Fresh calibration curves were produced for each separate set of experiments.

Chiral GC

Where it was also desirable to obtained information about the *ee* of a particular sample, a GC method using a chiral column was used to allow determination of *ee* and the percentage conversion. An example trace is shown in Figure A.15.

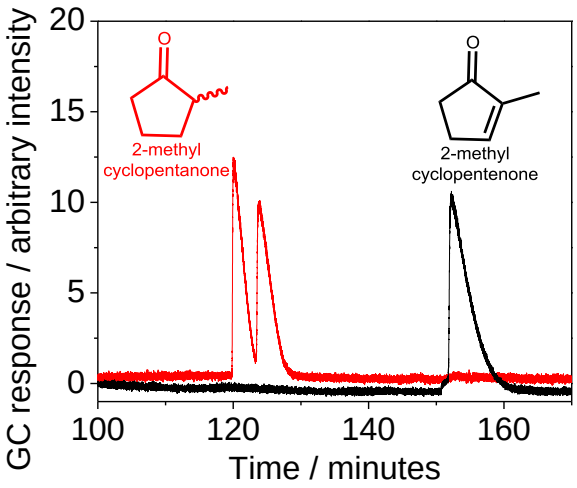

Figure A.15: (a) GC trace showing the retention times for 2-methyl-2-cyclopentenone (153 min) and 2-methyl cyclopentanone (120 and 125 mins). Samples were prepared using the following method: A 100 µL aliquot of reaction mixture was extracted into 200 µL of ethyl acetate (containing 0.1 µL/mL toluene as an internal standard). Extraction of the product was achieved by adding the ethyl acetate, vortexing to ensure efficient mixing, centrifuging, separating the layers, and then repeating the process several times to give a total volume of 400 µL of ethyl acetate. The collected ethyl acetate fractions were then dried using excess $MgSO_4$ and filtered through cotton wool. A 0.3 µL injection was used for GC analysis.

The retention time of 2-methyl cyclopentenone is 153 min and of 2-methyl cyclopentanone 120 min for the first enantiomer and 125 mins for the second enantiomer. An example of the calibration curve used to determine the concentration of 2-methyl-cyclopentanone is shown in Figure A.16.

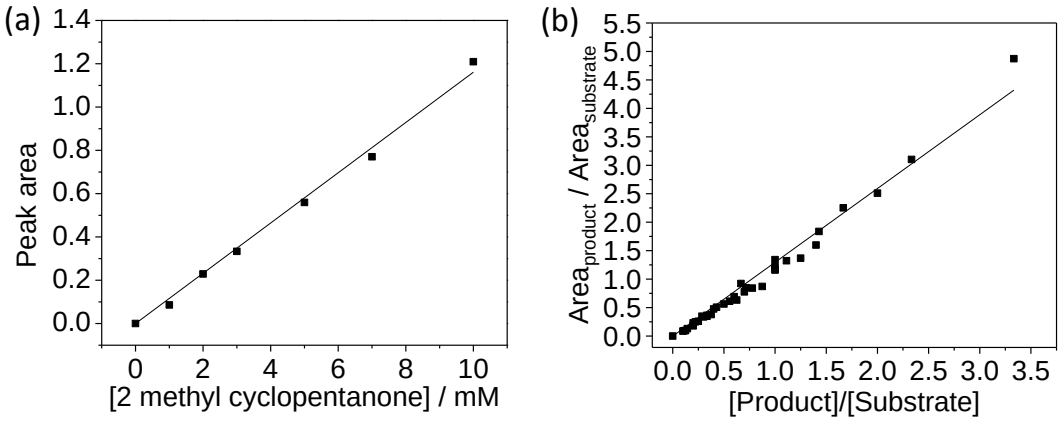

Figure A.16: (a) Standards of 2-methyl cyclopentanone against the area of the peaks observed in the FID trace divided by the internal standard in the GC chromatogram. A linear fit was applied to this data with an R^2 value of 0.999 and a gradient of 0.116. This trace was used to calculate the concentration of unknown samples of 2-methyl cyclopentanone (b) A ratio of the area of substrate and product peaks (corrected for the internal standard). A linear fit was applied to this data, which gave an R^2 value of 0.995 and a gradient of 1.296. This graph was used to determine the percentage conversion of unknown samples.

The calibration curve shown in Figure A.16 (a) was used to determine the concentration of 2-methyl cyclopentanone in an unknown sample. The calibration curve was produced using commercially available racemic samples of 2-methyl cyclopentanone, it was assumed that both enantiomer produce peaks of the same intensity. The plot of [2-methyl cyclopentanone] / [2-methyl-2-cyclopentenone] *vs* (the area of the peak for 2-methyl cyclopentanone) / (the area of the peak for 2-methyl-2-cyclopentenone) shown in Figure A.16 (b) was used to determine the percentage conversion.

Appendix D **Additional attempts at demonstrating the effect of having the *Vf ω-transaminase* immobilised on particles *versus* in solution**

At high L-alanine concentrations as shown in Figure A.17 (a) higher percentage conversions were obtained for samples with the *Vf-ω-transaminase* in solution. However, in Figure A.17 (b), where lower concentrations of L-alanine were used, higher conversions were observed at 5 mM L-alanine concentration when the *Vf-ω-transaminase* was immobilised. This supports the findings shown in Figure 3-20, which suggest that there is some beneficial effect to having the *Vf-ω-transaminase* immobilised when low concentrations of L-alanine are used.

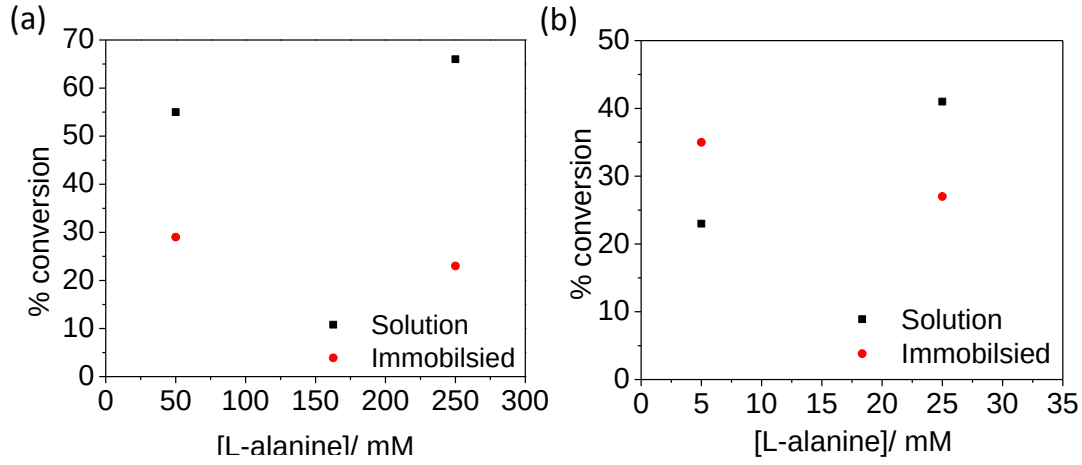

Figure A.17: Graphs comparing the percentage conversion obtained for experiments run in parallel with the *Vf ω-transaminase* enzyme both immobilised (red) and in solution (black). Graphs (a) and (b) were conducted on different occasions. In (a) the concentration of L-alanine was varied from 250 mM to 50 mM and in (b) from 25 mM to 5 mM.

Particles were made with 140 µg Hyd 2, 51 µg Hox~~H~~Y~~F~~U (*R. eutropha)*, 13 µL L-alanine dehydrogenase, 1.8 mg BP 2000 particles; these were then divided into two equal portions and 9 mg of *Vf ω-transaminase* was added to one aliquot. The particles were then left at 4 ^{o}C for one hour, washed twice, and each aliquot was further split into 2 equal aliquots respectively. A 100 µL portion of reaction mixture made of 100 mM Tris-HCl pH 8, containing 1 mM NAD^{+}, 10 mM 4-phenyl-2-butanone, 0.5 mM PLP, 150 mM NH_4Cl was added to each tube. Finally 4.5 mg of *ω-transaminase* was added to each of the tubes containing particles which had not had *ω-transaminase* initially immobilised on them. Reactions were carried out at 22 ^{o}C, under 2 bar H_2-pressure overnight (*ca.* 16 hours).

Appendix E : **Effect of L-alanine on NAD^+ reduction activity**

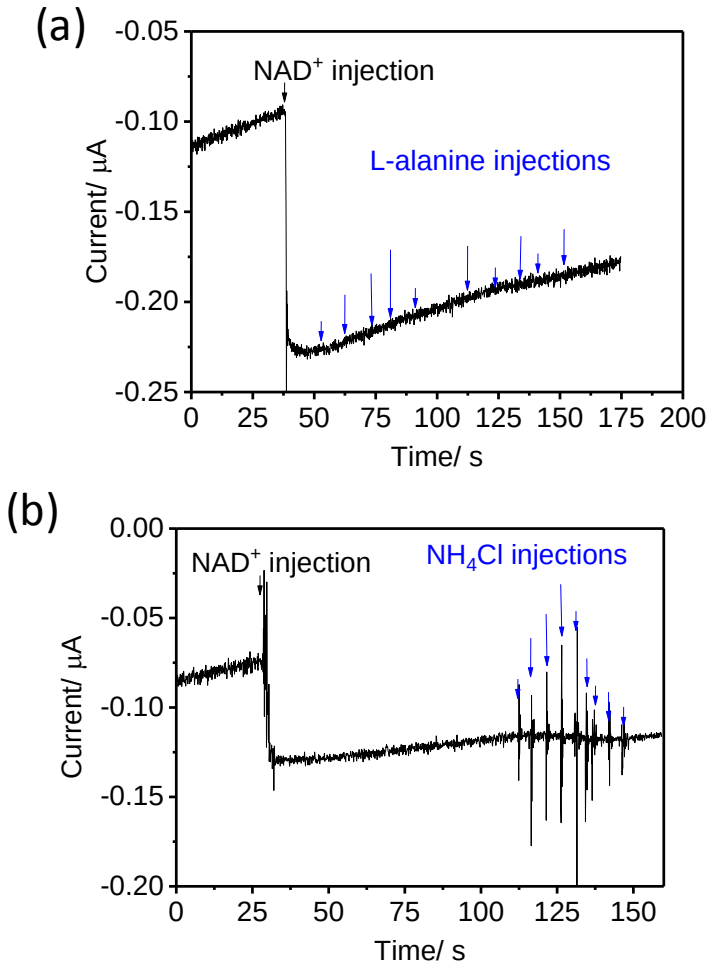

Figure A.18: Inhibition plots for an *R. eutropha* Hox~~HY~~FU functionalised electrode. The electrode was rotated at 2000 rpm and held at a potential of -380 mV *vs* SHE. (a) An aliquot of NAD^+ was injected into the electrochemical cell solution to give a final concentration of 666 µM NAD^+. This was followed by sequential aliquots of L-alanine, shown by each of the blue arrows the concentration was 1.6, 3.3, 5, 6.6, 8.3, 10, 11.7, 13.3, 15, 16.7 mM. (b) A 132µM aliquot of NAD^+ was injected into the electrochemical cell solution. This was followed by sequential aliquots of NH_4Cl, shown by each of the blue arrows the concentration was 1.6, 3.3, 5, 6.6, 8.3, 10, 11.7, 13.3, 15, 16.7 mM.

The scans in Figure A.18 show experiments in which a PGE RDE was modified with *R. eutropha* Hox~~HY~~FU. An aliquot of NAD^+ was then added to the solution resulting in an increase in catalytic current. Subsequently, aliquots of NH_4Cl or L-alanine were added to the electrochemical cell, indicated by the blue arrows. As the catalytic current

remains constant in the chronoamperometry traces in Figure A.18, this demonstrate that below concentrations of 16.7 mM the *R. eutropha* Hox~~HY~~FU is not inhibited by either NH_4Cl or L-alanine.

Appendix F **Establishing the *ee* of 1-methyl-3-phenylpropylamine prepared by the *Vf* *ω-transaminase* by ^{1}H NMR spectroscopy**

The *ee* for the 1-methyl-3-phenylpropylamine was determined using NMR spectroscopy in combination with a chiral shift reagent (chiral solvating agent) ((S)-(+)-O-acetylmandelic acid), in a modification of the method of Parker.[180] This allows rapid determination of the *ee* of a number of chiral amine molecules.

The ^{1}H NMR spectrum of (rac)-1-methyl-3-phenylpropylamine gives a doublet between 0.9 and 1.20 ppm. Addition of the (S)-(+)-O-acetylmandelic acid shift reagent splits this doublet into two doublets. In a fully racemic sample (*ee* = 0), these doublets have the same integration, see Figure A.19.

Following a reaction with *Vf*-ω-transaminase, the analyte solution was first basified by addition of 10 M NaOH (30 µL/mL). A 300 µL aliquot of $C^{2}HCl_3$ (containing a TMS standard) was then added to the reaction solution, followed by agitation by vortex mixing, and centrifugation to rapidly separate the aqueous and organic fractions. The layer of $C^{2}HCl_3$ was then removed and the extraction procedure repeated twice more. The combined organic fractions were dried over $MgSO_4$ and analysed by ^{1}H NMR spectroscopy on a Brücker 400 MHz instrument. Finally an aliquot of (S)-(+)-O-acetylmandelic acid was added (such that the concentration of (S)-(+)-O-acetylmandelic acid in the tube was 7.13 mM), and the NMR spectrum was re-acquired. Characteristic doublets were obtained at 1.03 ppm and 1.05 ppm with the ^{1}H NMR spectra being referenced to the signal from the protonated solvent, $C\underline{H}Cl_3$ (δ = 7.26 ppm).

The peaks were assigned based on the known (S)-selectivity of the *Vf ω-transaminase* which is widely described in the literature both for 1-methyl-3-phenylpropylamine and a range of other chiral amines products,[136] based on the assumption that using the

enzyme modified particles as part of an L-alanine recycling system would not lead to a complete change in enantioselectivity of this enzyme.

Consequently, the peak at 1.03 ppm was tentatively assigned to the (S)-enantiomer. Additionally, Parker *et al.* suggest that it is possible to "assign the absolute configuration (of a molecule) within a related series of compounds,"[318] using this method of *ee* determination. It has been shown that the shift of the methyl group of (S)-2-phenylethylamine complexed with (S)-(+)-O-acetylmandelic acid would be found at lower ppm values than the methyl group of (R)-2-phenylethylamine.[180,318,319] This therefore, provides further support for assigning the peak at 1.03 ppm for 1-methyl-3-phenylpropylamine to the (S) enantiomer.

The larger doublet at 1.03 ppm demonstrates that the *Vf ω-transaminase* gives a high *ee*. However, it is difficult to determine this precisely.

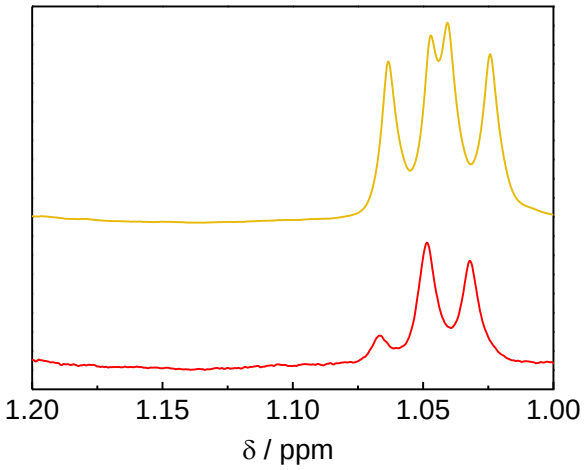

Figure A.19: Red trace shows the spectrum of sample produced by the *Vf ω-transaminase* system extracted into C^2HCl_3 by basifying the reaction mixture with 30 µL 10 N NaOH, adding 300 µL C^2HCl_3 to the reaction mixture, vortexing and then centrifuging down and removing the bottom layer. This procedure was repeated twice. A 7.13 mM aliquot of (S)-(+)-O-acetylmandelic acid was then added before the NMR spectrum was obtained. The spectrum in yellow shows a racemic sample of 1-methyl-3-phenylpropylamine in C^2HCl_3 with 7.13 mM (S)-(+)-O-acetylmandelic acid.

Deconvolution of the 1-methyl-3-phenylpropylamine sample from the *Vf-ω-transaminase*

This deconvolution was performed by Dr Jack Rowbotham (Post-Doc in the Vincent group)

The deconvolution is shown in Figure A.20.

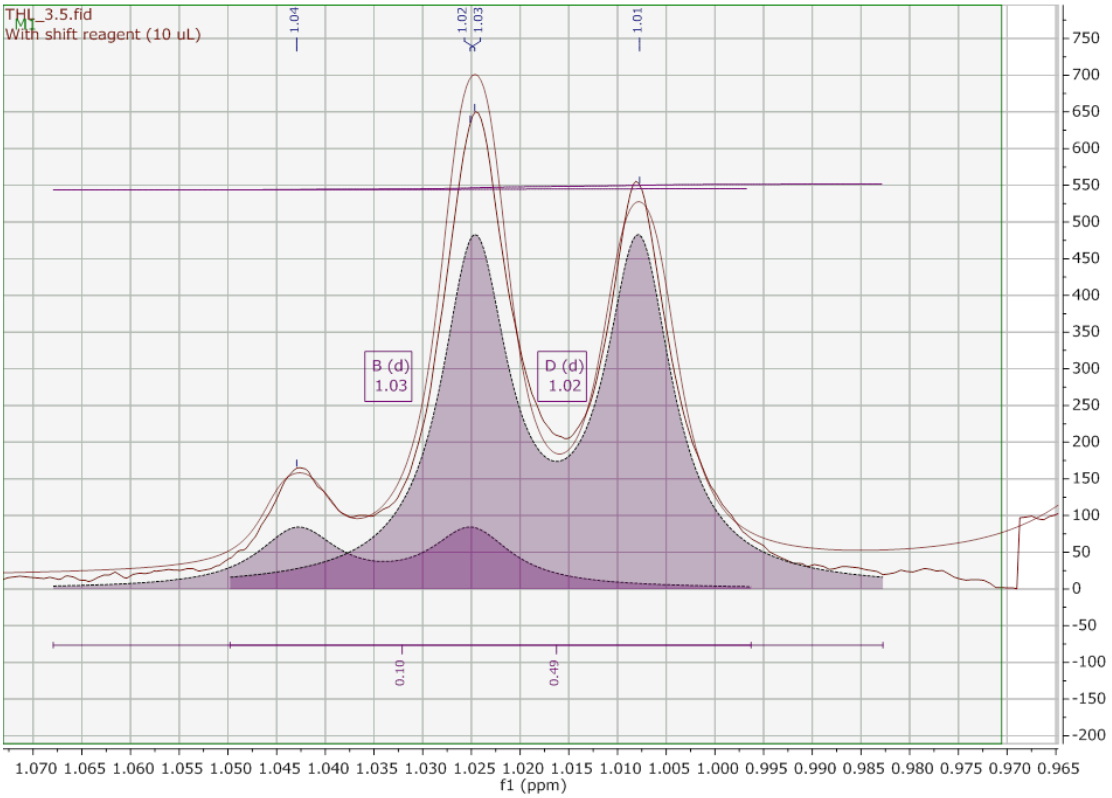

Figure A.20: Deconvolution of peaks in the doublet used to calculate the respective area of each of the peaks.

Firstly, a standard baseline correction was applied across the spectral region of interest. The peak intended for deconvolution was then fitted as an overlapping pair of doublets (both with J = 6.9 Hz), assuming Lorentzian line-shapes. Optimisation of the fitted curves was achieved by adjusting their intensities to minimise the residual peak area following subtraction of the original experimental trace. The enantiomeric excess (*ee*) was subsequently determined from the ratio of the integrated areas of the two doublets. The graph in Figure A.20 shows that it is possible to mathematically separate the two peaks for each of the enantiomers of 1-methyl-3-phenylpropylamine. Hence, the two signals were found to have an area ratio of 10:49, which equates to an *ee* of 66 % for the 1-methyl-3-phenylpropylamine product.

Appendix G **: Maleimide hydrolysis**

Paul *et al*. have used both phenyl and ethyl maleimides as substrates for ene-reductases in their work with artificial cofactors. It is known that both of these substrates undergo hydrolysis, shown in Figure A.21.[66,263] Recent unpublished work by Okamoto *et al*. has demonstrated that hydrolysis of the N-phenyl maleimide represents a significant competing reaction under aqueous conditions.

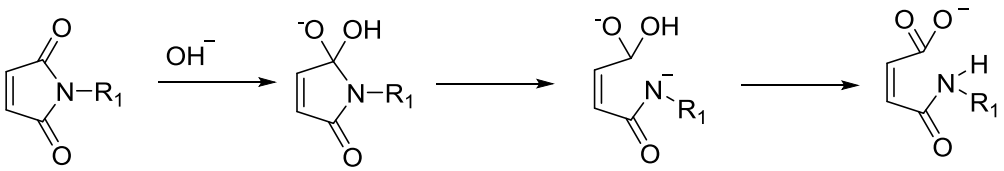

R_1 = Phenyl (N-phenyl maleimide)
R_1 = H (Maleimide)
R_1 = Ethyl (N-ethyl maleimide)

Figure A.21: The mechanism of hydrolysis of maleimide substrates in alkaline media, with addition of HO^- to the carbonyl (usually the rate determining step) and subsequent formation of a tetrahedral intermediate.[278]

These experiments were performed with the assistance of Dr Jack Rowbotham (Post-Doc in the Vincent group)

Machida et al. have demonstrated that in phosphate buffer at pH 7 the half-life of N-ethyl maleimide is 25×10^{-2} min, one order of magnitude greater than that of phenyl maleimide at 1×10^{-2} min.[278] The rate of hydrolysis of maleimide derivatives has been demonstrated to be faster under basic conditions, though the phenyl-derivative is still the most rapidly hydrolysed. Due to the limited amounts of HoxFU/HoxHYFU enzyme available in the laboratory it was essential to work on small scales and to run reactions for extended periods. Therefore it was necessary to find a substrate that does not evaporate significantly on the timescale of the reaction and which does not hydrolyse.

To investigate the rate of hydrolysis of Maleimide, N-ethyl maleimide and N-phenyl maleimide in Tris-HCl buffer at pD 8.1 an NMR study was carried out.

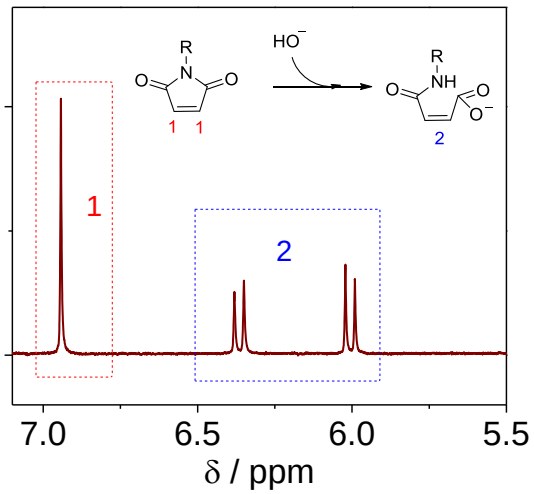

Figure A.22: A ^{1}H NMR spectrum (400 MHz) of N-phenyl maleimide after *ca.* 8 hours in deuteriated 50 mM Tris-HCl buffer pD 8.1. This spectrum demonstrates that during the course of the hydrolysis reaction the peaks due to the protons on the maleimide C=C bond (labelled 1) shift downfield in the hydrolysed product (peaks labelled 2). This means by integrating the areas of the peaks it is possible to obtain a percentage conversion for the amount of hydrolysed product.

Figure A.22 demonstrates that it is possible to calculate the extent of hydrolysis by monitoring the increase in the intensity of the two doublets between 6.0 and 6.5 ppm relative to the doublet at around 7.0 ppm (which represents the protons on the non-hydrolysed maleimide ring).

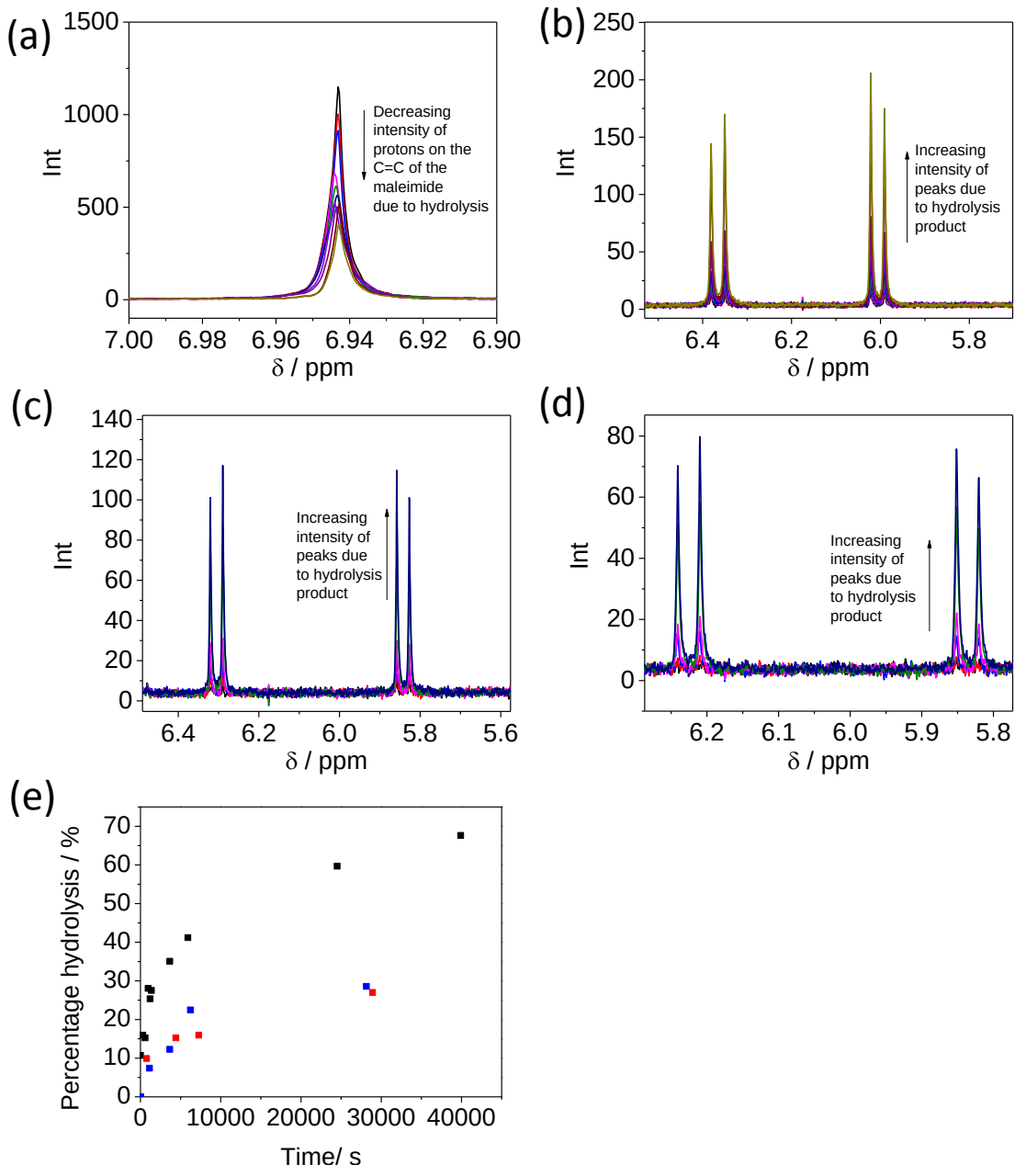

Figure A.23: ^{1}H NMR spectra showing maleimide hydrolysis. (a) The peak at around 6.9 ppm corresponding to N-phenyl maleimide decreasing in intensity as a function of time due to hydrolysis of the maleimide ring. (b) The peaks between 6.0 and 6.5 ppm corresponding to N-phenyl maleimide increasing as a function of time due to the increased concentration of hydrolysis product. (c) The peaks between 6.4 ppm and 5.8 ppm corresponding to maleimide increasing as a function of time due to the increased concentration of hydrolysis product. (d) The peaks between 6.3 ppm and 5.8 ppm corresponding to N-ethyl maleimide increasing as a function of time due to the increased concentration of hydrolysis product. All reactions were carried out in 50 mM deuteriated Tris-HCl pH 8.1 with 10 mM of the relevant maleimide and 5 vol. % DMSO. (e) The percentage hydrolysis for each of the maleimide substrates as a function of time, black: N-phenyl maleimide, blue: maleimide, red: N-ethyl maleimide.

Figure A.23 (a) to (d) shows the spectra used to determine the percentage hydrolysis of each of the maleimide derivatives. The graph in Figure A.23 (e) demonstrates the

percentage hydrolysis observed for each of the derivatives. It is clear to see that the N-phenyl maleimide shows the highest degree of hydrolysis under these conditions, with approximately 70 % being hydrolysed after 11 hours. In contrast the rate of hydrolysis for N-ethyl maleimide is much lower with only about 30 % being hydrolysed after 8 hours. Maleimide shows a similar rate, albeit slightly higher rate of hydrolysis to N-ethyl maleimide.

Appendix H : **Analysis of cofactors using LC-MS**

The following liquid chromatography-mass spectrometry (LC-MS) program and settings were used in this thesis to determine the product from direct reduction of mAC^+ at the surface of the carbon particles functionalised with Hyd 2, but without NAD^+-reductase.

The mass spectrometer used was a Waters LCT Premier XE equipped with an electrospray interface. The LC consists of a Waters Acquity Binary solvent manager, a PAL CTC Autosampler, and Waters Acquity Column oven. The software is Masslynx 4.1 (with openlynx open access)

A sample (5 μL) was injected onto the system. The column was a 2.1 × 50 mm (3 μm) ACE equivalence C18.

A flow rate of 0.4 mL min^{-1} was used. A gradient LC program was employed with solvent A (acetonitrile) and solvent B (MilliQ water with 0.1 % formic acid). Starting concentrations of 5 % A and 95 % B were maintained for 1 minute. The concentration of solvent A was then linearly increased to 100 % over 6 minutes, where it was held for 1 minute before returning to the starting conditions (5 % A, 95 % B) and held for 2 minutes.

Appendix I : **NMR experiments to confirm conversion of pyruvate to L-alanine**

In chapter 3 (Figure 3-6) particular regions of the ^{1}H NMR spectra are presented. The full NMR spectra used to produce each of these figures is presented below for reference. The residual signal of the proton on the solvent $^{2}H_2O$ ($^{2}H\underline{H}O$, δ = 4.79 ppm) was used as a reference.

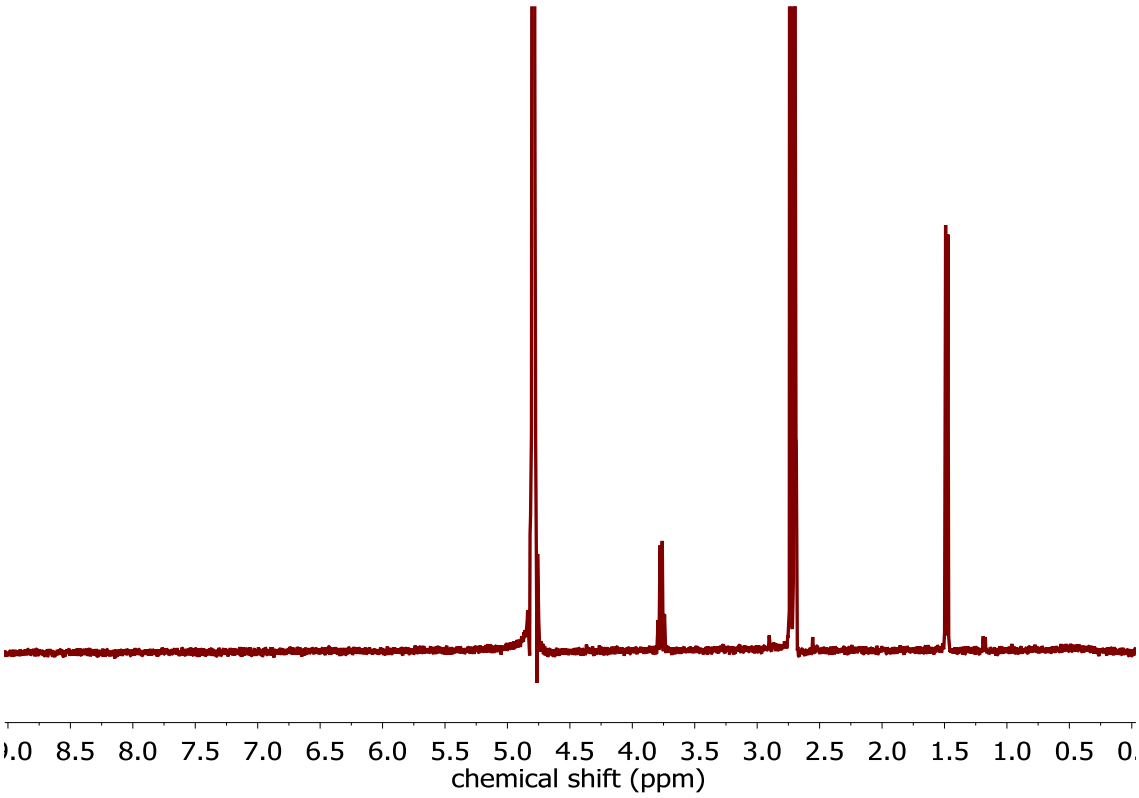

Figure A.24: Full NMR spectra of L-alanine in deuteriated phosphate buffer pH 8 corresponding to Figure 3-6 (a). The peaks at 1.4 ppm and 3.7 ppm are due to L-alanine the spectra of which has already been reported in the literature.[320,321]

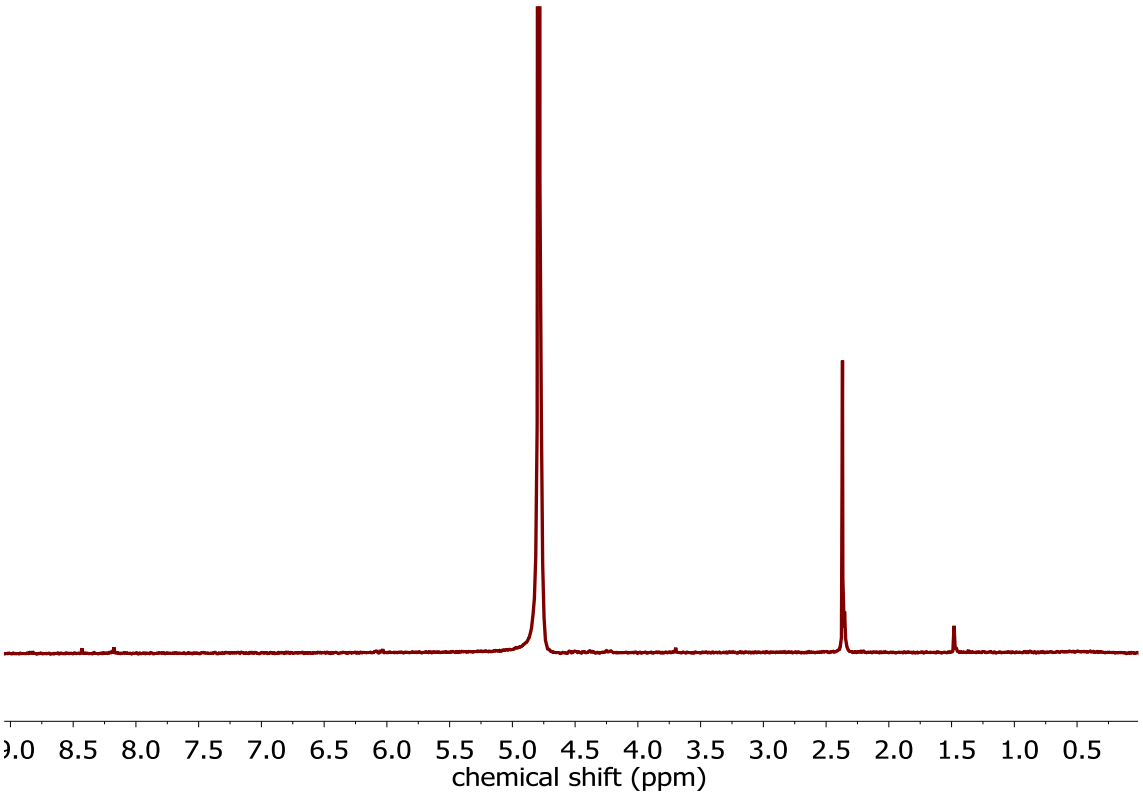

Figure A.25: Full NMR spectra of pyruvate in deuteriated phosphate buffer pH 8.0 corresponding to Figure 3-6 (b)

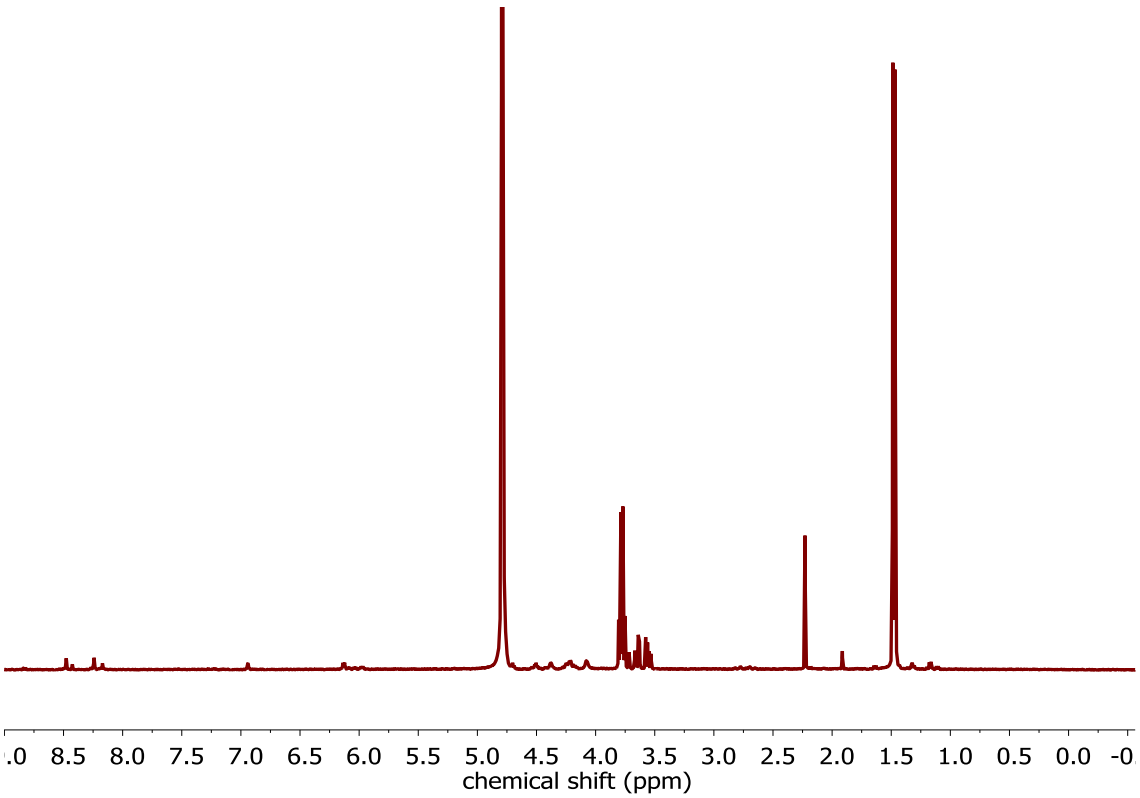

Figure A.26: Full NMR spectra of the L-alanine sample produced using the enzyme-modified particles corresponding to Figure 3-6 (c)

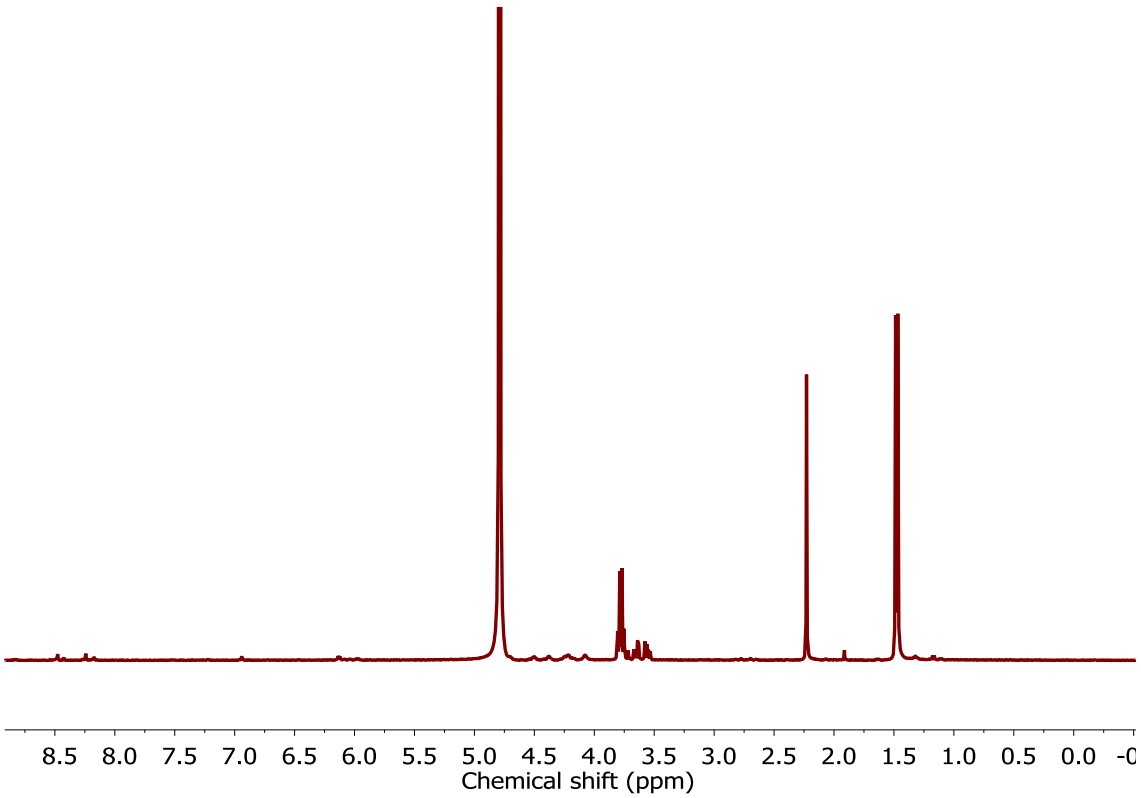

Figure A.27: Full NMR spectra the L-alanine sample produced using the enzyme-modified particles spiked with a further aliquot of acetone corresponding to Figure 3-6 (d)

Appendix J **:NMR spectroscopic analysis of deuteriated chemicals**

In chapter 7 particular regions of the NMR spectra are presented throughout the chapter. The full NMR spectra used to produce each of these figures is presented below for reference. Samples for NMR spectroscopy were contained in Norell® SelectSeries™ 5 mm 400 MHz sample tubes, with data being collected at 293 ± 2 K on a Bruker AVIIIHD 400 nanobay instrument (equipped with a 5 mm z-gradient broadband multinuclear probe). Generally, ^{1}H spectra (obtained at 400.17 MHz) were acquired across an 8000 Hz range using a standard zg30 pulse sequence (14 μs, 30˚ pulse) with an acquisition time of 4.0 s and a relaxation delay of 1.0 s. In the first instance, 8 scans were recorded, with the number of transients being increasing to 64 when an improved signal to noise ratio was required. ^{1}H-^{1}H COSY experiments were also performed under similar conditions, with the spectral width in both dimensions varying as necessary. For samples dissolved in C^{2}HCl3, the residual signal of the proton on C$\underline{H}$Cl$_3$ (δ = 7.26 ppm) was used as a reference, and in D_2O a small amount of acetone (C$\underline{H}_6$O, δ = 2.22 ppm) was used instead.

J.1 Standards

The section contains the full spectra of a number of standards used throughout Chapter 7.

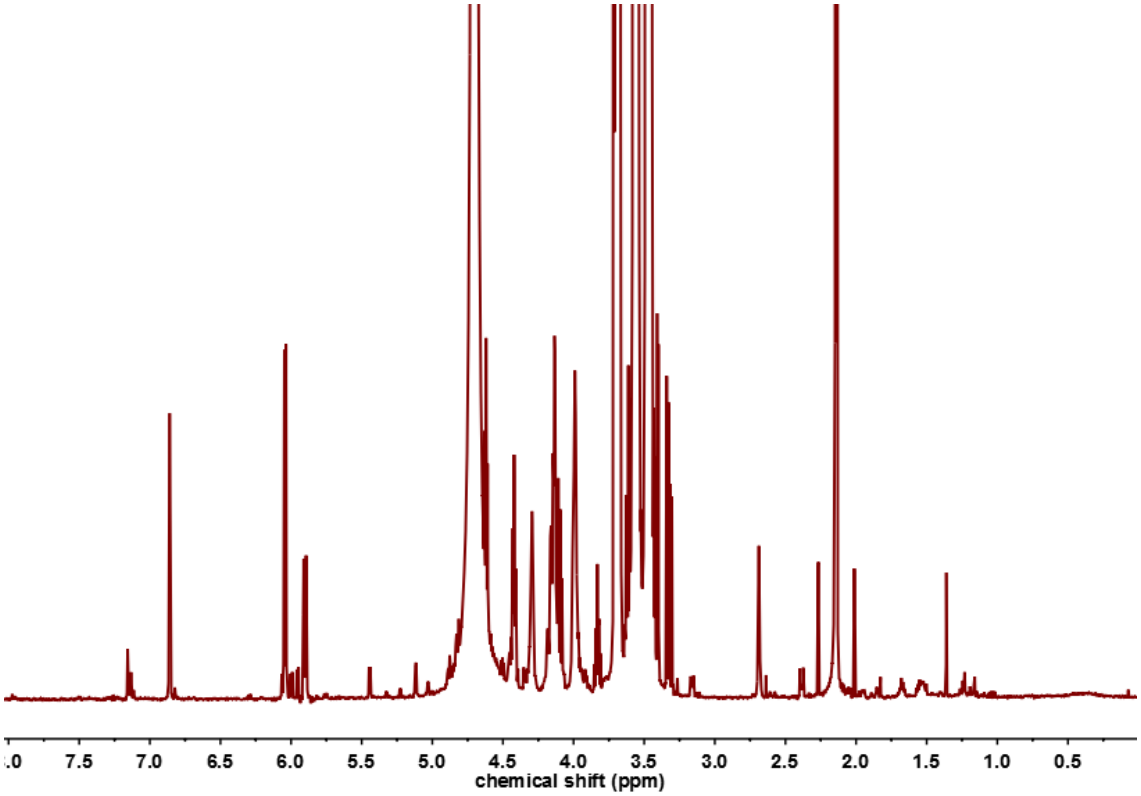

Figure A.28: Full NMR spectra of [4S-^{2}H]NADH in $^{2}H_2O$ corresponding to Figure 7.6 (b) in main text.

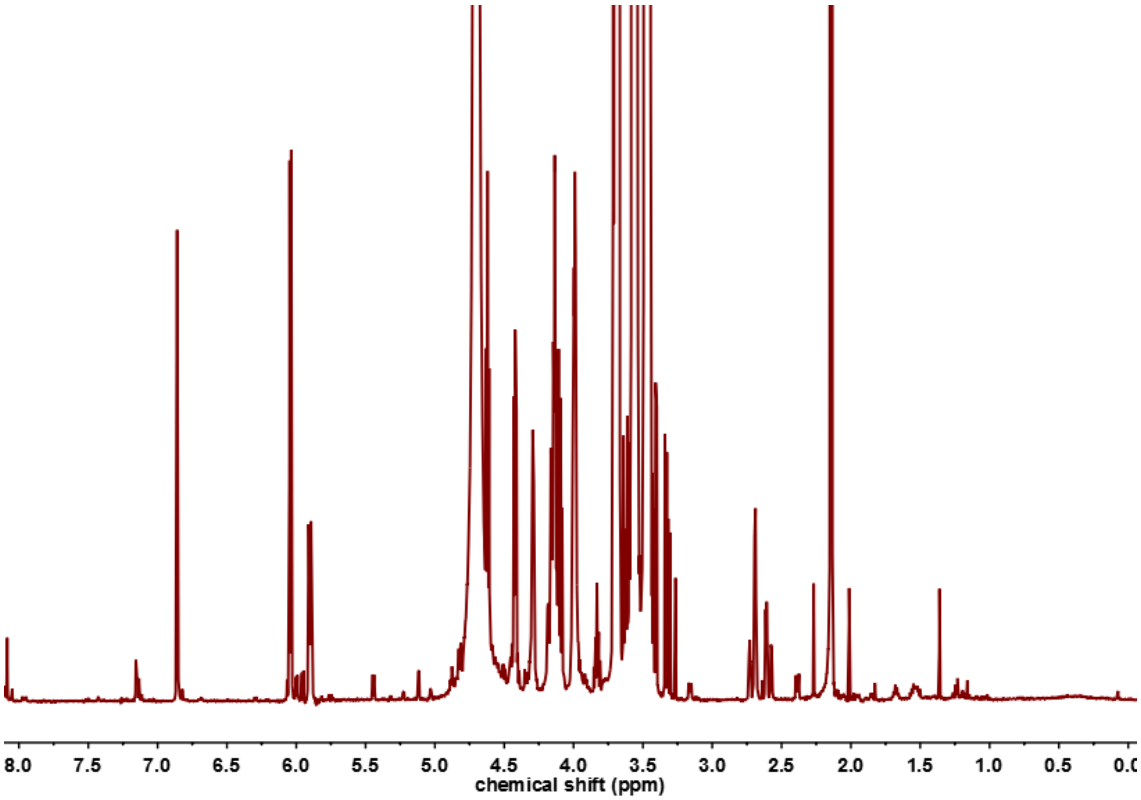

Figure A.29: Full NMR spectra of [4S-^{2}H]NADH spiked with commercially available non-deuteriated [4-2H]NADH in $^{2}H_2O$ corresponding to Figure 7.6 (c) in main text

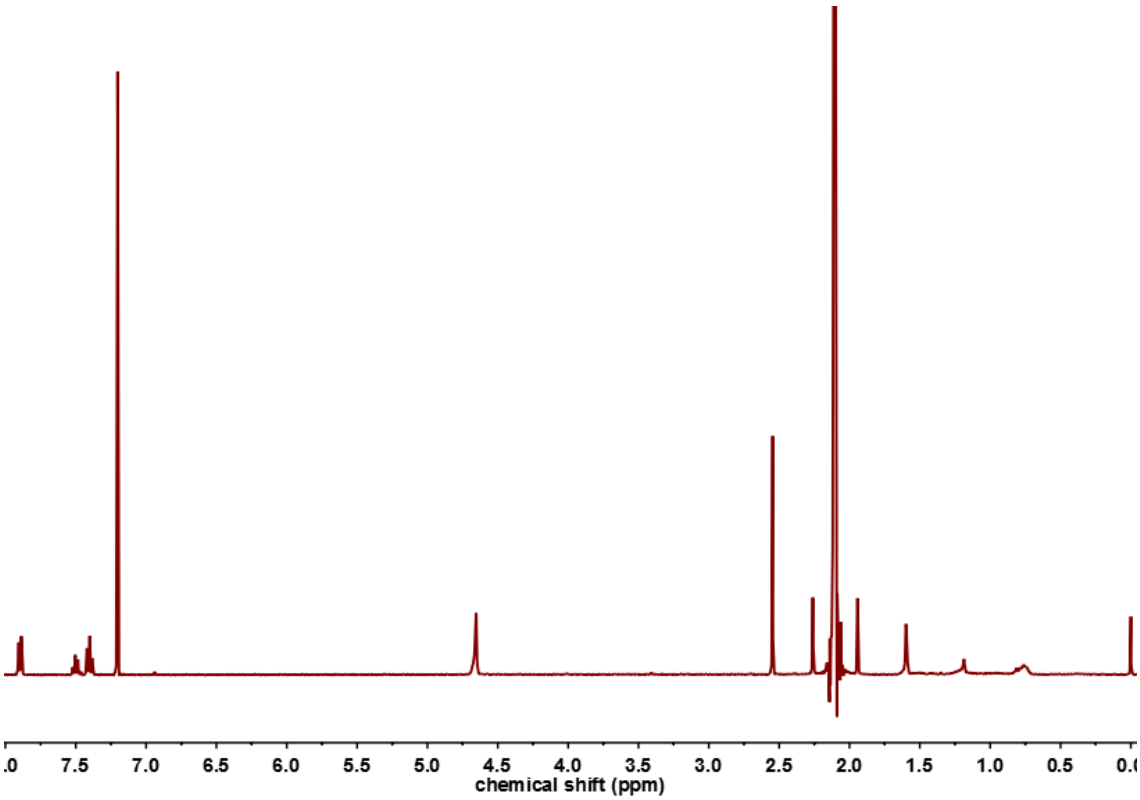

Figure A.30: Acetophenone in C^2HCl_3. The peak at ca. 4.7 ppm corresponds to water in the solvent and the peak at ca. 2.1 ppm corresponds to acetone.

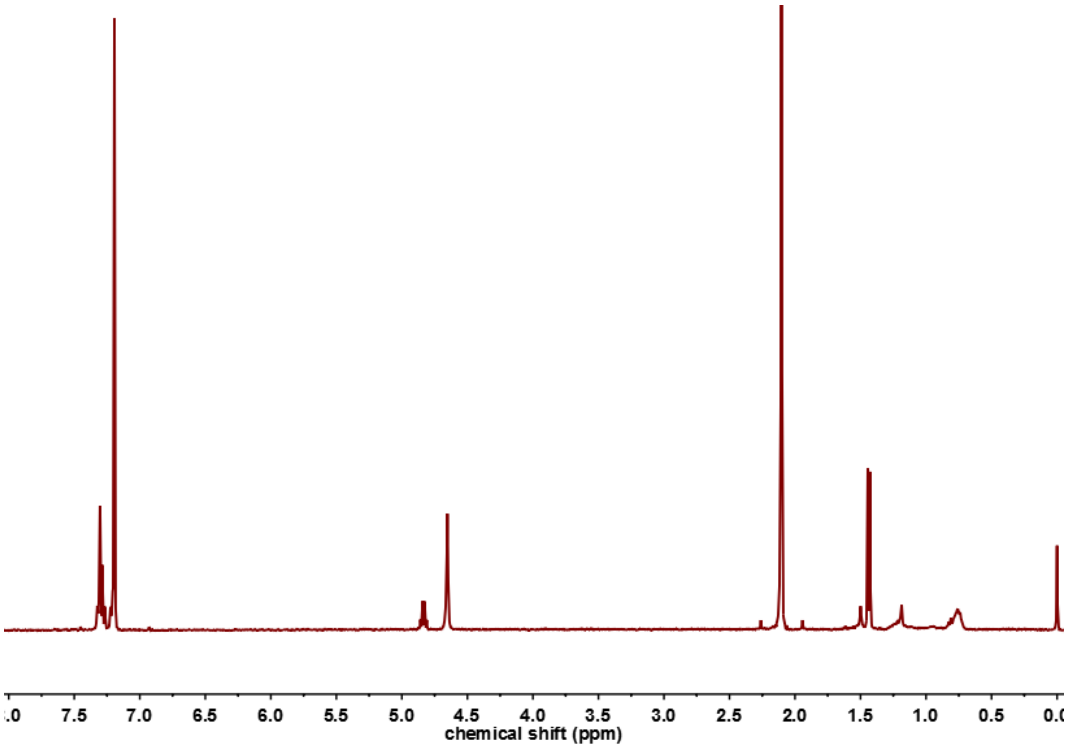

Figure A.31: Phenylethanol in C^2HCl_3 corresponding to Figure 7-10 (a) in main text. The peak at ca. 4.7 ppm corresponds to H_2O in the solvent and the peak at ca. 2.1 ppm corresponds to acetone.

J.2 Reaction analysis

This section contains the spectra of samples produced enzymatically in the work carried out in chapter 7.

Spectra from Figure 7-11 in main text

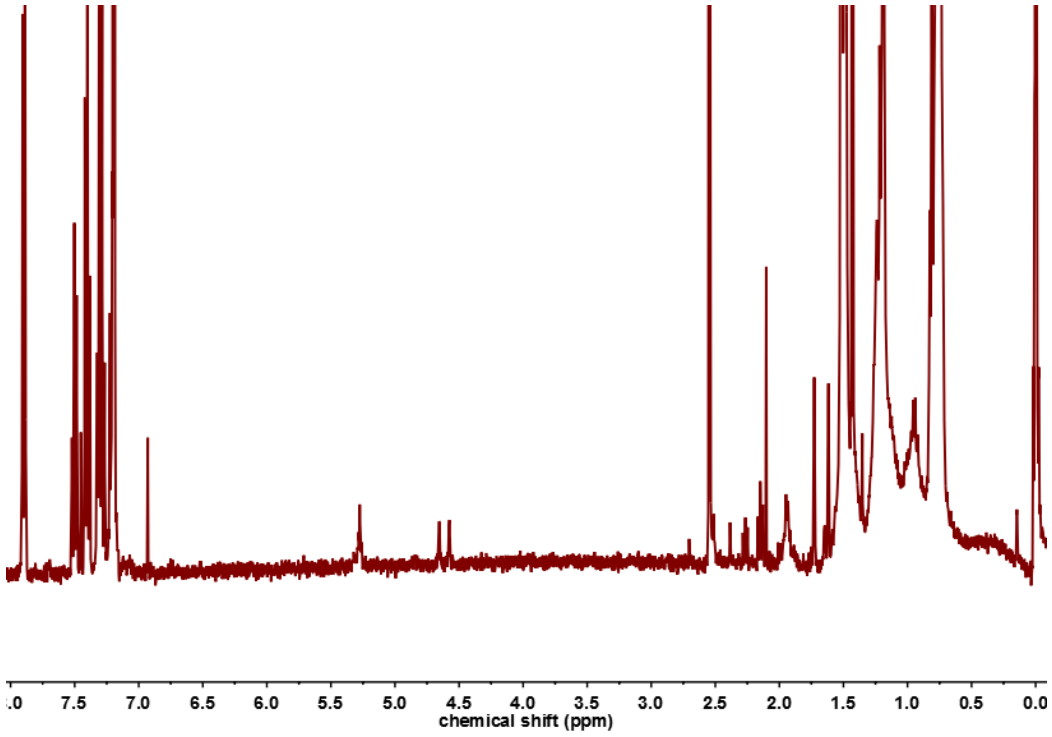

Figure A.32: Spectrum of phenylethanol produced by an (R)-selective ADH with [4S-^{2}H]NADH. Product was extracted into C^2HCl_3.

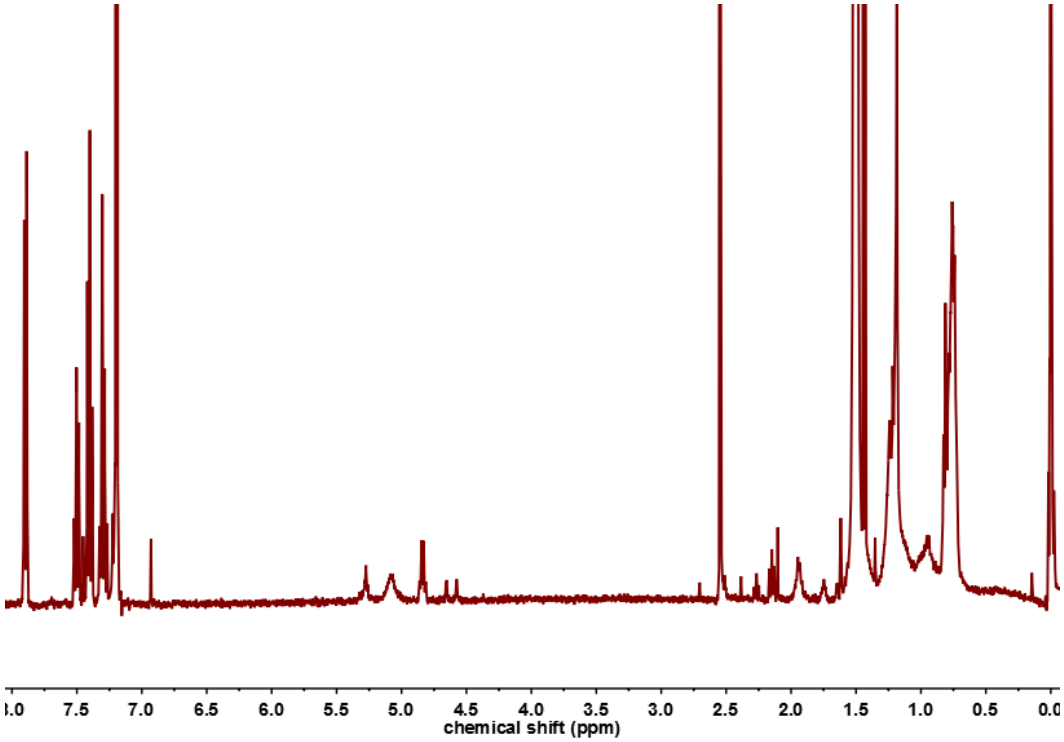

Figure A.33: Spectrum of phenylethanol produced by an (S)-selective ADH with [4S-^{2}H]NADH. Product was extracted into C^{2}HCl$_{3}$.

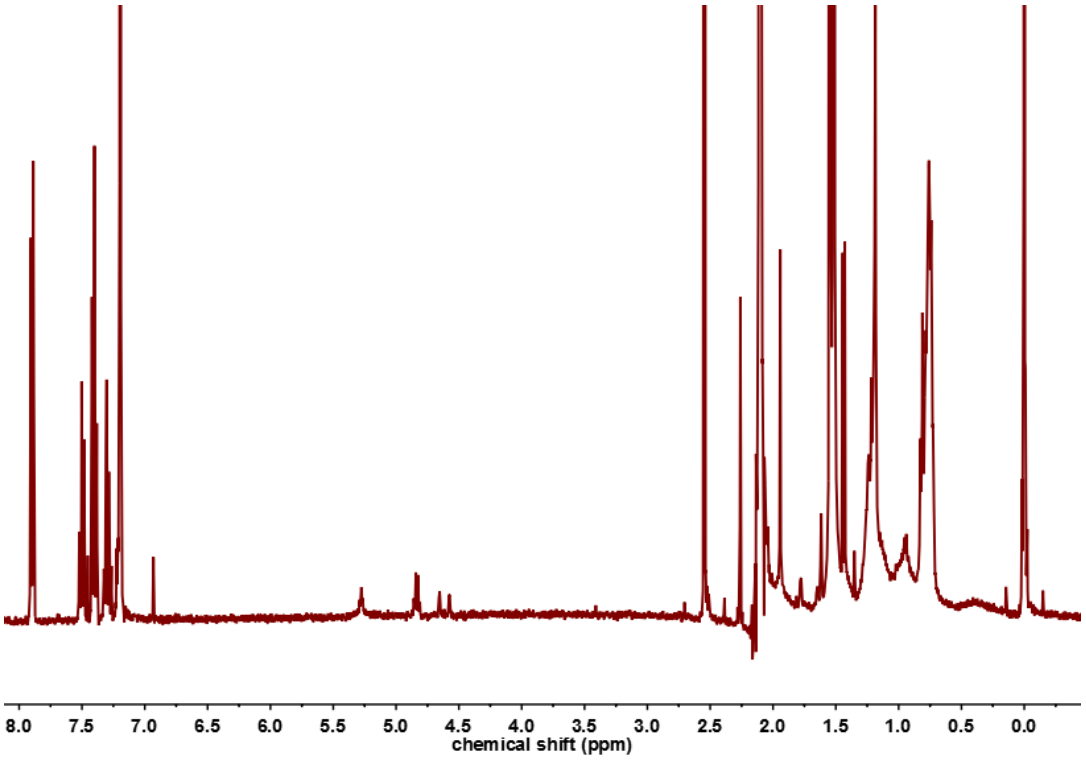

Figure A.34: Spectrum of phenylethanol produced by an (R)-selective ADH with [^{1}H]NADH. Product was extracted into C^{2}HCl$_{3}$.

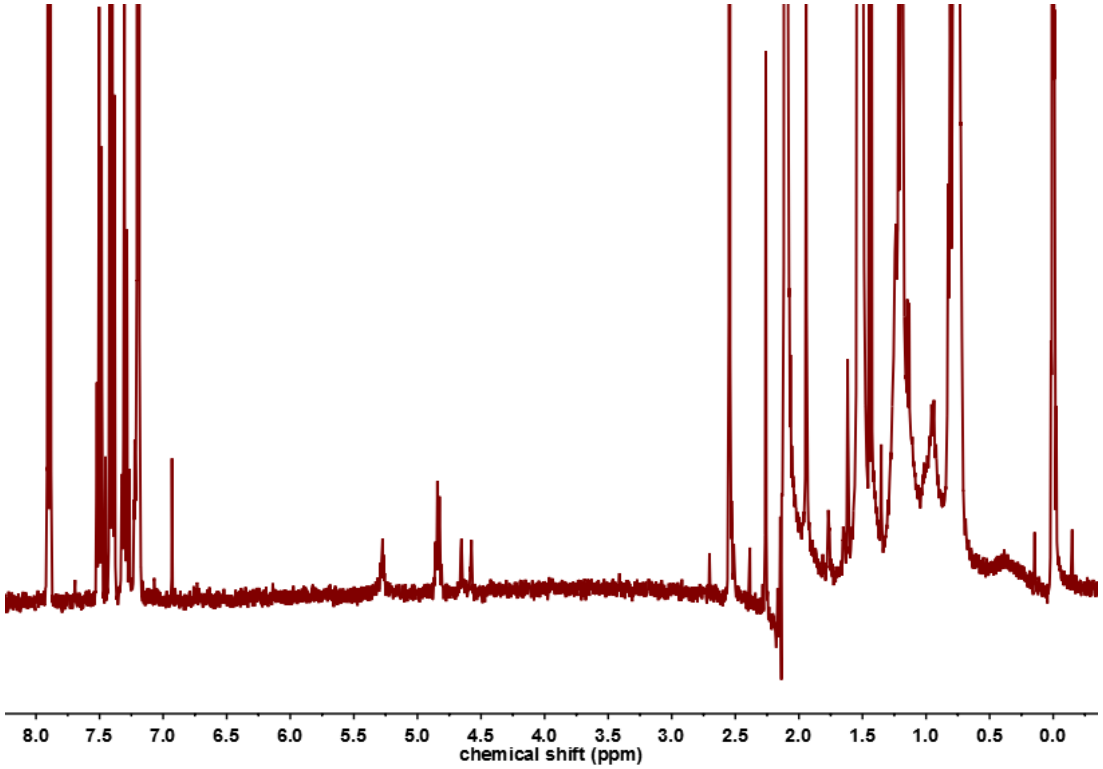

Figure A.35: Spectrum of phenylethanol produced by an (S)-selective ADH with [^{1}H]NADH. Product was extracted into C^{2}HCl$_3$.

Spectra from Figure 7-13 in main text

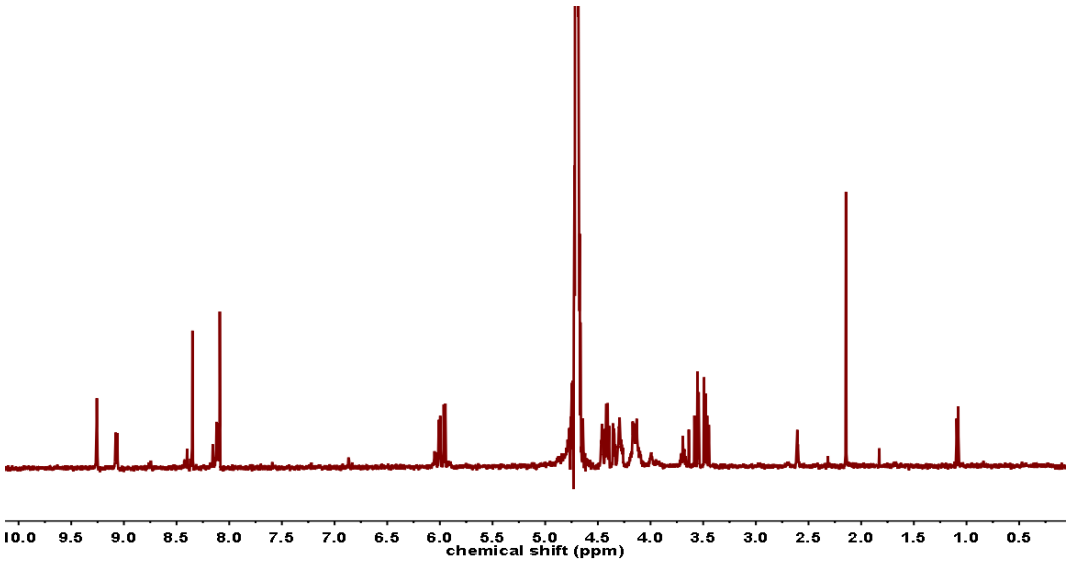

Figure A.36: Spectrum of the aqueous fraction after addition of [4S-^{2}H]NADH to an (S)-selective ADH reaction converting acetophenone to phenylethanol. The phenylethanol product was later extracted with C^{2}HCl$_3$.

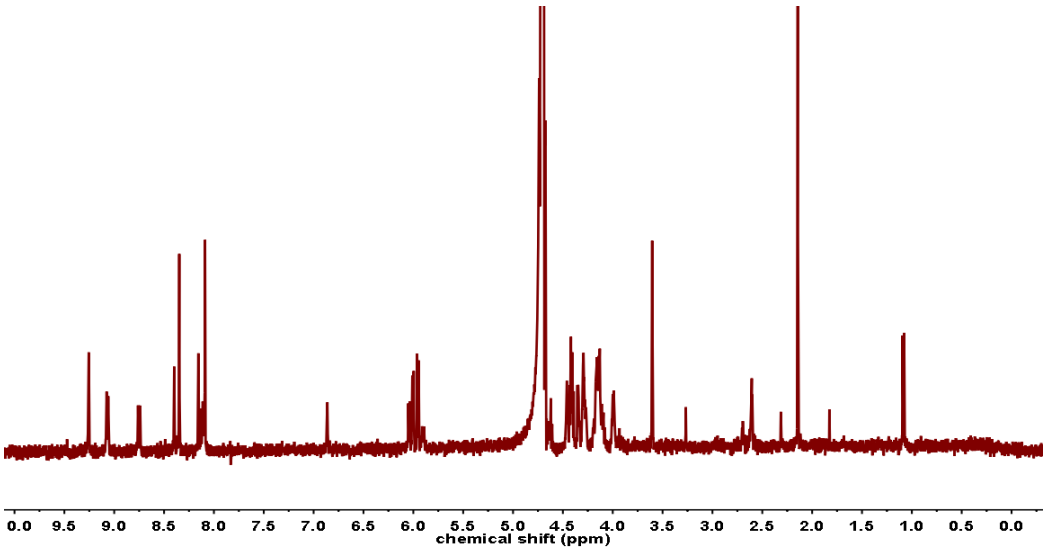

Figure A.37: Spectrum of the aqueous fraction after addition of [4S-^{2}H]NADH to a (R)-selective ADH reaction converting acetophenone to phenylethanol. The phenylethanol product was later extracted with $C^{2}HCl_{3}$.

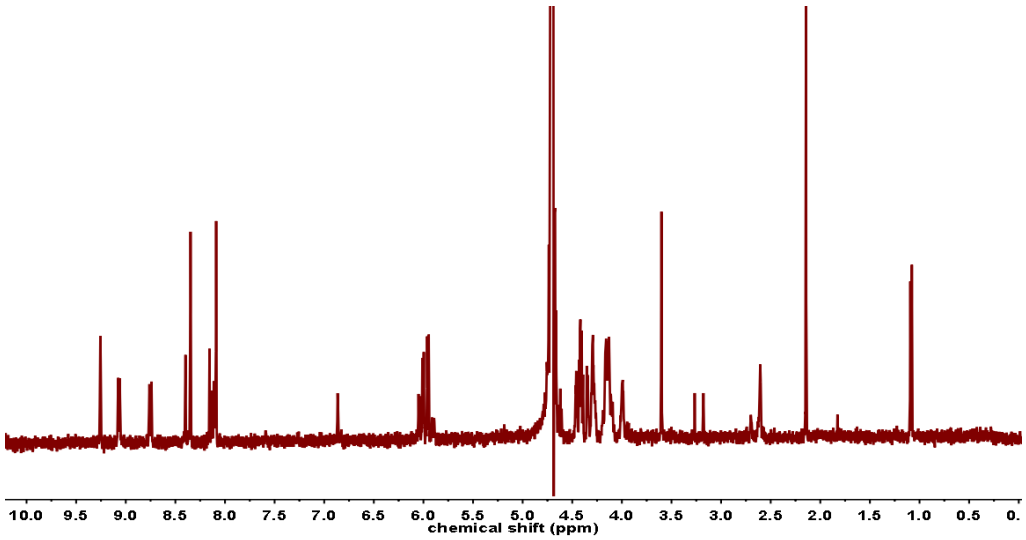

Figure A.38: Spectrum of the aqueous fraction after addition of [^{1}H]NADH to a (S)-selective ADH reaction converting acetophenone to phenylethanol. The phenylethanol product was later extracted with $C^{2}HCl_{3}$.

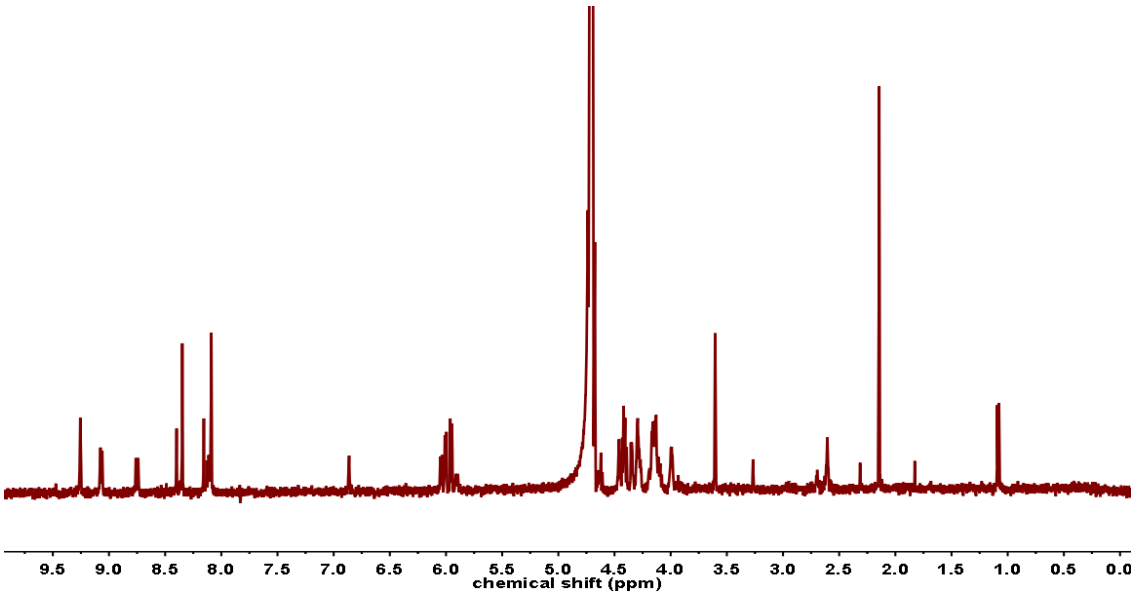

Figure A.39: Spectrum of the aqueous fraction after addition of [^{1}H]NADH to a (R)-selective ADH reaction converting acetophenone to phenylethanol. The phenylethanol product was later extracted with C^{2}HCl$_3$.

Spectra from Figure 7-15 in main text

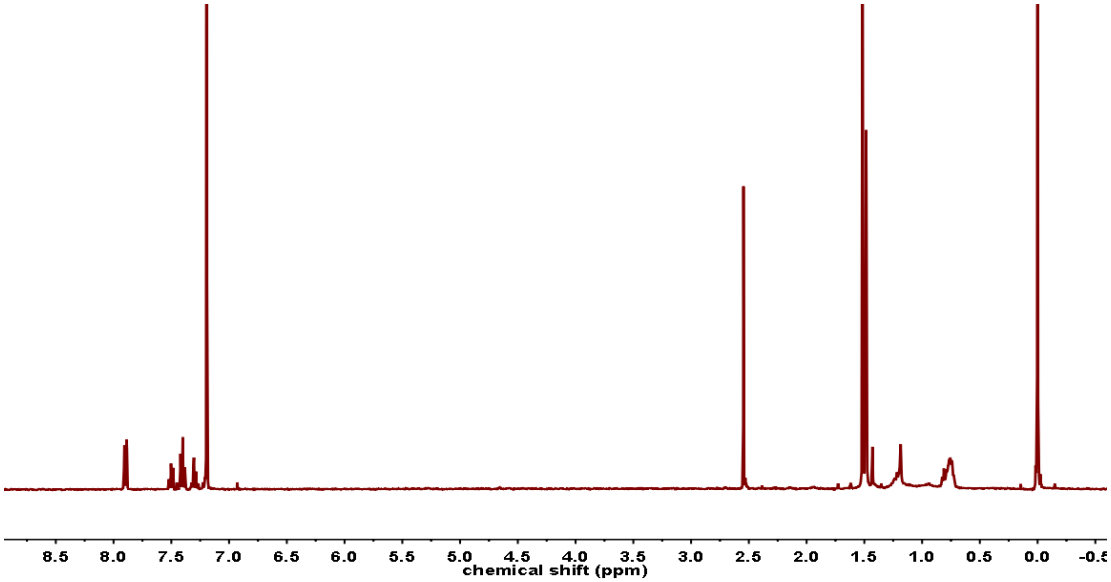

Figure A.40: Spectrum of phenylethanol produced with an (S)-selective ADH with cofactor recycling *in situ*. Sample was subsequently extracted into C^{2}HCl$_3$.

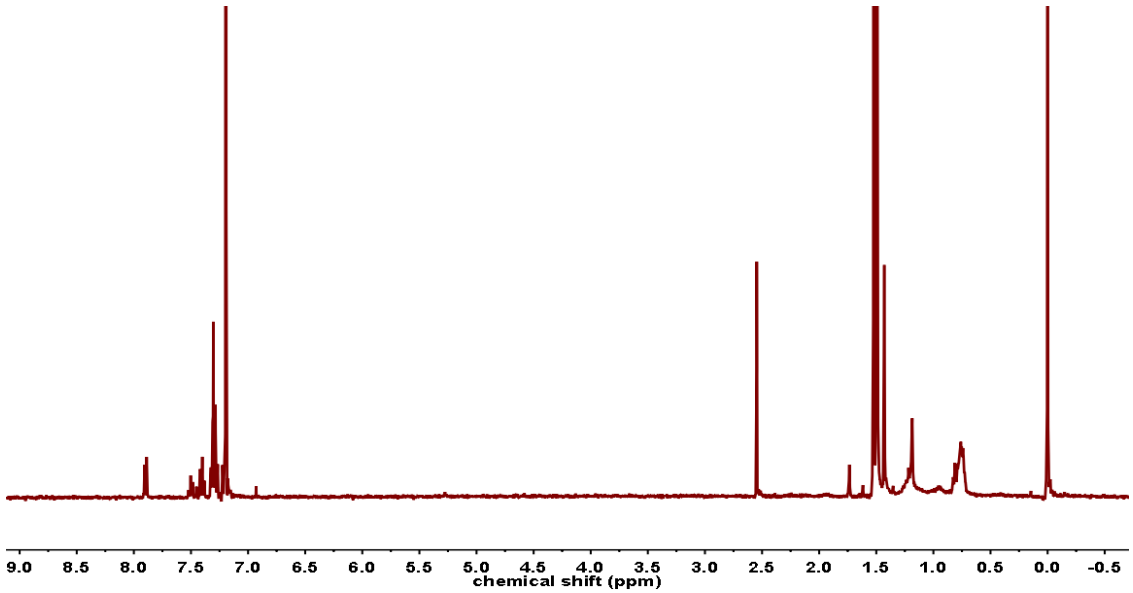

Figure A.41: Spectrum of phenylethanol produced with an (R)-selective ADH with cofactor recycling *in situ*. Sample was subsequently extracted into C^2HCl_3.

Spectra from Figure 7-16 in main text

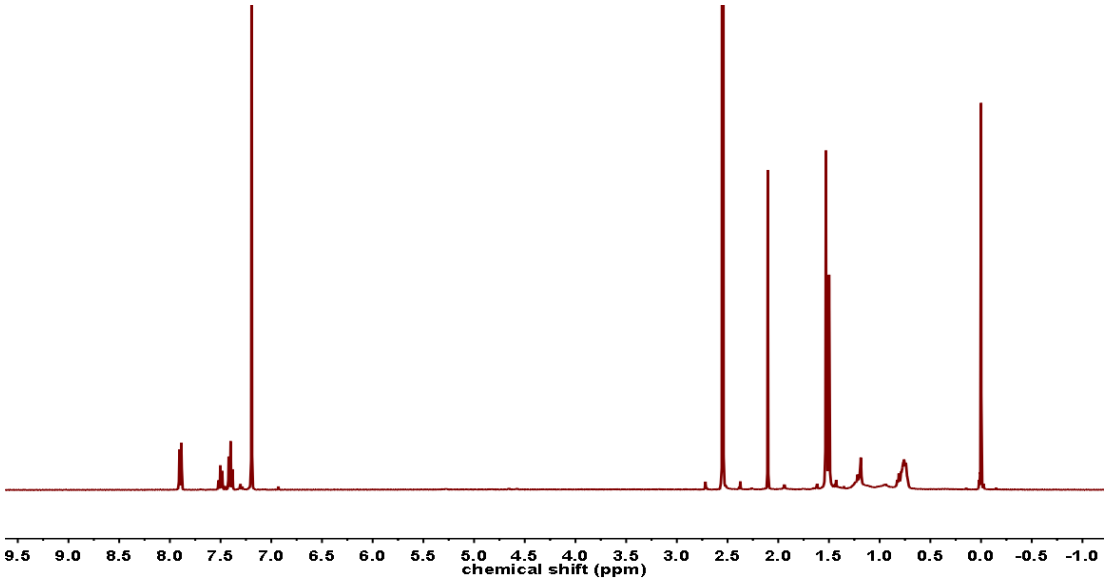

Figure A.42: Spectrum of (S)-phenylethanol produced with *in situ* cofactor recycling in the presence of $^2H_2$. This reaction was carried out in un-buffered H_2O.

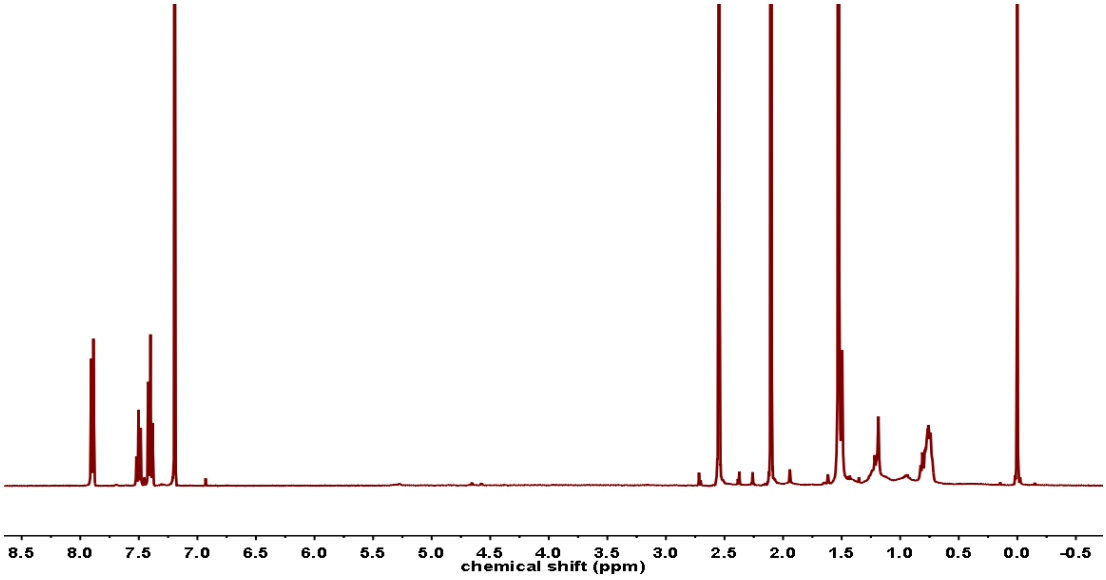

Figure A.43: Spectrum of (S)-phenylethanol produced with *in situ* cofactor recycling in the presence of D_2. This reaction was carried out in un-buffered ^2H_2O.

Appendix K : *ee* of ADH 101 and ADH 105 using a glucose dehydrogenase cofactor recycling system

Chiral HPLC was carried out to determine the *enantiomeric excess (ee)* for each of the ADH enzymes used in Chapter 7, in the presence of a glucose dehydrogenase cofactor recycling system. The traces from each of these tests are shown in Figure A.44. From these traces it is clear that both enzymes give >99 % *ee* with the GDH system.

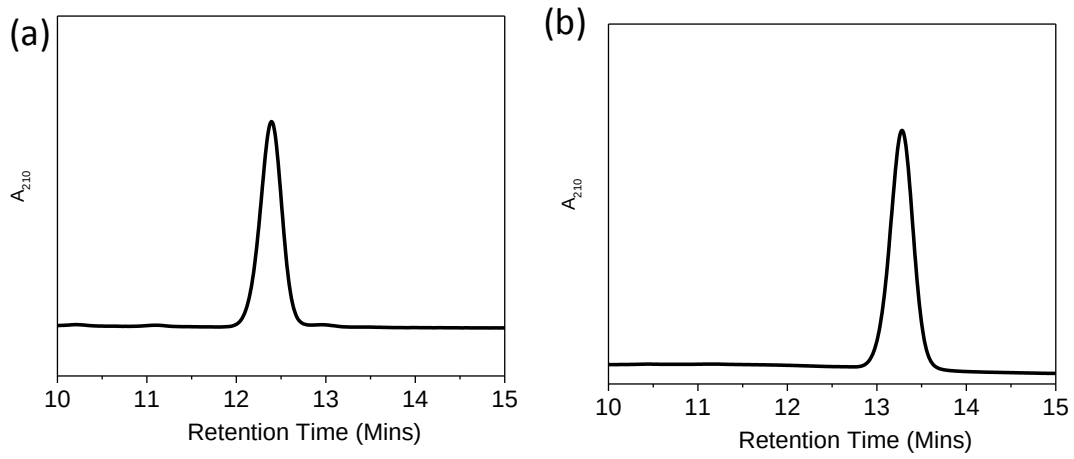

Figure A.44: The alcohol dehydrogenase enzymes with glucose dehydrogenase as a cofactor recycling system. Reactions were carried out on a 1 mL scale with 500 µg of glucose dehydrogenase, 200 µg of each alcohol dehydrogenase, 1 mM NAD^+, 10 mM Acetophenone and 50 mM d-glucose. (a) HPLC trace at 210 nm for the product of the reaction using ADH 101 (b) HPLC trace at 210 nm for the product of the reaction using ADH 105.

The HPLC method used to perform this analysis is described in Appendix C.